

Department of Pure and Applied Chemistry

**STUDIES AND IMPROVEMENT OF MOLECULAR DOCKING METHODS  
IN RIGID AND FLEXIBLE RECEPTORS**

by

**ARMELLE LE GALL**

A thesis submitted to the Department of Pure and Applied Chemistry, University of Strathclyde, in part fulfillment of the regulations for the degree of Doctor of Philosophy in Chemistry.

January 2017



## **Declaration of Ownership**

This thesis is the result of the author's original research. It has been composed by the author and has not been previously submitted for examination which has led to the award of a degree.

The copyright of this thesis belongs to the author under the terms of the United Kingdom Copyright Acts as qualified by University of Strathclyde Regulation 3.50. Due acknowledgement must always be made of the use of any material contained in, or derived from, this thesis.

Signed:

Date:

## **Acknowledgements**

I would firstly like to thank Colin Edge, my industrial supervisor at GSK, for useful and lively discussions about science but also English grammar, for his support throughout these four years and for making me smile when the motivation evaded me. I would also like to thank Tell Tuttle, my supervisor at the University of Strathclyde, for insightful discussions and guidance and for welcoming me in his lab.

I would also like to thank my colleagues in Computational Chemistry at GSK for their support and in particular I would like to thank Andrew Leach and Darren Green, for encouraging me to join the GSK/University of Strathclyde collaborative PhD programme and for their support, Gianpaolo Bravi for his advice and encouragement, Chris Luscombe, for his help with experimental design and Ian Wall for his feedback and for helping me with my revisions.

I would like to thank the students in Tell Tuttle's lab for welcoming me and looking after me during my trips to Glasgow.

Finally, I would like to thank my family and my friends for their continuing support without which I would not have come so far and of course, a special thank-you to Martin for keeping me smiling and for providing me with invaluable and numerous cups of tea.

## Abstract

Computational chemistry is a field of chemistry that uses computers to model chemical structures and properties and as such has been used in drug discovery since the eighties.<sup>1</sup> Computational chemistry within the field of Drug Design can be sub-divided into a number of different areas, including target identification, high-throughput screening analysis, *de novo* design, molecular docking, activity predictions, etc. These methods aim to predict the properties of molecular systems, such as the energy, the activity profile or the physico-chemical properties.

The main objective of computational chemistry in the pharmaceutical industry context is to help decision making by guiding research scientists as to which molecules to synthesise or test.<sup>2</sup> In the case of structure-based drug design, computational chemistry relies on structural biology to provide structural data, for instance crystal structures of protein-ligand complexes. These crystal structures give information about the interaction of the ligand and the protein binding site and can be used in the design of subsequent and more optimised molecules.

The use of rigid receptor molecular docking is exemplified in this work through the investigation of the LTA4H system. A number of analogue compounds of **5** were docked in LTA4H successfully and it was shown that molecular docking could be used as a tool for stereochemistry assignment for the closely related LTA4H ligands **10a-d**. In this work, molecular docking predicted the isomers associated with measured potencies and these predictions were confirmed by subsequent experimental data.

One drawback of rigid receptor docking is that it does not account for the flexibility of the target. The investigation of protein flexibility in molecular docking, therefore, followed. Standard protocols from the Schrödinger modelling suite were investigated first and the results were benchmarked for the fXa and CDK2 dockings, which were compared to the published Schrödinger results. The Induced Fit Docking (IFD) protocol was tested with default settings, and with automated and manual truncations of amino acids. These experiments concluded that the selection of amino acids could be improved as was also the case for the scoring function, IFDScore. Therefore, in this work a new approach for the automatic selection of amino acids for flexible exploration of the binding site was introduced. In addition, a modified scoring function was investigated and applied to fXa, CDK2 and UPPS systems. The new selection and scoring protocols showed some advantages over the standard Schrödinger IFD protocol.

## Abbreviations

2D	Two-dimensional
3D	Three-dimensional
5-LO	5-Lipoxygenase
Å	Angström
AA	Arachidonic Acid
AMBER	Assisted Model Building with Energy Refinement
AP	Aminopeptidase
CDK2	Cyclin-Dependent Kinase 2
CHARMM	Chemistry at HARvard Macromolecular Mechanics
COPD	Chronic Obstructive Pulmonary Disease
COX-2	Cyclooxygenase-2
CSAR	Community Structure-Activity Resource
CSD	Cambridge Structural Database
fXa	Factor Xa
GA	Genetic Algorithm
GOLD	Genetic Optimisation for Ligand Docking

Glide	Grid-based Ligand Docking with Energetics
GSK	GlaxoSmithKline
IC <sub>50</sub>	Half maximal Inhibitory Concentration
IFD	Induced Fit Docking
kDa	kiloDalton
Ki	Inhibition constant
LT	Leukotriene
LTA4	Leukotriene A4
LTA4H	Leukotriene A4 Hydrolase
LTB4	Leukotriene B4
LTC4	Leukotriene C4
MMFF	Merck Molecular Force Field
MM4	Molecular Mechanics 4
NMR	Nuclear Magnetic Resonance
OPLS	Optimized Potential for Liquid Simulations
OPLS-AA	Optimized Potential for Liquid Simulations – All Atoms
PDB	Protein Data Bank



PE	Prime Energy
PPAR $\gamma$	Peroxisome proliferator activated receptor gamma
RMSD	Root-Mean Square Deviation
SMILES	Simplified Molecular Input Line Entry Specification
SP	Standard Precision
UA	Unified Atoms
UPPS	Undecaprenylpyrophosphate Synthase
$\mu$ M	Micromolar
vdW	Van der Waals
XP	eXtra Precision

#### Amino Acids

Ala	Alanine
Arg	Arginine
Asn	Asparagine
Asp	Aspartic acid
Cys	Cysteine
Gln	Glutamine
Glu	Glutamic acid
Gly	Glycine

His	Histidine
Ile	Isoleucine
Leu	Leucine
Lys	Lysine
Met	Methionine
Phe	Phenylalanine
Pro	Proline
Ser	Serine
Thr	Threonine
Trp	Tryptophan
Tyr	Tyrosine
Val	Valine

## Table of Contents

Declaration of Ownership .....	I
Acknowledgements.....	II
Abstract.....	III
Abbreviations.....	V
Table of Contents.....	IX
1. Introduction .....	1
2. Theory .....	4
2.1. Molecular mechanics force fields .....	4
2.2. Molecular docking.....	17
2.3. Protein flexibility .....	31
2.4. Statistical methods.....	45
2.5. Water molecules in crystal structures .....	53
3. Protein systems studied .....	70
3.1. Leukotriene A4 hydrolase .....	70
3.2. Cyclin-dependent kinase 2.....	80
3.3. UPPS.....	91
3.4. Factor Xa .....	101
4. Methods .....	108
4.1. Preparation of the protein .....	108
4.2. Preparation of ligands.....	110
4.3. Predicting water locations .....	111
5. Rigid docking in LTA4H .....	113
5.1. LTA4H protein and ligand preparation .....	113
5.2. Conformations of the [3.3.1] system .....	116
5.3. Comparing rigid receptor docking programs .....	119
5.4. Comparison of simulation length.....	128
5.5. Conformational search in rigid receptor docking .....	141
5.6. Predicting stereochemistry with rigid receptor docking .....	147
5.7. Application to molecular diversity in rigid receptor docking.....	161

5.8.	The role of water in rigid receptor docking .....	177
5.9.	Conclusion.....	205
6.	From rigid to induced fit docking .....	208
6.1.	Glide docking.....	208
6.2.	Standard induced fit docking .....	213
6.3.	Induced fit docking with automatic mutations.....	219
6.4.	The effect of different chain lengths on the Prime energy.....	227
6.5.	Induced fit docking with manual amino acid mutations .....	230
6.6.	Conclusion.....	238
7.	An improved IFD protocol .....	243
7.1.	Development of improved IFD protocol .....	243
7.2.	Testing of improved IFD protocol .....	260
7.3.	Application of improved IFD protocol.....	285
7.4.	Conclusion.....	331
8.	Conclusions .....	334
9.	Outlook.....	339
	References .....	341
	Appendices.....	351
	Appendix 1 – automated_IFD_process.pl.....	351
	Appendix 2 – binding_site_RMSD.pl.....	362
	Appendix 3 – New IFDScores calculations .....	369

## 1. Introduction

Drug discovery aims to find new molecules that will modify a binding event between a protein and a substrate, whether that be a small molecule or another protein. This modification could induce the inhibition of the event, i.e., to stop it happening to prevent the associated biological response, to modulate it, i.e., to produce a lesser biological response, or to enhance it, i.e., to increase the biological response. Modern medicinal chemistry uses techniques such as high throughput screening (HTS) to identify new active molecules, often referred to as hits. Hits are then modified in an iterative fashion in order to optimise the biological as well as the safety profile leading to the identification of leads and then drug candidates.<sup>3-4</sup>

Computational chemistry has had an increasingly central role to play in drug discovery over the past decades.<sup>5</sup> One of the techniques that is often used is molecular docking, with the objective of predicting the binding mode of known active molecules, but also potentially to discriminate binders from non-binders. Molecular docking relies on molecular mechanics force fields to accurately predict the energy of molecules. This can enable binding modes to be predicted and, therefore, critical interactions with the protein binding site can be identified. Molecular docking has been used and evaluated extensively and has been successful at generating correct poses but less successful at scoring them accordingly so that the right binding pose is found at the top of the rank-order. This is known as the “docking problem” and has been reported in the literature.<sup>5-7</sup>

This thesis will first cover the theory behind molecular mechanics force fields, their parameterisation and classification. This will be followed by a description of how molecular mechanics is used in molecular docking. Scoring functions will be discussed in more detail. In particular, an example of a force-field based scoring function, such as GoldScore which is available for the docking programme GOLD, will be detailed. Force-field based scoring functions are based on a molecular mechanics equation in order to estimate the energy of the ligand pose. On the other hand, empirical or regression based scoring functions, such as ChemScore or GlideScore, attempt to approximate the binding affinity of ligand poses and, therefore, should be able to discriminate between binders and non-binders.<sup>8</sup>

Rigid receptor molecular docking will then be described for a set of closely related ligands of leukotriene 4 hydrolase (LTA4H). The docking programme GOLD, which is based on a genetic algorithm, was the programme of choice for these ligands. Redocking was investigated first, followed by cross-docking of new molecules, that is docking molecules in their non-native crystal structures. Molecular docking was then used to predict stereoisomers and these predictions are compared to subsequent experimental characterisation.

In real life systems, the protein and its binding site are not rigid. Amino acids can occupy different rotamer states, loops can move in and out making the binding site larger or smaller, thus accommodating ligands of different sizes. Predicting protein flexibility is still today a very computationally challenging issue, in terms of computer power and time. Therefore, most docking methods which include protein flexibility are limited to amino acids within the binding site.<sup>9</sup> With these

programmes, such as Schrödinger's Induced Fit Docking (IFD)<sup>9</sup> or AutoDock,<sup>10</sup> the user is able to choose amino acids of interest and the conformation of these can be explored either prior to, or during, the docking run. Schrödinger's IFD protocol was investigated in detail, with public domain structures of CDK2 which are known to show some movement in the binding site.

The choice of amino acids whose conformations will be explored during a docking run is often subjective and relies on the user's knowledge of the protein system. The automated selection of amino acids can also be used in the IFD protocol and this selection is based on the temperature factor. An alternative selection of amino acids is also explored in this work as a comparison to the Schrödinger approach. In addition, the Schrödinger IFD scoring function is also analysed. Scoring is a challenge in docking programmes and it is instructive to evaluate how the standard Schrödinger IFD scoring function performs and whether it can be modified and perhaps improved. The standard protocol as well as the modified one is applied to a number of public as well as GSK proprietary systems.

## 2. Theory

### 2.1. Molecular mechanics force fields

Molecular mechanics methods<sup>5</sup> consider a 'ball-and-spring' representation of chemical entities, where balls are the atoms and springs are the bonds between them. Molecular mechanics methodologies give information about the energy of the system in a computationally efficient manner and as such, are very attractive when computer time and power are limited.

The speed of the method results from the ability to evaluate the potential energy of the system, using a pre-defined energy function, which defines the force field.

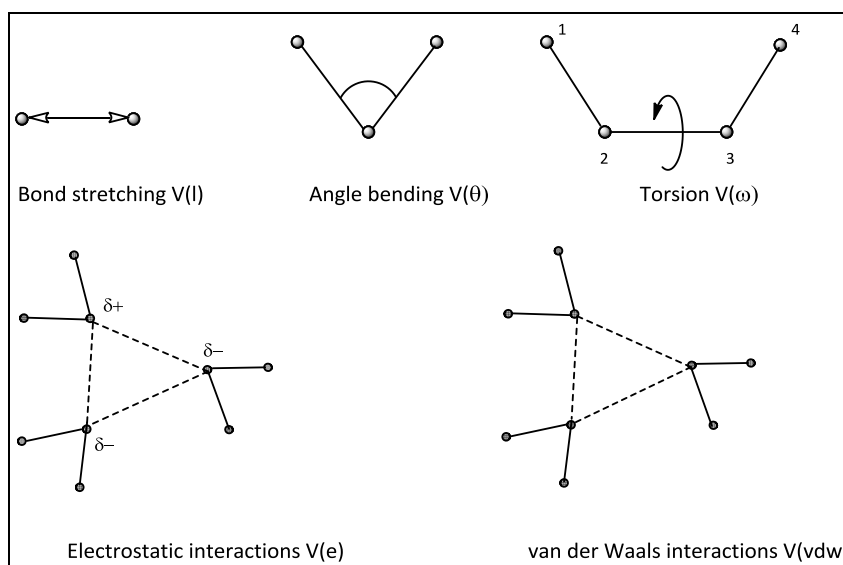


*Figure 1: Representation of five key force field terms*



### 2.1.1. Force field description

A generic force field can be described by the following equation:<sup>11</sup>

$$V = V(l) + V(\theta) + V(\omega) + V(\text{non bonded}) \quad (1)$$

+ specific terms

*Figure 1* shows a schematic representation of five key terms of a force field.

In Equation 1, the first term  $V(l)$  is used to model the stretching or compression of bonds. It is described by a harmonic oscillator:

$$V(l) = \sum_{\text{bonds}} \frac{k_r}{2} (l_i - l_{i,0})^2 \quad (2)$$

In this case, it is analogous to Hooke's law.  $k_r$  is the stretching force constant which indicates the stiffness of the spring (strength of the bond) and  $l_{i,0}$  is the reference equilibrium bond length.  $l_i$  is the instantaneous bond length value observed for bond  $i$ . When  $l_i$  moves away from  $l_{i,0}$ , i.e., the bond stretches or compresses, the energy of the system deviates from its local minimum and increases as can be seen in *Figure 2*. Another way of describing bond stretching would be to use a Morse potential<sup>5</sup> defined as follows:

$$V(l) = D_e \{1 - \exp[-a(l - l_0)]\}^2 \quad (3)$$

$$\text{where } a = v \sqrt{\frac{\mu}{2D_e}} \quad (4)$$

$D_e$  is the depth of the potential energy minimum,  $\nu$  is the vibration frequency of the bond and  $\mu$  is the reduced mass of the vibrating system. Although using a Morse potential could be advantageous, e.g., it includes bond breaking,<sup>5</sup> it is not usually used in molecular mechanics as it requires more computer time to calculate and also three parameters to be defined for each type of bond, rather than two for the harmonic oscillator.

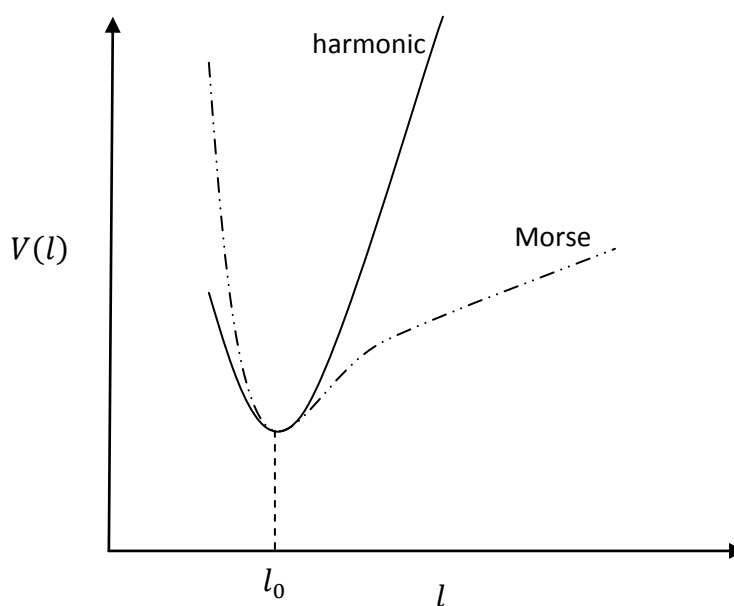


Figure 2: Illustration of harmonic oscillator and Morse potentials

The second term  $V(\theta)$  in Equation 1 models angle bending and is calculated as:

$$V(\theta) = \sum_{\text{angles}} \frac{k_{\theta}}{2} (\theta_i - \theta_{i,0})^2 \quad (5)$$

The angle bending expression is also a harmonic oscillator, where  $k_{\theta}$  is the angle force constant and  $\theta_{i,0}$  is the equilibrium angle value.  $\theta_i$  is the current observed angle between the three bonded atoms. When  $\theta_i$  moves away from  $\theta_{i,0}$ , i.e., the

angle opens or closes, the energy of the system increases. This term can be represented by a figure equivalent to the harmonic potential in *Figure 2*.

The third term  $V(\omega)$  in Equation 1 is the bond rotation - also known as the torsion - term which models the energy variation with the rotation of atoms 1 and 4 around a central bond (*Figure 1*). It is computed as follows:

$$V(\omega) = \sum_{\text{torsions}} \frac{V_n}{2} (1 + \cos(n\omega - \gamma)) \quad (6)$$

$V_n$  represents the barriers of rotation.  $n$  is the multiplicity, i.e., the number of minima as the bond is rotated around  $360^\circ$ .  $\gamma$  is the phase angle which offsets the cosine function to allow the minimum and maximum to occur at pre-defined angles; and  $\omega$  is the torsion angle being considered. As an example, for an ethane molecule,  $n$  is 3,  $\gamma$  is  $0^\circ$  and  $\omega$  can be  $60^\circ$ ,  $180^\circ$  or  $300^\circ$  to get a minimum value.

The fourth term  $V(\text{non bonded})$  in Equation 1 models non-bonded interactions, i.e., electrostatics and van der Waals interactions. They are calculated for all atoms of the molecule which are not bonded to each other, or to a common atom, or separated by two atoms (these interactions are already taken into consideration in the bond stretching, angle bending and torsion terms). A typical non-bonded energy term is shown in Equation 7.

$$V(\text{non bonded}) = \sum_{i=1}^{N-1} \sum_{j=i+1}^N \left( 4\epsilon_{ij} \left[ \left( \frac{\sigma_{ij}}{r_{ij}} \right)^{12} - \left( \frac{\sigma_{ij}}{r_{ij}} \right)^6 \right] + \frac{q_i q_j}{4\pi\epsilon_0 r_{ij}} \right) \quad (7)$$

The electrostatic potential is modelled using Coulomb's law (Equation 8), which represents the magnitude and charge of the electrostatic force for two idealised point charges  $q_i$  and  $q_j$ .

$$V(e) = \sum_{i=1}^{N-1} \sum_{j=i+1}^N \left( \frac{q_i q_j}{4\pi\epsilon_0 r_{ij}} \right) \quad (8)$$

where  $\epsilon_0$  is the dielectric constant (or the permittivity of free space in vacuum) and  $r_{ij}$  is the separation between atoms  $i$  and  $j$ .

If we ignore polarisation, an atom can be considered as a point charge as its charge is evenly spread across its surface and, therefore, the centre of charge can be considered to be the centre of the atom.  $V(e)$  decreases with  $\frac{1}{r_{ij}}$ .

Van der Waals interactions are represented by a Lennard-Jones potential:

$$V(vdW) = \sum_{i=1}^{N-1} \sum_{j=i+1}^N \left( 4\epsilon_{ij} \left[ \left( \frac{\sigma_{ij}}{r_{ij}} \right)^{12} - \left( \frac{\sigma_{ij}}{r_{ij}} \right)^6 \right] \right) \quad (9)$$

where  $\epsilon_{ij}$  is the well depth and  $r_{ij}$  is the distance between atoms  $i$  and  $j$ .  $\sigma_{ij}$  is the collision diameter for the interaction between atoms  $i$  and  $j$ . It is calculated as the arithmetic mean of the values of the atomic radii of  $i$  and  $j$  taken as isolated entities.

The Lennard-Jones potential is an approximation of the interaction between two neutral atoms or molecules. There are two terms, representing attractive and repulsive interactions. London dispersion forces describe the attraction between

two entities. Momentary electronic phenomena arise in atoms due to the movement of their electrons. When the distribution of the electron density of a given atom shifts to one side, it becomes slightly negative ( $\delta^-$ ) while the opposite side of the atom becomes slightly positive ( $\delta^+$ ), creating a dipole. Because electrons are very mobile, the direction of the dipole changes all the time with the change in electron density. The electron density in a neighbouring atom responds to this dipole, producing an *induced* dipole, and their brief interaction results in the attraction of the two atoms. This attraction term of the Lennard-Jones potential can be described as a potential proportional to  $r^{-6}$ .

The repulsion between two entities increases rapidly when  $r_{ij}$  becomes small. Repulsion originates from the Pauli Exclusion Principle, which is a quantum mechanical principle stating that any two electrons in a system cannot have the same quantum numbers. When two atoms approach each other, their orbitals overlap. In the case of two helium atoms, the electron-occupied 1s orbitals would overlap. Two  $\sigma$  orbitals are created, one bonding and one anti-bonding. There are four electrons to accommodate in these two orbitals and these four electrons cannot be held by the bonding orbital because of the Pauli Exclusion Principle.<sup>12</sup> The resulting energy of the system is higher and it continues to increase quickly as the two entities get closer (*Figure 3*). This is the cause of the repulsion. It can be approximately described as a potential proportional to  $r^{-12}$ .

The Lennard-Jones potential defined above can also be referred to as a 12-6 potential, which refers to the values of the exponents in Equation 9. Both 9-6 and 10-6 potentials, i.e., respectively proportional to  $r^{-6}$  and  $r^{-9}$ , and  $r^{-6}$  and  $r^{-10}$ ,

have been used in some force fields which give a softer curve.<sup>5</sup> However, 12-6 potentials are more widely used due to the computational efficiency of obtaining the  $r^{-12}$  term from the  $r^{-6}$  term (by squaring).

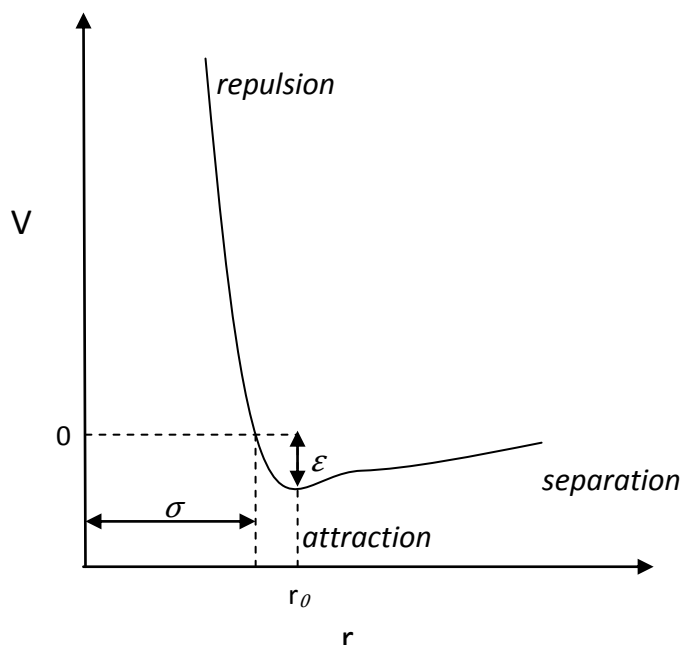


Figure 3: Illustration of the Lennard-Jones potential

Other terms (described as *specific terms* in Equation 1) can be added to estimate more subtle interactions within the system. These can include, for example, out-of-plane bending and hydrogen bonding terms. Out-of-plane bending terms are used to reach an acceptable energy for substructures that should lie in a coplanar manner. One way of modelling this is to apply improper torsions. An improper torsion is a torsion for which the atoms are not consecutively bonded to each other. A typical example (Figure 4) is of a ketone functionality in which the carbonyl group should sit coplanar to the adjacent carbon atoms:

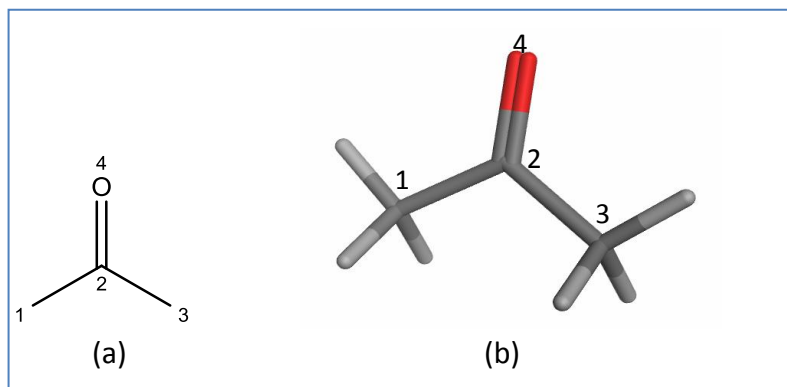
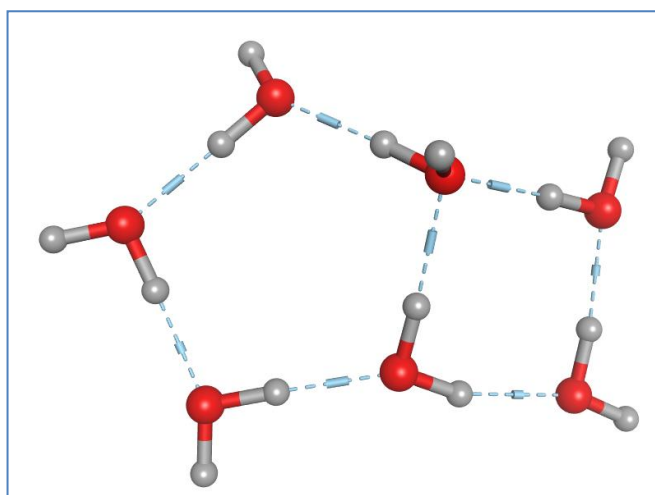


Figure 4: a) Two-dimensional depiction of propanone (without hydrogens); b) its low energy conformation after application of force field OPLS-AA

An improper torsion angle in this case would be, for example, 4-1-2-3. A torsional potential (e.g., Equation 6) is then applied to give a minimum value of the torsion at  $180^\circ$  in this instance.

Hydrogen bonds occur between a hydrogen atom, which is slightly positive, and an electronegative atom, such as nitrogen or oxygen, which has a lone pair (Figure 5). This is due primarily to the electrostatic attraction between the atoms. H-bonds are involved in the stability of the three-dimensional structure of proteins, e.g., secondary structures like  $\alpha$ -helices and  $\beta$ -sheets are characterised by their hydrogen bonding pattern. Hydrogen bonds are also important in the interaction of a protein binding site and a ligand. Therefore, hydrogen bonding is an important physical interaction to describe accurately in biochemical force fields.



*Figure 5: An example of hydrogen bond interactions between water molecules, oxygen atoms in red, hydrogen atoms in light grey and hydrogen bonds shown in light blue dotted lines*

The accurate description of hydrogen bonding can be achieved by adding a specific term which can be expressed as a 12-10 Lennard-Jones potential, used to describe hydrogen bond interactions, as is the case in the AMBER force field.<sup>13</sup> An alternative method to describing hydrogen bonds is exemplified in the GRID programme,<sup>14</sup> which identifies favourable interaction locations in a protein binding site using a chemical probe. The GRID force field uses an 8-6 potential as part of the term describing hydrogen bonds (Equation 10), as it produced the closest concordance with experimental data:<sup>15</sup>

$$E_r = \frac{C}{r^8} - \frac{D}{r^6} \quad (10)$$

$$\text{where } C = -3E_m r_m^8 \text{ and } D = -4E_m r_m^6 \quad (11)$$



In this case,  $r$  is the distance between the acceptor and the donor non-hydrogen atoms,  $E_m$  is the parameterised hydrogen bond energy and  $r_m$  is the ideal hydrogen bond length for the interacting heavy atoms. These parameters differ depending on the atoms engaged in the hydrogen bond interaction (m).

### 2.1.2. Force field parameterisation

Force fields are defined by their functional form (Equation 1) and their parameterisation. It is important before attempting any calculation to choose the force field appropriately. Indeed, force fields have been developed for particular systems, e.g., AMBER<sup>13</sup> for macromolecules, MMFF<sup>16-17</sup> for small molecules. They have different parameters and are only suitable for systems similar to those used to develop them.

Observations, e.g., bond length, provide the reference values for a number of terms, like the bond stretching term, and are required in order to solve Equation 1. This means that the force field should be accurate at predicting the energy and geometry of the specific chemical arrangements that were used to parameterise it. However, when the atom type under consideration has not been parameterised, then the force field cannot predict its geometry and the calculation would fail. As an example, biochemical force fields do not have atoms like boron parameterised. Therefore, they are unable to predict the energy of small molecules containing boron.

Evaluations of force fields have been reported in the literature, in particular in comparison to MMFF force fields.<sup>16</sup> Halgren showed in his evaluation of MMFF94 and MMFF94s to seven other force fields<sup>16</sup> that a number of force fields perform poorly, some generating the wrong conformers, others making errors of over 7 kcal/mol. The benchmark data set used was of small organic molecules which were similar to the ones used to derive the parameters of the force field. This could explain why the MMFF force fields performed well in comparison to the others

evaluated in this study. Even though MMFF force fields performed the best, Halgren showed that they also suffered from a lack of parameterisation, notably for halocyclohexanes, favouring axial over equatorial substitution.<sup>16</sup>

### 2.1.3. Force field classification

Force fields can be classified depending on the presence of cross-terms in their functional form.<sup>18</sup> A force field of class I, like OPLS (see Section 2.1.4), includes harmonic terms but does not have any cross-term whilst a class II force field includes anharmonic terms, such as Morse potential and quartic terms for the description of bond stretching and angle bending, and cross terms, such as stretch-bend, torsion-stretch and bend-bend terms. These additional terms enable a greater accuracy in property predictions, like vibrational frequencies. An example of a class II force field is MM3.<sup>19-21</sup> A class III force field is even more accurate and is able to incorporate electronegativity and hyperconjugation, as is the case for the MM4 force field.<sup>5, 22</sup>

To decrease the running time, some force fields<sup>23</sup> are designed so that hydrogens are included with the non-hydrogen atoms, also known as heavy atoms, to which they are linked. This is the case for OPLS<sup>23</sup> and AMBER.<sup>13</sup> These types of atoms are known as unified atoms (UA). Polar hydrogens are not typically considered in the unification process so that they can take part in hydrogen bonding events.

#### 2.1.4. Force field example

OPLS<sup>23</sup> (Optimized Potential for Liquid Simulations) is a force field very similar to AMBER,<sup>13</sup> which is a general force field developed to model proteins and nucleic acids. The functional form of OPLS is equivalent to Equation 1. The OPLS force field differs from AMBER by the removal of the hydrogen bond specific term. It was found by Jorgensen and Tirado-Rives that the specific term was not necessary to describe hydrogen bonds accurately in polypeptide crystals and therefore was not included in the OPLS force field.<sup>23</sup> OPLS was primarily designed to describe proteins in solution, rather than in gas phase. The original OPLS force field used a united atom (UA) model, which made it very popular as the number of atoms to be considered was smaller. Its development was focused on non-bonded interactions and the parameterisation was based on Monte Carlo simulations. The OPLS-AA (all atoms) force field was then developed to take into account all the atoms of the system, i.e., including non-polar hydrogen atoms.<sup>24</sup>

## 2.2. Molecular docking

Molecular docking consists of placing a ligand in a particular conformation within a protein binding site, which results in a particular orientation, often referred to as a pose.<sup>25</sup> Each pose is then scored in order to identify the most complementary arrangement of the ligand in the binding site from a shape and contact point of view.<sup>25</sup> The aim of the docking protocol is to find the right conformation and orientation of the ligand in the binding site and be able to discriminate this solution against other poses via a scoring function.

### 2.2.1. Scoring functions

Scoring functions attempt to assess the interactions between the active site and the ligand pose. Docking and particularly scoring are very challenging because of the flexibility of the ligand and of the protein and because of the accuracy of scoring functions. These challenges have been reported in the literature as the “docking problem”.<sup>5-7</sup> However, it is a method that is regularly used in drug discovery when the three-dimensional structure of the target is known.<sup>25</sup>

The potential energy that is calculated from a molecular mechanics force field (Equation 1) is used to characterise the energy of a system. In docking experiments, many ligand conformations are generated and need to be assessed to find the ones with the lowest energy or the highest predicted binding affinity.

There are three main groups of scoring functions, force field based, empirical or regression-based and knowledge-based. Force field based scoring functions are described using a force field to estimate the energy of the complex and of the ligand

itself (strain and steric). GoldScore is an example of this class and, as a force field based scoring function, has a similar functional form to Equation 1.<sup>26</sup> GoldScore attempts to reproduce geometries observed in crystal structures using a force field. It was not developed to reproduce binding affinities but has been shown to correlate with them to some extent.<sup>27</sup> It consists of three terms (Equation 12): the protein-ligand H-bond energy and the protein-ligand energy (non-bonded interactions), and the ligand internal energy (non-bonded interactions and torsional term).

$$GoldScore = -H\_bond\_Energy - \quad (12)$$

$$(Internal\_Energy + Complex\_Energy)$$

The protein-ligand hydrogen bond term (H\_bond\_Energy) is calculated by examining all possible hydrogen bonds between the protein and the ligand configuration (Equation 13).

$$E_{pair} = (E_{da} + E_{ww}) - (E_{dw} + E_{aw}) \quad (13)$$

where  $E_{dw}$  and  $E_{aw}$  are the hydrogen bond energy of the donor ( $d$ ) and acceptor ( $a$ ) in solution and  $E_{da}$  is the hydrogen bond energy of the complex ( $da$ ) whilst  $E_{ww}$  is the hydrogen bond energy of the water molecules being removed upon complexation.  $E_{pair}$  is then scaled by a weight between 0 and 1, depending on the geometry of the hydrogen bond.  $E_{pair}$  is pre-computed based on model fragments.<sup>28</sup>

The internal energy term consists of a steric term described by a 12-6 Lennard-Jones potential, and a torsional term, represented by an equation identical to Equation 6.

The *Complex\_Energy* term is the protein-ligand energy and is described by an 8-4 Lennard-Jones potential. An 8-4 potential, described in Equation 14, was chosen as it was much softer, i.e., the curve on the repulsion side is less steep, than the usual 12-6 potential.<sup>29</sup>

$$E_{ij} = \frac{A}{d_{ij}^8} - \frac{B}{d_{ij}^4} \quad (14)$$

where  $d_{ij}$  is the distance between atoms  $i$  and  $j$ , and  $A$  and  $B$  are two parameters that were optimised to reproduce the minimum of a 12-6 potential.

The second group of scoring functions are empirical or regression-based methods, such as ChemScore. ChemScore estimates the total free energy change occurring on ligand binding,  $\Delta G'_{binding}$ . It was derived from a set of 82 known protein-ligand complexes for which binding affinities have been measured and it was trained against these data.<sup>30</sup> A penalty term ( $E_{clash}$ ), which takes into account potential steric conflicts with the protein binding site, was added to the estimate of the  $\Delta G_{binding}$ , as well as a torsional term ( $E_{int}$ ) to account for unfavourable conformations (Equation 15).<sup>27</sup>

$$\Delta G'_{binding} = \Delta G_{binding} + E_{clash} + E_{int} + E_{cov} \quad (15)$$

$E_{cov}$  is optional and only used when dealing with a ligand covalently bound to the protein.

$\Delta G_{binding}$  is described in Equation 16:<sup>30</sup>

$$\begin{aligned} \Delta G_{binding} = \Delta G_0 + \Delta G_{hbond} S_{hbond} + \Delta G_{metal} S_{metal} \\ + \Delta G_{lipophilic} S_{lipophilic} + \Delta G_{rot} H_{rot} \end{aligned} \quad (16)$$

The  $\Delta G$  coefficients are obtained from the regression against affinity data.  $S_{hbond}$ ,  $S_{metal}$  and  $S_{lipophilic}$  are based on a block function  $f(x)$  with two constants  $x_1$  and  $x_2$  as shown in *Figure 6*.  $x$  is the value under consideration, it being either a distance between two atoms or an angle. If  $x$  is less than  $x_1$ , then  $f(x)$  is 1. If  $x$  is greater than  $x_2$ , then  $f(x)$  is 0. Otherwise,  $f(x)$  is calculated as a function of  $x_1$  and  $x_2$ .

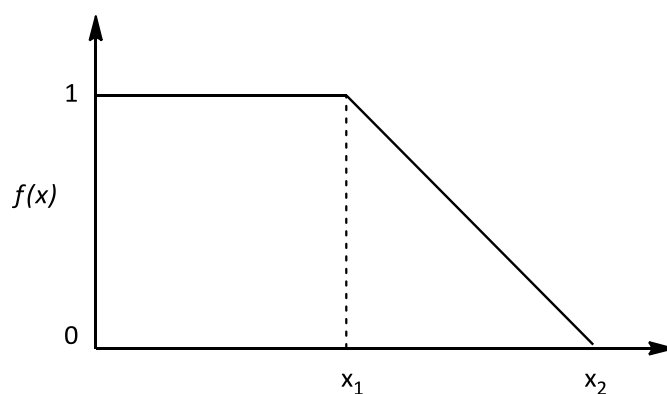


*Figure 6*: Schematic description of block function  $f(x)$

GlideScore (Equation 17) is an expanded version of ChemScore with two options. GlideScore Standard Precision (SP) is more suited to identify ligands that are likely to bind, whereas GlideScore eXtra Precision (XP) has a harder potential and assigns severe penalties to violation of conventional physical chemistry principles,<sup>8</sup> e.g., charged moieties should point into solvent. GlideScore is described by Equation 17



and differs from ChemScore by the addition of new terms. For example, the hydrogen bond term is split in three and the block functions vary depending on the nature of the donor and acceptor groups. The Coulomb and van der Waals terms were also added.  $f, g$  and  $h$  are block functions,  $r$  and  $\alpha$  are distances and angles respectively, the  $l, r$  and  $m$  indices are to indicate ligand, receptor and metal atoms respectively.

$$\begin{aligned}
 & \Delta G_{bind} & (17) \\
 & = C_{lipo-lipo} \sum f(r_{lr}) \\
 & + C_{hbond-neut-neut} \sum g(\Delta r)h(\Delta \alpha) \\
 & + C_{hbond-neut-charged} \sum g(\Delta r)h(\Delta \alpha) \\
 & + C_{hbond-charged-charged} \sum g(\Delta r)h(\Delta \alpha) \\
 & + C_{max-metal-ion} \sum f(r_{lm}) + C_{rotb}H_{rotb} \\
 & + \Delta G_{polar-phob}V_{polar-phob} + C_{coul}E_{Coul} + C_{vdw}E_{vdw} \\
 & + solvation terms
 \end{aligned}$$

ChemPLP is also an empirical scoring function<sup>31</sup> and is available within GOLD. In addition to the empirical terms to describe binding affinity, ChemPLP includes a statistical potential to describe the steric complementarity of the ligand and the protein. A publication from the CCDC concluded that ChemPLP was the best scoring function within the GOLD software suite.<sup>32</sup> This study was run against the Astex Diverse Set, in a pose prediction mode.<sup>32</sup> The Astex Diverse Set consists of 85 diverse protein-ligand complexes, with more representation in the major protein

families, such as for example, kinases and nuclear receptors.<sup>33</sup> There is no sequence similarity between the remaining 57 structures in the set. When sampling the docking poses which were within 2 Å of the correct binding mode, all force-field based and empirical scoring functions studied (which included ChemPLP, GoldScore and ChemScore) performed similarly. If considering only the top scoring pose or the closest pose out of the top 25 poses, ChemPLP somewhat outperforms GoldScore and ChemScore. Nonetheless, there is not one scoring function that is best for generic use and that different docking programmes and scoring functions should be assessed in any new work to find the best one.<sup>27, 34-37</sup> This was confirmed in a study by Xu *et al.* which found that GoldScore was on of the two best performing scoring function and that ChemPLP correlated negatively with binding affinities and therefore, did not predict well the correct binding mode.<sup>38</sup>

The third category of scoring functions is knowledge-based. Such scoring functions are based on a statistical potential and are derived from experimental structural data and atom-type interactions in specific environments. Rules are derived from these data to generate most common geometries observed in experiments. An example of such scoring function is ASP (Astex Statistical Potential).<sup>26</sup> Such scoring function can generally be described as follows:<sup>39</sup>

$$\Delta W_{ij}(r) \propto -\ln \frac{g_{ij}(r)}{g_{ref}} \quad (18)$$

where  $\Delta W_{ij}(r)$  is a pair-potential,  $g_{ij}(r)$  is a probability or frequency distribution of atom pairs  $i$  and  $j$  separated by a distance  $r$  and  $g_{ref}$  is a reference distribution. The sum of these pair-potentials yields a score for the protein-ligand complex studied. In comparison to force field functions, these are softer as they do not rely on simulated parameters and geometries.<sup>39</sup> However, a disadvantage of using experimental data to derive a scoring function is that it is not possible to predict geometries which have not been observed before. In the first instance, knowledge-based scoring functions showed some success in reproducing binding poses for known protein-ligand complexes.<sup>40</sup> Since then, it was reported that these scoring functions do perform well in terms of reproducing known binding modes and when correlated with binding affinities can achieve equivalent or sometimes better predictions than other classes of scoring functions.<sup>39, 41</sup> New and improved knowledge-based scoring functions are an active area of research in line with the regular release of new and quality data in the public domain (e.g. CSAR<sup>42</sup>). One of the CSAR benchmark exercise, which used unpublished data, concluded that there was not one type of scoring function that stood out in terms of reproducing the native binding mode.<sup>43</sup> They all performed similarly, including knowledge-based. This type of large scale assessment is very valuable and allow for the comparison of docking programs and scoring functions in a more independent fashion, as opposed to relying on publications from developers of scoring functions. The availability of different data in the PDB, for example halogenated ligands, also enables the development of more sophisticated knowledge-based scoring function, such as the halogen bonding scoring function by Liu *et al.*<sup>44</sup> Xu *et al.* who compared a set of

sixteen scoring functions on six different target systems found that knowledge-based scoring functions such as ASP perform reasonably well.<sup>38</sup> Overall, the authors concluded that GoldScore<sup>26</sup> together with FlexX<sup>45</sup> were the best performing scoring functions, although for systems which were hydrophobic none of the scoring functions studied did particularly well. This study reinforces the fact that there is not a scoring function that is generic enough to be effective on any systems.

### 2.2.2. Examples of commercial docking programmes

GOLD (Genetic Optimisation for Ligand Docking) is a docking program based on a genetic algorithm (GA), which means that it is inspired by the process of evolution.<sup>46</sup> Ligand configurations, each of which is a potential solution, are generated at random and they are encoded as chromosomes. A chromosome stores information about the interactions of a given orientation of the ligand and the binding site.<sup>29</sup> Potential hydrogen bonding from the ligand to the active site for both acceptors and donors is recorded. At each iteration, selected chromosomes are subjected to operations, i.e., mutations and/or cross-over. The mutation operation is applied to one chromosome, whilst a cross-over (*Figure 7*) requires two chromosomes. The mutation operator mutates a value at a selected location on the chromosome to another allowed value. The cross-over operator swaps data from each parent after a given cross-over point. A cross-over can be one-point or two-point. The output of such operations gives one or two new chromosomes and they are retained if their fitness is greater than one of the least fit parents.

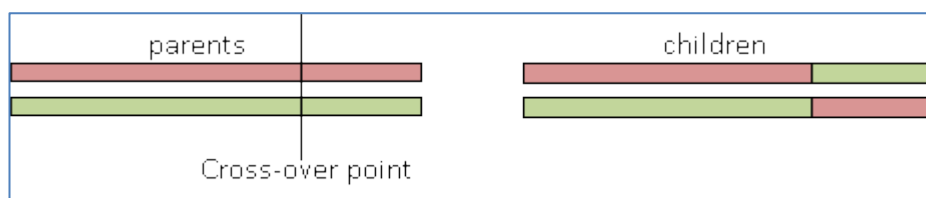


*Figure 7: Schematic representation of a cross-over operation.*

A least-squares fitting method is used to place the ligand into the binding site. A virtual fitting point is projected at 2.9 Å from each donor hydrogen. A virtual fitting point is also generated at the centre of each acceptor atom. A chromosome encodes mappings of possible hydrogen bonds between the ligand and the protein. A first least-squares fit is performed which minimises the distance between the ligand and the protein virtual fitting points. A second least-squares fit is then performed to minimise the distance between pairs of virtual points less than 1.5 Å apart.<sup>28-29</sup>

Glide (Grid-based Ligand Docking with Energetics) is a docking program that performs an exhaustive search of the conformational space of the ligand whilst maintaining computational speed.<sup>8</sup> It is therefore well suited to screen large libraries of compounds. A grid of the protein is generated to characterise its shape and properties using various sets of fields. The conformational space of the ligand is then searched and a selection of conformations is made by applying screens that enable the location of potential poses. Each pose is then minimised within the protein field using a molecular mechanics function, of the type described in the previous section. The final step is to refine three of the six lowest energy poses using a Monte Carlo method to explore other torsion angle minima.

### 2.2.3. Molecular docking as a tool in the context of drug discovery

#### 2.2.3.1. Accuracy of biological assays and relationship with binding energies

The accuracy of docking algorithms and scoring functions is typically assessed against a variety of experimental data. The type of data can be quite varied (e.g. crystallography,  $K$ ,  $IC_{50}$ , etc.), as can the accuracy, making these comparisons even more challenging given the known shortcomings of scoring functions themselves. In this work, we are assuming that  $K \approx IC_{50}$ , the half maximal inhibitory concentration, which is realistic in cases where the concentration of the substrate is very low compared to the protein concentration.<sup>47</sup> In order to be able to objectively evaluate the significance of changes in docking scores between compounds, we need to be able to relate the change in binding energy to the difference in biological activity (and *vice versa*). To this effect, we can use the equation  $\Delta G = -RT\ln K$ , where  $R$  is the gas constant and is  $8.314 \text{ J.K}^{-1}.\text{mol}^{-1}$  and  $T$  is the temperature  $298 \text{ K}$  (for  $25^\circ\text{C}$ ). From this, we calculate that for a difference in  $\Delta G$  of  $1 \text{ kcal/mol}$ , there is a factor of 5 in  $IC_{50}$  or a difference of about 0.7 log units in  $pIC_{50}$ ; and for a difference of 1 log unit in  $pIC_{50}$  (also equivalent to a 10 fold difference in  $IC_{50}$ ), there is roughly a difference of  $1.4 \text{ kcal/mol}$  in  $\Delta G$ . For example, the difference in free energy between a compound with a  $pIC_{50}$  of 6 and a compound with a  $pIC_{50}$  of 7 is around  $1.4 \text{ kcal/mol}$ . Similarly, two compounds with a  $pIC_{50}$  of 6 and 6.7, respectively, should be  $1 \text{ kcal/mol}$  apart in free energy.

There is often an error of about  $\pm 0.3$  log unit in  $pIC_{50}$  on biological assay measurements, which is equivalent to a factor of 0.5 in terms of  $IC_{50}$  on either side

of the assay value. For example, a compound which shows a pIC<sub>50</sub> value of 7 means that its true IC<sub>50</sub> value would not be exactly 100 nM, but is likely to fall somewhere between 50 and 200 nM. (However, these boundaries are not absolute and the IC<sub>50</sub> value could fall just outside.). The more replication of measurement, i.e., assay run on different days, the more accurate and the more confidence in the assay value. In terms of free energy, this error in the assay is equivalent to  $\pm 0.4$  kcal/mol. Given the relationship between the IC<sub>50</sub> and the free energy, it is difficult to differentiate definitively between compounds that have very similar IC<sub>50</sub> values. This is particularly the case when docking methods are used to calculate the free energy for docking between compounds, where the errors in the docking methods are typically in the order of 2-3 kcal/mol. However, when comparing closely related systems the errors in the absolute binding energies are considered to be about equal and, therefore, the relative binding energies of the series are more reliable.

#### 2.2.3.2. *Predictivity of scoring functions*

There are still to this day major issues with scoring functions.<sup>38, 41, 48-50</sup> Indeed, most of them only take the enthalpic component of the binding event into account and ignore the entropic effects, despite the fact that they are intended to model the binding event.<sup>51</sup> Indeed, in a docking and scoring experiment, only one static protein-ligand complex is considered as opposed to an ensemble or an average of them which would be generated during a molecular dynamics (MD) run and the unbound state is not considered either.<sup>34</sup> This is one drawback of a docking and

scoring methodology but it is also an advantage as they are much quicker to run compared to more sophisticated methods such as MD or free energy perturbation (FEP).

A number of publications have reported over the years thorough examinations of widely used scoring functions for the cases of binding mode prediction, virtual screening and affinity prediction.<sup>34, 36-37, 43, 48-54</sup> It was shown that scoring functions are successful at generating the correct binding mode but that often it was not a top scoring docking pose. Cheng et al. even recommended to inspect a number of top scoring docked poses of a ligand as good practice, reinforcing the fact that the top scoring pose is unlikely to represent the correct binding mode.<sup>34</sup> Warren et al. also highlighted that none of the scoring functions that they studied could differentiate the best docked pose as the top scoring pose.<sup>37</sup> With this observation in mind, the user should inspect several of the docking poses output by the programme in order to find the correct one. However, it is very likely that they would find it in this list.

It was also shown in these studies that scoring functions are good at retrieving active chemotypes amongst decoys in the context of virtual screening. Indeed, it was found that the enrichment when using docking as a virtual screening methodology was in general better than random.<sup>37, 51</sup> This was also true even if the decoys were inactive analogues closely related to active molecules.<sup>37</sup> There have been a number of successful virtual screening campaigns reported in the literature that could identify active chemotypes within a set of inactive molecules, as summarised by Kitchen et al.<sup>51</sup>



The third exercise that reviewers generally undertook was to assess the ability of scoring functions to predict biological affinity. In this instance, all reviews concluded that scoring functions failed in this context. The various authors even highlight this as the main and most pressing issue with scoring functions.<sup>34, 51</sup> Cheng et al. go further by stating that aiming for a generic scoring function that could work for any system might be too ambitious a goal and that perhaps developing tailored scoring functions might be more realistic and more attainable.<sup>34</sup> There is no difference in the type of scoring functions that perform better than others in predicting binding affinity. Even the empirical scoring functions derived using measured binding data do not seem to offer a significant advantage.

There is a much lower requirement for precision in medicinal chemistry relative to that required to predict binding affinity. Indeed, in the docking setting, the main requirement of a docking tool, when applied in the lead optimisation stage of a drug discovery project, is to roughly place the molecule in the binding site to allow the design of new active molecules. If there is a slight translation of the docking pose, which would in reality affect the binding affinity, the good fit obtained would be sufficient to guide a medicinal chemistry effort. For instance, in the case of a kinase target, the correct placement of the hinge binding moiety and of the vector leading to the back pocket enable the elaboration of new molecules.

#### 2.2.3.3. *Root Mean Square Deviation*

Root mean square deviation or RMSD is widely used to assess the accuracy of a docking pose in comparison to the expected crystal pose.<sup>55</sup> A low RMSD value

indicates a docking pose which is very close to the crystal pose, whereas a large RMSD denotes a docking pose which is very different to the crystal pose.

RMSD is obtained by computing the square of the difference between the coordinates of pairs of atoms. All squared differences are then summed and divided by the number of atom pairs. The square root of this number is the RMSD.

The simplicity of the RMSD evaluation makes it a fast and unbiased approach to assessing different docking poses of the same ligand. However, it is important to bear in mind that the simplicity of the RMSD value also implies a number of limitations.<sup>55</sup> Indeed, plausible docking poses which maintain key interactions with the binding site, e.g., to the hinge for kinases, and for which the key binding moiety is in the right location but flipped will show a high RMSD. This is also the case for symmetric molecules as RMSD is calculated based on the atom index, rather than the atom type. Moreover, flexible chains which are not involved in the binding and are in a different conformation to the experimental pose will lead to a high RMSD. Small ligands are more likely to achieve a lower RMSD, because of their size and, therefore, while the use of RMSD for the same ligand is unbiased, when comparing across different ligands the relative size of the ligands may mask differences in the quality of the alignments.

Given the limitations to RMSD mentioned above, the diagnostic is mostly used within this research in conjunction with a qualitative visual assessment of the docking poses. Three levels were devised to explain the outcomes of the visual assessment: 'good' corresponds to an orientation that results in the key interactions of a binding pose being maintained, with the additional feature of the remainder of

the molecule also being well-aligned to the crystal pose; 'OK' describes the situation where the docking pose maintains the key interactions but the ligand is shifted in some respect from the crystal pose; and 'wrong' describes a docking pose that does not maintain key interactions or interactions are made from a different moiety. The visual assessment for a docking pose does not necessarily correlate with its RMSD.

### 2.3. Protein flexibility

The lock-and-key theory of the protein-ligand complex was first described by Fischer in 1894.<sup>56</sup> In his theory, the protein binding site represents the lock and its ligand, the key. The ligand requires some complementarity both in shape and properties to be able to "unlock" the protein and produce an event. This theory assumes that the protein binding site is rigid and, therefore, the shape complementarity of the ligand is very important for binding to occur. The theory was widely accepted until the 1950s, when Koshland challenged it due to its inability to explain all protein-ligand binding phenomena.<sup>57</sup> For example, the lock-and-key theory could not explain why some ligands would bind but not induce a response, as in non-competitive inhibition, unless the substrate is present.<sup>56</sup>

Koshland proposed the induced fit theory, which stated that binding of a substrate can involve a change in the three dimensional conformation of the site. This movement should bring together catalytic groups responsible for the enzymatic reaction. Even though this new theory was initially met with some reservations, it is now well accepted. Koshland and his co-workers managed to prove through experiments that induced fit was indeed happening.<sup>56</sup> They introduced the "hand in

glove” analogy, which encompasses Fischer’s lock-and-key theory together with the flexibility of proteins. Current models are moving towards the concept that proteins exist in an ensemble of conformations, with some being more populated than others.<sup>58</sup> Binding of a ligand to a specific protein conformation can increase its percentage in the total population.<sup>59</sup>

It is now well understood that proteins do not exist in a unique conformation and that protein flexibility is required for them to perform their function.<sup>59</sup> A challenge for structure-based drug design is to incorporate protein flexibility into the ranking and scoring algorithms for new candidate compounds. Currently, most modelling programmes consider the protein fixed. These rigid methods are still the first resort, simply because taking protein flexibility into account is expensive in computer power and time.<sup>60</sup>

Over the years, many techniques - such as, flexible side-chains,<sup>61</sup> binding-site flooding,<sup>62</sup> simulated annealing,<sup>63</sup> strategic mutations,<sup>9</sup> ensemble docking,<sup>58, 64-65</sup> etc. - have been developed to try to overcome the problem of protein flexibility. It is not the purpose of this work to provide an exhaustive review of these methods and the interested reader is directed to the excellent reviews about incorporating protein flexibility in structure-based drug design,<sup>60, 66-67</sup> but also more specific reviews by Essex *et al.*,<sup>7</sup> Carlson,<sup>58</sup> Korb,<sup>68</sup> Teague,<sup>59</sup> Shoichet,<sup>69</sup> etc. In the following, a brief overview of methods, pivotal to the approach used in this work is provided.

One of the first methods to be reported in the field of flexible docking was to allow some flexibility of amino acid side chains. Leach described an algorithm for ligand

docking that he developed keeping the backbone of the protein fixed and letting the side chains of amino acids have a degree of flexibility.<sup>61</sup> The conformations of the amino acid side chains were limited to rotameric states, described in a rotamer library. The energy of the rotamer combinations was evaluated using AMBER. The ligand was allowed only certain restricted conformations, derived from a conformational search performed in isolation. The algorithm also output a set of protein-ligand complexes, which were within a given energy threshold of the global energy minimum. Leach applied this protocol to the docking of benzamidine to trypsin and of phosphocholine to antibody McPC603.<sup>61</sup> In both cases, the algorithm predicted that there would be some conformational changes in the side chains of the binding site upon binding of the ligand. For the benzamidine-trypsin complex, they found that the lowest energy complex obtained with side chain flexibility was the one with the lowest RMSD to the crystal structure. However, for the phosphocholine-McPC603 complex, none of the structures obtained were close to the crystal structure.<sup>61</sup>

Miranker and Karplus developed the multiple copy simultaneous search (MCSS) method to characterise protein binding sites.<sup>62</sup> A number of small chemical groups, or probes, were used to flood the protein binding sites. These fragments were chosen as a representation of most organic molecules; examples of such chemical groups are methyl ammonium or acetate. At first, a large number of probes (between 1,000 and 5,000) are diffused randomly in the defined binding site. The interaction energy between the probe and the binding site is computed and if it is greater than a defined threshold, i.e., the interaction is estimated to be

unfavourable, then the probe is removed. The probes are then minimised using an approximation algorithm, which excludes interactions between the probes and estimates the force on the protein from only one probe. The minimisation is achieved in turn on 100 fragment subsets. After every 1,000 steps, results are analysed and redundancies, i.e., probes that accumulate in a similar minimum defined by an RMS threshold, are removed. This procedure is repeated until convergence, i.e., when the RMS gradient  $\leq 0.01$  kcal/mol/Å. When minimisation is complete, a small number of low minima are investigated further, usually using a grid search for each minimum. Miranker and Karplus applied this method to influenza virus hemagglutinin and used the water, methane, methanol, acetate and methyl ammonium probes to characterise the binding site.<sup>62</sup> They then compared the probes hotspots with the functionalities of the sialic acid ligand. They found that there was not an absolute agreement between the probe calculations and the functional groups of sialic acid. They explained this difference by a potential inability of sialic acid to occupy optimal positions for its functional moieties.<sup>62</sup>

Damm and Carlson compared the use of experimental and computer generated multiple protein structures in order to develop pharmacophore models of the binding site.<sup>70</sup> Small chemical probes, such as benzene and methanol, were used to flood the binding site and were then minimised using a low temperature Monte Carlo sampling. Clusters, where the same probe was found multiple times, were then identified. Structures were superimposed and consensus clusters were identified, where each cluster represented a pharmacophore point. These

pharmacophore models were then used to screen three-dimensional databases of compounds.<sup>70</sup>

In this study, we have focused on investigating an induced fit docking method and improving the current protocol. Indeed, even though there are a number of other ways of assessing or exploring protein flexibility, as discussed above, induced fit docking was a logical extension to the rigid receptor docking studies performed in the first half of this work. The Schrödinger Induced Fit Docking (IFD) protocol, in particular, which is described in the following Section 2.3.1, will be examined. Currently, there is not a way of objectively assessing the binding site through temporary truncations of residues to alanine, which is restricting the use of such a method to known systems and relies on the user's knowledge of the target. This will be the focus of studies reported in Chapter 7. Such an improvement of the method would enable a wider use of the tool and a basic understanding of the binding site plasticity.

Proteins exist in a number of conformations and ligands bind to a subset of these conformations.<sup>59</sup> However, the most common approach for docking studies is to focus on a single crystal structure, which is most applicable to the system of interest.<sup>71</sup> This is an assumption made when using a docking approach, i.e., that the protein is represented by a single conformation. This standard approach was employed in the current work and, therefore, a study of alternative methods was outside the scope of this work.

### 2.3.1. Schrödinger Induced Fit Docking protocol

In 2006, Sherman et al. demonstrated a new method of docking ligands into protein binding sites.<sup>9</sup> The ligands were allowed full flexibility, whilst some degree of flexibility in the protein was also maintained. This kind of approach is particularly useful when rigid docking fails. It has often been seen as a problem in cross docking, i.e., docking ligands in non-native protein crystal structures, when there are known or suspected movements of amino acids in the binding site. The authors' Induced Fit Docking protocol (IFD) uses Glide and Prime from Schrödinger's Maestro molecular modelling suite.<sup>9</sup> Glide is used to dock the ligand into the binding site, and Prime to optimise and minimise the protein. Glide has been described previously in Section 2.2.2.

Prime is Schrödinger's protein structure prediction tool and, of particular relevance for this work, can be used to predict amino acid side chain conformations.<sup>72</sup> Within these studies, the OPLS2005 force field is used by Prime to determine the most favourable orientations of the amino acid side chains. The orientation of the side chains is determined by their addition to the fixed protein backbone in a random rotamer state. Each side chain is then optimised in turn, whilst the rest of the protein and the other side chains are kept fixed.

To sample the rotameric states of side chains, an extensive rotamer library is employed. Screening of this library using a hard sphere overlap is performed prior to the more expensive sampling in order to alleviate the use of such a rotamer library. Once the lowest energy rotamer is found, the energy of the side chain is minimised. Once all side chains have been optimised, i.e., convergence has been



reached, their energy is minimised concurrently. This process is repeated five times, each time starting from different random rotamers. The lowest energy system is ultimately chosen.

A Python script has been developed by Schrödinger in order to automate the steps of the protocol and settings can be modified in a window interface within Maestro. The standard protocol can be divided into five steps.<sup>9</sup>

- 1) The first step consists of docking the ligand, using Glide, into the protein binding site, with a softened potential. The van der Waals radii of the ligand and the protein are scaled by 50%, in order to allow some steric clashes in the binding site. The potential downsides of using a 50% van der Waals scaling is that it creates a much larger effective volume for the binding site and thus more space for the ligand to explore. Therefore, it is more likely to get to the wrong binding pose. Mutation of highly flexible amino acids to alanine is also possible, with a maximum of three mutations. The residues can be selected automatically based on the temperature factor, or manually. In the case of automatic selection, the SP scoring function is used to score the docking poses. The top scoring twenty poses are retained for the next step.
- 2) For each pose generated in step 1, a Prime refinement run is performed on the new protein-ligand complexes using the OPLS parameters. Amino acids within 5 Å of the ligand docking pose, generated previously, go through a conformational search, followed by a minimisation. The amino acids selected are used to compare the energy of the different structures

generated. Amino acids, which were mutated to alanine in step 1, are mutated back to the original amino acid prior to starting the refinement. The ligand is not optimised in this first part. After convergence, a final minimisation was performed to relax the whole protein-ligand complex system.

- 3) The ligand is then re-docked in each of the new structures using Glide with no softened potential in Standard Precision (SP) mode with default settings.
- 4) The GlideScore for each docking pose is altered by the addition of one twentieth of the Prime energy, in order to take into account the energy of the system. This score is called the IFDscore. It is used to score each docking pose. The authors claimed that combining these two numbers gave a high robustness in finding the correct binding mode. The IFDscore is detailed in Equation 19.<sup>9</sup>

$$IFDscore = GlideScore + 0.05 * PrimeEnergy \quad (19)$$

- 5) After the first round of the protocol, if the top ranked structures exhibit scores that are very similar ( $\Delta IFDscore < 0.2$ ), a second round is initiated starting from the results of the first round. However, this time the first step uses rigid docking (no softened potential).

Glide defines two types of potentials, hard and soft.<sup>73</sup> A hard potential is the standard Lennard-Jones potential with a repulsive and an attractive component. A

soft potential, however, is a Lennard-Jones potential where the repulsive term is calculated using van der Waals radii modified by a scaling factor. If the soft potential is used to place the ligand in the binding site but it is switched back to a hard potential when minimising the pose before scoring, then it does not have an impact on the final score, because it is calculated with the hard potential.

If docking is run on a set of ligand conformers, then it could be argued that a soft potential is not necessary as the conformational space that the ligand can explore should be sufficient to obtain a docking pose without having to modify the potential. Moreover, there is a risk of over fitting when using a soft potential as the ligand is forced to bind in the pocket and the binding site is actually changed in order to do so. Therefore, applying a soft potential in virtual screening can be detrimental and produce false positives. However, in the context of IFD, where it is used to generate a set of starting docking poses to be fed through the rest of the protocol, the downsides are mitigated by the fact that the last step is a standard docking step with a hard potential.

Experimental irreversible mutation of amino acids to alanine is used in site-directed mutagenesis. One case, known as alanine scanning, is used to assess the role of specific amino acids in the activity and stability of proteins of interest.<sup>74</sup> Another use for alanine mutation is to mutate certain residues to alanine in order to identify which are important for binding.<sup>74</sup> Mutation of amino acids to alanine in binding sites has also been investigated to modify targets and induce selectivity of inhibitors designed to occupy this newly formed cleft for the target of interest.<sup>75</sup> However, while these experimental approaches present some similarity in their use of alanine

to probe the binding site, there is no direct correlation with the use of alanines in docking as an intermediate step to truncate the binding site. That is, the residues that are truncated are re-introduced during the docking step, so that the ligand is docked into the native binding site, rather than the alanine mutant.

Schrödinger applied their IFD procedure to 21 example systems. They found, with rigid docking, an average RMSD of 5.5 Å, whilst with induced fit docking the average RMSD was 1.4 Å.<sup>9</sup> There were three cases, where the RMSD was greater than 1.8 Å, but the ligand was correctly orientated and the hydrogen bond interactions maintained. Two of these cases occurred when docking into two protein structures of PPAR $\gamma$ .<sup>9</sup> Both of the ligands studied produced docking poses with RMSDs of 1.8 Å and 3.0 Å. In the first instance, the authors explained the higher RMSD to be due to the difference in size between the original ligand crystallised in the protein structure and the ligand to be docked. Therefore, a number of residues had their side chains protruding in the binding site. In addition, the ligand contained a flexible tail, which was misplaced in IFD, whilst the core of the ligand was in a good orientation. In the second case, the ligand to be docked was much smaller than the ligand crystallised, which gave too much space in the binding site for the ligand to explore. The third case was when docking into thermolysin. Out of the two ligands studied for this target, one produced an RMSD of 3.2 Å. The authors explained this result by the difference in size between the ligand crystallised and the ligand to be docked, and the presence of amino acid side chains in the binding site. These observations lead to the issue of whether the size similarity of the ligands to be studied in comparison to the ligand crystallised in the protein structure of interest is

important. The ultimate aim of IFD is to dock unknown ligands, not necessarily similar to the original one, and to predict their binding mode whatever the conformational movement occurring upon binding. Following on from Sherman et al.'s article,<sup>9</sup> a number of groups published their work using Schrödinger's Induced Fit Protocol.<sup>76-80</sup>

Due to the problem of resistance to current drugs and the lack of structural information, Barreca et al. were interested in predicting the binding modes and the mode of actions of HIV integrase inhibitors.<sup>76</sup> The authors used the IFD protocol of Schrödinger to dock these compounds. Some of their findings could be confirmed by results from other research groups. The binding mode they obtained for integrase strand transfer inhibitors (INSTIs), where inhibitor binding prevents loop mobility and catalytic activity, were confirmed by other groups. They also obtained IFD results confirming that the inhibitors bound preferably to the HIV integrase active site and hence blocked the binding of the host DNA. This hypothesis had previously been put forward by two other groups.<sup>76</sup> The authors believed that their results shed some light on the mechanism of resistance and could help future medicinal chemistry efforts for the discovery of new HIV integrase inhibitors. Through their experiments, they showed that with the use of IFD it was possible to predict the binding mode of ligands when there is a lack of structural data available.

Zhong et al. used IFD to study inhibitors of tyrosine kinases, and in particular EGFR, and ABL (in active and inactive states).<sup>80</sup> Their objective was to identify amino acids of interest that should be targeted for the design of new inhibitors. In this work, 18

different ligands were studied against the three protein targets. They found that it was possible to reproduce the ligand binding poses by cross docking and the results were consistent with experimental data. This process also allowed the authors to identify amino acids that are important for activity. The only disadvantage that was faced using IFD compared to rigid docking was the time cost. However, the superior results obtained with IFD were considered to be worth the extra cost.<sup>80</sup>

Lauria et al. used Schrödinger IFD to study eight known inhibitors of the heat shock protein Hsp90, all eight belonging to different chemotypes.<sup>77</sup> Although it is not clear whether a single crystal system was used as a starting point for the IFD experiments, excellent RMSDs for all eight ligands studied were reported, with the worst result obtained for docking ATP (RMSD = 3.46 Å). This was explained by the fact that, in this particular structure, there was a phosphate group missing in the electron density of the ligand crystal pose and, therefore, ADP was modelled instead. When the authors docked ADP, the RMSD went down to 0.54 Å, which was within the range of the results for the other ligands. Through the use of IFD, the authors were able to validate structural models of Hsp90 and simulate the plasticity of the binding site in order to better reproduce ligand binding.

Wang and co-workers used IFD to investigate the binding mode of mometasone furoate, a ligand of the glucocorticoid receptor, for which there was no crystal structure.<sup>79</sup> In this work, the induced fit protocol was successfully validated to preserve the structure of the binding site, but also to open up the known 17 $\alpha$  pocket induced with larger ligands. Met560, Leu563 and Met646 underwent conformational changes in order to open the 17 $\alpha$  pocket. These residues were not

selected for mutations in the IFD run. However, it was possible to identify important amino acids involved in interactions with mometasone furoate through hydrogen bonds, which could explain the high potency of this ligand for the glucocorticoid receptor. In addition, it was demonstrated that the 17 $\alpha$  pocket could spread even more in order to accommodate larger ligands than mometasone furoate. Thus, it was concluded that the IFD protocol was very valuable in predicting side chain movement and, therefore, was beneficial for modelling studies.

Repo et al's work highlighted the use of IFD to explain the promiscuity of constitutive androstane receptor (CAR), and to understand the effects of mutations on ligand binding across two species of CAR, human and mouse.<sup>78</sup> Different mutations were evaluated in functional assays and docking was used to identify the location of the ligands in the binding site. Multiple runs of IFD were used, with different parameter sets, in order to identify the best docking poses. This work focussed on the effect of the definition of the binding site (from ligand location or centroid of specific residues), the mutation of specific residues and the scoring function (SP or XP). The authors concluded that for each ligand it was a different protocol that produced the best results and there was not a single protocol that could be applied to all ligands. It was also found that the runs with the XP scoring function generated more docking poses than with the SP scoring function. In this instance, IFD was useful to use alongside mutation experiments in order to predict the binding mode of ligands, in the absence of structural data.

Recently, a consensus induced fit docking approach has been published by Kalid et al.<sup>81</sup> The Schrödinger IFD protocol was modified in order to perform virtual

screening. As opposed to rigid receptor docking, this method takes into account the flexibility of the binding site, given that there are known ligands to the target. This new protocol came from the authors' experience of rigid body docking failing to retrieve known ligands during virtual screening experiments. The idea was to generate a single model from the docking of multiple ligands to the same rigid binding site, and then allow the side chains of amino acids to move in order to accommodate the hybrid ligand. The result is a single binding site, which could potentially accommodate a wider range of ligand shapes. The authors successfully applied this protocol to known difficult targets, such as COX-2, but also to an active drug discovery project. In the case of HIV reverse transcriptase, a decrease in performance compared to rigid docking was noted, which was believed to be due to the different binding modes of the ligands used.<sup>81</sup> One potential issue with this approach is the generation of a large binding site which could accommodate a wide range of ligands, with not much discrimination between specific ligands and false positives.



## 2.4. Statistical methods

### 2.4.1. Molecular Similarity

#### 2.4.1.1. *Representing molecules*

There are many ways of representing molecular structures. Simplified Molecular Input Line Entry Specification (SMILES) strings can be used to describe molecules in the two-dimensional space. They are strings of alphanumeric characters representing atoms and how they are bonded together. Atoms are described by their atomic symbols, with a capital letter for an aliphatic atom and a lower case for an aromatic atom. Single as well as aromatic bonds can be omitted, double bonds and triple bonds are represented by “=” and “#”, respectively. Ring closures are symbolised by pairs of numbers, as seen in the benzene example of *Figure 8*, and branched substitution is added in parentheses, as in the propanone example of *Figure 8*.

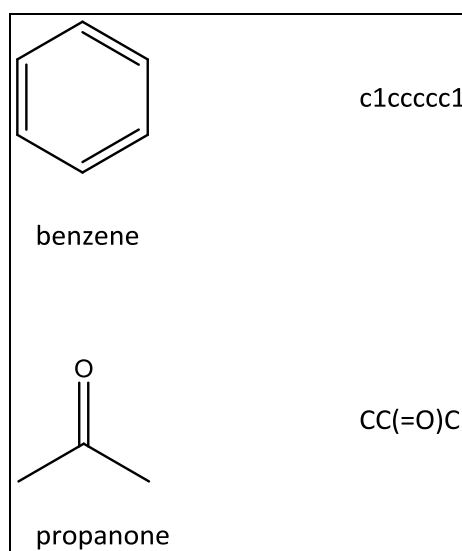


Figure 8: Two examples of SMILES strings

Molecules can also be represented by binary strings, known as bitstrings or fingerprints, which consist of “0”s and “1”s and are therefore very easy to manipulate. Bitstrings are the natural currency of computers, and as such they are a very fast way of comparing chemical structures computationally.

Dictionary fingerprints, also known as structural keys, are bitstrings where each bit corresponds to a specific chemical substructure in the molecule and, therefore, are directly and easily interpretable (Figure 9).

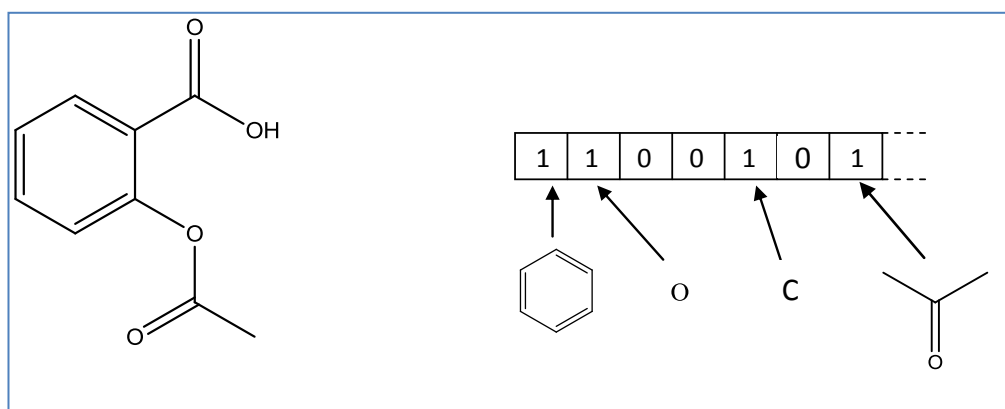


Figure 9: Example of a dictionary fingerprint

Dictionary fingerprints are based on a fragment dictionary, in which fragments are stored and the *ith* fragment in the dictionary corresponds to the *ith* bit in a fingerprint. An obvious limitation of this type of fingerprints is that they rely on a suitable design of the dictionary, i.e., applicable to the molecules under consideration.

A hashed fingerprint does not depend on a dictionary. It is based on the enumeration of all possible paths, from length 0 to a specific number, of connected atoms in a molecule. Each path is processed through a hashing algorithm in order to set a defined number of bits, typically four or five, to "1" in the fingerprint (*Figure 10*).<sup>82</sup> Collisions can happen when two different paths set the same bit on, but it is unlikely that two distinct paths set all the same bits. The standard Daylight fingerprints are hashed fingerprints containing 1024 bits and a maximum path length of 7. These fingerprints were used in this study.

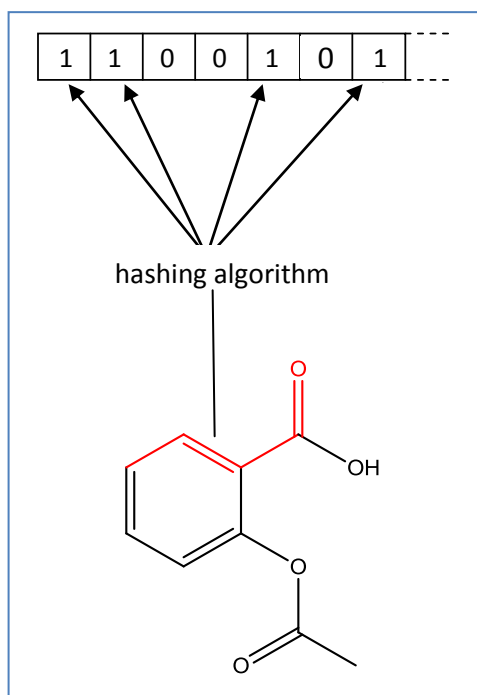


Figure 10: Example of a possible path in red, setting four bits in a hashed fingerprint

Fingerprints were designed as a first step for screening out molecules in a database prior to performing a substructure search using graph matching algorithms.<sup>83</sup> As the graph matching step is slow, the objective of screening was to rapidly remove from consideration molecules that could not match the query. Subsequently, they have been used in similarity searching, clustering, etc.

#### 2.4.1.2. *The Similarity Principle and its meaning in Drug Discovery*

The Similarity Principle states that structurally similar molecules tend to present similar properties.<sup>84</sup> The Similarity Principle is an important concept in Drug Discovery and is the basis of virtual screening. It enables one to find close analogues of an active molecule when screening large databases of compounds. However, it

also allows one to jump from one chemical series to another, known as scaffold hopping, when fuzzier molecular descriptors are used. Dissimilarity is the converse of similarity and can be calculated by subtracting the similarity score from unity. As dissimilarity is based on the definition of similarity, it is also of use in Drug Discovery. Namely, one could infer that dissimilar molecules might exhibit dissimilar properties. This is the starting point for molecular diversity selection, where molecules are selected because of the fact that they are dissimilar. In a Drug Discovery context, this can be used to put together a set of compounds in order to probe the activity space of a specific series.

There are many ways to compute similarity between two objects and the Tanimoto coefficient is the most widely used similarity coefficient in Drug Discovery.<sup>85</sup> What is nowadays referred to as the Tanimoto coefficient was first published by Jaccard.<sup>86</sup> In the publication describing his research on the distribution of the alpine flora, Jaccard uses a coefficient of commonality to assess the number of common species between alpine regions. The number of common species was subtracted from the total number of species in the two regions. Dividing the number of common species by this number gave the coefficient of commonality as a percentage.

Later, Rogers and Tanimoto described how a similarity ratio was used to classify plants with specific attributes.<sup>87</sup> The yes/no label of each attribute was converted into 1/0 respectively by an IBM computer. The computer program was then able to calculate the similarity ratio as the number of attributes common to both plants over the number of discrete attributes to compare two plants.

In a chemical context, the Tanimoto coefficient is calculated from the fingerprints of the molecules as follows (Equation 20):<sup>82, 88</sup>

$$T = \frac{c}{a + b - c} \quad (20)$$

where  $a$  is the number of bits set to 1 in the fingerprint for molecule A,  $b$  the number of bits set to 1 in the fingerprint for molecule B and  $c$  is the number of bits set to 1 in common to molecules A and B. The Tanimoto coefficient is between 0 and 1, with 1 representing very similar molecules. However, it must be noted that a Tanimoto score of 1 does not necessarily mean that they are identical. Indeed, it could be that the two molecules under consideration are made up of the same substructures but are connected in a different manner.

#### 2.4.2. Student $t$ -test

Before performing a statistical test on two sets of data points, a hypothesis is required, which will be verified, or not, by the statistical test. Usually, two hypotheses are stated and they are referred to as the null and the alternate hypothesis. The null hypothesis is the hypothesis of no difference, whilst the alternate hypothesis is the hypothesis of the observation of a difference. Most of the time, a statistical test produces a value called a test statistic. This number can then be looked up in a probability table and the corresponding probability (or  $p$ -value) compared to the threshold for statistical significance in order to accept or reject the null hypothesis. The larger the difference between the  $p$ -value and the threshold for statistical significance, the more confidence there is in the outcome.

Nowadays, most statistical packages output the  $p$ -value rather than the test statistic, so there is no need to use look-up tables.

In 1954, Fisher suggested that if the probability of getting a difference between the predicted (which is the null hypothesis) and the actual results was less than 5% (or 0.05), then it was possible to deduce that the difference was statistically significant.<sup>89</sup> Since then, the threshold of 0.05 for statistical significance is used as a standard in research and is recognised to be an acceptable level of risk.

Statistical tests can be separated into two distinct sets, the parametric and the non-parametric tests. Parametric tests make several assumptions, and in particular they assume that the data fit a defined distribution – usually a normal distribution.<sup>89</sup> A normal distribution can be described by its mean and its standard deviation. The normal distribution is relevant to many situations and statistical tests utilising the parameters of the normal distribution are easy to use and implement.<sup>89</sup>

A two-tailed statistical test is a test where the direction of the difference is not specified. In such a case, the alternate hypothesis is that there is a difference between the two data sets. For a one-tailed test, the alternate hypothesis could be that the mean of data set X is greater than the mean of data set Y.

The Student's  $t$ -test is an example of a parametric test and can be used to assess whether the mean difference between two populations is zero. It is applicable to populations that follow a Student distribution, i.e., if the data set contains few data points then its distribution will be wide and flat but as more samples are added, the distribution comes closer and closer to a normal distribution. A  $t$ -test assumes that

the data is normally distributed, that the variance between the two populations is equivalent and the data points in each population are independent.

When these assumptions cannot be made, a paired *t*-test can be used instead between pairs of data matched into appropriate groups. Notably, it can be utilised in the case of an experiment measuring a parameter before and after an event. However, it can also be used to pair two experimental results together provided that they are drawn from a similar group, e.g., in a clinical trial, results from two different patients but from the same age group or as is the case here, ranked docking pose scores for two different compounds.

The *t* statistic for a paired test is used to test whether two sets of data are statistically different from each other and is calculated as follows:

$$t = \frac{\bar{X}}{\frac{\sigma}{\sqrt{n}}}$$

where  $\bar{X}$  is the mean of the differences between the pairs,  $\sigma$  is the standard deviation of the differences and  $\sqrt{n}$  is the square root of the number of pairs. The *t* statistic was used in this work on populations of docking scores to objectively assess whether there was a statistical significant difference between them and to subsequently draw conclusions on, for example, characterising stereocentres with confidence.



## 2.5. Water molecules in crystal structures

When the crystal structure of a protein-ligand complex is solved, it is very common to also find water molecules, or other chemical entities that were part of the crystallisation buffer, such as glycerol. When the resolution of the crystal structure is high, it is possible to locate some of these water molecules. However, it becomes difficult to differentiate between the locations of water molecules and artefacts in the electron density, when the resolution is not high enough.<sup>90</sup> Water locations can provide useful information on the interactions of the ligand with the protein binding site and also on potential interactions. Indeed, it is very common to observe water mediated interactions between a ligand and a binding site.<sup>91</sup> The role of water molecules, in that case, is to stabilise the protein-ligand complex.<sup>91-92</sup> In the absence of a protein, water molecules form extensive networks, hydrogen bonding to each other.<sup>93</sup> These networks are very dynamic with hydrogen bonds continuously rearranging. In large binding sites, these networks can also be present. Some water molecules are conserved through a number of different crystal structures of homologous proteins, perhaps implying a structural function.<sup>94</sup> Some water locations are not always observed, therefore, inferring that they could be displaceable.

Characterising water molecules becomes particularly important when using molecular docking to predict the putative binding mode of new ligands in an existing crystal structure. Several methods have been reported in the literature to this end and two of these methods, SuperStar<sup>95</sup> and GRID<sup>14</sup> will be described here in further detail.

### 2.5.1. Water molecules in proteins

The three-dimensional structure of a protein is determined predominantly by the intramolecular hydrogen bonds occurring between its residues, but also by the intermolecular interactions it makes with water molecules.<sup>96</sup> A protein-ligand complex in solution is surrounded by water molecules. Those on the outside of proteins are not detected by X-ray crystallography because they are very mobile and have a short time-span interaction with the protein surface.<sup>97</sup> Of the ones that can be detected by crystallography, some are seen to be trapped within the protein site. Water molecules can interact directly with the ligand and the protein; however, they can also make indirect interactions with the ligand and the protein by keeping other water molecules in the right position.<sup>97-100</sup>

The presence of water molecules in protein binding sites means that they influence the shape and the properties of the binding site. This is an important consideration for drug design, as the ligand might not interact directly with all of the binding site residues. However, it is not straightforward to predict which water molecules will be present in the protein-ligand complex. It is difficult to identify the waters that are conserved and the ones that are displaceable.<sup>92, 97</sup> Moreover, displacing a water molecule by a ligand functional group is not always beneficial, which adds to the complexity of the problem. Therefore, water molecules are often removed from the binding site when designing new ligands.<sup>92</sup>

In an attempt to characterise water molecules in protein binding sites, Poonima and Dean studied twenty-six high resolution crystal structures.<sup>101</sup> They concluded that conserved waters were more tightly bound and were found in deep grooves,

whereas displaced waters were found in shallow grooves where they did not make many polar contacts.

Poonima and Dean also studied the conservation of hydration sites across orthologues.<sup>94</sup> In this work, five sets of homologous proteins were considered from different species in order to identify if water molecules in binding sites could be conserved during evolution. Moreover, the conserved waters were characterised to assess whether they were tightly bound in deep grooves, as observed in a previous study.<sup>101</sup> It was found that conserved water molecules existed in homologous protein binding sites and that these waters showed similar properties, i.e., they made polar contacts with the proteins and they were buried in deep grooves. This confirmed the conclusion of the previous study.<sup>101</sup> In addition, it was observed that the protein residues interacting with conserved waters were all conserved across a set of homologous proteins.<sup>94</sup>

In the last few years, there has been a lot more interest in computing the energy of waters and predicting displaceability based on energies. These more advanced methods have not been used in this work and the reader is directed, for example, to publications by Miranker,<sup>62</sup> Yang et al.,<sup>102</sup> Sindhikara and Hirata,<sup>103</sup> or Ross et al..<sup>104</sup>

### 2.5.2. Water molecules and molecular docking

Targeting water molecules when designing new ligands has proven successful in some medicinal chemistry programmes.<sup>105</sup> However, dealing with waters in a computational context is still a matter of debate. Recently, a number of studies have been published on the potential advantage of including water molecules in

docking experiments to improve docking result accuracy.<sup>97-98, 100, 106</sup> Roberts and Mancera report a study of a large dataset of protein-ligand crystal structures containing water molecules.<sup>97</sup> The preparation of the systems, prior to docking, involved an optimisation of the water network with and without the ligand. Keeping the ligand could bias the water network to form the most favourable hydrogen bonds with the protein-ligand complex. Comparing docking results when the systems did not contain any waters to the same systems with optimised water networks clearly showed that including waters improved the accuracy of docking results. However, comparing docking results between water optimisation methods showed that the optimisation method did not have an effect on the docking results. Indeed, statistical *t*-tests were performed in order to assess whether the water optimisation method had an impact on the docking accuracy: there was no significance difference between the two sets of results. Therefore, it was concluded that the water network optimisation without the ligand in the binding site provided similar docking accuracy.<sup>97</sup> This means that there would be no bias of the water network caused by the native ligand when docking new ligands. It was also noted that the inclusion of waters had greater impact on the docking results of lower resolution crystal structures.<sup>97</sup> One important limitation was the scoring function, which ideally would need to be adjusted to account for water-ligand hydrogen bond interactions.

Thilagavathi and Mancera followed up on the previous study with cross-docking experiments in the presence of water molecules.<sup>106</sup> Cross-docking consists of docking different ligands that have been crystallised in different structures of the

same protein to the same rigid protein conformation. It is important to note that changes in the conformation of the protein, notably around the binding site, make cross-docking experiments inappropriate,<sup>106</sup> unless protein flexibility is taken into account in some way. The structure with the highest resolution was used as a template and all other crystal structures of the same protein were aligned to the template. Water locations in a 5 Å radius around the ligand were compared and when several waters fell in the same cluster (i.e., within 1.5 Å of the template water), those locations were retained for the docking simulations. Six different proteins were used for this study and statistical tests showed that the docking accuracy increased with the inclusion of conserved water molecules. It was also highlighted that the choice of water molecules for inclusion in docking experiments was crucial to the improvement of docking results.

Huang and Shoichet studied water molecules as part of flexible protein regions.<sup>98</sup> Each water molecule was characterised by an “off” or “on” state and they were all equally displaceable. For each water molecule, an electrostatic and a van der Waals potential map were computed. Docked molecules were then scored against these maps as well as a grid map of the protein. Waters are turned “on” or “off” depending on their impact on the interaction between the protein and the waters and the ligand, i.e., if the interaction is improved then the water molecules are turned “on”. Twenty-four proteins from the Directory of Useful Decoys (DUD) dataset<sup>107</sup> were used in the docking experiments. Within the DUD dataset, for each molecule active against a given protein, there are thirty-six decoys which present similar physico-chemical properties to the active molecule but are structurally

dissimilar. The enrichment was compared when docking without waters and docking with displaceable water molecules. The enrichment was calculated from the number of true active molecules found in the top of the ranked list of scored molecules, i.e., the method is able to discriminate between true actives and decoys. For half of the proteins studied, including displaceable waters did not affect the enrichment, whilst it slightly worsened for one of the targets. The simulation was repeated with fixed waters in the protein binding sites. The enrichment was much poorer for fifteen proteins, unchanged for eight of them and better for one.<sup>98</sup>

Lie et al. proposed an Attached Water Model (AWM) where water molecules were attached to the ligand at its hydrogen bonding groups.<sup>100</sup> The ligand was fully solvated at each hydrogen bonding point. For example, each hydroxyl group had two water molecules donating hydrogen bonds to it and one water molecule accepting one hydrogen bond from it. These waters attached to the ligand of interest can be displaced by the protein during docking. A water molecule was part of the final docking pose if it interacted in a favourable manner with its neighbours, its neighbours being the protein, the ligand, and other attached waters. An entropy penalty constant, accounting for the loss of entropy of water, was added for each water molecule that was retained to encourage their displacement. The entropy term encourages the displacement of the waters attached to the ligand. Indeed, the release of waters which are not in an ideal environment in terms of interactions should be removed from the protein-ligand complex, producing an entropy gain. Therefore, an entropy penalty was associated with each water to encourage their displacement. The study was performed on twelve protein-ligand complexes from

the PDB, which presented water mediated interactions between the ligand and the protein. The AWM was able to reproduce the crystallographic poses of the ligands, even though not always as the top ranked docking solution. An optimal value of three for the entropy penalty constant was also found.

These recent studies of water molecules in the context of molecular docking show that including waters is often beneficial to the accuracy of docking poses. However, one issue that has been raised lies with the scoring functions.<sup>97, 100</sup> Also, Hartshorn et al. pointed out that including water molecules can limit the search space by leaving room for only a few conformations of the ligand, especially when docking back into its native protein crystal structure.<sup>108</sup> A final question is around the applicability of a system with fixed crystal waters to be used prospectively in the docking of novel ligands.

Ideally, only water molecules which are involved in stabilising the protein-ligand complex and interact with both the ligand and the protein binding site through bridging hydrogen bonds would be retained for molecular docking studies. To this end, two programs which aim to identify favourable hydration sites will be described in the subsequent section.

### 2.5.3. Prediction of hydration sites

#### 2.5.3.1. *Superstar*

Superstar is a tool provided by the Cambridge Crystallographic Data Centre (CCDC). It is a knowledge based approach to identify favourable interactions points, propensity maps, in protein binding sites, or around small molecules.<sup>95</sup> It uses as a knowledge base the small molecule crystallographic information of the Cambridge Structural Database (CSD).<sup>109</sup> It is also possible to use crystal information from the PDB,<sup>110-111</sup> although it is reported to be of lower accuracy and reliability due to the lower resolution of protein structures, compared to small molecules, and to the absence of hydrogen atoms.<sup>95</sup> Indeed, the crystallographic information available from the CSD is of much higher resolution than that from the PDB. Thus, interactions such as hydrogen bonds are precisely defined. Also the amount of data in the CSD is much greater than in the PDB (800,000 vs ~100,000, respectively). Combining the size of the database with the quality of the data means that the statistics and interactions derived from the CSD are more robust than from the PDB. It has been shown that crystal packing does not have an effect on the interactions derived from either databases, but the solvent used does.<sup>112-114</sup> However, the chemical make-up of these two databases is different. It has been shown that interaction patterns derived from the CSD agree well with those of the PDB.<sup>115</sup> It has been claimed, however, that one of potential drawbacks of the CSD is that it does not represent hydrophobic interactions between ligand and protein well as small molecules are often crystallised from non-aqueous solvents.<sup>115</sup> Therefore, an extra



hydrophobic factor has been added to the SuperStar maps to account for this known deficiency.<sup>115</sup>

SuperStar uses IsoStar distributions to generate propensity maps. IsoStar is a library that stores information, i.e., type of contact, geometry, energy, of about 250 chemical groups.<sup>116</sup> It uses crystallographic information from the CSD or the PDB to generate scatterplots describing intermolecular contacts. A contact is defined as any distance shorter than the sum of the van der Waals radii of the atoms plus 0.5 Å. The CSD was searched for interactions between specific pairs of functional groups. The PDB was also searched for specific interactions between protein residues and ligand atoms, water molecules and ligand atoms and water molecules and protein residues. The resulting contacts were aligned using the central group as reference and were displayed as scatterplots (*Figure 11*).

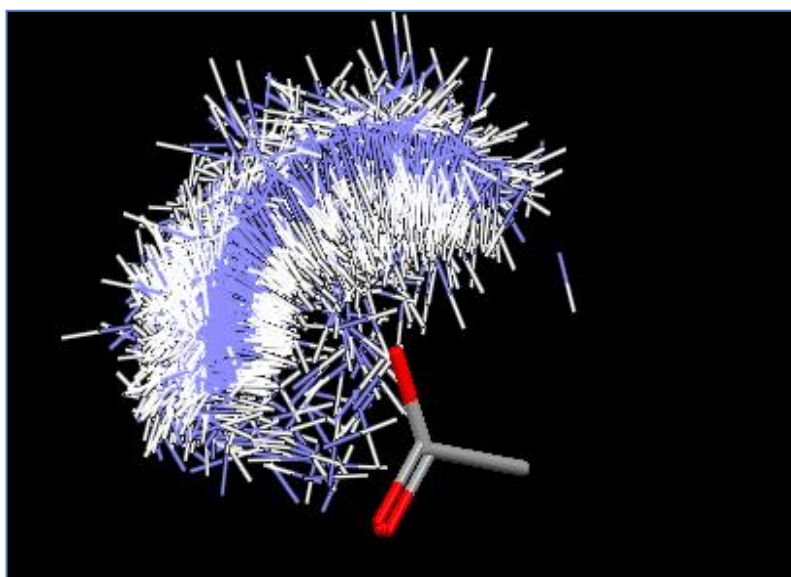


*Figure 11:* IsoStar scatterplot showing any NH around a charged carboxylic acid

A scatterplot represents the distribution of a contact group around a central group. It is also possible to convert a scatterplot to a contoured density surface.

Scatterplots are linked to the CSD or PDB data and it is possible for the user to select a contact group and visualise the crystal structures where it was found. A comparison of the CSD and the PDB scatterplots has revealed that there is a good agreement between the two sources of data.<sup>115</sup>

In SuperStar, the preparation of the protein binding site lies with the user. It is important to make sure that the hydrogen atoms are added, the hydrogen bond network optimised and the charges checked to ensure the appropriate interactions are computed. Once the protein is prepared, a probe needs to be selected. A probe is an IsoStar contact group and is chosen from a set of eleven for CSD data, such as alcohol oxygen or methyl carbon, and six for PDB data. Some probes are not included when the PDB option is selected because of the lack of sufficient crystallographic data – for example in the case of halogen probes.<sup>95, 117</sup> The template protein is then placed in a 3D grid and broken up into fragments. Such a fragment is equivalent to an IsoStar central group. Atoms in the central group are target atoms, whilst the remaining atoms are treated as ‘hard spheres’. In order to assess which IsoStar central group matches the fragment the best, a match quality coefficient is computed. Each permutation of the atoms on to the IsoStar central group is performed. The central group with the highest score is chosen. IsoStar scatterplots of central groups are superimposed onto the protein and each scatterplot is translated into a density map, which is the number of probes per unit of volume. The contributions for each probe at each grid point around it are computed and summed to give a probe density  $d(i, j)$  at each grid point (Equation 21).

$$d(i,j) = \frac{1}{\Delta^3} \sum_{k=1}^{N_{p(j)}} w(i,j,k) \quad (21)$$

where  $i$  is the grid point,  $j$  the scatterplot,  $k$  the probe,  $\Delta$  the grid spacing (the default is 0.7 Å),  $N_{p(j)}$  the number of probes in scatterplot  $j$  and  $w(i,j,k)$  the contribution, described in Equation 22:

$$w(i,j,k) \propto e^{\left(-\frac{|r_i - r(j,k)|^2}{2\sigma_s^2}\right)} \quad (22)$$

$r_i$  is the position of grid point  $i$ ,  $r(j,k)$  is the position of probe  $k$  in scatterplot  $j$ .  $\sigma_s$  is the fall-off of the contribution to each grid point with its distance to the probe;  $\sigma_s = 0.25$  Å. The weights are distributed using a Gaussian smearing function and their sum equals one.

The density maps are then normalised by computing an average density for each scatterplot, which would be the density obtained at random. Once this is achieved a propensity  $p(i,j)$  can be computed for each grid point (Equation 23).

$$p(i,j) = \frac{d(i,j)}{d_{av}(j)} \quad (23)$$

where  $d_{av}(j)$  is the average density for scatterplot  $j$ .

Density maps from different central groups can overlap. In order to reflect this in the final composite map, the propensities are multiplied as shown in Equation 24:

$$P(i) = P_o(i) \prod_{j=1}^{N_s} p(i,j) \quad (24)$$

where  $N_s$  is the number of scatterplots contributing to the composite map and  $P_o(i)$  is the propensity of the protein atoms that were not used to compute the map. This is set to one for all grid points apart from those points which are within a defined distance from any 'hard sphere'. This prevents the map being calculated inside unmatched atoms.

SuperStar is also able to deal with some metal atoms, namely zinc, calcium and magnesium, in the protein binding site in the same way as other central groups are handled.<sup>117</sup> However, the coordination data need to be managed as well as the geometries. Searching the CSD for metal complexes led the authors to the conclusion that zinc atoms have a preferred coordination pattern of four, whilst for magnesium it is six and calcium is less selective with six, seven or eight-coordinate complex. Associated to the coordination, the geometries of the metal complexes vary from tetrahedral for a four-coordinate complex to dodecahedral for an eight coordinate complex. The authors set up templates of the most common metal complexes and compared the metal complex of the CSD central group to assign its likely coordination and geometry. It is often the case that in protein binding sites, metal atoms are only partially coordinated by the protein itself. The other coordination sites are occupied by water molecules or ligand atoms. This means that the templates need to have several corresponding central groups, for example central groups with partial coordination of two up to five correspond to the zinc atom when it is found in trigonal bipyramidal geometry. Scatterplots are then produced for all central groups thus defined.

### 2.5.3.2. GRID

GRID is a force-field based method that identifies favourable interaction sites of a template by running a specified probe, which is a small chemical group such as ammonium or water, along a three dimensional grid.<sup>14</sup> GRID computes the interaction energy at each GRID point between the probe and the template molecule. Once the energy has been computed, contour surfaces can be displayed. Negative energy levels indicate attraction between the probe and the protein.

The GRID energy function has a similar functional form to the non-bonded terms in molecular mechanics force fields described in Section 2.1. The Lennard-Jones term models van der Waals interactions between the probe and the protein, whilst the electrostatic term account for charge interactions and the hydrogen bond term models hydrogen bond contacts. The GRID energy function is presented in Equation 25.

$$E_{xyz} = \sum E_{lj} + \sum E_{el} + \sum E_{hb} \quad (25)$$

where  $E_{lj}$  is the Lennard-Jones function,  $E_{el}$  is the electrostatic term and  $E_{hb}$  the hydrogen bond term.

The Lennard-Jones energy function is represented by a 12-6 potential of the form described in Equation 26.

$$E_{ij} = \frac{A}{d^{12}} - \frac{B}{d^6} \quad (26)$$

where  $d$  is the distance between two atoms under consideration,  $A$  and  $B$  are parameters derived from the number of electrons, the polarisability and the van der Waals radius of the atoms. As  $d$  becomes small, the repulsive term  $\frac{A}{d^{12}}$  increases rapidly as represented in *Figure 3*. Conversely, the attraction term  $\frac{B}{d^6}$  approaches zero very quickly as  $d$  becomes large. Therefore, a distance threshold of 8 Å, above which  $E_{ij}$  is assigned the value zero, is chosen.

The electrostatic potential is not as influenced by the distance separating the two atoms as the Lennard-Jones potential is. It is computed for all pairs of atoms and is never set to zero, as opposed to the Lennard-Jones potential. The electrostatic function is described in Equation 27.

$$E_{el} = \frac{pq}{\kappa\zeta} \left[ \frac{1}{d} + \frac{(\zeta - \varepsilon)/(\zeta + \varepsilon)}{\sqrt{d^2 - 4s_p s_q}} \right] \quad (27)$$

where  $p$  is the electrostatic charge of the probe and  $q$  the electrostatic charge of the protein atom,  $d$  the distance between the probe and the atom,  $\varepsilon$  the dielectric of a homogeneous solution and  $\zeta$  the protein phase dielectric.  $s_q$  is the depth of the protein atom in the protein phase and  $s_p$  the depth of probe at position xyz in the protein phase. These depths are assigned a value depending on the number of atoms within a radius of 4 Å. The author showed that when the probe had less than

seven neighbouring atoms in its 4 Å radius, then it was in solution as opposed to in the protein phase. Therefore,  $4s_p s_q$  is assigned the value zero when the probe is surrounded by less than seven protein atoms within a 4 Å radius around it.

In the first publication on GRID, the hydrogen bond energy term was described using a direction dependent 6-4 potential.<sup>14</sup> Boobbyer et al. subsequently found that the 6-4 potential presented too long hydrogen bonds compared to experimental data, whilst a 12-10 function gave a too restricted array of hydrogen bond lengths.<sup>15</sup> They concluded that an 8-6 potential was the most suited to describe hydrogen bonds accurately (Equation 28).<sup>15</sup>

$$E_r = \frac{C}{r^8} - \frac{D}{r^6} \quad (28)$$

where  $E_r$  is the distance dependent function of the hydrogen bond energy function  $E_{hb}$  described in Equation 29.  $C$  and  $D$  are described Equation 11.

$$E_{hb} = E_r \times E_t \times E_p \quad (29)$$

$E_t$  and  $E_p$  are the angle dependent functions for the target protein atom and the probe respectively, with  $t$  the angle made by the hydrogen bond at the target atom and  $p$  the angle at the probe atom (*Figure 12*).<sup>118</sup>

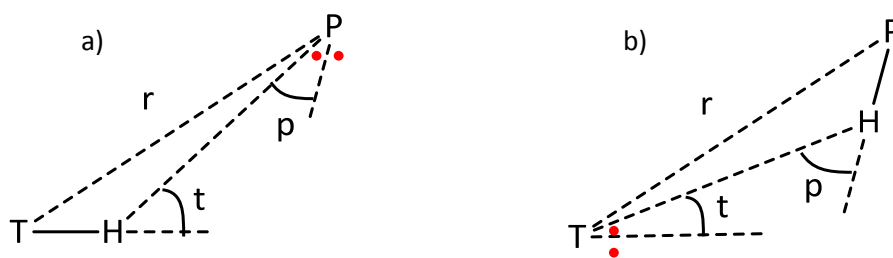


Figure 12: Definition of angles  $t$  and  $p$ , a) when the target atom is the hydrogen bond donor; b) when the probe is the hydrogen bond donor. Lone pairs in red

These functions are dependent on the chemical nature of the atoms involved in the hydrogen bonding event and are selected by fitting to experimental data.

For any target atom which donates a hydrogen,  $E_t$  is described as (Equation 30):

$$E_t = \cos^n t \quad (30)$$

where  $n$  is 2, 4, or 6 depending on the nature of the target atom.

When the target atom accepts hydrogen bonds,  $E_t$  can be represented by a number of functions in order to account for the diversity of hydrogen bond geometries, from an acceptor perspective.<sup>15</sup>

If the probe is able to make only one hydrogen bond then  $E_p = 1$  as the probe can orient itself in such a way that it makes the most optimal interaction. In such cases,  $p$  would be zero. However, if it makes more than one hydrogen bond, then it is possible that not all hydrogen bonds are optimal. Wade et al. found that the



expression of  $E_p$ , shown in Equation 31, was the best to reproduce experimental data when two or more hydrogen bonds were made by the probe.<sup>118-119</sup>

$$E_p = \cos^2 p \quad \text{with } 0 < p < 90^\circ \quad (31)$$

$$E_p = 0 \quad \text{for } p > 90^\circ$$

In this case,  $E_p$  is equal to one when the probe makes optimal hydrogen bonds.

The parameters used to assess the empirical energy functions are based on the CHARMM force field and its extended atom model.<sup>120</sup>

### 3. Protein systems studied

#### 3.1. Leukotriene A4 hydrolase

##### 3.1.1. Leukotriene pathway

Leukotrienes (LT) are important lipid mediators in inflammatory and allergic responses. They are synthesised through the arachidonic acid (AA) pathway, with the initial reaction being the conversion of AA by 5-lipoxygenase (5-LO) into leukotriene A4 (LTA4). LTA4 is very unstable and is converted into leukotriene B4 (LTB4) by LTA4 hydrolase (LTA4H) but also into leukotriene C4 (LTC4) by LTC4 synthase (*Figure 13*).<sup>121</sup>

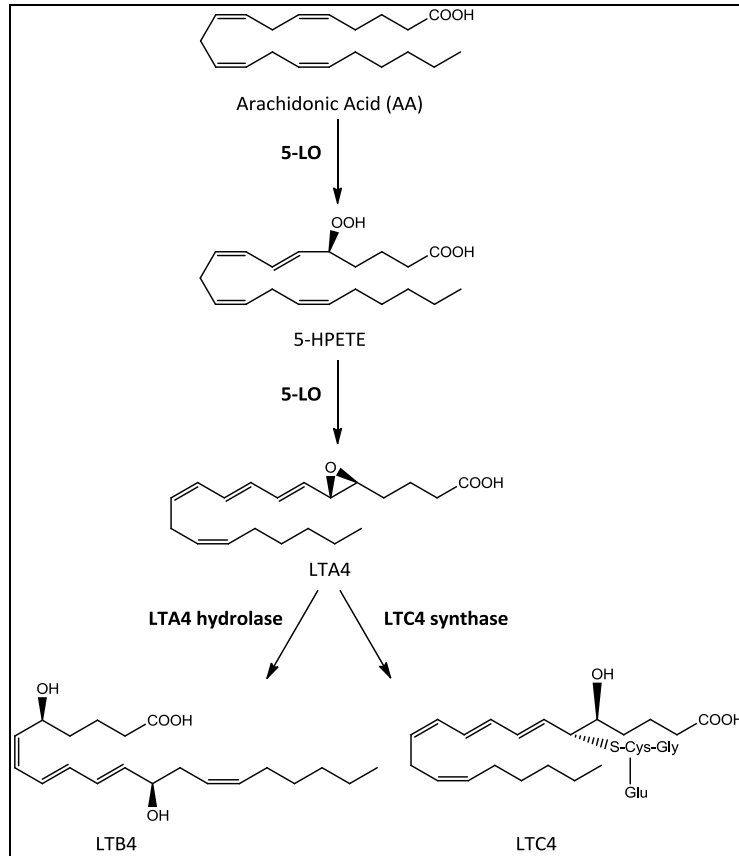


Figure 13: Leukotriene synthesis - inspired from Haeggström et al<sup>121</sup>

The immune system is a biological system which enables the protection of an organism against diseases through killing of foreign entities entering it. The immune response can be divided into two types, the innate response and the adaptive response. Innate response to inflammation is non-specific. It comprises general systems which attack xenobiotics and is the primary response to infection. Adaptive response is activated by the innate immune system and provides protective immunity. It consists of very specialised cells, like T-cells, and protects the host against future attacks. LTB<sub>4</sub> is involved in adherence and aggregation of leukocytes. It can also induce the attraction of T-cells to the site of infection. These belong to a

group of white blood cells called lymphocytes and are part of the adaptive response. Thus, LTB<sub>4</sub> is a link between innate and adaptive immune response to inflammation.<sup>121</sup> LTB<sub>4</sub> is an important mediator in various inflammatory diseases and the inhibition of its synthesis through LTA<sub>4</sub>H is an attractive target in the treatment of lung inflammation such as asthma and Chronic Obstructive Pulmonary Disease (COPD).

### 3.1.2. LTA4H and its biological activities

LTA4H is a 69 kDa metalloenzyme, which is made up of three domains, with a zinc atom in its binding site (*Figure 14*) and it has two functions, as a hydrolase and as an aminopeptidase.<sup>121-123</sup>

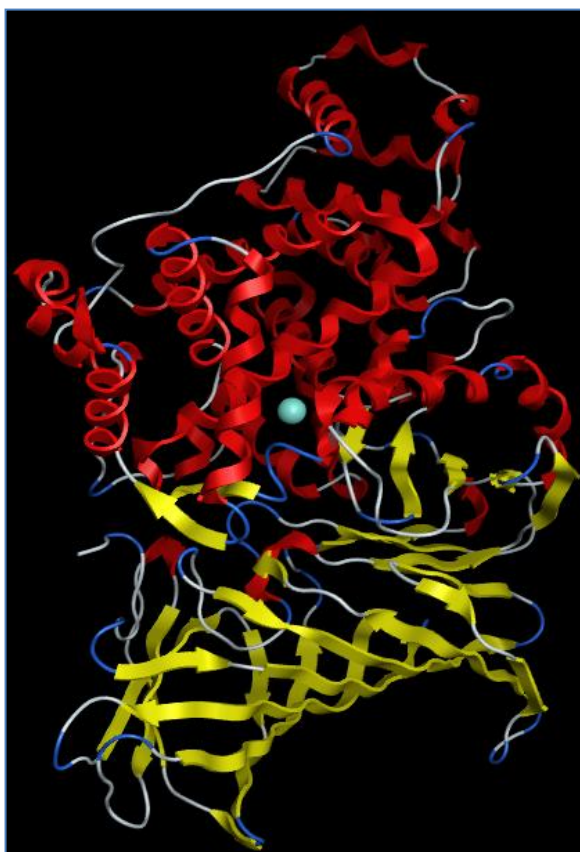


*Figure 14:* Ribbon representation of LTA4H enzyme with  $\alpha$ -helices in red and  $\beta$ -sheets in yellow. The zinc atom is highlighted in turquoise

The hydrolase activity is observed in the hydrolysis of LTA4 into LTB4. The biological role of LTA4H as an aminopeptidase is not yet well understood, but it is thought to be associated with the processing of peptides in immune response.<sup>121</sup> A comparison of its primary structure with other zinc hydrolases exposed a catalytic zinc site which binds synthetic peptidic ligands. In this work, the focus is on inhibiting the hydrolase activity of LTA4H.

To assess whether a molecule has an inhibitory effect on the hydrolase activity of LTA4H, the project biologists developed a biochemical assay to measure  $IC_{50}$ 's (half maximal inhibitory concentration).

In this project, an aminopeptidase assay was used to measure the activity of the compounds designed and synthesised by the chemistry team, as the hydrolase and the aminopeptidase activities of LTA4H occur in the same binding site. The primary assay is a fluorescence assay which quantifies LTA4H aminopeptidase inhibition. A fluorescence assay is an assay in which a light source emits at a given wavelength on to a solution containing the enzyme, a substrate and the test compound, either of which is tagged with a fluorescent moiety. Changes in fluorescence are associated with an interaction between the test compound and the enzyme. In this instance, the substrate is an amino acid specific to the enzyme coupled with a fluorescent compound, which fluoresces only if the bond between the amino acid and itself is cleaved. The fluorogenic substrate is excited at a certain wavelength. If there is no inhibition of the enzyme, i.e., the bond is cleaved, then there is fluorescence which is measured at a different wavelength. If the test compound inhibits the enzyme, then the bond is not cleaved and there is no fluorescence to be measured. The output of the assay is usually expressed as  $pIC_{50}$ .

$IC_{50}$  is the half maximal inhibitory concentration, i.e., the amount of a particular compound needed to inhibit half of the target activity *in vitro*.  $pIC_{50}$  is the negative log base 10 of  $IC_{50}$  and the greater the  $pIC_{50}$ , the more active the compound under consideration. Similarly,  $K_i$ , the inhibition constant, is sometimes used to represent the activity of molecules.  $K_i$  is the ratio of the concentration of free inhibitor and of

the protein over the concentration the protein complexed with the inhibitor:  $K_i = [P][I]/[PI]$ , where P is the protein and I the inhibitor. The lower the  $K_i$ , the more active a compound is.

The LTA4H hydrolase inhibition was also checked in a hydrolase inhibition assay on a subset of compounds. However, no specificity was observed between the two assays for the lead series. Hence, the aminopeptidase assay was selected as the first pass. Only compounds of interest were tested in the hydrolase assay to check that the inhibition in the aminopeptidase assay translated into the similar level of inhibition in the hydrolase assay (*Figure 15*).

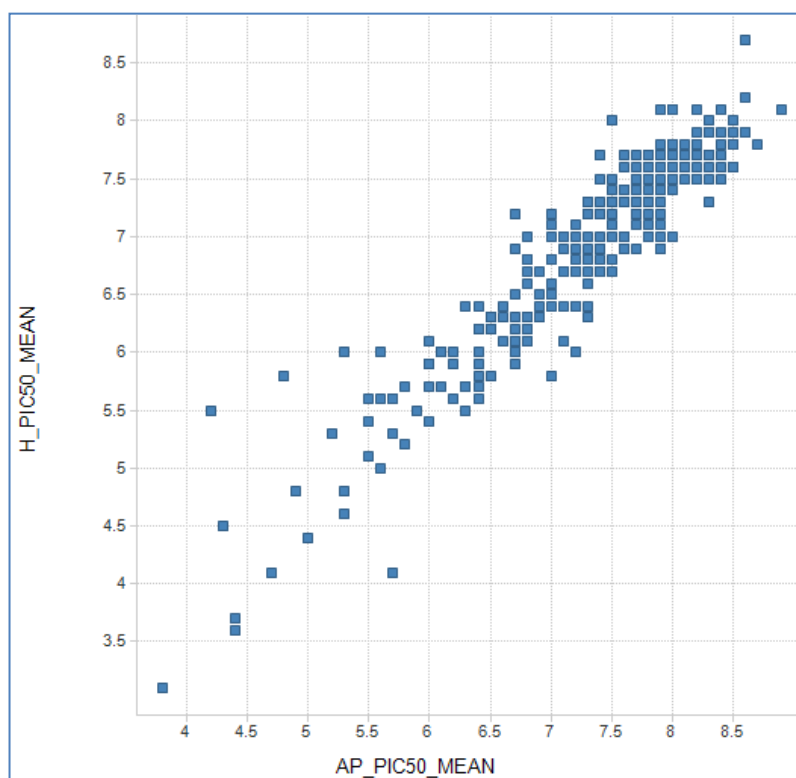


*Figure 15:* Comparison of activity values in the aminopeptidase assay (AP\_PIC50\_MEAN) and the hydrolase assay (H\_PIC50\_MEAN)

### 3.1.3. LTA4H and protein crystallography

From a solution, it is sometimes possible to crystallise a molecule, whether it is a small ligand or a macromolecule such as a protein, or molecules in complex with each other. A single crystal X-ray diffraction experiment can then be used to obtain diffraction data from which a three-dimensional structure can be derived. Such structures will be referred to, hereafter, as crystal structures. Each crystal structure has a resolution associated with it, which gives an indication of its quality. The higher the resolution of the data, the more detail can be observed in the electron density map. The resolution is reported in angstroms ( $\text{\AA}$ ). For example, if a protein crystal structure has a resolution of around  $3 \text{\AA}$ , only the contour of the amino acids can be seen on the electron density map; some atoms are not well defined (*Figure 16a*). The crystal structure of a protein with a resolution of less than  $2 \text{\AA}$  is considered of good quality and atoms are well defined on the electron density map (*Figure 16b*). Small molecule crystal structures usually have a resolution of less than  $1 \text{\AA}$ , which means that even hydrogen atoms can be seen on the electron density map.



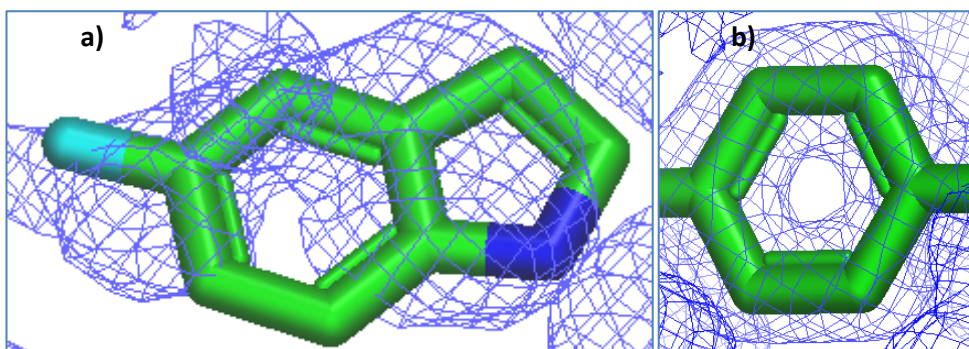


*Figure 16:* a) 3FUF with resolution of 2.6 Å focussing on the ligand, where not all atoms can be seen on the electron density map; b) 3FUN with a resolution of 1.58 Å focussing on the electron density of a benzene ring.

The crystal structure of LTA4H in complex with a competitive inhibitor bestatin **1** (*Figure 17*) was solved in 2001.<sup>124</sup> Since then, around forty crystal structures of LTA4H with different ligands have followed and have been released in the public domain. This represents helpful information that can be used in the context of structure-based design. A selection of ligands from the public domain is depicted below. It can be noted that the chemical diversity of LTA4H inhibitors is not large. Molecules often present a lipophilic side made up of one or two aromatic rings, sometimes separated by a linker, followed by an amine functionality and a carbon chain terminated by a carboxylic acid.

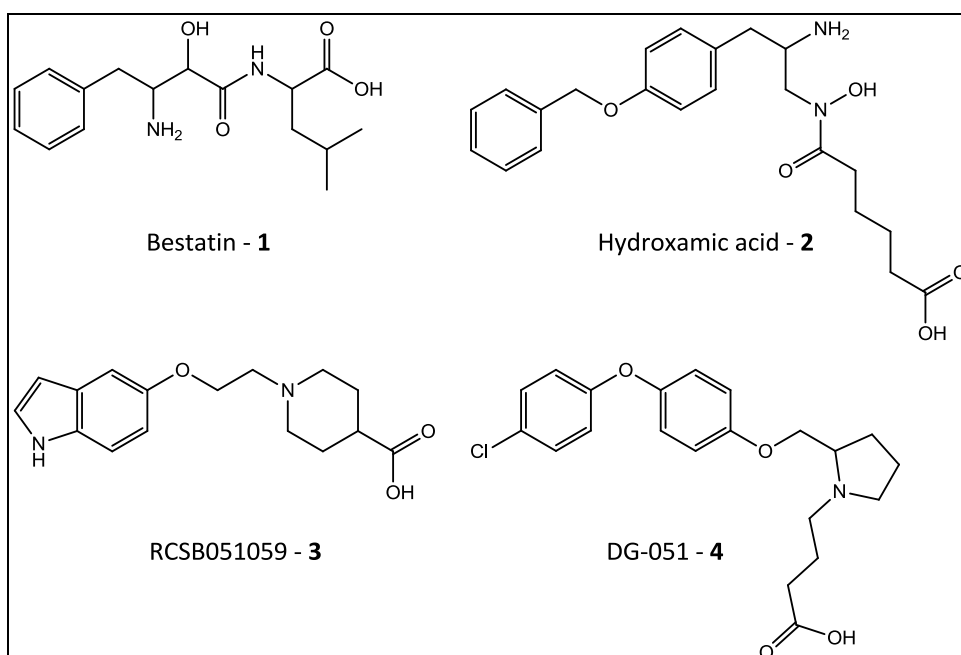


*Figure 17:* A selection of ligands from the public domain crystallised in complex with LTA4H, bestatin being the first compound to have successfully been crystallised

An analysis of crystal structures showed that the zinc atom interacts with His295, His299 and Glu318. The zinc is often tetrahedral and most of the time, it is a water molecule that provides the fourth contact. However, it can also be made by a carboxylic acid, as the case is for **4** (PDB entry 3FH7 – *Figure 18*) and in this case, the zinc atom adopts a 5-coordinate configuration.<sup>125</sup> This is typical of the zinc atom which is frequently observed to be either tetrahedral or in a 5-coordinate configuration as it is a soft, easily polarisable ion as opposed to harder metal ions, such as magnesium, which is always octahedral.<sup>117</sup>

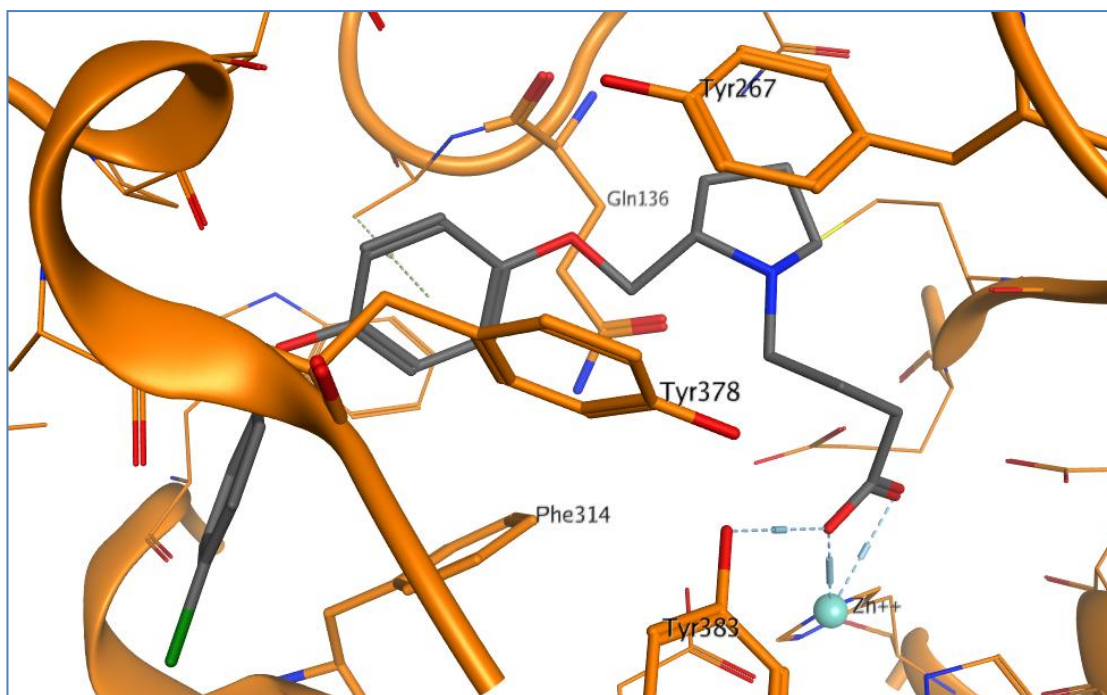


*Figure 18:* Compound **4** interacts with the zinc atom through its carboxylic acid moiety in a bidentate fashion

The following proprietary LTA4H ligands were studied in this work (*Table 1*).

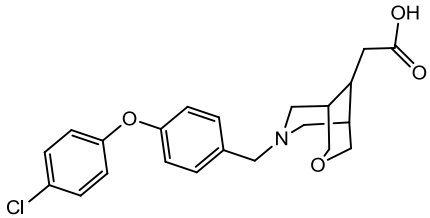
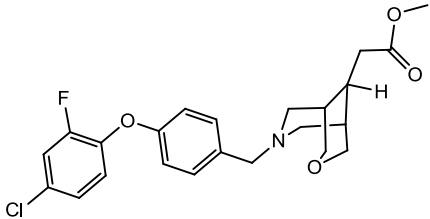
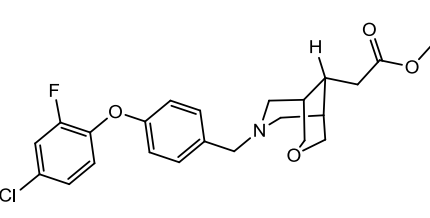
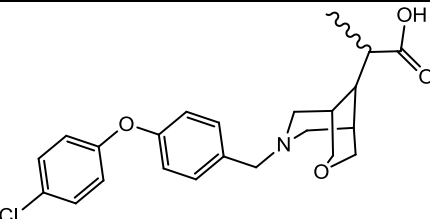
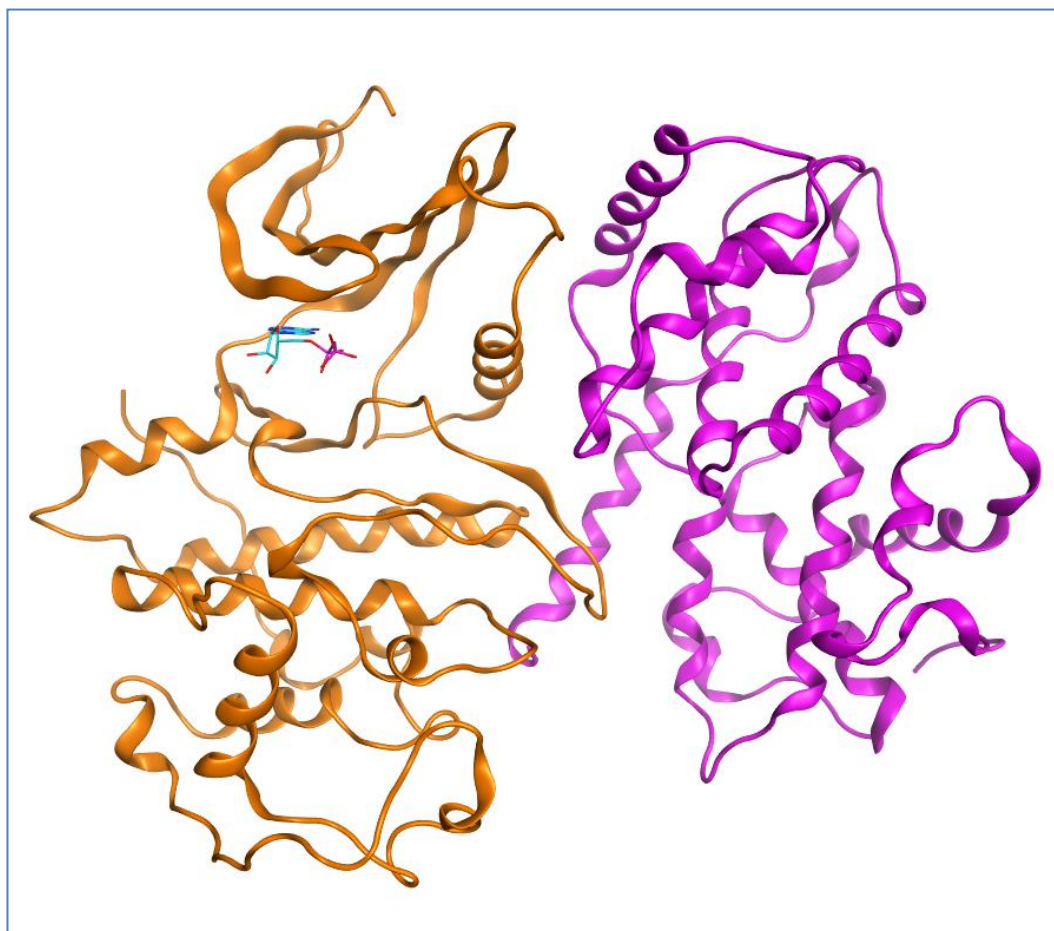
Ligand	Structure	Aminopeptidase pIC50	heavy	MW	clogP
7		8.1	28	402	1.9
8		7.6	30	434	4.5
9		7.2	30	434	4.5
10		7.7	29	416	2.2

Table 1: Proprietary LTA4H ligands studied and physico-chemical properties; pIC50 values given for compounds **7** and **10** are for the unprotected carboxylic acids

### 3.2. Cyclin-dependent kinase 2

Cyclin-dependent kinase 2 (CDK2) is a protein which is part of the kinase family. It is involved in the cell cycle and is activated by binding of cyclin E (or A) and phosphorylation of a conserved threonine.<sup>126</sup> The protein has a typical kinase architecture, where the N-terminal is made of  $\beta$ -sheets, whilst the C-terminus is made of  $\alpha$ -helices. In between these two domains is the hinge. CDK2 is a Ser/Thr kinase, which means that it transfers a phosphate group from adenosine triphosphate (ATP) to these specific amino acids, which have a similar side chain, of

the substrate protein. In the absence of cyclin, CDK2 is in an inactive state. When cyclin binds, it induces a movement in one of the  $\alpha$ -helices, which brings together Lys33 and Glu51 in a salt bridge interaction (*Figure 19*).<sup>127</sup> This interaction is thought to make this side of the ATP binding site more rigid.



*Figure 19:* Structure of CDK2 in orange with ADP bound (turquoise) in complex with cyclin A in magenta (as resolved in public crystal structure 4I3Z)

There are over 400 structures of CDK2 in the public domain. Four different CDK2 crystal structures and two ligands were studied in this work. All three protein crystal structures were obtained without cyclin bound. Thus, the salt bridge between Lys33 and Glu51 was not formed. This implies that Lys33 is more mobile and can protrude

into the binding site, making it smaller. The objective of these experiments was to assess the Induced Fit Docking (IFD) protocol to reproduce the results obtained by the Schrödinger group and to devise improvements to the methods.<sup>9</sup> The Schrödinger group do not state in their publication the reason why they chose specific systems. However, we have chosen the 1BUH structure because it was crystallised with no ligand bound and it is the only structure in the public domain, to date, with a significant movement of Phe80. The 1DM2 structure is a more typical conformation of CDK2 bound to a drug-like molecule, whilst in 1AQ1 CDK2 was crystallised bound to a large ligand in a very similar conformation to 1DM2 but with slight movements near the hinge. There are other amino acid movements in the binding site seen in other structures, especially around the hinge but the amino acid side chains are pointing out of the binding site, e.g., His84 or Gln85, making them less interesting to study.

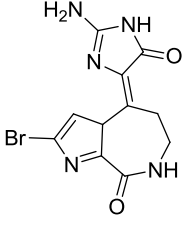
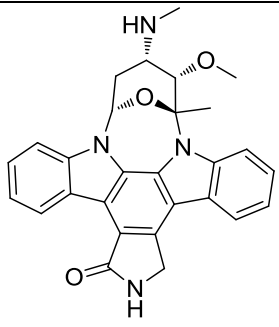
Ligand	Structure	Heavy	MW	clogP
<b>11</b>		19	324	-1.6
<b>12</b>		35	466	4.2

Table 2: Physico-chemical profile of CDK2 ligands **11** and **12** (Heavy = number of heavy atoms, MW = molecular weight, clogP = calculated logP)

## 1BUH

The CDK2 protein crystal structure 1BUH was solved in 1996 by Bourne et al.,<sup>126</sup> at a resolution of 2.6 Å. It was in complex with CksHs1, the human cell cycle regulatory protein, which binds to the C-terminal domain of CDK2. The effect of binding of these two proteins is not well understood, but is thought to be involved in the inhibition of Tyr15 dephosphorylation.<sup>126</sup> The cyclin and ATP binding sites were not affected by the binding of CksHs1. The ATP binding site did not contain any ligand, therefore, the protein was in an apo state. Instead, the site is filled with water molecules.

*Figure 20* shows the ATP binding site, with some key residues highlighted in a thick stick representation. Glu81 and Leu83 constitute the hinge binding region, where the adenine ring of ATP would usually bind. Phe80 is the last residue of the hinge domain and, in the kinase family, is referred to as the gatekeeper;<sup>128</sup> in this structure, it is found in an unusual conformation relative to other CDK2 structures where Phe80 does not protrude into the binding site. Bourne et al. claimed that this flipped conformation may interact with the side chain of Ala31.<sup>126</sup> There is a salt bridge between Lys33 and Asp145, which is different to the salt bridge induced by the binding of cyclin to CDK2. In this instance, the salt bridge reduces the size of the binding site, which may cause some issues when cross-docking ligands in the rigid binding site.



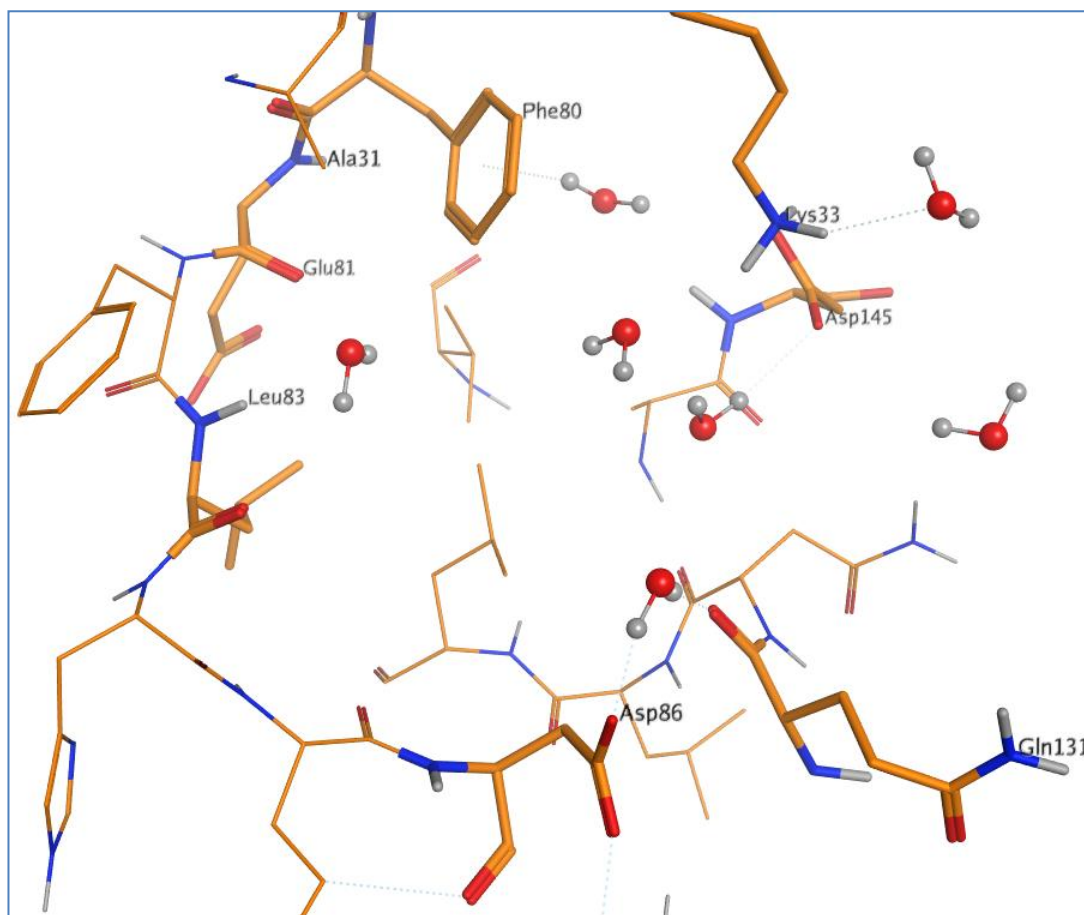


Figure 20: The binding site in 1BUH; amino acids of interest highlighted in thick stick representation

The 1BUH crystal structure of CDK2 contains 287 amino acids. Residues 40-46 and 295-298 are missing, due to missing electron density. Residues 40-46 are part of a flexible loop, which is also missing in the following crystal structures.

### 1DM2

The CDK2 protein crystal structure 1DM2 was solved in 2000, by Meijer et al., with a resolution of 2.1 Å.<sup>129</sup> CDK2 was crystallised in complex with ligand **11** (Figure 21), hymenialdisine, a marine-sponge derived natural product. The pyrroloazepinone core is an atypical hinge binder. It is a weak binder due to its semi-saturated

aromatic nature in comparison to the usual flat aromatic moieties. Ligand **11** interacts with Glu81 through the nitrogen of the amide moiety and with Leu83 through the amide carbonyl and the pyrrole nitrogen (*Figure 21*). The nitrogen on the pyrroloazepinone ring hydrogen bonds to the backbone carbonyl of Gln131 through water 580, whilst the amine on the same ring interacts with the side chain carboxylic acid of Asp145. There are some van der Waals contacts between the side chain of Ile10 and the core and the side chain of Val18 and the imidazolone ring. Unfortunately, the electron density of 1DM2 was not released by the authors;<sup>129</sup> therefore, it was not possible to verify the binding mode of ligand **11**.

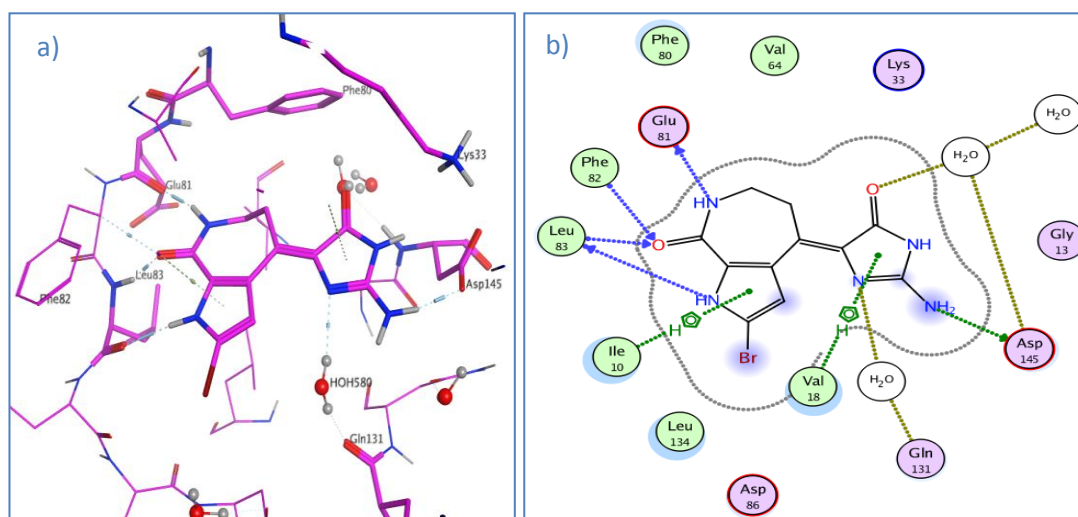


*Figure 21:* a) The binding site in 1DM2, with ligand **11** bound; b) 2D representation of the ligand interactions

Residues 36 to 44 and 149 to 163, part of two flexible loops, were not modelled due to weak or missing electron density. Crystal structure 1DM2 is thus 274 amino acids in length.

## 1AQ1

The CDK2 protein crystal structure 1AQ1 was solved in 1997, by Lawrie et al., with a resolution of 2 Å.<sup>127</sup> The protein was resolved in complex with staurosporine (ligand **12**, Table 2), a known non-specific inhibitor of kinases.<sup>127</sup> It interacts with the binding site of CDK2 through hydrogen bonds to Glu81 and Leu83 on the hinge. However, the carbonyl of Leu83 is not involved in any interaction with the ligand as was seen in crystal structure 1DM2. It is rotated away from the binding site in order to accommodate **12**. This is not a commonly observed movement for CDK2 and is due to the size of **12**. It will be instructive to assess whether IFD will be able to reproduce this movement. The protonated secondary amine interacts with the backbone carbonyl of Gln131 and the side chain carboxylic acid of Asp86, through hydrogen bonds. There are also some van der Waals contacts between the side chain of Val18 and the core. An inspection of the electron density showed that the binding pose reported by the authors was plausible.<sup>127</sup>

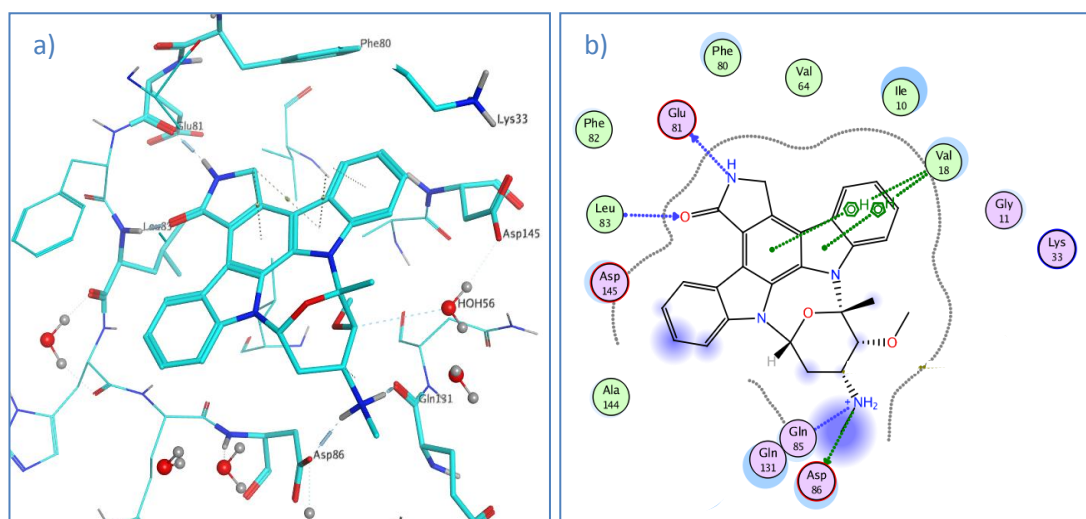


Figure 22: a) The binding site of 1AQ1, with ligand **12** bound; b) 2D representation of the ligand interactions

Residues 36-44 and 149-161 showed poor electron density and were not modelled. These residues are part of the same flexible loops mentioned for the crystal structure 1DM2. Crystal structure 1AQ1 is 277 amino acids in length.

#### 4EK3

This apo structure of CDK2 was solved in 2013 by Kang and Stuckey, at a resolution of 1.34 Å.<sup>110</sup> There is currently no publication associated with this crystal structure and as such, minimal information could be gathered about it. The protein is 291 residues long and was crystallised in the absence of a ligand. *Figure 23* shows the conformation of the binding site and it is quite clear that Lys33 is protruding into the binding site. This could affect docking outcomes. Residues 36 to 44 were not resolved.

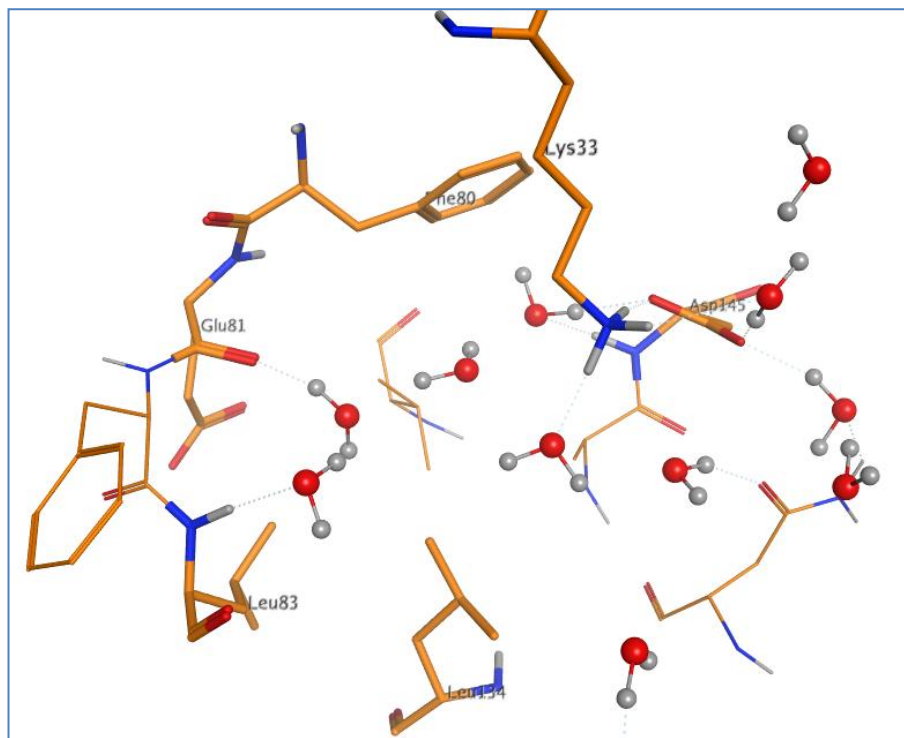


Figure 23: Binding site of apo structure 4EK3

Figure 24 shows the superposition of the binding site from all four CDK2 protein crystal structures. There are some large movements of side chains in the binding site, such as Phe80, Lys33, Asp145, but also of side chains pointing out of the binding site, such as His84. In the apo protein crystal structures 1BUH and 4EK3, there is a salt bridge between Lys33 and Asp145, which is not present in the other two structures. Phe80 moves out of the binding site to accommodate the ligands in 1DM2 and 1AQ1, but also in 4EK3. The same applies to Lys33 and Asp145, especially in 4EK3 in which Lys33 protrudes into the binding site. The conformation of the amino acids on the hinge is consistent across all four protein structures, apart from the carbonyl of Leu83 which points up and away from the binding site in 1AQ1. This

could be due to the size of ligand **12**, which would overlap with Leu83 if its carbonyl did not move out.

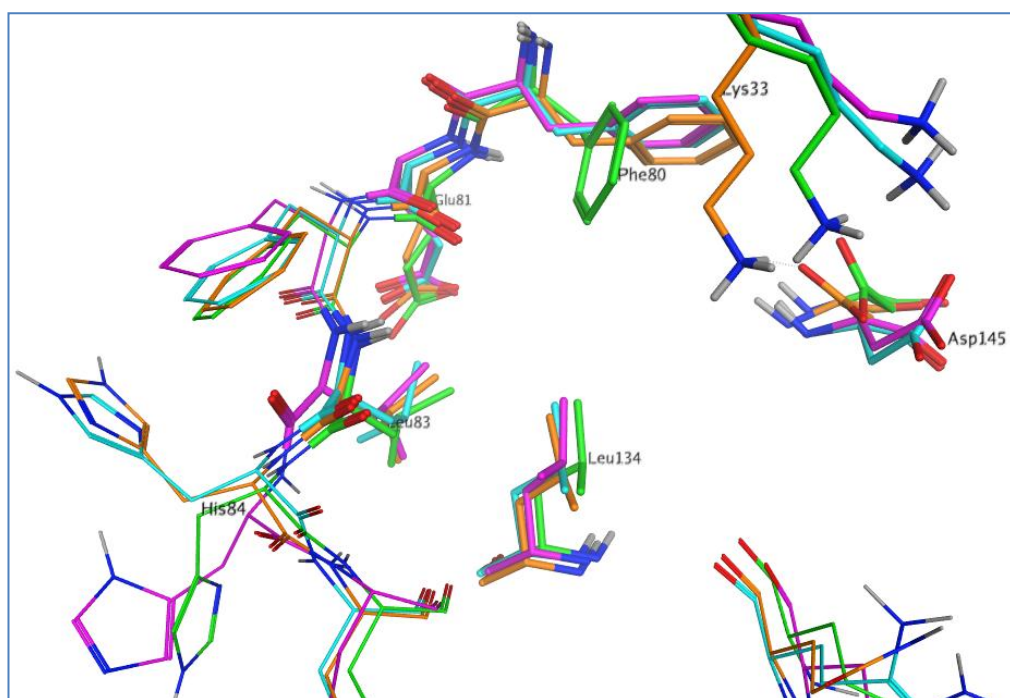


Figure 24: Superposition of 1BUH (green), 1DM2 (turquoise), 1AQ1 (magenta) and 4EK3 (orange)

It is expected that docking of ligands across different protein crystal structures of the same kinase and even across different kinases should yield good results in terms of ligand orientation and interactions, given the conserved hinge binding region.<sup>130</sup>

The only hindrance to this would be substantial conformational changes of the binding site. In the case of the apo CDK2 structures, 1BUH and 4EK3, there are indeed large conformational changes of the side chains. Thus, it might be expected that cross-docking of ligands from other crystal structures would fail in those

instances. One aim of this work is to confirm that this is the case and then to explore flexible docking methods as a means of resolving this problem.

The four CDK2 protein crystal structures were prepared using the Protein Preparation Wizard<sup>131-132</sup> available in Maestro, as described in Section 4.1, although in this instance water molecules were removed from the model systems.

The ligands were prepared with LigPrep,<sup>133</sup> also available in Maestro. The procedure is described in Section 4.2.

### 3.3. UPPS

Undecaprenyl pyrophosphate synthase (UPPS) is an anti-bacterial target, which is involved in the synthesis of the bacterial membrane. Its role is to make undecaprenyl pyrophosphate (UPP) from farnesyl pyrophosphate (FPP) by eight successive multiple additions of isopentenyl diphosphate (IPP).<sup>134</sup> These consecutive condensations lead to UPP, which is a C55 long diphosphate polymer (*Figure 25*). UPP is a building block implicated in the synthesis of precursors to peptidoglycan, a polymer layer found on the outside membrane of bacteria, also known as the bacterial cell wall.<sup>135</sup> Therefore, by inhibiting the ability of UPPS to create UPP for the synthesis of its membrane, the bacteria is unable to survive and proliferate. Furthermore, UPPS is not found in humans and, therefore, finding a drug with specific activity against this target reduces the chance of side effects. Thus, UPPS could be an important antibacterial target in order to affect these types of cells.

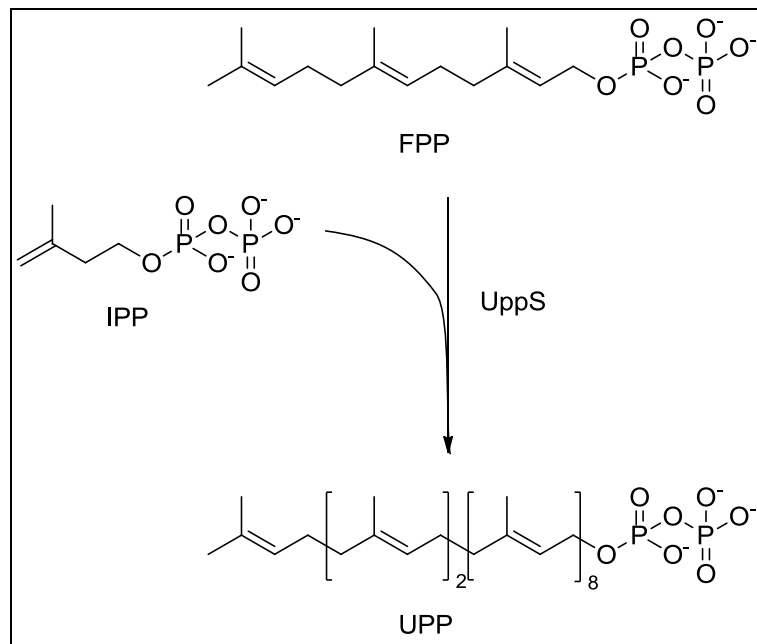
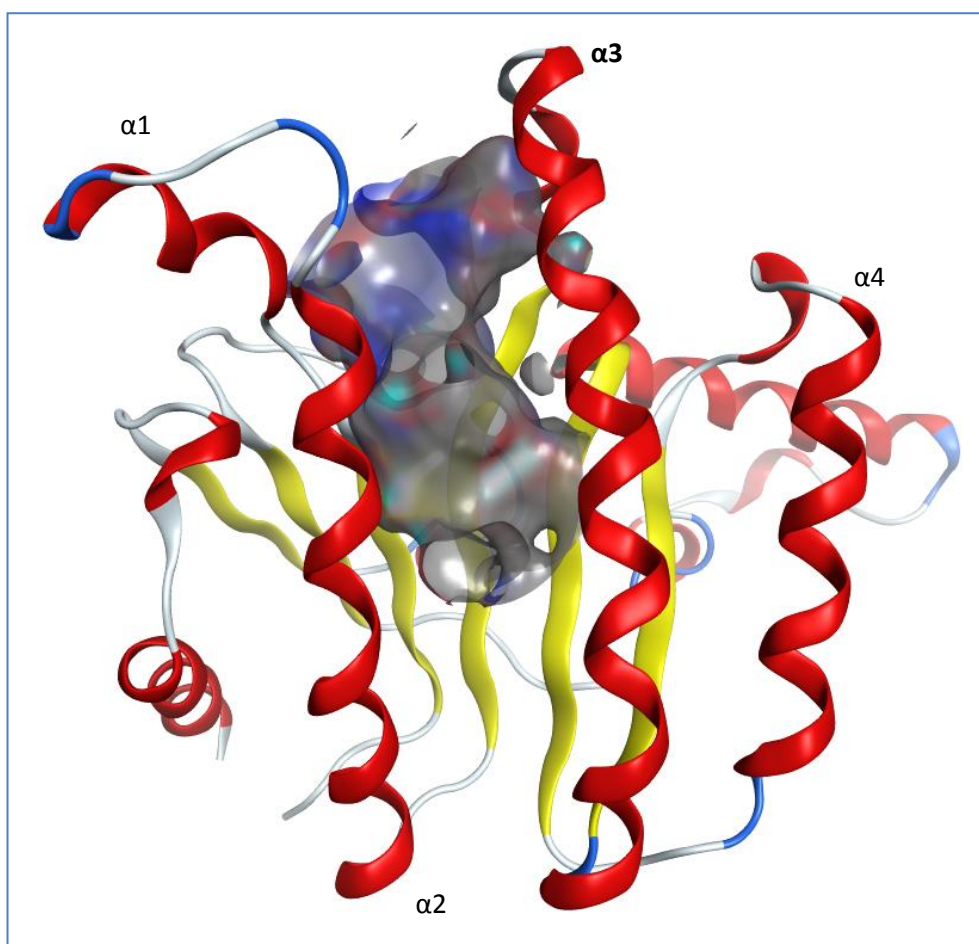


Figure 25: UPP synthesis

UPPS is a flexible protein. There is a loop that is often not visible in crystal structures, when no ligand is bound in the binding site.<sup>135</sup> When a ligand is bound, including FPP, the protein adopts a closed conformation with  $\alpha$ -helix 3 ( $\alpha$ 3) moving in (Figure 26).<sup>136</sup>





*Figure 26:* UPPS structure showing the location of helix  $\alpha 3$

The FPP and IPP binding sites can be seen in *Figure 27*. In this crystal structure, IPP was found bound in the FPP binding site. Nevertheless, this structure was able to shed some light on the key interactions of both FPP and IPP in the UPPS active site, given that these two molecules share common features. The diphosphates of the FPP and IPP are thought to coordinate a magnesium dication found between them. The magnesium dication also interacted with the side chain of Asp28 and with two water molecules, adopting an octahedral coordination, the preferred coordination geometry of magnesium II.<sup>137</sup> IPP in the FPP pocket also made hydrogen bonds to

the side chain and backbone of Arg32, the backbones of Asn30, Asn31 and Gly29 and on the other side of the phosphate with the side chain of Arg79. In the IPP pocket, IPP hydrogen bonds to the side chains of Arg196, Arg202 and Ser204 as well as the side chain of Asn76 and Arg79 on the other side of the phosphate group.

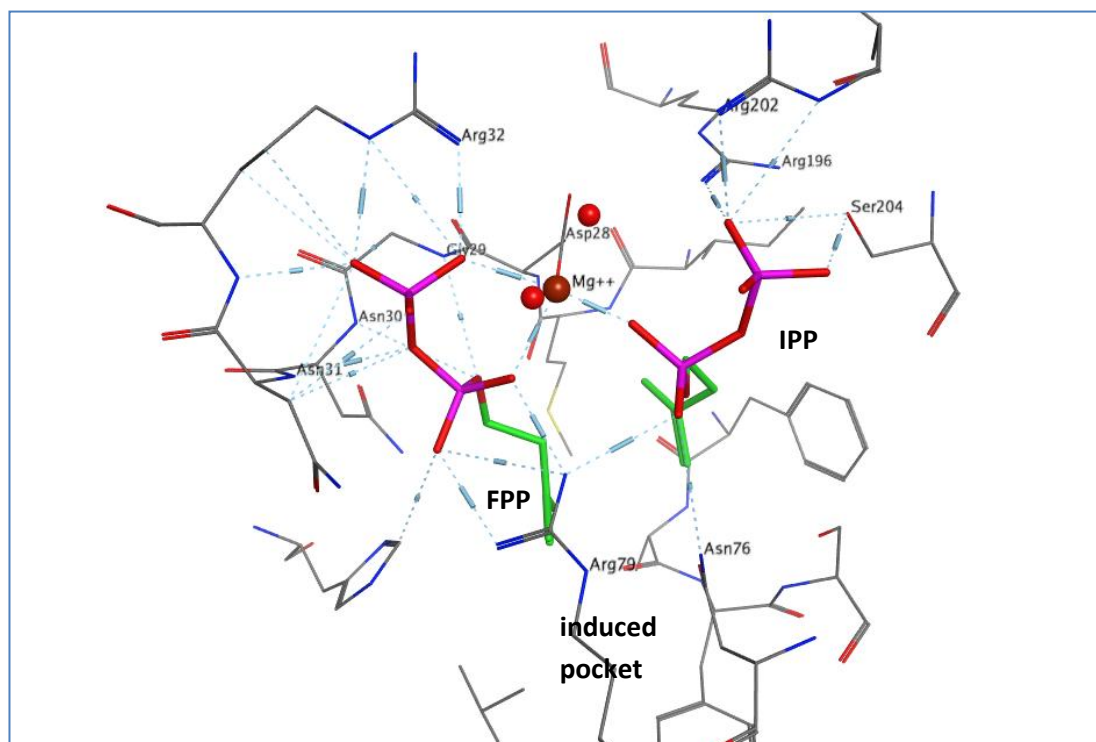


Figure 27: FPP and IPP binding sites highlighted, with IPP binding in both sites on this occasion. Proprietary crystal structure 6HNEW

In the following docking experiments, three UPPS ligands were investigated (Table 3). These ligands have been made in GSK as well as their corresponding protein-ligand crystal structures. The three ligands and their protein crystal structures were used in induced fit docking experiments.

Table 3 shows some physico-chemical properties for ligands **13**, **14** and **15**. Ligand **15** is much larger and more lipophilic than **13** and **14**, with a molecular weight of

534 and a calculated clogP of 3.9. The larger size of **15** presents a significant challenge to dock into the other two structures.

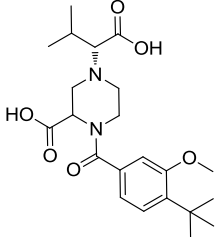
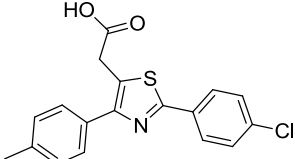
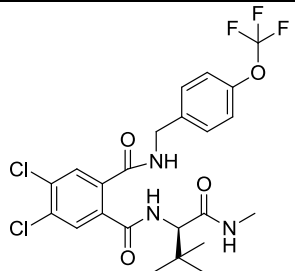
Ligand	Structure	pIC50	heavy	MW	clogP
13		3.1	30	420	2.9
14		<4	23	344	4.9
15		n.d.*	35	534	3.9

Table 3: Summary of some physico-chemical properties for **13**, **14** and **15**

\* no data - analogue bearing tBu instead of CF<sub>3</sub> tested with a pIC<sub>50</sub> = 7.7

#### 4NCKH

Ligand **13** was crystallised in complex with UPPS in crystal structure 4NCKH, at a resolution of 1.67 Å. There were two complexes in the asymmetric unit. There was a slight difference in binding mode for **13**, between chains A and B. In chain A, the isopropyl of **13** pointed towards the side chain of Phe70 and the neighbouring carboxylic acid made a hydrogen bond to the side chain of Asn76 (*Figure 28*). In chain B, this moiety was rotated and bound slightly higher than in chain A. The acid was still interacting with Asn76 but also with the backbone NH of Ser73, which was

too far away in chain A. The conformation of the core piperazine of **13** was less favourable, adopting a strained twisted-boat arrangement.

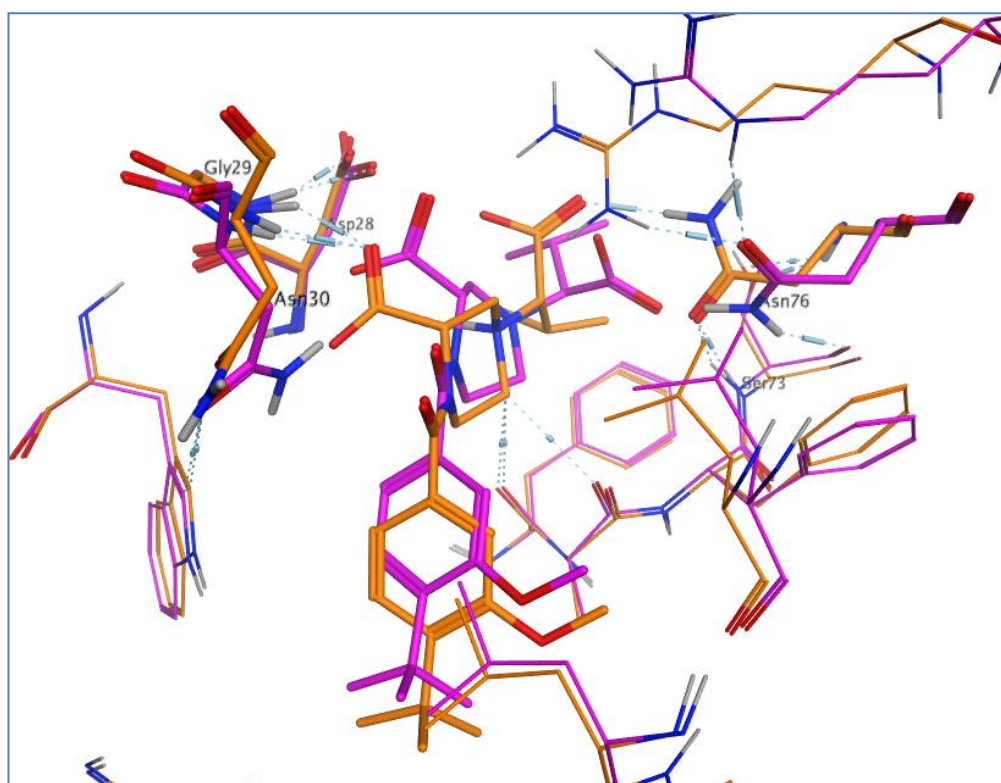


Figure 28: Comparison of ligand conformations in chain A (orange) and chain B (magenta) in 4NCKH

Chain A is 205 residues in length, whilst chain B is 215 residues long. Residues 1 to 4, 31 to 49 and 211 to 215 were not resolved. Because of the good agreement between chain A and chain B in terms of superposition, only chain A was used in the docking experiments.

Ligand **13** makes several hydrogen bond interactions, mainly through its carboxylic acids (Figure 29). The central acid interacted with the backbone NHs of Asn30 and Gly29 and the terminal one with the side chain of Asn76. The *p-t*-butyl-*o*-methoxy phenyl bound in the lipophilic pocket is located at the bottom of the site.

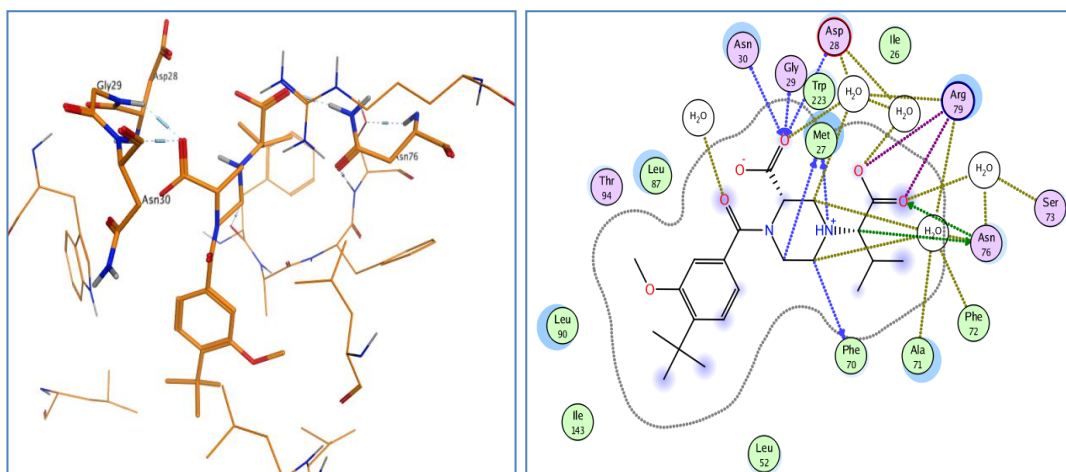


Figure 29: Binding mode and interactions of **13** in crystal structure 4NCKH and its ligand interaction diagram

### 1ZHUB

Ligand **14** was crystallised in complex with UPPS in crystal structure 1ZHUB, at a resolution of 1.9 Å. In this instance, there were again two chains of UPPS bound in the asymmetric unit, but only chain A bound **14**. For this reason, chain A is used in the docking experiments.

Ligand **14** made several hydrogen bond interactions from its carboxylic acid moiety to the backbone NHs of Asn30 and Asn31, to water 355 and also to the side chain of Asn30 (Figure 30). There is also a potential interaction between the nitrogen of the thiazole core to the backbone carbonyl of Phe70 through water 286.

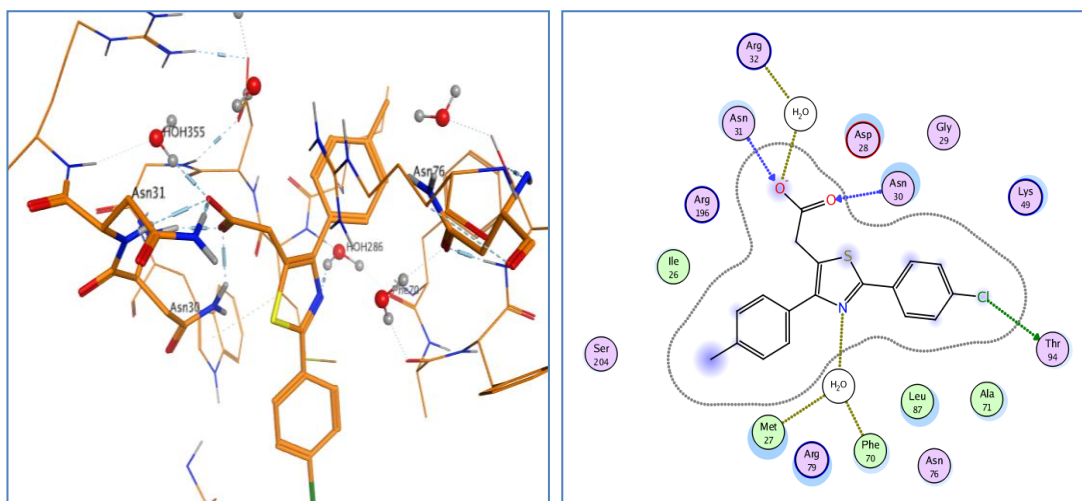


Figure 30: Binding mode and interactions of **14** in 1ZHUB and its ligand interaction diagram

### 7WZYC

Ligand **15** was crystallised in complex with UPPS in crystal structure 7WZYC, at a resolution of 2.3 Å. In this instance, there are four chains of UPPS bound in the asymmetric unit. **15** was bound in all four chains. The carbonyl of the benzamide between the two phenyl rings interacts with the amide side chain of Asn30 and its NH with the backbone carbonyl of Ala71. The NH of the central benzamide hydrogen bonds to the carbonyl of the side chain of Asn76, as does the NH of the terminal methyl amide. There is also a through-water interaction between the second benzamide and Gly29 and Asp28 at the top of the pocket. The dichlorophenyl moiety binds a pocket induced upon binding with a noticeable movement of Leu87 to create this pocket. This will be referred to as the induced pocket, hereafter.

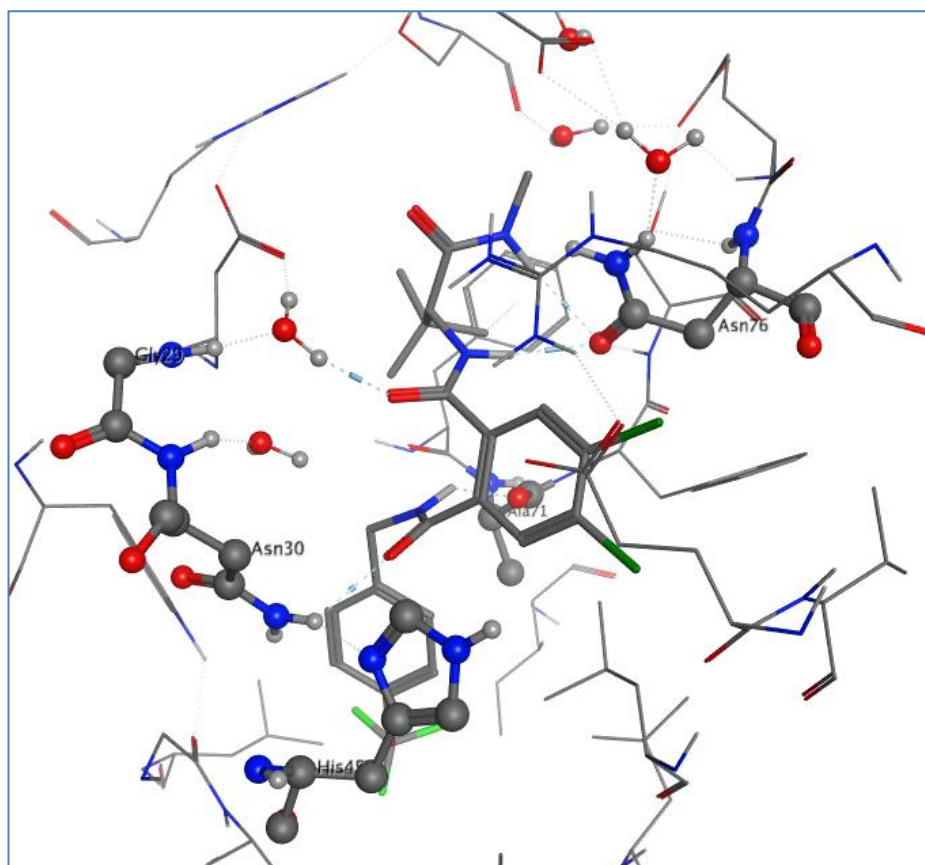


Figure 31: Binding mode of **15** in crystal structure 7WZYC

A comparison of all three proprietary crystal structures showed that there is little difference in conformation between the complexes 4CNKH (ligand **13**) and 1ZHUB (ligand **14**), but there is some movement in 7WZYC (ligand **15**) (*Figure 32*). In particular, lipophilic amino acids such as Leu87, Leu90 and Leu91, are found in different rotamers. Also the region between helix  $\alpha 1$  and the top of helix  $\alpha 2$ , disordered in 4CNKH and 1ZHUB, is ordered in 7WZYC and could be modelled (*Figure 33*). The presence of these extra amino acids, leading to a more constrained binding site, is expected to pose a realistic challenge to the IFD simulations in this particular structure. However, the reverse could also be true, i.e., the absence of

these residues in the other two structures creates a large binding site for docking studies, which can lead to more false positives.

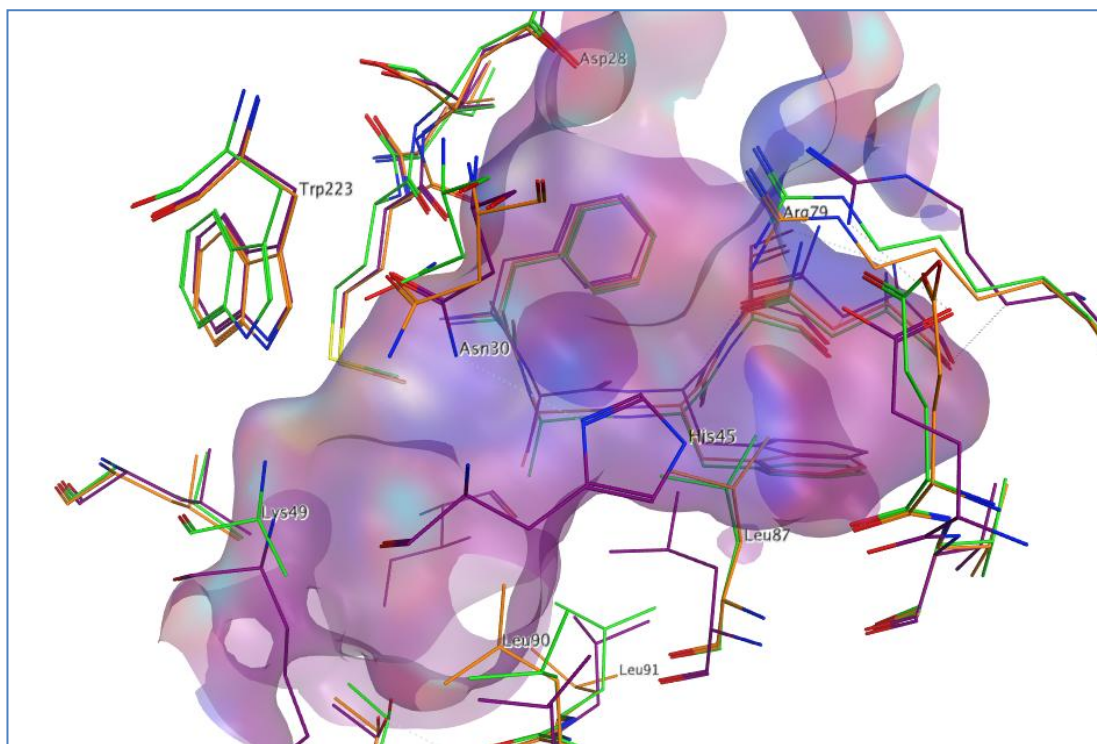


Figure 32: Binding site comparison between 4CNKH in orange, 1ZHUB in green and 7WZYC in purple

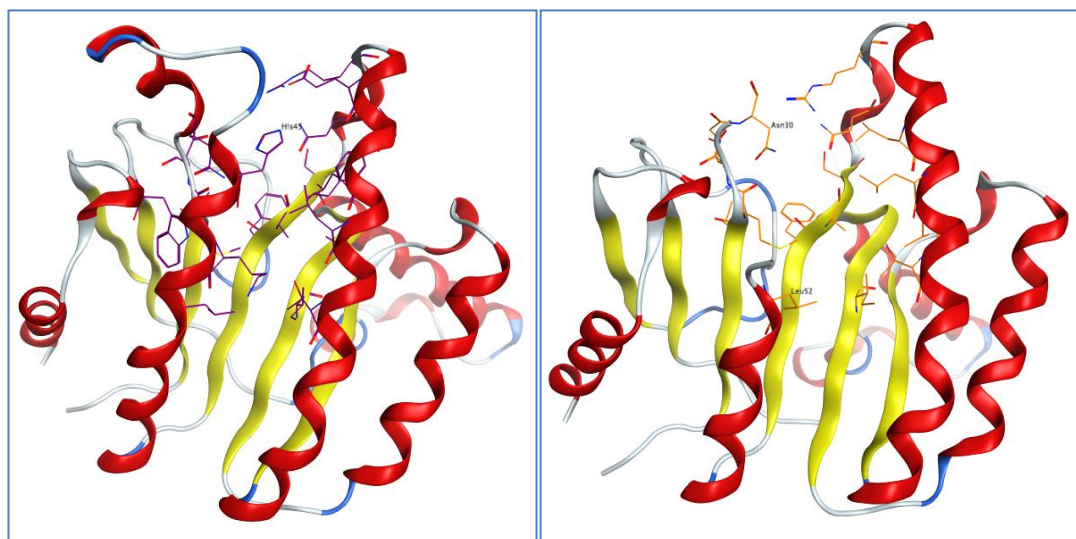


Figure 33: UPPS structures showing the a) presence in 7WZYC and b) absence in 4CNKH of residues 31 to 51 in the top left of the pictures



The three UPPS protein crystal structures were prepared using the Protein Preparation Wizard available in Maestro, as described in Section 4.1. Water molecules were removed from the model systems. The ligands were prepared with LigPrep, also available in Maestro using the procedure is described in Section 4.2.

### 3.4. Factor Xa

Factor Xa (fXa) is an enzyme that converts pro-thrombin to thrombin.<sup>138</sup> It has been investigated as a potential treatment to prevent the formation of blood clots. In the cascade leading to blood clot formation, thrombin transforms fibrinogen into fibrin, which is the last step of the process.<sup>138</sup> Traditional ways to counteract this phenomena is to find inhibitors of thrombin. An alternative approach is to target fXa to stop the formation of thrombin itself. This could be a safer way to tackle this disease, as many thrombin inhibitors have undesirable side effects, such as abnormal bleeding.<sup>138</sup>

fXa consists of two chains, a light one and a heavy one (*Figure 34*). The light chain consists of the N-terminal Gla domain (made of eleven glutamic acid residues) and two epidermal growth factor-like (EGF-like) domains. The heavy chain is the catalytic domain, which is a serine protease.<sup>138</sup>

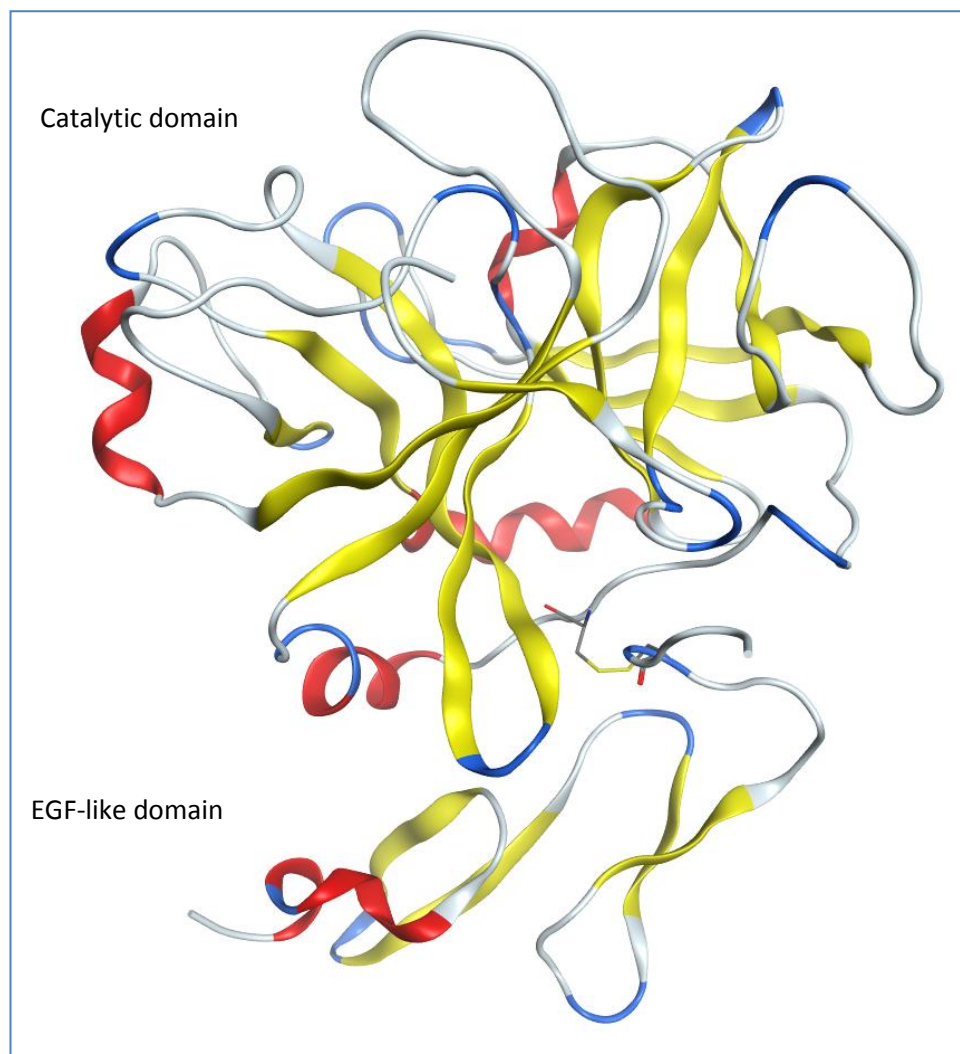


*Figure 34:* Structure of fXa showing the two domains linked by a disulfide bridge

Two known fXa inhibitors that were studied and are shown in *Table 4*. They are similar in size, as demonstrated by their heavy atom counts; and they both present a benzamidine moiety, which is important for binding.

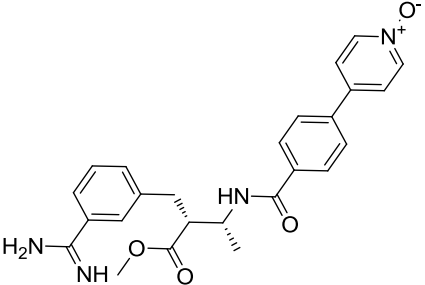
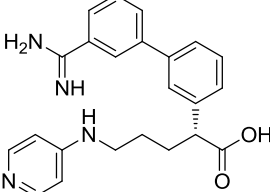
Ligand	SMILES	heavy	MW	clogP
16		33	446	0.6
17		29	389	2.1

Table 4: Summary of some physico-chemical properties for **16** and **17**

### 1KSN

fXa was crystallised in complex with **16** with a resolution of 2.1 Å at a pH of 5.7 by Maignan and Guilloteau.<sup>139</sup> Ligand **16** presented a protonated benzimidazole moiety, as predicted by LigPrep at this pH, which interacted through a bidentate hydrogen bond to the side chain carboxylic acid of Asp189 and also to the backbone carbonyl of Gly219 and to a resolved water molecule, water16 (*Figure 35*). This bidentate interaction is the anchor of the binding mode for this compound, with the remaining interactions contributing relatively less to the stability of the complex. Indeed, the remaining interactions, visible at this resolution, are from the amide NH to water133, from the amide carbonyl to water100 and the backbone NH of Gly219. There is also a  $\pi$ - $\pi$  interaction between the N-oxide pyridine and Phe174. The authors of the original publication where this chemical series was described explain the interaction between the N-oxide pyridine and the aromatic amino acids as “extensive van der Waals contacts”.<sup>139</sup> A bare pyridine ring is an electron deficient ring. When moving to an N-oxide pyridine, the aromatic ring itself becomes more

electron-deficient due to the addition of the oxygen atom. This would concur with the possible existence of  $\pi$ - $\pi$  interactions with nearby electron rich aromatic amino acids. The other interactions that could be possible with this kind of ring are from the positive charge on the nitrogen to a  $\pi$  cloud of electrons.

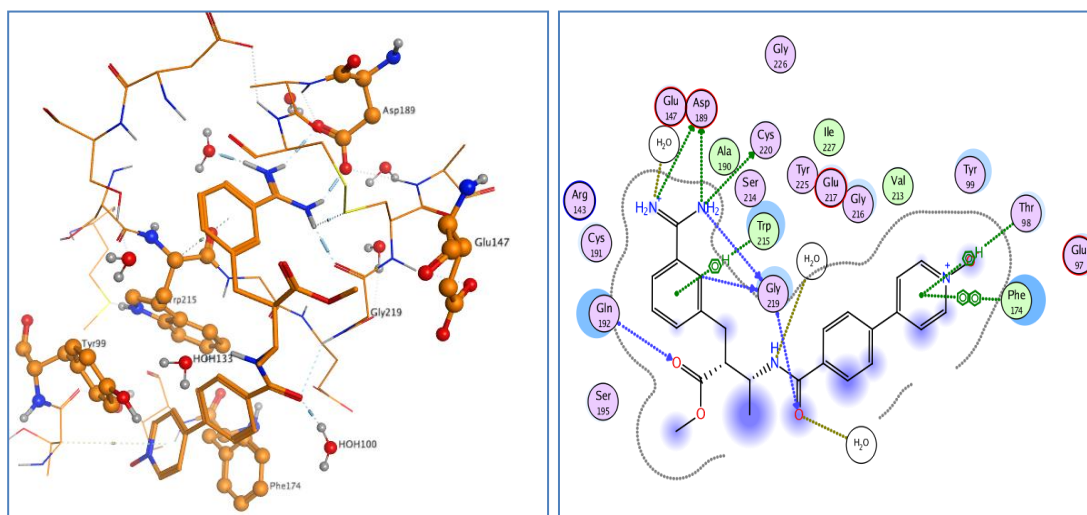


Figure 35: Binding mode of **16** in 1KSN and its ligand interaction diagram

### 1XKA

fXa was crystallised in complex with **17** with a resolution of 2.3 Å by Kamata and Kim.<sup>138</sup> The benzamidine as well as the pyridine are protonated at the pH at which the crystallisation experiment was run (pH = 5.5), as predicted by LigPrep. Chain L in this crystal structure represents the first and second epidermal growth factor (EGF)-like domains.<sup>138</sup> Chain L is linked by a disulfide bridge to Chain C, the catalytic domain. Ligand **17** is bound in chain C, making the same strong bidentate interaction from its benzamidine to the side chain carboxylic acid of Asp189 (Figure 36). The amidine interacts with the backbone carbonyl of Gly218 and the oxygen of water517. There is a hydrogen bond from the carboxylic acid of **17** to water603. The

amino pyridine hydrogen bonds to water583 and the nitrogen of the pyridine hydrogen bonds to Ile175 through water578. There is also a  $\pi$ - $\pi$  hydrophobic interaction between Trp215 and the aminopyridine ring.

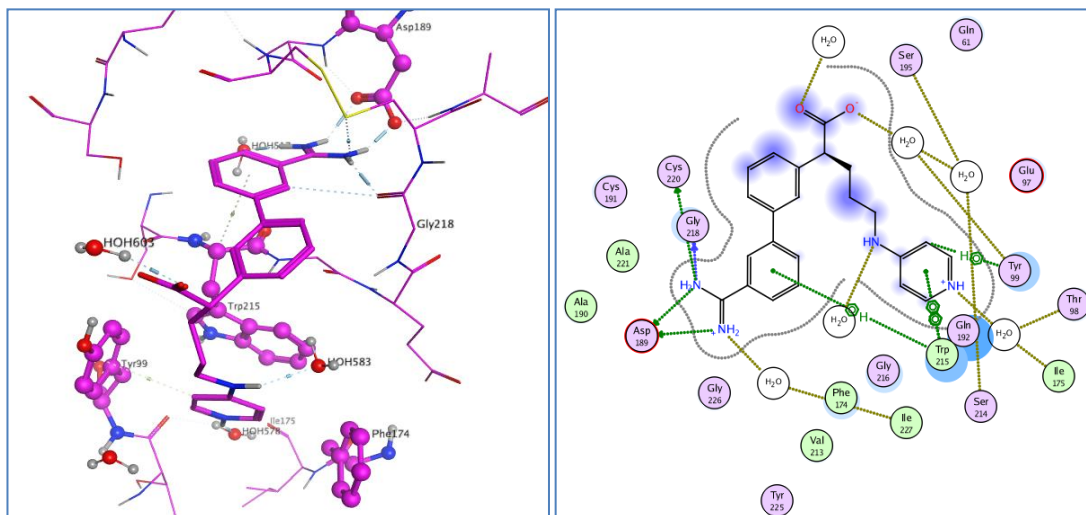
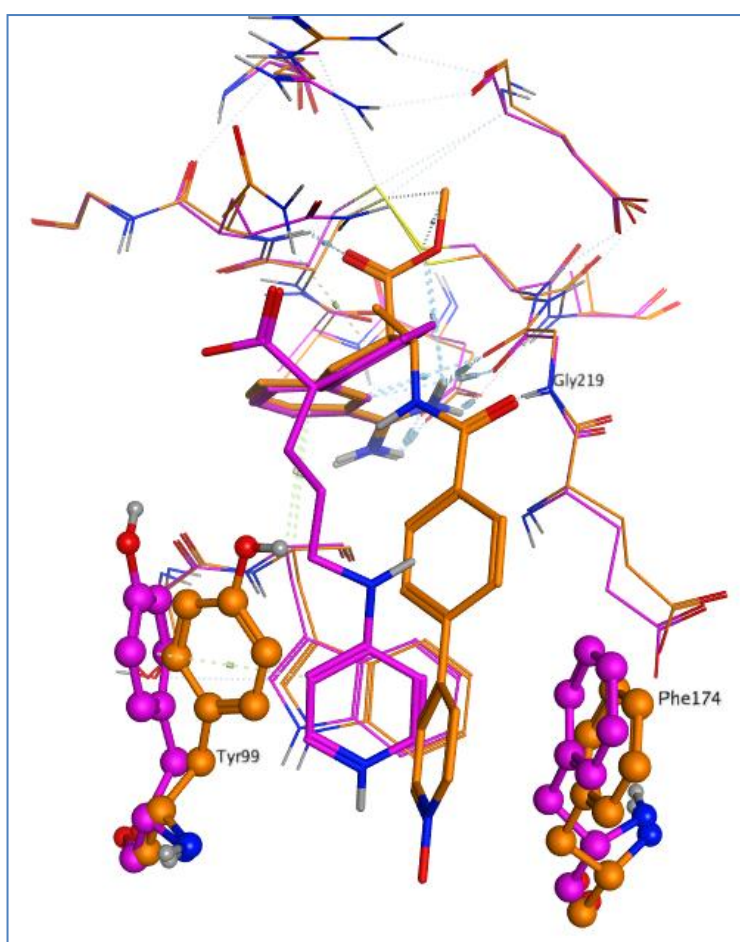


Figure 36: Binding mode of **17** in 1XKA and its ligand interaction diagram, blue smudges represent solvent accessible parts of the molecule

A comparison of structures 1KSN and 1XKA indicates that Tyr99 occupies a slightly different conformation and is rotated away from the binding site in 1XKA (*Figure 37*). Ligand **16** was less flexible than **17** and Tyr99 is rotated into the binding site to possibly allow a long edge to face interaction with the N-oxide-pyridine. For 1XKA, **17** is more flexible with a five atom linker between the biphenyl warhead and the terminal pyridine. In this case, Tyr99 rotated away from the binding site and is still able to maintain an edge-to-face interaction with the terminal pyridine.



*Figure 37:* Comparison of binding sites of 1KSN in orange and 1XKA in magenta

The two fXa protein crystal structures were prepared using the Protein Preparation Wizard available in Maestro, as described in Section 4.1. Water molecules were removed from the model systems. The ligands were prepared with LigPrep, also available within Maestro with the procedure is described in Section 4.2.

## 4. Methods

### 4.1. Preparation of the protein

Protein crystal structures need to be prepared before setting up docking experiments. Even if the resolution of the X-ray structure is high, it is often not sufficient to assign appropriate protonation states or the conformation of some residues, such as glutamine or asparagine. In those cases, the oxygen and the nitrogen atoms have the same connectivity, i.e., they are connected in the same way to neighbouring atoms. In addition, they differ by only one electron. This means that they often cannot be differentiated in the resolution range at which protein structures are usually solved.

Schrödinger's Protein Preparation wizard<sup>131</sup> is a stepwise tool that guides the user to prepare a protein structure in view of subsequently applying other modelling tools. The first stage is to pre-process the structure. This is where the hydrogen atoms are added, but also where the potential presence of metal atoms is highlighted, i.e., whether metal ions are present in the crystal structure and whether they need to be included in the preparation. These could be metals in part of the binding site or metal ions from the buffer used to crystallise the protein. Termini can be capped and if there are missing amino acids (either single residues or loops) they can be modelled using Prime,<sup>140</sup> which is a protein structure prediction program.

In the second step, the protonation states are enumerated using Epik, Schrödinger's pKa prediction tool,<sup>141</sup> and ionisations states are also generated. These need to be



checked before moving to the following stage, as they will have an impact on the subsequent step of the protein preparation. The protonation state of the ligand can affect the protonation and the conformation of binding site residues. Appropriate protonations and ionisations for the ligand can typically be chosen from a list of possible states for a specified pH range. It is important to choose the correct protonation state for the ligand to ensure that the subsequent steps of optimisation of the protein, notably hydrogen bond optimisation, can be performed accurately. The conformation of the ligand is not affected during this step.

The third step is the hydrogen-bond assignment. An exhaustive sampling of hydrogen bonds between residues is performed as well as sampling of orientations of water molecules crystallised in the protein. Some residues have the possibility to adopt different conformations. They can be flipped as the case is for glutamine and asparagines (*Figure 38*). The conformations of glutamine and asparagine are usually not determined from the electron density map of the crystal structure, as described above. However, their conformations can be deduced from the hydrogen bond network and their interaction with neighbouring residues or the ligand. This is also true for the hydrogen on the imidazole ring of histidine, the position of which may be deduced from the environment.

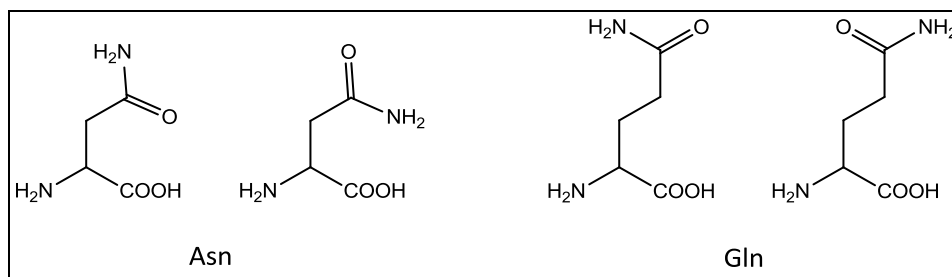


*Figure 38:* Depiction of residues that can be flipped, asparagine (Asn) and glutamine (Gln)

Flipped residues are visually checked on completion to make sure that the glutamine and asparagine near the binding sites are in the correct conformation, as defined by presenting the best hydrogen bonding arrangement.

The fourth and final stage involves a geometry optimisation by minimisation of the molecular mechanics energy, referred to hereafter as energy minimisation. This can be carried out on hydrogen atoms only, which was the case in this work, and the OPLS\_2005 force field was used for this purpose. The energy minimisation is performed on hydrogens only as they were missing from the crystal structures and it is important to optimise the hydrogen bond network between the amino acids in order to have a robust and reliable system to work from in the subsequent docking experiments.

#### 4.2. Preparation of ligands

LigPrep<sup>133</sup> is a Schrödinger tool which is used to convert two-dimensional (2D) ligand structures into three-dimensional (3D) ones. In addition, this program removes salts and can also generate tautomers, stereoisomers, and protonation states for a particular pH range. It can also include energy minimisation.

### 4.3. Predicting water locations

The predictions of water locations was performed for the LTA4H model system.

#### 4.3.1. Running SuperStar

SuperStar is accessed through CCDC's Hermes interface.<sup>142</sup> In order to make the SuperStar computation quicker, the amino acids for LTA4H within 10 Å of ligand **7** were selected and saved in a mol2 file. This also included the zinc. However, the ligand and the water molecules were excluded.

The mol2 file was then uploaded into Hermes and in the SuperStar window, Gln136 was chosen to be the centre of the binding site. Propensity maps were then computed first on CSD data and then on PDB data using the water oxygen probe. The option to let the O-H, N-H and S-H bonds of amino acids, for example tyrosine, freely rotate was turned off and on to assess whether it would make a difference to the resulting map.

A propensity map was also generated for ligand **7** still using the water oxygen probe but from CSD data only, as PDB scatterplots are not available for ligands.

#### 4.3.2. Running GRID

Within the program GRID, GRUB is the table of parameters that assesses the energy functions, such as the Lennard-Jones function, and GRIN attaches the parameters for each atom to the input protein file, typically a PDB file. The protein was prepared as described previously and the ligand as well as all water molecules were

removed. GRID was run from the GREATER interface, where the GRIN programme runs instantly in the background upon loading of template molecule file. This outputs two files, one of which is the .kout file containing the properties of the template molecule and is used as input to GRID. In order to set up a GRID run properly, it is necessary to check the default parameters and modify them as required. For example, in the case of LTA4H, the number of heteroatoms was changed to one as the LTA4H protein binding site includes a zinc atom. The grid spacing was chosen to be 0.5 Å and the water probe was selected. From the resulting output, it is possible to visualise the energy hot-spots within GREATER or any other software of choice, upon conversion to an appropriate file format, e.g. a .grid file for viewing in MOE.<sup>143</sup>

## 5. Rigid docking in LTA4H

### 5.1. LTA4H protein and ligand preparation

Proprietary crystal structure 1LOZX which has been solved by the GSK protein crystallography group was used as a starting point. Because it has a resolution of 1.97 Å, the positions of the hydrogen atoms could not be determined. Therefore, it was put through the Schrödinger Protein Preparation protocol, as described in Section 4.1.

Missing residues were modelled. The ionisation state of the zinc atom was verified to be 2+. The ligand protonation state was chosen to be protonated at the amine functionality and deprotonated at the carboxylic acid functionality (*Figure 39*).

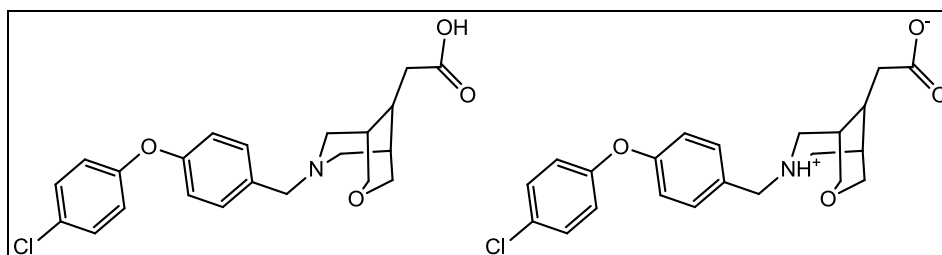


*Figure 39:* Ligand **7** and its appropriate protonation state

Special attention was taken for Gln136 (*Figure 40*), which is known to interact with lead series compounds through a hydrogen-bond acceptor interaction from its carbonyl group to the protonated amine of the ligand.

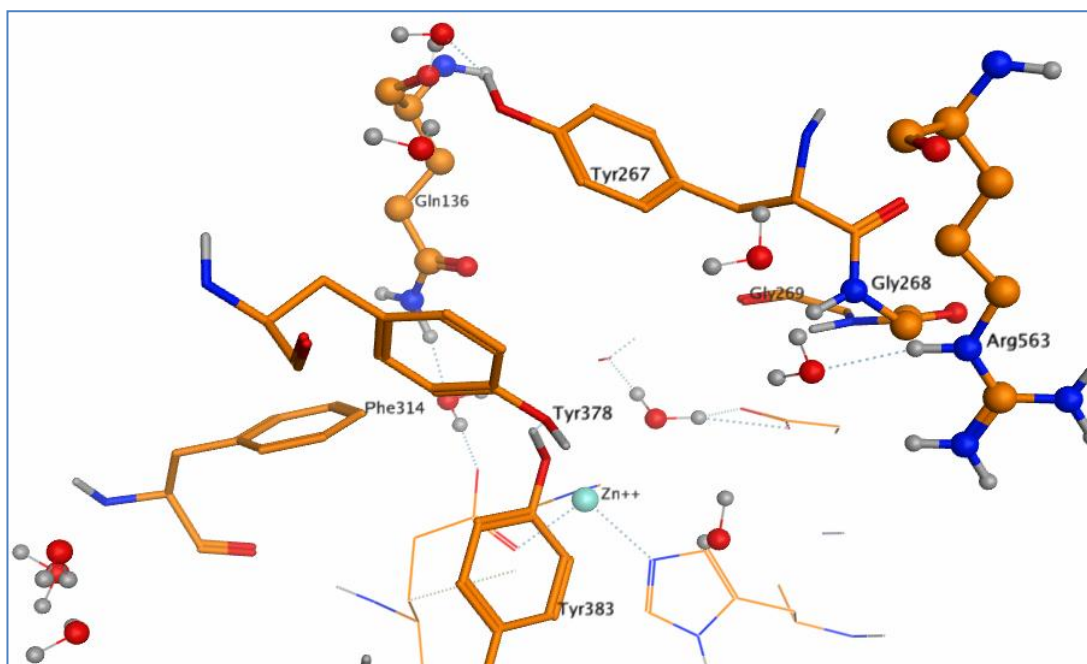


*Figure 40:* LTA4H binding site extracted from 1LOZX with key residues highlighted (Gln136, Gly268, Arg563)

The optimised water network was also verified: the fourth contact to the zinc atom was with a water molecule that was located close to another water. After inspection of the electron density map for 1LOZX, it was noted that there was no density for a water positioned directly above the zinc. Therefore, this water was removed from the model system, thus creating a potential interaction site for the ligand. It is hypothesised that this water is displaceable and this is supported by the fact that there are crystal structures of ligands which interact directly with the zinc atom at this locus. As will be described in Section 5.4, its absence does not affect the outcome of the docking experiments.

Even though in this instance, a three-dimensional structure of ligand **7** is already available from the crystal structure 1LOZX, it is not ready to be used for docking experiments as hydrogen atoms are missing. It is expected to present a protonated amine functionality and deprotonated carboxylic acid and this is one of the solutions that LigPrep generated (*Figure 41*). It has to be noted, in the case of 1LOZX, the unusual conformation of the bicyclo[3.3.1]nonane moiety of the ligand, referred to as the [3.3.1] system hereafter, which is typically found in a chair-chair conformation. In this instance, it adopts a chair-boat conformation and this is conserved in the conformation with the correct protonation assignments from LigPrep. However, LigPrep is able to flip ring corners and the chair-chair conformation was also obtained. As will be described in Sections 5.3 and 5.4, the starting conformation is not a constraining factor. A substructure search of the Cambridge Structural Database<sup>109</sup> (CSD) showed that [3.3.1] systems, in majority, sit in a chair-chair conformation which is confirmed by crystal structures solved in-house.

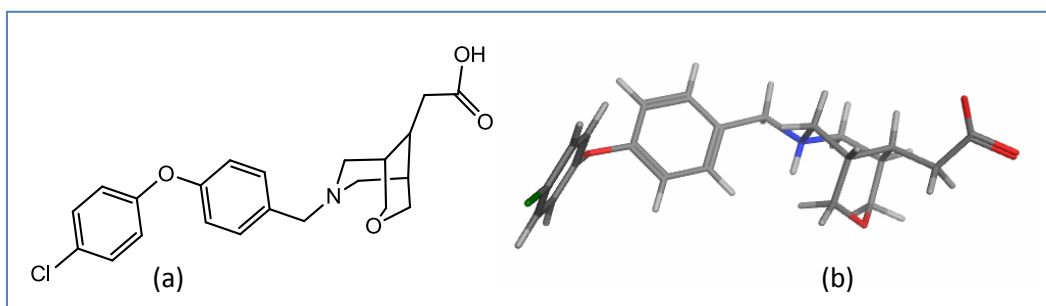


*Figure 41:* a) A two-dimensional depiction of **7** in a chair-chair conformation and b) a three-dimensional structure of **7** in a chair-boat conformation, resulting from a LigPrep run. Oxygen atoms are shown in red, nitrogens in blue and the chlorine atom in green.

In the interest of clarity, the 2D depictions of [3.3.1] systems will represent it in a chair-chair conformation.

## 5.2. Conformations of the [3.3.1] system

The [3.3.1] ring can theoretically adopt four conformations: chair-chair, chair-boat, boat-chair and boat-boat. Small molecule crystal structures published to the CSD and containing a [3.3.1] ring were investigated to determine the most likely arrangement. It was found that the [3.3.1] systems were in a chair-chair conformation in a majority of crystal structures. This observation was also corroborated by protein-ligand crystal structures solved at GSK. Indeed, thirty crystal structures containing a [3.3.1] system have been solved in-house and of those twenty-seven were in a chair-chair conformation, two in a chair-boat and one in a boat-chair. None of the crystal structures were in a boat-boat conformation, which is expected to be the highest energy one of the four arrangements.

It was also necessary to determine if the modelling approach employed could reproduce this experimentally observed preference. Therefore, the four conformers were built in Maestro,<sup>140</sup> which is Schrödinger's interface to all their tools (*Figure 42*). All four conformers were energy minimised using the Minimization tool within Macromodel.<sup>144</sup> OPLS\_2005 was the force field of choice and the solvent was water. The conformer with the lowest energy is in the chair-chair arrangement, whilst the highest energy conformer is the boat-boat conformer (*Table 5*). The chair-boat and the boat-chair conformations are ranked 3 and 2, respectively.



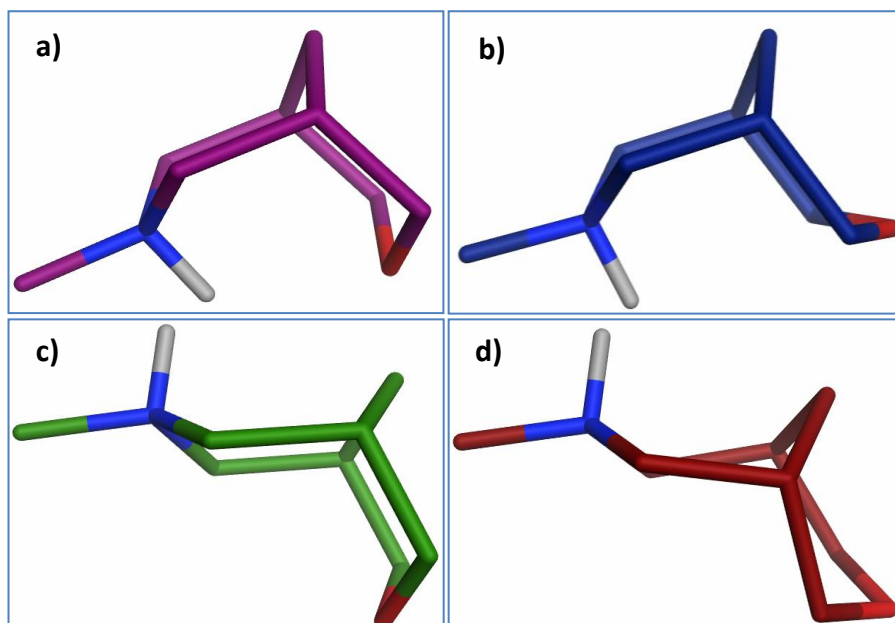


Figure 42: The four conformations of the [3.3.1] ring: a) chair-chair, b) chair-boat, c) boat-chair, d) boat-boat

Conformation	Energy (kcal/mol)	Relative Energy (kcal/mol)	Rank
chair-chair	-12.15	0.00	1
chair-boat	-1.55	10.59	3
boat-chair	-4.27	7.88	2
boat-boat	4.88	17.02	4

Table 5: Summary of energies and relative energies for all four conformations; the lowest energy conformer is ranked 1

The experiment was repeated but without any solvent during the geometry optimisation step, in order to check whether the solvent had an impact on the

results. It was expected that the resulting energies would be different but the overall ranking of the conformers should be retained; and this was observed (*Table 6*).

<b>Conformation</b>	<b>Energy (kcal/mol)</b>	<b>Relative Energy (kcal/mol)</b>	<b>Rank</b>
chair-chair	42.09	0.00	1
chair-boat	59.28	17.19	3
boat-chair	53.45	11.36	2
boat-boat	66.93	24.84	4

*Table 6:* Resulting energies for each conformer with no solvent during the energy minimisation stage

These results correlated with the experimental observation from crystal structures that the chair-chair conformation was the preferred conformation for this system. The chair-boat conformation seen in two proprietary protein-ligand crystal structures is not favoured energetically and it was anticipated that there must be an energy penalty for this conformation to be the bioactive one. In crystal structure 1LOZX, the oxygen atom of the chair-boat [3.3.1] system pointed toward the zinc atom, which may explain the observation of the chair-boat conformation in crystal structure 1LOZX.

### 5.3. Comparing rigid receptor docking programs

There is not a single docking programme together with a specific scoring function that is recommended for all possible systems. It has been advised in the literature to test a set of programmes and scoring functions to find the best one for the studied system.<sup>71, 145</sup> In this work, the focus was on reproducing the correct binding mode rather than estimating the binding affinity. However, both force field based and empirical scoring functions have been evaluated with the aim to determine which one was the most suitable for the system under consideration. In addition to the ca. 40 structures released in the public domain, a number of crystal structures of LTA4H in complex with a selection of proprietary ligands have also been solved at GSK. Very similar compounds can sometimes show a dissimilar activity profile, as is the case for isomers in the lead series studied (*Figure 43* for compound structures). The hypothesis is that these observations could be explained by docking studies.

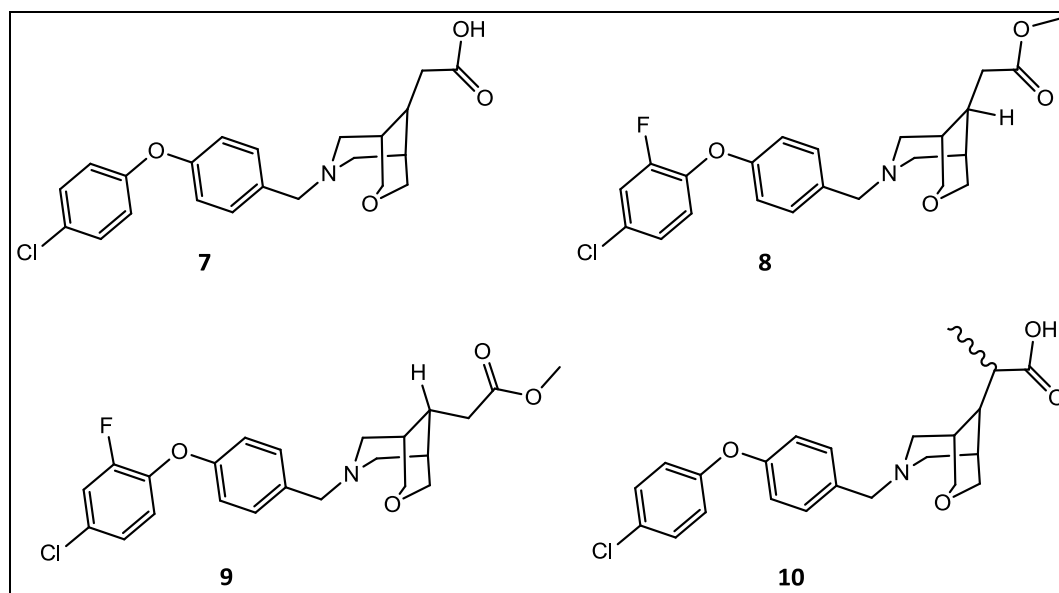


*Figure 43:* Summary of proprietary LTA4H ligands included in this study

Once the protein and the ligand were prepared, GOLD and Glide were used to set up the docking experiments. The first task was to try to reproduce the crystal pose of **7** as crystallised in 1LOZX. Indeed, this is an important step to perform in order to assess the performance of the docking program under consideration. If it is unable to reproduce a pose close to the one observed in the crystal structure, then it is not suitable to carry out docking experiments for the system of interest.

Once a suitable docking protocol was found, it was used to dock analogue compounds of **7** as well as known LTA4H ligands from the public domain.

#### 5.3.1. Docking of **7** using GOLD

Docking and scoring of **7** using GoldScore gave good results with all resulting five docking poses being very close to the crystal pose (*Table 7*). Pose1 was scored slightly lower than the other four due to a close contact with Gln136.

Pose number	GoldScore
pose2	98.48
pose3	98.17
pose4	97.41
pose5	97.36
pose1	91.14

*Table 7: Summary of GoldScores for **7***

The closest docked pose, pose2, presents an additional hydrogen bond from its carboxylic acid to the backbone nitrogen of Gly268, as shown in *Figure 44a*. The only major difference with the crystal pose is the conformation of the [3.3.1] system which is in a chair-chair conformation in all of the docking poses identified.

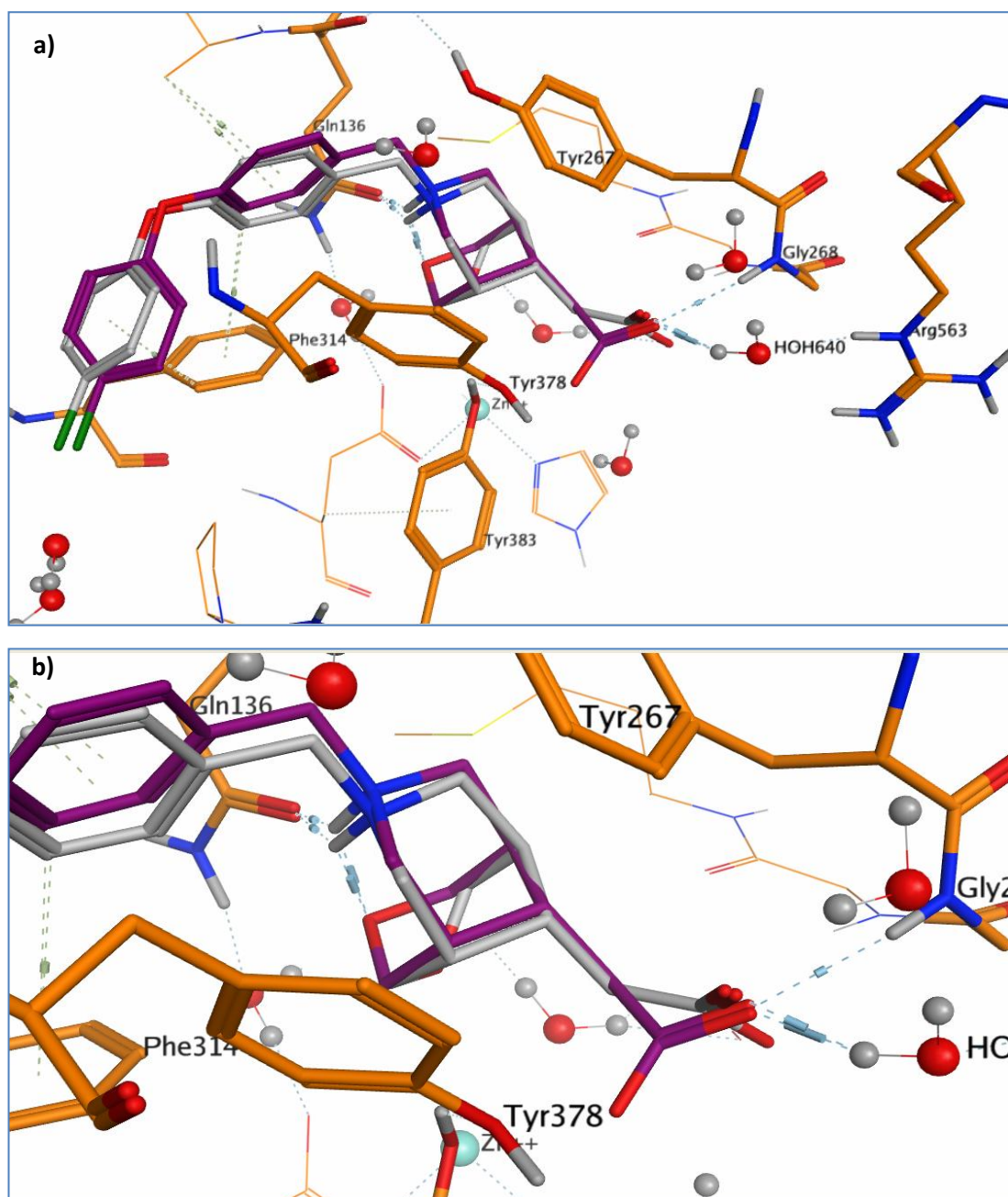


Figure 44: a) Closest docking pose of **7** (pose2) in purple and its crystal pose in light grey; b) a close-up on the conformation of the [3.3.1] moiety and the hydrogen bonds that it makes with the binding site. Hydrogen bonds are highlighted by light blue dotted lines, whilst favourable contacts are highlighted in light green dotted lines.

The same process using ChemScore gave similar docking poses to the ones observed when scoring with GoldScore (*Figure 45a*). All five docking poses are very close to the crystal pose of **7**.

Pose number	ChemScore
pose5	50.75
pose1	49.83
pose4	49.7
pose3	48.77
pose2	47.51

*Table 8:* Summary of ChemScores for **7**

The top scoring docking pose (pose5, *Figure 45b*) is engaged in the same interaction with the binding site as observed in the previous experiment with GoldScore.

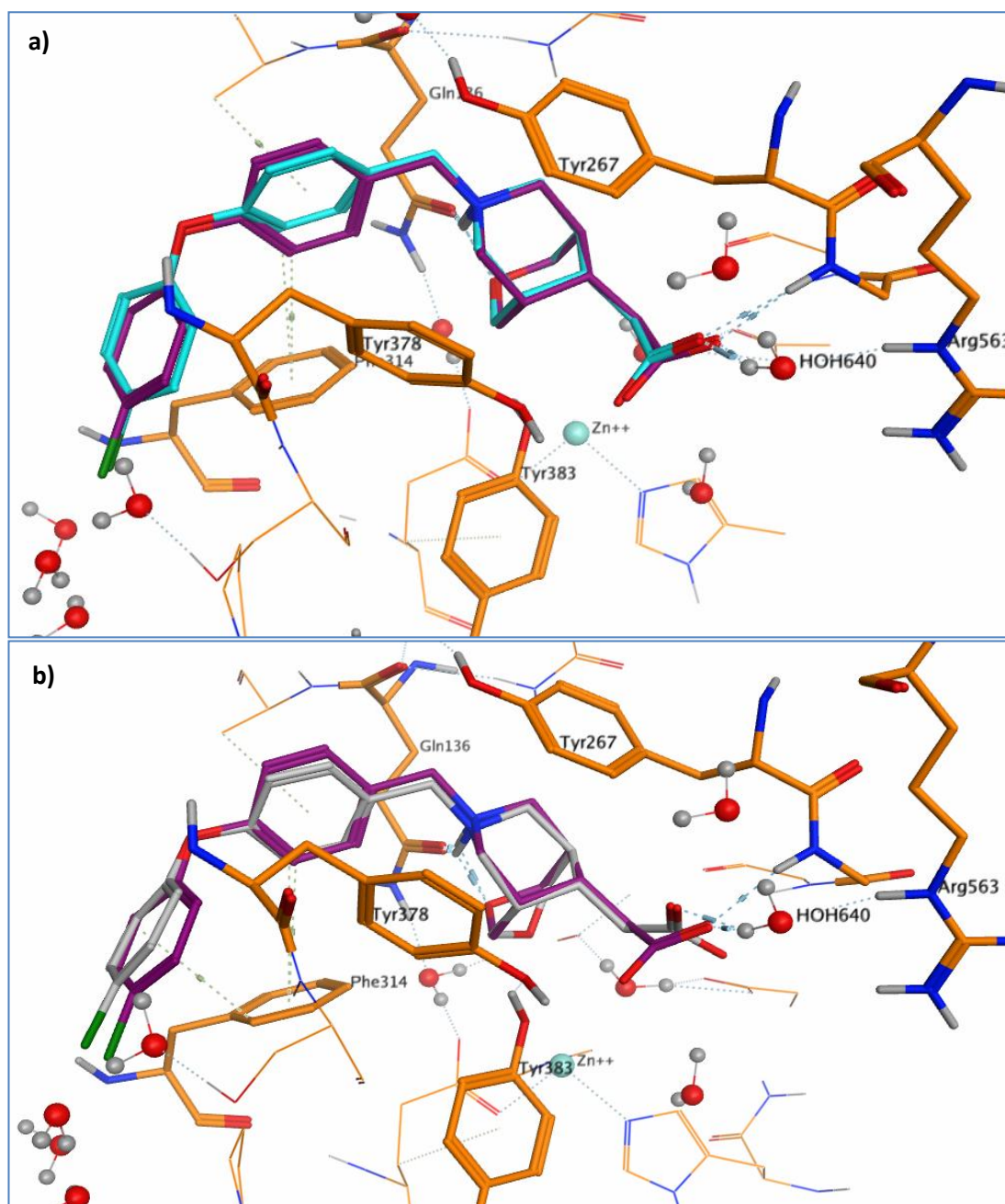


*Figure 45:* a) Comparison of best scoring pose with ChemScore in purple and with GoldScore in turquoise; b) best scoring pose for **7** using ChemScore in purple and crystal pose in light grey

It was not possible to choose between GoldScore and ChemScore based on the above results. However, GoldScore was used in previous experiments (not reported



here) and as there are no obvious advantages in using ChemScore, it was decided to continue with GoldScore.

### 5.3.2. Docking of **7** using Glide

Docking with Glide was used next to assess whether it could present any advantages over GOLD. Although the docking poses obtained in GOLD are of good quality, running future, related docking studies in Glide could be beneficial due to an easier setup and shorter running time. Glide would be the program of choice for the docking studies, in this context, if the results can match the quality of the GOLD output.

Before setting up a docking experiment, a grid of the protein was generated. Glide was run in SP mode, keeping all parameters as default in a first instance to get an initial indication of its performance. All five poses produced non-planar aromatic rings (*Figure 46*). This was thought to be due to the final energy minimisation step of the docking protocol. Therefore, the docking experiment was run again without this step; however, the program failed to output any docking poses under these conditions.

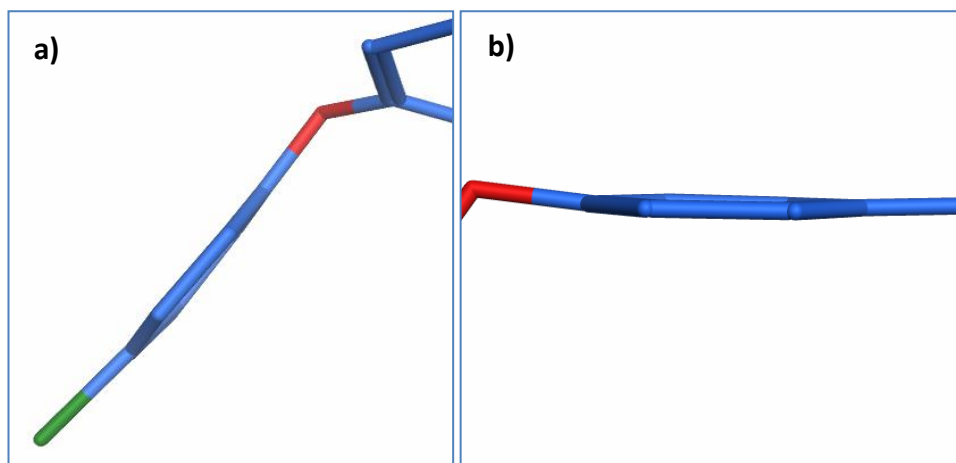


Figure 46: Focus on aromatic rings of **7**, a) terminal phenyl ring and b) middle phenyl ring

As reported by Friesner et al,<sup>8, 146</sup> some issues can be encountered with ligand docking into a tight and rigid binding site due to the van der Waals radii of the non-polar protein atoms. They recommend decreasing the van der Waals radii of the protein and possibly the ligand to allow more space in the binding site and advise using a 0.9/0.8 ratio for the protein/ligand atoms as opposed to the default 1.0/0.8. Therefore, this was applied to the 1LOZX system and the receptor grid was computed again prior to ligand docking. Again, the program output five docking poses but with bent phenyl rings, when keeping the post-docking energy minimisation step. The visual analysis of the docking poses showed that the chlorine atom protruded out of the binding pocket as did the carboxylic acid. The lowest scoring docking pose was placed in reversed mode, i.e., the [3.3.1] system was found in the lipophilic pocket where the phenoxy moiety usually binds, and vice versa.

When repeating the experiment without the post-docking energy minimisation, only one docking pose was output. Upon visual inspection, the planarity of the phenyl rings was observed and it resulted that it was the same as the lowest scoring pose seen in the previous run. This meant that the other four docking poses obtained with the minimised system were possibly rejected due to steric clashes.

Glide was unable to output appropriate docking poses for **7**. It would be possible to derive a tailored scoring function for this specific system. These are scoring functions which are derived from a set of known binders to a specific protein system to be applied to this system with new ligands. Rognan et al.<sup>147</sup> have used this method to develop a scoring function in order to predict the free energy of binding of new ligands to Class I major histocompatibility proteins. They derived two scoring functions, one based on crystallographic data and another one on homology models. They started off by using the default ChemScore, which provided a good starting point and modified the coefficients to fit their data. This could have been attempted in the current work, but it relies on accurate biological data and a larger data set in terms of number of molecules for the derivation of such a function. In addition, the function is only applicable to the specific protein conformation and a specific chemical series, if the ligands chosen are all congeneric.

GOLD was chosen as the docking programme of choice for this system. Within GOLD, the binding site can be defined by selecting the ligand. The amino acids considered were within 6 Å of the location of the ligand. During docking, the ligand was allowed complete flexibility whereas the amino acid side chains of the binding site were fixed. In this study, the number of iterations for the genetic algorithm was set to 10 and then 100 to ascertain whether it had an impact on the quality of the docking poses. Similarly, GoldScore and ChemScore were used and compared, to gauge the robustness of the predictions as a function of the scoring method.

#### 5.4. Comparison of simulation length

Two analogue compounds to **7** were docked into 1LOZX. They differ in the bridge substitution, with one of the isomers (**8**) being *anti* and the other one (**9**) *syn*, with respect to the oxygen atom of the [3.3.1] moiety (Figure 47). They are the separated methyl esters of **7**, with an extra fluorine atom on the terminal phenyl ring.

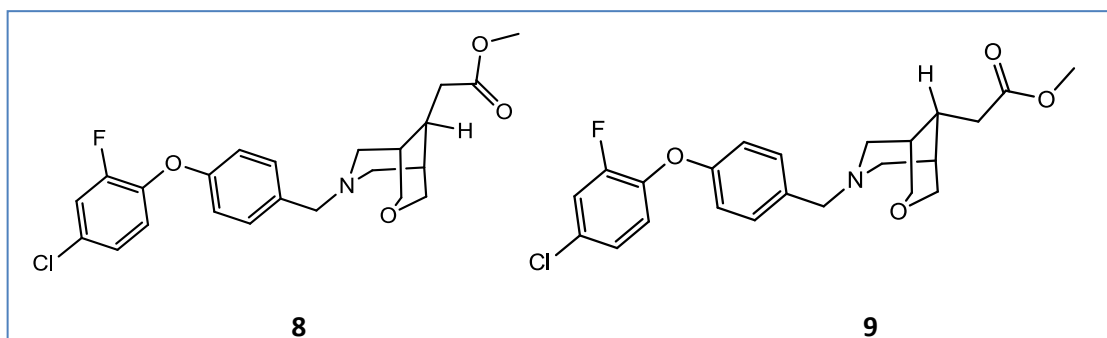


Figure 47: Anti isomer **8**: pIC50 = 7.6 and syn isomer **9**: pIC50 = 7.2

Molecule **8** showed a pIC50 of 7.6 in the aminopeptidase primary assay, whereas **9** had a pIC50 of 7.2 in the primary assay. The structural difference between these

two isomers could be considered minimal, although they exhibit a 0.5 log unit difference in potency in the primary assay.

#### 5.4.1. Running GOLD for 10 GA iterations

GOLD was first run for 10 iterations of the genetic algorithm with the possibility for early termination if the top five poses were within 1.5 Å RMSD (root-mean square deviation). The results are summarised in the following two tables.

Pose number	GoldScore
pose4	79.98
pose5	75.48
pose1	74.14
pose7	74.12
pose2	73.09
pose3	70.54
pose6	70.01

*Table 9:* Summary of docking poses for **8** and their GoldScores after 10 iterations

The seven docking poses of **8** presented more spread in their GoldScores with a difference of 9 (*Table 9*), between the highest and the lowest scoring poses, compared to the GoldScores of **7** with a difference of 7. The best scoring pose (pose4, *Figure 48a*) maintained all interactions that were observed for **7**. However,

all poses show some steric clashes with the binding site typically with Phe314 and Tyr267; an example is shown in *Figure 48b*.

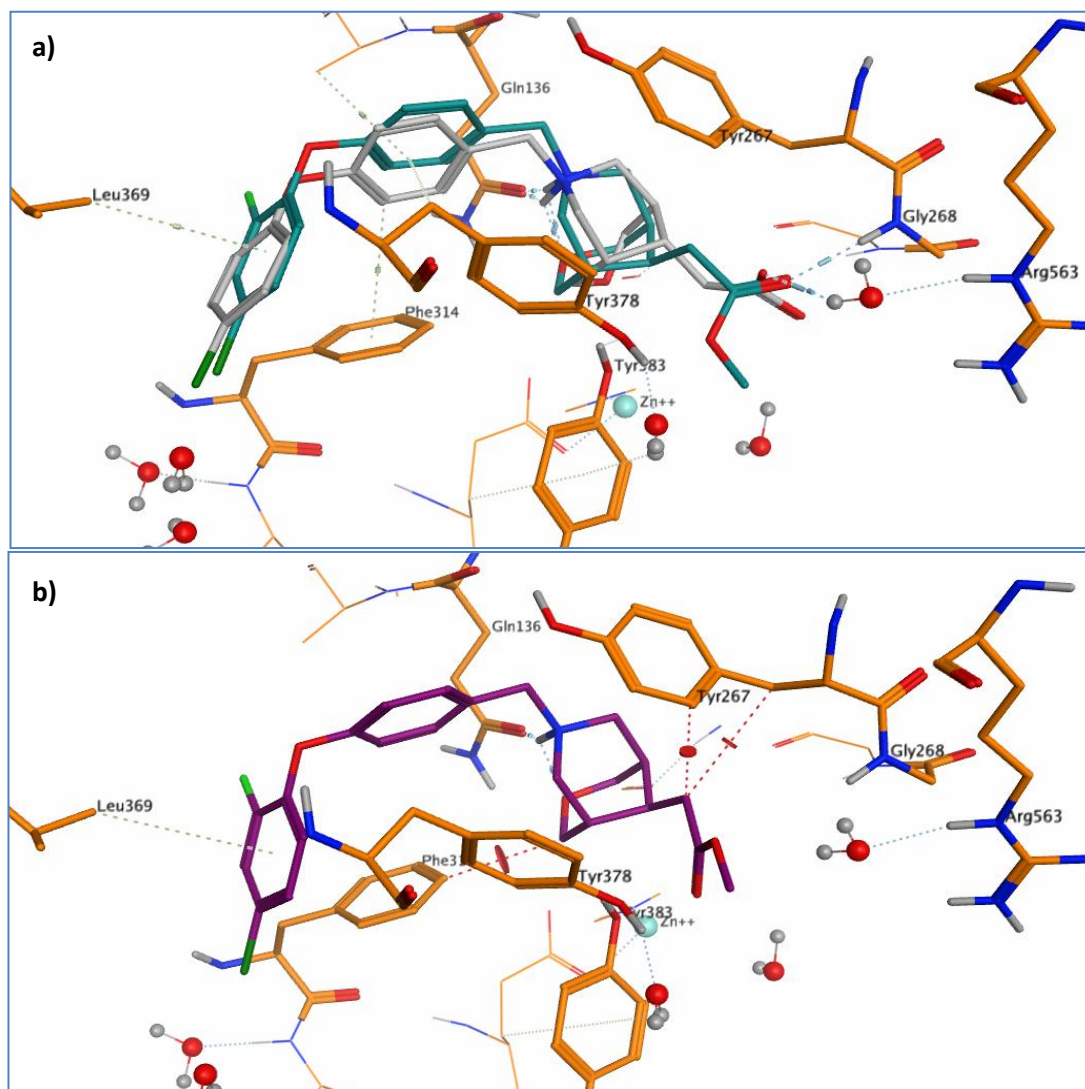


*Figure 48:* a) Best scoring docking pose (pose4) for **8** in turquoise and crystal pose of **7** in light grey; b) An example pose (pose3) of **8** which causes some steric clashes with Phe314 and Tyr267; clashes are represented by red disks on dotted lines.

This observation can be confirmed by the *Complex\_Energy* term (Equation 12) which accounts for attractive van der Waals interactions between the protein and

the ligand. The external van der Waals scores for **8** are lower than the ones for **9**, indicating that there are less favourable interactions between the protein and ligand **8** (*Table 10*).

Vdw scores for <b>8</b>		Vdw scores for <b>9</b>	
pose4	58.52	pose6	62.08
pose5	58.31	pose3	63.01
pose1	53.86	pose2	58.4
pose7	56.74	pose1	61.35
pose2	57.75	pose5	61.16
pose3	54.93	pose4	64.42
pose6	55.11		

*Table 10:* Summary of van der Waals scores between the ligand and the protein

Six docking poses were obtained for **9** and they presented a difference of 8 in their GoldScores (*Table 11*). In the best scoring pose (pose6, *Figure 49*) the ligand interacts with Glu136 through its protonated tertiary amine.

Pose number	GoldScore
pose6	83.98
pose3	82.46
pose2	82.12
pose1	80.99
pose5	79.22
pose4	75.42

*Table 11:* Summary of docking poses for **9** and their GoldScores after 10 iterations

This tertiary amine is also engaged in an intra-molecular hydrogen bond with the terminal oxygen of the [3.3.1] system. This was not observed in the crystal structure of **7**, due to its unusual conformation as a chair-boat. The interaction of the carbonyl of the ester with Arg563 through a water-mediated interaction, as seen in the crystal structure, is not accessible in this pose, even though it is present in three of the other poses. Additional close interactions, with for example Leu369 and Phe314, were also found with the other poses.



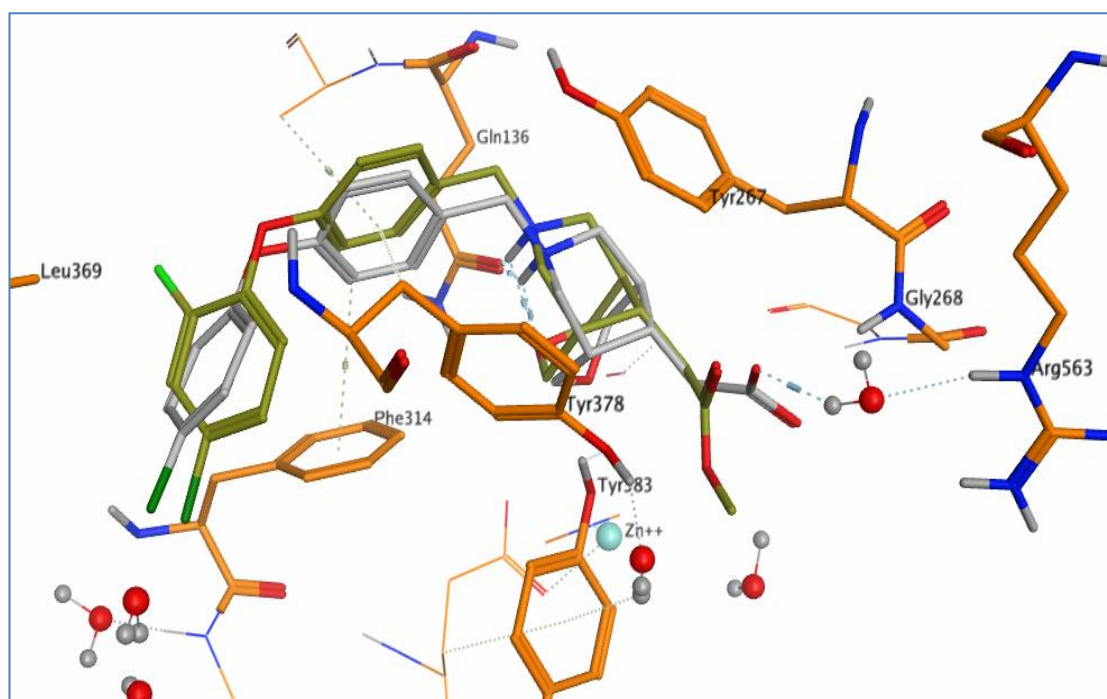


Figure 49: Best scoring docking pose (pose6) for **9** in yellow and crystal pose of **7** in light grey

A statistical analysis was carried out using a *t*-test to assess whether the difference in GoldScores between the two isomers was significant. A *t*-test is a statistical procedure which can be used to compare mean values for a population, as described in Section 2.4.2. It starts from a null hypothesis that the difference in the means is the same and produces a probability value (*p*-value) which is compared to the threshold of statistical significance – here 0.05. The use of a statistical technique to compare docking scores is considered prudent given the recognised inability of scoring functions to assign the best score to the best docked conformation, as described in Section 2.2.3. Therefore, it is necessary to take into account a number of top scoring poses as recommended by Cheng et al.<sup>34</sup>

The null hypothesis, here, was that there is no difference in means between the two sets of GoldScores. The test statistics are summarised in *Table 12*. The paired *t*-test returned a *p*-value of 0.0002, which is below the threshold for statistical significance. This means that the null hypothesis is rejected, and therefore that the GoldScores for **8** and **9** are statistically different. This means that we are able to derive hypotheses from the GoldScores, together with the actual conformations of the poses, on the compounds biological activities.

	GoldScore for <b>8</b>	GoldScore for <b>9</b>
Mean	74.6	80.7
Variance	9.8	9.2
Observations	6	6

*Table 12: Statistics summary for 10 iterations*

#### 5.4.2. Running GOLD for 100 GA iterations

GOLD was then run for 100 iterations of the genetic algorithm, also with the possibility for early termination if the top five poses were within 1.5 Å of each other.

Docking of **8** returned eight poses after 100 iterations of the algorithm (*Table 13*).

Pose number	GoldScore
pose8	78.84
pose7	77.59
pose1	76.28
pose6	73.33
pose5	71.05
pose3	69.68
pose2	69.57
pose4	67.50

*Table 13:* Summary of docking poses for **8** and their GoldScores after 100 iterations.

Here again, as noted in the 10-iteration run, the GoldScores are spread over a larger range (11.34) and are slightly lower than the ones obtained for **9**. All poses clash with the binding site and particularly with Phe314 and Tyr267. The best scoring pose (pose8) is shown in *Figure 50*.

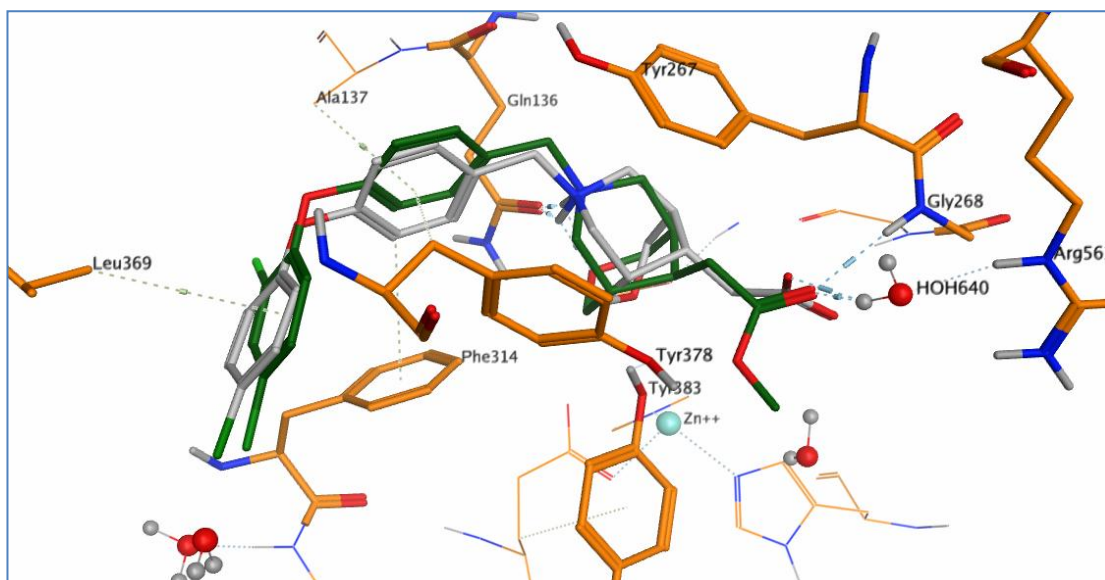


Figure 50: Best scoring pose (pose8) of **8**, after 100 iterations, in green and crystal structure of **7** in light grey.

Pose number	GoldScore
pose6	82.84
pose2	82.09
pose1	80.59
pose4	80.35
pose5	78.05
pose3	75.75

Table 14: Summary of docking poses for **9** and their GoldScores after 100 iterations

Six poses were obtained for **9**, after a docking run of 100 iterations, and they exhibited a difference of 7.09 in their GoldScores (Table 14). In the best scoring pose (pose6, Figure 51), the ligand interacts similarly with the binding site as observed in the 10-iteration run described previously.

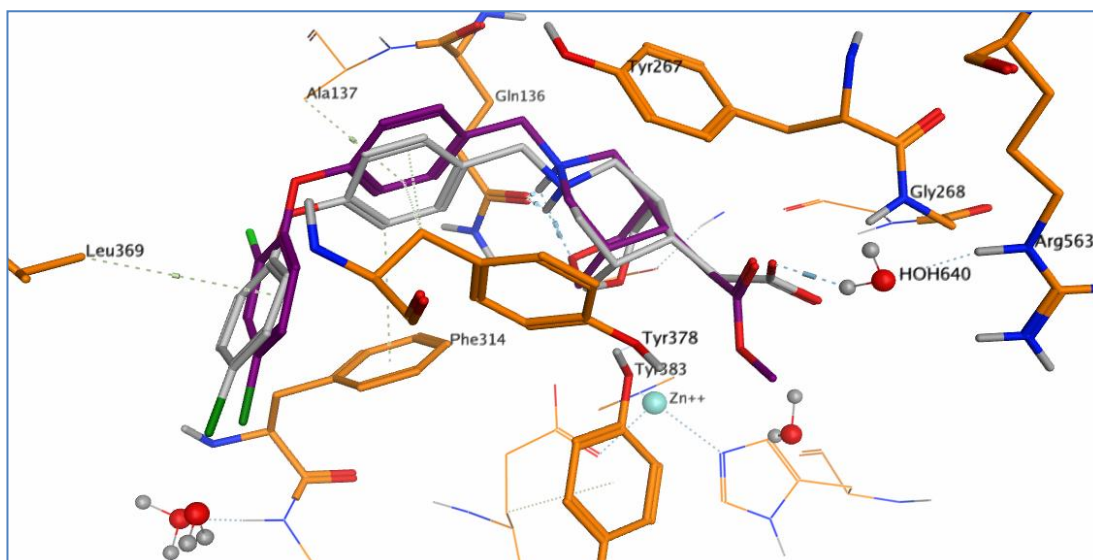


Figure 51: Best scoring pose (pose6) for **9** in purple after 100 iterations. Crystal structure of **7** is in light grey.

A paired *t*-test was also run for this set of scores to verify the hypothesis that the GoldScores for **8** are statistically different to the ones of **9** (Table 15).

	GoldScore for <b>8</b>	GoldScore for <b>9</b>
Mean	74.5	79.9
Variance	13.6	6.9
Observations	6	6

Table 15: Statistics summary for 100 iterations

The paired *t*-test returned a *p*-value of 0.0002, which is below the threshold for statistical significance of 0.05. This means that the null hypothesis is rejected, and therefore that the GoldScores for **8** and **9** are statistically different.

#### 5.4.3. Comparison of the results based on the number of iterations

After visual inspection of the docking poses and sets of GoldScores, it is clear that the increase in the number of iterations of the genetic algorithm does not affect the results. However, to perform a more robust assessment of the two sets of scores, two paired t-tests were carried out on GoldScores between GOLD runs for the same molecules as opposed to between molecules for the same runs.

Pose rank	GoldScore after 10 iterations	GoldScore after 100 iterations
1	79.98	78.84
2	75.48	77.59
3	74.14	76.28
4	74.12	73.33
5	73.09	71.05
6	70.54	69.68
7	70.01	69.57

*Table 16:* Summary of GoldScores for **8** after 10 and 100 iterations

A paired *t*-test was performed on the data in *Table 16* to assess whether the number of iterations had an impact on the GoldScores. If the null hypothesis stating that the difference between the means of the two sets of GoldScores is zero is accepted, then the number of iterations does not impact on the results of the docking experiment. The output of the paired *t*-test is presented in *Table 17*.

	GoldScore after 10 iterations	GoldScore after 100 iterations
Mean	73.91	73.76
Variance	11.11	14.76
Observations	7	7

*Table 17: Summary of paired t-test statistics for 8*

The paired *t*-test returned a *p*-value of 0.82, which is greater than the threshold for statistical significance of 0.05. This means that the null hypothesis is accepted, and therefore that the GoldScores for **8** after 10 or 100 iterations are statistically identical.

The same assessment was carried out for compound **9**. A paired *t*-test was performed on the data in *Table 18* to assess whether the number of iterations had an impact on the GoldScores. The output of the paired *t*-test is presented in *Table 19*.

Pose rank	GoldScore after 10 iterations	GoldScore after 100 iterations
1	83.98	82.84
2	82.46	82.09
3	82.12	80.59
4	80.99	80.35
5	79.22	78.05
6	75.42	75.75

*Table 18: Summary of GoldScores for 9 after 10 and 100 iterations*

The paired  $t$ -test returned a  $p$ -value of 0.041, which is below the threshold for statistical significance of 0.05. Even if the  $p$ -value is very close to the threshold for statistical significance, it means that the null hypothesis is rejected, but with less confidence, and therefore that the GoldScores for **9** after 10 or 100 iterations are statistically different. The threshold of statistical significance of 0.05 chosen throughout this study is the most used and is considered an acceptable level of risk. The value of 0.05 means that one time out of twenty the null hypothesis is rejected when it should have been accepted. Twenty tests which are required for this statement to be true were not performed within this study. One can argue that, in this instance, either we are in the situation where the null hypothesis should have been accepted or the difference between the GoldScores is real.

	GoldScore after 10 iterations	GoldScore after 100 iterations
Mean	80.70	79.95
Variance	9.21	6.95
Observations	6	6

*Table 19: Summary of paired t-test statistics for 9*

Given the high confidence in the  $t$ -test statistics for **8** and the low confidence for **9**, it was decided to continue the subsequent docking experiments with ten iterations of the genetic algorithm.



### 5.5. Conformational search in rigid receptor docking

In the set-up of the GOLD docking experiments, the option allowing the flipping of a saturated ring (e.g., in the case of a six-membered ring, flip from chair to boat) was switched on. In order to confirm that GOLD is able to flip the conformation of the [3.3.1] system, the input 3D structure and all the output docking poses were inspected. This is summarised in *Table 20*.

Compound	Input structure	Number of docking poses output	Docking poses	
			chair-chair	chair-boat
7	chair-chair	5	5	0
8 (10 iter)	chair-chair	7	7	0
8 (100 iter)	chair-chair	8	8	0
9 (10 iter)	chair-chair	6	4	2
9 (100 iter)	chair-chair	6	6	0
10a	chair-boat	10	9	1
10b	chair-chair	5	5	0
10c	chair-chair	5	5	0
10d	chair-boat	5	5	0

*Table 20:* Summary of the [3.3.1] ring conformation in the input and output structures

Even though, in the majority of cases, the conformation of the [3.3.1] ring was the same in the input and the output structures, there are some examples where the [3.3.1] ring is flipped. For compound **9** with 10 iterations of the genetic algorithm,

the input structure was in a chair-chair conformation and four docking poses were also in a chair-chair conformation whilst two docking poses were in a chair-boat conformation. Similarly, for compound **10a**, the starting conformation was chair-boat and nine docking poses were in the flipped chair-chair conformation and one docking poses still in the chair-boat conformation.

These observations show that while GOLD is able to flip the rings of the [3.3.1] system, the energetically favoured chair-chair conformation is predominantly favoured in the docked structure.

As can be seen from *Table 20*, no boat-chair or boat-boat conformations were identified in the output docking poses. This observation led to the question of whether this was due to the high energies of these two conformations (see *Table 5* in Section 5.3) or whether these two conformers cannot physically fit in the binding site. To answer this question, an additional docking experiment was run on compound **7**. The two runs started from two different conformations of compound **7** (in boat-chair and in boat-boat).

#### 5.5.1. Docking of **7** starting from a boat-chair conformation

The 3D conformation of **7** generated for an earlier experiment was modified to produce a boat-chair conformation of the [3.3.1] ring. It was then optimised through energy minimisation. The same docking protocol was used. Four docking poses out of the five output were in a chair-chair conformation, whilst one was in a chair-boat conformation (*Figure 52*). Therefore, GOLD is clearly able to access the boat-chair conformation region of the potential energy surface for **7**. As such, we

conclude that the lack of boat-chair isomers in the docking results is due to the higher energy of these isomers relative to the chair-chair and chair-boat isomers.

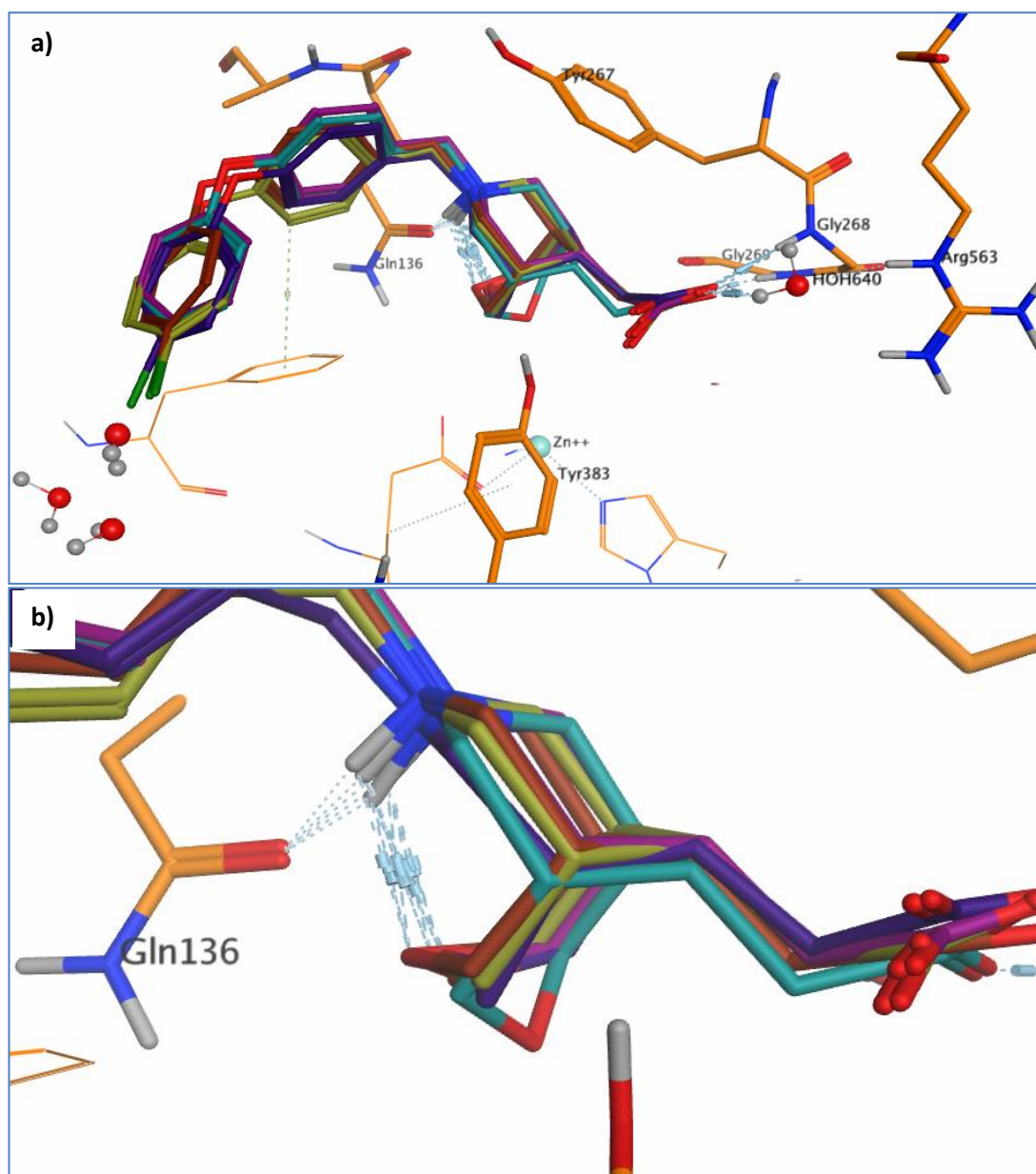


Figure 52: a) Five docking poses of 7 when starting from a boat-chair conformation and b) close up on the conformations of the [3.3.1] system

### 5.5.2. Docking of **7** starting from a boat-boat conformation

The 3D conformation of **7** generated for an earlier experiment was again amended to produce a boat-boat conformation of the [3.3.1] ring. It was then optimised through energy minimisation. The same docking protocol was used. Five docking poses were output and they were all in a boat-boat conformation (*Figure 53*). In this arrangement, the important hydrogen bond to the carbonyl of Gln136 cannot occur. The protonated amine interacts then with the phenyl ring of Tyr267 through a  $\pi$ -cation interaction, as seen in *Figure 53a*.

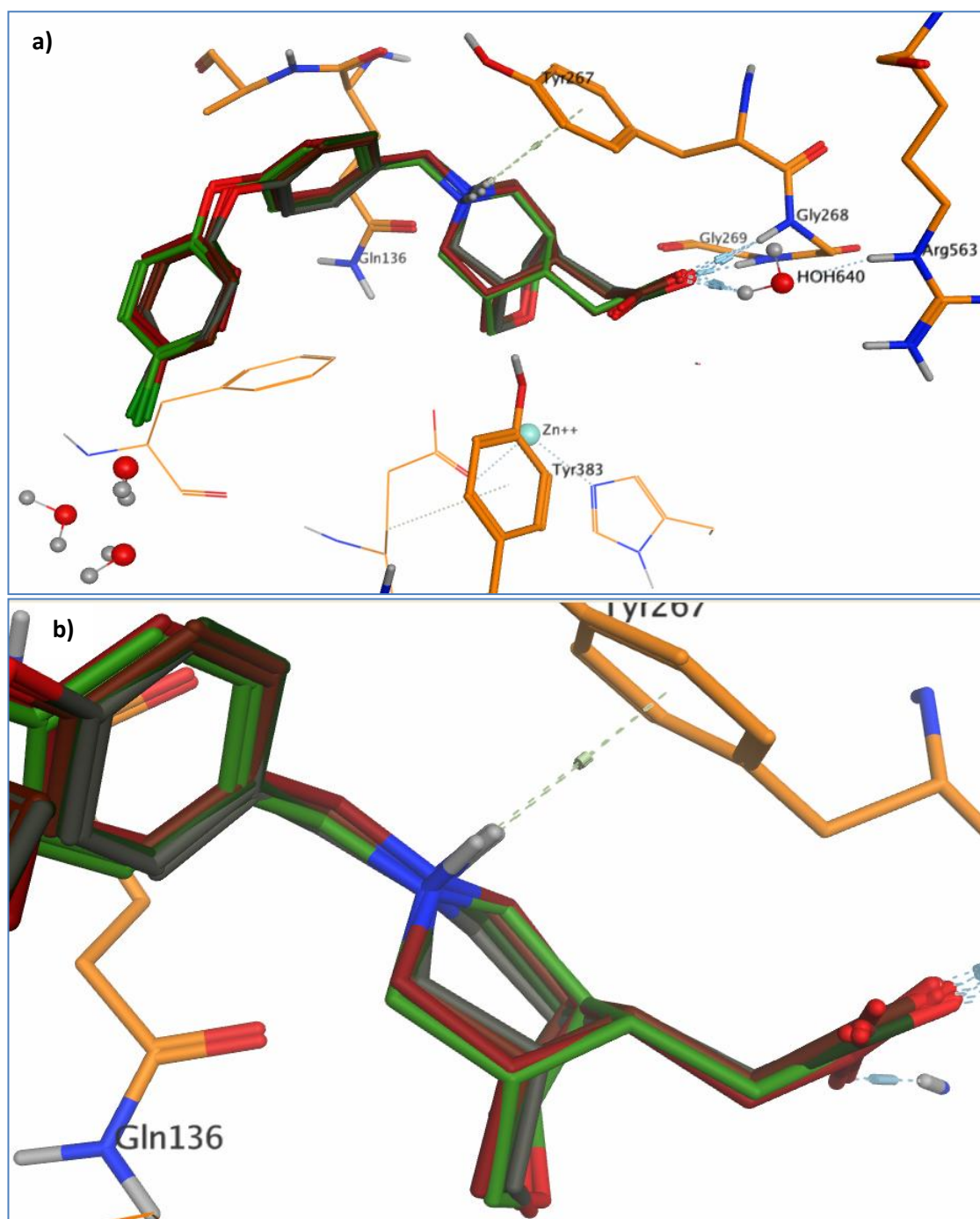


Figure 53: a) All 5 docking poses in a boat-boat conformation; b) close-up on the [3.3.1] rings

The docking experiment was repeated but with 100 iterations of the genetic algorithm to check whether, in this case, it had an impact on the outcome. However, the results were the same as obtained with 10 iterations. A last docking

run was set up to force a hydrogen bond between the ligand and the carbonyl oxygen of Gln136. Again, the starting boat-boat conformation of the ring was not flipped and all resulting docking poses were in boat-boat.

### 5.5.3. Conclusion

The only problematic initial conformation is the boat-boat. All other three ring conformations as starting points can be flipped by GOLD. From the energies obtained when optimising the conformations, the boat-boat conformation was significantly higher in energy. Given the much larger internal destabilisation energy of the boat-boat conformation, the docking experiments for each ligand were not repeated starting with all four different conformations of the input structure.

## 5.6. Predicting stereochemistry with rigid receptor docking

Compound **10** is a mixture of methyl substituted isomers (*Figure 54*) and exhibited a pIC50 of 7.7 in the aminopeptidase assay.

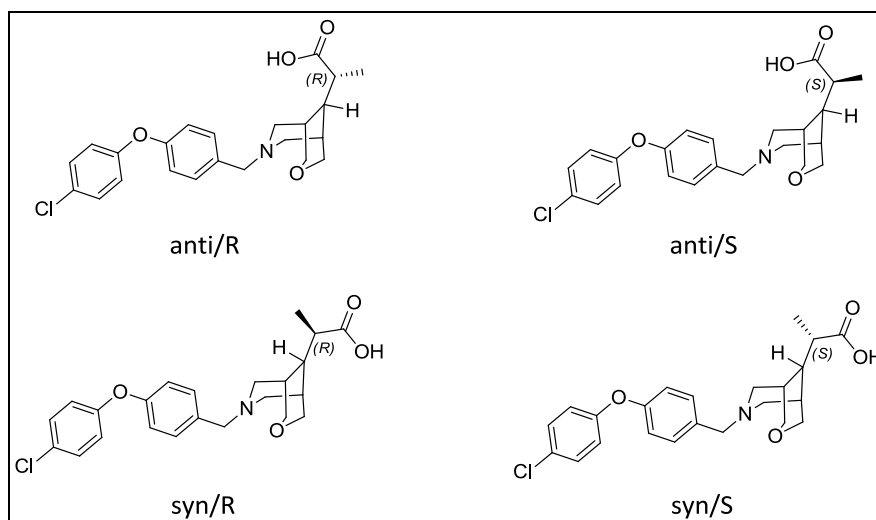


*Figure 54:* Compound **10** is a mixture of four isomers

The mixture was separated and all isomers were tested in the aminopeptidase assay (*Table 21*). They were characterised by NMR but only the bridge position could be identified, not the stereochemistry. Therefore, docking experiments in GOLD were performed in an attempt to assign the stereochemistry of each isomer.

Compound number	Isomer	Aminopeptidase pIC50
<b>10a</b>	Anti	6.7
<b>10b</b>	Anti	7.7
<b>10c</b>	Syn	8.0
<b>10d</b>	Syn	6.6

*Table 21:* Summary of separated isomers and their activities

The same protocol as described previously was followed, however, with only ten iterations as it was shown that increasing the number of iterations did not produce better results.

#### 5.6.1. Anti-R/S pair

There is a potency difference of 1 log unit between the two enantiomers as summarised in *Table 21*. Therefore, the two enantiomers were constructed, docked and their GoldScores determined. These scores showed a difference in the molecule fit into the active site, as summarised in *Table 22*.

Pose rank	anti/R GoldScore	anti/R vdW score	anti/S GoldScore	anti/S vdW score
1	68.01	50.64	71.36	54.69
2	67.64	49.7	69.78	54.12
3	57.69	41.76	69.05	53.61
4	55.69	32.47	68.96	53.34
5	55.25	44.23	61.66	37.1
6	55.03	43.92		
7	54.43	43.43		
8	52.44	41.84		
9	52.34	44.21		
10	44.53	38.14		

*Table 22: Summary of docking scores for the anti isomers*



A paired *t*-test was performed to determine whether the two sets of GoldScores were different. Only the first five GoldScores were used for isomer anti/R in order to maintain comparable data set sizes for the statistical comparison. The test statistics are shown in *Table 23*.

	GoldScore for anti/R	GoldScore for anti/S
Mean	60.86	68.16
Variance	41.34	14.14
Observations	5	5

*Table 23*: Summary of the statistics for anti isomers

The paired *t*-test returned a *p*-value of 0.03, which is below the threshold for statistical significance of 0.05. This means that the null hypothesis stating that both sets of GoldScores had a mean difference of zero, i.e., the values are similar, is rejected. Therefore, the GoldScores for the anti/R and anti/S isomers are statistically different.

Both isomers interact with Gln136 through the protonated amine of the [3.3.1] moiety (*Figure 55*).

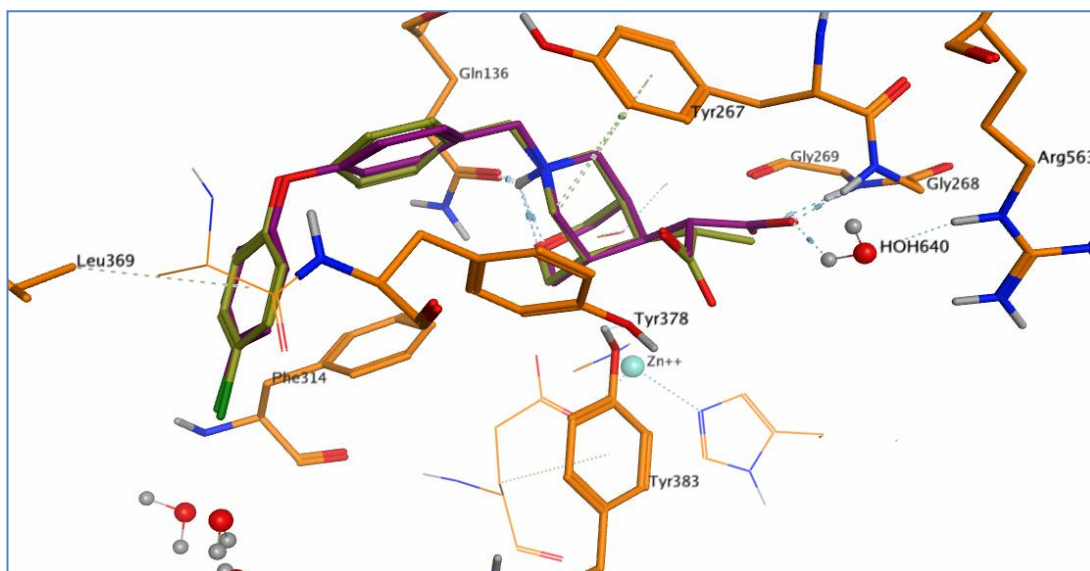


*Figure 55:* Comparison of docking poses between both anti stereoisomers; in orange, LTA4H binding site, in purple, the R stereoisomer and in yellow, the S stereoisomer

In addition to the interaction of the amine with Gln136, the carboxylic acid group of the anti/S stereoisomer interacts directly with the backbone nitrogens of Gly268 and of Gly269 and through a water-mediated interaction with Arg563. In most poses, the terminal aromatic ring also interacts with Leu369 through a favourable van der Waals contact. However, the fifth docking pose for this stereoisomer presented some steric clashes with the binding site as shown in *Figure 56*. This is reflected in its GoldScore, which is lower than the first four, and also in its van der Waals score (*Table 24*).

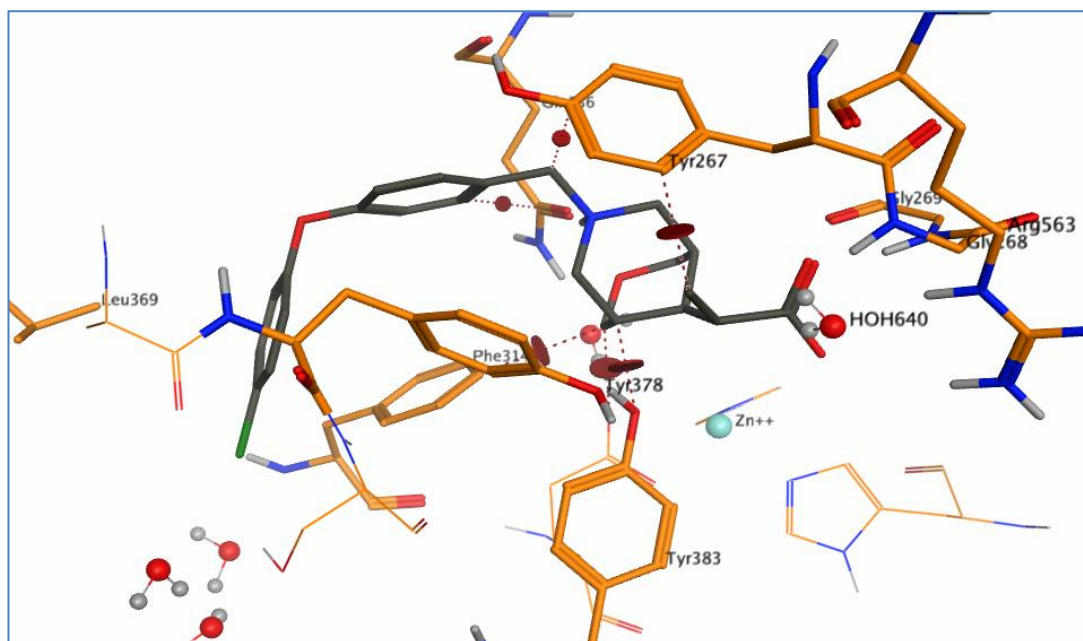


Figure 56: Anti/S stereoisomer fifth scoring pose clashing with residues Phe314, Tyr378, Gln136 and Tyr267; clashes are highlighted in dark red disks on dotted lines.

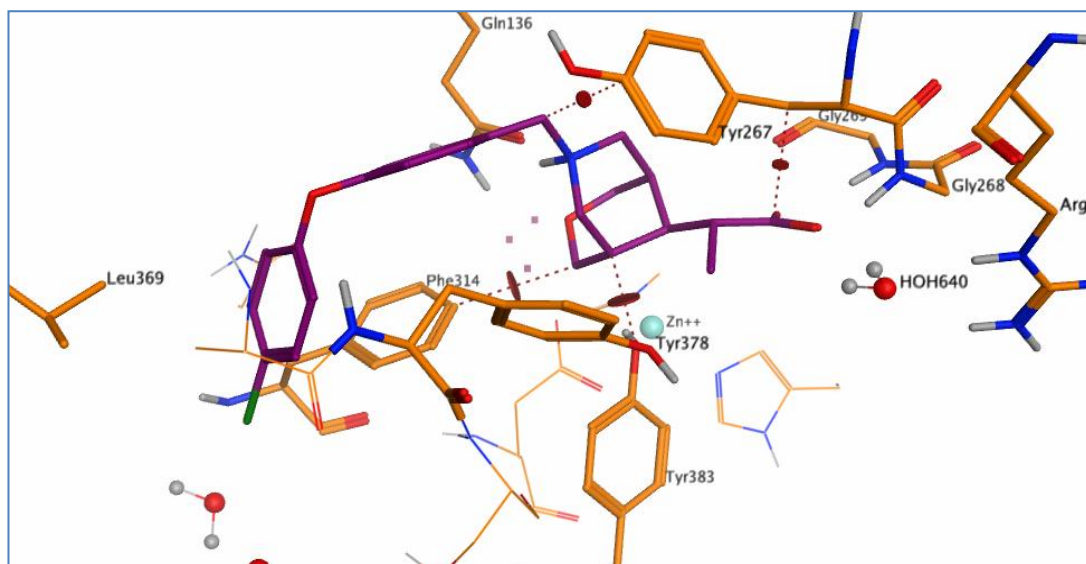
anti/S GoldScore	anti/S vdW score
71.36	54.69
69.78	54.12
69.05	53.61
68.96	53.34
61.66	37.1

Table 24: Summary of GoldScores and van der Waals scores for the anti/S isomer

The anti/R stereoisomer does not fit well in the binding site and presents steric clashes (*Figure 57*) as reflected in its GoldScores and van der Waals scores (*Table 25*).

anti/R GoldScore	anti/R vdW score
68.01	50.64
67.64	49.7
57.69	41.76
55.69	32.47
55.25	44.23
55.03	43.92
54.43	43.43
52.44	41.84
52.34	44.21
44.53	38.14

*Table 25:* Summary of GoldScores and van der Waals scores for anti/R isomer



*Figure 57:* Best scoring pose for anti/R isomer presents steric clashes with residues Tyr267, Tyr378 and Phe314

Based on the quality of the fit and the different ranges in the GoldScores, it is hypothesised that the anti/S enantiomer is **10b** the anti/R enantiomer is **10a** (*Figure 58*). Indeed, the anti/S isomer fits well into the binding site and only one docking pose out of five presented clashes. On the other hand, the anti/R isomer does not fit well and its poses produced clashes with the binding site. Hence, it is assumed that the anti/R isomer is the less potent one.

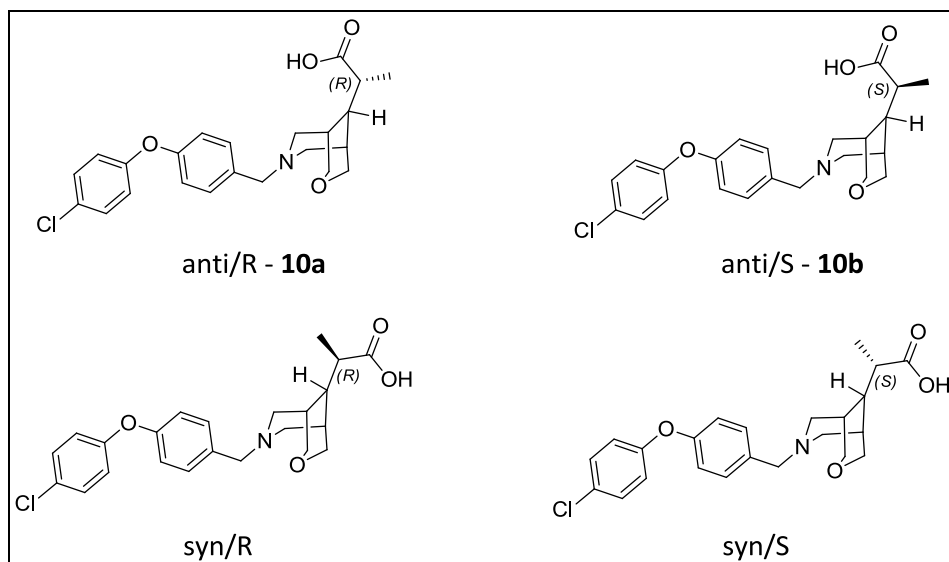


Figure 58: Anti isomers were assigned to their possible chemical structures

### 5.6.2. Syn-R/S pair

There is a potency difference of 1.4 log units between the two enantiomers (*Table 21*). Both enantiomers were built and subsequently docked into the LTA4H binding site using the same protocol in GOLD. The GoldScores of the docking poses did not show a large difference. However, the distribution of the scores for the syn/R isomer are shifted upwards compared to the score for the syn/S isomer, as summarised in *Table 26* below.

Syn/R GoldScore	Syn/S GoldScore
89.90	85.94
88.89	84.11
88.04	82.90
87.30	82.77
85.54	81.54

*Table 26: Summary of GoldScores for all poses of both syn isomers*

A paired *t*-test was performed to verify whether the assumption that both isomers have different docking scores is correct. The statistics are summarised in *Table 27*.

	GoldScore for <b>syn/R</b>	GoldScore for <b>syn/S</b>
Mean	87.93	83.45
Variance	2.73	2.76
Observations	5	5

*Table 27: Statistics summary for the syn isomers*

The paired *t*-test returned a *p*-value of  $3.9 \times 10^{-5}$ , which is below the threshold for statistical significance of 0.05. This means that the null hypothesis stating that both sets of GoldScores had a mean difference of zero, i.e., the values are similar, is rejected. Therefore, the GoldScores for the syn/R and syn/S isomers are statistically different. The top scoring poses for both isomers are shown in *Figure 59*.

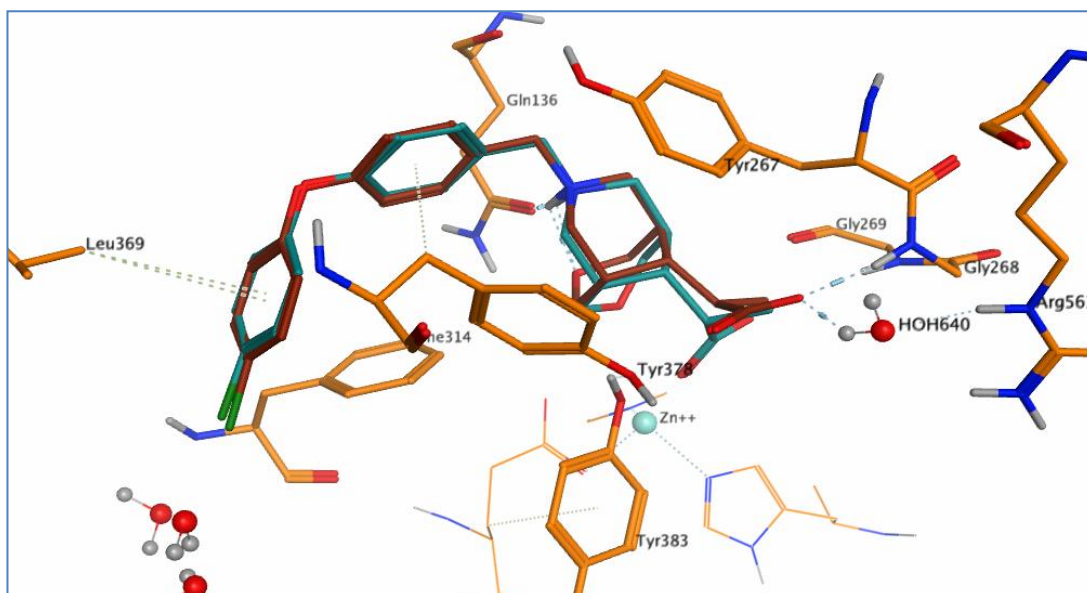


*Figure 59:* Comparison of best docking poses between both syn stereoisomers, in brown, the R stereoisomer, and, in green, the S stereoisomer.

The syn/R stereoisomer interacts with Gln136 through its protonated amine and the carboxylic acid moiety is engaged in hydrogen bonds with the NH of Gly268 and through a water mediated hydrogen bond with Arg563 (*Figure 60a*), as seen in previous docking poses of analogue molecules. There is also an intramolecular hydrogen bond interaction between the protonated amine of the oxygen of the [3.3.1] system which is in a chair-chair conformation. All five docking poses make the same interactions with the binding site and differ in the orientation of the terminal phenyl ring (*Figure 60b*).



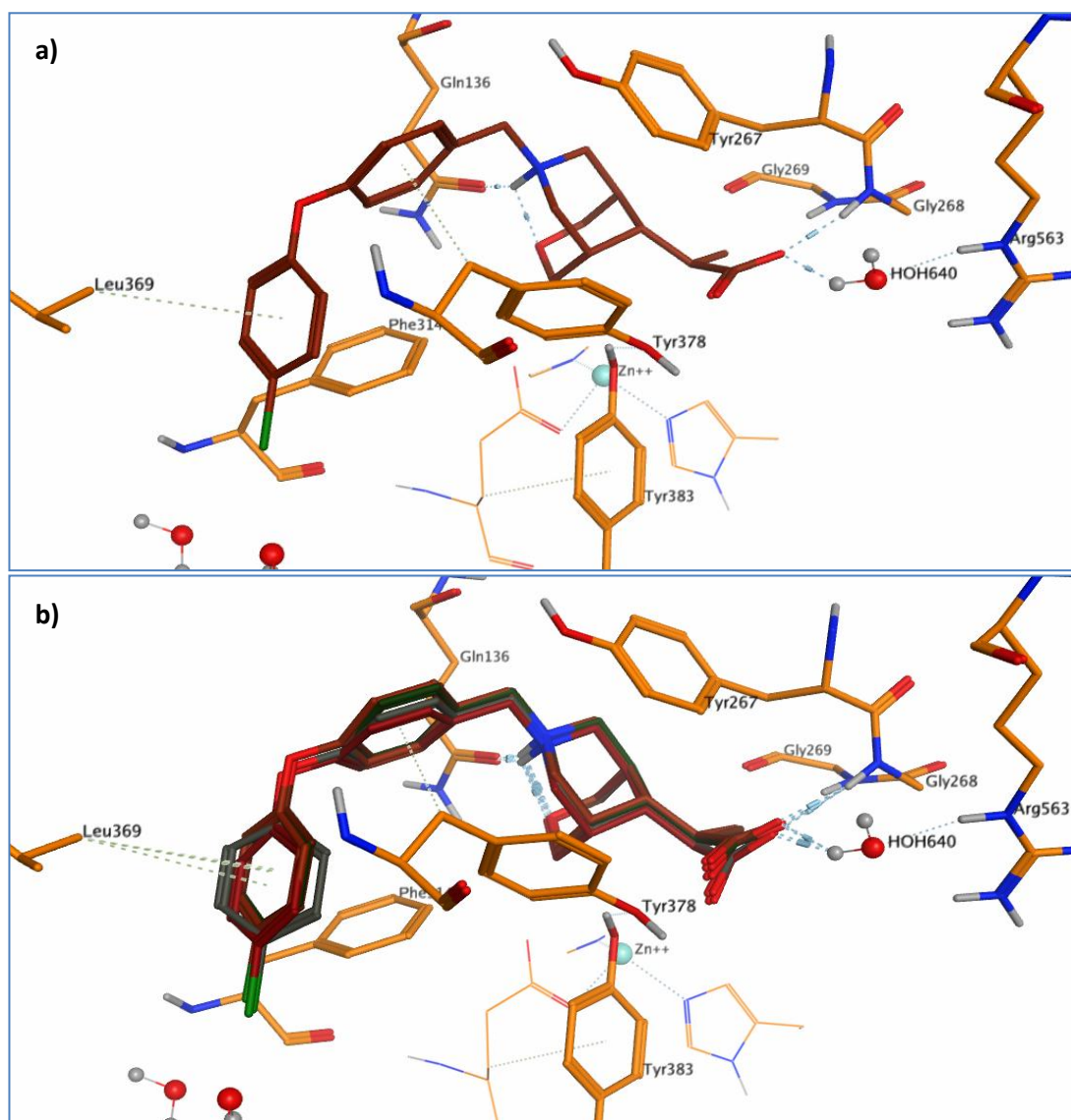


*Figure 60:* a) Top scoring poses for the syn/R stereoisomer showing hydrogen bond interactions; b) all five docking poses for the syn/R stereoisomer.

The syn/S stereoisomer, which is the one with a set of lower GoldScores fits well in the binding site. Its top scoring pose is shown in *Figure 61a*. The only hydrogen bond interaction that the top scoring docking pose can make is from its protonated amine to Gln136. The methyl substitution on the bridge group means that for this stereoisomer the carboxylic acid moiety is not able to interact in a bidentate fashion with both Gly268 and the water640 as seen in other docking poses of analogue

molecules. Two of the five docking poses can make one hydrogen bond to Gly269, which is the residue next to Gly268 (Figure 61b). This could explain the slightly lower GoldScores for this stereoisomer.

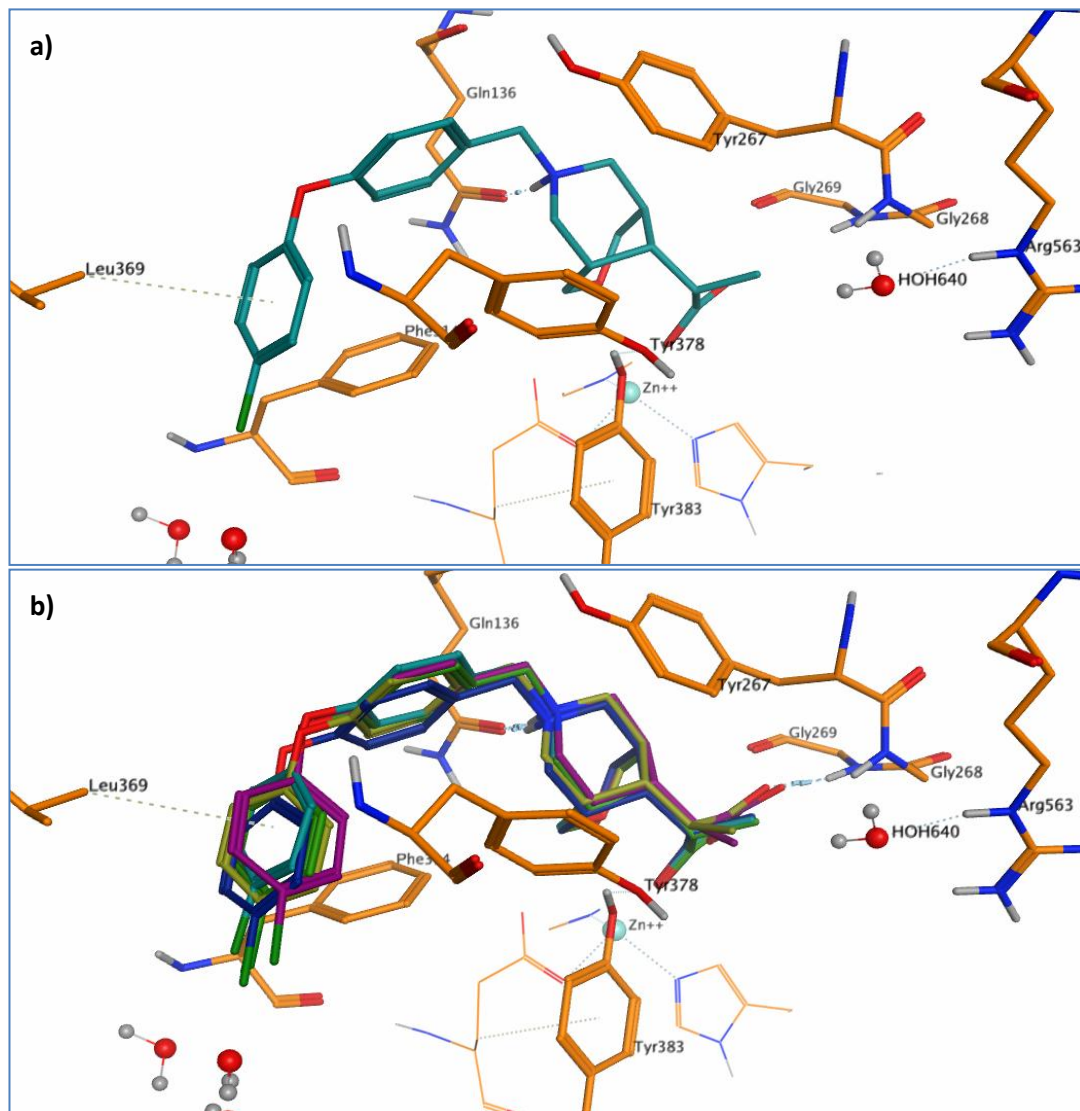


Figure 61: a) Top scoring pose for the syn/S stereoisomer in turquoise; b) all five docking poses for the syn/S stereoisomer with only two of them hydrogen-bonding to Gly269.

Both isomers fit well in the binding site. However, based on their GoldScores and the interactions made with the binding site, it is hypothesised that the syn/R is **10c** the syn/S is **10d** (Figure 62).

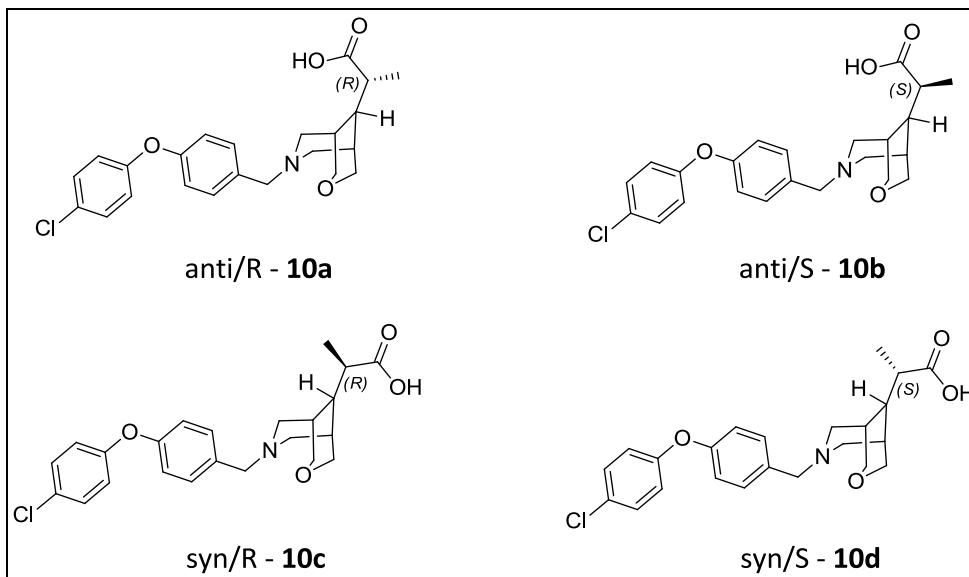


Figure 62: The two remaining syn isomers were associated with their possible chemical structures **10c** and **10d**

	pIC50	Best GoldScore
<b>10c</b> - syn/R	8.0	89.9
<b>10b</b> - anti/S	7.7	71.4
<b>10a</b> - anti/R	6.7	68.0
<b>10d</b> - syn/S	6.6	85.9

Table 28: Summary of pIC50s and GoldScores for all four isomers

### 5.6.3. Conclusion

All separated isomers of **10** were successfully docked into 1LOZX. Plausible docking poses were produced for all four compounds and a hypothesis was put forward as to which chemical structure is associated to a particular potency.

This hypothesis could be verified by crystallising the ligands in order to characterise their stereocentres. Therefore, one example of each pair was submitted to the small molecule crystallography group at GSK. The syn isomer submitted was **10d** ( $pIC_{50} = 6.6$ ). This was successfully crystallised and characterised as the syn/S enantiomer. This experimental result validates the prediction made on the syn pair.

The methyl ester analogue of anti isomer **10a** ( $pIC_{50} = 6.7$ ) was submitted for Vibrational Circular Dichroism (VCD) analysis. Compound **10a** could not be submitted for this analysis because of solid unavailability. However, it is possible to link **10a** back to its methyl ester analogue. Therefore, it was appropriate to characterise the methyl ester and then infer the configuration of **10a**. The methyl ester was reliably characterised as the anti/R enantiomer, and the configuration of **10a** is deduced to also be anti/R. This result shows the accuracy of the prediction of the stereocentre configuration from the docking experiment, as does the previous example.

### 5.7. Application to molecular diversity in rigid receptor docking

Thirty-nine crystal structures of known LTA4H have been released to the public domain over the past 13 years, with the crystal structure of bestatin **1** in complex with LTA4H being the first one to be solved in 2001.<sup>124</sup> Many of these known inhibitors present the same pharmacophore.

A pharmacophore is a collection of chemical and electronic features that enable the recognition of a ligand by a binding site. In this case, a possible pharmacophore for LTA4H ligands is a lipophilic left-hand side (often a biaryl moiety), a protonated amine and a carboxylic acid, separated by a linker of variable length. It was anticipated that docking studies on all thirty nine ligands are not necessary due to their chemical similarity. Nevertheless, this assumption needed to be verified.

The SMILES strings of all thirty nine LTA4H inhibitors were used as input to select a set of chemically diverse molecules for inclusion in the docking studies. Daylight fingerprints were used to represent the compounds together with the Tanimoto coefficient to assess their similarity. Twenty two molecules were selected based on a Tanimoto threshold of 0.7, i.e., between them, the selected molecules had a Tanimoto score of less than 0.7 (*Figure 63*).

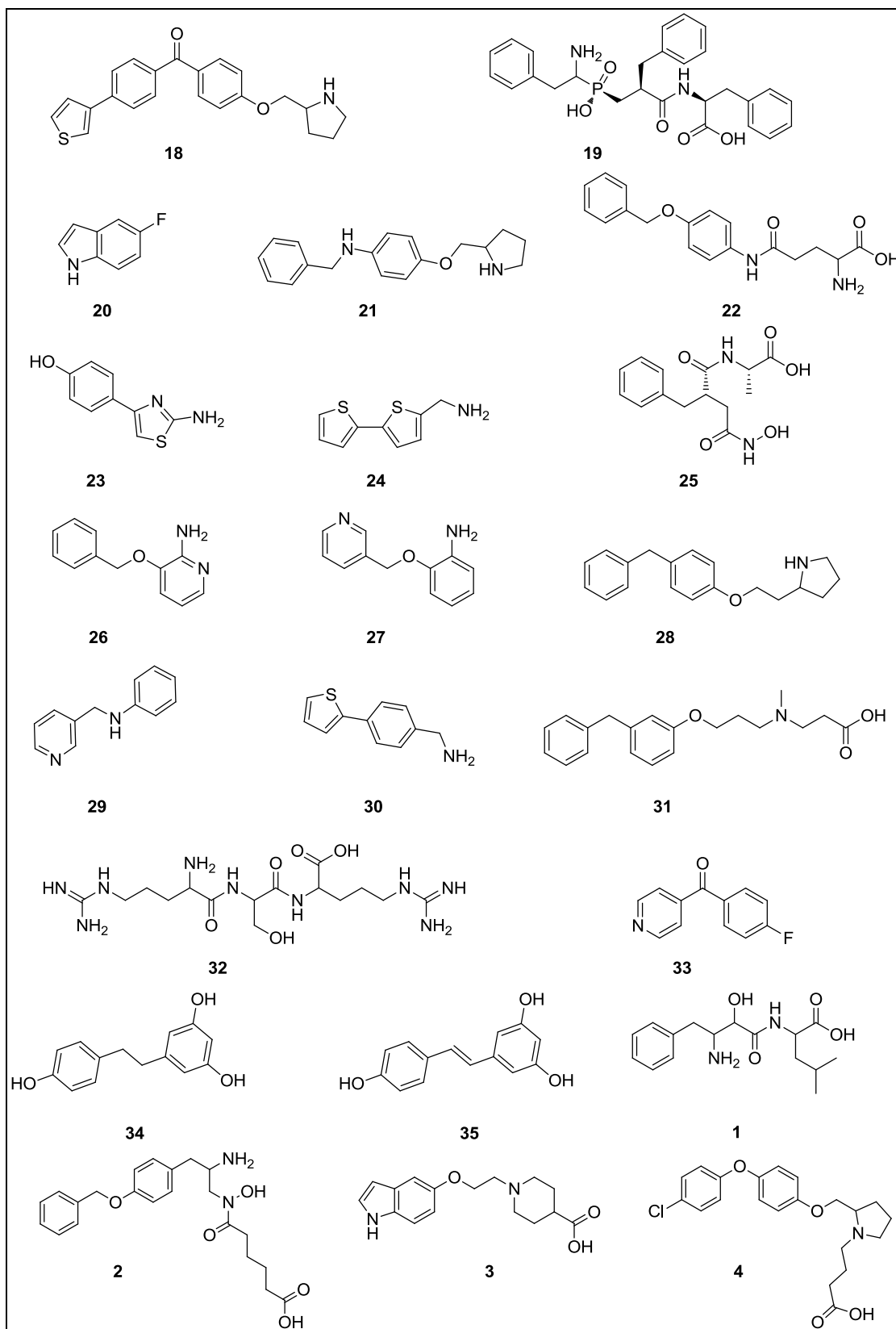


Figure 63: 2D depiction of the selection of 22 known LTA4H inhibitors

The 22 ligands were docked into the LTA4H binding site using the GOLD protocol set up in the previous experiments and the 1LOZX crystal structure. The GoldScore for the best pose of each compound are summarised in *Table 29* (see further analysis of docking scores and molecular weight in Section 5.8).

<b>Ligand Name</b>	<b>mw</b>	<b>GoldScore</b>
<b>22</b>	328.4	91.15
<b>32</b>	417.5	89.77
<b>31</b>	327.4	86.02
<b>4</b>	389.9	85.76
<b>18</b>	363.5	85.56
<b>2</b>	400.5	82.20
<b>28</b>	281.4	80.28
<b>21</b>	282.4	76.02
<b>3</b>	288.3	74.53
<b>1</b>	308.4	73.51
<b>25</b>	294.3	70.13
<b>24</b>	195.3	61.69
<b>30</b>	189.3	59.07
<b>35</b>	228.2	58.80
<b>34</b>	230.3	58.55
<b>26</b>	200.2	55.80
<b>19</b>	494.5	55.17
<b>27</b>	200.2	53.97
<b>29</b>	184.2	53.46
<b>23</b>	192.2	51.72
<b>33</b>	201.2	51.41
<b>20</b>	135.1	40.25

*Table 29:* Summary of best GoldScore for each ligand, ranked in order of the highest to the lowest scoring ligand

### 5.7.1. Bestatin

The crystal structure of LTA4H in complex with bestatin **1** was the first crystal structure of LTA4H to be solved (PDB entry 1HS6). **1** is a small reversible inhibitor of LTA4H (*Figure 64*) with a  $K_i$  of  $0.2 \mu\text{M}$ .<sup>148</sup>

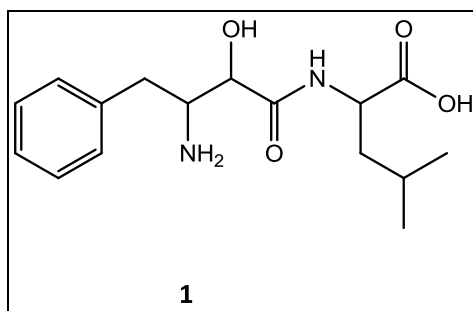


*Figure 64*: 2D depiction of **1**

In crystal structure 1HS6, **1** interacts through its primary amine moiety to Gln136. The hydroxyl functionality interacts with the zinc atom as does the carbonyl oxygen of the amide, causing a pentavalent conformation for the zinc atom. The amide carbonyl also interacts with Tyr383. The carboxylic acid moiety interacts with the NH of Gly268 and through a water mediated hydrogen bond to Arg563 (*Figure 65*).



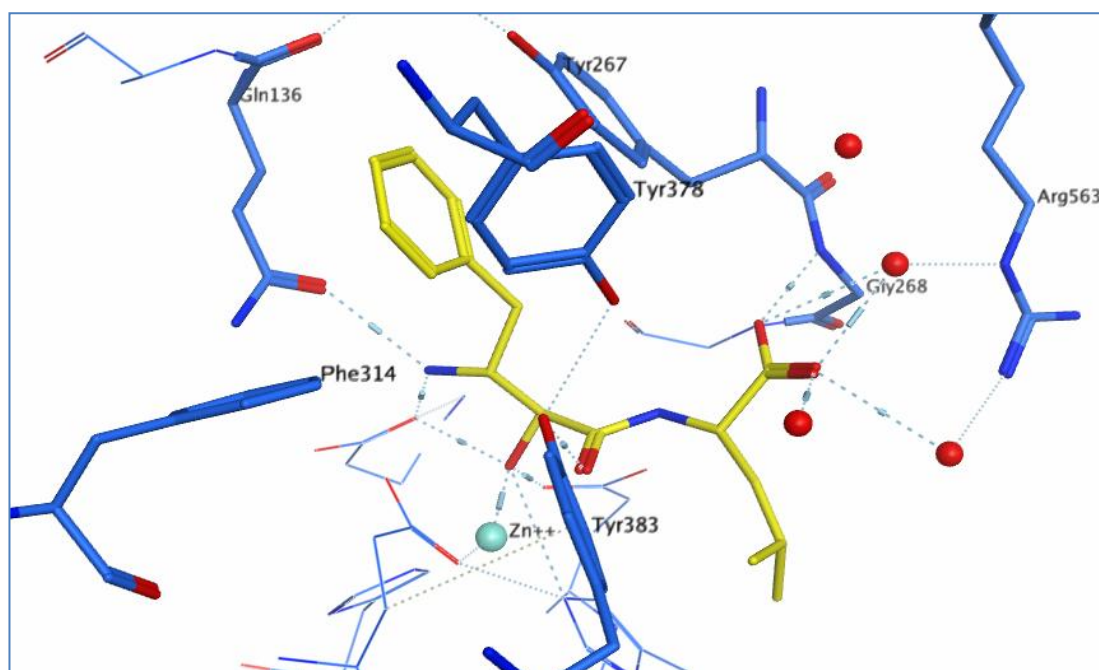


*Figure 65: Crystal pose of 1 in X-ray structure 1HS6 (without hydrogens)*

Compound **1** was docked into the 1LOZX system. Ten docking poses were obtained and none of these reproduced the crystal pose observed in 1HS6. This is due to the fact that the location where **1** crystallised in 1HS6 is occupied by water molecules in 1LOZX (*Figure 66a*). The top scoring docking pose binds where proprietary molecules usually bind (*Figure 66b*).

All but one docking poses were found to be reversed and shifted in comparison to the crystal pose due to the presence of waters close to the zinc. Moreover, the poses do not interact with any key residues, e.g., Gln136, Arg563 and Gly268.

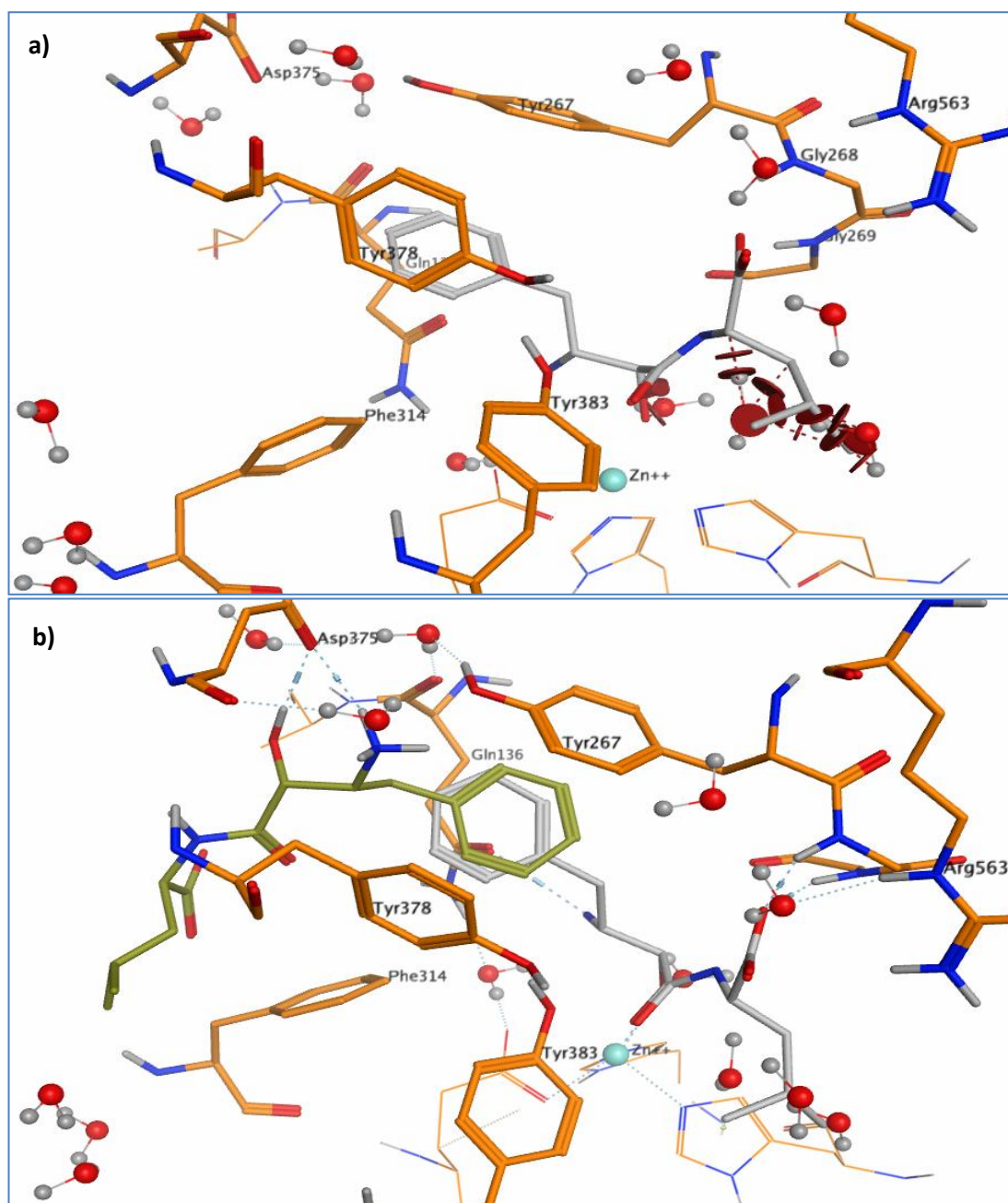
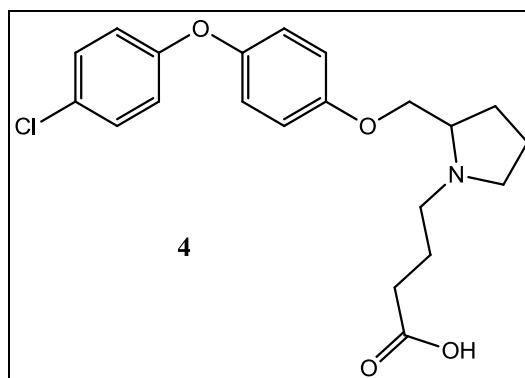


Figure 66: a) Crystal pose of **1** showing clashes with waters crystallised in the 1LOZX system; b) Top scoring docking pose of **1** in yellow and crystal pose in grey

### 5.7.2. DG-051

The crystal structure of LTA4H in complex with DG-051 **4** was published in 2010 (PDB entry 3FH7). DG-051 is an inhibitor of LTA4H with an  $IC_{50}$  of  $0.069 \mu\text{M}$ .<sup>125</sup> It is depicted in *Figure 67*.



*Figure 67*: 2D depiction of ligand **4**

In crystal structure 3FH7, the ligand **4** makes only one hydrogen bond interaction with the binding site, i.e., from its carboxylic acid moiety to Tyr383. The carboxylic acid also interacts with the zinc atom in a bidentate fashion, making it pentavalent as observed in the previous structure (*Figure 68*).

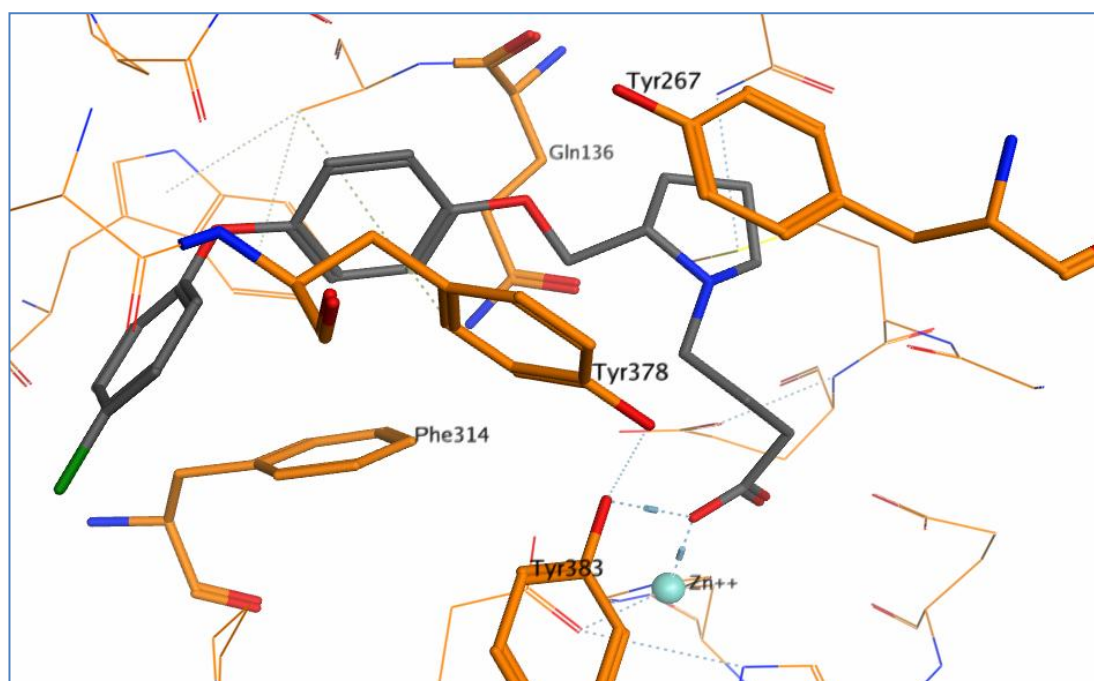


Figure 68: Ligand **4** in complex with LTA4H (3FH7)

When the crystal pose of **4** is placed in the 1LOZX system, its carboxylic acid group sits over a water molecule which was crystallised in the 1LOZX system (Figure 69a). When docking **4** into 1LOZX, five poses were obtained. In the top scoring docking pose (Figure 69b), the biphenyl moiety superposed well on the crystal pose whereas the cyclic amine and carboxylic acid did not. This is due to the presence of waters in close proximity to the zinc atom. This was observed for all five docking poses of **4**. Overall, the docking poses for this ligand are only partially acceptable due to the presence of the water molecule near the zinc atom.

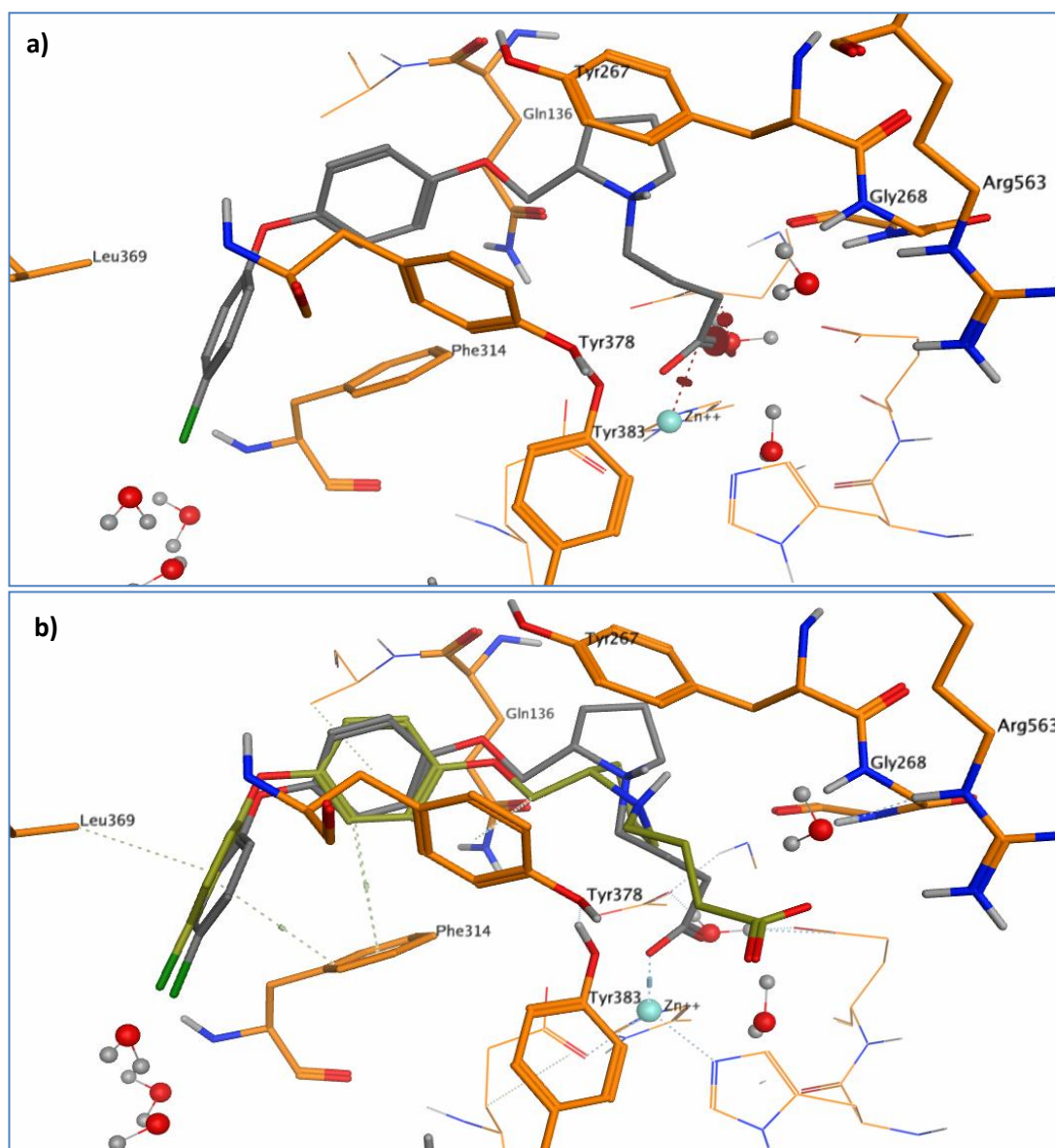
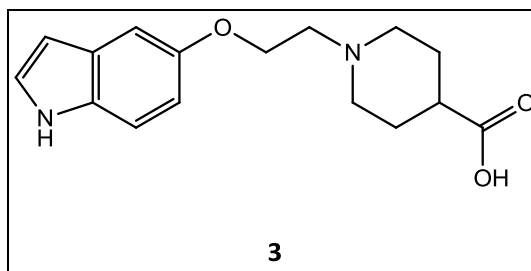


Figure 69: a) Ligand **4**, as crystallised in 3FH7 shown, in the 1LOZX system with clashes with crystallised water shown in dark red disks; b) top scoring pose of **4** in yellow and crystal pose in light grey

### 5.7.3. RCSB051059

The crystal structure of LTA4H in complex with RCSB051059 **3** was published in 2009 (PDB entry 3FUK). Compound **3** is an inhibitor of LTA4H with an  $IC_{50}$  of 1491  $\mu$ M, which means that it is not as potent an inhibitor as the previous examples.<sup>123</sup> Its structure is represented in *Figure 70*.



*Figure 70*: 2D depiction of **3**

In crystal structure 3FUK, the tertiary amine functionality of the ligand interacts with Gln136 while the carboxylic acid is engaged in a hydrogen bond with Tyr383 and also interacts with the zinc atom in a bidentate manner (*Figure 71*). This means that the zinc is pentavalent as well.

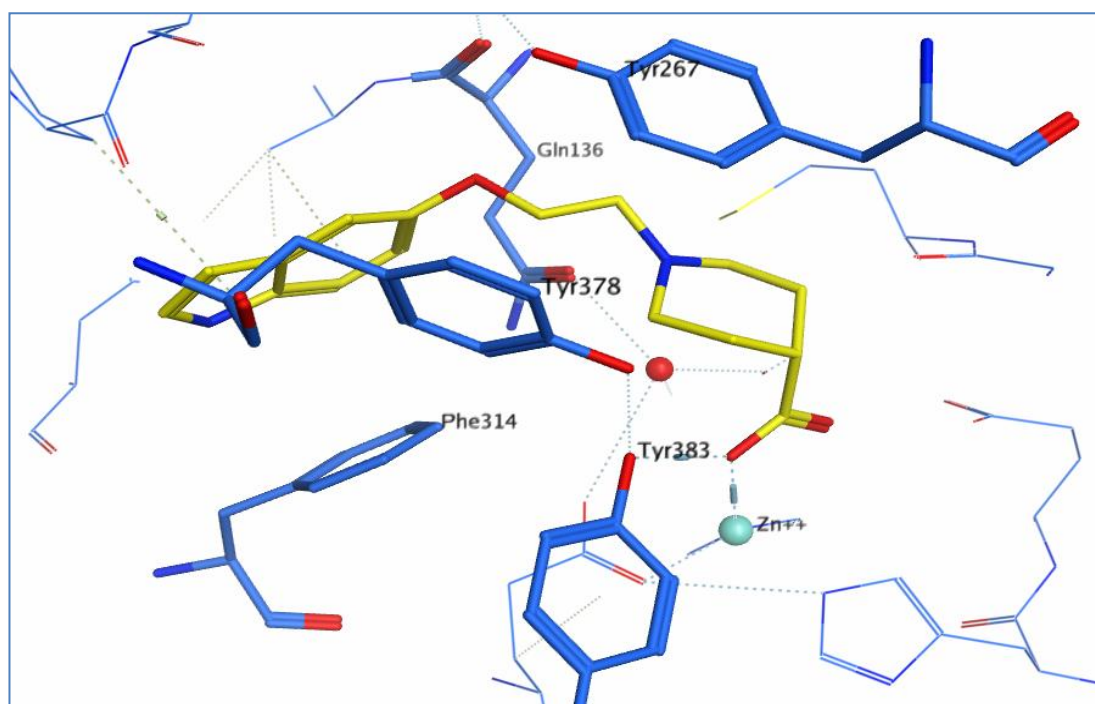


Figure 71: Ligand **3** in X-ray structure 3FUK

An important observation to make is that the pendant carboxylic acid is in an axial substitution on the piperidine ring. This is an unusual conformation as an equatorial substitution is preferred. When searching the CSD<sup>109</sup> to confirm this, the twelve hits found with 3D coordinates presented an equatorial substitution of the carboxylic acid. Therefore, it could become an issue for GOLD to find the correct docking pose. When placing **3**, as crystallised in 3FUK, in the 1LOZX binding site, it is sitting over a water molecule which is close to the zinc atom (*Figure 72a*).

Docking this ligand into 1LOZX produced ten docking poses. The top scoring docking pose was slightly shifted to the left of the binding site compared to the crystal pose (*Figure 72b*). It interacted with Gln136 through its protonated amine and with Trp311 through the NH of the indole ring. The carboxylic acid was equatorial to the piperidine ring and pointed in the direction of the zinc atom. In such a case, where

there is no X-ray information available, one could conclude that it is a plausible docking pose. Out of the ten docking poses generated, four of them presented an axial substitution. However, this unfavourable conformation allowed an interaction with the zinc atom only in one instance (*Figure 72c*).

Overall the docking poses for this ligand are satisfactory.



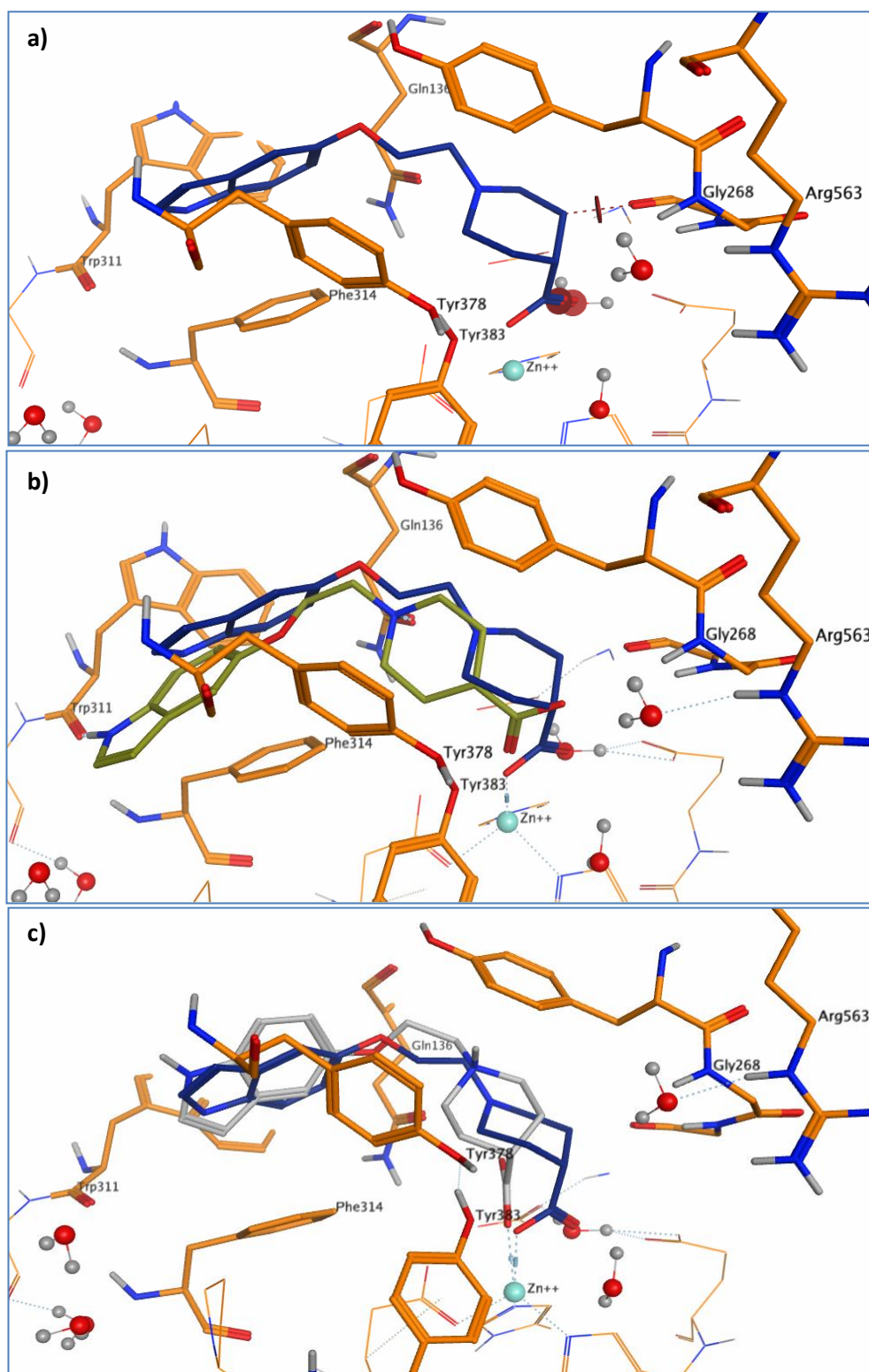


Figure 72: a) Crystal pose of **3** in 1LOZX system with carboxylic acid sitting over a water molecule; b) top scoring docking pose of **3** in yellow and crystal pose in blue; c) in light grey, a docking pose with an axial substitution on the piperidine ring.

#### 5.7.4. Hydroxamic acid

The crystal structure of LTA4H in complex with hydroxamic acid **2** was published in 2002 (PDB entry 2VJ8). Compound **2** is an inhibitor of LTA4H with a  $K_i$  of  $0.002 \mu\text{M}$  (Figure 73).<sup>149</sup>

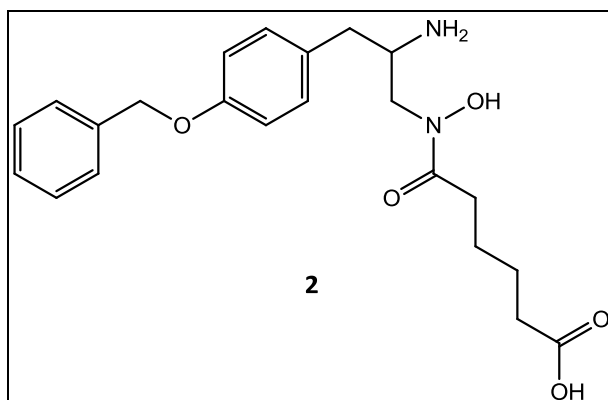


Figure 73: 2D depiction of **2**

In crystal structure 2VJ8, the ligand protonated amine interacts with Gln136 while the hydroxyl of the hydroxamide interacts with the zinc atom and with Tyr383. The zinc is in a tetrahedral configuration in this instance. The carboxylic acid interacts with a water molecule and also with Arg563 (Figure 74).

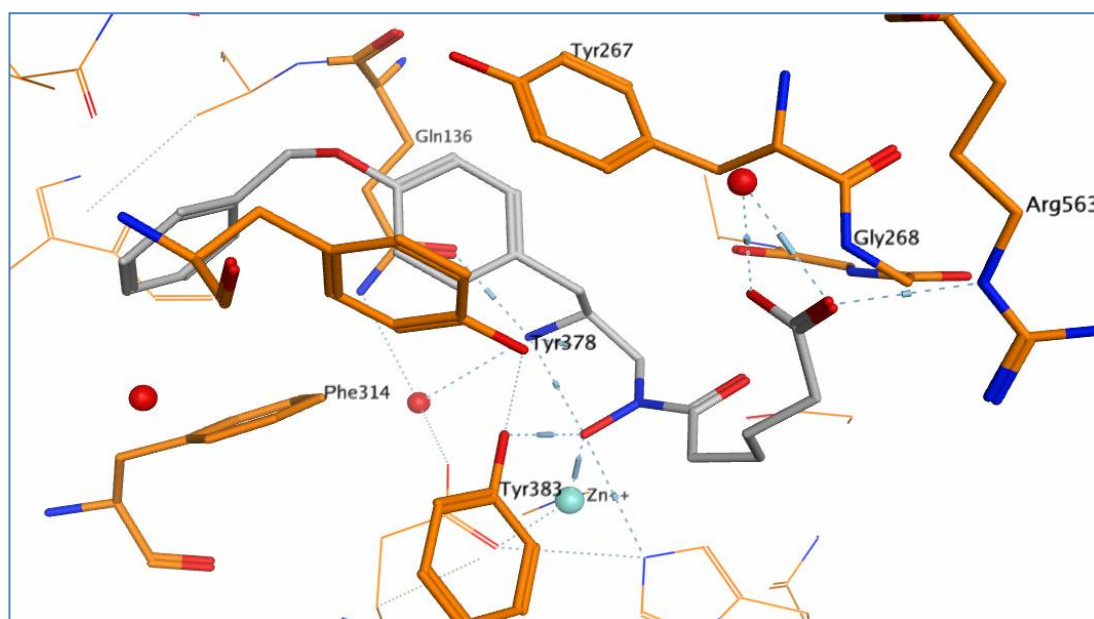


Figure 74: **2** in crystal structure 2VJ8

Compound **2** was placed in the 1LOZX system and as observed with previous ligands, it sat over one water molecule and very close to two others (*Figure 75a*).

When docking it in GOLD, ten poses were output and four were found to be in the same reversed and shifted pose as seen for **1**. Only two docking poses can make an interaction with the zinc atom through the ligand carbonyl group. The top scoring docking pose binds further down the binding site and its carboxylic acid moiety interacts with Gly268 through a hydrogen bond (*Figure 75b*).

Overall, the docking poses for this ligand are not satisfactory due to the presence of waters close to the zinc atom.

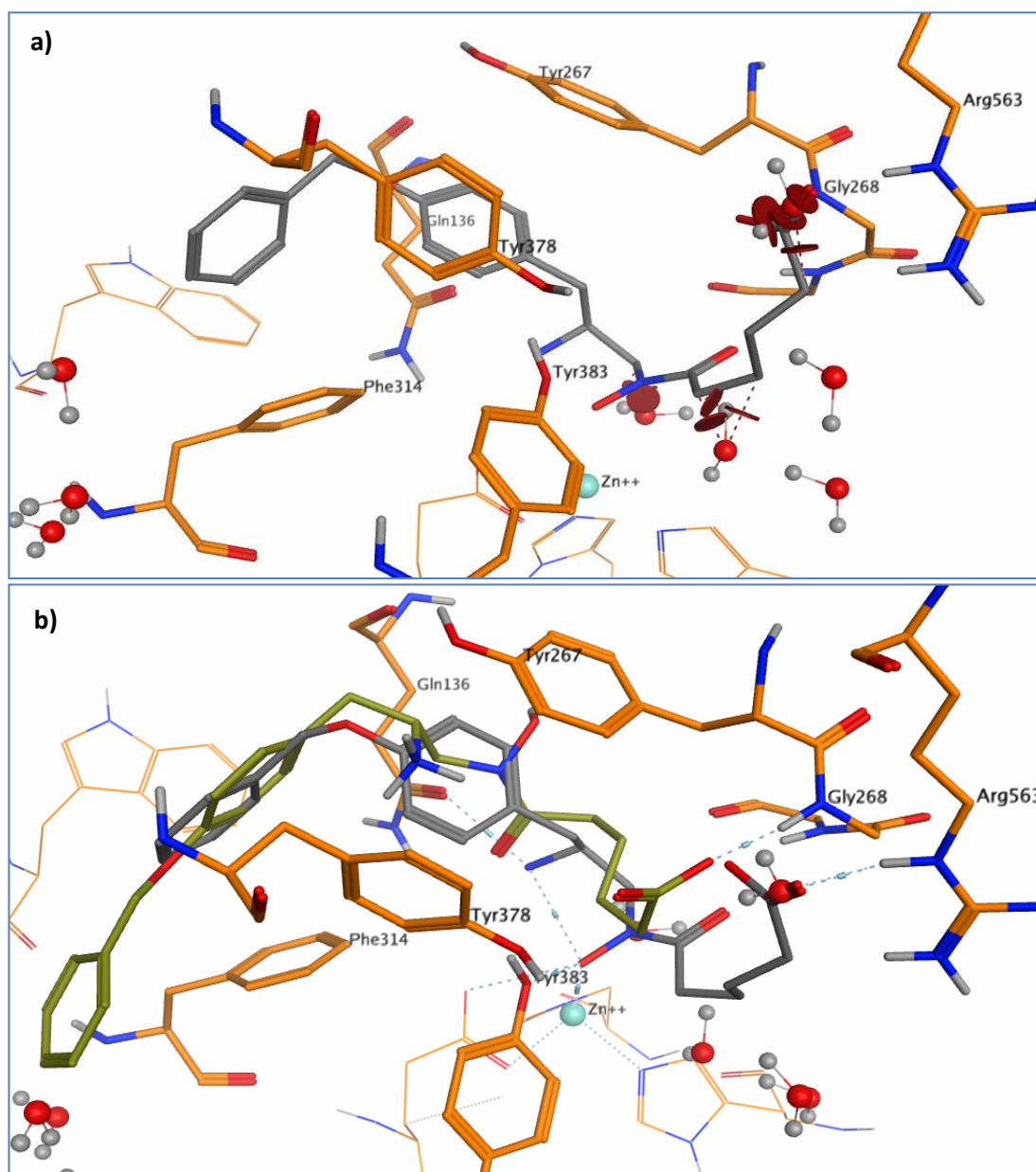


Figure 75: a) crystal pose of 2 in the 1LOZX system; b) top scoring pose in yellow binds further down the active site and crystal pose in light grey.

## 5.8. The role of water in rigid receptor docking

### 5.8.1. Rationale

The unmodified 1LOZX system was not suitable for most known LTA4H ligands due to the presence of water molecules near the zinc atom. This was shown by the inability of GOLD to reproduce the binding mode of **1**, **2**, **3** and **4** in this model. Therefore, 1LOZX was re-prepared, after removing all water molecules within 10 Å of the zinc atom, following the same protocol as described in Section 4.1.

### 5.8.2. Known LTA4H inhibitors

The same LTA4H known molecules as in Section 5.6.6 will be the focus of this section. The molecules were docked into the modified 1LOZX system and the GoldScore for the best scoring pose of each compound can be found in *Table 30*.

Ligand Name	mw	GoldScore (no water)	GoldScore (with water)
32	417.5	109.92	89.77
19	494.5	104.45	55.17
2	400.5	97.44	82.2
4	389.9	91.64	85.76
18	363.5	90.87	85.56
1	308.4	88.99	73.51
22	328.4	83.58	91.15
21	282.4	83.44	76.02
31	327.4	83.09	86.02
25	294.3	77.11	70.13
28	281.4	72.56	80.28
3	288.3	69.46	74.53
24	195.3	66.91	61.69
35	228.2	65.29	58.8
34	230.3	65.06	58.55
30	189.3	61.91	59.07
26	200.2	55.72	55.8
27	200.2	54.58	53.97
29	184.2	53.67	53.46
33	201.2	53.48	51.41
23	192.2	52.69	51.72
20	135.1	36.00	40.25

*Table 30:* Comparison of best GoldScore for each ligand when docking with and without water molecules near the zinc atom, sorted in decreasing order of GoldScore (no water)

It is interesting to note that in the absence of water, larger ligands (higher molecular weight (mw)) achieve a higher GoldScore. This could suggest that larger ligands, which have more atoms to contribute to the scoring function, are favoured over smaller ligands. The two scatter plots below show the correlation between GoldScore and molecular weight. There is more of a correlation between the docking score and molecular weight in the case where there were no water molecules included in the docking experiment (right-hand side plot) which could suggest that the scoring function does not add value over using only molecular weight to differentiate between binders. In the case where waters were included there is less correlation, although the larger molecules still seem to have higher GoldScores. This is not so surprising given the functional form of the scoring function. The more interactions docking poses make in the binding site, the better the chance of a high the score. In the absence of steric clashes, typically larger molecules will make more interactions than small ones.

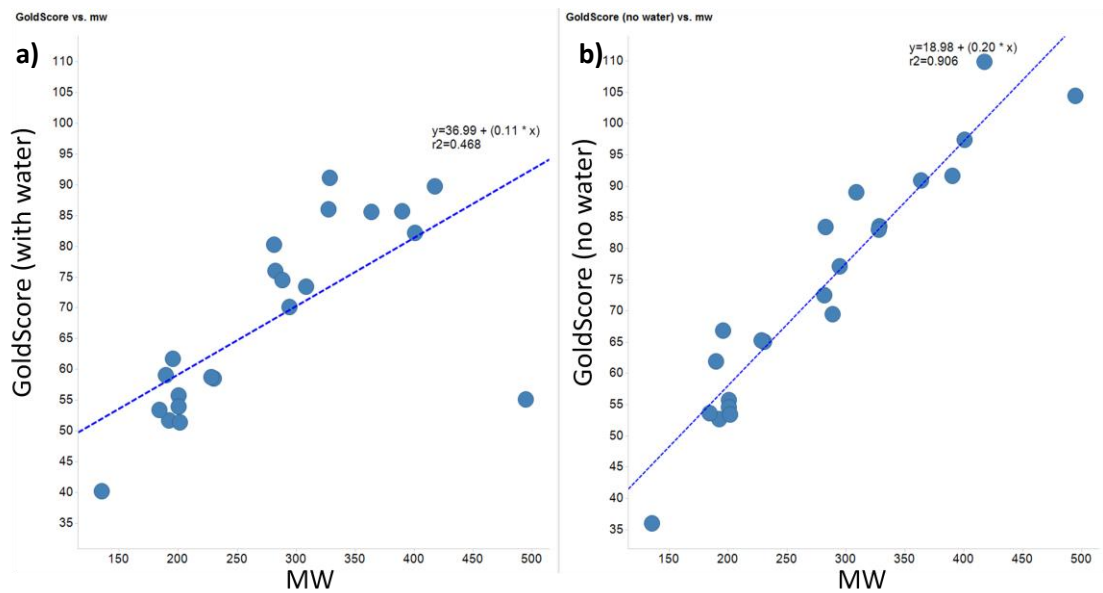


Figure 76: Correlation between GoldScore and molecular weight: a) GoldScore with water and b) GoldScore without water



#### 5.8.2.1. *Bestatin*

The top scoring pose of **1** with a GoldScore of 88.99 interacts with the binding site through hydrogen bonds from its carboxylic acid to Gly268, from its amide carbonyl to Gly269, from its primary amine to Gln136, Glu318 and Glu271 and from its hydroxyl to Glu296 (*Figure 77a*). After inspection of all ten docking poses, it appeared that the fourth and fifth docking poses, scoring respectively 73 and 72, were closer to the crystal pose than the top scoring one (*Figure 77b*). Indeed, they interact with the zinc atom through the hydroxyl moiety. Whilst the hydrogen bonding from the carboxylic acid and the amide carbonyl are maintained, the primary amine interacts with Glu271 and Gly269 in both cases. Their hydrogen bond score is lower (27 and 28 respectively) compared to the top scoring pose with a hydrogen bond score of 38.

The comparison of the top scoring poses when docking with and without waters shows that the removal of water molecules near the zinc atom was beneficial. It was possible to reproduce the crystal pose (*Figure 77c*).

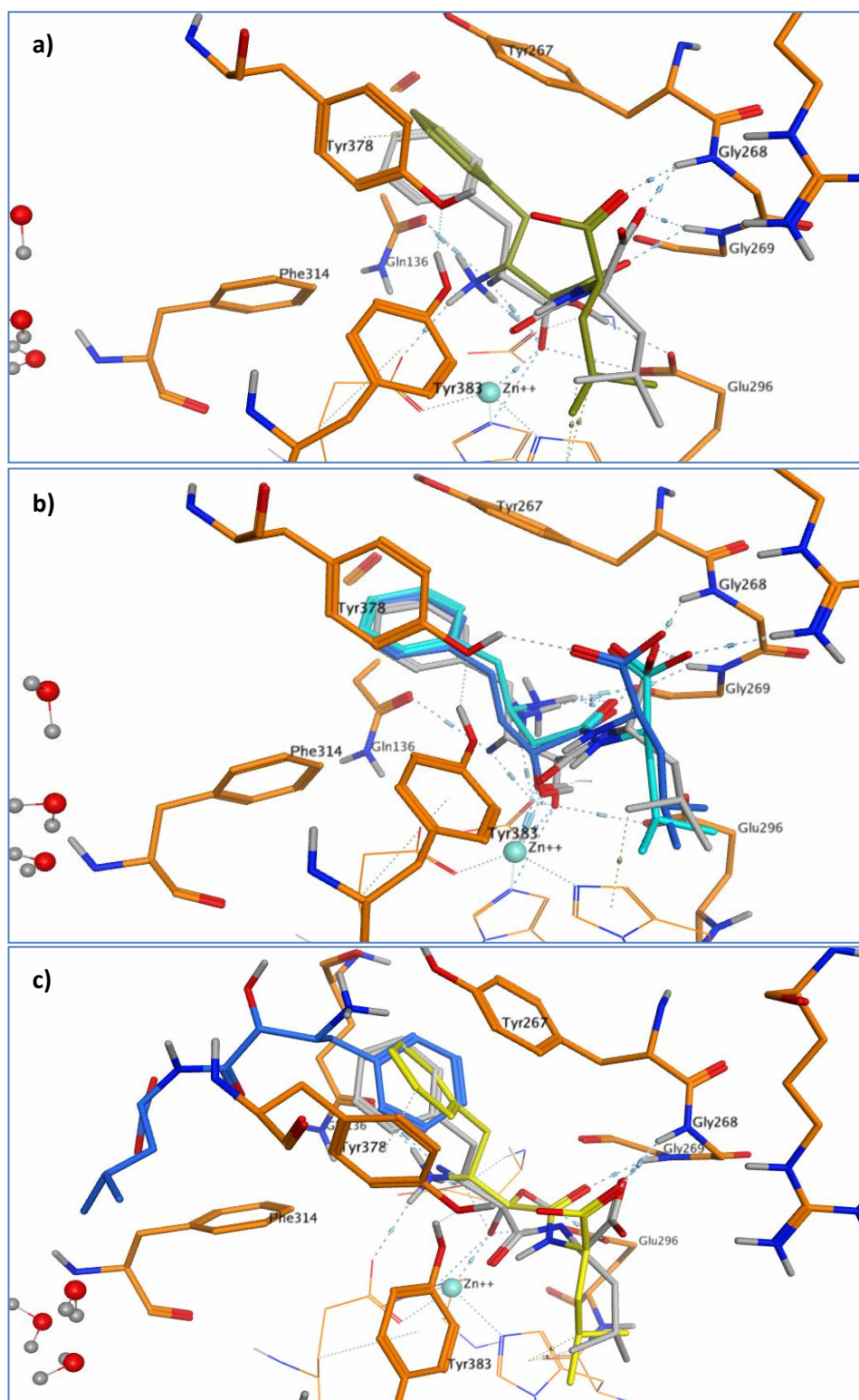


Figure 77: a) Top scoring docking pose of **1** in yellow and its crystal pose in light grey; b) 4<sup>th</sup> docking pose in turquoise and fifth docking pose in blue; c) Top scoring pose without water in yellow and with water in blue, crystal pose in light grey.

#### 5.8.2.2. DG-051

From the set of known LTA4H ligands docked into the 1LOZX system, compound **4** is the most similar to GSK compounds **7**, **8**, **9** and **10a-d**. Docking of **4** into the modified 1LOZX system did not produce poses closer to the crystal pose than the unmodified model. The top scoring pose interacts with the binding site through hydrogen bonds from its carboxylic acid moiety to Arg563, and not with the zinc atom as seen in the crystal structure, and from its protonated amine to Gly269 (*Figure 78a*). However, the placement of the biaryl moiety is slightly shifted to the right compared to the top scoring pose when docking with waters (*Figure 78b*). Four out of nine docking poses generated are reversed compared to the crystal pose. In this case, removing water molecules near the zinc does not improve the docking poses.

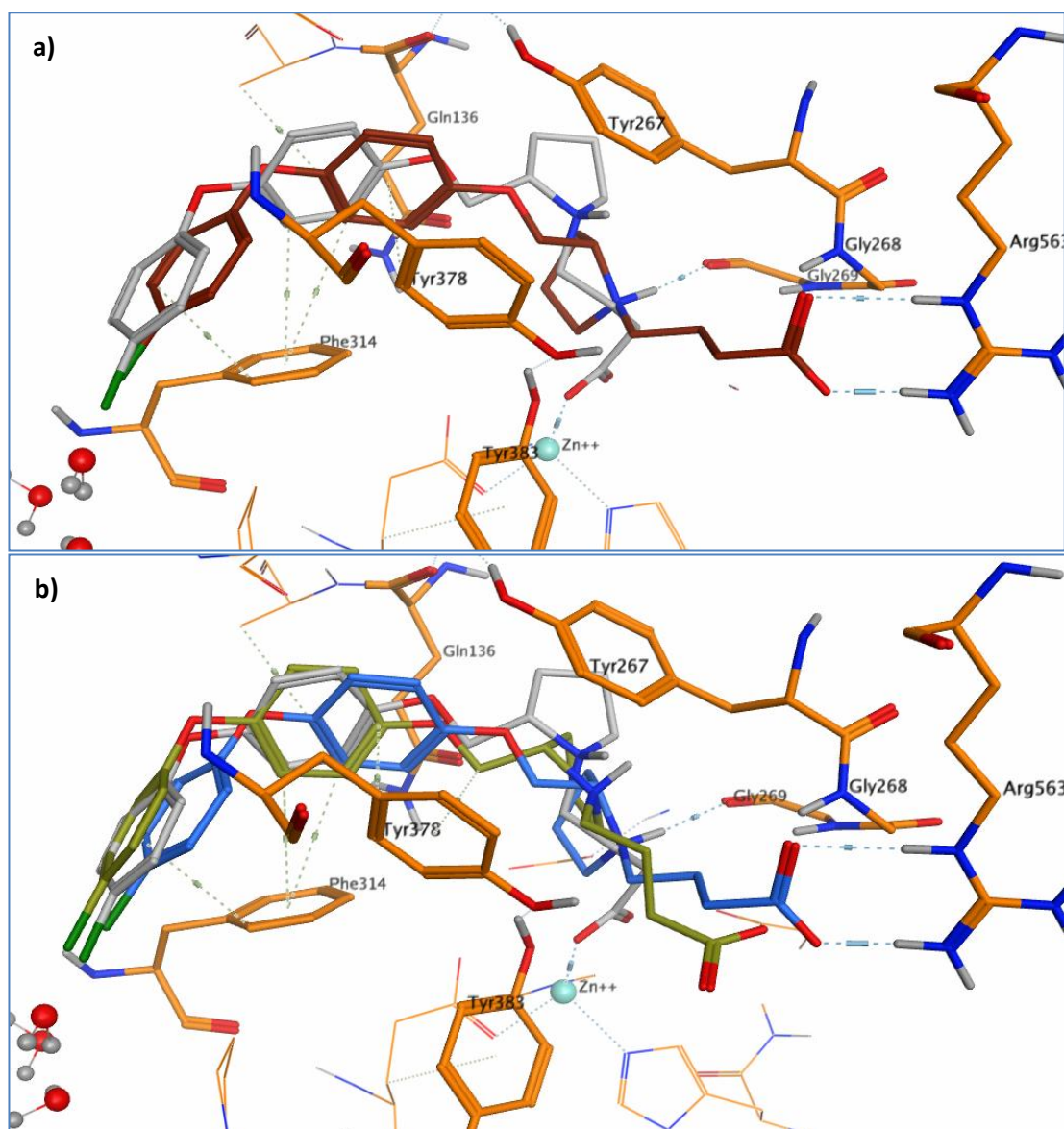


Figure 78: a) Top scoring docking pose of **4** in brown and its crystal pose in light grey; b) top scoring docking pose with waters in yellow and without waters in blue, crystal pose in light grey

### 5.8.2.3. RCSB051059

The top scoring docking pose for this ligand, with a GoldScore of 69.46, is reversed compared to the crystal pose. It interacts through only one hydrogen bond from the indole NH to Glu296 in the binding site (*Figure 79a*). This is reflected in a poor hydrogen bond score of only 10. All five docking poses produced are in this orientation. All but one docking pose presents an axial substitution of the carboxylic acid on the piperidine ring.

In comparison, the top scoring pose when docking with waters was more plausible with its carboxylic acid interacting with the zinc atom (*Figure 79b*). This molecule is problematic due to its unusual conformation. However, docking in a system with no water molecules near the zinc atom did not improve the docking poses.

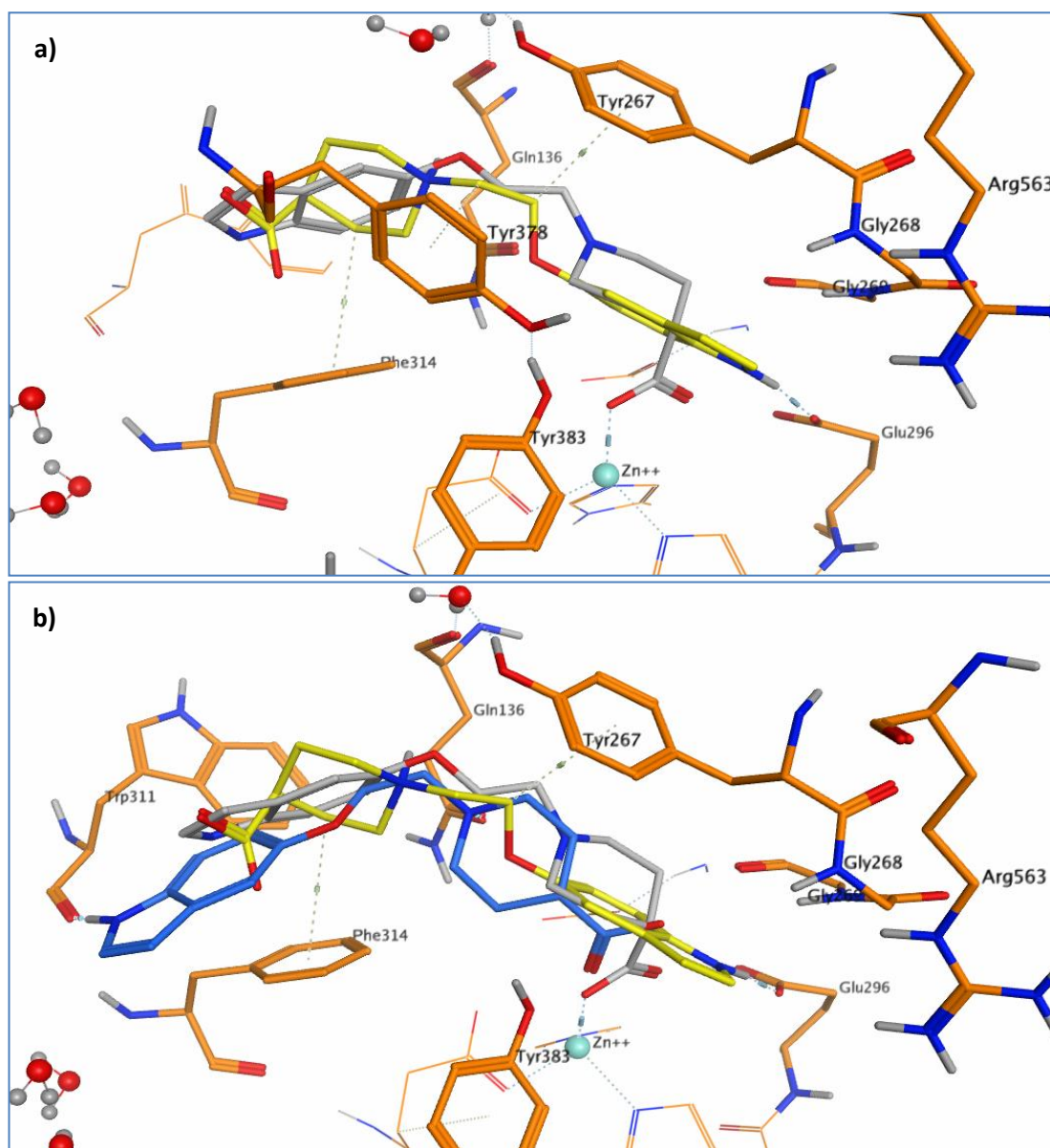


Figure 79: a) Top scoring docking pose of **3** in yellow and its crystal pose in light grey; b) Top scoring pose without waters in yellow and with water in blue, crystal pose in light grey.

#### 5.8.2.4. *Hydroxamic acid*

The top scoring docking pose of **2** is reversed when the crystallographic waters in 1LOZX are removed. The ligand interacts with the binding site from its protonated primary amine to Gln136, Glu271 and Glu318 (*Figure 80a*). There is an intramolecular hydrogen bond between the hydroxyl group and the carboxylic acid. Moreover, none of the ten docking poses generated were placed in the same orientation as the crystal pose. In contrast, the top scoring docking pose generated when keeping the water molecules in the binding site was at least in the same orientation as the crystal pose (*Figure 80b*).

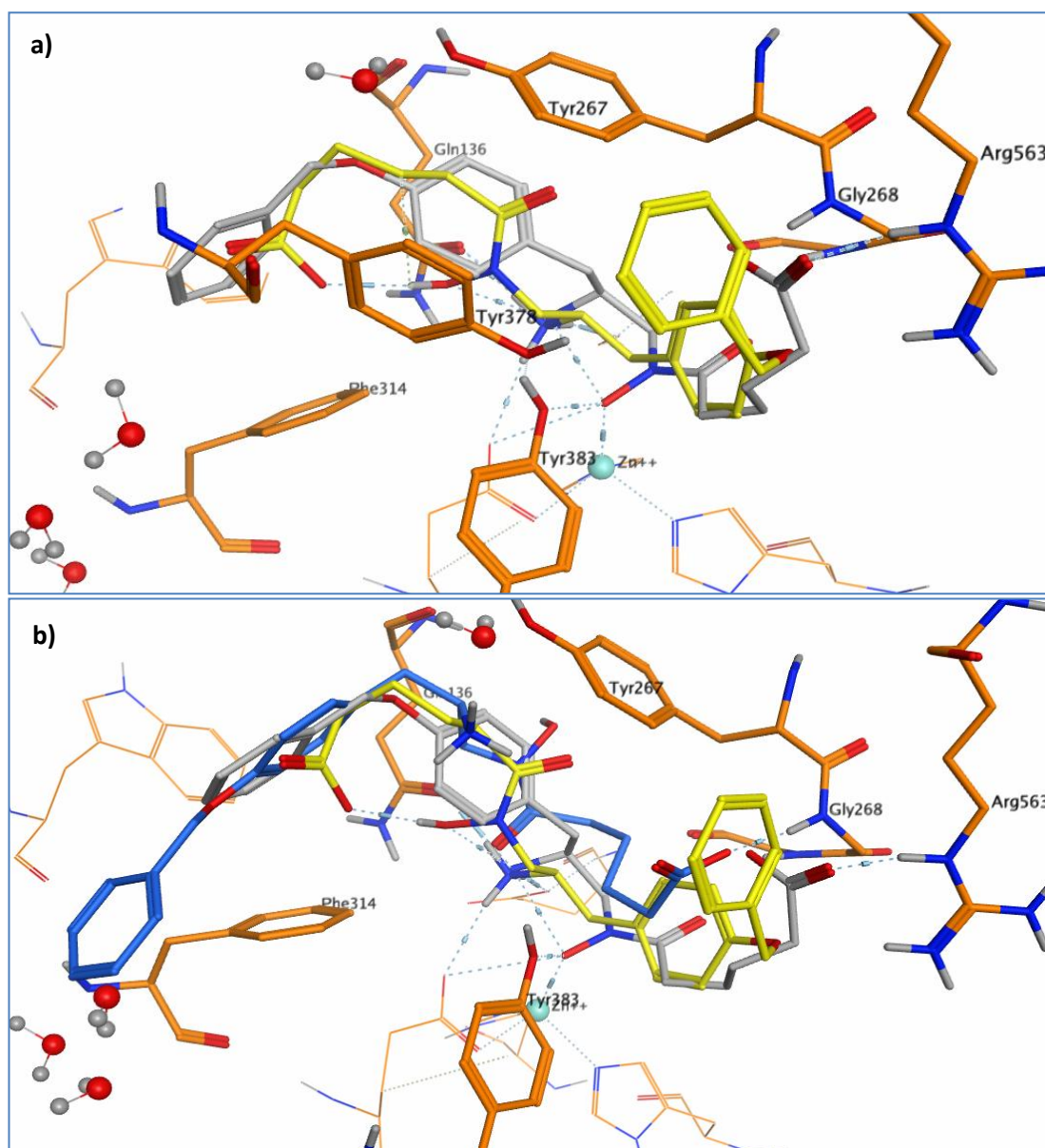


Figure 80: a) Top scoring pose of **2** in yellow and its crystal pose in light grey; b) top scoring pose without waters in yellow and with water in blue, crystal pose in light grey



### 5.8.3. GSK ligands

As the 1LOZX system was modified by the removal of waters, it is also important to verify and assess whether this alteration affects the docking of GSK ligands. Therefore, **7**, **8** and **9** were re-docked in the modified 1LOZX model.

#### 5.8.3.1. *Docking of 7 in modified 1LOZX*

The top scoring pose of **7** interacts with Gln136 through its protonated amine and there is also an intramolecular hydrogen bond between the oxygen and the NH of the [3.3.1] system. The carboxylic acid is engaged in a hydrogen bond with Gly268 (*Figure 81a*). When comparing the top scoring poses in the hydrated and the dehydrated systems, they are identical apart from a slight rotation of the terminal phenyl (*Figure 81b*).

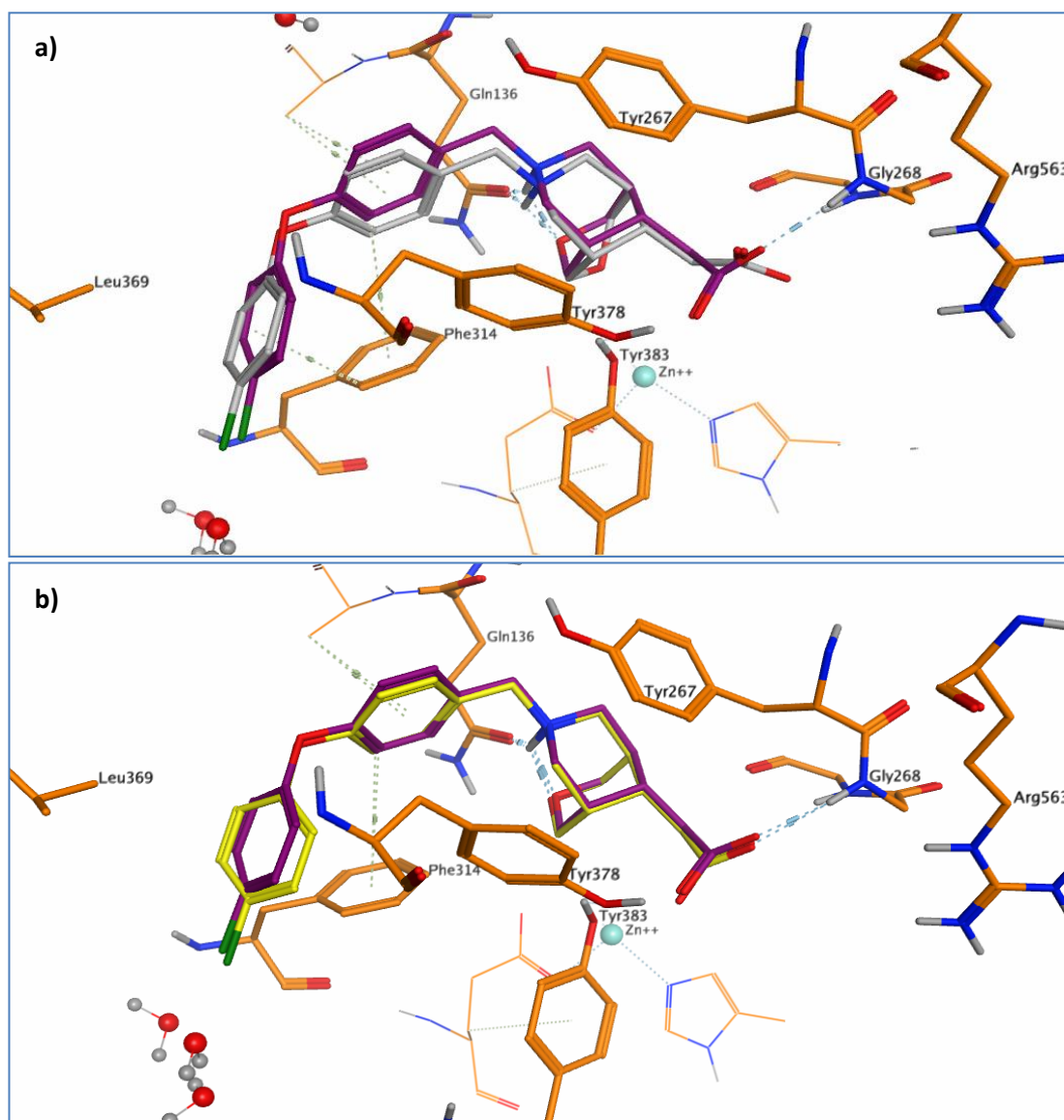


*Figure 81:* a) Top scoring docking pose for **7** in purple when waters near the zinc are removed and its crystal pose in light grey; b) Comparison of top scoring docking poses with waters in yellow and without waters in magenta.

### 5.8.3.2. Docking of **8** and **9**

The top scoring pose of **8** interacts with Gln136 through its protonated amine and with Tyr378 through the carbonyl of its carboxylic acid moiety (*Figure 82a*). There is also an intramolecular hydrogen bond between the oxygen and NH of the [3.3.1] system. Comparing the top scoring poses when docking with and without waters showed that the only difference was the orientation of the ester moiety and the terminal phenyl ring being flipped, as seen in *Figure 82b*.

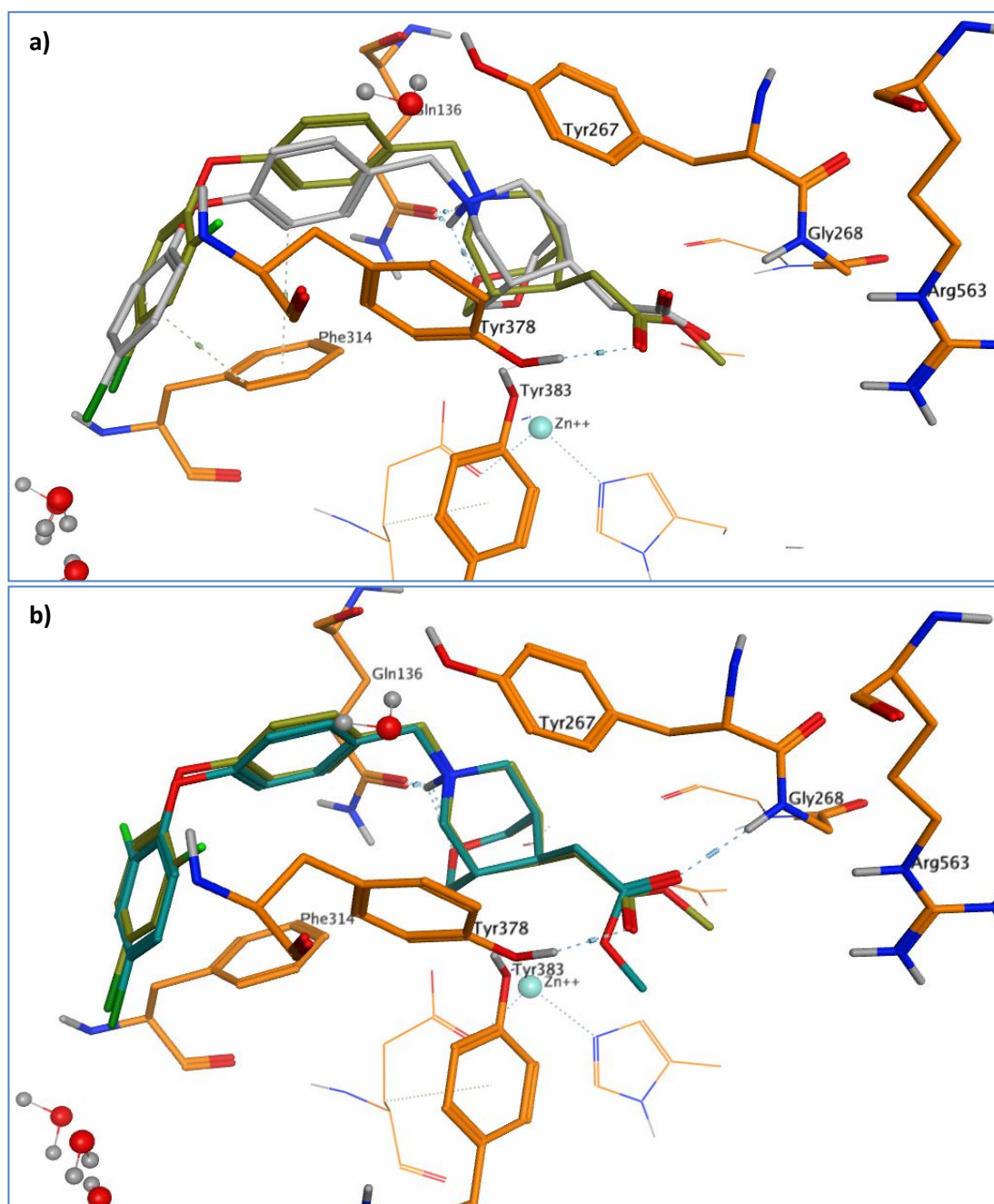


*Figure 82:* a) Best scoring pose for **8** in yellow and crystal pose for **1** in light grey; b) comparison of top scoring pose with waters in turquoise and without waters in yellow.

The top scoring pose of **9** interacts with the binding site through its protonated amine to Gln136 and through the carbonyl of its ester functionality to Gly268 and

Gly269 (Figure 83a). There is an intramolecular hydrogen bond between the oxygen and the NH of the [3.3.1] system. Comparing top scoring poses when docking with and without waters demonstrates that they are equivalent, with the ester group rotating to interact with Gly268 and Gly269 in the system without waters (Figure 83b).

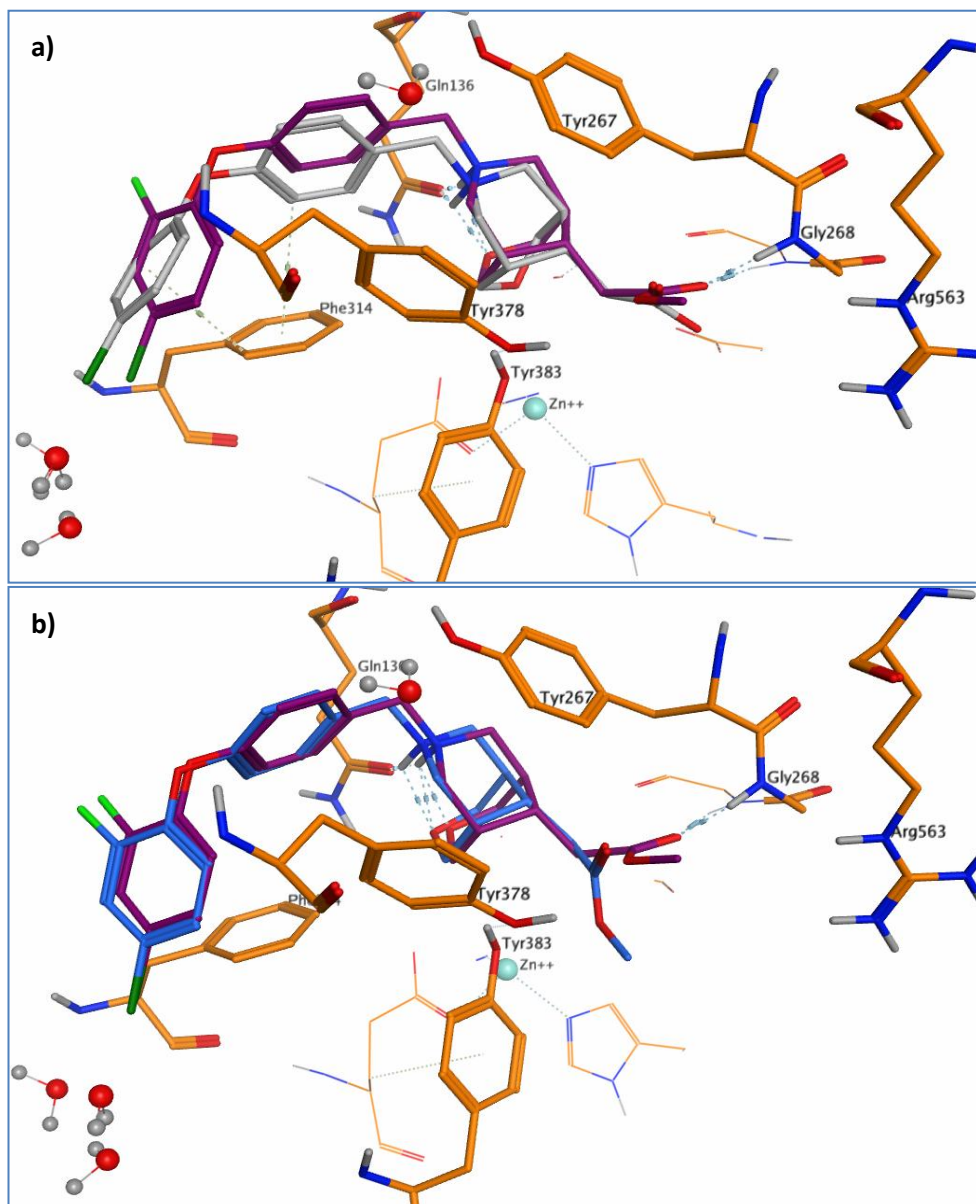


Figure 83: a) Best scoring pose 9 in purple and crystal pose for 1 in light grey; b) comparison of top scoring pose with waters in blue and without waters in purple

#### 5.8.4. Conclusion

Both systems studied are suitable for docking of GSK compounds. However, neither system is particularly appropriate for the docking of known LTA4H ligands. The known ligands are sometimes rather different structurally to the proprietary ligands and in all cases are more flexible. Removal of water molecules near the zinc atom can help in some instances but also gives too much free space for the program to explore. Indeed, often the molecules were placed in the opposite orientation to the crystal pose and the correlation of the score with molecular weight suggests that there are no specific constraints on the system that could otherwise prefer one pose over another.

## 5.8.5. Finding water hot-spots in 1LOZX

### 5.8.5.1. *Using SuperStar*

The truncated crystal structure 1LOZX was loaded into SuperStar and the oxygen water probe was selected to generate composite propensity maps. The first run was performed on CSD data with the rotatable (O, N, S)-H bond option turned off. The resulting map is shown in *Figure 84*.

The crystal waters from 1LOZX were uploaded to allow a straightforward evaluation with the propensity map. The comparison between the composite propensity map and the crystal water molecules showed that seven of the crystal waters corresponded to a high density point. When bringing the crystal pose of ligand back in, two of the predicted water high density points are occupied by the carboxylic acid moiety of the ligand (*Figure 84b*). Also, there is a high density point above the zinc atom that is unoccupied by any crystal waters. It is important to note that a water molecule that was positioned above the zinc in the original 1LOZX crystal structure was removed during preparation of the protein due to short contacts with other surrounding waters as well as the ligand. The propensity map shows that the oxygen of the ligand is also close to another nearby high density point. This particular area of the binding site is well occupied by two crystal waters and the oxygen of the ligand. One of the waters was found by the propensity map, whilst the other water sat near to two density points, one of which is positioned above the zinc. These observations support the decision that the crystal water directly positioned above the zinc should have been removed prior to the protein preparation stage.

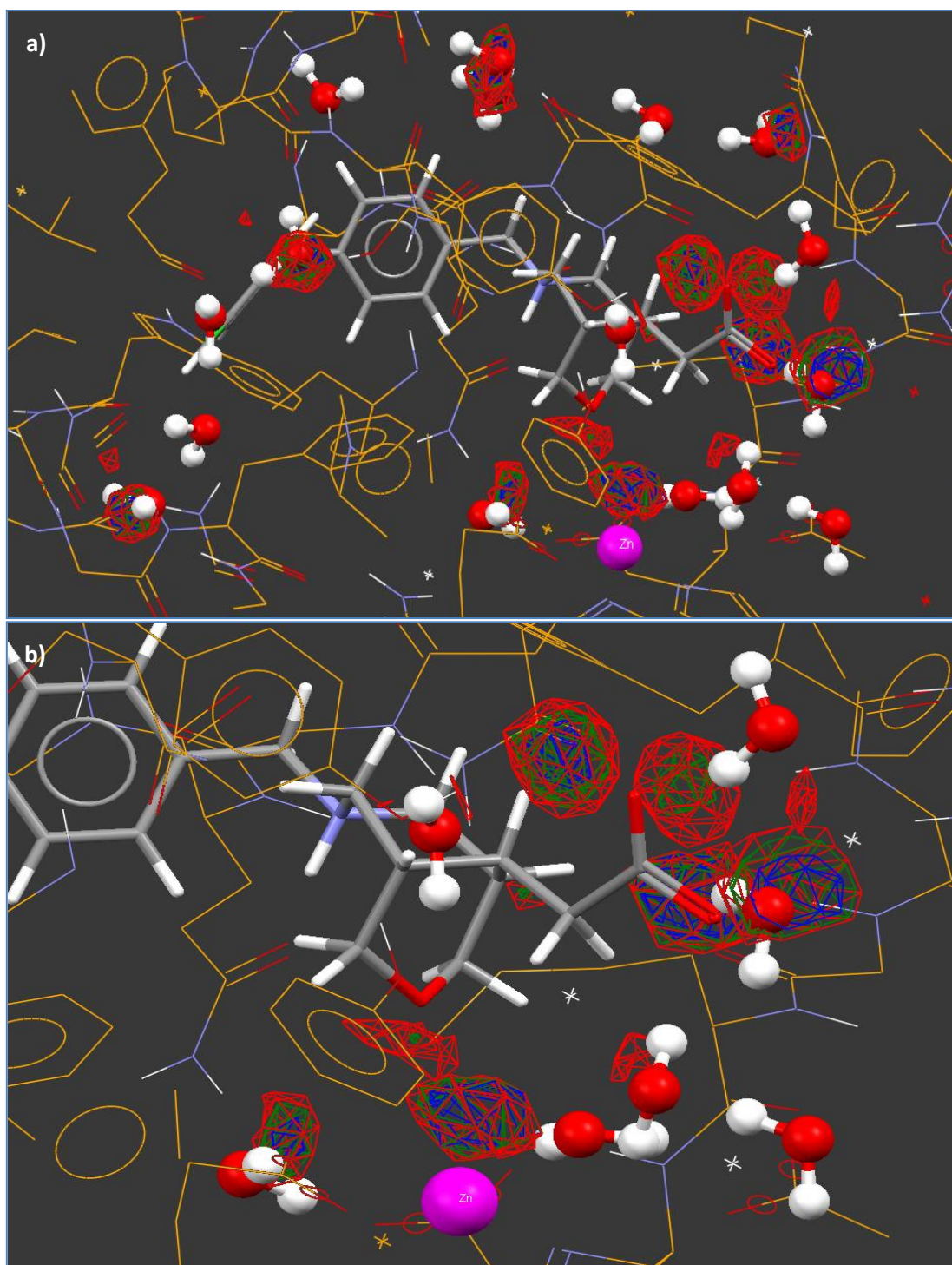
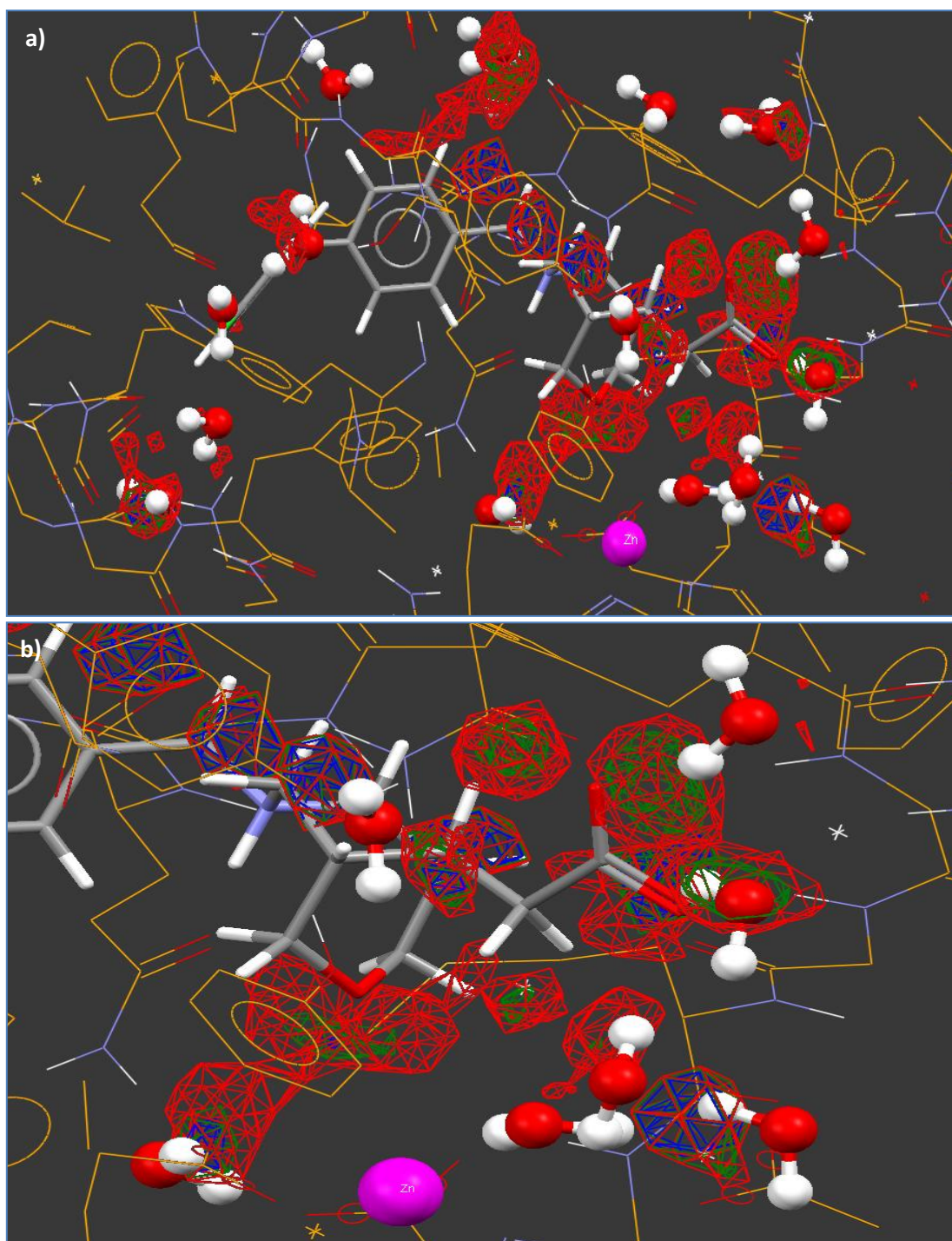


Figure 84: a) Composite propensity map using the water probe and CSD data; crystal waters were also added (shown as balls and sticks); b) close up on the area near the zinc atom

The same experiment was repeated using PDB data as opposed to CSD data to generate the propensity map in order to assess whether the two different sources would have an effect on the resulting maps. The propensity map obtained from PDB data using the water oxygen



probe is shown in *Figure 85*. The propensity map matched nine crystal water molecules, hence performing better than the map generated from the CSD data. Again on this map, there is high density area above the zinc atom. This area of high density is also very close to the oxygen atom of the ligand. The location where the carboxylic acid of the ligand is positioned was also represented by two high density points. An additional observation that can be made for this map was that some water densities can be observed were the ligand is bound, suggesting the displacement of water molecules upon binding.



*Figure 85:* a) Composite propensity map for the water probe in 1LOZX using PDB data; crystal waters were added for comparison (shown in balls and sticks); b) close up on area near the zinc atom

Overall, there is a good agreement between the CSD and the PDB data, with more correspondence of the PDB based propensity map with the experimental data.

In order to assess whether the ligand can add any information to the water network of the protein, it was used as the template to compute a propensity map, using the oxygen water probe and CSD data. The resulting map is shown in *Figure 86*. There were only a small number of density points: a main area around the ether oxygen, another one near one of the oxygens of the carboxylic acid group and the last one near the protonated amine. When adding the protein binding site back, the propensity map of the ligand for the water probe did not correspond to any of the crystal waters. However, the density point near the protonated amine corresponded to the position of the carbonyl oxygen of Gln136. The other two high density areas did not match with any of the binding site atoms.

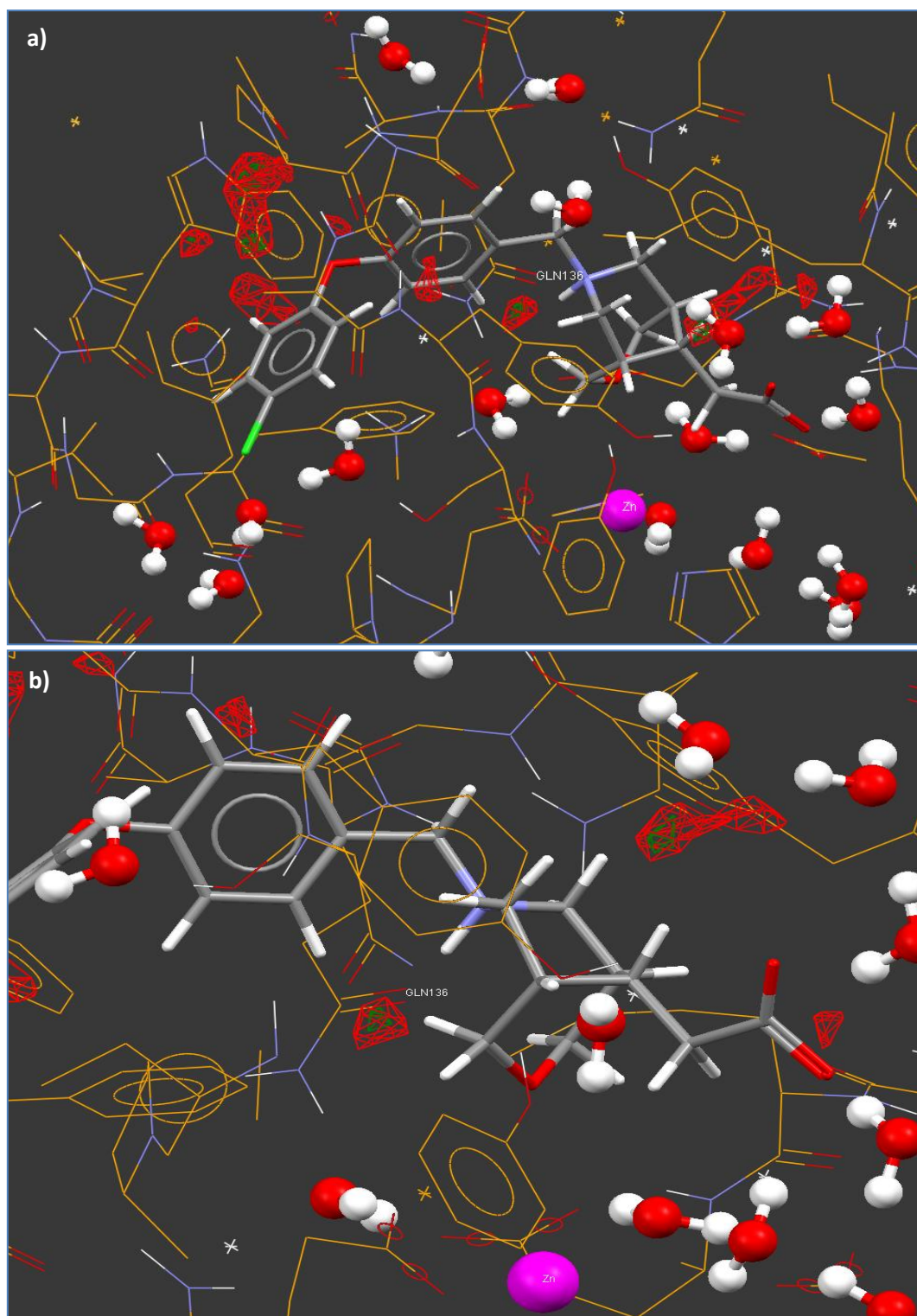


Figure 86: a) Composite propensity map using the water probe around compound **7** against CSD data; crystal waters were added for comparison; b) close up on density near the carbonyl of Gln136

#### 5.8.5.2. Using GRID

The water probe was run in the 3D grid of 1LOZX binding site. The resulting energy map was displayed over the binding site and ligand **7** as well as the crystal waters were imported back in order to compare the computed hot-spots to experimental observations (*Figure 87* where the contouring was displayed at -10 kcal/mol). Eight of the crystal waters were matched by an energy hot-spot. It is important to note that the crystal water adjacent to the zinc that was also identified by GRID, whereas the water located directly over the zinc atom was not (this water is highlighted in the yellow box in *Figure 87a*). This confirms the observation made when running SuperStar and again supports the decision to remove the water molecule. The oxygen atom of the [3.3.1] system also fell into the hot-spot above the zinc atom, as seen in the SuperStar maps.

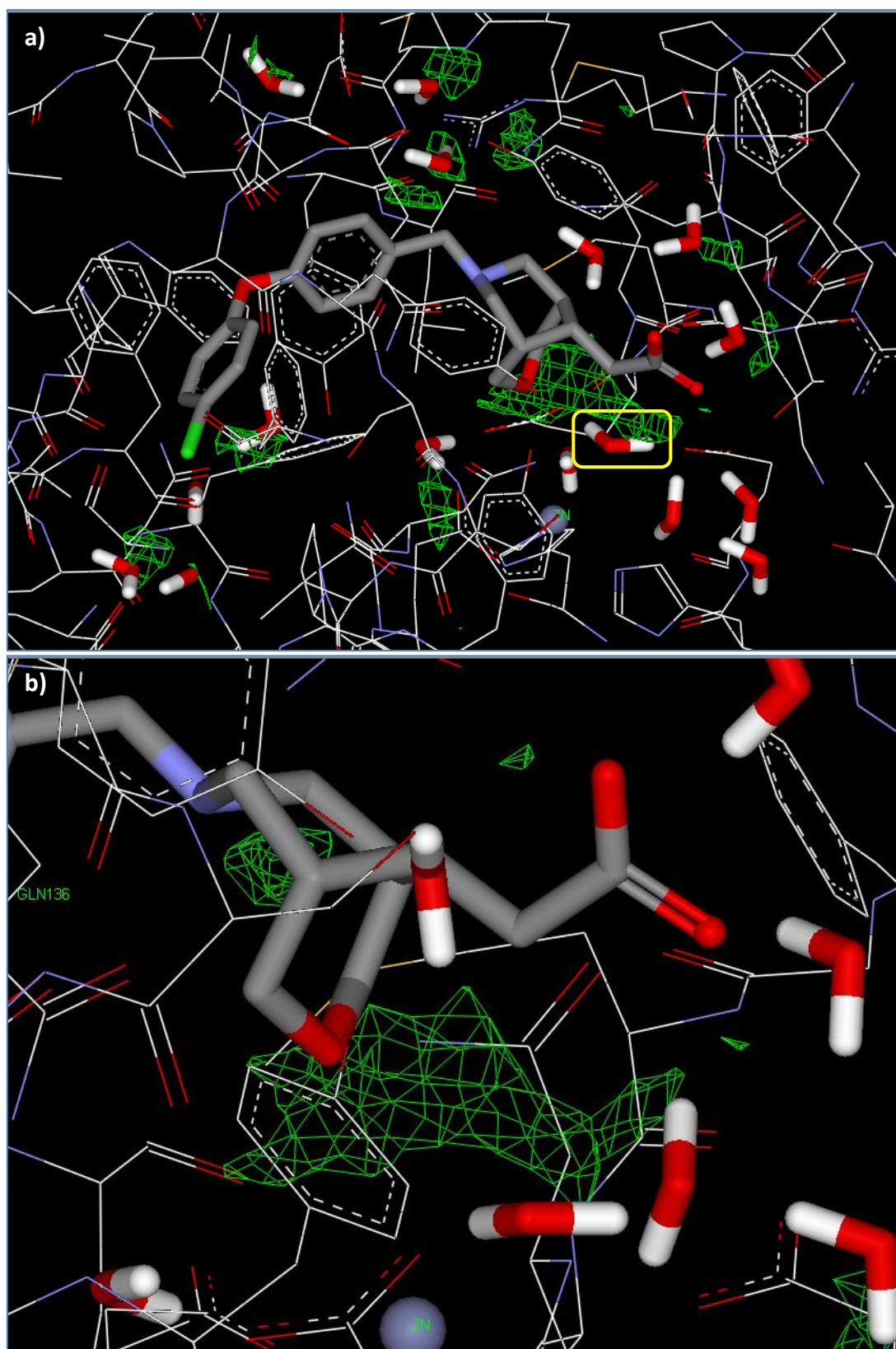


Figure 87: a) Energy map for the water probe, in green mesh, in 1LOZX binding site, crystal waters were added back for comparison purposes; b) close up on [3.3.1] system

The ligand was also used as an input to GRID to verify whether running the water probe around it would add more information about the water network in 1LOZX. The resulting energy map is shown in *Figure 88*, with the contouring at -3 kcal/mol. The area near the [3.3.1] system is completely surrounded by an energy hot-spot. In particular, several amino acids, i.e., Gln136, Gly268 and Gly269, two crystal waters and the zinc atom overlay on this specific area of the energy map. As observed when using SuperStar on ligand **7**, there is a favourable energy point around the oxygen atom of the biaryl moiety. This did not correspond to any protein atom or any water molecule. When increasing the contouring to -4 kcal/mol, this hot-spot disappeared from the map whereas the one around the [3.3.1] remained practically unchanged.

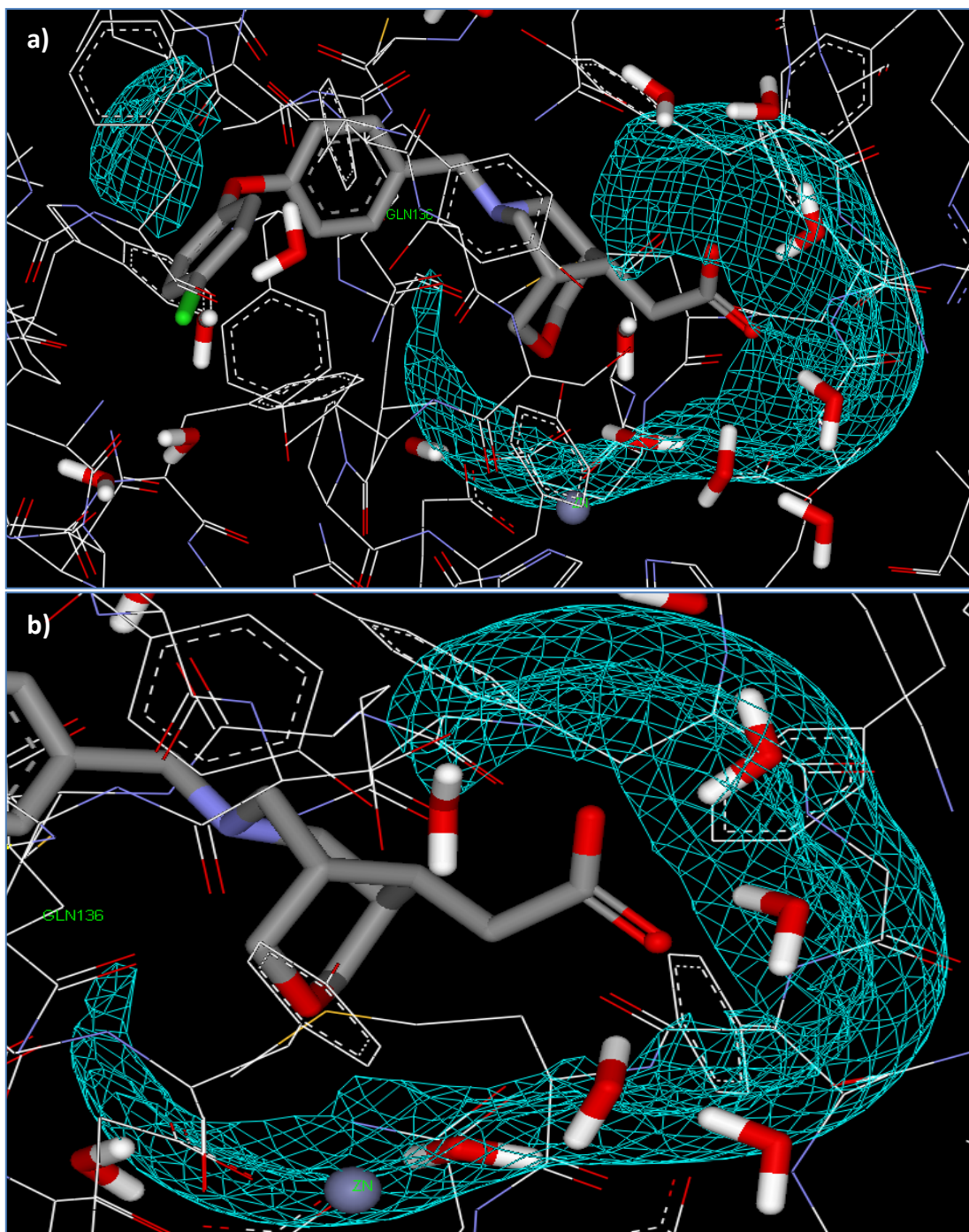


Figure 88: a) Energy map for the water probe at -3 kcal/mol, in turquoise mesh, around crystal pose of ligand **5**, crystal waters, shown in stick were added back for comparison purposes; b) close up on [3.3.1]



### 5.8.5.3. *Conclusion*

There is a good agreement between the knowledge-based (SuperStar) and the empirical energy methods (GRID) for locating possible “hot-spots” for water molecules in protein binding sites. Indeed, both methods found a number of water molecules that compared well to the crystallographic information, from the protein and the ligand perspective. When using the ligand as an input, it is also possible to find a union between the favourable interaction points and some amino acids key to the protein-ligand interaction complex. This information and information derived from other types of chemical probes can be used to modify the ligands during lead optimisation to yield ligands with higher potency. It is important to note that there are docking programmes which enable the switching on and off of water molecules in the binding site, e.g. GOLD. This has not been investigated in these studies and would be a logical extension to this work. This would enable a direct comparison between tools like GRID and Superstar and docking programmes in terms of predicting important water locations.

### 5.9. Conclusion

In this chapter, we investigated whether rigid docking methods could be used to differentiate between stereoisomers of known compounds. This was achieved through the docking of proprietary ligands in LTA4H. The GOLD and Glide docking software packages were evaluated to ensure that it was possible to re-dock the native ligand into the protein crystal structure. This benchmarking exercise demonstrated that GOLD was successful at identifying the correct binding pose for this system, whereas Glide was not. It was also observed that Glide was unable to maintain planarity of the aromatic rings in the ligand and

as such GOLD was used for all subsequent docking simulations of the GSK proprietary, as well as public domain, ligands.

The issues observed with maintaining the correct ring geometries in the case of the native ligand, raised the possibility of whether GOLD would be able to reproduce the correct conformation for the unusual [3.3.1] saturated tricyclic moiety that is present in the GSK proprietary ligands. Therefore, all possible conformations of the tricyclic moiety were constructed and docking simulations were carried out to determine whether the lower energies conformations could be reached during the docking run, regardless of the starting conformation. These simulations revealed that the chair-chair conformation was the lowest energy conformation, followed by chair-boat, which is consistent with the conformation for this system that is observed in the crystal structure, 1LOZX. Furthermore, it was found that only the boat-boat starting conformation could be problematic as GOLD was unable to flip the ring corners in this instance. However, the other starting conformations were not a constraining factor for docking in GOLD.

The next factor that was evaluated in our benchmarking of the docking process was the number of iterations of the genetic algorithm that were used in the docking simulations. It emerged that there was no difference in terms of results between 10 and 100 iterations. This was tested on a number of ligands to dock in 1LOZX. In addition, *t* tests were run to confirm the qualitative observations of the docking scores. As a result, the remainder of the docking studies were performed with 10 iterations of the genetic algorithm.

Having carried out these evaluations and established the limits of the methodology and the required parameters to achieve accurate docking results, the ultimate goal of this study – to assess whether docking could be used to characterise stereocenters – was investigated. The four isomers of ligand **10** were used to this end, differing by the bridge substitution

(*anti/syn*) and the carbon stereocenter on the bridge bearing a methyl group. The four isomers were docked in pairs, i.e., the two *anti* isomers were compared and similarly for the two *syn* isomers. Predictions were made based on the Goldscores and the fit of the docked poses in the binding site. Compounds were subsequently submitted for experimental verification (either via small molecule crystallography or VCD), which confirmed the predictions that were made using the docking protocol. This result demonstrates the power of rigid docking methods to discriminate between a set of closely related ligands when the docking methods are carefully evaluated and benchmarked against related systems. However, it also highlights the potential limitations of these methods as choices of scoring functions and very subtle differences in the setup of the system can drastically affect the quality of the results obtained.

To demonstrate this point the docking of public domain ligands in 1LOZX was investigated in order to assess the ability of the finely tuned model system and chosen methodology to be able to dock a wider variety of ligands. This study highlighted the fact that subtle changes in the binding site, such as the decision to retain or remove crystallographically resolved water molecules could have a significant effect on the ability of the docking method to identify the correct poses.

Given the important role of the water molecules around the zinc atom in the binding site, the decision to retain or remove waters was evaluated using two well known software packages, GRID and SuperStar. Both tools, which predict water location using different methods (empirical energy vs knowledge-based), were in agreement with crystallographic data. This encouraging result suggests that the use of such software is critical when developing a system for the docking of a diverse array of ligands into a given receptor using a rigid docking approach.

## 6. From rigid to induced fit docking

Proteins are not rigid bodies and the fact that the flexibility of the ligand only is taken into account in standard docking protocols is not representative of the reality. Induced fit docking was developed with this in mind as described in Section 2.3. The protocol designed by the Schrödinger group<sup>9</sup> has been investigated here to start with and modified depending on the outcomes from the preliminary experiments. In this chapter, the CDK2 system is examined to provide a comparison with the results published by Schrödinger.

### 6.1. Glide docking

Ligands **11** and **12** were docked into the three CDK2 crystal structures using the standard docking protocol in Glide, with SP precision as a scoring function. This experiment was performed in order to assess the results obtained from docking and to compare them with the results from the induced fit docking protocol, in terms of quality and accuracy, measured in RMSD, relative to the crystal poses. The results of the top scoring docking poses for each run can be found in *Table 31*.

Model system	Ligand	GlideScore (kcal/mol)	Ligand RMSD (Å)	Visual Assessment
1BUH	<b>11</b>	-3.5	5.8	Wrong
	<b>12</b>	-4.5	6.3	Wrong
1DM2	<b>11</b>	-6.8	0.3	Good
	<b>12</b>	-3.3	7.0	Wrong
1AQ1	<b>11</b>	-6.1	5.2	Wrong
	<b>12</b>	-12.3	0.1	Good

*Table 31:* Best docking poses for each system and their associated docking scores and RMSDs; redocking experiments highlighted in blue

The crystal poses for ligands **11** and **12** were not found in the docking poses with model system 1BUH, which is an apo structure. They could not make the correct hinge interactions and in general the docking poses were found away from the top of the site, defined by Phe80 and Lys33, because of these amino acids protruding in the binding site. It is known from other crystal structures, such as 1DM2 and 1AQ1, that Phe80 and Lys33 can occupy other conformations. They can move away from the binding site to accommodate ligands. It is expected that with the inclusion of some flexibility in the site, the quality of the docking poses should improve.

*Figure 89* shows the top docking pose of **11** compared with the crystal pose. One can see from the crystal pose that it would have clashed with amino acids Phe80 and Lys33, as shown by the orange disc representation of close contacts. Therefore, the top docking pose was found further away from Phe80 and Lys33, in order to avoid unfavourable steric contacts with the binding site. The whole molecule was flipped by 180 degrees compared to the crystal pose and was able to make one hydrogen bond interaction with the hinge, from the NH of the imidazolone to the carbonyl of Leu83.

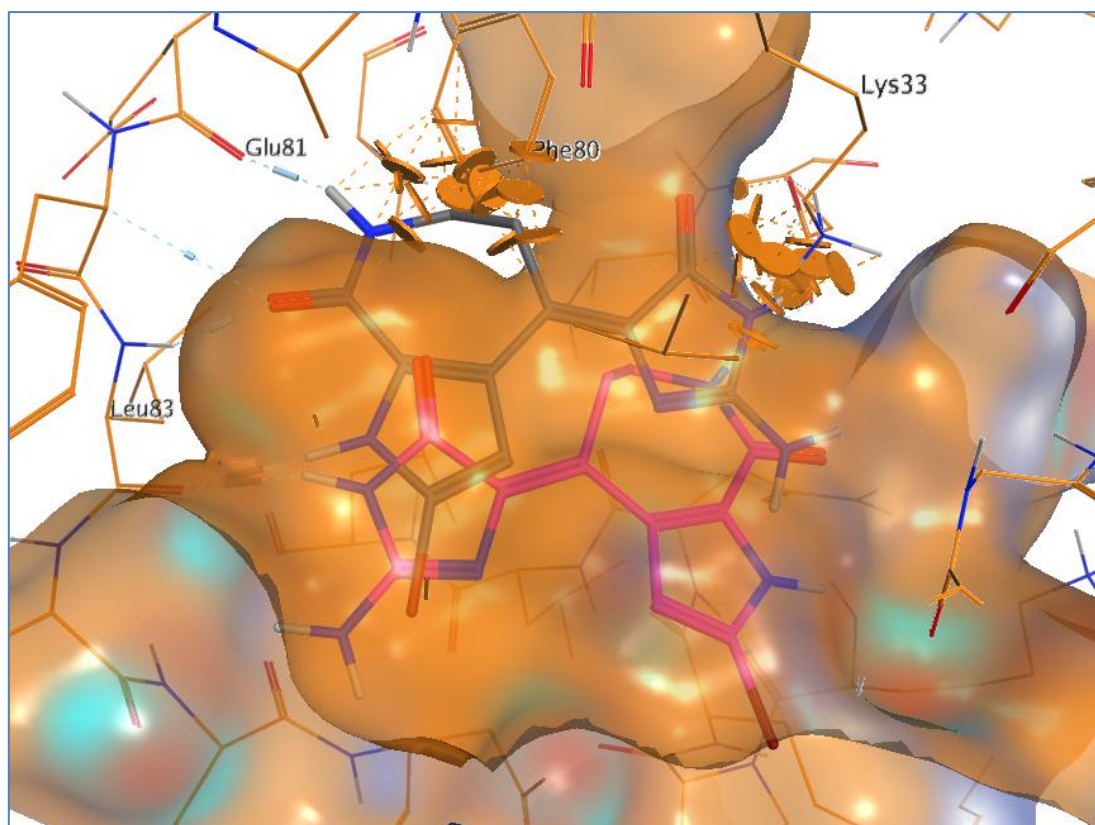


*Figure 89:* Top scoring pose of **11** docked into 1BUH in pink; crystal pose of **11** in 1DM2 in grey; the orange discs represent close contacts

In *Figure 90*, the crystal pose of **12** shows that the ligand can fit in the binding site of crystal structure 1DM2. However, docking of this ligand demonstrated that the entrance of the binding site was too tight for it to be able to occupy the same space as its crystal pose, without generating some unfavourable steric contacts. This translated into a decrease in the docking score and also a larger RMSD of 7 Å.

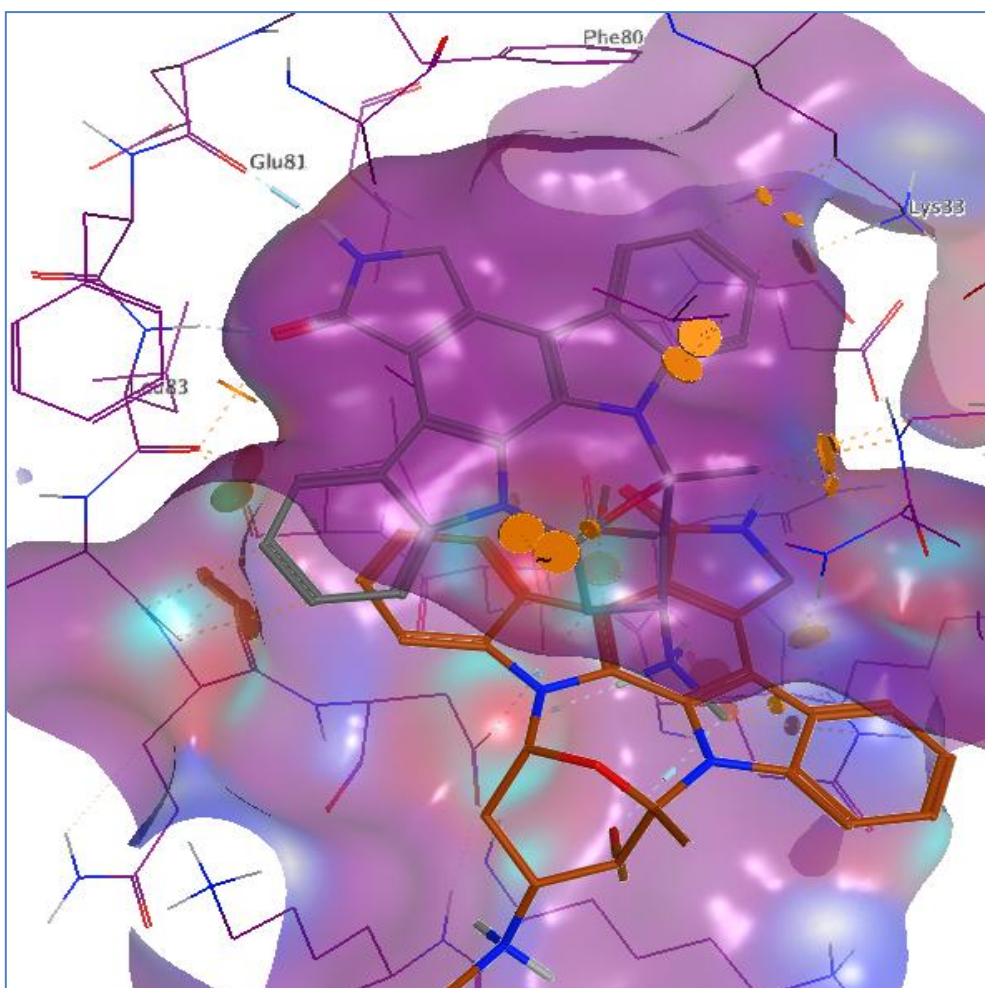
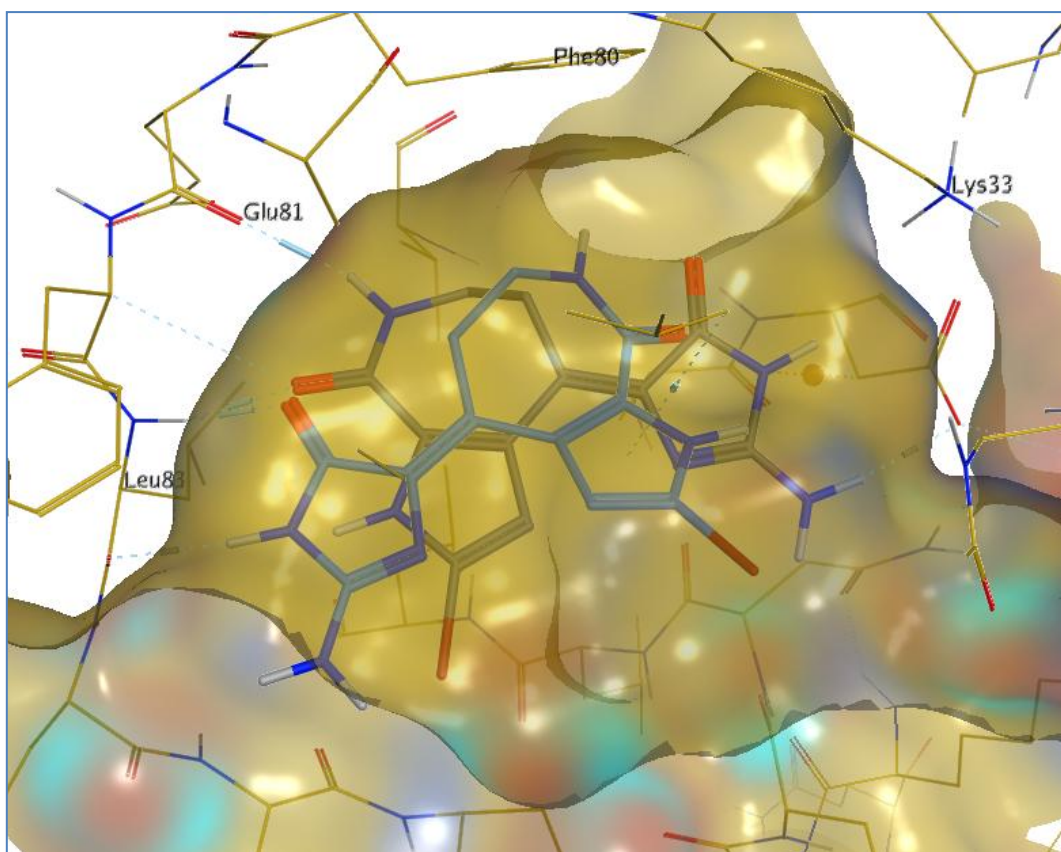


Figure 90: Top scoring pose of **12** in 1DM2 in orange; crystal pose of **12** in 1AQ1 in grey

Figure 91 displays the superposition of the top scoring pose of ligand **11** in crystal structure 1AQ1 and its crystal pose. One can see that the binding site in this case is much larger than in the two previous crystal structures. Therefore, the poses for ligand **11** were easily accommodated. The top scoring pose, even though able to make two of the three hydrogen bond interactions with the hinge, was flipped by 180 degrees from left to right compared to the crystal pose. The hydrogen bonds contributed to a better docking score (-6.1 kcal/mol), but the wrong orientation of the pose means that the RMSD was high (5.3 Å). A docking pose very close to the crystal pose could be found further down the list, in position three (GlideScore = -5.1 kcal/mol; RMSD = 0.8 Å).



*Figure 91: Top scoring pose of **11** docked into 1AQ1 in blue; crystal pose of **11** in 1DM2 in grey*

In conclusion, rigid docking was able to reproduce the crystal poses of ligands when re-docking into their original CDK2 protein crystal structure. It is important to re-dock a ligand into its native crystal structure to assess whether the docking programme and scoring function are able to reproduce the crystal pose and rank it as the top scoring pose. The main objective of docking is to dock virtual compounds, which typically have not been synthesised yet and the above results confirm that 1DM2 and 1AQ1 are suitable systems to dock other known and potential CDK2 inhibitors using Glide, as long as there are no protein movements needed for binding. Docking in the apo form of CDK2 failed on both occasions due to Phe80 protruding into the binding site. The presence of the Phe80 side chain in the site penalises poses similar to those found in 1DM2 and 1AQ1, because of steric clashes, resulting in



poorer scores. Cross-docking of **12** in 1DM2 was also unsuccessful due to the narrowness of the entrance of the binding site. However, cross-docking of **11** produced an acceptable docking pose, located in the right region of the binding site but in the wrong orientation. From these results, it was concluded that allowing some flexibility in the binding site would be beneficial for the docking of these ligands. Side chain, and to a lesser extent backbone, flexibility are the two areas to be investigated.

## 6.2. Standard induced fit docking

Following on from the results obtained in the previous section, the Induced Fit Docking protocol in Maestro was run on the same systems. This set of experiments was performed using the default parameters of IFD, and in particular none of the amino acids in the binding site were mutated to alanine during the initial soft docking step. The binding site was chosen as the centroid of the following amino acids: Gly13, Thr14, Glu81, Phe82 and Leu83. The receptor van der Waals scaling was set to the default 0.50 for the soft docking step, and twenty poses were output to be carried forward to the next stage. Residues within 5 Å of the ligand poses were optimised during the Prime refinement stage. The re-docking step was performed using SP precision as the scoring function for GlideScore.

*Table 32* summarises the results obtained for each protein model and each ligand. In all cases, only the top scoring pose according to the IFDScore is shown.

Model system	Ligand	IFDscore (kcal/mol)	GlideScore (kcal/mol)	Ligand RMSD (Å)	Visual Assessment
1BUH	<b>11</b>	-761	-6.3	3.8	Ok
	<b>12</b>	-756	-9.8	4.0	Wrong
1DM2	<b>11</b>	-588	-8.7	1.1	Good
	<b>12</b>	-584	-12.4	1.7	Good
1AQ1	<b>11</b>	-588	-7.2	4.4	Ok
	<b>12</b>	-587	-12.4	0.5	Good

Table 32: Results from the IFD run with no amino acid mutation; re-docking experiments highlighted in blue

Induced fit docking of **11** in 1BUH gave a better docking pose than in rigid receptor docking. The pyrroloazepinone core was found in a good orientation near the hinge and was able to interact through hydrogen bonds to Leu83 and Glu81. There was also a hydrogen bond from the amine on the pyrroloazepinone ring to Lys33. However, the core was flipped by 180 degrees compared to the crystal pose in 1DM2, which explained a higher RMSD of 3.8 Å. *Figure 92* also shows the movements observed from the starting protein crystal structure in red and the final induced structure in orange. Mainly Phe80 and Lys33 moved during the induced fit run. There were also some clashes between the crystal pose of **11** and the induced protein structure, notably with Lys33 and to a lesser extent with Phe80, which could explain the difference in poses.

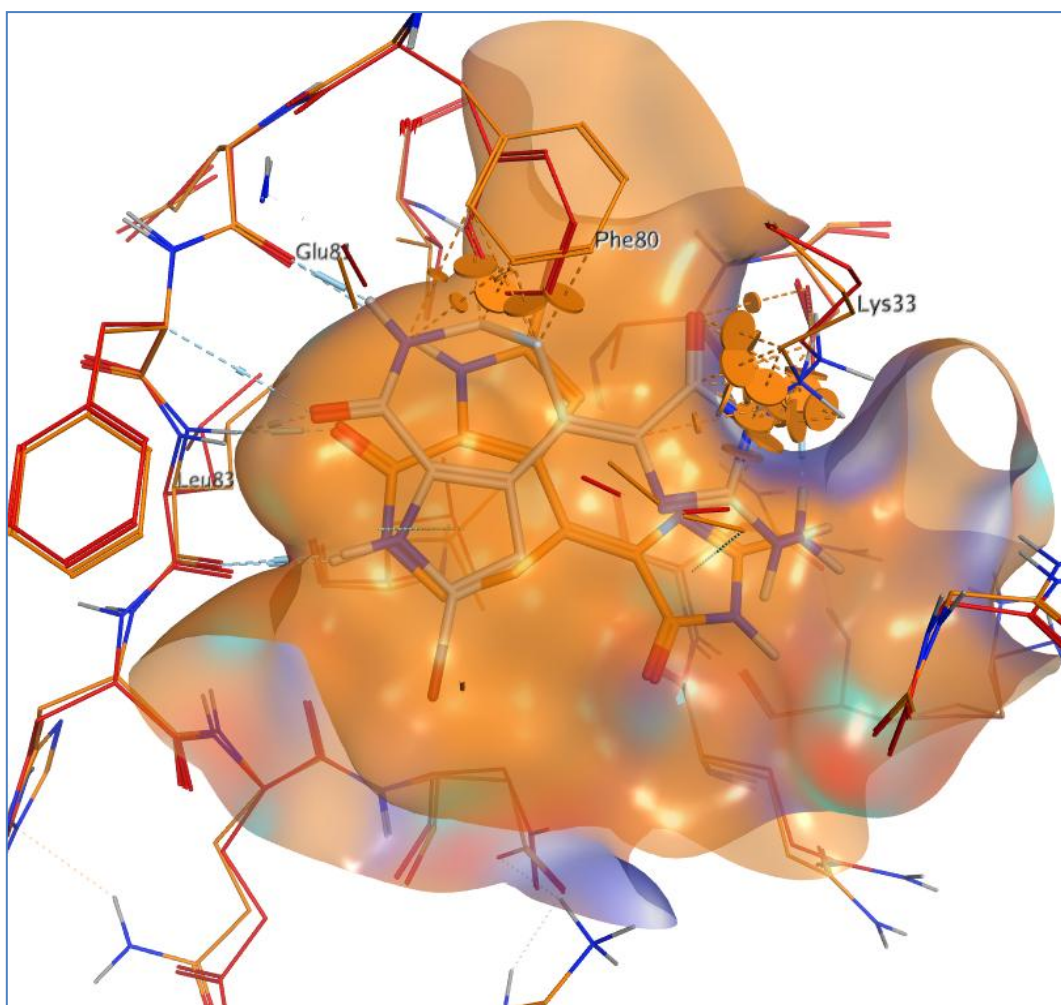


*Figure 92:* Ligand **11** docked flexibly in 1BUH in orange; original 1BUH crystal structure in red; crystal pose of **11** in grey

Ligand **12** was then docked in 1DM2 using the same default IFD protocol. The top scoring docking pose, shown in *Figure 93*, was good with the hydrogen bond interactions from the lactam to the hinge maintained. There was an additional hydrogen bond from the secondary amine substituent to the side chain carbonyl of Asn132. The RMSD of the top scoring pose was 7 Å in the rigid receptor docking experiment compared to 1.7 Å with induced fit docking. In this case, using induced fit docking proved beneficial compared to rigid body docking, both in terms of pose orientation (generating beneficial interactions) and RMSD.

The movement of the binding site amino acids here are slightly larger than seen in previous experiments. This could be due to the size of **12**, which is a large molecule.

Steric clashes between the crystal pose and the induced protein structure would have been mainly present with residues located above the plane of the docking pose, such as Ile10, Gly11, Val18 (not shown; only orange disks can be seen in *Figure 93*). This means that these amino acids should have moved out more in order to obtain a docking pose closer to the crystal pose.

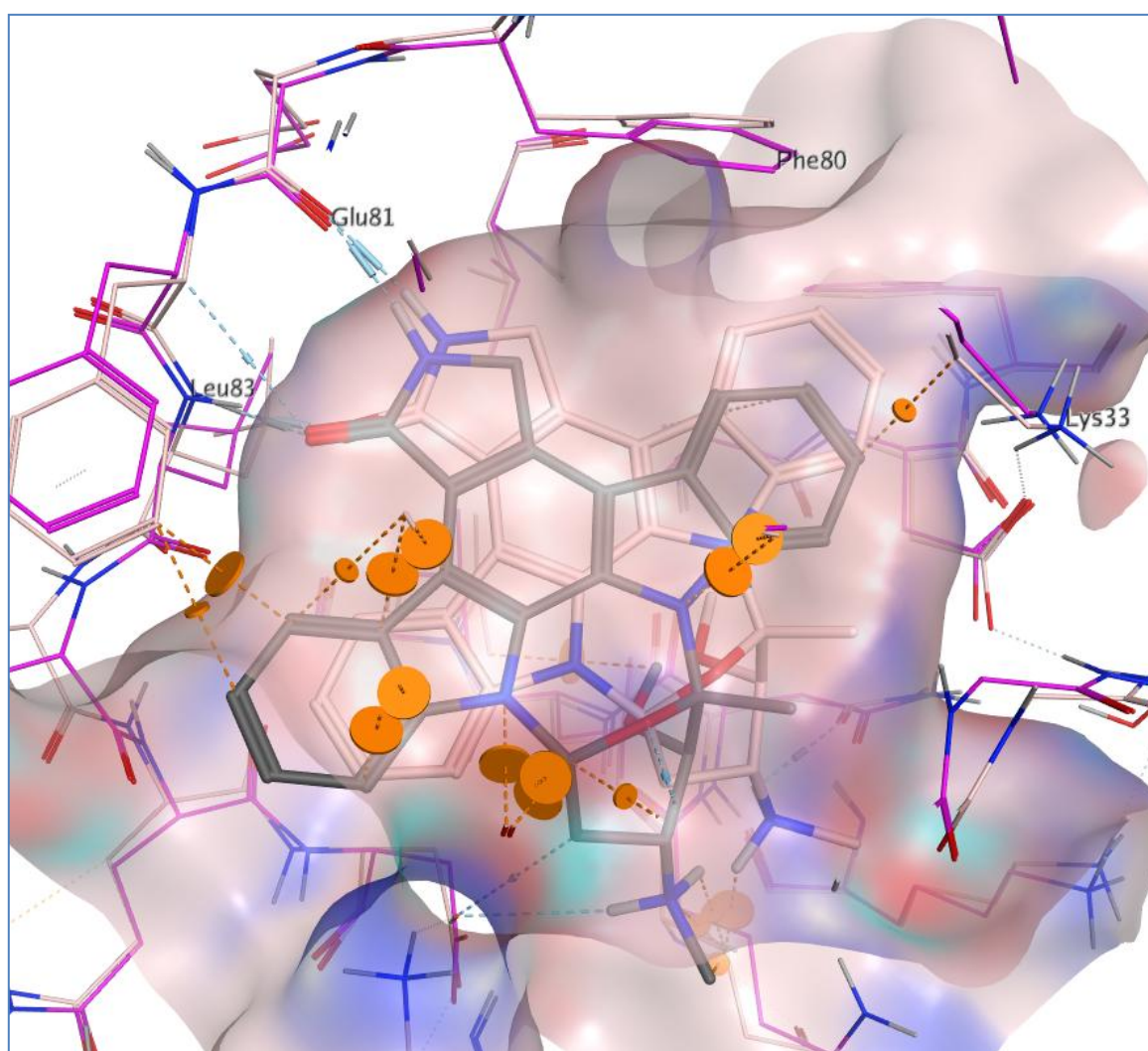


*Figure 93*: Ligand **12** docked in 1DM2 in light pink; crystal structure of 1DM2 in pink; ligand **12** crystal pose in grey

The induced fit docking of **11** in protein structure 1AQ1 did not produce a good top scoring docking pose, because the core was flipped by 180 degrees compared to the crystal pose (*Figure 94*). However, the docking pose was nevertheless closer to the crystal pose than when docking in a rigid receptor. The amide group of the azepinone ring could interact through hydrogen bonds to both the backbone NH and the carbonyl of Leu83. The amide moiety of the pyrroloazepinone ring hydrogen bonded to Lys89 and Asp86, whilst the amine interacted with the backbone carbonyl of Gln131 and with the side chain carboxylic acid of Asp145. The main amino acid movements in the binding site is the side chain of Asp145, Lys89 and Asp86, which moved in to interact with **11** as described previously. Steric clashes between the ligand crystal pose and the induced protein structure would have been found between the imidazolone and Asp145 and Lys33. This could be the origin of core flip. If the side chain of Asp145 had stayed in place, there would have been enough space to dock the ligand in a pose similar to the crystal pose.

There is a slight improvement in the RMSD when moving from rigid receptor docking (5.3 Å) to induced fit docking (4.4 Å). However, in both cases the top scoring pose was not satisfactory in terms of orientation. When inspecting docking poses further down the list, the second ranked pose was much closer to the crystal pose (IFDscore = -588 kcal/mol; GlideScore = -7.0 kcal/mol; RMSD = 1.0 Å). From an IFDscore and GlideScore perspective, the difference is minimal whereas the difference in RMSD is large. This highlights that finding the correct pose is often not an issue with placing the ligand in the binding site, but rather with scoring.

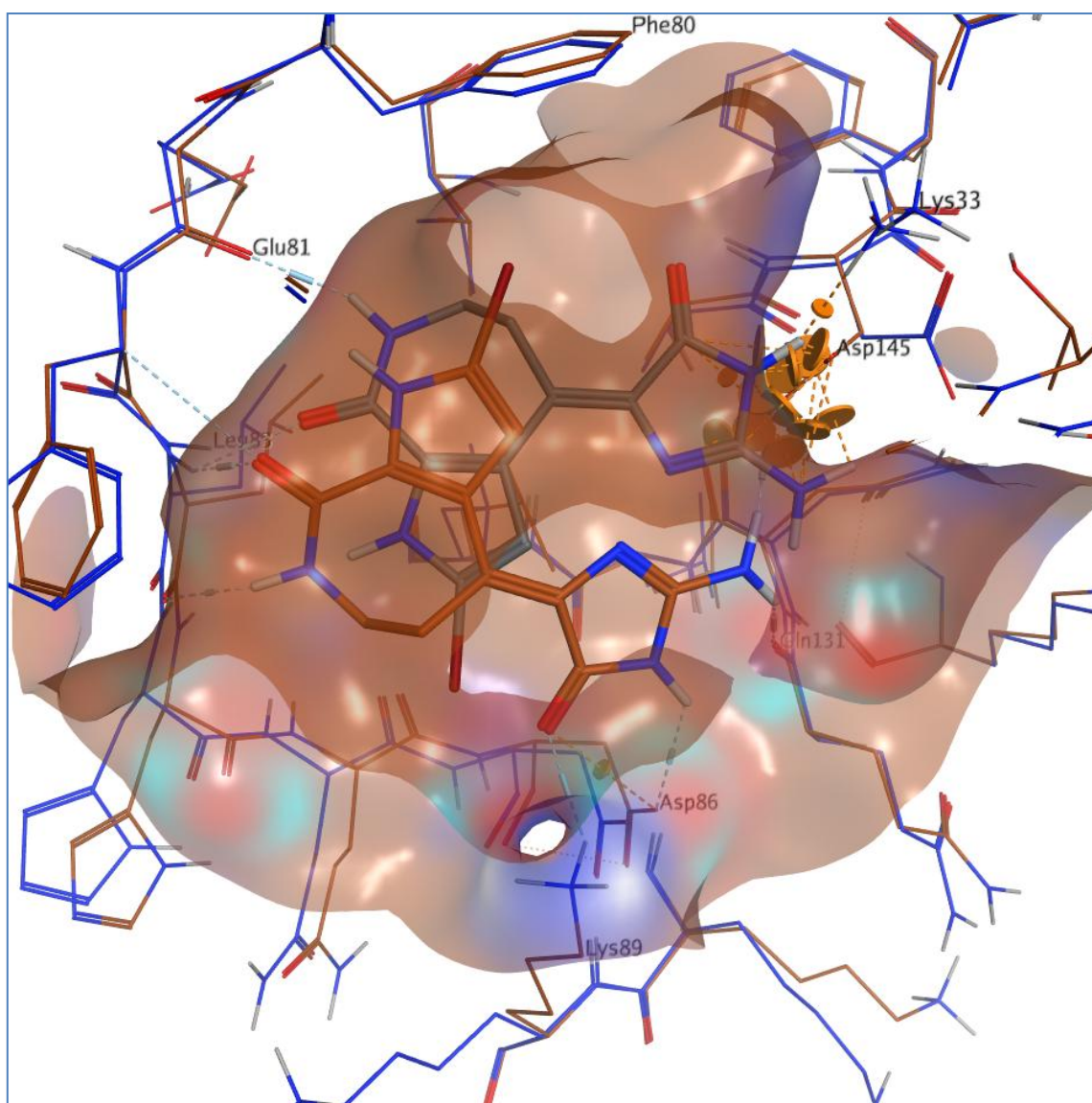


*Figure 94:* Ligand **11** docked in 1AQ1 in brown; crystal structure of 1AQ1 in blue; crystal pose of **11** in grey

In conclusion, there were some improvements in the quality of the docking poses in all cases, apart from re-docking a ligand in its own protein crystal structure for which rigid receptor docking is superior. Including some flexibility in the binding site is, therefore, beneficial for docking non-native ligands into binding sites, even though the computation time and cost is much higher than traditional rigid docking.

Residues that moved significantly during the IFD run are summarised in *Table 33*. There is a large overlap between the three systems studied (residues highlighted in bold font). There are also some residues, such as Phe80, which occur in only one system (1BUH for Phe80). Given this variation, it is critical to identify a systematic way of selecting potentially problematic residues.

System	Residues
1BUH	Ile <b>10</b> , Lys20, Lys33, Phe80, <b>Phe82</b> , His84, Gln85, <b>Lys89</b>
1DM2	Ile <b>10</b> , Glu12, Lys20, <b>Phe82</b> , <b>Lys89</b> , Gln131, Lys129
1AQ1	Ile <b>10</b> , Glu12, Lys33, <b>Phe82</b> , <b>Lys89</b> , Asp145

*Table 33:* Summary of residues that moved significantly in IFD runs when cross-docking

### 6.3. Induced fit docking with automatic mutations

It is possible to truncate amino acid side chains near the ligand in order to prevent them from interfering with the search for the correct binding pose. This could be beneficial with the CDK2 protein structures studied as amino acids such as Phe80 or Lys33 sometimes protrude in the binding site and impact on the quality of the docking poses.

A modified Induced Fit Docking protocol was, therefore, run on all of the systems. It is not clear why certain specific parameter thresholds were chosen by the Schrödinger group.<sup>9</sup> A discussion about their IFD protocol and the way they developed it did not bring any light on the rationale behind the thresholds used as defaults.<sup>150</sup> However, for the sake of consistency, the following set of experiments was performed using the default parameters of IFD, based on the Schrödinger paper.<sup>9</sup> Selected residue side chains within 5 Å of the ligand can be truncated and mutated to alanine during the initial soft docking step. They are then mutated back to the original side chain before the optimisation step. The amino acids

which undergo mutation were automatically selected based on the temperature factor (B-factor) in a 5 Å radius from the binding site. The threshold for the B-factor is 40 and the maximum number of residues to mutate is three – these limits are hard-coded. It was argued in the Schrödinger paper that mutating more than three residues at any one time creates too big a binding site and the docking poses obtained are consequently far away from the crystal poses. When the option of truncating amino acids is selected, the van der Waals scaling for the protein is re-adjusted to 0.70 for the soft docking step, as opposed to 0.50 in the default settings, as there should be less probability of steric clashes with the protein. This is because mutating amino acids to alanines should open the binding site and, therefore, there should result in a higher chance of finding an acceptable docking pose during step 1 of the protocol.

Table 34 summarises the results obtained for each protein model and each ligand. In all cases, only the top scoring pose according to the IFDscore is shown.

Model system	Ligand	IFDscore (kcal/mol)	GlideScore (kcal/mol)	Ligand RMSD (Å)	Visual Assessment
1BUH	11	-757	-5.3	4.1	Wrong
	12	-758	-10.8	1.8	Ok
1DM2	11	-588	-9.7	0.9	Good
	12	-771	-12.7	0.5	Good
1AQ1	11	-587	-7.4	4.4	Ok
	12	-588	-13.4	0.5	Good

Table 34: IFD results using automatic amino acid mutations; only top scoring poses shown. Re-docking experiments are highlighted in blue

Ligand **11** was docked into apo protein structure 1BUH using this procedure. As seen in the two previous docking experiments with **11** in this protein structure, the top docking pose



was flipped by 180 degrees compared with the crystal pose (*Figure 95*). There was one hydrogen bond interaction with the hinge, from the NH of the pyrrole ring to the backbone carbonyl of Leu83. The amide moiety in the azepinone ring interacted with Lys89 and Asp86, whereas the amide NH of the pyrroloazepinone hydrogen-bonded to Lys33 and the amine on the ring to Asp145. The residues that were mutated to alanine were Thr160, Val154 and Glu162, which were not found in the binding site. They were located within the first shell of amino acids around the binding site. Nonetheless, mutating these residues might have an impact of the conformation and orientation of the amino acids of the active site. However, there was not much movement when comparing the original 1BUH protein structure and the induced structure, apart from Lys33 and Lys89 which moved into the binding site to interact with the ligand. As can be seen from *Figure 95*, there were some steric clashes between the crystal pose of **11** and the induced structure of 1BUH, notably with Phe80, Lys33 and Asp145. The main hindrance to obtaining a good docking pose was Phe80, which needed to move out of the binding site. The poor choice of amino acids to mutate and the conformation of Phe80 translated to a ligand RMSD of 4.1 Å, comparable to the one obtained in the previous IFD experiment (3.8 Å, *Table 32*) but better than with rigid body docking (5.8 Å, *Table 31*).

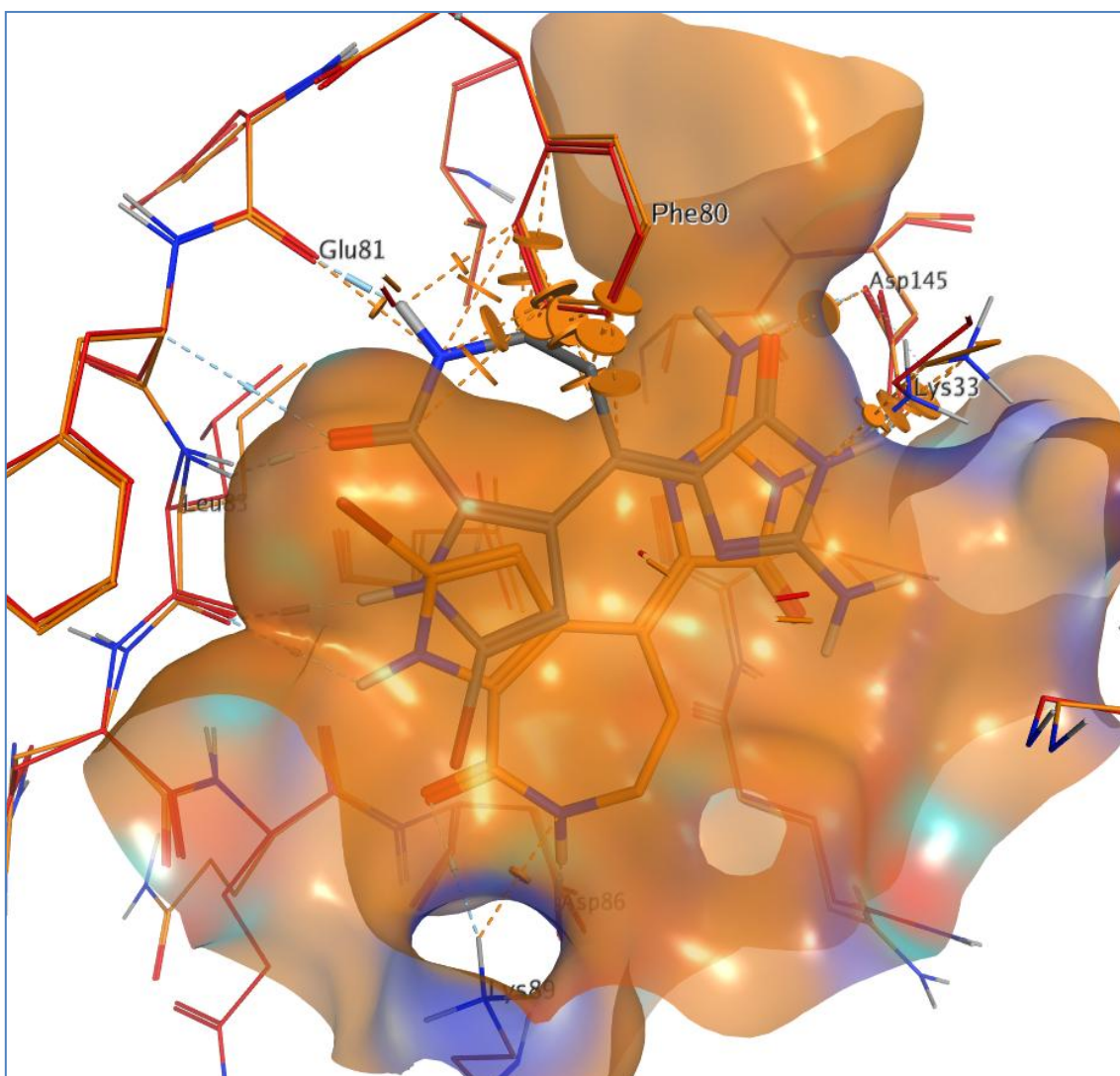
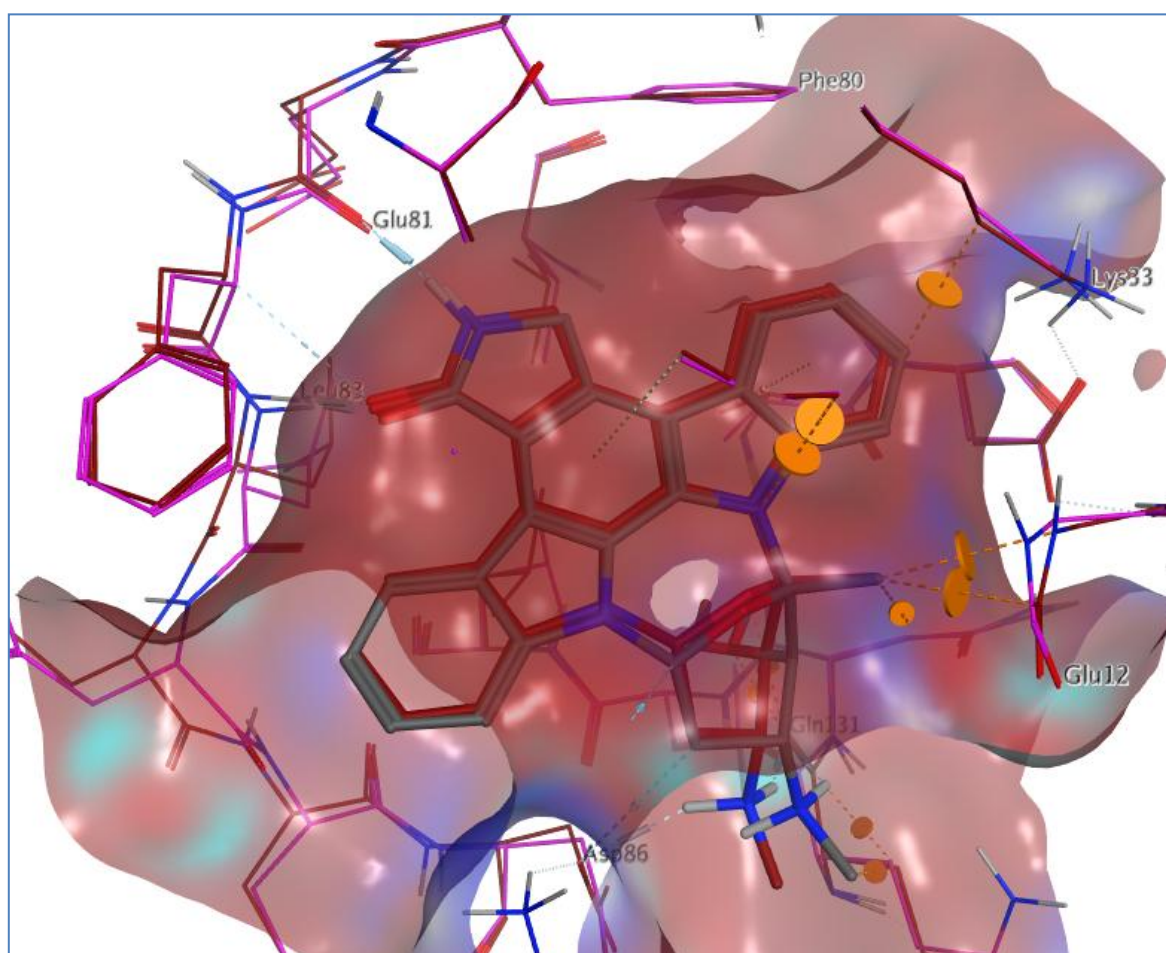


Figure 95: Ligand **11** docked flexibly in 1BUH in orange; original 1BUH crystal structure in red; crystal pose of **11** in grey

Induced fit docking of **12** in protein structure 1DM2 produced good results, with the top scoring docking pose in a good orientation compared to the crystal pose (Figure 96). In addition, it was able to make all hydrogen bond interactions expected with the hinge and with Gln131 and Asp86. From the point of view of the flexibility of the binding site, there is not much movement in the side chains but a slight movement of the backbone below the hinge region (Figure 96). The same amino acid side chains were mutated as for the other ligand, that is Glu12, Thr14 and Tyr15. The steric clashes between the ligand crystal pose

and the induced structure were minimal, notably with the side chain of Lys33, Glu12 and Val18 (not shown). The RMSD of this docking pose (0.5 Å, *Table 34*) supports the quality of the fit. This is an improvement over IFD with no mutation (RMSD = 1.7 Å, *Table 32*) and rigid body docking (RMSD = 7 Å, *Table 31*).



*Figure 96:* Ligand **12** docked flexibly in 1DM2 in red; original 1DM2 crystal structure in pink; crystal pose of **12** in grey

Ligand **11** was then docked into 1AQ1 using IFD. The top scoring docking pose obtained (*Figure 97*) showed a flipped core as seen in previous experiments. However, the hydrogen bonds to the hinge could be maintained apart from the one to Glu81. The amide of the pyrroloazepinone ring could interact with Lys89 and Asp86, whereas the amine hydrogen

bonded to Gln131 and Asp145. The side chain movements were minimal in this case, with amino acids Glu12, Leu148 and Val164 mutated to alanines. Glu12 and Leu148 are located at the edge of the binding site near Lys33, whilst Val164 was outside the site. Asp145 rotated towards the interior of the binding site which caused steric clashes, as seen with the crystal pose resulting in the flipped pose. All three experiments produced poses with similar RMSDs (4-5 Å) and none were able to reproduce the crystal pose.

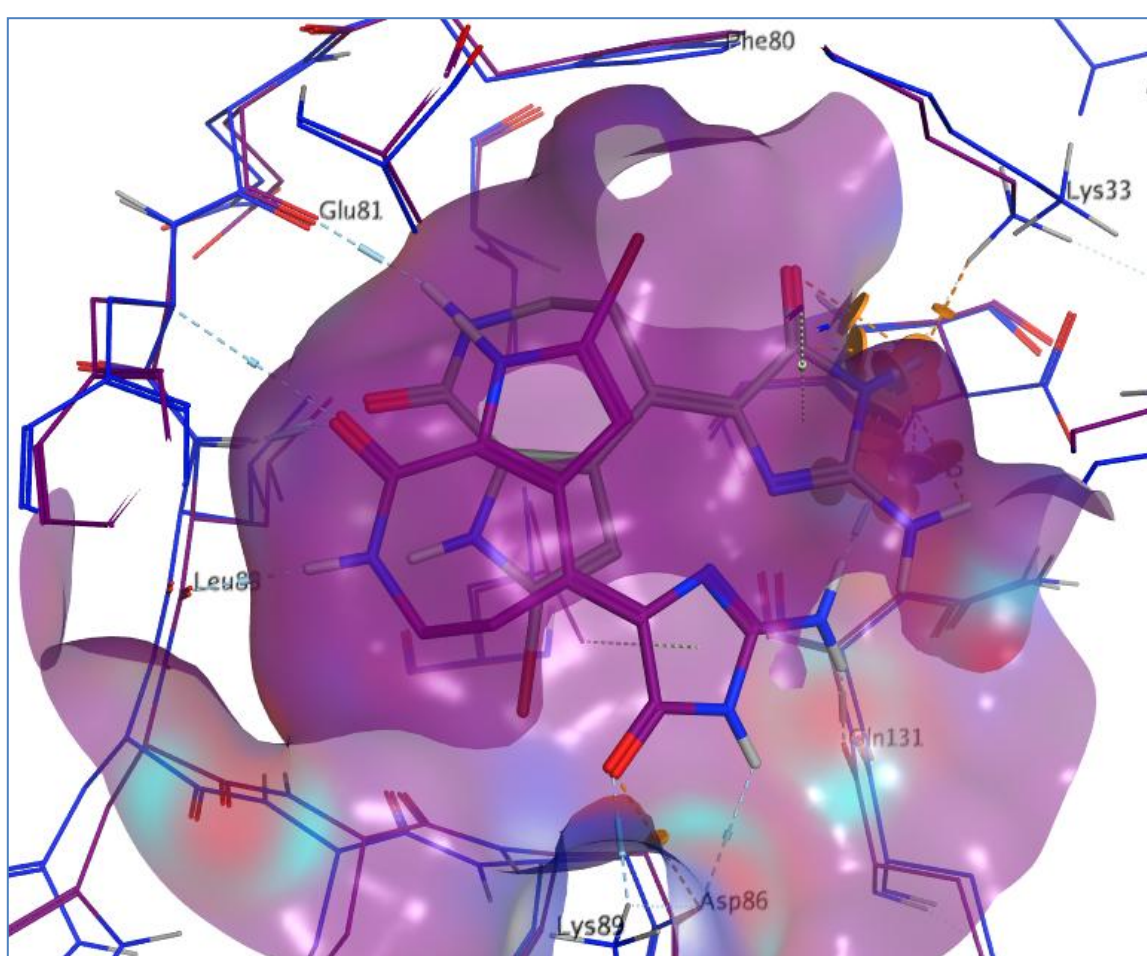


*Figure 97:* Ligand **11** docked flexibly in 1AQ1 in purple; original 1AQ1 crystal structure in blue; crystal pose of **11** in grey

In conclusion, the IFD protocol with mutations provided some improvement over the default IFD process for some of the model systems. In particular, this was the case for cross-docking of **12** in 1BUH and **12** in 1DM2. Docking of **11** in its own protein structure 1DM2 produced a better docking pose, whilst docking of **12** in its native structure 1AQ1 gave similar results. Cross-docking of **11** in model system 1BUH generated a top scoring pose which was further away from the crystal pose than the one obtained with the standard IFD protocol. Cross-docking of **11** in 1AQ1 gave equivalent poses. When the top scoring pose was different to the crystal pose, the correct pose could be found further down the list of docking poses output in the majority of cases.

The inclusion of some flexibility has had varied results on the three model systems studied here. Overall, adding protein flexibility to the docking protocol has been beneficial in all cases, apart from re-docking of ligands into their original protein crystal structure. The outcome for re-docking was not unexpected, as it was also found previously when using GOLD (see Section 5.4). The fact that amino acids were protruding in the binding site, especially in the apo crystal structure, meant that flexibility of the protein binding site was expected to improve the quality of the docking poses. This was indeed the case for model system 1BUH, with some improvement in RMSDs when using the procedure with more flexibility (*Table 35*). The same observation could be made for cross-docking **12** into 1DM2, and to a lesser extent **11** into 1AQ1.

Model system	Ligand	RMSD rigid docking (Å)	RMSD default IFD (Å)	RMSD IFD with automatic mutations (Å)
1BUH	<b>11</b>	5.8	3.8	4.1
	<b>12</b>	6.3	4.0	1.8
1DM2	<b>11</b>	0.3	1.1	0.9
	<b>12</b>	7.0	1.7	0.5
1AQ1	<b>11</b>	5.3	4.4	4.4
	<b>12</b>	0.1	0.5	0.5

Table 35: Summary of ligand RMSDs obtained with all three protocols; re-docking experiments highlighted in blue

There did not appear to be much difference in outcome between the IFD protocol with and without amino acid mutations, with the exception of docking **12** in the apo crystal structure 1BUH and 1DM2. For the smaller ligand **11**, there was not a noticeable advantage in using IFD in the standard modes.

The results obtained were different from the ones from the Schrödinger's group (Table 36).<sup>9</sup> The reasons for these discrepancies have not been fully identified. We can speculate that Schrodinger have not used the default settings and it is more likely that they have used specific parameters for these docking experiments. Direct communication with them did not provide any clarifications around these differences.

Model system	Ligand	RMSD rigid docking	Schrödinger RMSD rigid docking	RMSD IFD with mutations	Schrödinger RMSD IFD with mutations
1BUH	<b>11</b>	5.8	6.4	4.14	1.1
1DM2	<b>12</b>	7.0	6.2	0.54	0.8
1AQ1	<b>11</b>	5.2	0.6	4.39	0.8

Table 36: Comparison of ligand RMSDs to the ones obtained by Schrödinger<sup>140</sup>

#### 6.4. The effect of different chain lengths on the Prime energy

The three crystal structures have a different number of amino acids. This will have an impact on the Prime energy and in order to assess the extent of this, the common sequence between the three protein structures was studied. The three sequences were compared and any residues that were not common to the three structures were removed from consideration.

The extra 79 residues in 1BUH were deleted (marked as chain B in the PDB file): these represent CksHs1, the protein bound at the C-terminus domain of CDK2, as described in Section 3.2. Additionally, residues 36 to 39 and 149 to 163 were missing in 1DM2 and to some extent in 1AQ1, and they were deleted from the 1BUH sequence. In 1BUH, the terminal residues 295 to 299 were missing compared to 1DM2 and 1AQ1 and, therefore, they were removed from the 1DM2 and 1AQ1 sequences. In addition, residues 44 to 45 and 162 to 163, which were not solved in 1DM2, were deleted from the 1AQ1 sequence. Similarly, residues 36 to 39 and 149 to 163 were not present in 1DM2 and to some extent in 1AQ1, and therefore, were discarded from the 1BUH sequence. The common sequence between the three systems was 268 amino acids long. The terminal nitrogens and carbons of amino acids were capped with a N-methyl amide or a N-acetyl using the Protein Preparation tool in Maestro. In all cases, the residues removed from the sequences are remote from the binding site. *Table 37* gives a summary of the residues removed in the three different systems.

Model system	Residues removed	Number of residues removed
1BUH	Arg36 – Thr39, Ala149 – Val163	19 (not including CksHs1)
1DM2	Pro45-Ser46, His295 – Leu298	6
1AQ1	Val44, Pro45, Glu162 – Val163, His295 – Leu298	8

Table 37: Summary of residues which were deleted from the different protein structures

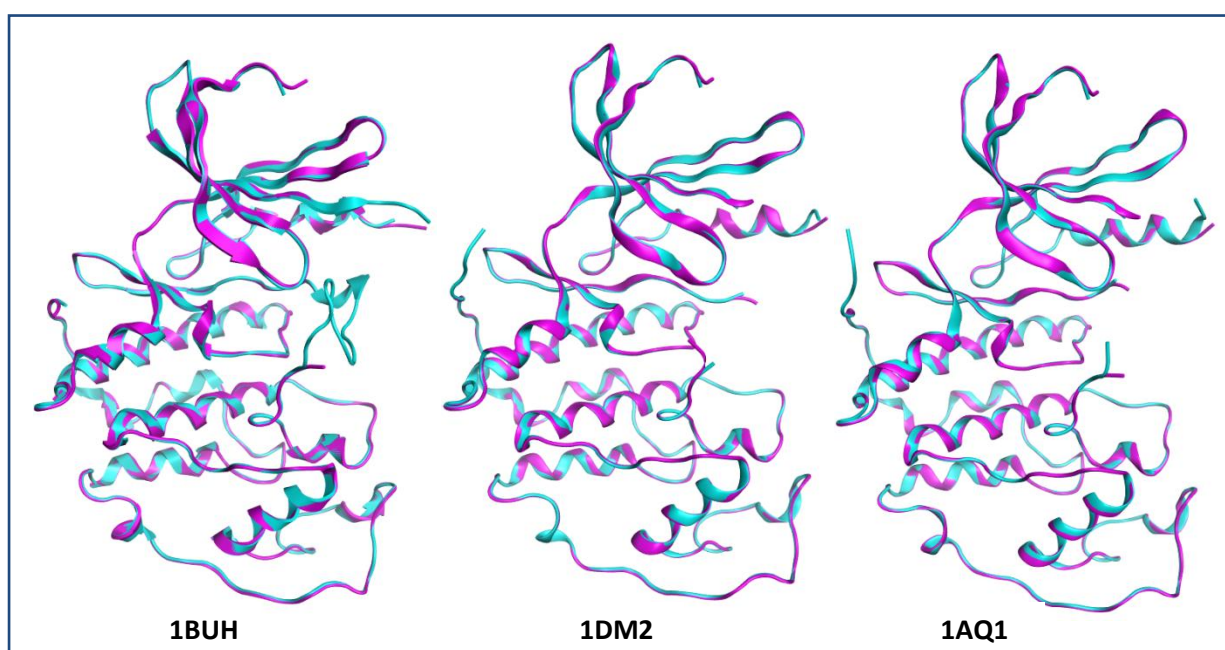


Figure 98: Comparison of all three CDK2 structures before (turquoise) and after normalisation (magenta)

The Prime energies for the three systems before and after normalisation were computed (Table 38). A larger increase in Prime energy can be noticed after normalisation of the sequence in the 1BUH system. This could be justified by the fact that 19 amino acids were removed from the sequence. There is a lesser increase in Prime Energy for the 1AQ1 system, which lost eight amino acids from the normalisation step. The Prime Energy is not affected as much by the normalisation for 1DM2 either, for which six amino acids were removed.



When comparing the 1DM2 and 1AQ1 systems, the main difference in sequence from the normalisation is the removal of Glu162 and Val163. It could be argued that the difference in Prime Energy between these two systems is due to the removal of these two residues. The initial Prime Energies were already 100 kcal/mol apart and ended up within 45 kcal/mol of each other. The Prime Energy data suggests that the normalised 1DM2 system is the most unstable of all three, followed closely by 1BUH and 1AQ1 being the most stable.

<b>Model system</b>	<b>PE before normalisation (kcal/mol)</b>	<b>PE after normalisation (kcal/mol)</b>	<b><math>\Delta</math>PE (kcal/mol)</b>
1BUH	-11866	-11135	731
1DM2	-11332	-11131	201
1AQ1	-11427	-11176	251

*Table 38:* Summary of Prime energies. PE = Prime Energy

In order to further understand the effect of the difference in amino acid length, a comparison of the docking scores was performed. Ligand **11** was chosen as an example and it was docked flexibly in the three model systems starting from the common sequence. These results were then compared to the ones obtained previously in the equivalent set of experiments (see Section 6.2). They are summarised in *Table 39*. The GlideScores in the three systems have all improved, whilst the IFDScores have increased in line with the change in sequence length.

The largest difference in IFDScores is seen for 1BUH. The new IFDScores are now all comparable. This experiment shows that there can be some large differences in Prime Energy and IFDScore, depending on the sequence length.

Model system	Sequence	IFDscore (kcal/mol)	GlideScore (kcal/mol)
1BUH	Full	-761	-6.3
	Common	-575	-9.2
1DM2	Full	-588	-8.7
	Common	-577	-11.1
1AQ1	Full	-588	-7.2
	Common	-576	-9.1

*Table 39:* Comparison of scores when docking **11** in the three model systems depending on the sequence length

From this limited data, it transpires that there should be a drop in IFDscore when docking in the normalised system.

Normalisation of sequence length would be important when docking ligands in different model systems and comparing IFDScores. When comparisons need to be performed, then normalisation is recommended to allow a fair assessment of model systems studied.

#### 6.5. Induced fit docking with manual amino acid mutations

Based on the results from the previous two sets of IFD experiments (Section 6.2 and 6.3), manual selection of amino acids was investigated. The selection was driven by the clashes observed between the ligand crystal poses and the induced protein structures generated previously, i.e., amino acids that are preventing the correct binding pose being obtained. This selection may seem slightly artificial, as in most other cases the correct pose is not known, but it can be seen as an examination of the best possible selection of amino acids. A summary of residue selection for each system is presented in *Table 40*. A maximum of two residues were mutated at any one time and the same two residues were investigated for

both ligands, even if they were not seen to hinder docking each time in previous experiments. The same IFD set-up parameters were used to perform the induced fit docking experiments.

Model	Mutation	Ligand	IFDscore (kcal/mol)	GlideScore (kcal/mol)	Prime Energy (kcal/mol)	Ligand RMSD (Å)	Visual Assessment
1BUH	Phe80	<b>11</b>	-577	-10.6	-11330	0.9	Good
		<b>12</b>	-570	-9.9	-11212	5.0	Wrong
	Lys33	<b>11</b>	-574	-8.0	-11318	4.1	Wrong
		<b>12</b>	-572	-11.4	-11206	1.5	Good
	Phe80 + Lys33	<b>11</b>	-577	-10.7	-11319	0.8	Good
		<b>12</b>	-572	-10.3	-11239	3.4	Wrong
1DM2	Asp145	<b>11</b>	-577	-10.8	-11317	5.1	Wrong
		<b>12</b>	-576	-13.1	-11249	0.6	Good
	Lys33	<b>11</b>	-577	-11.2	-11322	5.2	Wrong
		<b>12</b>	-575	-12.9	-11249	0.7	Good
	Asp145+ Lys33	<b>11</b>	-576	-10.7	-11315	1.1	Good
		<b>12</b>	-575	-12.8	-11243	0.6	Good
1AQ1	Asp145	<b>11</b>	-576	-9.7	-11335	5.2	Wrong
		<b>12</b>	-575	-12.2	-11254	0.6	Good
	Lys33	<b>11</b>	-577	-9.9	-11336	4.5	Ok
		<b>12</b>	-575	-12.1	-11255	0.6	Good
	Asp145 + Lys33	<b>11</b>	-577	-9.9	-11335	4.5	Ok
		<b>12</b>	-575	-11.9	-11260	0.4	Good

Table 40: Summary of IFD results with targeted residue mutations, with re-docking experiments highlighted in blue

Ligand **11** was first docked into 1BUH, mutating Phe80, which is the main residue protruding in the binding site of 1BUH and hindering the correct docking of CDK2 ligands. The top

scoring docking pose is shown in *Figure 99*. The side chain of Phe80 is rotated up by around 45 degrees, allowing **11** to be docked in the right location of the binding site and form hydrogen bonds with the residues in the hinge region, namely Glu81 and Leu83. The mutation of Phe80 made a large positive difference in the correct docking of **11** in 1BUH, reflected in the very good GlideScore.

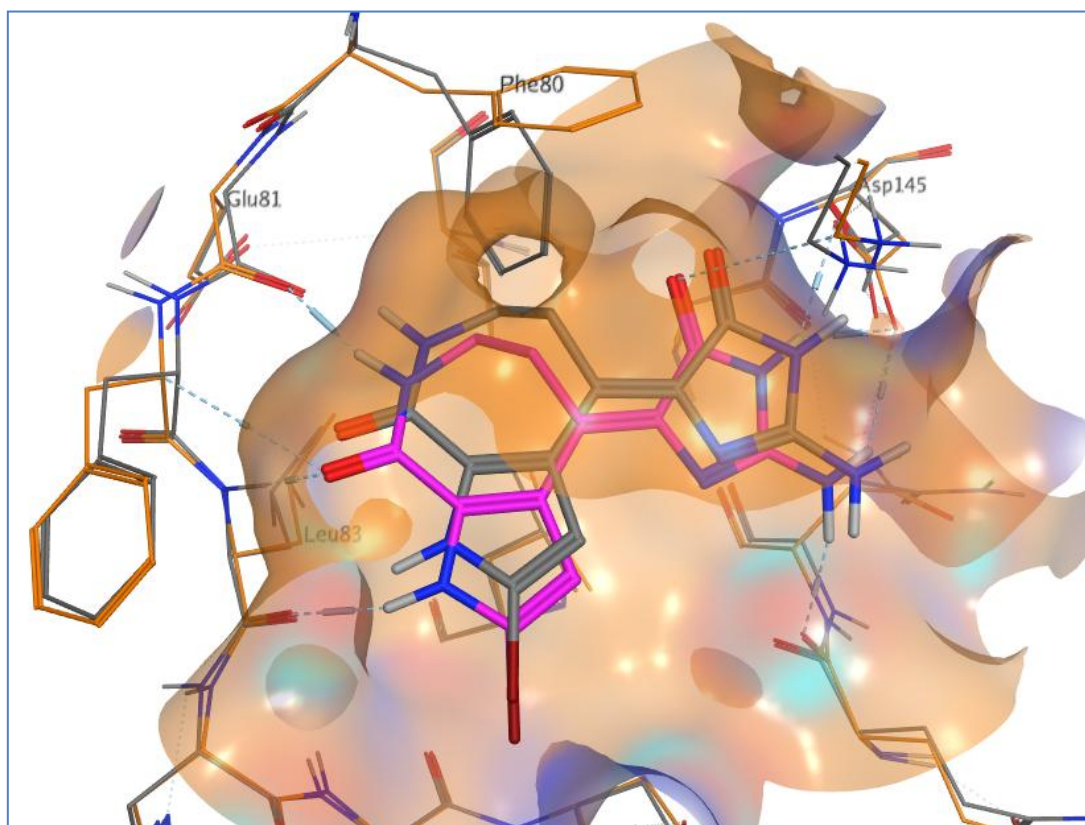


*Figure 99*: Top scoring pose of **11** (pink) in an induced conformation of 1BUH (orange) when mutating Phe80; crystal pose of **11** and crystal conformation of 1BUH shown in grey

Mutation of Lys33 was then investigated. The top scoring pose of **11** for this mutation is shown in *Figure 100*. The docking pose is not found in the right orientation and is not able to interact through hydrogen bonds with the hinge. The hydrogen bond between the pyrroloazepinone ring and Asp145 at the back of the binding site is, however, maintained. In

addition, the core of the ligand interacts through hydrogen bonds to Lys89 and Asp86 at the bottom of the pocket. The side chain of Phe80 is obstructing the binding site and preventing the right docking pose being found, as seen in previous experiments. This is reflected in the slightly lower scores compared to the previous experiment.

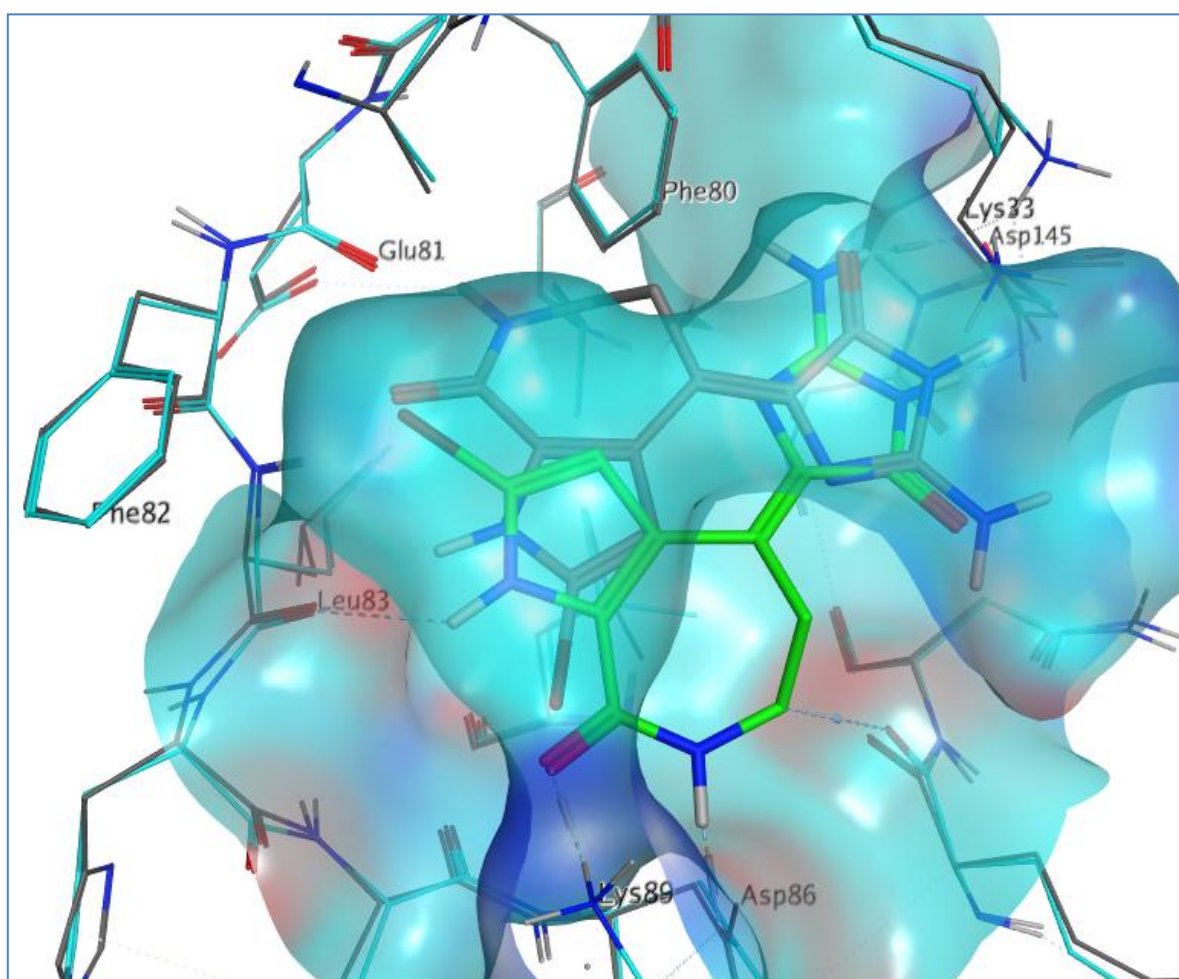


*Figure 100:* Top scoring pose of **11** (green) in the induced conformation of 1BUH (turquoise) when mutating Lys33; crystal pose of **11** and crystal structure of 1BUH shown in grey

It is worth noting that it is sometimes possible to obtain the right binding pose, even when a protruding residue is not mutated. This is the case when docking **12** in an induced conformation of 1BUH (*Figure 101*). The correct binding pose is found when mutating Lys33.

Phe80 is tilted towards the top of the binding site during the optimisation step, allowing **12** to occupy the correct region of the binding site and in the correct orientation.

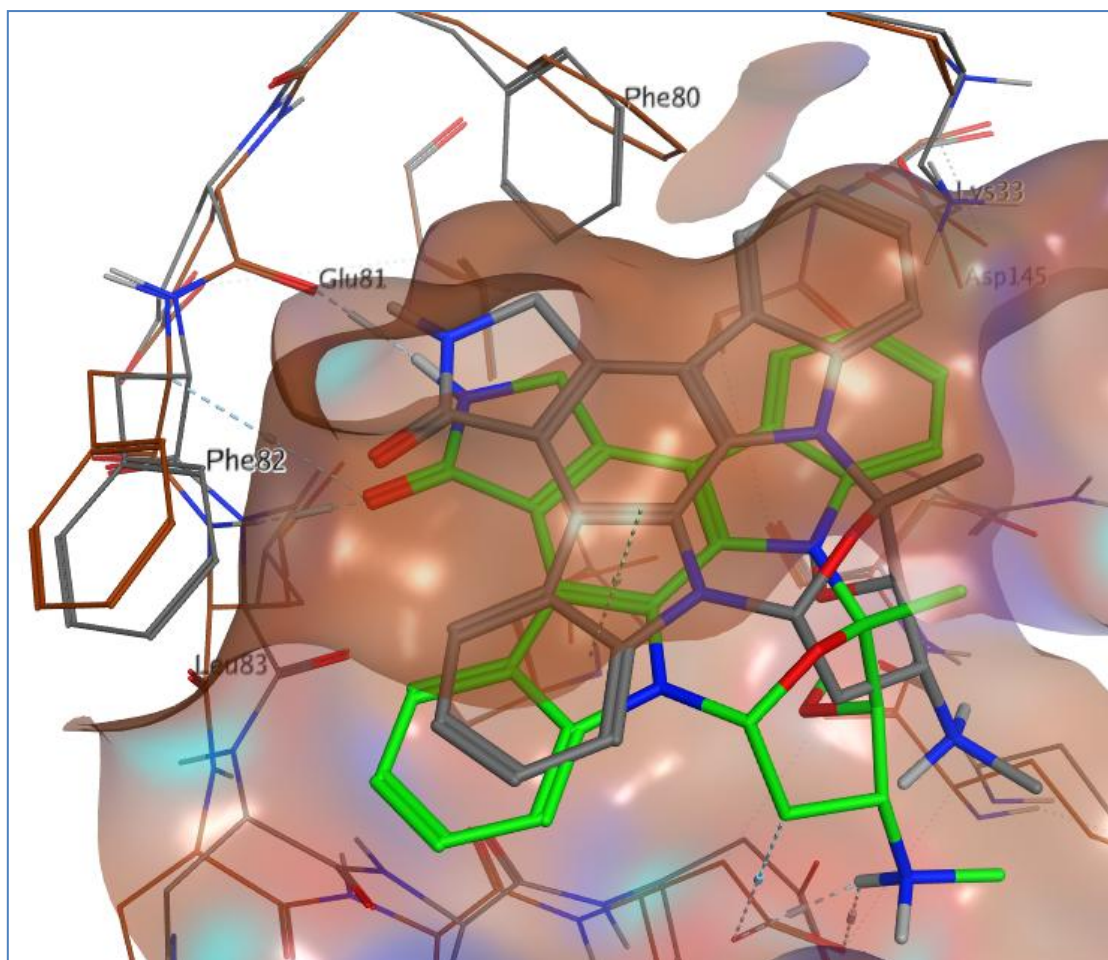


*Figure 101:* Top scoring pose of **12** (green) in an induced conformation of 1BUH (brown) when mutating Lys33; crystal pose of **12** and crystal structure of 1BUH shown in grey

Next, both residues Phe80 and Lys33 were mutated at the same time in order to assess the impact of a double mutation on the docking poses. The top docking pose of **11** (*Figure 102*) presents a good orientation within the binding site and makes the expected hydrogen bonds, i.e., to the hinge and at the back of the pocket with Asp145 and Lys33. However, a comparison of the IFD and GlideScores with those obtained for the single Phe80 mutation

indicate that the quality of this docking pose is due to the inclusion of Phe80 in the set of mutations, rather than a cooperative effect of the double mutation.

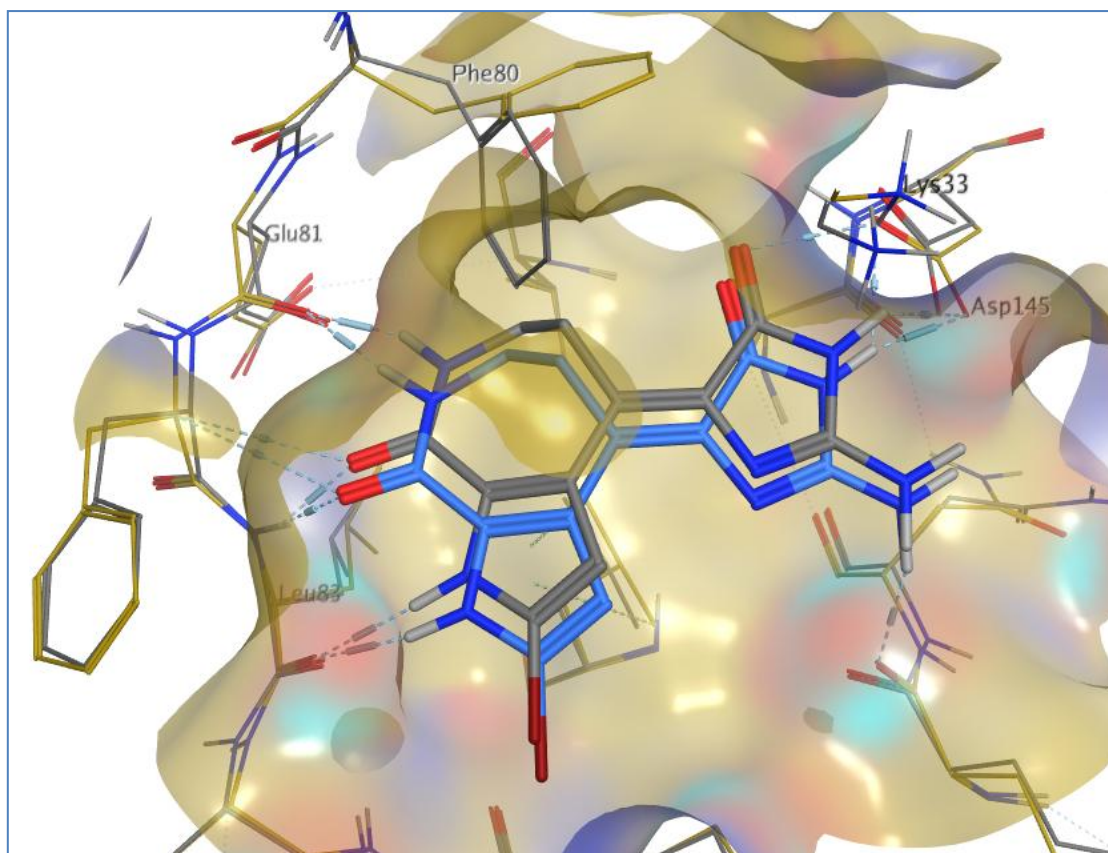


*Figure 102:* Top scoring pose of **11** (blue) in an induced conformation of 1BUH (gold) when mutating Phe80 and Lys33; crystal pose of **11** and crystal structure of 1BUH shown in grey

Double mutation does not always yield the correct pose as the top scoring docking pose, even if the correct binding site conformation has been reached, e.g. docking **12** in 1BUH when mutating both Phe80 and Lys33.

When comparing the results when mutating Lys33 in all three systems and docking **12** (Figure 103), there is a good overlay between all induced binding sites and the crystal structure of 1AQ1 (apart from Phe80 in 1BUH). The top scoring docking poses are in the correct orientation and make the expected hydrogen bonds with the hinge. Overall, whatever the chosen crystal structure, it is possible to obtain the correct binding pose of **12** when mutating only Lys33.

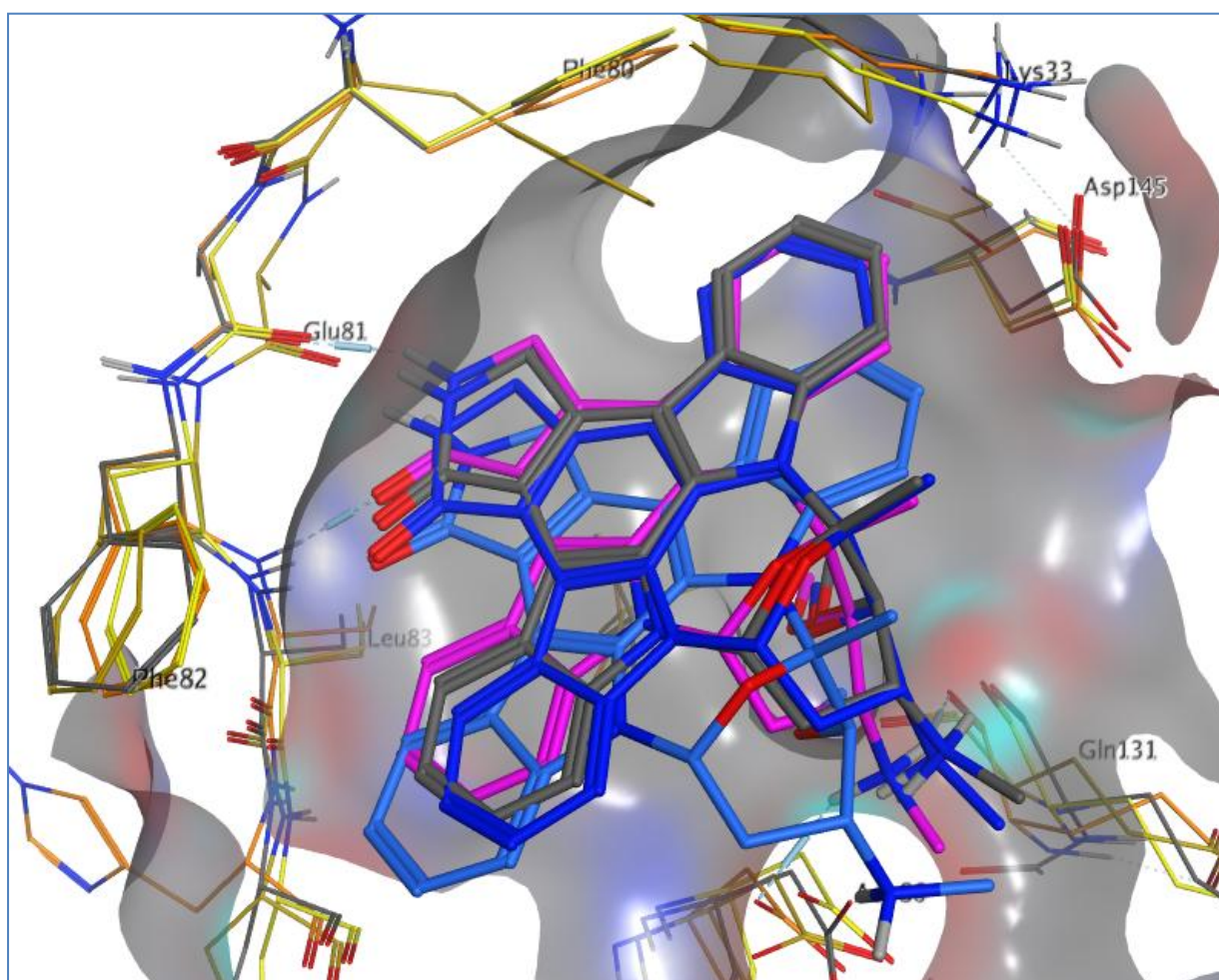
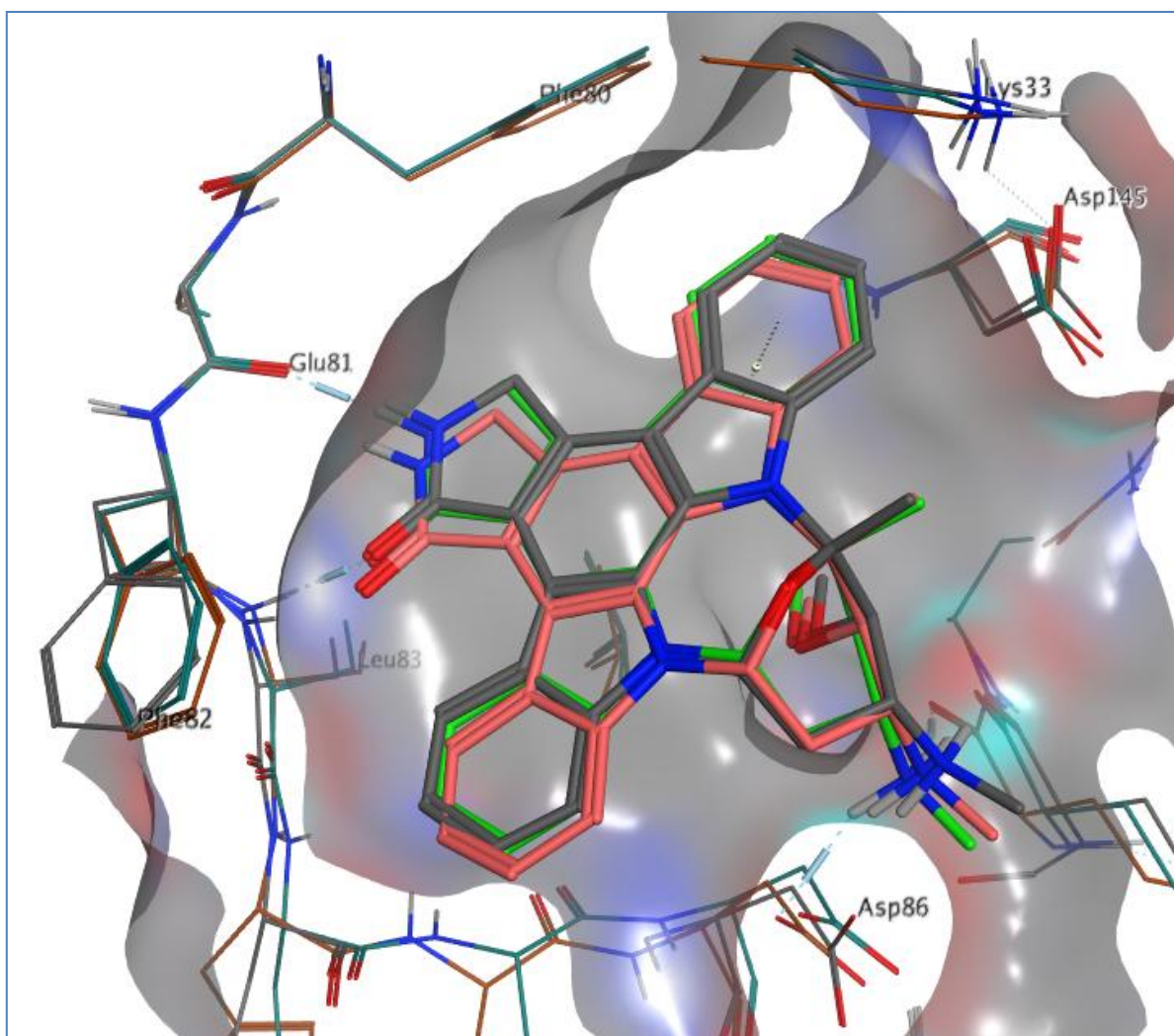


Figure 103: Comparison of docking poses and induced conformations of the binding site when mutating Lys33: induced 1BUH in gold and its docking pose of **12** in light blue, induced 1DM2 in orange and its docking pose of **12** in magenta, induced 1AQ1 in yellow and its docking pose of **12** in dark blue, crystal structure of 1AQ1 and crystal pose of **12** in grey



Similarly, mutation of Asp145 in the 1DM2 and 1AQ1 systems led to comparable results in terms of the conformations of the binding site and of the docking poses compared to the crystal structure (*Figure 104*). The chosen model system does not have an effect on the ability to dock and score **12**.



*Figure 104*: Comparison of docking poses and induced conformations of the binding site when mutating Asp145: induced 1DM2 in brown and its docking pose of **12** in green, induced 1AQ1 in dark green and its docking pose of **12** in pink, crystal structure of 1AQ1 and crystal pose of **12** in grey

When both these residues, Asp145 and Lys33, are truncated, similar results are obtained (docking poses not shown). This was not the case when the same protocol was applied to docking **11** and more variability is noted in the binding site conformations and in the docking poses in the case of the double mutation. One reason for this difference could be due to the size of the two ligands (*Table 2*). This observation suggests that more than one single residue mutation for small ligands produces too large a binding site for the initial docking step. This is the most important step of the whole IFD protocol, as subsequent steps depend on it. Therefore, a poor initial docking pose is likely to lead to a poor IFD pose. However, the docking of larger ligands is less likely to be affected by a double mutation. The quantification of this effect needs to be confirmed by additional experiments.

In conclusion, good results have been obtained for single mutations of targeted residues. This shows that manual selection of residues can add some value over automatic selection based on the temperature factor, for example. However, it would be instructive to investigate the mutation of binding site residues in a systematic manner, without any manual intervention from the user. Also, the effect of double mutations needs to be examined further, in order to confirm or invalidate the hypothesis put forward previously regarding the size of the ligand. Another consideration to take into account is the location of the residues in the case of multiple mutations.

## 6.6. Conclusion

Rigid receptor docking has been shown to be successful when the target ligand and the binding site are well matched. However, when non-native ligands are docked into a well-defined binding site, the resulting poses are often poorly aligned with the crystallographic poses. Therefore, in this work we have carried out an initial evaluation of flexible docking,

where selected amino acids within the binding site are given the freedom to move during the docking simulations. In order to determine the effect of the flexible docking protocol, rigid receptor docking was first investigated as a baseline for the IFD experiments that followed. This work confirmed that while re-docking of ligands into their own protein crystal structures was very successful, the docking of ligands into distorted binding sites was largely unsuccessful, primarily due to the protrusion of sidechains into the binding site, which affected the possible binding pose for a given ligand.

Having confirmed that the rigid docking method was unable to locate the correct binding pose when cross docking the ligands into the alternative binding sites the first set of IFD experiments was performed with the default settings and no amino acid side chains were truncated. In general, the results from this set of experiments were mixed. In particular, it was noted that docking in 1BUH, in which the Phe80 residue protrudes into the binding site, produced disappointing docking poses. However, overall, there were some improvements in the RMSDs of the ligand poses relative to rigid receptor docking. For example, docking of **12** in 1DM2 was much improved (RMSD from 7.0 to 1.7 Å).

The initial IFD experiments relied on the default parameters of the docking program, and did not allow truncation of the residues. Therefore, a second set of experiments was performed that considered the automatic mutation of amino acids within the binding site to alanine (truncation). The automatic selection of the amino acids within the binding site is based on the temperature factor of the residues, with the rationale that the higher temperature factor will have a higher degree of uncertainty in the position of the residue and, therefore, is more likely to be incorrectly positioned and require repositioning. These experiments showed that, for the systems under study, the ligand RMSDs were either similar or slightly better than in the previous set of experiments. That is, the introduction of the truncation

approach had no negative effects on the ability of the program, but it was not particularly successful at solving problem cases. The main reason for this inability to correct problem cases is that the amino acids selected for truncation were always relatively removed from the binding site, which posed the question of the utility of this option, especially when there are obvious amino acids in the binding site that are hindering the identification of the correct binding mode.

The issue encountered with the use of temperature factors to identify the amino acids to truncate is that it is based on the concept that there is a resolution problem with the structure that needs correcting. However, the systems under study had well defined binding sites, with all amino acids within the binding sites having relatively low temperature factors. Nonetheless, because these binding sites were crystallised in the presence of specific ligands, some residues within the binding sites (e.g., Phe80), while being well-defined within the crystal structure, are mis-aligned for the docking of different ligands. Therefore, manual mutations selected on visual inspection of the binding site to determine which residues may be hindering the docking of ligands were carried out. Based on the results obtained in the previous set of experiments, a maximum of two amino acids were picked for each system. Overall, the resulting docking poses RMSDs were similar to previous IFD experiments in model system 1AQ1 (*Table 41*). In 1DM2, the docking poses RMSDs are worse when re-docking **11** unless both truncations of Asp145 and Lys33 are simultaneously carried out. In the case of 1BUH, the truncation of Phe80 is beneficial for the docking of **11**, whilst it is detrimental for **12**. Truncation of Lys33 in this system does not impact the RMSDs, probably pointing to the fact that lysine can move out of the way during the Prime refinement step. Overall, this study showed that the truncation of certain residues and docking using the IFD procedure could be successful. However, the selection of which residues to truncate is

critical to the success of this process. The use of temperature factors to make this selection often identifies residues that are remote to the well-defined binding sites, while the process of visual inspection is tedious and not efficient enough to be employed across an automated docking screen. Therefore, a more objective and efficient way of selecting amino acids for truncation is needed – this will be investigated in the next chapter.

Model	Mutation	Ligand	RMSD IFD with automatic mutations (Å)	RMSD rigid docking (Å)	RMSD default IFD (Å)	RMSD IFD with automatic mutations (Å)
1BUH	Phe80	11	0.9	5.8	3.8	4.1
		12	5.0	6.3	4.0	1.8
	Lys33	11	4.1	5.8	3.8	4.1
		12	1.5	6.3	4.0	1.8
	Phe80 + Lys33	11	0.8	5.8	3.8	4.1
		12	3.4	6.3	4.0	1.8
1DM2	Asp145	11	5.1	0.3	1.1	0.9
		12	0.6	7.0	1.7	0.5
	Lys33	11	5.2	0.3	1.1	0.9
		12	0.7	7.0	1.7	0.5
	Asp145+ Lys33	11	1.1	0.3	1.1	0.9
		12	0.6	7.0	1.7	0.5
1AQ1	Asp145	11	5.2	5.3	4.4	4.4
		12	0.6	0.1	0.5	0.5
	Lys33	11	4.5	5.3	4.4	4.4
		12	0.6	0.1	0.5	0.5
	Asp145 + Lys33	11	4.5	5.3	4.4	4.4
		12	0.4	0.1	0.5	0.5

Table 41: Summary of RMSDs for all IFD set-ups and rigid receptor docking; re-docking experiments highlighted in blue. RMSD values in green indicate an obvious improvement when using manual truncations and in red an obvious deterioration

## 7. An improved IFD protocol

### 7.1. Development of improved IFD protocol

#### 7.1.1. Prioritisation of binding site amino acids

It is important to assess which amino acids, if any, are likely to move to allow binding of a ligand. It is, however, neither feasible nor efficient to make all possible single truncations and sets of multiple truncations of the amino acids present in the binding site.

In the Schrödinger induced fit docking protocol, it is possible to truncate amino acid side chains back to alanine to make more space in the binding site in the first docking step, before building them up again during the refinement step. However, it is not efficient to investigate, in this way, every single amino acid or all possible combinations, when the manual selection of side chains is used. Also, in the Schrödinger protocol, there is a hard-coded limit of three amino acid side chains to be truncated at the same time and it would be informative to verify whether more, although not all, could be truncated without negatively impacting on results and performance.

A protocol to automate the selection of residues for mutation for induced fit docking experiments has been investigated. A look-up table has been created in order to enable the prioritisation of binding site amino acids of interest for mutation (*Table 42*). This prioritisation has been implemented through the use of a score, which will be described in further details below.

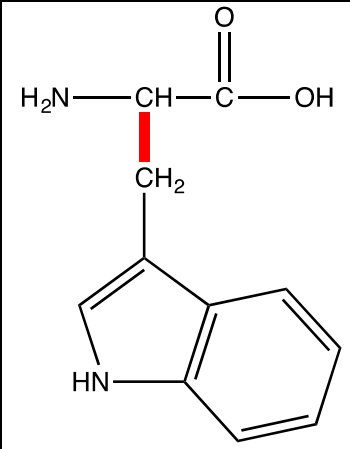
The hypothesis put forward here is that amino acids with a larger side chain, i.e., with a greater number of heavy atoms, and that are not flexible are more likely to protrude into binding sites and not be dealt with during the refinement step and, therefore, hinder finding correct docking poses. In addition, it is assumed that amino acids with more flexible side

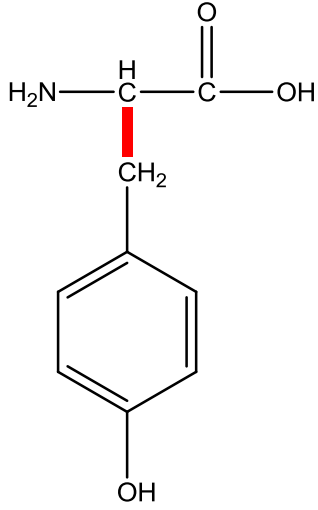
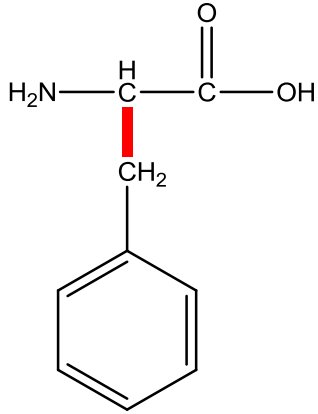
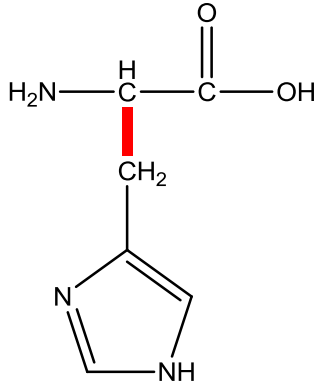
chains are less likely to be a hindrance due to the number of different rotameric states they can adopt. Therefore, a scoring function was devised, whereby for each side chain the number of heavy atoms was normalised by the number of dominant rotatable bonds, hereafter referred to as “dominant rotors”, to account for flexibility. The number of rotatable bonds and dominant rotors can be calculated from the 2D structure of a molecule to obtain an indication of its flexibility. Obviously, this is not the only way of assessing flexibility of amino acids; for example, the number of rotamers for each could be used. For example, the hybridisation of the atoms could be taken as a measure as  $sp^2$  hybridised atoms are less flexible. Thus, an  $sp^2-sp^2$  bond is not very flexible, if at all, compared to an  $sp^2-sp^3$  bond, which is itself less flexible than an  $sp^3-sp^3$  bond. Therefore, only  $sp^3-sp^3$  bonds were counted in the dominant rotor descriptor. This neglects  $sp^2-sp^3$  bonds, such as  $C_\beta$  to  $C_\gamma$  in Trp, as their ‘spinning’ movement can be dealt with during the Prime optimisation step of IFD. The more influential  $C_\alpha$  to  $C_\beta$  bond cranking motion cannot be so well explored by IFD, therefore, it is counted in the dominant rotor descriptor. Internal hydrogen bonds in a ligand or between amino acid side chains in a binding site could decrease the flexibility of these entities and the number of rotatable bonds as a surrogate for flexibility in these instances could be misleading. The SMILES strings of the side chains of all twenty natural amino acids were used as starting points. The number of dominant rotors was adapted from Lovell’s publication.<sup>151</sup> Lovell *et al.* use clusters of side chain  $\chi$  angles to derive the Penultimate Rotamer Library for use in modelling protein crystallographic data but also derive homology models.<sup>151</sup> A  $\chi$  angle is equivalent to a torsion. Each  $\chi$  angle is named as  $\chi_1$ ,  $\chi_2$ ,  $\chi_3$ , etc. This can be adapted to represent dominant rotors. They started from a high quality database of protein crystal structures. Their objective was to derive a rotamer library that did not present the pitfalls of previous libraries, i.e., using low quality data for the



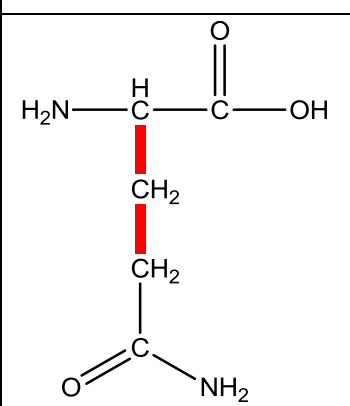
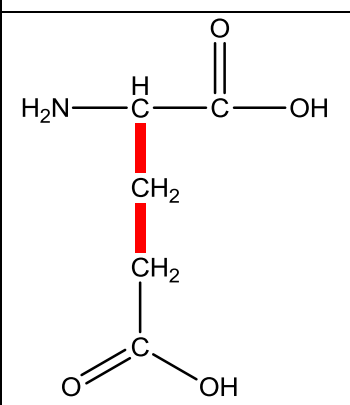
derivation which gets propagated to new protein crystal structures and homology models, and so on. The  $\chi$  angle information was clustered and representative rotamers from these clusters, corresponding to different combinations of the  $\chi$  angle values, composed the rotamer library. The number of dominant rotors that are presented in *Table 42* are inspired from this publication and were used to calculate the amino acid scores as a surrogate for a flexibility assessment.

The aromatic amino acids are at the top of the table, as they have the largest number of heavy atoms and the least number of dominant rotors. Similarly, more flexible amino acids, such as lysine, are found further down the rank-order. Alanine has a score of zero, since it has only one heavy atom and no rotatable bond. Glycine was the lowest scoring amino acid as it does not have any heavy atom nor any rotatable bond in its side chain.

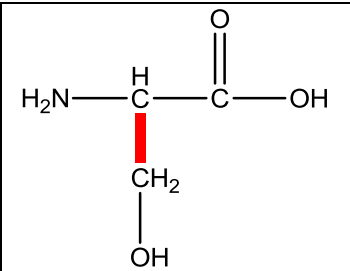
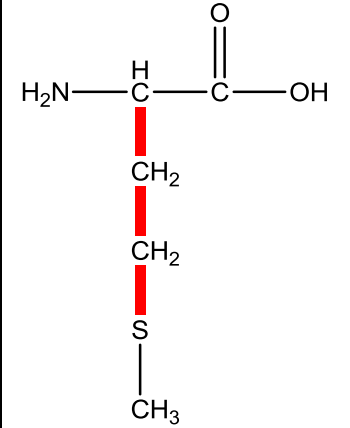
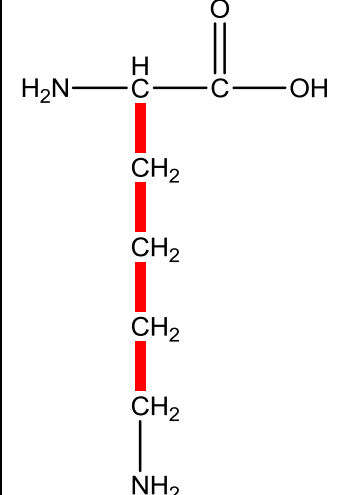
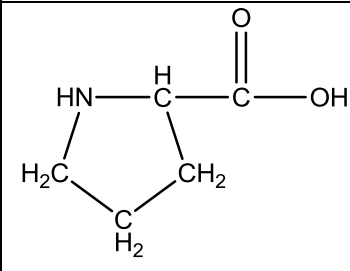
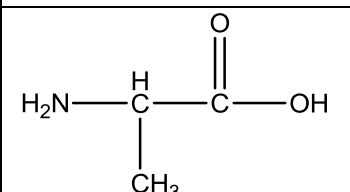
Name	Structure	#DR	Rationale	Heavy Atoms	Score
Trp		1	The bonds within the indole ring are not considered rotatable, as the ring system is aromatic and fixed. The bond from C <sub>β</sub> to C <sub>γ</sub> is not included in the count because it is the terminal rotatable bond linking a Csp <sup>3</sup> to Csp <sup>2</sup> , easily optimisable with Prime, and thus was not deemed 'rotatable' in this scheme.	10	10/1 = 10

Tyr		1	<p>The bonds within the phenyl ring are not considered rotatable, as the ring system is aromatic and fixed. The bond from <math>C_\beta</math> to <math>C_\gamma</math> is not included in the count because it is the terminal rotatable bond linking a <math>C_{sp^3}</math> to <math>C_{sp^2}</math>, and thus was not deemed 'rotatable' in this scheme. The bond between the phenyl and the hydroxyl is not considered rotatable because the hydroxyl is terminal.</p>	8	8/1 =8
Phe		1	<p>The bonds within the phenyl ring are not considered rotatable, as the ring system is aromatic and fixed. The bond from <math>C_\beta</math> to <math>C_\gamma</math> is not included in the count because it is the terminal rotatable bond linking a <math>C_{sp^3}</math> to <math>C_{sp^2}</math>, easily optimisable with Prime, and thus was not deemed 'rotatable' in this scheme.</p>	7	7/1 =7
His		1	<p>The bonds within the imidazole ring are not considered rotatable, as the ring system is aromatic and fixed. The bond from <math>C_\beta</math> to <math>C_\gamma</math> is not included in the count because it is the terminal rotatable bond linking a <math>C_{sp^3}</math> to <math>C_{sp^2}</math>, easily optimisable with Prime, and thus was not deemed 'rotatable' in this scheme.</p>	6	6/1 =6

Asn		1	The rotatable bond is the single bond between $C_{\alpha}$ and $C_{\beta}$ . The bond from $C_{\beta}$ to $C_{\gamma}$ is not included in the count because it is the terminal rotatable bond linking a $Csp^3$ to $Csp^2$ and there is a delocalization of electrons on the amide group, which results in this moiety occupying roughly similar space in all expected conformations and thus was not deemed 'rotatable' in this scheme.	4	4/1 =4
Asp		1	The rotatable bond is the single bond between $C_{\alpha}$ and $C_{\beta}$ . The bond from $C_{\beta}$ to $C_{\gamma}$ is not included in the count because it is the terminal rotatable bond linking a $Csp^3$ to $Csp^2$ and there is a delocalization of electrons on the carboxylic acid group, which results in this moiety occupying roughly similar space in all expected conformations and thus was not deemed 'rotatable' in this scheme.	4	4/1 =4
Val		1	The rotatable bond is the single bond between $C_{\alpha}$ and $C_{\beta}$ . The bonds between $C_{\beta}$ and the terminal methyls are not considered rotatable because of the symmetry of these respective groups and because they are terminal.	3	3/1 =3
Thr		1	The rotatable bond is the single bond between $C_{\alpha}$ and $C_{\beta}$ . The bonds between $C_{\beta}$ and the terminal methyl and hydroxyl are not	3	3/1 =3

			considered rotatable because of the symmetry of the methyl and because these groups are terminal.		
Gln		2	The rotatable bonds are the single bonds between $C_\alpha$ and $C_\beta$ , and $C_\beta$ and $C_\gamma$ . The bond between $C_\gamma$ and $C_\delta$ is not included in the count because it is the terminal rotatable bond linking a $Csp^3$ to $Csp^2$ and there is a delocalization of electrons on the amide group, which results in this moiety occupying roughly similar space in all expected conformations and thus was not deemed 'rotatable' in this scheme.	5	5/2 =2.5
Glu		2	The rotatable bonds are the single bonds between $C_\alpha$ and $C_\beta$ , and $C_\beta$ and $C_\gamma$ . The bond between $C_\gamma$ and $C_\delta$ is not included in the count because it is the terminal rotatable bond linking a $Csp^3$ to $Csp^2$ and there is a delocalization of electrons on the carboxylic acid group, which results in this moiety occupying roughly similar space in all expected conformations and thus was not deemed 'rotatable' in this scheme.	5	5/2 =2.5

Arg		3	The rotatable bonds are the single bonds between $C_\alpha$ and $C_\beta$ , $C_\beta$ and $C_\gamma$ , and $C_\gamma$ and $C_\delta$ . Because of the possible delocalization of electrons on the guanidinium moiety, the subsequent bonds are not considered rotatable.	7	$7/3 = 2.3$
Leu		2	The rotatable bonds are the single bonds between $C_\alpha$ and $C_\beta$ , and $C_\beta$ and $C_\gamma$ . The bonds between $C_\beta$ and the terminal methyls are not considered rotatable because of the symmetry of these respective groups and because they are terminal.	4	$4/2 = 2$
Ile		2	The rotatable bonds are the single bonds between $C_\alpha$ and $C_\beta$ , and $C_\beta$ and $C_\gamma$ . The bonds between $C_\beta$ and the terminal methyl and $C_\gamma$ and the other terminal methyl are not considered rotatable because of the symmetry of these respective groups and because they are terminal.	4	$4/2 = 2$
Cys		1	The rotatable bond is the single bond between $C_\alpha$ and $C_\beta$ . The bond between $C_\beta$ and $S_\gamma$ is not considered rotatable as the thiol is a terminal group.	2	$2/1 = 2$

Ser	 <p>Chemical structure of Serine showing the rotatable bond between the alpha carbon (<math>C_\alpha</math>) and the beta carbon (<math>C_\beta</math>).</p>	1	The rotatable bond is the single bond between $C_\alpha$ and $C_\beta$ . The bond between $C_\beta$ and $O_\gamma$ is not considered rotatable as the hydroxyl is a terminal group.	2	$2/1 = 2$
Met	 <p>Chemical structure of Methionine showing the rotatable bonds between <math>C_\alpha</math> and <math>C_\beta</math>, <math>C_\beta</math> and <math>C_\gamma</math>, and <math>C_\gamma</math> to <math>S_\delta</math>.</p>	3	The rotatable bonds are the single bonds between $C_\alpha$ and $C_\beta$ , $C_\beta$ and $C_\gamma$ , and $C_\gamma$ to $S_\delta$ . The bond between $S_\delta$ and the terminal methyl is not considered rotatable because of the symmetry of this group and the methyl is the terminal group.	4	$4/3 = 1.3$
Lys	 <p>Chemical structure of Lysine showing the rotatable bonds between <math>C_\alpha</math> and <math>C_\beta</math>, <math>C_\beta</math> and <math>C_\gamma</math>, <math>C_\gamma</math> to <math>C_\delta</math>, and <math>C_\delta</math> to <math>C_\epsilon</math>.</p>	4	The rotatable bonds are the single bonds between $C_\alpha$ and $C_\beta$ , $C_\beta$ and $C_\gamma$ , $C_\gamma$ to $C_\delta$ , and $C_\delta$ to $C_\epsilon$ . The bond between $C_\epsilon$ and the terminal amine is not considered rotatable because the amine is a terminal group.	5	$5/4 = 1.3$
Pro	 <p>Chemical structure of Proline showing the cyclic structure where the alpha carbon (<math>C_\alpha</math>) and beta carbon (<math>C_\beta</math>) are part of the ring.</p>	0	All single bonds are involved in forming the cyclic structure, and are not considered rotatable. However, it is worth noting that Proline is able to adopt a cis or trans conformation, unlike other residues.	3	0
Ala	 <p>Chemical structure of Alanine showing the <math>C_\alpha</math> to <math>C_\beta</math> single bond.</p>	0	The $C_\alpha$ to $C_\beta$ single bond is not considered rotatable because of the symmetry of the methyl and because it is a terminal group.	1	0

Gly	$  \begin{array}{c}  \text{O} \\  \parallel \\  \text{H}_2\text{N}-\text{C}-\text{C}-\text{OH} \\    \\  \text{H}  \end{array}  $	0	The side chain is a hydrogen. There are no heavy atoms.	0	0
-----	---	---	---	---	---

*Table 42:* Master table of all natural amino acid side chains and the number of heavy atoms, number of dominant rotors (DR) and the score (heavy atoms/DR). Bonds corresponding to the dominant rotors are highlighted in bold red.

Amino acids within a 4 Å radius of the ligand centroid, within the crystal pose geometry, were selected. This was defined as the binding site of the protein. The Schrödinger IFD defines the binding site automatically by an enclosing box, based on the ligand selected. Only the side chains of the selected amino acids were of interest here. This ensured that only amino acids, with side chains pointing towards the interior of the binding site, were considered, as it was assumed that the residues pointing outwards would not contribute or affect the docking pose of the ligand.

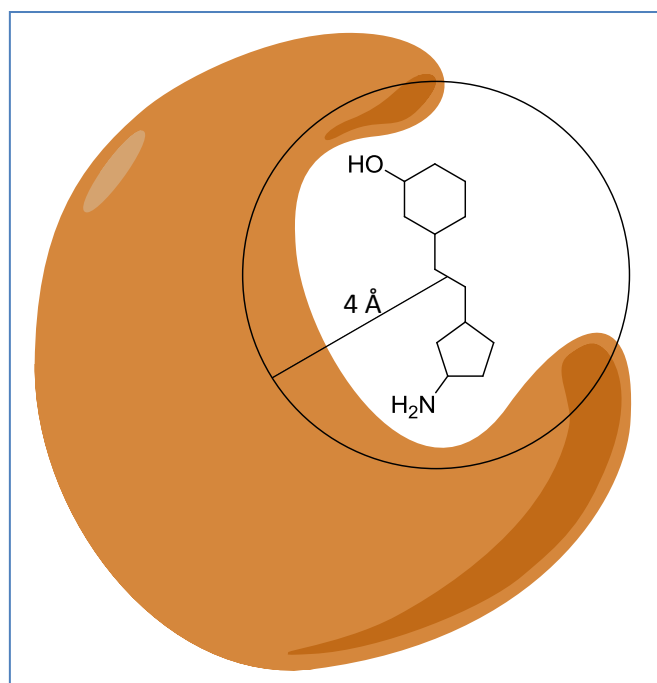


*Figure 105:* definition of the binding site

This list of selected residues was then compared to the master list, shown in *Table 42*, in order to extract their score and prioritise the temporary truncation. The side chains of the top scoring amino acids would be the first ones to be mutated to alanine in the modified IFD process. In the case where more than four amino acids can be prioritised using the score, i.e., there is a tie, an additional criteria needs to be used. From the list of amino acids in a tie, the closest to the ligand are considered until the complete list of four can be drawn – see Section 7.2.4 for an example.



### 7.1.2. Efficient exploration of the binding site using experimental design

There is not a one-to-one relationship between the number of experiments conducted and the amount of information generated, as the experimental space might not be explored further for each new experiment.<sup>152</sup> In addition, the cost of experiments increases with the number of experiments. Therefore, only a limited number of experiments will give an optimal amount of information in a cost effective manner. Traditionally, in a multi-parameter problem, one approach may be to change a single parameter at a time until there is no more improvement to the results, and then move on to the next until no parameters are left to investigate. This way, the optimum point might be found only if all parameters are independent. Often, this is not the case. An alternative could be to modify all parameters at the same time, as is performed in experimental design.<sup>152</sup> This approach requires fewer experiments to be conducted and is more efficient in terms of generating information. Analysis of the data produced this way is more likely to lead to the identification of the optimal conditions and can also identify which parameters are important to get to the result.<sup>152</sup>

To ascertain which amino acids will more likely impact on the docking of ligands through temporary truncations, experimental design was investigated. This way of characterising the binding site would minimise the number of IFD experiments and still enable enough information to be generated and potentially highlight the important amino acids within the binding site. There are a number of ways to create an experimental design. Factorial design is an example, where each parameter has a low and high level. This method is well suited to the truncations of selected amino acids. Because there was a pre-set limit at three for the number of amino acid truncations in the Schrödinger IFD protocol, it was decided to

investigate the potential truncation of four binding site amino acids and assess whether this really produces the wrong binding mode due to the space created. A four-factor experimental design leads to a  $2^4$  full factorial design, i.e., two levels for each factor, which equates to 16 experiments. Such a number of experiments, although manageable on paper, would take a lot of computer time and power to investigate one system only. Therefore, a  $\frac{1}{2} 2^4$  fractional factorial design was selected instead, in which only half of the experiments would need to be conducted, i.e., 8 experiments in this case.

Such a fractional factorial design was derived using Design Expert,<sup>153</sup> with a maximum of four residue truncation, performed in eight different experiments. These experiments are summarised in the table below (*Table 43*).

Run	Factor 1	Factor 2	Factor 3	Factor 4
1	Truncate	Truncate	Truncate	Truncate
2	Keep	Keep	Keep	Keep
3	Truncate	Keep	Truncate	Keep
4	Keep	Truncate	Truncate	Keep
5	Keep	Truncate	Keep	Truncate
6	Truncate	Keep	Keep	Truncate
7	Keep	Keep	Truncate	Truncate
8	Truncate	Truncate	Keep	Keep

*Table 43:* Four amino acid points of change fractional factorial design

Factors 1, 2, 3 and 4 are the prioritised residues which will be considered for truncation. As can be seen from *Table 43*, the first experiment consists of truncating all four amino acids,

whilst the second experiment does not involve any truncation. In the following six experiments, a maximum of two residues are mutated at any one time.

The experimental design chosen is made of 8 experiments. The input information are the 4 points of change – in this case 4 amino acids – and their two levels – “keep” and “truncate”.

The results from such a set of 8 experiments is analysed as a whole to ascertain what the impact of each factor is. The objective of these experiments was to generate as much information as possible with a minimum number of experiments. This is enabled by a fractional factorial experimental design, which results in 2 points of change at a time, except for the reference experiments, i.e., no change and all change. The way the information is input does not have any impact on the experimental design itself. Additionally, the experiments are randomised and the order in which they are run does not matter. This design is balanced, i.e., each amino acid is kept 4 times and truncated 4 times. This means that all factors can be independently assessed, as the impact of any interaction terms can be separated from the impact of the factors as part of the statistical analysis. For example, for factor 4 in *Table 43*, for each experiment where factor 4 is truncated, factor 3 is truncated twice and kept twice. The same applies to factors 1 and 2 and also when a factor is kept, which means that the impact of factor 4 can be assessed independently from the other factors. This means that we can use all 8 results to determine the impact of factor 4. If we had chosen to run a design where the first two baseline experiments are the same as these ones and the next four are (truncate 1 keep 234), (truncate 2 keep 134), (truncate 3 keep 124) and (truncate 4 keep 123) or the next four are (truncate 123 keep 4), (truncate 124 keep 3), (truncate 134 keep 2) and (truncate 234 keep 1), there would be only two experiments which could be compared. Indeed, continuing the example of factor 4, only the (keep all) and (truncate 4 keep 123) or (truncate all) and (truncate 123 keep 4) could be

compared, relying on only two results instead of eight to assess the impact of factor 4. The alternative approach of carrying out single mutations is an inefficient way of exploring space in general; moreover, a design of experiments would not be necessary in the case of single mutations. Running the full experimental design (16 experiments) as opposed to a fraction (8 experiments) would not generate more information about the factors but would enable the separation of the interaction terms from each other, which is not one of the objectives here.

In the Schrödinger paper, it is stated that more than three simultaneous mutations would create too large a binding site and it would be unlikely to reach the right binding pose due to the larger space for exploration.<sup>9</sup> A preliminary investigation of other experimental designs with a higher number of mutations was carried out. However, the computational cost associated with this was prohibitive. It is anticipated that four truncations will give an indication of whether a maximum of three truncations in the standard Schrödinger IFD protocol is appropriate.

If using different starting structures of the same target, it is possible to add the starting conformation as an additional factor in addition to the 4 amino acids, with two levels – conformation1 and conformation2. Additional conformations would have to be added as blocking variables, which would complicate the statistical analysis. In the case of two conformations, we would move to a  $2^5$  fractional factorial design. Eight experiments would not be enough anymore to independently assess the impact of each factor, therefore, we would have to run 16 experiments, which would not be an issue in itself necessarily. The impact of each amino acid may or may not be dependent on the starting conformation, e.g., truncating Phe80 in CDK2 1BUH would be more impactful than truncating it in 1DM2 (*Table*

51 vs Table 53, variability of results vs. consistently finding good poses). This would lead to the problem of choosing which conformations to include in the design.

### 7.1.3. Change to IFDScore

Due to questions over the derivation of the standard Schrödinger IFDScore,<sup>9</sup> changes to this scoring function have also been investigated. The Schrödinger paper stated that the IFDScore was driven mainly by the GlideScore and that the small amount of Prime Energy taken into account was to represent the conformation of the protein. We found during our experiments that this was not the case and that the Prime Energy, being a much larger energy than GlideScore, overwhelmed the IFDScore on several occasions. In order to counteract this and have the GlideScore driving the scoring function, we examined the difference in Prime Energy between the input conformation to IFD of the protein only and the induced ones. This  $\Delta$  Prime Energy was then used in the calculation of a new IFDScore, with 0.01 to 1 of the  $\Delta$  Prime Energy being added to the GlideScore, as described in Equation 32.

$$IFDScore = GlideScore + X * \Delta Prime Energy \quad (32)$$

Where  $X$  is a scaling factor for the  $\Delta$  Prime Energy, between

0.01 and 1

To facilitate the computation of the different IFDScores, a perl script was developed, which took as input files the .maegz Maestro file containing up to twenty protein ligand complexes from a specific IFD run and the starting protein-ligand PDB file. The perl script can be found in Appendix 1.

The script first goes through the induced protein-ligand complexes, removes the ligand pose and relaxes the protein conformation (i.e., restrained minimisation with and without fixing heavy atoms) before calculating the Prime Energy. This protocol is repeated for each protein ligand complex from the IFD run under consideration as well as the starting complex. The difference in Prime Energy between each induced protein conformation and the starting one is calculated. A number of IFDScores, i.e., by varying X, as described in *Equation 32*, are then computed in order to allow an analysis to be conducted with the objective to find a score that would be more predictive than the standard IFDScore. This process might prioritise a different induced protein-ligand complex as top scoring. An example output is shown in *Table 44*, where *Entry* is the original rank-order and *old\_IFDScore* is the original IFDScore. The following two columns show the new Prime Energy after IFD,  $PE_{IFD}$ , and the corresponding  $\Delta PE$ , which is the difference between  $PE_{IFD}$  and the Prime Energy before IFD,  $PE_{min}$ . The remaining columns then report the various IFDScores. The number at the end of the column headers represent the percentage of Prime Energy included in the score. The new IFDScores are also expressed in kcal/mol. The numbers highlighted in red are the worst within a column, whilst the green numbers are the best in that same column. The data in *Table 44* demonstrates that depending on the IFDScore computed the range can be large compared to the range of the original IFDScores, potentially affecting the rank-order considerably.

Entry	ligand RMSD	BS RMSD	old_IFD Score	Glide Score	PE <sub>IFD</sub>	ΔPE	new_IFD Score_1	new_IFD Score_5	new_IFD Score_10	new_IFD Score_20	new_IFD Score_30	new_IFD Score_40	new_IFD Score_50	new_IFD Score_60	new_IFD Score_70	new_IFD Score_80	new_IFD Score_90	new_IFD Score_100
1	1.1	0.7	-578	-12.5	-11319	-94.7	-13.5	-17.3	-22.0	-31.5	-40.9	-50.4	-59.9	-69.3	-78.8	-88.3	-97.7	-107.2
2	1.8	0.8	-578	-12.7	-11320	-95.5	-13.6	-17.5	-22.2	-31.8	-41.3	-50.9	-60.5	-70.0	-79.6	-89.1	-98.7	-108.2
3	2.3	0.9	-578	-12.9	-11305	-80.7	-13.7	-16.9	-20.9	-29.0	-37.1	-45.1	-53.2	-61.3	-69.3	-77.4	-85.5	-93.6
4	4.1	0.9	-577	-11.5	-11319	-94.6	-12.5	-16.2	-21.0	-30.4	-39.9	-49.3	-58.8	-68.3	-77.7	-87.2	-96.6	-106.1
5	4.2	1.0	-576	-10.3	-11333	-107.7	-11.4	-15.7	-21.0	-31.8	-42.6	-53.4	-64.1	-74.9	-85.7	-96.5	-107.2	-118.0
6	5.1	1.1	-576	-10.6	-11330	-105.1	-11.7	-15.9	-21.1	-31.6	-42.1	-52.7	-63.2	-73.7	-84.2	-94.7	-105.2	-115.7
7	2.0	1.0	-576	-10.5	-11330	-105.3	-11.6	-15.8	-21.0	-31.6	-42.1	-52.6	-63.1	-73.7	-84.2	-94.7	-105.2	-115.8
8	2.1	0.7	-575	-10.6	-11313	-88.5	-11.5	-15.0	-19.4	-28.3	-37.1	-46.0	-54.8	-63.7	-72.5	-81.4	-90.2	-99.1
9	4.9	1.1	-575	-10.4	-11326	-101.1	-11.4	-15.5	-20.5	-30.7	-40.8	-50.9	-61.0	-71.1	-81.2	-91.3	-101.4	-111.5
10	5.8	1.0	-575	-10.3	-11321	-95.8	-11.3	-15.1	-19.9	-29.5	-39.0	-48.6	-58.2	-67.8	-77.3	-86.9	-96.5	-106.1
11	6.4	1.0	-571	-5.7	-11332	-106.9	-6.8	-11.1	-16.4	-27.1	-37.8	-48.5	-59.2	-69.8	-80.5	-91.2	-101.9	-112.6
12	7.1	1.0	-569	-4.4	-11323	-98.6	-5.4	-9.4	-14.3	-24.2	-34.0	-43.9	-53.8	-63.6	-73.5	-83.4	-93.2	-103.1
13	6.6	1.1	-569	-4.2	-11328	-103.7	-5.3	-9.4	-14.6	-25.0	-35.3	-45.7	-56.1	-66.4	-76.8	-87.2	-97.6	-107.9

Table 44: Example of output from the *automated\_IFD\_process.pl* perl script; the numbers highlighted in red are the worst within a column, whilst the green numbers are the best in that same column

As well as the various new IFDScores, the ligand RMSD and the binding site RMSD were computed for each new induced fit complex. For the ligand RMSD, the Conformer Cluster tool available in Maestro was used for calculation. Within this tool, it is possible to compute the RMSD matrix of a set of ligands. The next step in this protocol would be to cluster the ligand conformations, but this was not conducted in this instance. The perl script *binding\_site\_RMSD.pl* was written in order to compute the binding site RMSDs (see Appendix 2), where the expected protein structure (i.e., if docking **12** in 1DM2, the expected protein structure is 1AQ1) and the induced fit complexes are compared. In order to maintain consistency between complexes within a same set of experiments, the exact same list of amino acids was used to represent the binding site, wherever the docking pose location was. The amino acids chosen to this end were the ones scored during the amino acid prioritisation step, as they were deemed to represent the binding site. Once these amino acids were obtained for the two systems to be compared, the standard Schrödinger *rmsd.py* script was run.<sup>154</sup>

## 7.2. Testing of improved IFD protocol

In order to move beyond a knowledge-based, or a B-factor based, selection of amino acids for temporary truncation, a modified IFD protocol has been investigated. In particular, an automated way of selecting amino acids is reported. In the following, the original IFDScore and Prime Energy are used. Two Factor Xa structures, which were part of the Schrödinger study, and the three CDK2 structures, used previously, made up the training set to test this improved protocol. The effect of the new IFD scoring function is further examined in Section 7.2.4 and 7.3.



### 7.2.1. Factor Xa structure 1KSN

Ligand **16** was crystallised in complex with fXa in crystal structure 1KSN. As conducted previously, the amino acid side chains, which were within 4 Å of **16**, were selected to go through the prioritisation step. The four selected amino acids are highlighted in *Table 45*. As required, it was the largest and least flexible aromatic amino acids that were prioritised. This model system was also studied by the Schrödinger group and the amino acids that they chose for truncation were Glu147, Gln192 and Arg222.<sup>9</sup> There was no overlap of amino acids with the below list. It is worth noting that the choice of amino acids selected for truncation in the Schrödinger paper was made from the B-factor parameter<sup>9</sup> and that Tyr99, which could be the problematic amino acid due to the rotation highlighted in Section 3.4, was not part of their list. In the case of our scoring function, Tyr99 was prioritised for truncation. With this list set, ligand **17** was docked in 1KSN using the standard IFD protocol.

AA_ID	Name	R SMILES	heavy	#DR	score
TRP215	TRP	[*]Cc1c[nH]c2ccccc12	10	1	10
TYR99	TYR	[*]Cc1ccc(O)cc1	8	1	8
PHE174	PHE	[*]Cc1ccccc1	7	1	7
ASP189	ASP	[*]CC(O)=O	4	1	4
VAL213	VAL	[*]C(C)C	3	1	3
GLU147	GLU	[*]CCC(O)=O	5	2	2.5
GLN192	GLN	[*]CCC(N)=O	5	2	2.5
ARG143	ARG	[*]CCCNC(N)=N	7	3	2.3
CYS220	CYS	[*]CS	2	1	2
CYS220	CYS	[*]CS	2	1	2
SER195	SER	[*]CO	2	1	2
ALA190	ALA	[*]C	1	0	0

Table 45: Prioritised amino acids for binding site 1KSN; selected amino acids shown in blue

The resulting scores of the eight IFD experiments are shown in Table 46. It is clear that the majority of experiments produced good poses when compared to the expected crystal pose, apart from Experiments 6 and 7. The visual inspection of the poses also reflects this. The IFDScores are comparable, as are the GlideScores. The Schrödinger group reported a top ranking pose with a ligand RMSD of 1.5 Å. The results reported here are comparable and even slightly better in terms of RMSD, if ignoring Experiments 6 and 7.

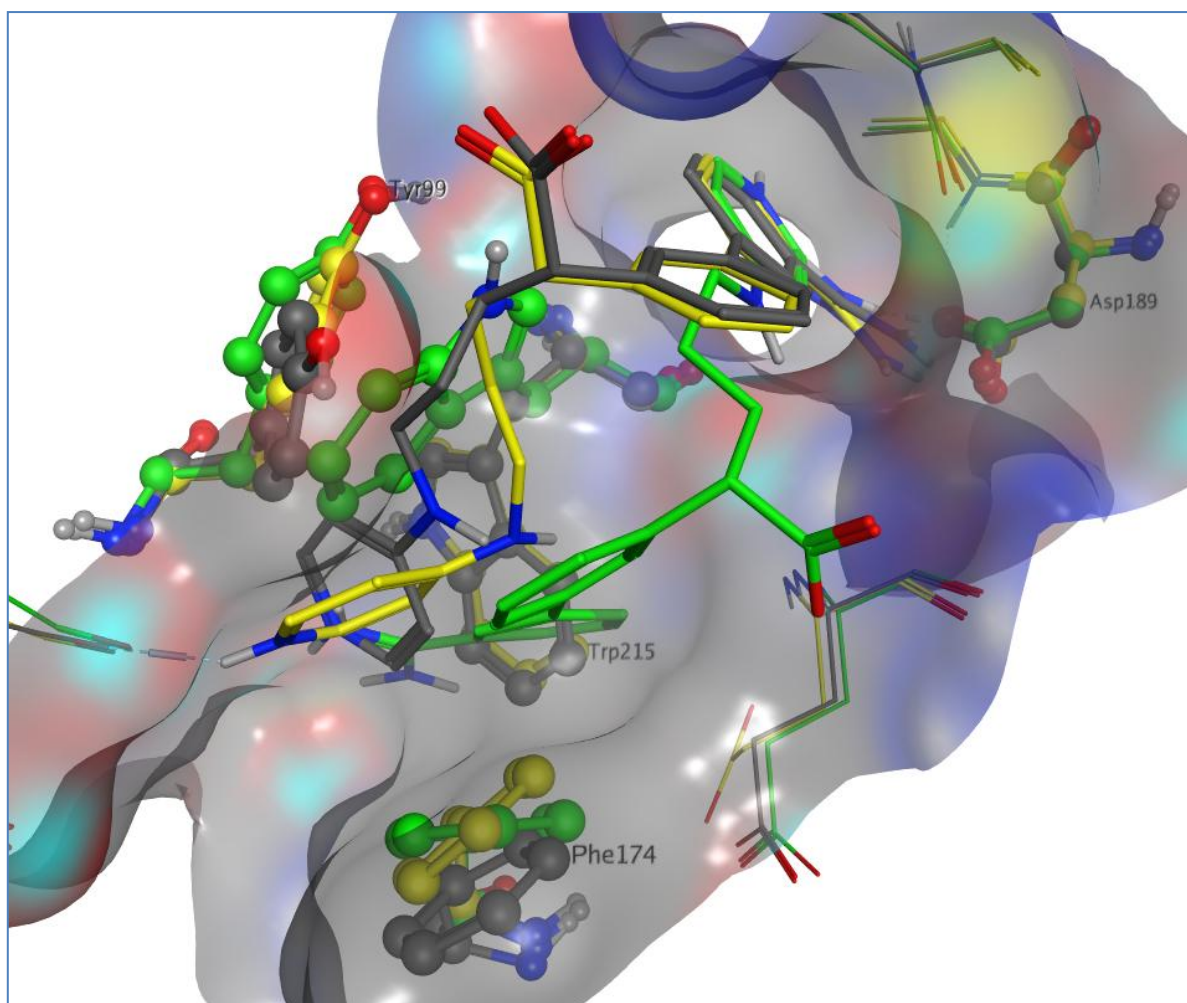
Exp design	Ligand	IFDScore	GlideScore	Prime energy	RMSD	Visual assessment
1	17	-664	-12.0	-13034	1.2	Good
2	17	-662	-11.6	-13015	1.2	Good
3	17	-664	-13.2	-13022	1.2	Good
4	17	-663	-12.3	-13020	1.1	Good
5	17	-661	-11.4	-13002	3.0	Ok
6	17	-661	-11.0	-12999	7.9	Wrong
7	17	-662	-11.8	-13013	8.6	Wrong
8	17	-662	-12.3	-13003	1.2	Good

Table 46: Summary of standard IFD results when docking **17** in 1KSN; "no change" experiment highlighted in blue

Figure 106 shows the top ranked docking pose for Experiments 1 and 6. Experiment 1 was the experiment where all four truncations were performed. The top scoring pose obtained for this experiment is reasonable maintaining the important bidentate interaction with Asp189. There is an additional interaction from the carboxylic acid of **17** to the NH<sub>2</sub> amide of the side chain of Gln192, not seen in the crystal structure, and also from the pyridinium to backbone carbonyl of Glu97. There is also a face-to-face  $\pi$ - $\pi$  interaction between the pyridine ring and Phe174 and possibly edge-to-face to Trp215 (although less clear), as opposed to edge-to-face to both Phe174 and Tyr99 and face-to-face to Trp215 in the crystal structure. Additional interactions observed in the crystal structure are to water molecules, which were removed from this model system.

In Experiment 6, Trp215 and Asp189 have been temporarily truncated. As can be seen in Figure 106, the top scoring pose for this experiment is back to front compared to the crystal pose of **17**, with the benzamidine moiety binding near Met180 on the opposite side to Asp189 in the binding site. There is an interaction between the benzamidine and the

backbone carbonyl of Thr98 and also a bidentate interaction between the carboxylic acid of **17** and Arg222 (not shown in *Figure 106*). A  $\pi$ - $\pi$  interaction between Tyr99 and Trp215 is observed, as Trp215 is rotated up compared to the crystal structure 1KSN (in grey in *Figure 106*). In 1XKA, Trp215 is found in a similar conformation to the one found in 1KSN. In this case, we could conclude that the truncation of Trp215 led to the incorrect binding pose, as Asp189 occupies a similar conformation to the one found in 1XKA. This observation could point to the size of the amino acid being truncated as being an issue as opposed to the Schrödinger comment that creating a larger binding site with too many truncations is detrimental to finding the correct binding pose.<sup>9</sup> However, other experiments, which also temporarily truncated Trp215 (such as experiments 1, 3 and 8), resulted in the correct binding mode. On the other hand, when truncating Asp189 (experiments 1, 5, 6 and 7), only one of the experiments lead to the right pose, with all other three experiments producing a docking pose with a much higher ligand RMSD. This could mean that Asp189 is necessary to reach the correct binding pose, and indeed Asp189 is very important for binding, as highlighted in Section 3.4. Therefore, rather than the number of truncations or the size of the residues being an issue, this would mean that truncation of amino acids essential for the binding of ligands, such as Asp189, is likely to impede the finding of the correct binding pose.



*Figure 106:* Comparison of 1KSN crystal structure in grey with induced protein-ligand complexes when docking **17**: in yellow, with all four truncation, and in green when truncating Trp215 and Asp189. Crystal pose of ligand **17** also shown in grey

### 7.2.2. Factor Xa structure 1XKA

Ligand **17** was crystallised in complex with fXa in 1XKA. For this binding site, the amino acids selected in the experimental design are highlighted in *Table 47*. The larger amino acids were found at the top of the rank and the fourth one was Asp189. In the Schrödinger publication, they chose not to truncate any amino acids in this system.<sup>9</sup> The binding site of 1XKA was larger than the previous one studied, given the movement of Tyr99. Therefore, in this case, one might not need to truncate any residue.

AA_ID	Name	R SMILES	heavy	#DR	score
TRP215	TRP	[*]Cc1c[nH]c2ccccc12	10	1	10
TYR99	TYR	[*]Cc1ccc(O)cc1	8	1	8
PHE174	PHE	[*]Cc1ccccc1	7	1	7
ASP189	ASP	[*]CC(O)=O	4	1	4
VAL213	VAL	[*]C(C)C	3	1	3
GLN192	GLN	[*]CCC(N)=O	5	2	2.5
GLN61	GLN	[*]CCC(N)=O	5	2	2.5
SER195	SER	[*]CO	2	1	2
CYS220	CYS	[*]CS	2	1	2
ALA190	ALA	[*]C	1	0	0

*Table 47:* Prioritised amino acids for binding site 1XKA

The IFD results from the eight experiments are presented in *Table 48*. The IFDScores as well as the GlideScores were comparable for the top ranked poses. However, the ligand RMSDs and the visual inspection of the poses compared to the crystal pose of **16** revealed that there was some disparity, not reflected by the scores.

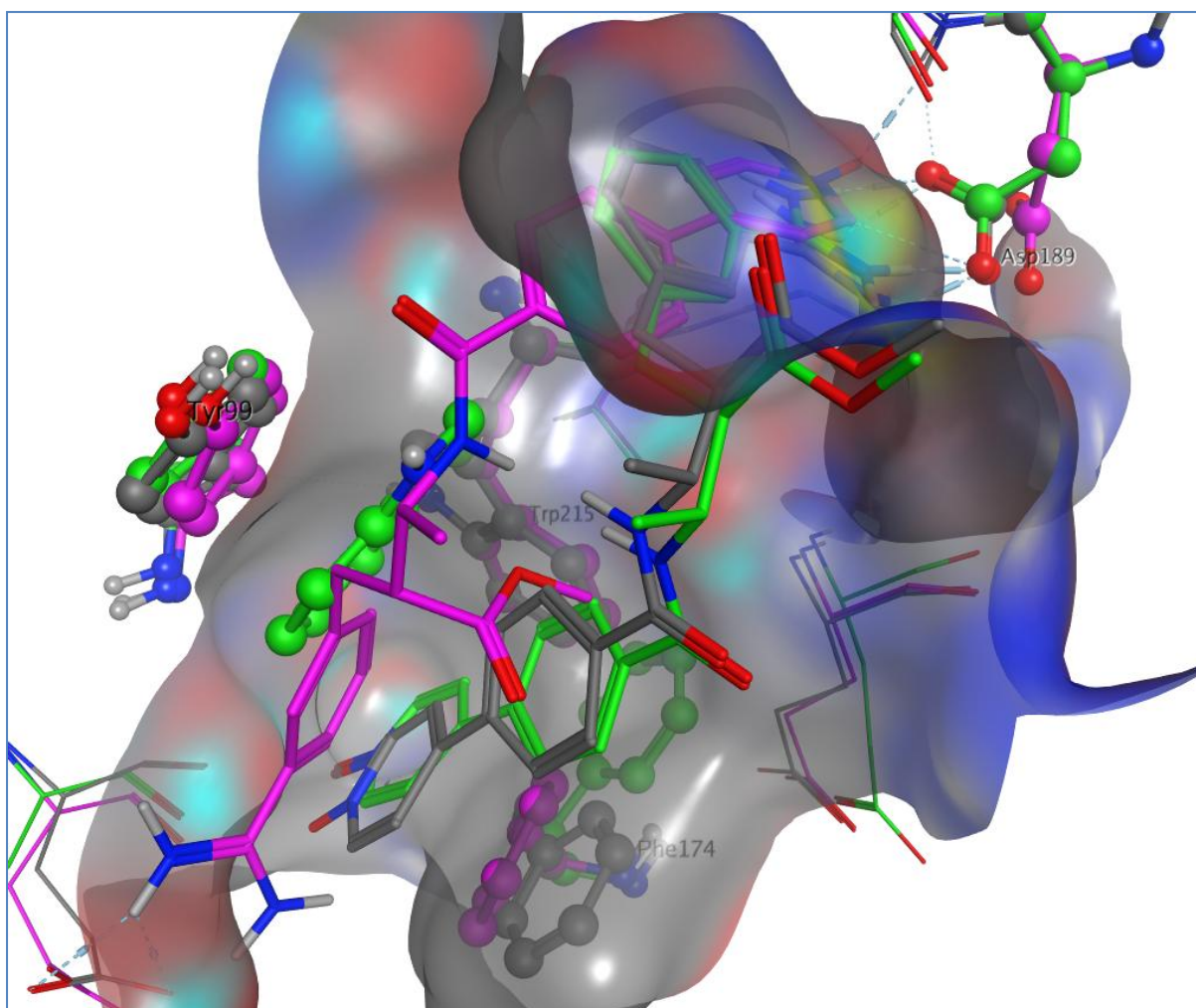
Exp	Ligand	IFDScore	GlideScore	Prime energy	RMSD	Visual assessment
1	16	-743	-10.0	-14654	9.7	Wrong
2	16	-745	-11.8	-14673	0.9	Good
3	16	-744	-10.3	-14678	3.3	Ok
4	16	-747	-11.6	-14701	2.2	Ok
5	16	-747	-12.8	-14692	2.5	Ok
6	16	-743	-10.4	-14656	9.6	Wrong
7	16	-743	-10.3	-14645	9.6	Wrong
8	16	-746	-11.2	-14696	2.4	Ok

Table 48: Summary of standard IFD results when docking **16** in 1XKA

Figure 107 shows the top ranked poses for Experiments 1 and 2 compared to the original conformation of 1XKA and the crystal pose of **16**. In Experiment 1, all four prioritised amino acids were truncated. Whilst the aromatic residues, which were Trp215, Tyr99 and Phe174, occupied a similar conformation to the starting crystal structure, the rotamer of Asp189 was different, rotated down compared to crystal structure 1XKA (in grey in Figure 107). The top scoring pose of **16** is found back to front compared to the expected crystal pose with the benzamidine moiety bound on the opposite side of the binding site with regards to Asp189.  $\pi$ - $\pi$  interactions between the benzamidine of **16** and Phe174, Tyr99 and Trp215 was observed as well hydrogen bonds from the amidine to the side chain of Glu97. The N-oxide pyridine interacts with the backbone NH of Ala190 situated next to Asp189. The ligand RMSD for this docking pose is large at 9.7 Å. Experiments 1, 6 and 7, in which Asp189 is truncated, are the ones with the worst RMSDs, which leads here also to the role of Asp189 in the binding event as observed in the previous set of experiments. Asp189 is the amino acid with the worst performance, with 3 experiments out of 4 leading to the wrong answer.

Experiment 2, for which no truncations were performed, also returned a very plausible docking pose. The benzamidine moiety was found in the correct location, interacting with Asp189. In order to accommodate **16**, residue Gln192 had to move away from the ester group. The hydrogen bond interaction between the amide carbonyl and the backbone NH of Gly219, seen in the crystal structure, is conserved. The  $\pi$ - $\pi$  interaction between the N-oxide pyridine and Phe174 is also maintained, although Phe174 is found in another rotamer (*Figure 107*). One unexpected movement noticed in this induced conformation of fXa, is the flip of Trp215 introducing a  $\pi$ - $\pi$  interaction with Tyr99. This could be due to the movement of Phe174.





*Figure 107: Comparison of 1XKA crystal structure in grey with induced protein-ligand complexes when docking **16**: in green, without any truncation, and in magenta when truncating all four prioritised residues. Crystal pose of ligand **16** also shown in grey*

The best ligand RMSD, which comes from one of the top three ranking poses, found by the Schrödinger group in this instance was 1.6 Å.<sup>9</sup> The results obtained for Experiment 2 are comparable in terms of ligand RMSD, giving an even better RMSD of 0.9 Å. As the Schrödinger group did not truncate any amino acids in their experiment, their results are directly comparable to Experiment 2 and a closer docking pose was achieved here. However, any combination of truncations performed yielded less satisfactory results, with respect to the RMSD.

### 7.2.3. Apo CDK2 structure 1BUH

As described in Section 7.1, side chains of amino acids within 4 Å of the ligand pose were selected. The resulting list can be matched to the look-up table (*Table 42*) and sorted in descending order of the score. This produces a list of binding site amino acid side chains, with the top scoring ones to be considered for temporary truncation.

*Table 49* shows the output for the binding site of structure 1BUH. The two phenylalanines present in its binding site are located at the top of the table.

AA_ID	Name	R SMILES	heavy	#DR	score	Distance from ligand centroid
PHE80	PHE	<chem>[*]Cc1ccccc1</chem>	7	1	7	
PHE82	PHE	<chem>[*]Cc1ccccc1</chem>	7	1	7	
ASP145	ASP	<chem>[*]CC(O)=O</chem>	4	1	4	
VAL18	VAL	<chem>[*]C(C)C</chem>	3	1	3	Within 4 Å
VAL64	VAL	<chem>[*]C(C)C</chem>	3	1	3	Within 4.5 Å
LEU134	LEU	<chem>[*]CC(C)C</chem>	4	2	2	
ILE10	ILE	<chem>[*]C(C)CC</chem>	4	2	2	
LYS33	LYS	<chem>[*]CCCCN</chem>	5	4	1	
ALA144	ALA	<chem>[*]C</chem>	1	0	0	
ALA31	ALA	<chem>[*]C</chem>	1	0	0	

*Table 49:* Prioritised amino acids for the binding site of 1BUH, sorted by decreasing score

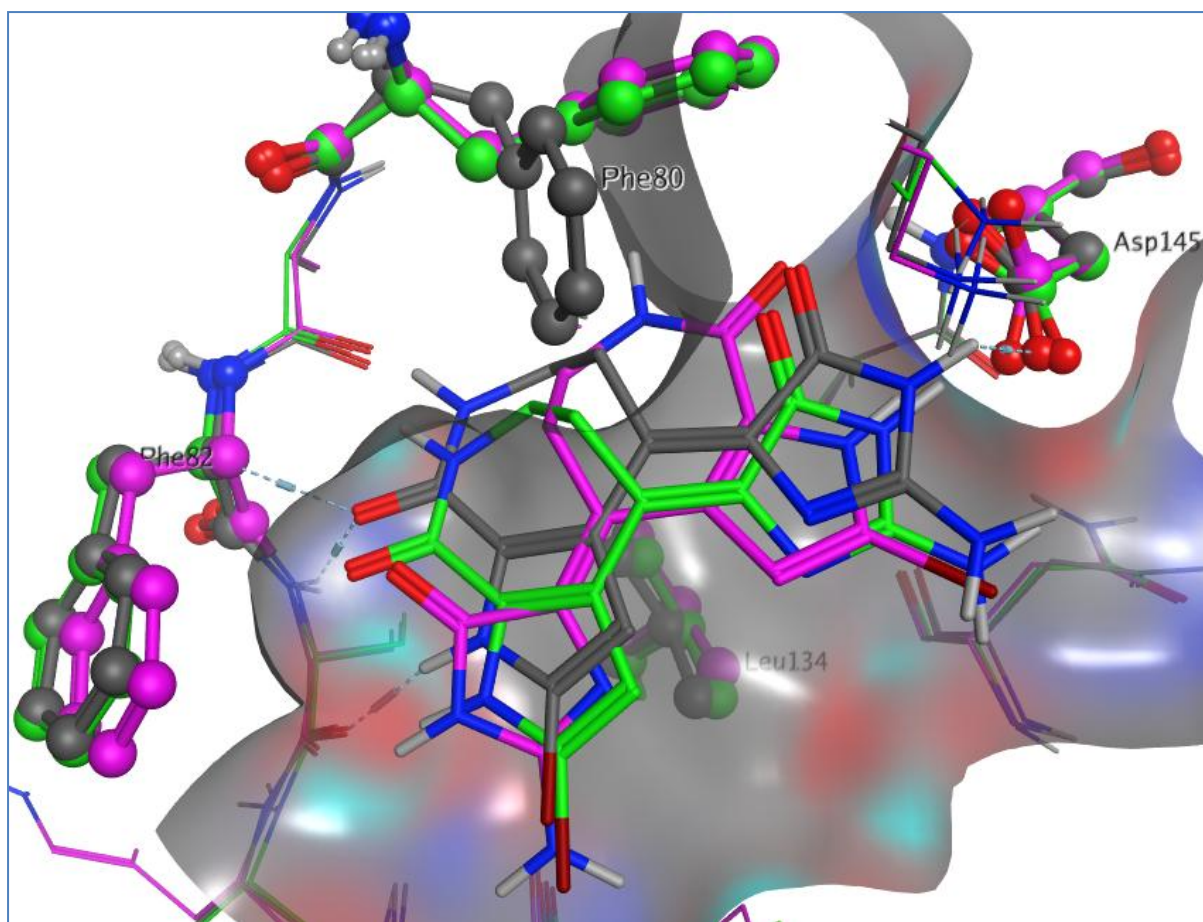
The four amino acids highlighted in *Table 49* were then used to run the eight experiments described in *Table 43*, with Factor1 being Phe80, Factor2 Phe82, Factor3 Asp145 and Factor4 Val18. With this prioritised list, IFD runs were set up keeping the same parameters as used in previous IFD experiments. The only change between runs was the amino acids picked for truncation.

Table 50 summarises the various scores obtained when docking **11** in 1BUH. The right binding pose was found as the top scoring pose for Experiment 2, 6, 7 and 8.

Experiment	Ligand	IFDScore	GlideScore	Prime Energy	Ligand RMSD	Visual assessment
1	11	-573	-9.4	-11286	5.1	Wrong
2	11	-575	-9.2	-11309	2.0	Ok
3	11	-574	-9.1	-11301	5.1	Wrong
4	11	-574	-7.8	-11318	6.0	Wrong
5	11	-574	-8.6	-11318	6.0	Wrong
6	11	-575	-10.5	-11292	0.9	Good
7	11	-573	-8.9	-11281	5.3	Ok
8	11	-577	-10.4	-11330	0.9	Good

Table 50: Summary of IFD results when docking ligand **11** in 1BUH, reporting only the top scoring pose for each, with the “no-change” experiment highlighted in blue

Two examples of output poses will be described in more details. The first one was generated when running Experiment 3 (truncating Phe80 and Asp145). The RMSD between the crystal pose of **11** and the docking pose in the induced complex is 5.1 Å. As can be seen from *Figure 108* in magenta, Phe80 was rotated away from its initial position in 1BUH following on from the truncation. This is the position that was expected to be found when **11** binds to CDK2.



*Figure 108:* Comparison of 1BUH crystal structure in grey with induced protein-ligand complexes when docking **11**: in magenta, when truncating Phe80 and Asp145 and in green, when truncating Phe80 and Phe82. Crystal pose of ligand **11** also shown in grey

The conformation of Phe80, however, was not sufficient to find the right binding pose, as the docking pose was flipped by 180 degrees (*Figure 108*). There was a bidentate hydrogen bond to the hinge, between the five membered ring amide and the backbone carbonyl and NH of Leu83. Overall, the docking pose was not plausible, even though Phe80 was flipped upwards to occupy the correct rotamer. It was noted that Asp145 was pointing into the binding site as opposed to out as seen in the 1DM2 crystal structure (*Figure 109*).

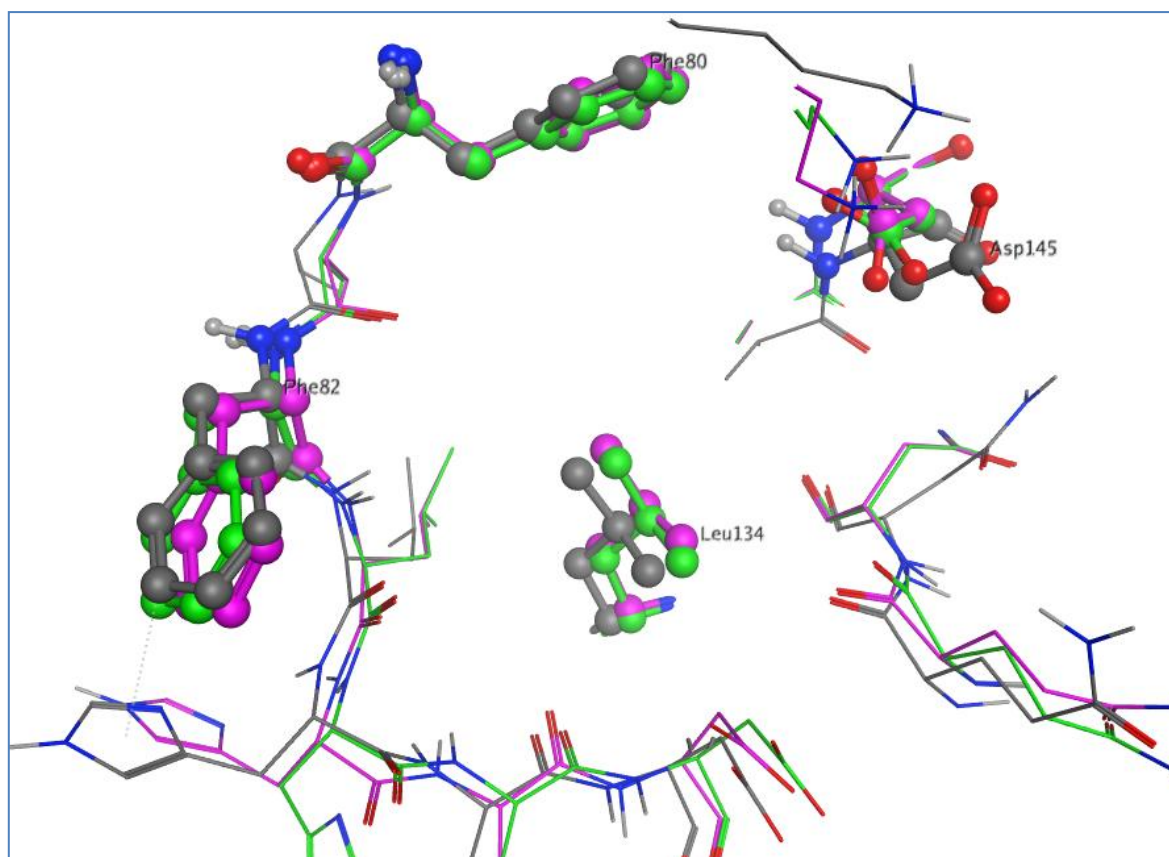


*Figure 109:* Comparison of the conformations of the four amino acids of interest: 1DM2 crystal structure in grey, induced proteins from Experiment 8 in green and from Experiment 3 in magenta

The second results are from Experiment 8, when mutating Phe80 and Phe82, which reproduced the right binding mode for **11**. The top scoring pose can be seen in *Figure 108*, in green. The conformation of Phe80 after the truncation and re-addition/optimisation step is very similar to the one obtained in the previous experiment and to the one found in 1DM2. The docking pose of **11** compared to its crystal pose gives an RMSD of 0.9 Å, which is very reasonable. This is also confirmed by the visual comparison with the crystal pose: the docking pose of **11** is in the right orientation and location and interacts with the hinge through hydrogen bonds to the backbones of Leu83 and Glu81.

The two experiments described above involved the truncation of Phe80. On one occasion, it was possible to get to the right binding pose as the top scoring docking pose (Experiment 8), but not in the other example (Experiment 3), although in both cases the right conformation for Phe80 was obtained. A plausible docking pose for **11** from Experiment 3 can however be found at rank 4 (IFDScore = -574 kcal/mol; GlideScore = -9.3 kcal/mol, Prime Energy = -11287 kcal/mol; RMSD = 1.1 Å). This highlights again the need for a better scoring function than the standard IFDScore.

*Table 51* summarises the findings when docking **12** in 1BUH and running the eight different experiments described in *Table 43*. The same four amino acids were prioritised.

Experiment	Ligand	IFDScore	GlideScore	Prime Energy	Ligand RMSD	Visual assessment
1	12	-571	-10.1	-11225	1.4	Good
2	12	-570	-9.9	-11195	4.1	Wrong
3	12	-569	-9.5	-11189	5.3	Wrong
4	12	x	x	x	x	Failed
5	12	-569	-9.8	-11176	6.1	Wrong
6	12	-572	-9.9	-11235	3.6	Wrong
7	12	-569	-10.6	-11171	6.0	Wrong
8	12	-571	-9.8	-11223	3.6	Wrong

*Table 51: Summary of IFD results when docking ligand **12** in 1BUH, with the “no-change” experiment highlighted in blue*

Docking of **12** in 1BUH generated disparate results, with three experiments leading to the correct binding mode, four others achieved the wrong pose and one failing to run. The results from Experiment 1, where all four amino acids were truncated, and Experiment 6, where residues Phe80 and Val18 were truncated, are described further. The top scoring

docking poses from both experiments can be found in *Figure 111* compared to the starting 1BUH crystal structure.

The truncation of all four prioritised amino acids led to finding a plausible top scoring docking pose. As can be seen from *Figure 111*, the orientation and location of **12** compared to its crystal pose were acceptable, even though not exact. The docking pose made a bidentate interaction with the carbonyl of Glu81 and the NH of Leu83 on the hinge. The RMSD between this pose and the crystal pose of **12** was 1.4 Å. This RMSD is satisfactory, and could have been smaller if the docking pose had not been shifted up the binding site towards Phe80 compared to the crystal pose. On the other hand, when truncating both Phe80 and Val18, the top scoring docking pose of **12** was rotated by 90 degrees and, therefore, not able to interact with the hinge. The RMSD for this docking pose compared to the crystal pose was 3.6 Å. When looking more closely at Phe80 in these two conformations, it was also flipped upwards as in the previous two examples when docking **11** and truncating Phe80.

From the results in *Table 51*, one can compare IFDScore to both GlideScore and Prime Energy. There is no real correlation between IFDScore and GlideScore as can be seen in *Figure 110a*. The less favourable IFDScore (-569, *Figure 110a*) corresponds to GlideScores ranging from -9.5 to -10.6 kcal/mol. Whereas, more favourable IFDScores (-570 → -572) match GlideScores clustered around -9.9 (*Figure 110a*). A linear regression analysis of the relationship between the GlideScore and the IFDScore result in a correlation coefficient of 0.003, which indicates that there is effectively no correlation between the two parameters. In contrast, there appears to be a direct correlation between the IFDScore and the Prime Energy (*Figure 110b*), even though one cannot conclude that the correlation between these numbers is particularly strong, due to the relatively restricted range of the IFDScores. The

calculated correlation coefficient measuring the relationship between the Prime Energy and the IFDScore is 0.94, indicating that the two variables are positively correlated. Nonetheless, this basic analysis indicates that the IFDScore is driven more by Prime Energy than GlideScore.

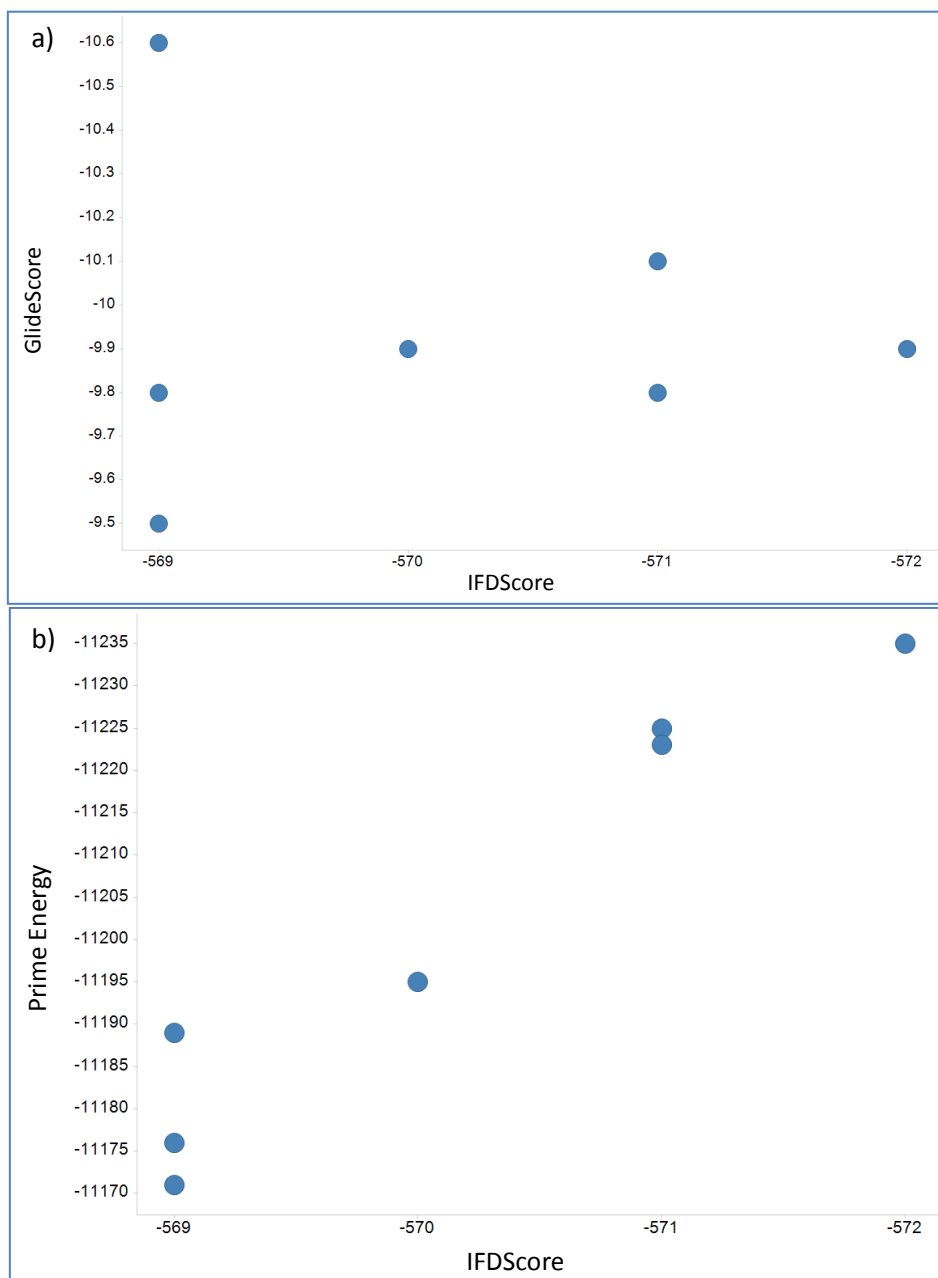
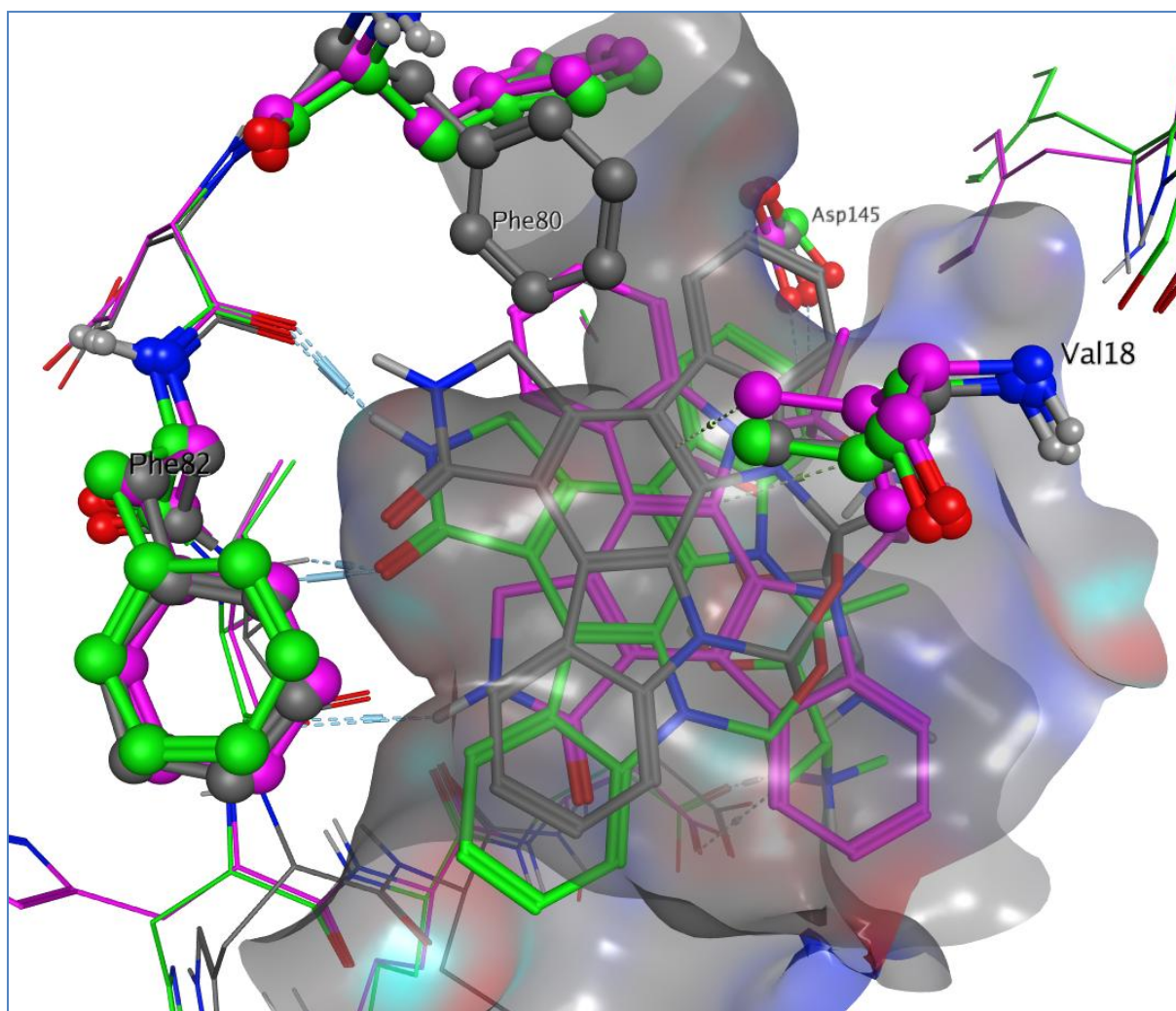


Figure 110: Correlation between IFDScore and a) GlideScore and b) Prime Energy for the top scoring docking poses when docking flexibly **12** in 1BUH





*Figure 111: Comparison of 1BUH crystal structure in grey with induced protein-ligand complexes when docking **12**: in magenta, when truncating Phe80 and Val18 and in green, when mutating all four amino acids. Crystal pose of ligand **12** also shown in grey*

The experiments that output the best scoring poses were Experiments 1, 6 and 8 (*Table 51*). A visual inspection of these docking poses showed that they were all in the wrong orientation compared to the crystal pose of **12**, with the exception of the pose from Experiment 1, and made only one interaction with the hinge region (with the backbone carbonyl of Leu83, on the outside of the hinge region).

#### 7.2.4. CDK2 structure 1DM2

Ligand **11** is bound to CDK2 in crystal structure 1DM2. Amino acid side chains for this binding site were selected following the previously described protocol. The list of amino acids can be found in *Table 52*. The top four scoring amino acids were used in the 4-factor experimental design. Phe80 and Phe82 were easily prioritised with a score of 7. However, in this instance, the other two amino acids could not be chosen from just the score. Indeed, three of them returned a score of 4 (*Table 52*). Therefore, the additional distance parameter was used to help in the selection. Asn132 and Asp145, the two residues closest to the ligand centroid, were prioritised.

Ligand **11** was crystallised bound to the 1DM2 crystal structure of CDK2. For this reason, this ligand was not part of the following set of experiments, as this would be equivalent to re-docking and would not contribute to assessing the validity of the altered protocol.

AA_ID	Name	R SMILES	heavy	#DR	score	Distance from ligand centroid
PHE80	PHE	[*]Cc1ccccc1	7	1	7	
PHE82	PHE	[*]Cc1ccccc1	7	1	7	
ASP145	ASP	[*]CC(O)=O	4	1	4	Within 7 Å
ASP86	ASP	[*]CC(O)=O	4	1	4	Within 9 Å
ASN132	ASN	[*]CC(N)=O	4	1	4	Within 8 Å
THR14	THR	[*]C(C)O	3	1	3	
VAL64	VAL	[*]C(C)C	3	1	3	
VAL18	VAL	[*]C(C)C	3	1	3	
LEU134	LEU	[*]CC(C)C	4	2	2	
LEU83	LEU	[*]CC(C)C	4	2	2	
ILE10	ILE	[*]C(C)CC	4	2	2	
LYS33	LYS	[*]CCCCN	5	4	1.3	
ALA144	ALA	[*]C	1	0	0	
ALA31	ALA	[*]C	1	0	0	

Table 52: Prioritised amino acids for the binding site of 1DM2, sorted by decreasing score; amino acids selected for temporary truncation highlighted in blue

Ligand **12** was docked in 1DM2, following the experimental design described in Table 43. The results of the eight IFD runs are reported in Table 53. All IFDScores are within 5 kcal/mol of each other, which is a rather narrow range. Four of the experiments produced the right binding mode as the top scoring pose, including Experiment 2 where no amino acids side chains were truncated.

Experiment	Ligand	IFDScore	GlideScore	Prime energy	$\Delta$ Prime Energy	Ligand RMSD	Visual assessment
1	12	-575	-13.2	-11240	-61	1.6	Good
2	12	-578	-12.5	-11317	-95	0.7	Good
3	12	-575	-12.9	-11249	-60	1.7	Good
4	12	-575	-13.2	-11236	-55	2.1	Good
5	12	-578	-13.4	-11290	-104	1.0	Good
6	12	-579	-13.1	-11316	-98	0.6	Good
7	12	-576	-13.0	-11251	-63	0.8	Good
8	12	-578	-12.8	-11304	-111	1.7	OK

Table 53: Summary of IFD results when docking ligand **12** in 1DM2, with the “no-change”

experiment highlighted in blue

The analysis of the decomposition of the IFDScore into its constituent components show a similar trend to that observed for the docking of **12** into 1BUH. Namely, that there is little to no correlation between the GlideScore and the IFDScore ( $R = 0.04$ , *Figure 112a*), while there appears to be a direct correlation between the Prime Energy and the IFDScore ( $R = 0.93$ , *Figure 112b*). Despite the apparent correlation between the IFDScore and the Prime Energy, the data from this simulation could also be interpreted as two distinct clusters. That is, there is a cluster of four structures that score well both in terms of their favourable Prime Energy and their IFDScore, whereas a second cluster of structures have lower IFDScores and also lower Prime Energies. It is interesting to note, that the two clusters (based on the IFDScores) remain independent of the GlideScore, with the higher scoring cluster containing both the best and worst results from the GlideScore (*Figure 112a*). Therefore, while the calculated correlation coefficient may not be particularly meaningful for the size of the data set and the range of scores attained, it is nevertheless clear that the IFDScore is driven primarily by the Prime Energy and the GlideScore has little effect.

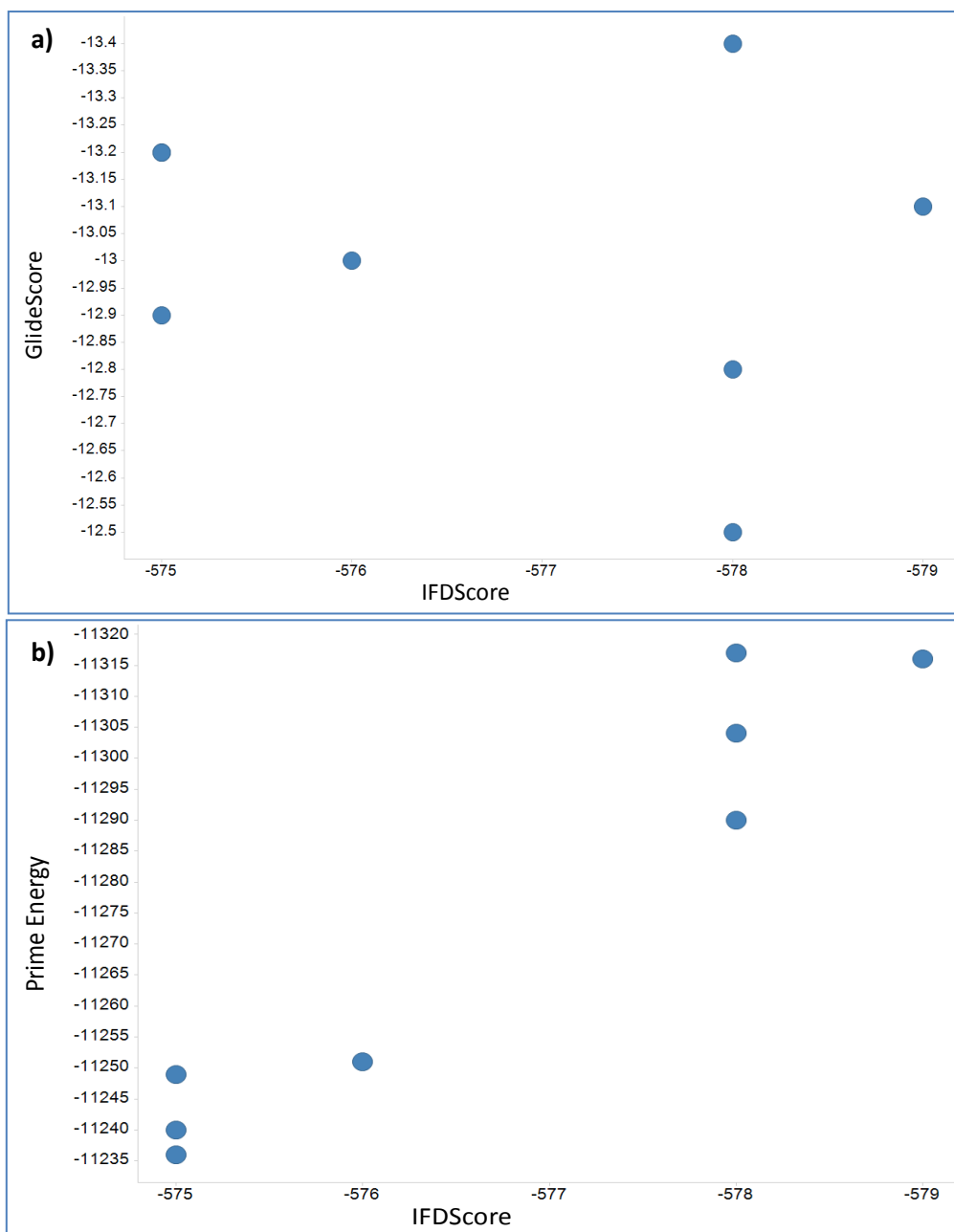
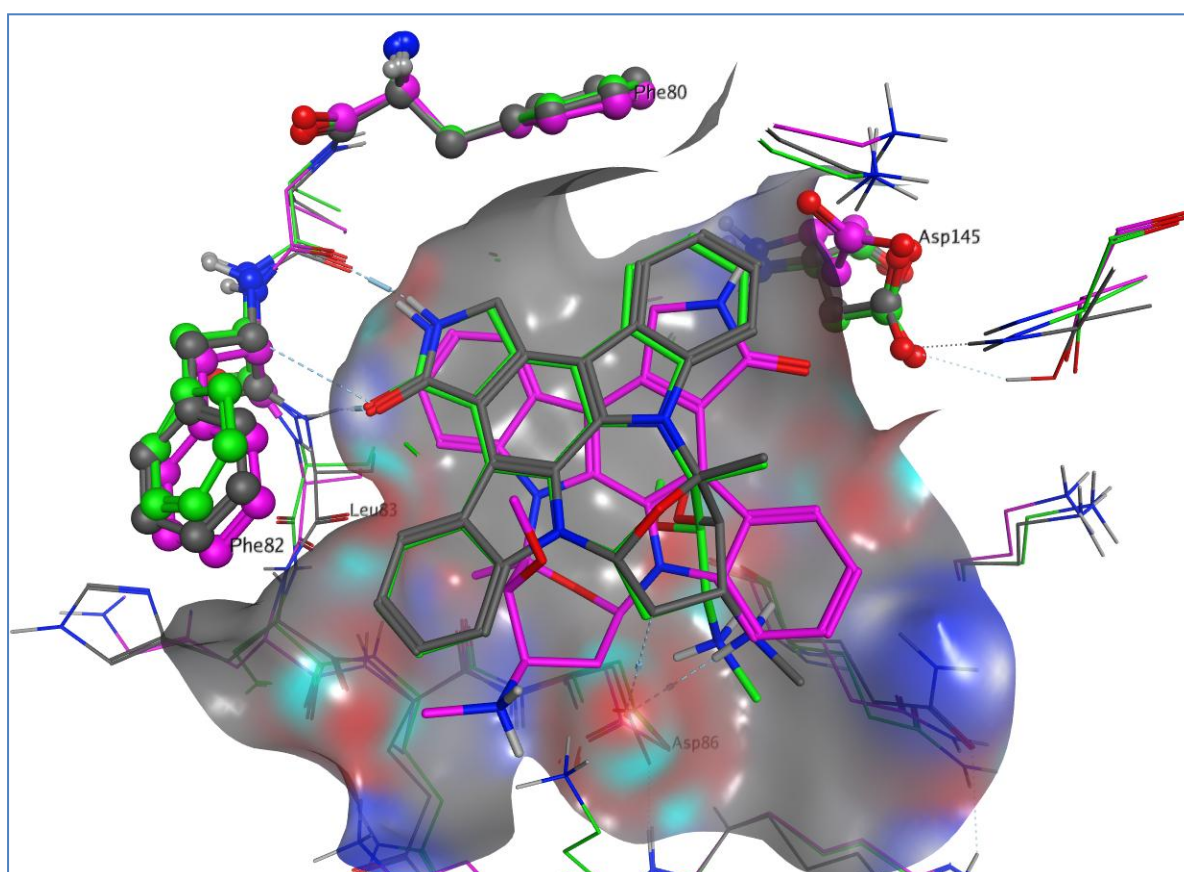


Figure 112: Correlation between a) IFDScore and GlideScore and b) IFDScore and Prime Energy for the top scoring docking poses from the eight experiments run when docking flexibly **12** in 1DM2

Figure 113 shows the top scoring poses of **12** from Experiments 1 and 6 compared to its crystal pose seen in structure 1AQ1. The pose from Experiment 1 was in the wrong orientation with the hinge-binding moiety interacting with Asp145, situated at the back of

the pocket compared to the hinge. In Experiment 1, all four prioritised amino acid side chains were truncated. On the contrary, in Experiment 6, the exact binding pose was found as the top scoring docking pose, with a very low RMSD of 0.6 Å. In this case, the side chains of amino acids Phe80 and Asp145 were truncated. It is important to note that Experiment 2, where no side chains were truncated, also produced the right binding mode as the top scoring pose. This might lead to the conclusion that with such a binding site, where there are no apparent problematic amino acids, it is not worthwhile truncating any side chains when using induced fit docking.



*Figure 113:* Comparison of 1DM2 crystal structure in grey with induced protein-ligand complexes when docking **12**: in magenta, when truncating all four amino acids and in green, when mutating Phe80 and Asp145. Crystal pose of ligand **12** also shown in grey

The modified IFDScores were computed for this set of experiments. The ligand pose RMSD as well as the binding site RMSD were also calculated for each experiment and each induced

fit complex within those, as described in Section 7.1. An example of output is shown in *Table 54*. The data shows that there are, for this experiment, notable differences between the old IFDScore and the new ones. In terms of RMSDs, the best combination is Entry 1 which had the best old IFDScore. However, Entry 2 which could be prioritised with new IFDScore\_5 and IFDScore\_10 also shows reasonable RMSDs. On the other hand, Entry 5, which would be prioritised with new IFDScore\_20 up to IFDScore\_100, presents a high ligand RMSD of 4.2 Å and would be too distant from the correct binding mode.

Entry	ligand RMSD	BS RMSD	old_IFD Score	Glide Score	PE <sub>IFD</sub>	ΔPE	new_IFD Score _1	new_IFD Score _5	new_IFD Score _10	new_IFD Score _20	new_IFD Score _30	new_IFD Score _40	new_IFD Score _50	new_IFD Score _60	new_IFD Score _70	new_IFD Score _80	new_IFD Score _90	new_IFD Score _100
1	1.1	0.7	-578	-12.5	-11319	-94.7	-13.5	-17.3	-22.0	-31.5	-40.9	-50.4	-59.9	-69.3	-78.8	-88.3	-97.7	-107.2
2	1.8	0.8	-578	-12.7	-11320	-95.5	-13.6	-17.5	-22.2	-31.8	-41.3	-50.9	-60.5	-70.0	-79.6	-89.1	-98.7	-108.2
3	2.3	0.9	-578	-12.9	-11305	-80.7	-13.7	-16.9	-20.9	-29.0	-37.1	-45.1	-53.2	-61.3	-69.3	-77.4	-85.5	-93.6
4	4.1	0.9	-577	-11.5	-11319	-94.6	-12.5	-16.2	-21.0	-30.4	-39.9	-49.3	-58.8	-68.3	-77.7	-87.2	-96.6	-106.1
5	4.2	1.0	-576	-10.3	-11333	-107.7	-11.4	-15.7	-21.0	-31.8	-42.6	-53.4	-64.1	-74.9	-85.7	-96.5	-107.2	-118.0
6	5.1	1.1	-576	-10.6	-11330	-105.1	-11.7	-15.9	-21.1	-31.6	-42.1	-52.7	-63.2	-73.7	-84.2	-94.7	-105.2	-115.7
7	2.0	1.0	-576	-10.5	-11330	-105.3	-11.6	-15.8	-21.0	-31.6	-42.1	-52.6	-63.1	-73.7	-84.2	-94.7	-105.2	-115.8
8	2.1	0.7	-575	-10.6	-11313	-88.5	-11.5	-15.0	-19.4	-28.3	-37.1	-46.0	-54.8	-63.7	-72.5	-81.4	-90.2	-99.1
9	4.9	1.1	-575	-10.4	-11326	-101.1	-11.4	-15.5	-20.5	-30.7	-40.8	-50.9	-61.0	-71.1	-81.2	-91.3	-101.4	-111.5
10	5.8	1.0	-575	-10.3	-11321	-95.8	-11.3	-15.1	-19.9	-29.5	-39.0	-48.6	-58.2	-67.8	-77.3	-86.9	-96.5	-106.1
11	6.4	1.0	-571	-5.7	-11332	-106.9	-6.8	-11.1	-16.4	-27.1	-37.8	-48.5	-59.2	-69.8	-80.5	-91.2	-101.9	-112.6
12	7.1	1.0	-569	-4.4	-11323	-98.6	-5.4	-9.4	-14.3	-24.2	-34.0	-43.9	-53.8	-63.6	-73.5	-83.4	-93.2	-103.1
13	6.6	1.1	-569	-4.2	-11328	-103.7	-5.3	-9.4	-14.6	-25.0	-35.3	-45.7	-56.1	-66.4	-76.8	-87.2	-97.6	-107.9

Table 54: Data generated for the 17 induced fit complexes output of Experiment 2 when docking **12** in 1DM2 – the table is ordered by increasing old\_IFDScore. The best IFDScores for each column is highlighted in green and the worst in red.



### 7.3. Application of improved IFD protocol

#### 7.3.1. Apo CDK2 structure 4EK3

4EK3 is another apo structure of CDK2. It is in a different conformation to the one found in structure 1BUH. Indeed, in this case, Phe80 occupies its most common rotamer (as seen in 1DM2 and 1AQ1), whilst Lys33 is protruding into the binding site. There are other CDK2 structures with Lys33 protruding in the binding site, such as 1PXL or 3QTS for example, but with lower resolution and less well defined electron density for the lysine side chain (the electron density for 4EK3 is 1.34 Å). This conformation is an attractive example to test the validity of our function that is designed to prioritise amino acids. *Figure 114* shows the difference in conformation between the two apo structures 1BUH and 4EK3 and an example of a structure with a ligand bound, such as 1DM2. It is clear from this representation that for 1BUH, Phe80 points towards the interior of the binding site, whilst for 4EK3, it is Lys33. In both cases, these amino acids reduce the size of the binding site quite considerably.

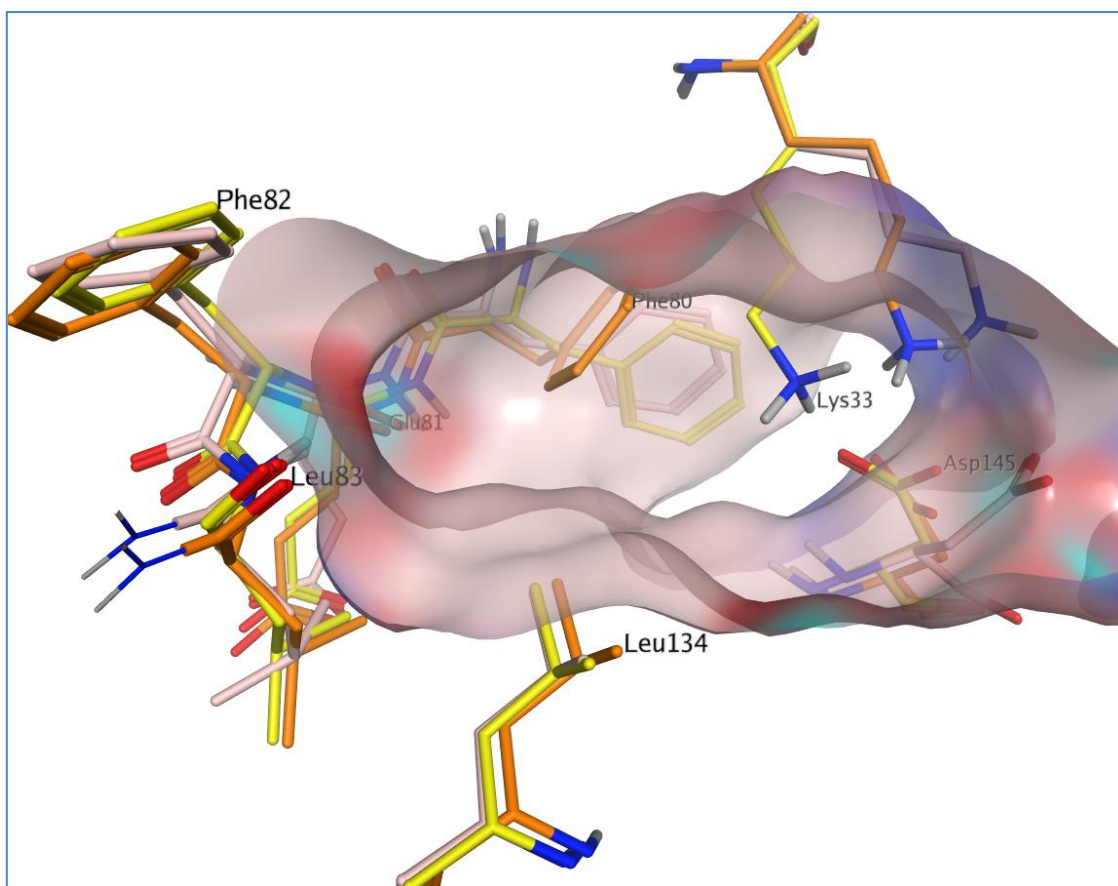


*Figure 114:* Comparison of apo binding sites 1BUH in orange and 4EK3 in yellow to the binding site in 1DM2 in light pink; the surface of 1DM2 binding site shown in solid light pink

The hypothesis behind the development of the amino acid scoring function was that flexible hindering amino acids were more likely to move away from the interior of the binding site during the Prime optimisation step and, therefore, be less problematic for the actual docking of ligands. Lysine is categorised as a flexible amino acids and has a score of 1.3, as seen in *Table 55*, and is, therefore, found at the bottom of the sorted list. If docking of ligands **11** and **12** is successful when protruding Lys33 is not truncated, then it will strengthen the validity of the scoring function derived for the prioritisation of amino acids. The validation will be even more robust if Experiment 2, in which no amino acids are truncated, cannot produce the respective correct binding modes.

AA_ID	Name	R SMILES	heavy	#DR	score	Distance from ligand centroid
PHE80	PHE	[*]Cc1ccccc1	7	1	7	
PHE82	PHE	[*]Cc1ccccc1	7	1	7	
ASP86	ASP	[*]CC(O)=O	4	1	4	Within 9 Å
ASP145	ASP	[*]CC(O)=O	4	1	4	Within 5 Å
ASN132	ASN	[*]CC(N)=O	4	1	4	Within 7 Å
VAL64	VAL	[*]C(C)C	3	1	3	
LEU134	LEU	[*]CC(C)C	4	2	2	
LYS33	LYS	[*]CCCCN	5	4	1.3	
LYS89	LYS	[*]CCCCN	5	4	1.3	
ALA31	ALA	[*]C	1	0	0	

Table 55: Prioritised list of amino acids for the binding site of structure 4EK3

The four amino acids that were truncated in turn in this set of experiments were Phe80, Phe82, Asp145 and Asn132 (highlighted in blue in Table 55). The first ligand to be studied in this system was ligand **11**. The results from the eight experiments are reported in Table 56. Only the top scoring docking pose for each experiment is reported. The range of IFDScore was rather narrow with IFDScores ranging from -623 kcal/mol to -621 kcal/mol. The correct binding mode was found as the top scoring pose in three cases, Experiments 4, 5 and 7, with the output from Experiments 4 and 5 being closer to the crystal pose (ligand RMSD = 1.4 Å). It is worth noting that these two docking poses exhibit similar IFDScores comparable to the IFDScore from Experiment 8, which output an incorrect pose.

Experiment	Ligand	IFDScore	GlideScore	Prime energy	$\Delta$ Prime Energy	Ligand RMSD	Visual assessment
1	11	-621	-7.9	-12264	-38	5.6	Wrong
2	11	-621	-9.2	-12242	-15	4.0	Wrong
3	11	-621	-8.4	-12245	-37	4.7	Wrong
4	11	-622	-9.5	-12258	-50	1.4	Good
5	11	-623	-9.8	-12256	-46	1.4	Good
6	11	-622	-9.1	-12259	-42	3.9	Wrong
7	11	-621	-8.0	-12258	-49	3.2	Ok
8	11	-623	-9.3	-12263	-47	3.4	Wrong

*Table 56:* Summary of results when docking ligand **11** into 4EK3 using the four points of change experimental design

*Figure 115* shows the top scoring docking poses for **11** for Experiments 2 and 5 compared to the starting conformation of 4EK3 and the crystal pose of **11**. The pose out of Experiment 5 was in the right orientation allowing the essential hydrogen bond interactions with the hinge. The pose was, however, slightly translated down compared to the crystal pose of **11**, although still yielding a satisfactory RMSD of 1.4 Å, which was the best RMSD among the eight top scoring poses in *Table 56*. The side chain of Lys33 has moved away from the inside of the binding site, although it was not truncated during the experiment. On the other hand, for the pose coming from Experiment 2 we can observe a binding mode flip (*Figure 115*). The interactions to the hinge were obtained and, therefore, it would have been a plausible pose, had the crystal pose not been known. In this induced protein-ligand complex, Lys33 is still pointing into the binding site, causing the generation of the incorrect binding pose due to a lack of space for the molecule to fit in the correct orientation. During this experiment, seventeen docking poses were produced. Upon inspection of all structures, it emerged that

none were in the correct binding pose and only four protein conformations had Lys33 moved away from the binding site. From other experiments conducted for this protein-ligand complex, it has been confirmed that Lys33 did not require truncation to reach the correct binding mode. In this instance, the issue could lie in the initial soft potential docking step not producing a reasonable enough pose to lead to the correct one later on, when no amino acids were truncated.

These results tend to agree with the rationale behind the amino acid scoring function. Indeed, Lys33 was able to move away from the centre of the binding site when other amino acids were truncated, whilst the no-change experiment yielded the incorrect binding pose indicating that truncations were indeed needed in this case to get to the right answer.

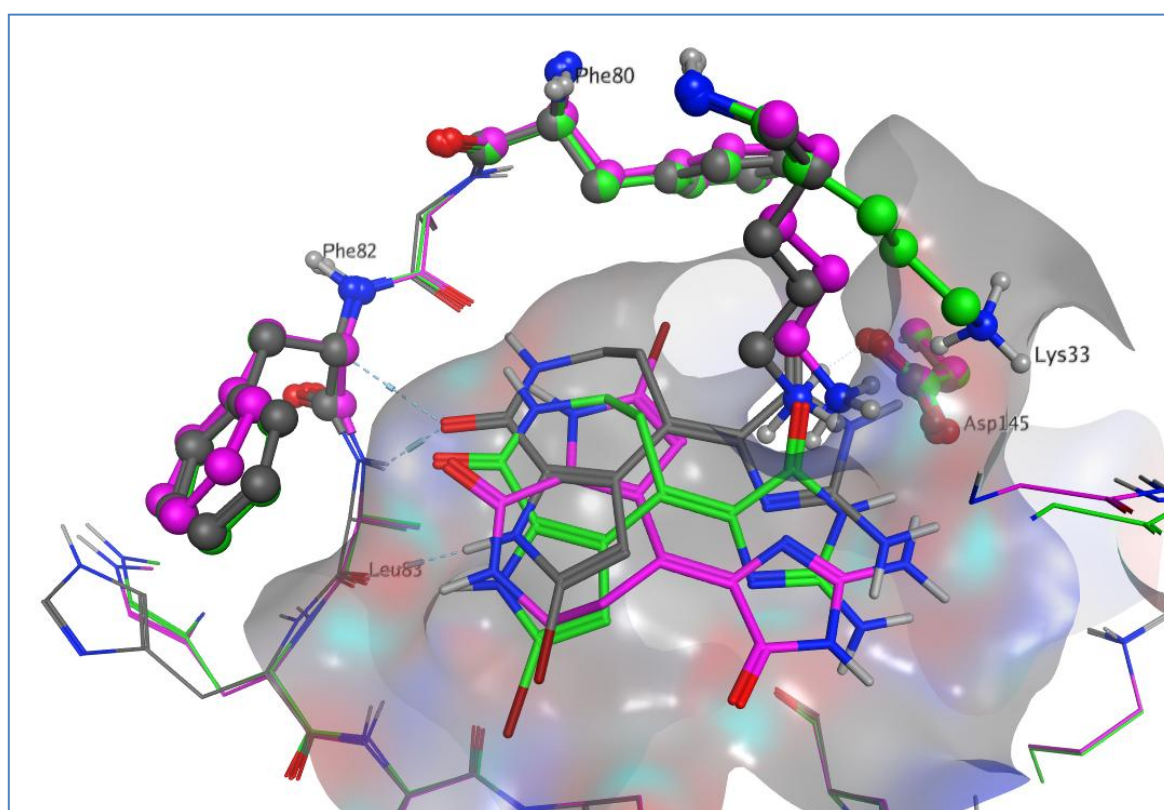


*Figure 115:* Comparison of 4EK3 crystal structure in grey with induced protein-ligand complexes when docking **11**: in magenta, when truncating all four prioritised amino acids and in green, when mutating Phe82 and Asp145. Crystal pose of ligand **11** also shown in grey

From the new IFDScores and ligand and binding site RMSDs shown in *Table 57*, the new IFDScore\_1 and IFDScore\_5 prioritise Entry 3, which presented the lowest ligand RMSD (2.5 Å), with also a reasonable binding site RMSD of 0.9 Å.

Entry	ligand RMSD	BS RMSD	old_IFD Score	Glide Score	PE <sub>IFD</sub>	ΔPE	new_IFD Score <sub>_1</sub>	new_IFD Score <sub>_5</sub>	new_IFD Score <sub>_10</sub>	new_IFD Score <sub>_20</sub>	new_IFD Score <sub>_30</sub>	new_IFD Score <sub>_40</sub>	new_IFD Score <sub>_50</sub>	new_IFD Score <sub>_60</sub>	new_IFD Score <sub>_70</sub>	new_IFD Score <sub>_80</sub>	new_IFD Score <sub>_90</sub>	new_IFD Score <sub>_100</sub>
1	4.2	1.1	-623	-9.3	-12132	-46.9	-9.8	-11.7	-14.0	-18.7	-23.4	-28.1	-32.8	-37.5	-42.2	-46.9	-51.6	-56.3
2	3.2	0.9	-622	-9.1	-12134	-49.4	-9.6	-11.6	-14.1	-19.0	-23.9	-28.9	-33.8	-38.8	-43.7	-48.6	-53.6	-58.5
3	2.5	0.9	-622	-9.5	-12130	-45.4	-10.0	-11.8	-14.0	-18.6	-23.1	-27.6	-32.2	-36.7	-41.3	-45.8	-50.3	-54.9
4	4.9	0.9	-622	-8.6	-12132	-46.8	-9.0	-10.9	-13.3	-17.9	-22.6	-27.3	-32.0	-36.6	-41.3	-46.0	-50.7	-55.3
5	4.4	0.8	-622	-8.7	-12123	-37.8	-9.0	-10.6	-12.4	-16.2	-20.0	-23.8	-27.6	-31.4	-35.1	-38.9	-42.7	-46.5
6	5.3	0.9	-621	-8.3	-12126	-41.3	-8.7	-10.3	-12.4	-16.5	-20.6	-24.8	-28.9	-33.0	-37.2	-41.3	-45.4	-49.5
7	5.8	1.2	-621	-8.1	-12124	-38.6	-8.5	-10.0	-12.0	-15.8	-19.7	-23.6	-27.4	-31.3	-35.1	-39.0	-42.9	-46.7
8	4.4	1.1	-621	-8.3	-12121	-36.3	-8.6	-10.1	-11.9	-15.5	-19.2	-22.8	-26.4	-30.1	-33.7	-37.3	-41.0	-44.6
9	4.5	1.2	-621	-7.8	-12125	-39.7	-8.2	-9.8	-11.8	-15.8	-19.7	-23.7	-27.7	-31.7	-35.6	-39.6	-43.6	-47.6
10	5.8	1.2	-621	-7.7	-12124	-39.3	-8.1	-9.7	-11.6	-15.6	-19.5	-23.4	-27.4	-31.3	-35.2	-39.2	-43.1	-47.0
11	5.0	0.9	-620	-7.5	-12130	-44.8	-8.0	-9.8	-12.0	-16.5	-20.9	-25.4	-29.9	-34.4	-38.8	-43.3	-47.8	-52.3
12	4.6	1.1	-620	-7.2	-12123	-37.9	-7.5	-9.1	-10.9	-14.7	-18.5	-22.3	-26.1	-29.9	-33.7	-37.5	-41.3	-45.1
13	5.0	1.7	-620	-7.4	-12130	-45.1	-7.8	-9.6	-11.9	-16.4	-20.9	-25.4	-29.9	-34.4	-38.9	-43.5	-48.0	-52.5
14	5.2	1.1	-620	-7.8	-12131	-45.9	-8.2	-10.0	-12.3	-16.9	-21.5	-26.1	-30.7	-35.3	-39.9	-44.5	-49.1	-53.7
15	5.0	1.1	-619	-7.4	-12126	-41.4	-7.8	-9.4	-11.5	-15.6	-19.8	-23.9	-28.1	-32.2	-36.4	-40.5	-44.6	-48.8
16	4.3	1.3	-619	-6.4	-12131	-45.7	-6.9	-8.7	-11.0	-15.6	-20.1	-24.7	-29.3	-33.9	-38.4	-43.0	-47.6	-52.1
17	4.8	1.1	-619	-6.4	-12132	-46.9	-6.9	-8.8	-11.1	-15.8	-20.5	-25.2	-29.9	-34.6	-39.2	-43.9	-48.6	-53.3
18	8.1	1.8	-618	-6.0	-12123	-37.7	-6.4	-7.9	-9.8	-13.5	-17.3	-21.1	-24.9	-28.6	-32.4	-36.2	-40.0	-43.7
19	8.8	1.3	-618	-5.8	-12130	-45.1	-6.3	-8.1	-10.4	-14.9	-19.4	-23.9	-28.4	-32.9	-37.4	-42.0	-46.5	-51.0

Table 57: Data generated for 19 induced fit complexes output from Experiment 8 when docking **11** in 4EK3, ordered by increasing old\_IFDScore. The best RMSDs and IFDScores are highlighted in green and the worst in red

New IFDScore\_10 to IFDScore\_100, however, prioritise an induced fit complex, Entry 2, with a less favourable RMSD of 3.2 Å. *Table 56* shows that the best induced complex from Experiment 8 was in the wrong orientation compared to the crystal pose of **11**, with a ligand RMSD of 4.2 Å. Entry 3 was found in the correct pose, with a slight translation of **11** towards the back of the binding site. Therefore, in this instance, new IFDScore\_1 or IFDScore\_5 would be able to identify the correct binding pose.

Ligand **12** was then docked in 4EK3 and *Table 58* reports the results.

Experiment	Ligand	IFDScore	GlideScore	Prime energy	Δ Prime Energy	RMSD	Visual assessment
1	12	-617	-10.0	-12149	-18	2.1	Ok
2	12	-619	-10.6	-12173	-30	4.7	Wrong
3	12	-617	-8.9	-12163	-50	2.1	Ok
4	12	-617	-8.9	-12157	-44	5.7	Ok
5	12	-618	-9.8	-12163	-47	1.8	OK
6	12	-618	-10.7	-12148	-35	1.2	Good
7	12	-618	-9.5	-12163	-51	2.1	Ok
8	12	-617	-9.8	-12150	-30	1.9	OK

*Table 58:* Summary of results when docking **12** flexibly in 4EK3 following the experimental design; the “no-change” experiment is highlighted in blue

*Figure 116* shows the results obtained for Experiments 2 and 6 when docking **12** in apo structure 4EK3. In both cases, Lys33 moved away from the inside of the binding site during the optimisation. Nevertheless, the two experiments led to two different poses. Experiment 6 produced the right binding mode, albeit translated slightly down compared to the crystal pose of **12**. Its RMSD of 1.2 Å confirms that it is an acceptable pose. In addition, the hydrogen bond interactions of the  $\gamma$ -lactam five membered ring with the hinge were maintained. Experiment 2, on the other hand, yielded an incorrect binding mode with the



hinge binding moiety of **12** pointing towards the front of the hinge, and not actually interacting with it (*Figure 116*). Upon visual inspection of the lower ranking poses, pose number 2 was close to the crystal pose expected for **12** with an RMSD of 2.2 Å. In addition, it is worth noting that the difference in IFDScore between these two poses is very small (IFDScore for pose number 2 was also -619 kcal/mol - *Table 59*). This indicates that the issue in this instance lies with the scoring function.

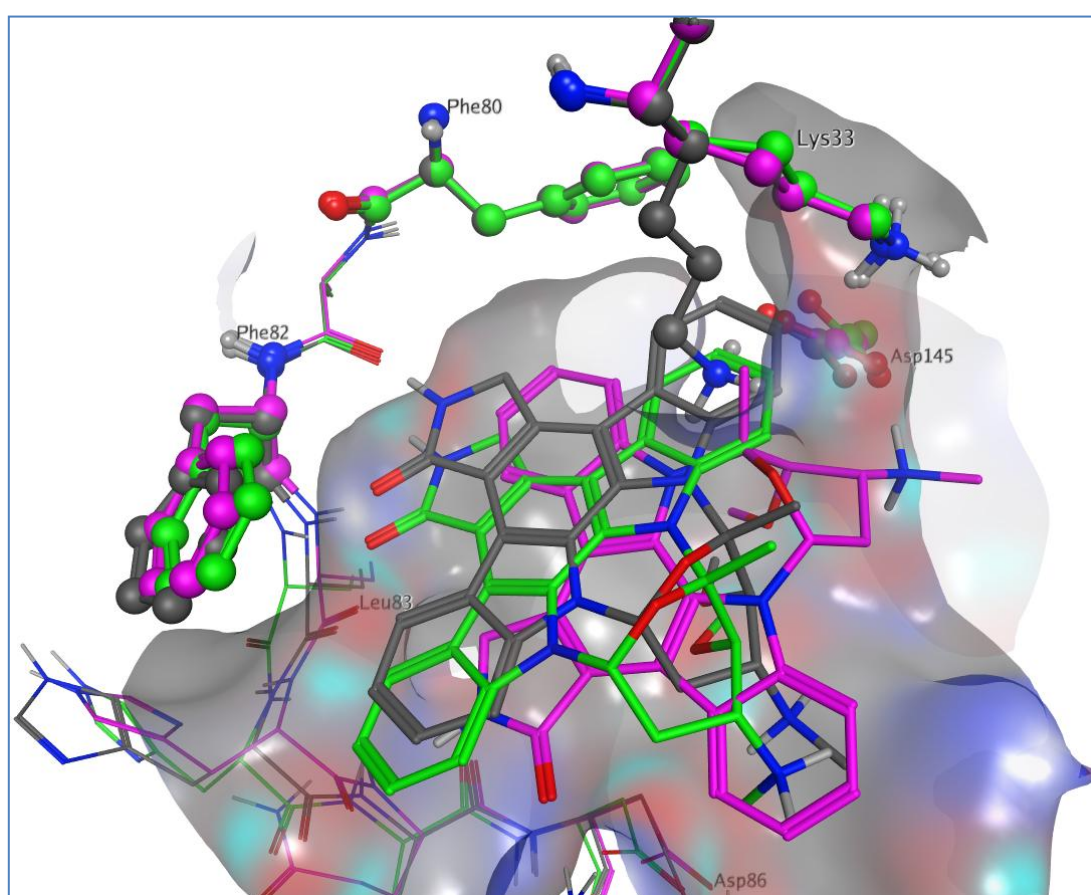


*Figure 116:* Comparison of 4EK3 crystal structure in grey with induced protein-ligand complexes when docking **12**: in magenta, without amino acid truncation and in green, when mutating Phe80 and Asp145. Crystal pose of ligand **12** also shown in grey

*Table 59* shows that, for Experiment 2, new IFDScore\_5 to IFDScore\_100 prioritise the same, Entry 2, found by visual inspection and which exhibits a reasonable ligand RMSD of 2.2 Å as well as binding site RMSD of 1.1 Å. This would be a better complex to select, whereas the old\_IFDScore prioritised Entry 1 with a ligand RMSD of 4.8 Å.

Entry	ligand RMSD	BS RMSD	old_IFD Score	Glide Score	PE <sub>IFD</sub>	$\Delta$ PE	new_IFD Score_1	new_IFD Score_5	new_IFD Score_10	new_IFD Score_20	new_IFD Score_30	new_IFD Score_40	new_IFD Score_50	new_IFD Score_60	new_IFD Score_70	new_IFD Score_80	new_IFD Score_90	new_IFD Score_100
1	4.8	1.0	-619	-10.7	-12115	-30.0	-11.0	-12.2	-13.7	-16.7	-19.7	-22.7	-25.7	-28.7	-31.7	-34.7	-37.7	-40.7
2	2.2	1.1	-619	-10.0	-12132	-46.6	-10.4	-12.3	-14.6	-19.3	-24.0	-28.6	-33.3	-37.9	-42.6	-47.3	-51.9	-56.6
3	5.9	1.1	-617	-8.9	-12120	-34.8	-9.3	-10.7	-12.4	-15.9	-19.4	-22.8	-26.3	-29.8	-33.3	-36.8	-40.3	-43.7
4	5.5	1.4	-616	-8.7	-12127	-41.9	-9.1	-10.7	-12.8	-17.0	-21.2	-25.4	-29.6	-33.8	-38.0	-42.2	-46.4	-50.6
5	2.2	1.4	-616	-8.1	-12133	-48.3	-8.6	-10.5	-12.9	-17.8	-22.6	-27.4	-32.3	-37.1	-41.9	-46.8	-51.6	-56.4
6	4.8	1.3	-615	-7.9	-12122	-37.5	-8.3	-9.8	-11.6	-15.4	-19.1	-22.9	-26.6	-30.4	-34.1	-37.9	-41.6	-45.4
7	8.8	1.3	-612	-4.2	-12127	-41.7	-4.6	-6.3	-8.4	-12.5	-16.7	-20.9	-25.1	-29.2	-33.4	-37.6	-41.8	-45.9

Table 59: Data generated for the 7 induced fit complexes output from Experiment 2 when docking **12** in 4EK3, ordered by decreasing old\_IFDScore. The best RMSDs and IFDScores are highlighted in green and the worst in red.

### 7.3.2. UPPS structure 4NCKH

The proprietary crystal structure 4NCKH is of UPPS in complex with **13**. To start with, this crystal structure was used in two re-docking experiments, using standard rigid receptor docking and IFD, in order to assess whether it would be suitable to use this model system for docking. The default parameters were used in both cases and no hydrogen bond constraints were included. In rigid receptor docking, the correct binding pose was found with a GlideScore of -8.5 kcal/mol (*Figure 117a*). As a reference for future experiments, the Prime Energy of the protein was computed as -19374 kcal/mol, which means that a corresponding IFDScore for this experiment would be -977 kcal/mol. In the case of default IFD, the correct binding pose was also obtained as the top scoring pose with an IFDScore of -986 kcal/mol, and a GlideScore of -9.4 kcal/mol and Prime Energy of -19534 kcal/mol (*Figure 117b*). It appeared that the induced conformation had a lower Prime Energy than the rigid receptor, which could perhaps be explained by some strain in the starting crystal structure. This model system seemed suitable for cross-docking experiments.

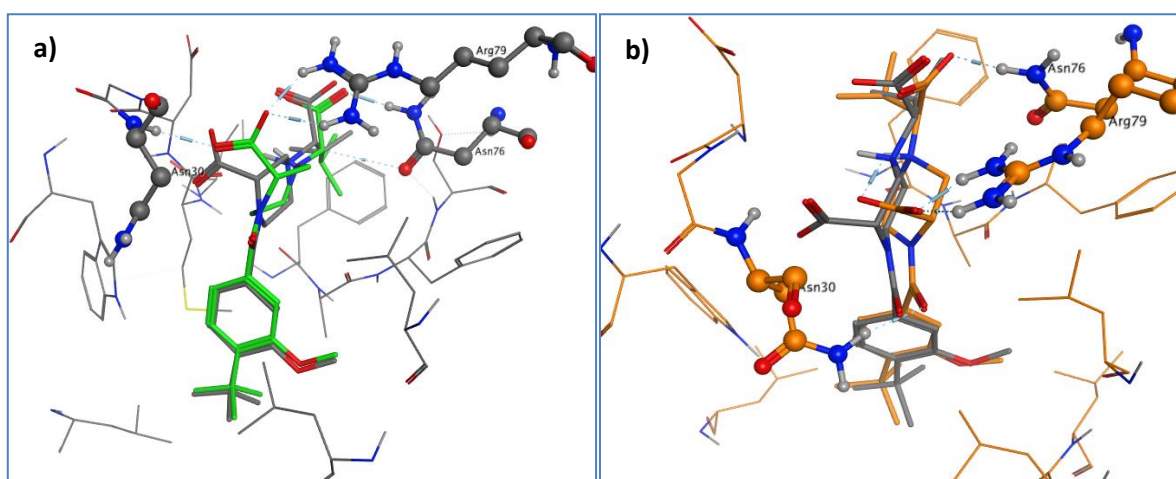


*Figure 117:* Re-docking of **13** in 4NCKH: a) rigid receptor docking with 4NCKH and crystal pose of **13** in grey and docked pose in green; b) Induced protein-ligand complex in orange with crystal pose of **13** in grey

Amino acids in 4NCKH within 4 Å of the ligand centroid were selected to be prioritised in the ranking of binding site amino acids (*Table 60*). Trp223 and Phe70 were the highest scoring, with a score of 10 and 7 respectively. However, the next two amino acids were selected from the set of three which had a score of 4. As discussed previously, a distance criterion to the ligand centroid, was used to differentiate between the equally ranked amino acids. In this way, Asn76 and Asn30 were selected to complete the list for the experimental design run.

AA_ID	Name	R SMILES	heavy	#DR	score	Distance from ligand centroid
TRP223	TRP	<chem>[*]Cc1c[nH]c2ccccc12</chem>	10	1	10	
PHE70	PHE	<chem>[*]Cc1ccccc1</chem>	7	1	7	
ASP28	ASP	<chem>[*]CC(O)=O</chem>	4	1	4	Within 4 Å
ASN76	ASN	<chem>[*]CC(N)=O</chem>	4	1	4	Within 3 Å
ASN30	ASN	<chem>[*]CC(N)=O</chem>	4	1	4	Within 3 Å
THR94	THR	<chem>[*]C(C)O</chem>	3	1	3	
ARG79	ARG	<chem>[*]CCCNC(N)=N</chem>	7	3	2.3	
LEU52	LEU	<chem>[*]CC(C)C</chem>	4	2	2	
LEU87	LEU	<chem>[*]CC(C)C</chem>	4	2	2	
LEU90	LEU	<chem>[*]CC(C)C</chem>	4	2	2	
ILE26	ILE	<chem>[*]C(C)CC</chem>	4	2	2	
SER73	SER	<chem>[*]CO</chem>	2	1	2	
MET27	MET	<chem>[*]CCSC</chem>	4	3	1	
ALA71	ALA	<chem>[*]C</chem>	1	0	0	

*Table 60:* Prioritised list of 4NCKH binding site amino acids

Ligand **14** was then docked in 4CNKH with these four prioritised amino acids as the parameters for the experimental design. The results are reported in *Table 61*. The range of

IFDScores is rather narrow, with only 3 kcal/mol difference at most between the docking poses. All but one experiment produced the incorrect binding pose as the top scoring pose. The large ligand RMSDs compared to the crystal pose of **14** show the large differences in atom coordinates. Experiment 2 yielded the correct binding pose, although the ligand RMSD was still rather large for a docking pose that is deemed right. For Experiment 5, 6 and 8, the correct poses could be found further down the list of induced fit structures. The  $\Delta$  Prime Energy varied significantly from +26 to -50. This would mean that the docking of the ligand in some cases gave a higher energy conformation of the protein than the starting state (positive  $\Delta$  Prime Energy) and in other cases, it gave a lower energy conformation of the protein (negative  $\Delta$  Prime Energy). In all cases though, the top ranking docking pose was in the wrong orientation, apart from Experiment 2 which had the lowest  $\Delta$  Prime Energy.

Exp design	Ligand	IFDScore	GlideScore	Prime energy	$\Delta$ Prime Energy	RMSD	Visual assessment
1	14	-983	-9.9	-19465	26	8.9	Wrong
2	14	-985	-8.7	-19532	-50	2.0	Ok
3	14	-985	-9.9	-19500	9	9.0	Wrong
4	14	-985	-8.9	-19517	-14	9.1	Wrong
5	14	-986	-8.8	-19543	-30	9.0	Wrong
6	14	-986	-9.8	-19516	0	9.4	Wrong
7	14	-985	-8.4	-19527	-21	8.8	Wrong
8	14	-986	-9.7	-19533	-10	8.2	Wrong

*Table 61:* Summary of IFD results when docking **14** in 4NCKH; the “no change” experiment is highlighted in blue

In Experiment 2, no amino acid side chains were truncated and this seemed to be the best set up to obtain the correct binding pose. In this orientation, **14** was able to make hydrogen bond interactions from its carboxylic acid moiety to the protonated nitrogens on the side chain of Arg79 and to the backbone NH of Asn30. The top scoring binding pose produced by this experiment was reasonable and relatively close to the crystal pose with a ligand RMSD of 2 Å (Figure 118).

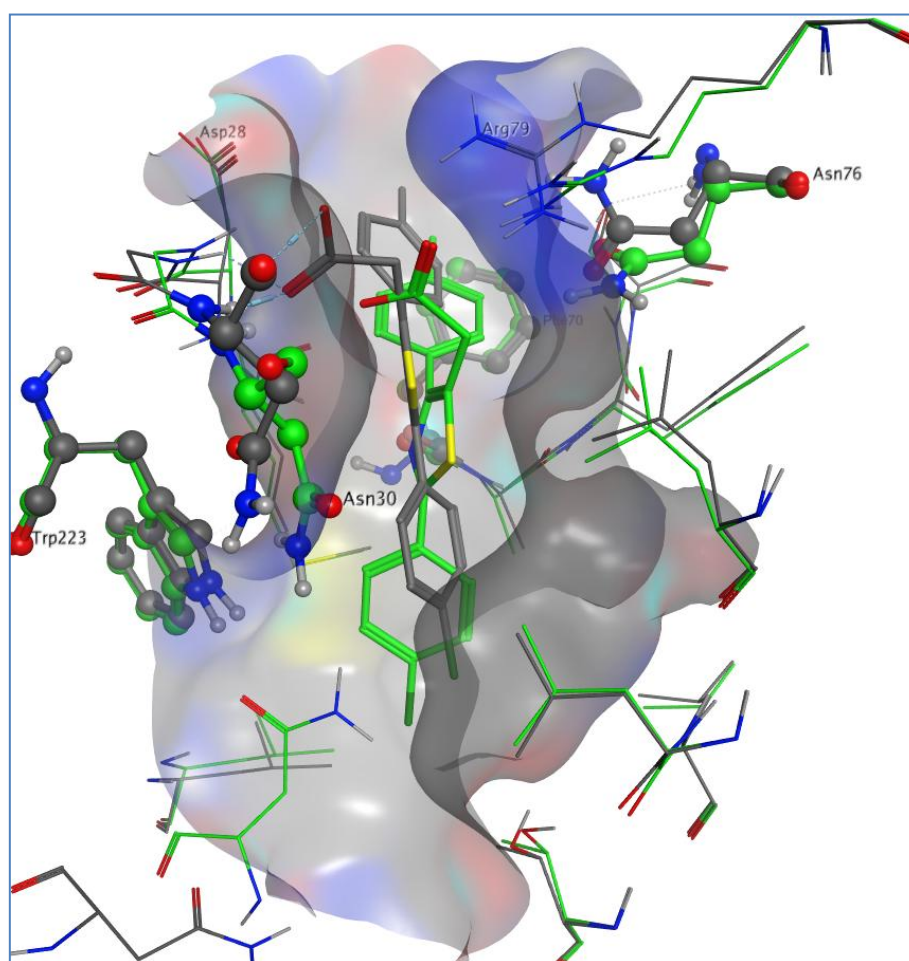
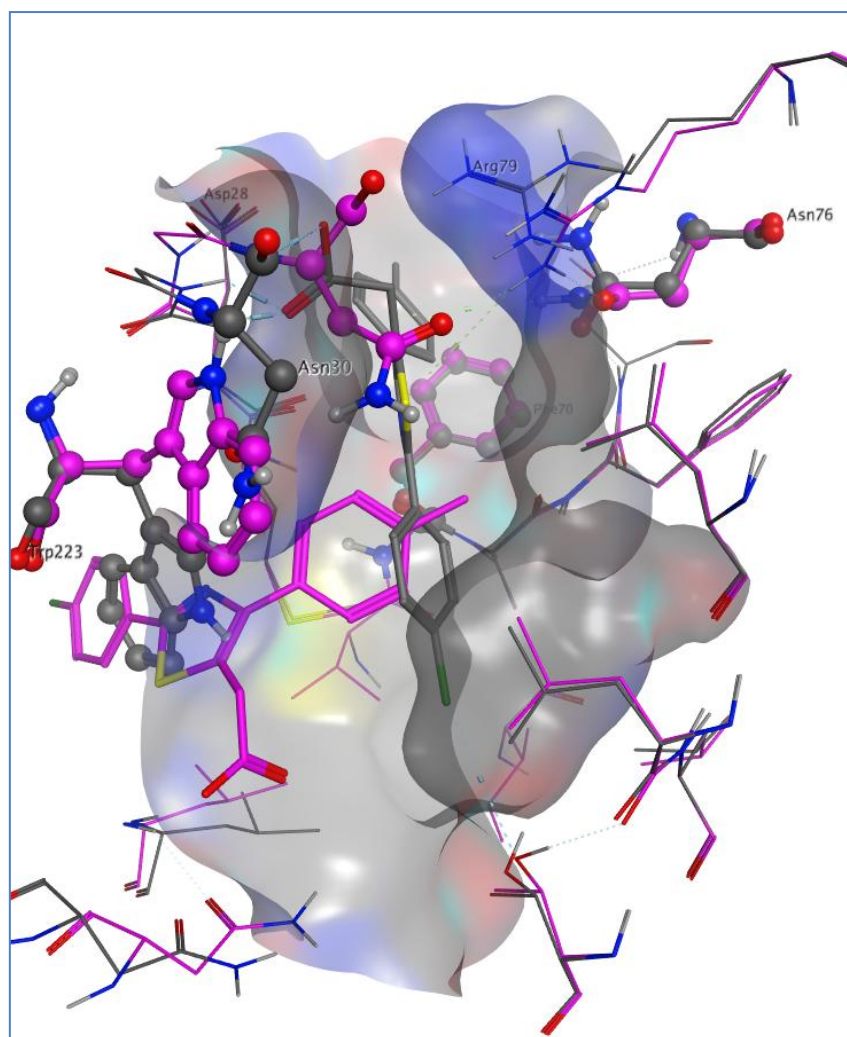


Figure 118: Comparison of 4NCKH crystal structure in grey with induced protein-ligand complex when docking **14**: in green, with no truncation. Crystal pose of ligand **14** also shown in grey

In the top scoring pose of Experiment 3, in which Trp223 and Asn30 were temporarily truncated, Trp223 was flipped upwards compared to its rotameric state in structure 4NCKH (*Figure 119*). This movement created a new pocket at the bottom of the binding site, where the docking pose of **14** was found, and also pushed Asn30 towards the inside of the “standard” binding site, blocking the top of it for ligand binding. The newly shaped binding site can be seen in *Figure 120*.

In terms of scores, these two docking poses from Experiments 2 and 3 had the same IFDScore of 985 kcal/mol, with the poses from Experiment 3 having a better GlideScore of 9.9 kcal/mol. The interactions of this pose with the binding site were from the carboxylic acid through hydrogen bonds to the NH backbone of Val51 and the side chain of Asn50. There were also hydrophobic contacts from the phenyl rings to hydrophobic residues such as Trp223, Phe226 and Ile25. It should be noted that the correct binding mode was not found further down the list of poses output in Experiment 3.





*Figure 119:* Comparison of 4NCKH crystal structure in grey with induced protein-ligand complex when docking **14**: in magenta, when truncating Trp223 and Asn30. Crystal pose of ligand **14** also shown in grey

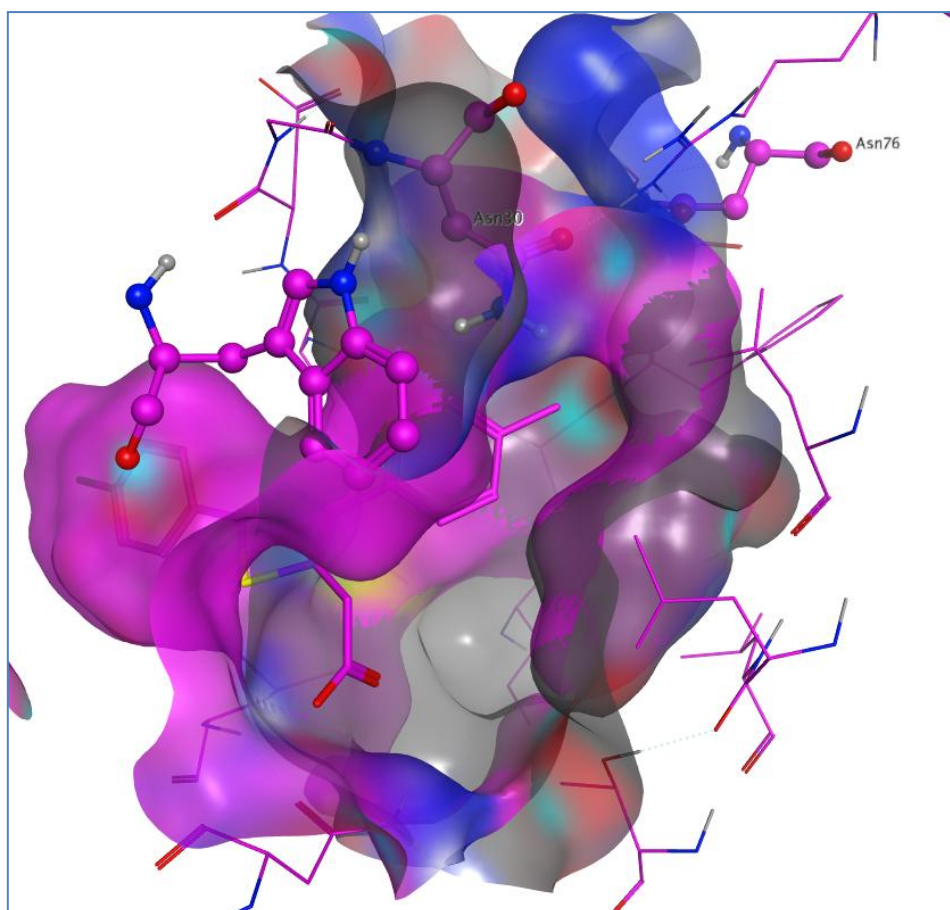


*Figure 120:* Close up on the induced binding site created by the flip of Trp223 in Experiment 3 and where **14** bound

The new IFDScores and RMSDs were also computed. *Table 62* shows the data generated for the induced fit complexes from Experiment 4. In this instance, all 13 complexes presented a rather large ligand RMSD, whilst the binding site RMSD was constant. New IFDScore<sub>10</sub> to IFDScore<sub>100</sub> would prioritise Entry 2, which exhibits a slightly lower ligand RMSD. However, the docking pose would still be in the wrong orientation and, therefore, the issue in this instance may lie with the choice of amino acids to be temporarily truncated.

Entry	ligand RMSD	BS RMSD	old_IFD Score	Glide Score	PE <sub>IFD</sub>	ΔPE	new_IFD Score <sub>_1</sub>	new_IFD Score <sub>_5</sub>	new_IFD Score <sub>_10</sub>	new_IFD Score <sub>_20</sub>	new_IFD Score <sub>_30</sub>	new_IFD Score <sub>_40</sub>	new_IFD Score <sub>_50</sub>	new_IFD Score <sub>_60</sub>	new_IFD Score <sub>_70</sub>	new_IFD Score <sub>_80</sub>	new_IFD Score <sub>_90</sub>	new_IFD Score <sub>_100</sub>
1	10.2	1.3	-985	-8.9	-19246	-13.8	-9.0	-9.6	-10.3	-11.7	-13.0	-14.4	-15.8	-17.2	-18.6	-19.9	-21.3	-22.7
2	9.2	1.3	-985	-8.1	-19259	-26.8	-8.4	-9.4	-10.8	-13.4	-16.1	-18.8	-21.5	-24.2	-26.8	-29.5	-32.2	-34.9
3	9.8	1.3	-985	-8.1	-19257	-24.8	-8.3	-9.3	-10.5	-13.0	-15.5	-18.0	-20.5	-22.9	-25.4	-27.9	-30.4	-32.9
4	9.8	1.3	-985	-8.0	-19252	-20.0	-8.2	-9.0	-10.0	-12.0	-14.0	-16.0	-18.0	-20.0	-22.0	-24.0	-26.0	-28.0
5	9.3	1.3	-984	-7.7	-19257	-24.9	-8.0	-9.0	-10.2	-12.7	-15.2	-17.7	-20.2	-22.7	-25.1	-27.6	-30.1	-32.6
6	9.5	1.3	-984	-7.6	-19258	-26.0	-7.8	-8.9	-10.2	-12.8	-15.4	-18.0	-20.6	-23.2	-25.8	-28.4	-31.0	-33.6
7	10.1	1.3	-984	-8.4	-19225	7.5	-8.4	-8.0	-7.7	-6.9	-6.2	-5.4	-4.7	-3.9	-3.2	-2.4	-1.6	-0.9
8	7.9	1.5	-984	-7.4	-19259	-26.8	-7.7	-8.8	-10.1	-12.8	-15.4	-18.1	-20.8	-23.5	-26.1	-28.8	-31.5	-34.2
9	11.7	1.3	-983	-7.1	-19255	-23.1	-7.3	-8.3	-9.4	-11.7	-14.0	-16.3	-18.6	-20.9	-23.2	-25.6	-27.9	-30.2
10	6.6	1.3	-982	-6.1	-19253	-21.1	-6.3	-7.2	-8.2	-10.3	-12.5	-14.6	-16.7	-18.8	-20.9	-23.0	-25.1	-27.2
11	8.7	1.4	-982	-6.5	-19248	-15.6	-6.6	-7.3	-8.0	-9.6	-11.2	-12.7	-14.3	-15.9	-17.4	-19.0	-20.5	-22.1
12	6.0	1.5	-982	-6.7	-19254	-21.6	-7.0	-7.8	-8.9	-11.1	-13.2	-15.4	-17.5	-19.7	-21.8	-24.0	-26.2	-28.3
13	5.0	1.5	-981	-5.9	-19252	-19.4	-6.1	-6.8	-7.8	-9.8	-11.7	-13.6	-15.6	-17.5	-19.5	-21.4	-23.3	-25.3

Table 62: Data generated for the 13 induced fit complexes output of Experiment 4 when docking **14** in 4NCKH, ordered by increasing old\_IFDScore. The best IFDScores and RMSDs are highlighted in green and the worst in red.

Ligand **15** was also docked in 4NCKH and results are reported in *Table 63*. As seen in the previous set of experiments, the variation of IFDScores was small. None of the experiments produced the right binding mode as the top scoring pose. The correct pose could be found further down the list of induced complexes for Experiment 3. The ligand RMSDs were significant and show how far away these poses were from the correct one. The GlideScores were reasonable and would tend to indicate good docking poses were obtained, although this was not the case. All top ranking docking poses made hydrogen bond interactions with the binding site, including to essential amino acids such as Asn30 and Ala71. However, the docking poses were often found bound back to front compared to the crystal pose or further down the binding site, with the dichlorophenyl in the lipophilic pocket as opposed to the induced pocket, as described in Section 3.3.

Exp design	Ligand	IFDScore	GlideScore	Prime energy	$\Delta$ Prime Energy	RMSD	Visual assessment
1	15	-992	-11.3	-19621	-7	10.0	Wrong
2	15	-991	-9.4	-19623	-30	6.8	Wrong
3	15	-992	-10.8	-19621	-15	10.1	Wrong
4	15	-991	-10.5	-19617	-20	6.9	Wrong
5	15	-990	-9.3	-19617	-29	7.2	Wrong
6	15	-990	-10.6	-19589	8	9.9	Wrong
7	15	-991	-10.1	-19615	-18	7.1	Wrong
8	15	-992	-10.4	-19628	-30	10.2	Wrong

*Table 63:* Summary of IFD results when docking **15** in 4NCKH; “no change” experiment highlighted in blue

Given that **15** was a much larger ligand than **13** and **14**, it might not be surprising that, upon binding to UPPS, it created a new lipophilic pocket. In order to recreate this effect Leu87 and Arg79 needed to move. This movement was not observed in any of this set of

experiments, leading to the incorrect binding pose. As an example, the top ranking pose from Experiment 4 will be described further. Phe70 and Asn30 were truncated during the IFD run for this experiment. As can be seen in *Figure 121*, Phe70 was found in the same rotamer as in the starting structure, whereas Asn30 moved further down the pocket to enable a hydrogen bond interaction with one of the amides of **15**. The terminal methyl amide interacted with Ala71 as well as Arg79. In comparison to the crystal pose of **15** that was expected, this docking pose of **15** bound further down the pocket and occupied an “L” shape conformation, whilst the crystal pose of **15** was extended. This difference in ligand conformation and location was demonstrated further by the ligand RMSD of 6.9 Å.

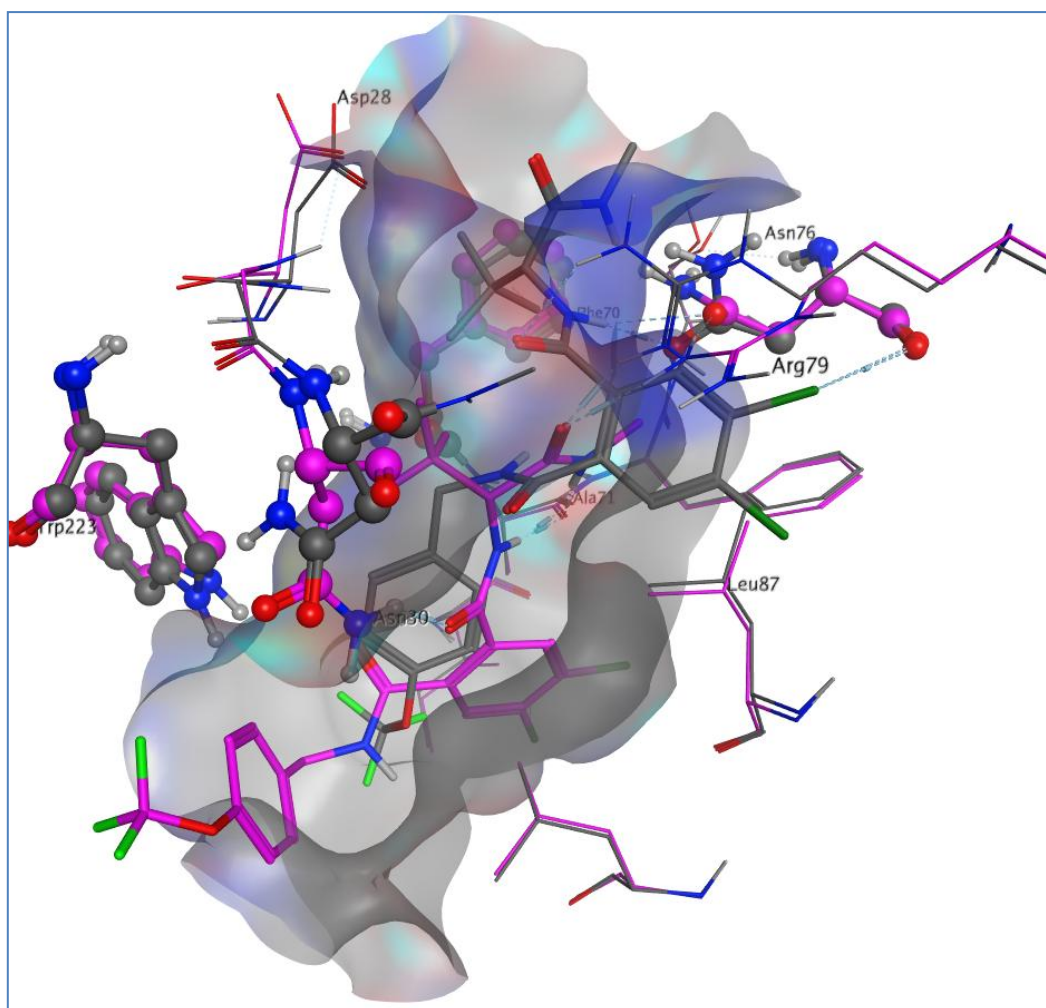


*Figure 121:* Comparison of 4NCKH crystal structure in grey with induced protein-ligand complex when docking **15**: in magenta, when truncating Phe70 and Asn30. Crystal pose of ligand **15** also shown in grey

The new IFDScores and RMSDs were computed and the results for Experiment 1 are shown in *Table 64*. New IFDScore\_10 highlighted Entry 3 as the best scoring complex. Entry 3 shows a lower ligand RMSD, but also the largest movement in the binding site, with an RMSD of 2.4 Å. Upon visual inspection of this docking pose, it emerged that the binding pose was also incorrect as indicated by the ligand RMSD value.

Entry	ligand RMSD	BS RMSD	old_IFD Score	Glide Score	PE <sub>IFD</sub>	$\Delta$ PE	new_IFD Score_1	new_IFD Score_5	new_IFD Score_10	new_IFD Score_20	new_IFD Score_30	new_IFD Score_40	new_IFD Score_50	new_IFD Score_60	new_IFD Score_70	new_IFD Score_80	new_IFD Score_90	new_IFD Score_100
1	10.6	1.2	-992	-11.3	-19239	-6.5	-11.4	-11.6	-11.9	-12.6	-13.2	-13.9	-14.5	-15.2	-15.8	-16.5	-17.1	-17.8
2	6.3	1.9	-991	-11.3	-19239	-6.5	-11.3	-11.6	-11.9	-12.6	-13.2	-13.9	-14.5	-15.2	-15.8	-16.5	-17.1	-17.8
3	5.5	2.4	-991	-10.6	-19246	-14.0	-10.7	-11.3	-12.0	-13.4	-14.8	-16.2	-17.6	-19.0	-20.4	-21.8	-23.2	-24.6
4	10.6	1.2	-991	-9.7	-19253	-21.1	-9.9	-10.7	-11.8	-13.9	-16.0	-18.1	-20.2	-22.3	-24.4	-26.5	-28.6	-30.7
5	10.7	2.1	-989	-9.6	-19247	-14.3	-9.7	-10.3	-11.0	-12.4	-13.9	-15.3	-16.7	-18.1	-19.6	-21.0	-22.4	-23.8
6	7.0	1.3	-988	-8.2	-19245	-12.2	-8.4	-8.8	-9.5	-10.7	-11.9	-13.1	-14.3	-15.6	-16.8	-18.0	-19.2	-20.5
7	8.8	1.3	-986	-6.4	-19242	-10.0	-6.5	-6.9	-7.4	-8.4	-9.4	-10.4	-11.4	-12.4	-13.4	-14.4	-15.4	-16.4

Table 64: Data generated for the 7 induced fit complexes output from Experiment 1 when docking **15** in 4NCKH, ordered by increasing old\_IFDScore. The best IFDScores and RMSDs are highlighted in green and the worst in red.

New IFDScore\_20 to IFDScore\_100 highlighted Entry 4 as the best scoring one. It presented ligand and binding site RMSDs similar to Entry 1, the top scoring complex using the old\_IFDScore.

### 7.3.3. UPPS structure 1ZHUB

After visual inspection, the crystal structure 1ZHUB of UPPS in complex with **14** did not exhibit great differences in conformation compared to 4NCKH (*Figure 122*). The only amino acids that have been affected were Leu90 and Leu91, whose side chains were found in a different rotameric state. Ligands **13** and **14** occupied a similar area of the binding site, although making slightly different interactions. The main hydrogen bond interactions of **14** with the binding site were through its carboxylic acid moiety to the side chains of Asn30 and Asn31 and also to their backbone NHs. However, there is likely an energetic penalty associated with these interactions, given the close proximity of Asp28, which could clash with the carboxylic acid of **14**.



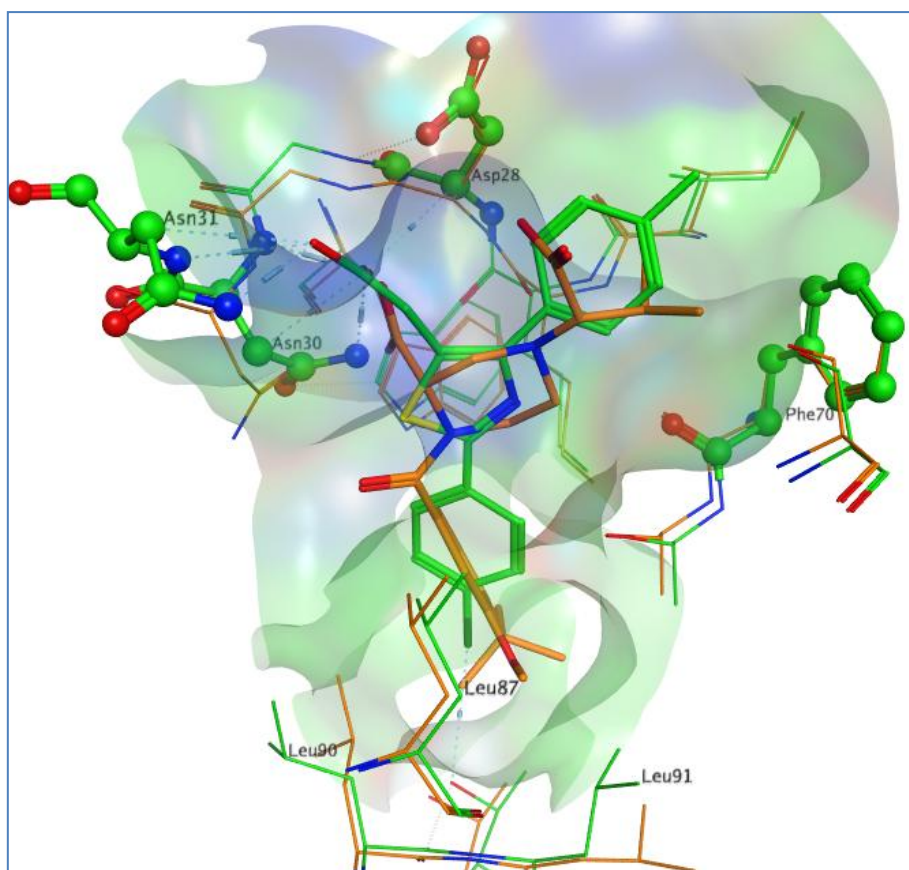


Figure 122: Comparison of 4NCKH binding site in orange and 1ZHUB binding site in green

As carried out for the previous structure 4NCKH, re-docking was investigated first. Default parameters and no hydrogen bond constraints were used. The rigid receptor docking experiment yielded the correct binding mode with a GlideScore of -8.8 kcal/mol (Figure 123a). The calculation of the Prime Energy produced a score of -19607 kcal/mol for the crystal structure, which would be equivalent to an IFDScore of -989 kcal/mol. Similarly, **14** was also docked in 1ZHUB using IFD and this resulted in the correct pose being found with an IFDScore of -997 kcal/mol, computed from a GlideScore of -8.7 kcal/mol and a Prime Energy of -19772 kcal/mol (Figure 123b). The GlideScores were comparable in both cases, whilst the Prime Energy was slightly lower in the default IFD case. This model system should be suitable for cross-docking experiments.

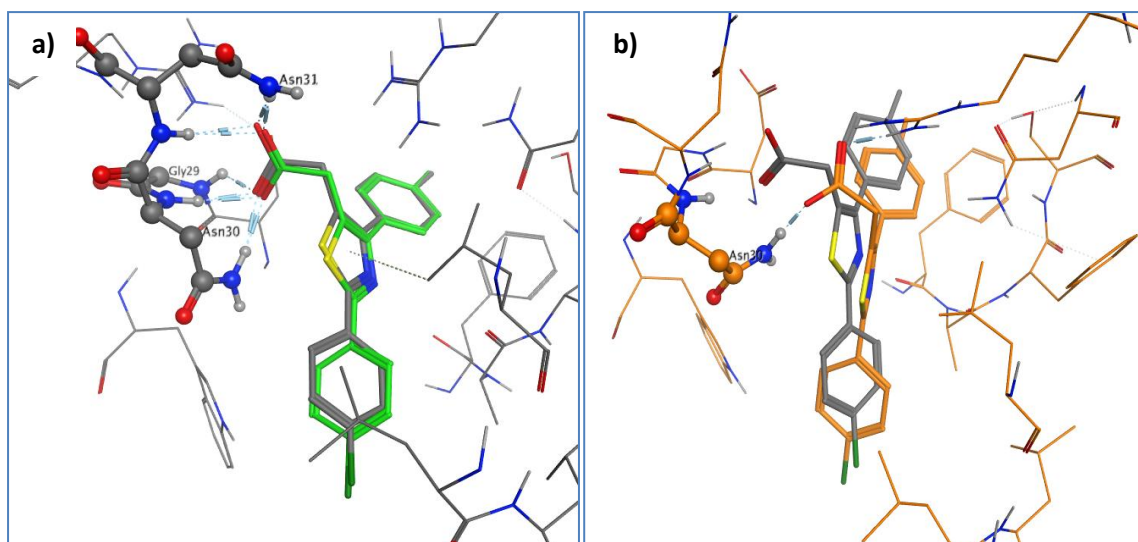


Figure 123: Re-docking of **14** in 1ZHUB: a) rigid receptor docking with 1ZHUB and crystal pose of **14** in grey and docked pose in green; b) induced protein ligand complex in orange and crystal pose of **14** in grey

The amino acids prioritised for IFD for this binding site are slightly different to the ones for 4NCKH. This was due to the ligands, which, despite occupying a similar area of the binding site, make slightly different interactions with the binding sites. The selected amino acids to be truncated for 1ZHUB are shown in *Table 65*. Phe70 was clearly the residue with the highest score. However, the following four amino acids needed to be further examined, given they all had a score of 4. The three residues closest to the ligand centroid were selected, that is Asn30, Asp28 and Asn31.

AA_ID	Name	R SMILES	heavy	#DR	score	Distance from ligand centroid
PHE70	PHE	[*]Cc1ccccc1	7	1	7	
ASN30	ASN	[*]CC(N)=O	4	1	4	Within 2 Å
ASN76	ASN	[*]CC(N)=O	4	1	4	Within 4 Å
ASP28	ASP	[*]CC(O)=O	4	1	4	Within 3 Å
ASN31	ASN	[*]CC(N)=O	4	1	4	Within 3 Å
THR94	THR	[*]C(C)O	3	1	3	
ARG79	ARG	[*]CCCNC(N)=N	7	3	2.3	
ARG196	ARG	[*]CCCNC(N)=N	7	3	2.3	
LEU91	LEU	[*]CC(C)C	4	2	2	
ILE26	ILE	[*]C(C)CC	4	2	2	
SER204	SER	[*]CO	2	1	2	
MET27	MET	[*]CCSC	4	3	1.3	
LYS49	LYS	[*]CCCCN	5	4	1.3	
ALA71	ALA	[*]C	1	0	0	

Table 65: Prioritisation of amino acids for binding site 1ZHUB; selection highlighted in blue

Ligand **13** was first docked flexibly in 1ZHUB and the results of the eight experiments are reported in Table 66. All eight experiments output a correct binding pose as the top scoring one. Although the “no change” experiment output the correct binding pose, it was the pose with the lowest IFDScore together with Experiment 5. Such good results were not unexpected, given the similarity in the way ligands **14** and **13** bind in the UPPS pocket.

Exp design	Ligand	IFDScore	GlideScore	Prime energy	Δ Prime Energy	RMSD	Visual assessment
1	13	-1001	-10.7	-19804	-20	0.8	Good
2	13	-998	-10.1	-19768	-8	1.1	Good
3	13	-1001	-10.6	-19812	-34	1.3	Good
4	13	-999	-10.2	-19784	-19	0.9	Good
5	13	-998	-9.2	-19781	-15	2.0	Ok
6	13	-1000	-10.1	-19794	-19	0.9	Good
7	13	-999	-9.6	-19780	-19	1.1	Good
8	13	-1002	-10.3	-19826	-54	0.9	Good

Table 66: Summary of IFD results when docking **13**; "no change" experiment in blue

The results of the two experiments at the two extremes of the design, that is 1 and 2 where, respectively, all four amino acids were truncated and no truncation was performed, will be described in more details. The top ranked poses for these two experiments can be found in *Figure 124*.

In Experiment 1, Phe70, Asn30, Asn31 and Asp28 were temporarily truncated and the top scoring docking pose was very good with a ligand RMSD of only 0.8 Å. Within this pose, hydrogen bond interactions were formed between the main carboxylic acid moiety of **13** to the backbone NHs of Asn30 and Asn31 and also to the side chain of Arg79. In addition, the carboxyl of the amide group was able to interact with the side chain of Asn31 and the terminal carboxylic acid to the side chain of Arg79. This was consistent with interactions observed in the crystal structure, given that water molecules were present in this instance (*Figure 29*).

From Experiment 2, the top ranked pose was very similar to the one obtained in Experiment 1. The conformation of **13** was also very similar and the same hydrogen bond interactions

occurred. The change in amino acid truncation between the different experiments did not have an impact on the docking of **13** in this case, which is due to the similarity in binding between **13** and **14**.

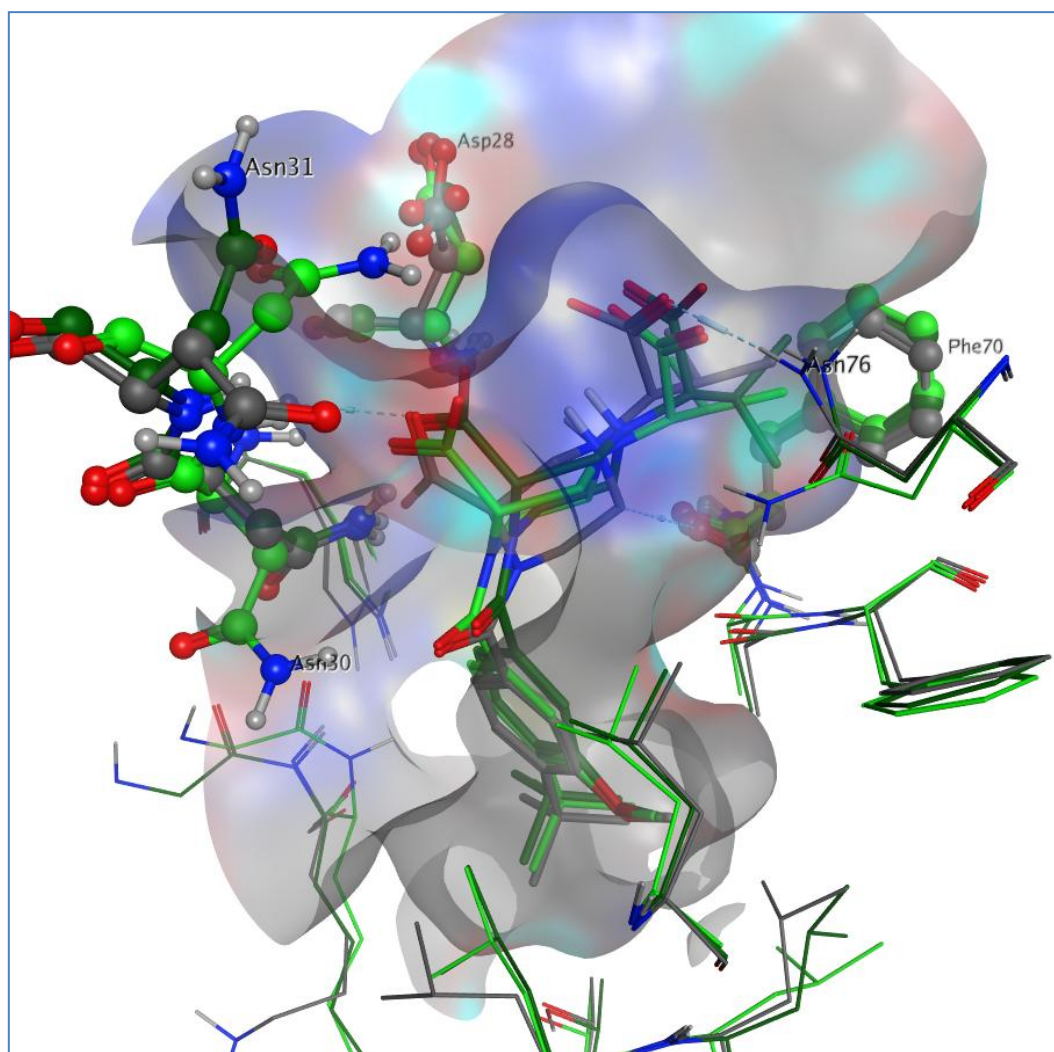


*Figure 124:* Comparison of 1ZHUB crystal structure in grey with induced protein-ligand complex when docking **13**: in light green, when truncating all four amino acids; in dark green, without any truncation. Crystal pose of ligand **13** also shown in grey

The new IFDScores and RMSDs were computed and an example is shown in *Table 67*. For Experiment 1, new IFDScore<sub>5</sub> to IFDScore<sub>60</sub> would prioritise Entry 3 which had an equivalent profile to Entry 1 in terms of RMSDs.

Entry	ligand RMSD	BS RMSD	old_IFD Score	Glide Score	PE <sub>IFD</sub>	ΔPE	new_IFD Score _1	new_IFD Score _5	new_IFD Score _10	new_IFD Score _20	new_IFD Score _30	new_IFD Score _40	new_IFD Score _50	new_IFD Score _60	new_IFD Score _70	new_IFD Score _80	new_IFD Score _90	new_IFD Score _100
1	2.0	0.7	-1001	-10.7	-19562	-19.5	-10.8	-11.6	-12.6	-14.6	-16.5	-18.5	-20.4	-22.4	-24.3	-26.3	-28.2	-30.2
2	2.1	0.8	-1001	-10.4	-19569	-27.0	-10.7	-11.7	-13.1	-15.8	-18.5	-21.2	-23.9	-26.6	-29.3	-32.0	-34.7	-37.4
3	2.2	0.6	-1001	-10.4	-19574	-32.4	-10.7	-12.0	-13.6	-16.9	-20.1	-23.4	-26.6	-29.8	-33.1	-36.3	-39.6	-42.8
4	3.2	0.7	-999	-9.3	-19565	-23.1	-9.6	-10.5	-11.6	-14.0	-16.3	-18.6	-20.9	-23.2	-25.5	-27.8	-30.1	-32.4
5	2.4	0.9	-998	-8.5	-19577	-35.4	-8.9	-10.3	-12.1	-15.6	-19.1	-22.7	-26.2	-29.7	-33.3	-36.8	-40.4	-43.9
6	2.9	0.8	-998	-9.4	-19561	-19.3	-9.6	-10.3	-11.3	-13.2	-15.2	-17.1	-19.0	-20.9	-22.9	-24.8	-26.7	-28.6
7	6.0	0.8	-998	-8.7	-19572	-29.5	-8.9	-10.1	-11.6	-14.6	-17.5	-20.5	-23.4	-26.4	-29.3	-32.3	-35.2	-38.2
8	2.9	0.8	-998	-8.5	-19572	-29.8	-8.8	-10.0	-11.5	-14.5	-17.5	-20.5	-23.4	-26.4	-29.4	-32.4	-35.4	-38.4
9	3.3	0.8	-998	-8.9	-19574	-32.5	-9.2	-10.5	-12.1	-15.4	-18.6	-21.9	-25.1	-28.4	-31.6	-34.9	-38.1	-41.4
10	5.8	0.9	-997	-8.1	-19577	-34.6	-8.5	-9.9	-11.6	-15.1	-18.5	-22.0	-25.4	-28.9	-32.3	-35.8	-39.3	-42.7
11	5.8	0.9	-997	-7.7	-19570	-27.8	-7.9	-9.0	-10.4	-13.2	-16.0	-18.8	-21.5	-24.3	-27.1	-29.9	-32.7	-35.4

Table 67: Data generated for the 11 induced fit complexes output of Experiment 1 when docking **13** in 1ZHUB, ordered by increasing old\_IFDScore. The best IFDScores and RMSDs are shown in green, and the worst in red.

New IFDScore\_70 to IFDScore\_100 highlighted Entry 5, which exhibited a slightly higher ligand RMSD and a slightly higher binding site RMSD. The GlideScore for this entry was 2 kcal/mol higher than either Entry 1 and Entry 3, which indicates that this docking pose was less satisfactory.

Ligand **15** was subsequently docked into 1ZHUB. Scores are reported in *Table 68* below. As opposed to results obtained from the previous set of experiments, the correct binding mode was not found by any of the experiments in this case. It is fair to say then that the issue here is not to do with the IFDScore, but possibly the size of **15** and of the binding site.

Exp design	Ligand	IFDScore	GlideScore	Prime energy	$\Delta$ Prime Energy	RMSD	Visual assessment
1	15	-1003	-10.5	-19846	-34	8.4	Wrong
2	15	-1004	-9.6	-19884	-46	8.9	Wrong
3	15	-1002	-9.0	-19859	-31	8.7	Wrong
4	15	-1002	-9.0	-19852	-33	8.6	Wrong
5	15	-1003	-10.2	-19848	-40	9.1	Wrong
6	15	-1004	-9.6	-19879	-44	9.3	Wrong
7	15	-1002	-9.1	-19850	-43	8.7	Wrong
8	15	-1004	-10.4	-19877	-38	9.1	Wrong

*Table 68:* Summary of IFD results when docking **15** in 1ZHUB; "no change" experiment in blue

Given that all experiments in this set produced the incorrect pose with a small range of IFDScores, only one result will be discussed in more details, that is of Experiment 4. In this experiment, Asn30 and Asn31 were truncated during the IFD run. *Figure 125* shows the resulting top ranked pose as well as the induced binding site compared to the crystal pose of **15** and crystal structure 1ZHUB. Instead of the dichloro phenyl binding in the groove near Leu87 and Arg79, this moiety is in the lipophilic bottom area of the binding site. There is no

significant movement of Leu87 between the crystal structure and the induced conformation of the protein, which would need to happen to allow the dichlorophenyl enough space to bind. The resulting docking pose, in this case, forms hydrogen bond interactions between the methyl amide of **15** and Asn31 and Glu83, whilst the amide on the same side of the central phenyl ring interacts with Arg79. There is also a weak face-to-face interaction between the trifluoromethoxyphenyl and Phe70. It is apparent in this instance, as it was also in the previous docking of **15** in 4NCKH, that the movement of Leu87 is crucial in determining the correct binding pose and that the truncation of larger amino acids is not enough to produce the binding mode expected.



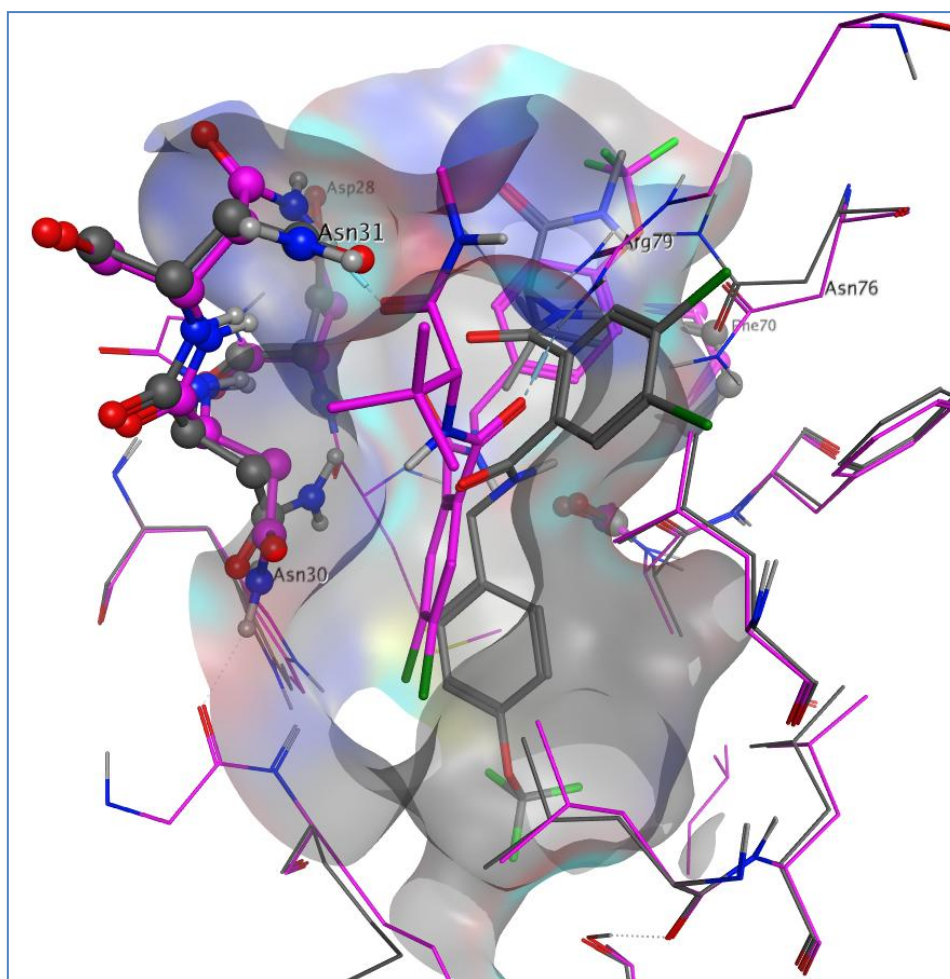


*Figure 125:* Comparison of 1ZHUB crystal structure in grey with induced protein-ligand complex when docking **15**: in magenta, when truncating Asn30 and Asn31. Crystal pose of ligand **15** also shown in grey

The new IFDScores and RMSDs were computed for this protein-ligand combination as well. An example of results obtained for Experiment 8 is shown in *Table 69*. The entry highlighted by the new IFDScore\_1 to IFDScore\_10 was Entry 2, showing exactly the same ligand and binding site RMSDs as Entry 1. Regarding new IFDScore\_20 to IFDScore\_100, they highlighted Entry 11, exhibiting a similar RMSD to Entry 1 and 2. However, the GlideScore for Entry 11 was less favourable than for the other two entries, indicating that this docking pose was making less significant interactions with the binding site. Indeed, this pose was

able to make only one hydrogen bond from the central benzamide to the side chain of Arg79 and the dichlorophenyl is bound at the entrance of the lipophilic pocket.

Entry	ligand RMSD	BS RMSD	old_IFD Score	Glide Score	PE <sub>IFD</sub>	ΔPE	new_IFD Score _1	new_IFD Score _5	new_IFD Score _10	new_IFD Score _20	new_IFD Score _30	new_IFD Score _40	new_IFD Score _50	new_IFD Score _60	new_IFD Score _70	new_IFD Score _80	new_IFD Score _90	new_IFD Score _100
1	9.3	1.1	-1004	-10.4	-19581	-38.2	-10.8	-12.3	-14.2	-18.0	-21.8	-25.6	-29.5	-33.3	-37.1	-40.9	-44.7	-48.6
2	9.3	1.1	-1004	-10.6	-19585	-41.9	-11.0	-12.7	-14.8	-19.0	-23.2	-27.4	-31.6	-35.8	-40.0	-44.2	-48.4	-52.6
3	9.0	1.0	-1004	-9.4	-19585	-41.7	-9.8	-11.5	-13.6	-17.7	-21.9	-26.1	-30.2	-34.4	-38.6	-42.8	-46.9	-51.1
4	9.4	1.1	-1004	-10.0	-19581	-37.7	-10.4	-11.9	-13.8	-17.6	-21.3	-25.1	-28.9	-32.6	-36.4	-40.2	-44.0	-47.7
5	9.3	1.1	-1003	-10.1	-19568	-24.9	-10.4	-11.4	-12.6	-15.1	-17.6	-20.1	-22.6	-25.1	-27.6	-30.0	-32.5	-35.0
6	9.6	1.1	-1003	-9.3	-19588	-45.2	-9.8	-11.6	-13.8	-18.4	-22.9	-27.4	-31.9	-36.4	-41.0	-45.5	-50.0	-54.5
7	9.0	1.1	-1002	-9.1	-19574	-30.8	-9.4	-10.6	-12.2	-15.2	-18.3	-21.4	-24.5	-27.5	-30.6	-33.7	-36.8	-39.9
8	8.8	1.2	-1002	-8.9	-19591	-48.2	-9.4	-11.3	-13.7	-18.5	-23.3	-28.2	-33.0	-37.8	-42.6	-47.5	-52.3	-57.1
9	9.3	1.1	-1002	-8.7	-19583	-39.8	-9.1	-10.7	-12.7	-16.7	-20.6	-24.6	-28.6	-32.6	-36.5	-40.5	-44.5	-48.5
10	9.3	1.2	-1002	-8.1	-19593	-50.1	-8.6	-10.6	-13.1	-18.1	-23.1	-28.1	-33.1	-38.2	-43.2	-48.2	-53.2	-58.2
11	9.5	1.0	-1001	-7.5	-19602	-58.9	-8.1	-10.5	-13.4	-19.3	-25.2	-31.1	-37.0	-42.8	-48.7	-54.6	-60.5	-66.4
12	9.3	1.0	-1001	-7.2	-19586	-42.8	-7.7	-9.4	-11.5	-15.8	-20.1	-24.4	-28.6	-32.9	-37.2	-41.5	-45.7	-50.0
13	9.6	1.1	-1001	-7.5	-19589	-46.5	-7.9	-9.8	-12.1	-16.8	-21.4	-26.1	-30.7	-35.4	-40.0	-44.7	-49.3	-54.0

Table 69: Data generated for the 13 induced fit complexes output for Experiment 8 when docking **15** in 1ZHUB, ordered by increasing old\_IFDScore. The best IFDScores and RMSDs are shown in green and the worst in red.

#### 7.3.4. UPPS structure 7WZYC

UPPS was crystallised in complex with ligand **15** in structure 7WZYC. This ligand was larger than ligands **13** and **14** and, as can be seen in *Figure 126*, induced a larger binding site for UPPS. In particular a new pocket is created by some movement of Arg79 and Leu87 in order to accommodate the dichlorophenyl moiety of **15**. Such differences had not been previously observed with any other known UPPS ligand.

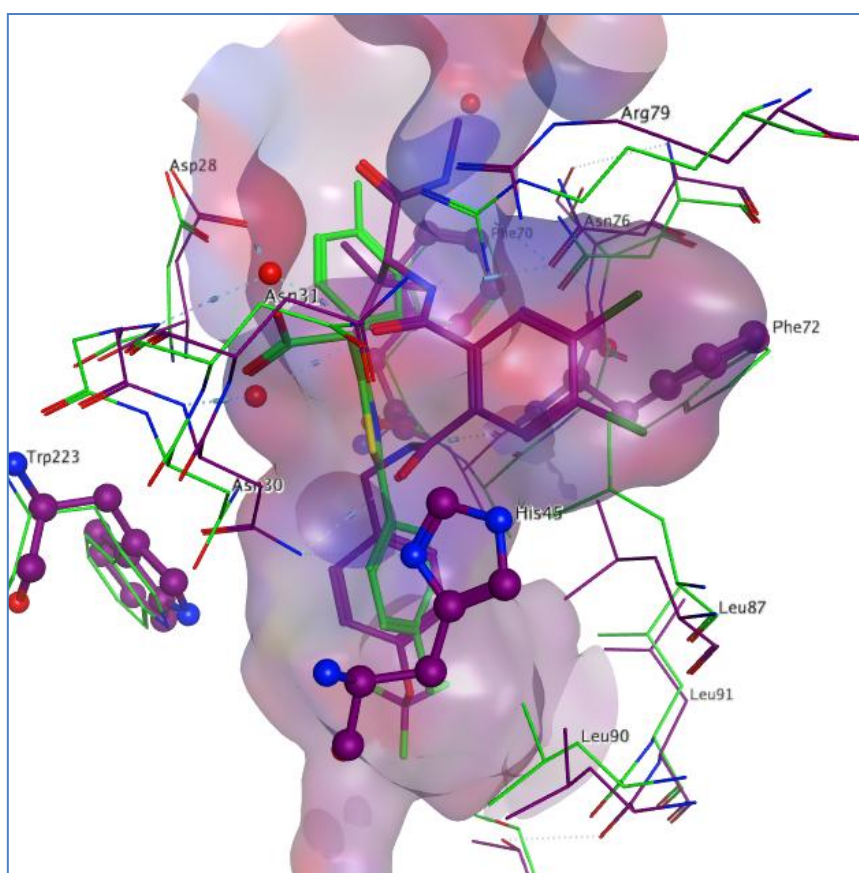


*Figure 126:* Comparison of 1ZHUB binding site in green and 7WZYC binding site in purple

The size of the binding site can also be appreciated further by the longer list of amino acids in close proximity to **15**. Indeed, eighteen amino acids were within 4 Å of the ligand pose and had to be prioritised for the IFD runs (*Table 70*). The selection of amino acids for truncation was straightforward, with no tie at the top of the sorted list, and Trp223, Phe70, Phe72 and His45 were progressed for use in the experimental design.

AA_ID	Name	R SMILES	heavy	#DR	score
TRP223	TRP	[*]Cc1c[nH]c2ccccc12	10	1	10
PHE72	PHE	[*]Cc1ccccc1	7	1	7
PHE70	PHE	[*]Cc1ccccc1	7	1	7
HIS45	HIS	[*]Cc1c[nH]cn1	6	1	6
ASP28	ASP	[*]CC(O)=O	4	1	4
ASN76	ASN	[*]CC(N)=O	4	1	4
ASN30	ASN	[*]CC(N)=O	4	1	4
THR94	THR	[*]C(C)O	3	1	3
GLU83	GLU	[*]CCC(O)=O	5	2	2.5
ARG79	ARG	[*]CCCN(C)=[NH2+]	7	3	2.3
LEU87	LEU	[*]CC(C)C	4	2	2
LEU52	LEU	[*]CC(C)C	4	2	2
LEU91	LEU	[*]CC(C)C	4	2	2
ILE26	ILE	[*]C(C)CC	4	2	2
SER73	SER	[*]CO	2	1	2
MET27	MET	[*]CCSC	4	3	1
LYS49	LYS	[*]CCCCN	5	4	1
ALA71	ALA	[*]C	1	0	0

Table 70: Prioritised amino acids for the binding site of structure 7WZYC

In the first instance, **13** was docked in 7WZYC. Table 71 summarises the scores obtained for these eight experiments. All experiments produced the correct binding mode as the top scoring pose, with reasonable ligand RMSDs compared to the crystal pose of **13**. In this set of experiments, the IFDScores and Prime Energies are twice as large as the ones obtained previously with 4NCKH and 1ZHUB. This is due to the fact that in 7WZYC, there are four copies of the protein in the asymmetric unit, whereas for the other two structures, there is only two. It is worth noting that the “no change” experiment was the experiment with the

least favourable IFDScore, albeit with only 1 kcal/mol difference to the next one up, and the largest ligand RMSD.

Exp design	Ligand	IFDScore	GlideScore	Prime energy	Δ Prime Energy	RMSD	Visual assessment
1	13	-2142	-9.2	-42655	-85	2.6	Good
2	13	-2140	-9.0	-42627	-15	2.8	Good
3	13	-2143	-10.9	-42643	-77	1.3	Good
4	13	-2141	-10.6	-42605	-37	1.8	Good
5	13	-2141	-8.9	-42650	22	1.3	Good
6	13	-2142	-10.8	-42627	-72	1.4	Good
7	13	-2143	-10.0	-42659	-93	1.4	Good
8	13	-2142	-10.4	-42630	-57	1.1	Good

*Table 71:* Summary of IFD results when docking **13** in 7WZYC; “no change” experiment shown in blue

The resulting top scoring pose from Experiment 2, for which no truncations were performed, and Experiment 8, where Trp223 and Phe70 were truncated during the IFD run, will be described in more details.

The top scoring pose from Experiment 2 forms three hydrogen bond interactions to the binding site: from its central carboxylic acid moiety to the side chain of Asn30 and from its terminal carboxylic acid to Arg79 and Asn76 (*Figure 127*). The *p-t*-butyl-*o*-methoxyphenyl is situated at the lipophilic bottom part of the site as expected. The two main movements, relative to the starting crystal structure 7WZYC, are the side chain of Asn30 coming into the centre of the binding site to interact with **13**; and Arg79 moving away from the site but interacting with **13** nonetheless. This is a plausible pose for **13**; however, as can be seen from *Table 71*, other experiments yielded poses closer to the crystal pose in terms of RMSD. This was the case for Experiment 8, with a very good ligand RMSD of 1.1 Å (*Figure 127*). The

pose forms several hydrogen bond interactions between the ligand's central carboxylic acid moiety and the backbone NHs of Asn31 and Gly29, as well as from the terminal carboxylic acid to Asn76 and Arg79. These interactions and this binding pose are very similar to the crystal pose of **13**, and this is reflected in the RMSD. It is notable, in this instance, that Experiment 2 produced the pose with the highest RMSD from the set, but this is not reflected in the IFDScore which is very similar to the rest.

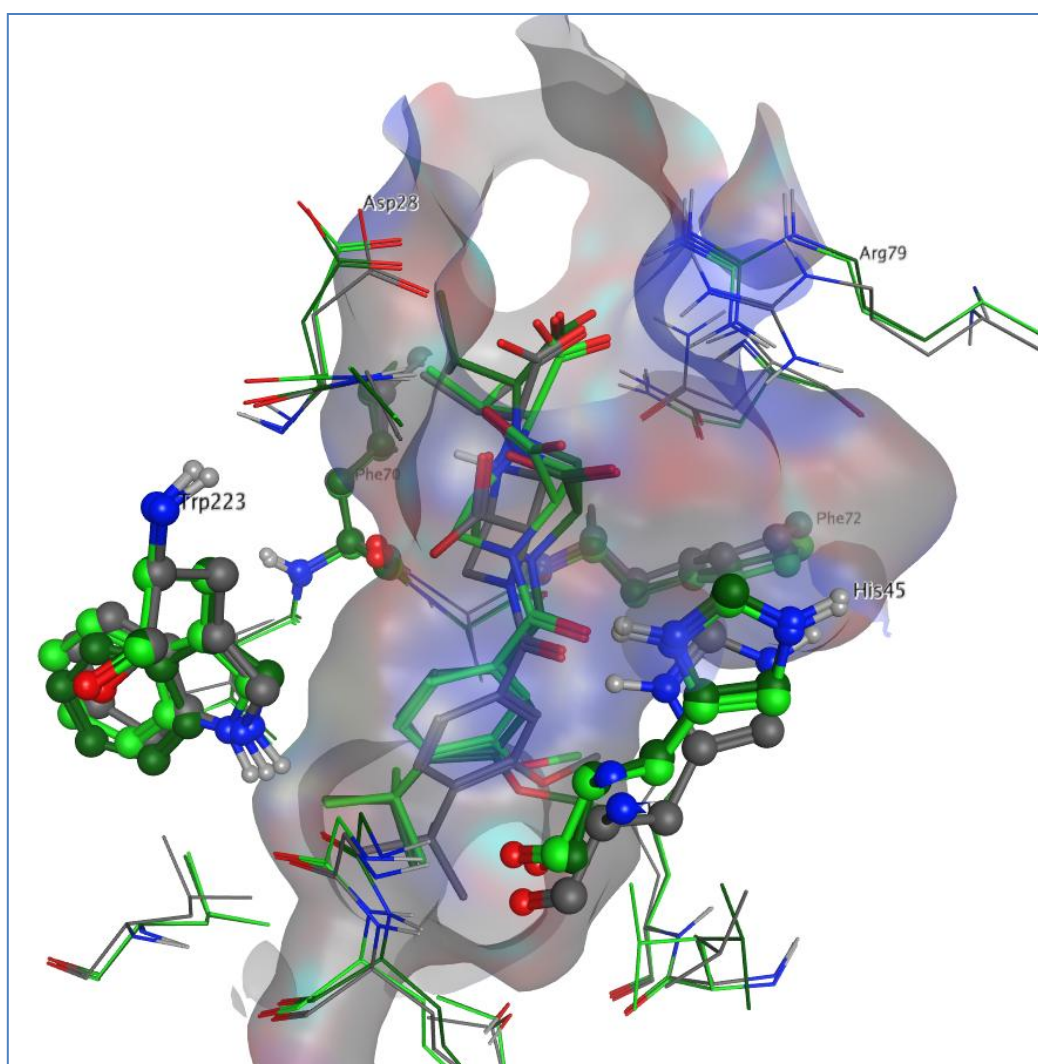


*Figure 127: Comparison of 7WZYC crystal structure in grey with induced protein-ligand complexes when docking **13**: in light green, when truncating Trp223 and Phe70; in dark green, when truncating no amino acids. Crystal pose of ligand **13** also shown in grey*

The new IFDScores and the ligand and binding site RMSDs were computed for this system and an example of results for Experiment 1 is presented in *Table 72*.



Entry	ligand RMSD	BS RMSD	old_IFD Score	Glide Score	PE <sub>IFD</sub>	ΔPE	new_IFD Score_1	new_IFD Score_5	new_IFD Score_10	new_IFD Score_20	new_IFD Score_30	new_IFD Score_40	new_IFD Score_50	new_IFD Score_60	new_IFD Score_70	new_IFD Score_80	new_IFD Score_90	new_IFD Score_100
1	1.6	1.1	-2142	-9.2	-41919	-84.6	-10.0	-13.4	-17.6	-26.1	-34.5	-43.0	-51.4	-59.9	-68.4	-76.8	-85.3	-93.7
2	1.8	1.1	-2142	-9.9	-41797	37.5	-9.6	-8.1	-6.2	-2.4	1.3	5.1	8.8	12.6	16.3	20.1	23.8	27.6
3	1.5	1.1	-2142	-10.0	-41860	-25.8	-10.2	-11.3	-12.6	-15.1	-17.7	-20.3	-22.9	-25.4	-28.0	-30.6	-33.2	-35.8
4	2.4	1.1	-2141	-9.9	-41848	-13.3	-10.0	-10.6	-11.2	-12.6	-13.9	-15.2	-16.6	-17.9	-19.2	-20.6	-21.9	-23.2
5	2.3	1.1	-2141	-9.1	-41862	-28.0	-9.4	-10.5	-11.9	-14.7	-17.5	-20.3	-23.1	-25.9	-28.7	-31.5	-34.3	-37.1
6	2.6	1.1	-2141	-9.1	-41862	-27.8	-9.4	-10.5	-11.9	-14.7	-17.4	-20.2	-23.0	-25.8	-28.5	-31.3	-34.1	-36.9
7	2.1	1.1	-2141	-9.4	-41855	-20.7	-9.6	-10.4	-11.4	-13.5	-15.6	-17.6	-19.7	-21.8	-23.9	-25.9	-28.0	-30.1
8	2.3	1.1	-2141	-9.4	-41803	30.8	-9.1	-7.8	-6.3	-3.2	-0.1	3.0	6.1	9.1	12.2	15.3	18.4	21.5
9	2.2	1.1	-2141	-8.8	-41903	-69.2	-9.5	-12.2	-15.7	-22.6	-29.5	-36.5	-43.4	-50.3	-57.2	-64.1	-71.1	-78.0

Table 72: Data generated for the 9 induced fit complexes output from Experiment 1 when docking **13** in 7WZYC, ordered by increasing old\_IFDScore. The best IFDScores and RMSDs are shown in green and the worst in red.

Most new IFDScores agreed with the old\_IFDScore, highlighting Entry 1 as the top scoring pose, apart from IFDScore\_1 which prioritised Entry 3. This makes sense given the low ligand and binding site RMSDs presented by this complex. In this case, there is apparently no advantage in using a different scoring function. However, it is encouraging to see that the new scoring functions are also able to identify the same correct binding pose as the standard IFDScore in this instance.

Ligand **14** was also docked into 7WZYC and the scores are reported in *Table 73*. The results are more varied in this case, although the IFDScores are somewhat comparable. Three out of the eight experiments produced the incorrect binding pose as the top scoring pose, including the “no change” experiment. Nevertheless, none of the experiments, which were able to output the correct binding mode, produced a pose with a ligand RMSD less than 1 Å. Experiment 7, where Phe72 and His45 had been truncated, was the experiment that generated the best result, in terms of RMSD. The poses from the three experiments, which produced the wrong binding mode, have a much higher RMSD than the rest. This was to do with the extra pocket that was created upon binding of **15** to UPPS in structure 7WZYC (it can be seen on the right hand side of the binding site in *Figure 128*). This new pocket, which was lipophilic in nature, could bind moieties similar to the dichlorophenyl of **15**. As can be seen for the docking pose of **14** in magenta in *Figure 128*, its *p*-methylphenyl is found in this pocket.

Exp design	Ligand	IFDScore	GlideScore	Prime energy	$\Delta$ Prime Energy	RMSD	Visual assessment
1	14	-2141	-9.3	-42635	-72	1.9	Ok
2	14	-2140	-9.1	-42624	-23	3.7	Wrong
3	14	-2139	-9.2	-42606	45	1.9	Ok
4	14	-2140	-9.0	-42617	-9	3.7	Wrong
5	14	-2141	-9.7	-42631	-26	1.9	Ok
6	14	-2141	-9.8	-42631	39	3.7	Wrong
7	14	-2141	-9.6	-42630	-26	1.8	Ok
8	14	-2140	-8.9	-42625	-22	1.9	Ok

Table 73: Summary of IFD results when docking **14** in 7WZYC; “no change” experiment shown in blue

As alluded to previously, the extra lipophilic pocket in 7WZYC created a larger binding site for docking. It is worth noting that this additional space did not pose any issue when docking **13**, which is of similar size to **14** albeit less flexible (Table 3).

In the case of Experiment 2 (no truncation), the methylphenyl moiety of **14** occupies the new lipophilic pocket, which was created by the binding of **15**, whereas the chlorophenyl binds in the expected lipophilic pocket at the bottom of the site (Figure 128). On top of these lipophilic interactions, this docking pose of **14** interacts with the binding site through hydrogen bond interactions from the carboxylic acid moiety to the backbone NH of Asn31 and the side chain of Asn30 on one side and the side chain of Arg79 and possibly His45 on the other side.

Even though the top ranked pose for Experiment 7 is not an absolute overlay of the crystal pose of **14**, the pose is plausible with interactions from the carboxylic acid to the side chains of Asn30 and Arg79 (Figure 128). The respective phenyl rings are found in the expected locations, with the chlorophenyl occupying the lipophilic pocket at the bottom of the site.

The ligand RMSD of 1.8 Å reflects these observations. Again, the IFDScores are not discriminatory when compared to the RMSDs and the same applies to GlideScores in this instance.

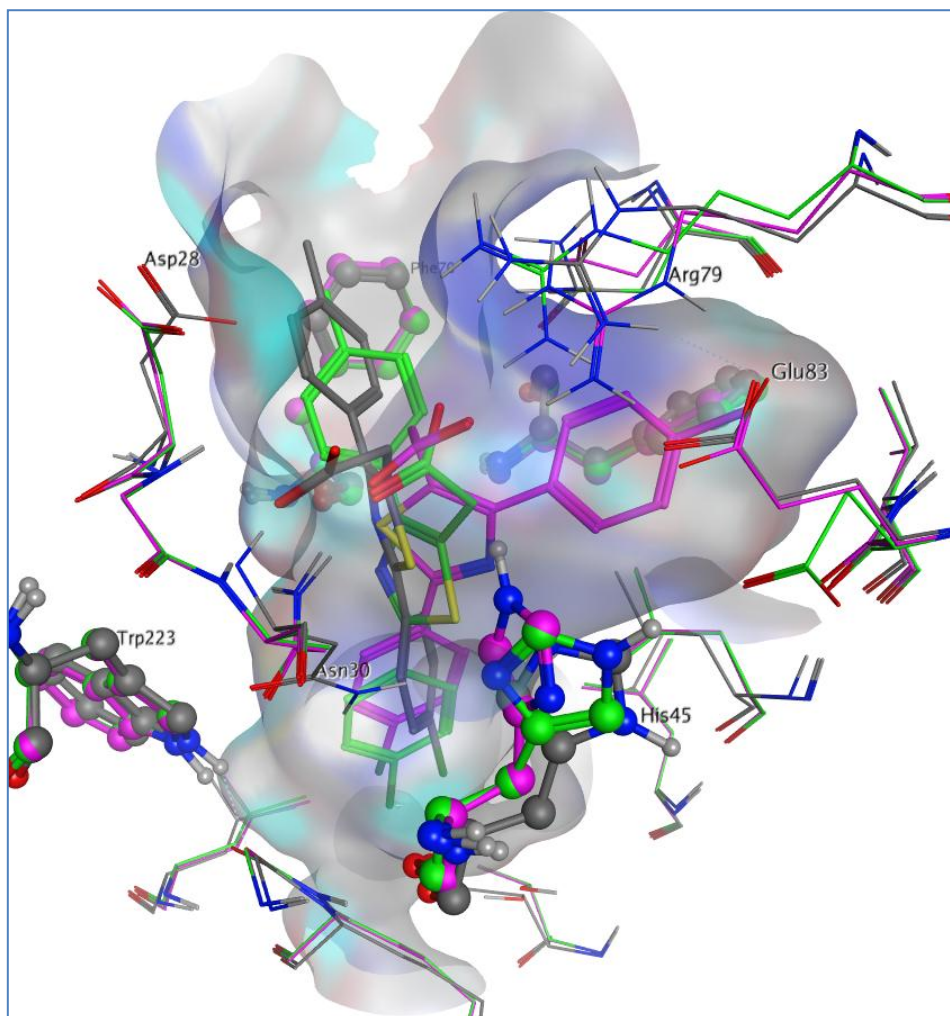


*Figure 128:* Comparison of 7WZYC crystal structure in grey with induced protein-ligand complexes when docking **14**: in magenta, without any truncation, and in green when truncating Phe72 and His45. Crystal pose of ligand **14** also shown in grey

The new IFDScores and RMSDs were computed for the above system and a set of results is shown in *Table 74*, as an example (Experiment 6). In this instance, all new IFDScores prioritised the same entry, Entry 5. This complex had a higher ligand RMSD and a similar binding site RMSD to Entry 1, although their GlideScores were comparable.

Entry	ligand RMSD	BS RMSD	old_IFD Score	Glide Score	PE <sub>IFD</sub>	ΔPE	new_IFD Score_1	new_IFD Score_5	new_IFD Score_10	new_IFD Score_20	new_IFD Score_30	new_IFD Score_40	new_IFD Score_50	new_IFD Score_60	new_IFD Score_70	new_IFD Score_80	new_IFD Score_90	new_IFD Score_100
1	<b>4.8</b>	0.8	<b>-2141</b>	-9.8	-41795	39.1	-9.4	-7.8	-5.9	-2.0	1.9	5.8	9.8	13.7	17.6	21.5	25.4	29.3
2	2.6	0.8	-2140	-9.4	-41798	36.0	-9.0	-7.6	-5.8	-2.2	1.4	5.0	8.6	12.2	15.8	19.4	23.0	26.6
3	4.7	0.9	-2140	-9.4	-41897	-62.4	-10.0	-12.5	-15.6	-21.8	-28.1	-34.3	-40.5	-46.8	-53.0	-59.2	-65.5	-71.7
4	2.5	<b>1.0</b>	-2140	-9.7	-41792	42.7	-9.3	-7.6	-5.4	-1.2	3.1	7.4	<b>11.7</b>	<b>15.9</b>	<b>20.2</b>	<b>24.5</b>	<b>28.7</b>	<b>33.0</b>
5	5.5	0.9	-2140	-9.4	-41898	-63.6	<b>-10.0</b>	<b>-12.6</b>	<b>-15.8</b>	<b>-22.1</b>	<b>-28.5</b>	<b>-34.8</b>	<b>-41.2</b>	<b>-47.5</b>	<b>-53.9</b>	<b>-60.3</b>	<b>-66.6</b>	<b>-73.0</b>
6	<b>2.4</b>	0.8	-2140	-9.3	-41799	35.6	-9.0	-7.5	-5.8	-2.2	1.4	4.9	8.5	12.1	15.6	19.2	22.7	26.3
7	3.0	0.9	-2140	-9.4	-41794	40.2	-9.0	-7.4	-5.4	-1.3	2.7	6.7	10.7	14.7	18.7	22.8	26.8	30.8
8	3.3	0.8	-2139	-8.8	-41857	-22.9	-9.0	-9.9	-11.1	-13.4	-15.7	-17.9	-20.2	-22.5	-24.8	-27.1	-29.4	-31.7
9	3.3	0.9	-2139	-8.8	-41793	40.8	-8.4	-6.7	-4.7	-0.6	<b>3.5</b>	<b>7.5</b>	11.6	15.7	19.8	23.9	28.0	32.0
10	2.8	<b>0.7</b>	-2139	-8.9	-41892	-58.1	-9.5	-11.8	-14.7	-20.5	-26.3	-32.1	-38.0	-43.8	-49.6	-55.4	-61.2	-67.0
11	3.0	0.9	-2139	-8.5	-41801	32.8	-8.1	-6.8	-5.2	-1.9	1.4	4.7	8.0	11.2	14.5	17.8	21.1	24.4
12	4.4	0.9	-2139	-7.9	-41860	-25.9	-8.2	-9.2	-10.5	-13.1	-15.7	-18.3	-20.9	-23.5	-26.1	-28.6	-31.2	-33.8
13	2.7	0.9	<b>-2139</b>	-8.0	-41799	34.9	<b>-7.6</b>	<b>-6.2</b>	<b>-4.5</b>	<b>-1.0</b>	2.5	6.0	9.5	13.0	16.4	19.9	23.4	26.9

Table 74: Data generated for the 13 induced fit complexes output of Experiment 6 when docking **14** in 7WZYC, ordered by increasing old\_IFDScore. The best IFDScores and RMSDs are shown in green and the worst in red

There were other entries with a more acceptable ligand RMSD, such as Entry 2 or Entry 6. But they were not picked up by the new scores. Therefore, the new IFDScores do not perform better than the standard IFDScore on this occasion.

Overall, UPPS was a very challenging target to use in flexible docking due mainly to the size of its binding site, which is long in order to accommodate the synthesis of UPP, a C55 polymer. In addition, the temporary truncation of selected amino acid side chains made this site even larger and, therefore, created even more space for the ligands to explore. However, flexible docking was successful in finding the right pose for **13** docked in 1ZHUB and in 7WZYC and to some extent for **14** in 7WZYC. The larger ligand **15** was more difficult and did not produce any reasonable poses for any of the 16 experiments run (8 experiments in 4NCKH and 8 experiments in 1ZHUB). The opening of the induced pocket could not be successfully predicted using IFD.

### 7.3.5. Conclusion

In total, nine protein structure-ligand combinations were investigated and eight experiments were run for each of them, with a minimum of four new protein-ligand complexes produced per experiment and a maximum of twenty. These different combinations are equivalent to 72 IFDScore data sets. They are all reported in Appendix 3. When the correct binding pose was identified by the standard IFDScore as the top scoring pose, the new IFDScores were not able to prioritise a correct binding pose on seven occasions. This was more often the case when docking **14** in UPPS 7WZYC (4 times). On the contrary, when the standard IFDScore was not able to identify the correct binding pose as the top ranking pose, the new IFDScores were able to do so on nine occasions. This

observation would show that there might be an advantage in using the new IFDScores. In particular, IFDScores\_1 to 10 were the most successful at identifying an equivalent or a better binding mode. Adding more PrimeEnergy, i.e., taking into account the conformation of the protein, is therefore not adding any value in finding the correct binding pose.

For the remainder of cases, the standard and new IFDScores were either both able to identify the correct binding pose or both failed to do so. Therefore, there was no advantage in using the new scoring system in these cases. Often, when the correct binding mode could not be reached, it was because it was not output from the IFD run, suggesting that the issue was not with the scoring function but with generating docking poses. For example, this was observed with docking **15** in either 4NCKH or 1ZHUB.

In summary, in most cases the new IFDScores and, in particular IFDScores\_1 to 10, gives comparable results to the standard IFDScore. In seven instances, it failed to find the right binding mode when the standard IFDScore could, but it managed to identify the correct one on nine occasions when the standard IFDScore failed. Therefore, there could be a slight advantage in using the new IFDScore\_1 to IFDScore\_10. More validation would need to be performed in order to ascertain which of these would be the best score.

#### 7.4. Conclusion

In this chapter, a new way of prioritising amino acids for temporary truncation has been presented. Each amino acid is given a score based on the number of heavy atoms in its side chain and the number of dominant rotors. This process was found to be efficient in automatically identifying amino acids within the binding site that could have an effect on the ability for correctly docking non-native ligands into a binding site. However, the set of

various combination for all potential truncations would still lead to a large number of simulations, leading to an inefficient process. To solve this problem, a  $2^4$  fractional factorial experimental design was introduced, resulting in an efficient process of running 8 experiments for each system.

To test the new automated selection and screening method several test systems were employed, including fXa, CDK2 and UPPS, with varied and informative results. In the fXa runs, it was observed that the truncation of Asp189, which is important for binding, produced the poorer results. Negative results of this kind also provide the potential for gaining insights into the system. For example, the truncation of Asp189 suggests the importance of this residue for binding. This concept can be easily extended to cases where little is known about the target.

In the case of CDK2, docking **12** was overall more successful than docking **11**. It is postulated that given the size of **12**, it is more likely to reach the right binding mode as it is less flexible and larger than typical drug-like molecules. Therefore, it can adopt only a limited number of conformations. The CDK2 binding site can only accommodate some of these conformations and it is somewhat easier to get to the correct answer with this ligand.

It was instructive to include two apo structures, one with Phe80 protruding in the binding site (1BUH) and the other with Lys33 (4EK3). Phe80 is an example of a large rigid amino acid, whilst Lys33 is a flexible one. In general, it was found that truncation of Phe80 in 1BUH led to the correct rotamer over half of the time and it did not move in 25% of cases. This does not necessarily mean that the correct binding pose for the ligand was found. Similarly, in 4EK3, Lys33 was found in the correct rotamer in over 80% of cases, with only no movement in around 20% of cases. This result led to the important observation that truncating large amino acids can help in reaching the correct rotamer and that flexible amino acids can move



away from the binding site during the refinement step and do not necessarily need to be truncated when protruding in binding sites, which is what the amino acid scoring function was based on.

In the case of UPPS, the results were disappointing as most of the time the wrong binding pose was obtained. The induced pocket created by the movement of Leu87 upon binding of **15** was not observed in any of the induced protein conformations. Instead new pockets were created with the truncations of larger residues, such as Trp223. In general, the poor results seen for this system could be due to the size of the binding site, which is long and lipophilic with important interactions made at the top where polar residues are found. When polar residues were truncated, such as Asn30 or Asp28, results were poor for three complexes out of four (see for example docking **14** in 4NCKH or **15** in 1ZHUB) which suggests that truncation of these amino acids is detrimental to finding the right binding mode.

Often, across these systems, it was observed that the failure in finding the correct binding mode did not lie with the amino acid conformations but rather with the scoring function used to score the different docking poses. Therefore, an attempt at modifying the existing IFDScore was investigated. The results from this exercise were mixed with the new IFDScores and were found to be superior in some instances, but not in others. More research would need to be performed in order to find a more suitable way of scoring induced fit docking poses.

## 8. Conclusions

This work began with the evaluation of rigid receptor docking protocols. In Chapter 5, the model system 1LOZX of LTA4H was used to dock proprietary ligands, with the ultimate objective of being able to assign the stereochemistry of chiral centres. Predictions were made from visual inspection and supported by statistics based on the docking scores. This was achieved successfully as confirmed by experimental data (small molecule crystallography and VCD). This type of rigorous analysis of docking scores with the aim to predict stereocentres provides a novel use of these established methods.

In the process of validating the methods that were applied for the determination of the stereocentres, several insights were also gained into which docking programmes, between GOLD and Glide, are best for specific model systems and what their shortcomings are, leading to the conclusion that GOLD was the preferred method for the systems under study. The thorough analysis that was carried out in this study also raised a number of questions regarding the general utility of these docking approaches for more varied systems.

In order to address these questions, a selection of known LTA4H ligands were studied and it was found that the 1LOZX system as set up to dock proprietary ligands was not suitable due to the presence of water molecules near the zinc atom. This finding led to a more detailed study of the importance, and potential problems, that result from the inclusion, or deletion, of water molecules that are crystallographically resolved within the binding site. A simple modification of the

model system (i.e. removal of water molecules) did not provide a generic system for docking public domain ligands, although the docking poses for the GSK ligands were not affected by this. Two different methods (GRID and SuperStar) were therefore used in order to characterise water molecules in the crystal structure. SuperStar, which is a knowledge-based approach, predicted some hydration sites correctly using the water probe around the binding site. When it was used on the ligand, some parts of the propensity map corresponded to the location of some amino acids, e.g. Gln136, which mostly denoted important polar interactions between the two entities. GRID, an energy-based approach, was equally successful, when studying the binding site and the ligand. Both methods were in agreement and as such the use of these methods together to pre-determine which water molecules should be retained or removed, before docking is carried out, is recommended for future studies.

Overall the rigid docking studies that were performed in this work highlight the importance of accurately selecting and preparing the system that will be used for a study. This is not a trivial point as it leads to the more fundamental question of how to select a system if very little is known about the preferred binding mode of target ligands. A system which is too specialised for a target ligand may not have the appropriate flexibility for screening a diverse range of ligands and the water network within a given binding site may further complicate this. Therefore, the second phase of this work focussed on one of the most challenging concepts in molecular docking – how to effectively introduce flexibility into a rigid receptor.

The initial aspect of the study into the importance of including flexibility into the binding sites of receptors focussed on the benchmarking of existing methods (Chapter 6). In this work it was shown that the inclusion of some flexibility during docking had varied results on the model systems studied. However, overall, adding protein flexibility to the docking procedure was beneficial in all cases, to a greater or lesser degree.

In the cases where amino acids were protruding into the binding site, especially in the case of apo crystal structures, the inclusion of flexibility meant that these residues could be rotated out of the binding site and improved docking poses were obtained. In particular, this was shown by the experiments run in CDK2 structures and to a lesser extent in fXa. The initial benchmarking studies also revealed that there was not a significant difference in outcome between the standard IFD protocol, with and without amino acid mutations – with the exception of docking ligand **12** in the apo crystal structure 1BUH, given its size and the truncation of Phe80.

In addition to providing evidence for the success of the existing flexible docking protocols, this work also revealed the essential role that the selection of the amino acids to be made flexible has. The current standard process is based on the amino acid temperature factors of a system. However, in several cases it was observed that the choices made using this approach did not necessarily result in mutations that were able to lead to the identification of the correct binding pose. Therefore, the use of manual selection of amino acids for truncation was examined. Clearly, a manual selection of the amino acids to be truncated requires a pre-existing

knowledge of the expected binding mode, which directly opposes the goals of this work. However, the idea behind this set of experiments was to develop a knowledge base of the key factors that could be used to automate the selection of amino acids to truncate. These targeted mutations were successful and revealed the impact of the number of truncations on the quality of the docking poses.

Based on the information obtained from the benchmark studies of existing docking methods, the development of an automated protocol for the selection of amino acids for mutation was investigated. A scoring function was developed based on the size of the amino acid side chain normalised by its number of rotatable bonds. This approach was built on the observations that bulkier and less flexible amino acids are less inclined to move away from the binding site during the refinement step. In addition to prioritising the amino acids to truncate, the new protocol also makes use of a design of experiments methodology to determine the optimal combinations of multiple amino acids to truncate in order to maximise the information generation together with enhancing the speed of the screening process. The developed protocol represents a new and important step forward for the use of flexible docking methods. Therefore, its development should prove beneficial to the scientific community and the drug discovery community in particular.

The protocol for selecting amino acids to truncate worked well when studying CDK2 and fXa structures. However, for systems with large and flexible binding sites, such as UPPS, the results were more varied. It was found that temporarily truncating

amino acids, in a binding site that is already significantly larger than required for the ligand, resulted in too many false positive docking poses.

Finally, this work highlighted the importance of balancing the destabilisation of the protein conformation and the binding energy of the ligand – which is currently calculated as the IFDScore. While the improved flexible docking approach was able to correctly locate the experimental binding pose, this binding pose was often considered less stable than alternative poses, according to the score. Therefore, an attempt to improve IFDScore was explored, but the results were not significantly better than with the standard IFDScore. This represents an important area for future work in this field. The inability of the overall protein to relax as a result of local temporary mutations in the binding site can result in significant destabilisation of the protein energy, which swamps the gain provided through ligand binding and, therefore, dominates the IFDScore. However, the development of a protocol that allows the relaxation of the full receptor/ligand system, while maintaining the ability to rapidly screen thousands of ligands is outside the scope of this research.

## 9. Outlook

The induced fit docking experiments described here were all performed without any hydrogen bond constraints. It would be instructive to investigate the addition of such constraints to the protocol, especially to the hinge region of CDK2 as these interactions are conserved across active chemotypes, and assess whether constraints have a beneficial impact on the scores and finding the right binding mode as the top scoring pose. This would enable a more complete evaluation of the IFD protocol. In the case of protein kinases, these hydrogen bond interactions are expected to happen for an ATP competitive ligand and would not substantially affect the objectivity of the experiment set up, which has been sought throughout this research. In the case of other proteins, it might not be possible to incorporate these hydrogen bonds during docking, especially if the systems are not well characterised.

The Schrödinger IFD protocol has been investigated in terms of improving the amino acid selection when temporary truncation is used. The new way of prioritising and selecting amino acids, presented here, proved successful in the majority of cases. It would also be informative to investigate what the optimal number of truncations of amino acids is, as computing time increases with the number of amino acids mutated. A maximum of four amino acids were mutated at a time in this study. Of the nine experiments run in that way, five of them found the correct binding pose. This contradicts the observation made by Schrödinger that three truncations were the maximum to obtain an acceptable size of the binding sites for the first docking step as well obtaining plausible poses.<sup>9</sup>

The insights and observations derived from this work provide regarding the deficiencies of the existing IFDScore provide an excellent starting point for the future development of this critical parameter. In particular, the results obtained in this research indicate that the scoring function for IFD needs to be re-developed and dissociated from Prime Energy.



## References

1. Lipkowitz, K. B.; Boyd, D. B., *Rev. Comp. Ch.* 1990.
2. Mason, J. S., Introduction to the Volume and Overview of Computer-Assisted Drug Design in the Drug Discovery Process. In *Comprehensive Medicinal Chemistry II*, Taylor, J. B.; Triggle, D. J., Eds. Elsevier: 2007; Vol. 4, pp 1-11.
3. Hughes, J. P.; Rees, S.; Kalindjian, S. B.; Philpott, K. L., *Brit. J. Pharmacol* **2011**, *162*, 1239-1249.
4. Pritchard, J. F.; Jurima-Romet, M.; Reimer, M. L. J.; Mortimer, E.; Rolfe, B. C., M.N., *Nat. Rev. Drug Discov* **2003**, *2*, 542-553.
5. Leach, A. R., *Molecular Modelling: Principles and Applications*. 2 ed.; 2001.
6. Kontoyianni, M.; McClellan, L. M.; Sokol, G. S., *J. Med. Chem* **2004**, *47*, 558-565.
7. Taylor, R. D.; Jewsbury, P. J.; Essex, J. W., *J. Comput. Aid. Mol. Des* **2002**, *16*, 151-166.
8. Friesner, R. A.; Banks, J. L.; Murphy, R. B.; Halgren, T. A.; Klicic, J. J.; Mainz, D. T.; Repasky, M. P.; Knoll, E. H.; Shelley, M.; Perry, J. K.; Shaw, D. E.; Francis, P.; Shenkin, P. S., *J. Med. Chem* **2004**, *47*, 1739-1749.
9. Sherman, W.; Day, T.; Jacobson, M. P.; Friesner, R. A.; Farid, R., *J. Med. Chem* **2006**, *49*, 534-553.
10. Goodsell, D. S.; Olson, A. J., *Proteins Struct. Funct. Genet* **1990**, *8*, 195-202.
11. Doucet, J. P.; Weber, J., *Computer-Aided Molecular Design*. 1996.
12. Atkins, P. W., *Quanta: A Handbook of Concepts*. 2 ed.; 1991.
13. Weiner, S. J.; Kollman, P. A.; Case, D. A.; Singh, U. C.; Ghio, C.; Alagona, G.; Profeta, S.; Weiner, P., *J. Am. Chem. Soc* **1984**, *106*, 765-784.
14. Goodford, P., *J. Med. Chem* **1985**, *28*, 849-857.
15. Boobbyer, D. N. A.; Goodford, P.; McWhinnie, P. M.; Wade, R. C., *J. Med. Chem* **1989**, *32*, 1083-1094.
16. Halgren, T. A., *J. Comput. Chem* **1999**, *20*, 730-748.

17. Halgren, T. A.; Murphy, R. B.; Friesner, R. A.; Beard, H. S.; Frye, L. L.; Pollard, W. T.; Banks, J. L., *J. Med. Chem* **2004**, *47*, 1750-1759.
18. Hwang, M. J.; Stockfisch, T. P.; Hagler, A. T., *J. Am. Chem. Soc* **1994**, *116*, 2515-2525.
19. Allinger, N. L.; Yuh, Y. H.; Lii, J.-H., *J. Am. Chem. Soc* **1989**, *111*, 8551-8566.
20. Lii, J.-H.; Allinger, N. L., *J. Am. Chem. Soc* **1989**, *111*, 8566-8575.
21. Lii, J.-H.; Allinger, N. L., *J. Am. Chem. Soc* **1989**, *111*, 8576-8582.
22. Allinger, N. L.; Chen, K.; Katzenellenbogen, J. A.; Wilson, S. R.; Anstead, G. M., *J. Comput. Chem* **1996**, *17*, 747-755.
23. Jorgensen, W. L.; Tirado-Rives, J., *J. Am. Chem. Soc* **1988**, *110*, 1657-1666.
24. Jorgensen, W. L.; Maxwell, D. S.; Tirado-Rives, J., *J. Am. Chem. Soc* **1996**, *118*, 11225-11236.
25. Stouten, P. F. W.; Kroemer, R. T., Docking and Scoring. In *Comprehensive Medicinal Chemistry II*, Taylor, J. B.; Triggle, D. J., Eds. Elsevier: 2007; Vol. 4, pp 255-281.
26. GOLD User Manual <http://www.ccdc.cam.ac.uk/support-and-resources/ccdcresources/gold.pdf>. <http://www.ccdc.cam.ac.uk/support-and-resources/ccdcresources/gold.pdf> (accessed 4/18/2016).
27. Verdonk, M. L.; Cole, J. C.; Hartshorn, M. J.; Murray, C. W.; Taylor, R. D., *Proteins* **2003**, *52*, 609-623.
28. Jones, G.; Willet, P.; Glen, R. C., *J. Mol. Biol* **1995**, *245*, 43-53.
29. Jones, G.; Willet, P.; Glen, R. C.; Leach, A. R.; Taylor, R., *J. Mol. Biol* **1997**, *267*, 727-748.
30. Eldridge, M. D.; Murray, C. W.; Auton, T. R.; Paolini, G.; Mee, R. P., *J. Comput. Aid. Mol. Des* **1997**, *11*, 425-445.
31. Korb, O., Stützle, T., Exner, T. E., *J. Chem. Inf. Model* **2009**, *49*, 84-96.
32. Liebeschuetz J.W., C., J.C., Korb, O., *J. Comput. Aid. Mol. Des* **2012**, *26*, 737-748.
33. Hartshorn, M. J., Verdonk, M. L., Chessari, G., Brewerton, S. C., Mooij, W. T. M., Mortenson, P. N., Murray, C. W., *J. Med. Chem* **2007**, *50*, 726-741.

34. Cheng, T., Li, X., Li, Y., Liu, Z., Wang, R., *J. Chem. Inf. Model.* **2009**, *49*.
35. Marsden, P. M. P., D.; Mitchell, J.B.O.; Glen, R.C., *Org. Biomol. Chem.* **2004**, *2*, 3267-3273.
36. Smith, R. D. D., J.B.; Ung, P.M.-U.; Esposito, E.X; Ynag, C.-Y.; Wang, S.; Carlson, H.A., *J. Chem. Inf. Model.* **2011**, *51*, 2115-2131.
37. Warren, G. L., Andrews, C.W., Capelli, A-M., Clarke, B., LaLonde, J., Lambert, M., Lindwall, M., Nevins, N., Semus, S.F., Senger, S., Tedesco, G., Wall, I.D., Woolven, J.M., Peishoff, C.E., Head, M.S., *J. Med. Chem* **2006**, *49*.
38. Xu, W. L., A.J.; Fairlie, D.P., *J. Mol. Graph. Model.* **2015**, *57*, 76-88.
39. Gohlke, H. K., G., *Curr. Opin. Struct. Biol.* **2001**, *11*, 231-235.
40. Gohlke, H. H., M.; Klebe, G., *J. Mol. Biol.* **2000**, *295*, 337-356.
41. Liu, J. W., R., *J. Chem. Inf. Model.* **2015**, *55*, 475-482.
42. Huang, S.-Y. Z., X., *J. Chem. Inf. Model.* **2011**, *51*, 2097-2106.
43. Carlson, H. A. S., R.D.; Damm-Ganamet, K.L.; Stuckey, J.A.; Ahmed, A.; Convery, M.A.; Somers, D.O.; Kranz, M.; Elkins, P.A.; Cui, G.; Peishoff, C.E.; Lambert, M.H.; Dunbar, J.B., *J. Chem. Inf. Model.* **2016**, *56*, 1063-1077.
44. Liu, Y. X., Z.; Yang, Z.; Chen, K.; Zhu, W., *J. Mol. Model.* **2013**, *19*, 5015-5030.
45. Rarey, M. K., B.; Lengauer, T.; Klebe, G., *J. Mol. Biol.* **1996**, *261*, 470-489.
46. GOLD <http://www.ccdc.cam.ac.uk/solutions/csd-discovery/components/gold/>. <http://www.ccdc.cam.ac.uk/solutions/csd-discovery/components/gold/> (accessed 4/18/2016).
47. Cer, R. Z.; Mudunuri, U.; Stephens, R.; Lebeda, F. J., *Nucleic Acids Res* **2009**, *37*, W441-W445.
48. Gathiaka, S. L., S.; Chiu, M.; Yang, H.; Stuckey, J.A.; Kang, Y.N.; Delproposito, J.; Kubish, G.; Dunbar, J.B.; Carlson, H.A.; Burley, S.K.; Walters, W.P.; Amaro, R.E.; Feher, V.A.; Gilson, M.K., *J. Comput. Aid. Mol. Des* **2016**, *30*, 651-668.
49. Kim, R. S., J., *J. Comput. Chem.* **2008**, *29*, 1316-1331.
50. Smith, R. D. D.-G., K.L; Dunbar, J.B.; Ahmed, A.; Chinnaswamy, K.; Delproposito, J.E.; Kubish, G.M.; Tinberg, C.E.; Khare, S.D.; Dou, J.; Doyle, L.; Stuckey, J.A.; Baker, D.; Carlson, H.A., *J. Chem. Inf. Model.* **2016**, *56*, 1022-1031.

51. Kitchen, D. B., Decornez, H., Furr, J.R., Bajorath, J., *Nat. Rev. Drug Discov* **2004**, *3*, 935-949.
52. Cross, J. B. T., D.C.; Rai, B.K.; Baber, J.C.; Fan, K.Y.; Hu, Y.; Humblet, C., *J. Chem. Inf. Model.* **2009**, *49*, 1455-1474.
53. Damm-Ganamet, K. L. S., R.D.; Dunbar, J.B.; Stuckey, J.A.; Carlson, H.A. , *J. Chem. Inf. Model.* **2013**, *53*, 1853-1870.
54. Li, Y. H., L.; Liu, Z.; Wang, R., *J. Chem. Inf. Model.* **2014**, *54*, 1717-1736.
55. Kirchmair, J.; Markt, P.; Distinto, S.; Wolber, G.; Langer, T., *J. Comput. Aid. Mol. Des* **2008**, *22*, 213-228.
56. Koshland, D. E., *Angew. Chem. Int. Ed* **1994**, *33*, 2375-2378.
57. Koshland, D. E., *Proc. Natl. Acad. Sci. U. S. A* **1958**, *44*, 98-104.
58. Carlson, H. A., *Curr. Opin. Chem. Biol* **2002**, *4*, 447-452.
59. Teague, S. J., *Nat. Rev. Drug Discov* **2003**, *2*, 527-541.
60. Antunes, D. A.; Devaurs, D.; Kaviraki, L. E., *Expert Opin. Drug Discov* **2015**, *10*, 1301-1313.
61. Leach, A. R., *J. Mol. Biol* **1994**, *235*, 345-356.
62. Miranker, A.; Karplus, M., *Proteins Struct. Funct. Genet* **1991**, *11*, 29-34.
63. Verkhivker, G. M.; Rejto, P. A.; Bouzida, D.; Arthurs, S.; Colson, A. B.; Freer, S. T.; Gehlhaar, D. K.; Larson, V.; Luty, B. A.; Marrone, T.; Rose, P. W., *Chem. Phys, Lett* **2001**, *337*, 181-189.
64. Hritz, J. d. R., A.; Oostenbrink, C., *J. Med. Chem.* **2008**, *51*, 7469-7477.
65. Totrov, M. A., R., *Curr. Opin. Struct. Biol.* **2008**, *18*, 178-184.
66. Buonfiglio, R.; Recanatini, M.; Masetti, M., *Chem. Med. Chem* **2015**, *10*, 1141-1148.
67. Lill, M. A., *Biochemistry* **2011**, *50*, 6157-6169.
68. Korb, O.; Olsson, T. S. G.; Bowden, S. J.; Hall, R. J.; Verdonk, M. L.; Liebeschuetz, J. W.; Cole, J. C., *J. Chem. Inf. Model* **2012**, *52*, 1262-1274.
69. Ferrari, A. M.; Wei, B. Q.; Costantino, L.; Shoichet, B. K., *J. Med. Chem* **2004**, *47*, 5076-5084.
70. Damm, K. L.; Carlson, H. A., *J. Am. Chem. Soc* **2007**, *129*, 8225-8235.

71. Morris, G. M.; Lim-Wilby, M., Molecular Docking. In *Molecular Modeling of Proteins*, Kukol, A., Ed. Springer: 2008; pp 365-382.
72. Jacobson, M. P.; Friesner, R. A.; Xiang, Z.; Honig, B., *J. Mol. Biol* **2002**, *320*, 597-608.
73. Schrödinger Release 2013-3: Glide, version 6.1, Schrödinger, LLC, New York, NY, 2013.
74. Morrison, K. L.; Weiss, G. A., *Curr. Opin. Chem. Biol* **2001**, *5*, 302-307.
75. Wang, H.; Shimizu, E.; Tang, Y.-P.; Cho, M.; Kyin, M.; Zuo, W.; Robinson, D. A.; Alaimo, P. J.; Zhang, C.; Morimoto, H.; Zhuo, M.; Feng, R.; Shokat, K. M.; Tsien, J. Z., *Proc. Natl. Acad. Sci. U. S. A* **2003**, *100* (4287), 4292.
76. Barreca, M. L.; Iraci, N.; De Luca, L.; Chimirri, A., *Chem. Med. Chem* **2009**, *4*, 1446-1456.
77. Lauria, A.; Ippolito, M.; Almerico, A. M., *J. Mol. Graph. Model* **2009**, *27*, 712-722.
78. Repo, S.; Jyrkkarinne, J.; Pulkkinen, J. T.; Laatikainen, R.; Honkakoski, P.; Johnson, M. S., *J. Med. Chem* **2008**, *51*, 7119-7131.
79. Wang, H.; Aslanian, R.; Madison, V. S., *J. Mol. Graphics Modell* **2008**, *27*, 512-521.
80. Zhong, H.; Tran, L. M.; Stang, J. L., *J. Mol. Graph. Model* **2009**, *28*, 336-346.
81. Kalid, O.; Toledo Warshaviak, D.; Shechter, S.; Sherman, W.; Shacham, S., *J. Comput. Aid. Mol. Des* **2012**, *26*, 1217-1228.
82. Daylight <http://www.daylight.com/dayhtml/doc/theory/theory.finger.html>. <http://www.daylight.com/dayhtml/doc/theory/theory.finger.html> (accessed 4/18/2016).
83. Leach, A. R.; Gillet, V. J., *An Introduction to Chemoinformatics*. 2003.
84. Martin, Y. C.; Kofron, J. L.; Traphagen, L. M., *J. Med. Chem* **2002**, *45*, 4350-4358.
85. Willett, P., *Drug Discov. Today* **2006**, *11*, 1046-1053.
86. Jaccard, P., *Bulletin de la Societe Vaudoise des Sciences Naturelles* **1901**, *37*, 241-272.

87. Rogers, D. J.; Tanimoto, T. T., *Science* **1960**, *132*, 1115-1118.
88. Willett, P.; Barnard, J. M.; Downs, G. M., *J. Chem. Inf. Comput. Sci* **1998**, *38*, 983-996.
89. McKillup, S., *Statistics Explained. An Introductory Guide for Life Scientists*. 2006.
90. Davis, A. M.; Teague, S. J.; Kleywegt, G. J., *Angew. Chem. Int. Ed* **2003**, *42*, 2718-2736.
91. Poornima, C. S.; Dean, P. M., *J. Comput. Aid. Mol. Des* **1995**, *9*, 500-512.
92. Barillari, C.; Taylor, J.; Viner, R.; Essex, J. W., *J. Am. Chem. Soc* **2007**, *129*, 2577-2587.
93. Fayer, M. D., *Acc. Chem. Res* **2012**, *45*, 3-14.
94. Poornima, C. S.; Dean, P. M., *J. Comput. Aid. Mol. Des* **1995**, *9*, 521-531.
95. Verdonk, M. L.; Cole, J. C.; Taylor, R., *J. Mol. Biol* **1999**, *289*, 1093-1108.
96. Raschke, T. M., *Curr. Opin. Struct. Biol* **2006**, *16*, 152-159.
97. Roberts, B. C.; Mancera, R. L., *J. Chem. Inf. Model* **2008**, *48*, 397-408.
98. Huang, N.; Shoichet, B. K., *J. Med. Chem* **2008**, *51*, 4862-4865.
99. Huggins, D. J.; Tidor, B., *Protein Eng. Des. Sel* **2011**, *24*, 777-789.
100. Lie, M. A.; Thomsen, R.; Pedersen, C. N. S.; Schiott, B.; Christensen, M. H., *J. Chem. Inf. Model* **2011**, *51*, 909-917.
101. Poornima, C. S.; Dean, P. M., *J. Comput. Aid. Mol. Des* **1995**, *9*, 513-520.
102. Yang, Y. L., F.C.; Wong, S.E., *Expert Opin. Drug Discov.* **2013**, *8*, 277-287.
103. Sindhikara, D. J. H., F., *J. Phys. Chem. B* **2013**, *117*, 6718-6723.
104. Ross, G. A. B., M.S.; Essex, J.W., *J. Am. Chem. Soc.* **2015**, *137*, 14930-14943.
105. Waszkowycz, B.; Clark, D. E.; Gancia, E., *WIREs Comput. Mol. Sci* **2011**, *1*, 229-259.
106. Thilagavathi, R.; Mancera, R. L., *J. Chem. Inf. Model* **2010**, *50*, 415-421.
107. Huang, N.; Shoichet, B. K.; Irwin, J. J., *J. Med. Chem* **2006**, *49*, 6789-6801.
108. Hartshorn, M. J.; Verdonk, M. L.; Chessari, G.; Brewerton, S. C.; Mooij, W. T. M., *J. Med. Chem* **2007**, *50*, 726-741.

109. CSD <http://www.ccdc.cam.ac.uk/solutions/csd-system/components/csd/>.  
<http://www.ccdc.cam.ac.uk/solutions/csd-system/components/csd/> (accessed 4/18/2016).
110. PDB <http://www.rcsb.org/pdb/>. <http://www.rcsb.org/pdb/> (accessed 4/18/2016).
111. Berman, H. M.; Westbrook, J.; Feng, Z.; Gilliland, G.; Bhat, T. N.; Weissig, H.; Shindyalov, I. N.; Bourne, P. E., *Nucleic Acids Res* **2000**, *28*, 235-242.
112. Cruz-Cabeza, A. J.; Liebeschuetz, J. W.; Allen, F. H., *CrystEngComm* **2012**, *14*, 6797-6811.
113. Cruz-Cabeza, A. J.; Bernstein, J., *Chem. Rev* **2014**, *114*, 2170-2191.
114. Taylor, R.; Allen, F. H.; Cole, J. C., *CrystEngComm* **2015**, *17*, 2651-2666.
115. Roeland Boer, D.; Kroon, J.; Cole, J. C.; Smith, B.; Verdonk, M. L., *J. Mol. Biol* **2001**, *312*, 275-287.
116. Bruno, I. J.; Cole, J. C.; Lommerse, J. P. M.; Rowland, R. S.; Taylor, R.; Verdonk, M. L., *J. Comput. Aid. Mol. Des* **1997**, *11*, 525-537.
117. Verdonk, M. L.; Cole, J. C.; Watson, P.; Gillet, V. J.; Willett, P., *J. Mol. Biol* **2001**, *307*, 841-859.
118. Wade, R. C.; Clark, K. J.; Goodford, P., *J. Med. Chem* **1993**, *36*, 140-147.
119. Wade, R. C.; Goodford, P., *J. Med. Chem* **1993**, *36*, 148-156.
120. Brooks, B. R.; Bruccoleri, R. E.; Olafson, B. D.; States, D. J.; Swaminathan, S.; Karplus, M., *J. Comput. Chem* **1983**, *4*, 187-217.
121. Haeggström, J. Z.; Tholander, F.; Wetterholm, A., *Prostag. Oth. Lipid M* **2007**, *83*, 198-202.
122. Haeggström, J. Z., *J. Biol. Chem* **2004**, *49*, 50639-50642.
123. Davies, D. R.; Mamat, B.; Magnusson, O. T.; Christensen, J.; Haraldsson, M. H.; Mishra, R. K.; Pease, B.; Hansen, E.; Singh, J.; Zembower, D. E.; Kim, H.; Kiselyov, A. S.; Burgin, A. B.; Gurney, M. E.; Stewart, L. J., *J. Med. Chem* **2009**, *52*, 4694-4715.
124. Thunnissen, M. G. M.; Nordlund, P.; Haeggström, J. Z., *Nat. Str. Biol* **2001**, *8*, 131-135.

125. Sandanayaka, V.; Mamat, B.; Mishra, R. K.; Winger, J.; Krohn, M.; Zhou, L. M.; Keyvan, M.; Enache, L.; Sullins, D.; Onua, E.; Zhang, J.; Halldorsdottir, G.; Sigthorsdottir, H.; Thorlaksdottir, A.; Sigthorsson, G.; Thorsteinnsdottir, M.; Davies, D. R.; Stewart, L. J.; Zembower, D. E.; Andresson, T.; Kiselyov, A. S.; Singh, J.; Gurney, M. E., *J. Med. Chem* **2010**, *53*, 573-585.
126. Bourne, Y.; Watson, M. H.; Hickey, M. J.; Holmes, W.; Rocque, W.; Reed, S. I.; Tainer, J. A., *Cell* **1996**, *84*, 863-874.
127. Lawrie, A. M.; Noble, M. E.; Tunnah, P.; Brown, N. R.; Johnson, L. N.; Endicott, J. A., *Nat. Str. Biol* **1997**, *4*, 796-801.
128. Huang, D.; Zhou, T.; Lafleur, K.; Nevado, C.; Caflisch, A., *Bioinformatics* **2010**, *26*, 198-204.
129. Meijer, L.; Thunnissen, A. M. W. H.; White, A. W.; Garnier, M.; Nikolic, M.; Tsai, L. H.; Walter, J.; Cleverley, K. E.; Salinas, P. C.; Wu, Y. Z.; Biernat, J.; Mandelkow, E. M.; Kim, S. H.; Pettit, G. R., *Chem. Biol* **2000**, *7*, 51-63.
130. Bamborough, P., Personal communication. 2014.
131. Schrödinger Release 2013-3: Schrödinger Suite 2013 Protein Preparation Wizard; Epik version 2.6, Schrödinger, LLC, New York, NY, 2013; Impact version 6.1, Schrödinger, LLC, New York, NY, 2013; Prime version 3.4, Schrödinger, LLC, New York, NY, 2013. 2013.
132. Sastry, G. M.; Adzhigirey, M.; Day, T.; Annabhimoju, R.; Sherman, W., *J. Comput. Aid. Mol. Des* **2013**, *27*, 221-234.
133. Schrödinger Release 2013-3: LigPrep, version 2.8, Schrödinger, LLC, New York, NY, 2013. 2013.
134. Peukert, S.; Sun, Y.; Zhang, R.; Hurley, B.; Sabio, M.; Shen, X.; Gray, C.; Dzink-Fox, J.; Tao, J.; Cebula, R.; Wattanasin, S., *Bioorg. Med. Chem. Lett* **2008**, *18*, 1840-1844.
135. Teng, K. H.; Liang, P. H., *Bioorg. Chem* **2012**, *43*, 51-57.
136. Chang, S. Y.; Ko, T. P.; Chen, A. P. C.; Wang, A. H. J.; Liang, P. H., *Protein Sci* **2004**, *13*, 971-978.



137. Black, C. B.; Huang, H. W.; Cowan, J. A., *Coordin. Chem. Rev* **1994**, *135/136*, 165-202.
138. Kamata, K.; Kawamoto, H.; Honma, T.; Iwama, T.; Kim, S. H., *Proc. Natl. Acad. Sci. U. S. A* **1998**, *95*, 6630-6635.
139. Guertin, K. R.; Gardner, C. J.; Klein, S. I.; Zulli, A. L.; Czekaj, M.; Gong, Y.; Spada, A. P.; Cheney, D. L.; Maignan, S.; Guilloteau, J. P.; Brown, K. D.; Colussi, D. J.; Chu, V.; Heran, C. L.; Morgan, S. R.; Bentley, R. G.; Dunwiddie, C. T.; Leadley, R. J.; Pauls, H. W., *Bioorg. Med. Chem. Lett* **2002**, *12*, 1671-1674.
140. Schrodinger <http://www.schrodinger.com/>. <http://www.schrodinger.com/> (accessed 4/18/2016).
141. Shelley, J. C.; Cholleti, A.; Frye, L.; Greenwood, J. R.; Timlin, M. R.; Uchimaya, M., *J. Comput. Aid. Mol. Des* **2007**, *21*, 681-691.
142. Hermes <http://www.ccdc.cam.ac.uk/support-and-resources/ccdcresources/hermes.pdf>. <http://www.ccdc.cam.ac.uk/support-and-resources/ccdcresources/hermes.pdf> (accessed 4/18/2016).
143. Inc., C. C. G. *Molecular Operating Environment (MOE) 2010.10*, 2010.
144. Macromodel <http://www.schrodinger.com/MacroModel>. <http://www.schrodinger.com/MacroModel> (accessed 4/18/2016).
145. Sousa, S. F.; Fernandes, P. A.; Ramos, M. J., *Proteins* **2006**, *65*, 15-26.
146. Halgren, T. A.; Murphy, R. B.; Friesner, R. A.; Beard, H. S.; Frye, L.; Pollard, W. T.; Banks, J. L., *J. Med. Chem* **2004**, *47*, 1750-1759.
147. Rognan, D.; Lauemoller, S. L.; Holm, A.; Buus, S.; Tschinke, V., *J. Med. Chem* **1999**, *42*, 4650-4658.
148. Orning, L.; Krivi, G.; Fitzpatrick, F. A., *J. Biol. Chem* **1991**, *266*, 1375-1378.
149. Thunnissen, M. G. M.; Andersson, B.; Wong, C. H.; Samuelsson, B.; Haeggström, J. Z., *Faseb J* **2002**, *16*, 1648.
150. Robinson, D., Personal Communication. 2013.
151. Lovell, S. C.; Word, J. M.; Richardson, J. S.; Richardson, D. C., *Proteins Struct. Funct. Genet* **2000**, *40*, 389-408.

152. Eriksson, L.; Johansson, E.; Kettaneh-Wold, N.; Wikstrom, C.; Wold, S., *Design of Experiments: Principles and Applications*. 2008.
153. Design-Expert® software, version 7.1.1, Stat-Ease, Inc., Minneapolis, MN USA, [www.statease.com](http://www.statease.com). 2015.
154. Schrödinger Release 2013-3, Schrödinger, LLC, New York, NY, 2013. 2013.

## Appendices

### Appendix 1 – automated IFD process.pl

```
#!/usr/central/bin/perl

# process .maegz file output from IFD run in Maestro

# use: perl ./automated_IFD_process.pl filename.maegz baseline_structure.pdb

use strict;

my($maestro_file,$prefix,$workdir_prefix,$pdb_f,$pdb_pref,$pdb_file,$pdb_prefix,$m,$command,$count,$n,$input_file,$fileHandle,$fileHandle2,$fileHandle4,$line,$line2,@F,$primeE,$fileHandle3,$output,$count2,@G,$input_pdbfile,$pdb_primeE,$firstLine,$new_score_file,$delta_primeE);

my
($new_IFDscore,$new_IFDscore_1,$new_IFDscore_10,$new_IFDscore_20,$new_IFDscore_30,$new_IFDscore_40,$new_IFDscore_50,$new_IFDscore_60,$new_IFDscore_70,$new_IFDscore_80,$new_IFDscore_90,$new_IFDscore_100);

# make sure schrodinger environment is set up

$command = "schrodinger-2013-3";

system($command);

# get filename from user input

$maestro_file = $ARGV[0];

print "maestro file is $maestro_file\n";

$maestro_file =~ m/(.*)\./;

$prefix = $1;

$prefix =~ s/[\.\/]//g;

print "file prefix is $prefix\n";

$prefix =~ m/(.*)\./;

$workdir_prefix = $1;
```

```

print "workdir prefix is $workdir_prefix\n";

# get pdb filename of baseline structure to compare PrimeEnergy to
$pdb_f = $ARGV[1];
$pdb_f =~ m/(.*)\./.*;/
$pdb_pref = $1;
$pdb_pref =~ s/[\.\/]//g;

# remove ligand from baseline PDB file
open (baseline_pdb, $pdb_f) || die "Can't open 'baseline_pdb': $!";
open $fileHandle, ">>", $pdb_pref."_nolig.pdb" or die "Can't open '$!'\n";
while(<baseline_pdb>)
{
    $line = $_;
    if ($line =~ /^ENDMDL/)
    {
        last;
    }
    else
    {
        #remove ligand
        if ($line =~ /^HETATM/)
        {
            next;
        }
        else
        {
            print $fileHandle $line;
        }
    }
}

```

```

    }
}
close $fileHandle;

# get baseline PDB new filename in variable
$pdb_file = $pdb_pref."_nolig.pdb";
$pdb_file =~ m/(.*)\.\.*/;
$pdb_prefix = $1;
$pdb_prefix =~ s/[\.\/]//g;

# extract pdb files from Maestro .maegz result file
$command = "\$SCHRODINGER/utilities/pdbconvert -imae $maestro_file -opdb $prefix"."pdb";
print "Converting maestro file to PDBs\n";
system($command);

# sort report.csv output from IFD on IFDScore
open (report, $workdir_prefix."_workdir/report.csv") || die "Can't open 'report': $!";
open $fileHandle, ">>", "report_sorted.csv" or die "Can't open '$!'\n";
$command = "(head -n 1 $workdir_prefix"."_workdir/report.csv && tail -n +2
$workdir_prefix"."_workdir/report.csv | sort -t, -k3 -n) > report_sorted.csv";
system($command);
print "I've printed sorted report file\n";
close report;
close $fileHandle;

# get number of PDB files that will be generated from the number of lines in the report file and
renumber entries in order of scores
open (report_sorted, "report_sorted.csv") || die "Can't open 'report_sorted': $!";
open $fileHandle4, ">>", "report_updated.csv" or die "Can't open '$!'\n";
while (<report_sorted>)

```

```

{
    $count++;

    chomp;

    $line = $_;

    @F = split(/,,$line);

    print $fileHandle4 "$count,$F[1],$F[2],$F[3],$F[4],$F[5]\n";
}

close report_sorted;

close $fileHandle4;

print "count of pdb files is: $count\n";

# split the Maestro output in the number of PDB files required (one per entry)
open (Maestro_results, $prefix.".pdb") || die "Can't open 'Maestro_results': $!";
for ($m=1;$m<=$count -1;$m++)
{
    print "pdb file number is $m\n";

    open $fileHandle, ">>", $prefix."_".$m.".pdb" or die "Can't open '$!'\n";

    while(<Maestro_results>)
    {
        $line = $_;

        if ($line =~ /^ENDMDL/)
        {
            last;
        }
        else
        {
            #remove ligand

            if ($line =~ /^HETATM/)
            {

```

```

        next;
    }
    else
    {
        print $fileHandle $line;
    }
}
}
close $fileHandle;
}

# print header in the results file
$output = $prefix."_new_rank.csv";
open my $fileHandle2, ">>", $output or die "Can't open '$output'\n";
print $fileHandle2
"Entry,Ligand,old_IFDScore,GlideScore,old_PrimeEnergy,new_PrimeEnergy,File\n";
close $fileHandle2;

# loop through all PDB files
for ($n=1; $n<= $count-1; $n++)
{
    print "loop number is $n\n";

    # convert each PDB file back to Maestro file format for manipulation
    $command = "\$SCHRODINGER/utilities/pdbconvert -ipdb $prefix"."_"."$n"."pdb -omae
$prefix"."_"."$n"."_1.mae";

    print "Converting PDB file to mae format...\n";
    system($command);
    print "Done!\n";

    # prepare PDB files prior to prime energy calculation

```

```

# sample waters and minimise hydrogens of altered species

$command = "\$SCHRODINGER/utilities/protassign -minimize -WAIT
$prefix"_"_"$n"_"_1.mae $prefix"_"_"$n"_"_2.mae";

print "Sampling waters and minimising hydrogens of altered species...\n";

system($command);

print "Done!\n";

# restrained minimisation (hydrogens only)

$command = "\$SCHRODINGER/utilities/impref -fix -WAIT $prefix"_"_"$n"_"_2.mae -op
$prefix"_"_"$n"_"_3.mae";

print "Restrained minimisation for hydrogens only...\n";

system($command);

print "Done!\n";

# restrained minimisation

$command = "\$SCHRODINGER/utilities/impref -WAIT $prefix"_"_"$n"_"_3.mae -op
$prefix"_"_"$n"_"_4.mae";

print "Restrained minimisation...\n";

system($command);

print "Done!\n";

$input_file = $prefix"_"_"$n".inp";

# prepare input file for Prime

open($fileHandle, '>', $input_file) or die "Could not open file '$input_file' $!";

print $fileHandle "STRUCT_FILE $prefix"_"_"$n"_"_4.mae\n";

print $fileHandle "JOB_TYPE      REFINE\nPRIME_TYPE
ENERGY\nUSE_CRYSTAL_SYMMETRY no\nUSE_RANDOM_SEED      no\nSEED
0\nOPLS_VERSION      OPLS2005\nEXT_DIEL  80.00\nUSE_MEMBRANE
no\nHOST      localhost\n";

close $fileHandle;

# run analyse energy in Prime

$command = "\$SCHRODINGER/prime -WAIT $input_file";

```



```

system($command);

# get new Prime energy from log file
open (prime_output, $prefix."_". "$n.log") || die "Can't open 'prime_output': $!";
while(<prime_output>)
{
    chomp;
    $line = $_;
    if ($line =~ /TOTALE/)
    {
        @F = split(/ /,$line);
        $primeE = $F[4];
    }
}

close(prime_output);

#print to the report file that corresponds to the the PDB file that we're looking at
open (report_updated, "report_updated.csv") || die "Can't open 'report_updated': $!";
open my $fileHandle2, ">>", $output or die "Can't open '$output'\n";
while(<report_updated>)
{
    $count2++;
    if($count2 == $n+1)
    {
        chomp;
        @G = split(/ /,$_);
        print $fileHandle2 "$G[0],$G[1],$G[2],$G[3],$G[4],$primeE,$G[5]\n";
    }
}

```

```

    }

    $count2 = 0;

    close(report_updated);

    close($fileHandle2);

}

# prepare baseline structure for Prime Energy to compare induced structures to
# convert each PDB file to Maestro file format for manipulation
$command = "\$SCHRODINGER/utilities/pdbconvert -ipdb $pdb_file -omae $pdb_prefix"."_1.mae";

print "Converting PDB file to mae format...\n";

system($command);

print "Done!\n";

# prepare PDB file prior to prime energy calculation
# sample waters and minimise hydrogens of altered species

$command = "\$SCHRODINGER/utilities/protassign -minimize -WAIT $pdb_prefix"."_1.mae
$pdb_prefix"."_2.mae";

print "Sampling waters and minimising hydrogens of altered species...\n";

system($command);

print "Done!\n";

# restrained minimisation (hydrogens only)

$command = "\$SCHRODINGER/utilities/impref -fix -WAIT $pdb_prefix"."_2.mae -op
$pdb_prefix"."_3.mae";

print "Restrained minimisation for hydrogens only...\n";

system($command);

print "Done!\n";

# restrained minimisation

$command = "\$SCHRODINGER/utilities/impref -WAIT $pdb_prefix"."_3.mae -op
$pdb_prefix"."_4.mae";

print "Restrained minimisation...\n";

```

```

system($command);

print "Done!\n";

# prepare input file Prime Energy for baseline structure to compare induced structures to

$input_pdbfile = $pdb_prefix.".inp";

open($fileHandle, '>', $input_pdbfile) or die "Could not open file '$input_pdbfile' $!";

print $fileHandle "STRUCT_FILE $pdb_prefix"."_4.mae\n";

print $fileHandle "JOB_TYPE      REFINE\nPRIME_TYPE
ENERGY\nUSE_CRYSTAL_SYMMETRYno\nUSE_RANDOM_SEED      no\nSEED
0\nOPLS_VERSION      OPLS2005\nEXT_DIEL  80.00\nUSE_MEMBRANE
no\nHOST      localhost\n";

close $fileHandle;

# run analyse energy in Prime

$command = "\"$SCHRODINGER/prime -WAIT $input_pdbfile\"";

print "Running Prime...\n";

system($command);

print "Done!\n";

# get new Prime energy from log file

open (prime_output, $pdb_prefix.".log") || die "Can't open 'prime_output': $!";

while(<prime_output>)

{

    chomp;

    $line = $_;

    if ($line =~ /TOTALE/)

    {

        @F = split(/ /,$line);

        $pdb_primeE = $F[4];

    }

}

```

```

}

# open results file to re-calculate IFDScore from delta prime energy

$new_score_file = $prefix."_new_ranked_list.csv";

$firstLine =1;

open (results, $output) || die "Can't open 'results': $!";

open($fileHandle, '>', $new_score_file) or die "Could not open file '$new_score_file' $!";

print $fileHandle
"Entry,Ligand,old_IFDScore,GlideScore,new_PrimeEnergy,delta_PrimeEnergy,new_IFDScore_1,new_IFDScore_5,new_IFDScore_10,new_IFDScore_20,new_IFDScore_30,new_IFDScore_40,new_IFDScore_50,new_IFDScore_60,new_IFDScore_70,new_IFDScore_80,new_IFDScore_90,new_IFDScore_100,File\n";

while(<results>)

{

    # skip the header

    if($firstLine){

        $firstLine = 0;

    }

    else

    {

        chomp;

        @F = split(/,/, $_);

        $delta_primeE = $F[5]-$pdb_primeE;

        print "delta primeE is $delta_primeE\n";

        $new_IFDscore_1 = $F[3]+(0.01*$delta_primeE);

        $new_IFDScore = $F[3]+(0.05*$delta_primeE);

        $new_IFDscore_10 = $F[3]+(0.10*$delta_primeE);

        $new_IFDscore_20 = $F[3]+(0.20*$delta_primeE);

        $new_IFDscore_30 = $F[3]+(0.30*$delta_primeE);

        $new_IFDscore_40 = $F[3]+(0.40*$delta_primeE);

        $new_IFDscore_50 = $F[3]+(0.50*$delta_primeE);

```

```

    $new_IFDscore_60 = $F[3]+(0.60*$delta_primeE);

    $new_IFDscore_70 = $F[3]+(0.70*$delta_primeE);

    $new_IFDscore_80 = $F[3]+(0.80*$delta_primeE);

    $new_IFDscore_90 = $F[3]+(0.90*$delta_primeE);

    $new_IFDscore_100 = $F[3]+$delta_primeE;

    print "new IFDScore is $new_IFDScore\n";

    print $fileHandle
"$F[0],$F[1],$F[2],$F[3],$F[5],$delta_primeE,$new_IFDscore_1,$new_IFDScore,$new_IFDscore_1
0,$new_IFDscore_20,$new_IFDscore_30,$new_IFDscore_40,$new_IFDscore_50,$new_IFDscore_6
0,$new_IFDscore_70,$new_IFDscore_80,$new_IFDscore_90,$new_IFDscore_100,$F[6]\n";

    }

    $delta_primeE = 0;

    $new_IFDScore = 0;

}

close(prime_output);

```

## Appendix 2 – binding\_site RMSD.pl

```
#!/usr/central/bin/perl

# process .maegz file output from IFD run in Maestro and compute binding site RMSD between each
# IFD structure and the input baseline structure.

# There can be a difference in the number of amino acids between the two structures being compared.

# use: perl ./binding_site_RMSD.pl filename.maegz baseline_structure.pdb residues.txt

use strict;

my($maestro_file,$prefix,$workdir_prefix,$pdb_f,$pdb_pref,$pdb_file,$pdb_prefix,$command,$resi
dues,$count,$m,$n,$line,$aa,$fileHandle,$residues,$res,
@residues,$maestro_f,$maestro_BS_file,$p);

# make sure schrodinger environment is set up

$command = "schrodinger-2013-3";

system($command);

# get IFD filename from user input

$maestro_file = $ARGV[0];

print "maestro file is $maestro_file\n";

$maestro_file =~ m/(.*)\..*/;

$prefix = $1;

$prefix =~ s/[\.\/]//g;

print "file prefix is $prefix\n";

$prefix =~ m/(.*)\-*/;

$workdir_prefix = $1;

print "workdir prefix is $workdir_prefix\n";

# get pdb filename of baseline structure for RMSD calculation
```

```

$pdb_f = $ARGV[1];

$pdb_f =~ m/(.*)\./.*;/

$pdb_pref = $1;

$pdb_pref =~ s/[\.\.\/]//g;

$pdb_file = $pdb_pref."_nolig.pdb";

#list of residues which represent the binding site

$residues = $ARGV[2];

#only keep residues that represent the binding site

open (baseline_pdb, $pdb_f) || die "Can't open 'baseline_pdb': $!";

open (residues, $residues) || die "Can't open 'residues': $!";

@residues = <residues>;

close residues;

open $fileHandle, ">>", $pdb_file or die "Can't open '$!\n";

while(<baseline_pdb>)

{

    $line = $_;

    chomp ($line);

    if ($line =~ /^ENDMDL/)

    {

        #found the end of the file

        last;

    }

    else

    {

        if ($line =~ /^ATOM/)

        {

```

```

my ($atom, $atom_nb, $atom_type, $residue, $chain, $res_nb, $x, $y, $z,
$occ, $Bfact, $atom_symb) = unpack 'a4 a7 a5 a4 a2 a5 a12 a8 a8 a6 a6 a12', $line;

s/^\s+|\s+$//g for ($residue, $chain, $res_nb);

$res = $residue.$res_nb;

#print " residue is $res\n";

if ($chain eq 'A')
{
    foreach $aa (@residues)
    {
        s/^\s+|\s+$//g for ($aa);
        #keep residues of interest
        if($aa =~ /$res/)
        {
            print $fileHandle "$line\n";
        }
    }
}

}

}

}

close baseline_pdb;

close $fileHandle;

# extract pdb files from Maestro .maegz result file
$command = "\$SCHRODINGER/utilities/pdbconvert -imae $maestro_file -opdb $prefix". ".pdb";
system($command);

# get number of PDB files that will be generated from the number of lines in the report file

```



```

open (report, $workdir_prefix."_workdir/report.csv") || die "Can't open 'report': $!";

$count++ while (<report>);

close report;

print "$count\n";

# go through Maestro pdb outout file and split into desired number of PDB files (one per entry)
open (Maestro_results, $prefix."_pdb") || die "Can't open 'Maestro_results': $!";

for ($m=1;$m<=$count -1;$m++)
{
    open $fileHandle, ">>", $prefix."_".$m."_pdb" or die "Can't open '$!'\n";

    while(<Maestro_results>)
    {
        $line = $_;

        if ($line =~ /^ENDMDL/)
        {
            last;
        }

        else
        {
            #remove ligand

            if ($line =~ /^HETATM/)
            {
                next;
            }

            else
            {
                print $fileHandle $line;
            }
        }
    }
}

```

```

    }

    close $fileHandle;
}

# go through pdb files to find residues of interest
for ($n=1; $n<= $count-1; $n++)
{
    print "loop number is $n\n";

    $maestro_f = $prefix."_".$n.".pdb";
    print "the filename is $maestro_f\n";
    $maestro_BS_file = $prefix."_BS".$n.".pdb";
    open (maestro_pdb, $maestro_f) || die "Can't open 'maestro_pdb': $!";
    open $fileHandle, ">>", $maestro_BS_file or die "Can't open '$!\n";

    while(<maestro_pdb>)
    {
        my($line) = $_;
        chomp ($line);
        if ($line =~ /^ENDMDL/)
        {
            last;
        }
        else
        {
            if ($line =~ /^ATOM/)
            {
                my ($atom, $atom_nb, $atom_type, $residue, $chain, $res_nb, $x,
                    $y, $z, $occ, $Bfact, $atom_symb) = unpack 'a4 a7 a5 a4 a2 a5 a12 a8 a8 a6 a6 a12', $line;
            }
        }
    }
}

```

```

s/^\s+\s+$/g for ($residue, $chain, $res_nb);

my($res) = $residue.$res_nb;

if ($chain eq 'A')
{
    foreach $aa (@residues)
    {
        s/^\s+\s+$/g for ($aa);
        #keep residues of interest
        if($aa =~ /$res/)
        {
            print $fileHandle "$line\n";
        }
    }
}

}

}

}

close $fileHandle;

unlink($maestro_f);

}

my($pdb_mae) = $pdb_pref."_nolig.mae";

#convert files to maestro format in preparation for rmsd calc

$command = "\$SCHRODINGER/utilities/pdbconvert -ipdb $pdb_file -omae $pdb_mae";

system($command);

# loop through all PDB files and calculate binding site RMSDs

```

```

for ($p=1; $p<= $count-1; $p++)
{
    print "loop number is $p\n";

    $maestro_BS_file = $prefix."_BS".$p".pdb";

    my($maestro_BS_mae) = $prefix."_BS".$p".mae";

    #convert files to maestro format

    $command = "\$SCHRODINGER/utilities/pdbconvert -ipdb $maestro_BS_file -omae
$maestro_BS_mae";

    system($command);

    unlink($maestro_BS_file);

    #compute RMSD

    $command = "\$SCHRODINGER/run rmsd.py $pdb_mae $maestro_BS_mae
>$prefix."_BS".$p".txt";

    system($command);

    unlink($maestro_BS_mae);
}

unlink($pdb_mae);

unlink($pdb_file);

```

## Appendix 3 – New IFDScores calculations

Ligand **12** in 1DM2

Entry	ligand RMSD	BS RMSD	old_IFD Score	Glide Score	PE <sub>IFD</sub>	ΔPE	new_IFD Score_1	new_IFD Score_5	new_IFD Score_10	new_IFD Score_20	new_IFD Score_30	new_IFD Score_40	new_IFD Score_50	new_IFD Score_60	new_IFD Score_70	new_IFD Score_80	new_IFD Score_90	new_IFD Score_100
1	1.6	0.9	-575	-13.3	-11295	-61	-13.9	-16.3	-19.3	-25.4	-31.5	-37.5	-43.6	-49.6	-55.7	-61.7	-67.8	-73.9
2	0.7	0.8	-574	-12.7	-11280	-46	-13.1	-15.0	-17.3	-21.9	-26.5	-31.1	-35.7	-40.3	-44.9	-49.5	-54.1	-58.7
3	2.0	0.9	-574	-12.3	-11289	-55	-12.9	-15.1	-17.9	-23.4	-28.9	-34.4	-39.9	-45.4	-50.9	-56.4	-61.9	-67.4
4	1.6	0.8	-573	-12.1	-11273	-39	-12.5	-14.0	-16.0	-19.9	-23.8	-27.7	-31.5	-35.4	-39.3	-43.2	-47.1	-51.0
5	5.6	1.0	-573	-11.2	-11326	-91	-12.1	-15.7	-20.3	-29.4	-38.5	-47.7	-56.8	-65.9	-75.0	-84.1	-93.2	-102.4
6	1.2	1.2	-572	-11.0	-11280	-45	-11.5	-13.3	-15.6	-20.1	-24.7	-29.2	-33.7	-38.3	-42.8	-47.3	-51.9	-56.4
7	5.6	1.1	-571	-10.2	-11284	-49	-10.6	-12.6	-15.1	-20.0	-24.9	-29.8	-34.7	-39.6	-44.5	-49.5	-54.4	-59.3
8	1.3	1.5	-571	-10.3	-11283	-49	-10.7	-12.7	-15.1	-20.0	-24.9	-29.7	-34.6	-39.5	-44.4	-49.2	-54.1	-59.0
9	5.9	0.9	-571	-9.2	-11297	-62	-9.8	-12.3	-15.4	-21.6	-27.9	-34.1	-40.4	-46.6	-52.8	-59.1	-65.3	-71.5
10	7.4	1.4	-570	-9.4	-11284	-49	-9.9	-11.9	-14.4	-19.3	-24.3	-29.2	-34.1	-39.1	-44.0	-49.0	-53.9	-58.8
11	7.2	1.3	-570	-9.7	-11281	-46	-10.2	-12.0	-14.3	-19.0	-23.6	-28.3	-32.9	-37.6	-42.2	-46.8	-51.5	-56.1
12	7.0	1.0	-568	-7.8	-11289	-54	-8.3	-10.5	-13.2	-18.6	-24.1	-29.5	-34.9	-40.4	-45.8	-51.2	-56.6	-62.1
13	2.2	0.9	-568	-7.4	-11302	-67	-8.1	-10.7	-14.1	-20.8	-27.6	-34.3	-41.0	-47.7	-54.4	-61.2	-67.9	-74.6

Table S1: 12 n 1DM2, Experiment 1

Entry	ligand RMSD	BS RMSD	old_IFD Score	Glide Score	PE <sub>IFD</sub>	ΔPE	new_IFD Score <sub>_1</sub>	new_IFD Score <sub>_5</sub>	new_IFD Score <sub>_10</sub>	new_IFD Score <sub>_20</sub>	new_IFD Score <sub>_30</sub>	new_IFD Score <sub>_40</sub>	new_IFD Score <sub>_50</sub>	new_IFD Score <sub>_60</sub>	new_IFD Score <sub>_70</sub>	new_IFD Score <sub>_80</sub>	new_IFD Score <sub>_90</sub>	new_IFD Score <sub>_100</sub>
1	1.1	0.7	-578	-12.5	-11319	-94.7	-13.5	-17.3	-22.0	-31.5	-40.9	-50.4	-59.9	-69.3	-78.8	-88.3	-97.7	-107.2
2	1.8	0.8	-578	-12.7	-11320	-95.5	-13.6	-17.5	-22.2	-31.8	-41.3	-50.9	-60.5	-70.0	-79.6	-89.1	-98.7	-108.2
3	2.3	0.9	-578	-12.9	-11305	-80.7	-13.7	-16.9	-20.9	-29.0	-37.1	-45.1	-53.2	-61.3	-69.3	-77.4	-85.5	-93.6
4	4.1	0.9	-577	-11.5	-11319	-94.6	-12.5	-16.2	-21.0	-30.4	-39.9	-49.3	-58.8	-68.3	-77.7	-87.2	-96.6	-106.1
5	4.2	1.0	-576	-10.3	-11333	-107.7	-11.4	-15.7	-21.0	-31.8	-42.6	-53.4	-64.1	-74.9	-85.7	-96.5	-107.2	-118.0
6	5.1	1.1	-576	-10.6	-11330	-105.1	-11.7	-15.9	-21.1	-31.6	-42.1	-52.7	-63.2	-73.7	-84.2	-94.7	-105.2	-115.7
7	2.0	1.0	-576	-10.5	-11330	-105.3	-11.6	-15.8	-21.0	-31.6	-42.1	-52.6	-63.1	-73.7	-84.2	-94.7	-105.2	-115.8
8	2.1	0.7	-575	-10.6	-11313	-88.5	-11.5	-15.0	-19.4	-28.3	-37.1	-46.0	-54.8	-63.7	-72.5	-81.4	-90.2	-99.1
9	4.9	1.1	-575	-10.4	-11326	-101.1	-11.4	-15.5	-20.5	-30.7	-40.8	-50.9	-61.0	-71.1	-81.2	-91.3	-101.4	-111.5
10	5.8	1.0	-575	-10.3	-11321	-95.8	-11.3	-15.1	-19.9	-29.5	-39.0	-48.6	-58.2	-67.8	-77.3	-86.9	-96.5	-106.1
11	6.4	1.0	-571	-5.7	-11332	-106.9	-6.8	-11.1	-16.4	-27.1	-37.8	-48.5	-59.2	-69.8	-80.5	-91.2	-101.9	-112.6
12	7.1	1.0	-569	-4.4	-11323	-98.6	-5.4	-9.4	-14.3	-24.2	-34.0	-43.9	-53.8	-63.6	-73.5	-83.4	-93.2	-103.1
13	6.6	1.1	-569	-4.2	-11328	-103.7	-5.3	-9.4	-14.6	-25.0	-35.3	-45.7	-56.1	-66.4	-76.8	-87.2	-97.6	-107.9

Table S2: 12 in 1DM2, Experiment 2

Entry	Ligand RMSD	BS RMSD	old_IFD Score	Glide Score	PE <sub>IFD</sub>	$\Delta$ PE	new_IFD Score_1	new_IFD Score_5	new_IFD Score_10	new_IFD Score_20	new_IFD Score_30	new_IFD Score_40	new_IFD Score_50	new_IFD Score_60	new_IFD Score_70	new_IFD Score_80	new_IFD Score_90	new_IFD Score_100
1	1.7	0.8	-575	-12.9	-11294	-59.9	-13.5	-15.9	-18.9	-24.9	-30.9	-36.9	-42.8	-48.8	-54.8	-60.8	-66.8	-72.8
2	0.7	0.9	-575	-13.0	-11277	-43.0	-13.5	-15.2	-17.3	-21.6	-25.9	-30.2	-34.5	-38.8	-43.1	-47.4	-51.7	-56.0
3	0.8	0.9	-575	-12.9	-11282	-47.2	-13.3	-15.2	-17.6	-22.3	-27.0	-31.8	-36.5	-41.2	-45.9	-50.6	-55.4	-60.1
4	0.5	1.0	-575	-12.1	-11289	-54.5	-12.6	-14.8	-17.6	-23.0	-28.5	-33.9	-39.4	-44.8	-50.3	-55.7	-61.2	-66.6
5	0.7	0.8	-575	-12.5	-11287	-52.8	-13.1	-15.2	-17.8	-23.1	-28.4	-33.6	-38.9	-44.2	-49.5	-54.8	-60.0	-65.3
6	2.0	1.0	-573	-11.8	-11283	-48.2	-12.3	-14.2	-16.7	-21.5	-26.3	-31.1	-35.9	-40.8	-45.6	-50.4	-55.2	-60.0
7	1.1	0.9	-573	-11.1	-11298	-63.8	-11.8	-14.3	-17.5	-23.9	-30.3	-36.7	-43.0	-49.4	-55.8	-62.2	-68.6	-75.0
8	4.9	1.1	-573	-11.0	-11283	-48.9	-11.5	-13.4	-15.9	-20.8	-25.7	-30.6	-35.5	-40.3	-45.2	-50.1	-55.0	-59.9
9	4.3	0.9	-573	-10.5	-11292	-57.6	-11.0	-13.4	-16.2	-22.0	-27.8	-33.5	-39.3	-45.1	-50.8	-56.6	-62.3	-68.1
10	0.9	1.0	-572	-10.7	-11290	-55.1	-11.3	-13.5	-16.2	-21.8	-27.3	-32.8	-38.3	-43.8	-49.3	-54.8	-60.4	-65.9
11	4.6	1.0	-572	-10.6	-11287	-52.9	-11.1	-13.2	-15.9	-21.2	-26.5	-31.8	-37.1	-42.3	-47.6	-52.9	-58.2	-63.5
12	4.5	0.9	-572	-10.1	-11282	-48.0	-10.6	-12.5	-14.9	-19.7	-24.5	-29.3	-34.1	-38.9	-43.7	-48.5	-53.3	-58.1
13	5.9	1.0	-571	-8.9	-11314	-79.6	-9.7	-12.9	-16.9	-24.8	-32.8	-40.7	-48.7	-56.6	-64.6	-72.6	-80.5	-88.5
14	5.5	0.9	-570	-9.0	-11294	-59.3	-9.6	-12.0	-15.0	-20.9	-26.8	-32.7	-38.7	-44.6	-50.5	-56.4	-62.4	-68.3
15	4.4	0.9	-570	-9.3	-11287	-52.6	-9.9	-12.0	-14.6	-19.9	-25.1	-30.4	-35.7	-40.9	-46.2	-51.4	-56.7	-62.0
16	3.9	0.8	-569	-8.4	-11295	-60.4	-9.0	-11.4	-14.4	-20.4	-26.5	-32.5	-38.5	-44.6	-50.6	-56.7	-62.7	-68.7

Table S3: 12 in 1DM2, Experiment 3



Entry	Ligand RMSD	BS RMSD	old_IFD Score	Glide Score	PE <sub>IFD</sub>	$\Delta$ PE	new_IFD Score <sub>_1</sub>	new_IFD Score <sub>_5</sub>	new_IFD Score <sub>_10</sub>	new_IFD Score <sub>_20</sub>	new_IFD Score <sub>_30</sub>	new_IFD Score <sub>_40</sub>	new_IFD Score <sub>_50</sub>	new_IFD Score <sub>_60</sub>	new_IFD Score <sub>_70</sub>	new_IFD Score <sub>_80</sub>	new_IFD Score <sub>_90</sub>	new_IFD Score <sub>_100</sub>
1	2.1	0.9	-575	-13.3	-11289	-54.9	-13.8	-16.0	-18.8	-24.3	-29.8	-35.3	-40.8	-46.2	-51.7	-57.2	-62.7	-68.2
2	0.7	0.8	-575	-12.7	-11273	-38.7	-13.1	-14.7	-16.6	-20.5	-24.3	-28.2	-32.1	-36.0	-39.8	-43.7	-47.6	-51.4
3	1.8	0.9	-574	-12.4	-11288	-53.4	-12.9	-15.1	-17.7	-23.1	-28.4	-33.8	-39.1	-44.5	-49.8	-55.2	-60.5	-65.8
4	1.7	1.0	-574	-12.1	-11293	-58.9	-12.7	-15.0	-18.0	-23.9	-29.7	-35.6	-41.5	-47.4	-53.3	-59.2	-65.1	-71.0
5	0.7	1.3	-574	-12.2	-11287	-53.1	-12.7	-14.8	-17.5	-22.8	-28.1	-33.4	-38.7	-44.0	-49.4	-54.7	-60.0	-65.3
6	1.6	0.8	-573	-12.0	-11281	-46.3	-12.4	-14.3	-16.6	-21.2	-25.9	-30.5	-35.1	-39.8	-44.4	-49.0	-53.6	-58.3
7	3.6	1.0	-573	-11.3	-11294	-60.1	-11.9	-14.3	-17.3	-23.3	-29.3	-35.3	-41.3	-47.3	-53.3	-59.3	-65.4	-71.4
8	3.8	1.0	-573	-10.5	-11297	-62.2	-11.1	-13.6	-16.7	-22.9	-29.1	-35.4	-41.6	-47.8	-54.0	-60.2	-66.5	-72.7
9	1.7	1.1	-573	-11.6	-11283	-48.6	-12.1	-14.0	-16.5	-21.3	-26.2	-31.1	-35.9	-40.8	-45.7	-50.5	-55.4	-60.3
10	5.8	1.0	-572	-10.7	-11292	-57.9	-11.3	-13.6	-16.5	-22.3	-28.0	-33.8	-39.6	-45.4	-51.2	-57.0	-62.8	-68.6
11	3.6	1.1	-571	-10.3	-11282	-47.3	-10.8	-12.7	-15.1	-19.8	-24.5	-29.3	-34.0	-38.7	-43.5	-48.2	-52.9	-57.7
12	3.1	0.9	-571	-9.6	-11301	-66.5	-10.3	-12.9	-16.3	-22.9	-29.6	-36.2	-42.8	-49.5	-56.1	-62.8	-69.4	-76.1
13	5.6	1.1	-571	-9.3	-11299	-64.6	-9.9	-12.5	-15.8	-22.2	-28.7	-35.1	-41.6	-48.0	-54.5	-61.0	-67.4	-73.9
14	4.7	1.0	-570	-9.7	-11274	-39.4	-10.1	-11.7	-13.7	-17.6	-21.6	-25.5	-29.5	-33.4	-37.3	-41.3	-45.2	-49.2
15	5.0	1.0	-569	-8.4	-11289	-54.8	-8.9	-11.1	-13.9	-19.3	-24.8	-30.3	-35.8	-41.3	-46.7	-52.2	-57.7	-63.2

Table S4: **12** in 1DM2, Experiment 4

Entry	ligand RMSD	BS RMSD	old_IFD Score	Glide Score	PE <sub>IFD</sub>	$\Delta$ PE	new_IFD Score _1	new_IFD Score _5	new_IFD Score _10	new_IFD Score _20	new_IFD Score _30	new_IFD Score _40	new_IFD Score _50	new_IFD Score _60	new_IFD Score _70	new_IFD Score _80	new_IFD Score _90	new_IFD Score _100
1	1.3	0.8	-578	-13.5	-11329	-104.0	-14.5	-18.7	-23.9	-34.3	-44.7	-55.1	-65.5	-75.9	-86.3	-96.7	-107.1	-117.5
2	1.7	0.9	-578	-12.5	-11318	-92.8	-13.5	-17.2	-21.8	-31.1	-40.4	-49.7	-58.9	-68.2	-77.5	-86.8	-96.1	-105.3
3	4.7	0.9	-576	-10.6	-11336	-111.7	-11.7	-16.2	-21.7	-32.9	-44.1	-55.2	-66.4	-77.6	-88.7	-99.9	-111.1	-122.2
4	4.6	0.8	-576	-10.8	-11326	-101.2	-11.8	-15.8	-20.9	-31.0	-41.1	-51.2	-61.3	-71.5	-81.6	-91.7	-101.8	-111.9
5	4.2	1.0	-576	-10.3	-11320	-94.9	-11.3	-15.1	-19.8	-29.3	-38.8	-48.3	-57.8	-67.3	-76.8	-86.3	-95.8	-105.3
6	5.7	1.3	-575	-10.1	-11323	-98.6	-11.0	-15.0	-19.9	-29.8	-39.6	-49.5	-59.4	-69.2	-79.1	-88.9	-98.8	-108.7
7	5.9	1.0	-575	-9.9	-11325	-100.4	-10.9	-15.0	-20.0	-30.0	-40.1	-50.1	-60.2	-70.2	-80.2	-90.3	-100.3	-110.4
8	6.0	1.1	-574	-9.1	-11326	-101.0	-10.1	-14.1	-19.2	-29.3	-39.4	-49.5	-59.6	-69.7	-79.8	-89.9	-100.0	-110.1
9	5.9	0.9	-573	-8.2	-11325	-100.6	-9.2	-13.3	-18.3	-28.4	-38.4	-48.5	-58.5	-68.6	-78.7	-88.7	-98.8	-108.9
10	2.9	1.2	-573	-8.5	-11337	-111.8	-9.6	-14.1	-19.7	-30.9	-42.1	-53.2	-64.4	-75.6	-86.8	-98.0	-109.2	-120.3
11	6.7	1.6	-570	-5.4	-11318	-93.0	-6.3	-10.0	-14.7	-24.0	-33.3	-42.6	-51.9	-61.2	-70.5	-79.8	-89.1	-98.4
12	6.4	0.9	-568	-3.9	-11320	-95.0	-4.8	-8.6	-13.4	-22.9	-32.4	-41.9	-51.4	-60.9	-70.4	-79.9	-89.4	-98.9

Table S5: 12 in 1DM2, Experiment 5

Entry	ligand RMSD	BS RMSD	old_IFD Score	GlideScore	PE <sub>IFD</sub>	ΔPE	new_IFD Score <sub>_1</sub>	new_IFD Score <sub>_5</sub>	new_IFD Score <sub>_10</sub>	new_IFD Score <sub>_20</sub>	new_IFD Score <sub>_30</sub>	new_IFD Score <sub>_40</sub>	new_IFD Score <sub>_50</sub>	new_IFD Score <sub>_60</sub>	new_IFD Score <sub>_70</sub>	new_IFD Score <sub>_80</sub>	new_IFD Score <sub>_90</sub>	new_IFD Score <sub>_100</sub>
1	1.0	0.7	-579	-13.1	-11323	-97.7	-14.1	-18.0	-22.9	-32.7	-42.5	-52.2	-62.0	-71.8	-81.5	-91.3	-101.1	-110.9
2	1.7	0.8	-578	-12.4	-11321	-96.6	-13.4	-17.2	-22.1	-31.7	-41.4	-51.0	-60.7	-70.4	-80.0	-89.7	-99.3	-109.0
3	4.6	0.7	-577	-11.1	-11320	-95.6	-12.0	-15.8	-20.6	-30.2	-39.7	-49.3	-58.8	-68.4	-78.0	-87.5	-97.1	-106.6
4	7.3	1.2	-576	-11.0	-11334	-109.6	-12.1	-16.5	-21.9	-32.9	-43.9	-54.8	-65.8	-76.7	-87.7	-98.6	-109.6	-120.6
5	2.0	1.0	-576	-10.6	-11328	-102.9	-11.6	-15.8	-20.9	-31.2	-41.5	-51.8	-62.1	-72.4	-82.6	-92.9	-103.2	-113.5
6	4.3	0.8	-576	-9.9	-11325	-100.2	-10.9	-15.0	-20.0	-30.0	-40.0	-50.0	-60.0	-70.1	-80.1	-90.1	-100.1	-110.1
7	2.2	1.1	-576	-10.3	-11332	-107.5	-11.4	-15.7	-21.1	-31.8	-42.6	-53.3	-64.1	-74.8	-85.6	-96.3	-107.1	-117.8
8	4.4	0.8	-575	-9.6	-11334	-109.0	-10.7	-15.1	-20.5	-31.4	-42.3	-53.2	-64.1	-75.0	-85.9	-96.8	-107.7	-118.6
9	5.7	1.1	-574	-9.6	-11335	-110.7	-10.7	-15.1	-20.7	-31.7	-42.8	-53.9	-64.9	-76.0	-87.1	-98.1	-109.2	-120.3
10	5.5	0.9	-574	-9.6	-11317	-92.6	-10.6	-14.3	-18.9	-28.2	-37.4	-46.7	-55.9	-65.2	-74.5	-83.7	-93.0	-102.3
11	5.8	1.0	-573	-8.0	-11330	-104.8	-9.0	-13.2	-18.4	-28.9	-39.4	-49.9	-60.3	-70.8	-81.3	-91.8	-102.2	-112.7
12	3.5	1.0	-573	-7.9	-11342	-117.1	-9.1	-13.8	-19.6	-31.3	-43.0	-54.7	-66.4	-78.2	-89.9	-101.6	-113.3	-125.0
13	6.1	1.0	-573	-8.0	-11332	-106.8	-9.1	-13.4	-18.7	-29.4	-40.0	-50.7	-61.4	-72.1	-82.8	-93.4	-104.1	-114.8
14	3.7	1.0	-572	-6.4	-11332	-106.9	-7.4	-11.7	-17.1	-27.7	-38.4	-49.1	-59.8	-70.5	-81.2	-91.9	-102.6	-113.3
15	6.1	1.0	-571	-5.1	-11327	-101.8	-6.1	-10.2	-15.2	-25.4	-35.6	-45.8	-56.0	-66.2	-76.4	-86.5	-96.7	-106.9
16	6.6	1.3	-569	-4.2	-11322	-96.7	-5.2	-9.1	-13.9	-23.6	-33.2	-42.9	-52.6	-62.3	-71.9	-81.6	-91.3	-101.0
17	9.6	0.9	-567	-2.1	-11324	-98.9	-3.1	-7.1	-12.0	-21.9	-31.8	-41.7	-51.6	-61.5	-71.3	-81.2	-91.1	-101.0
18	9.7	1.0	-567	-2.1	-11319	-94.5	-3.0	-6.8	-11.6	-21.0	-30.5	-39.9	-49.4	-58.8	-68.3	-77.7	-87.2	-96.6

Table S6: 12 in 1DM2, Experiment 6

Entry	Ligand RMSD	BS RMSD	old_ IFD Score	Glide Score	PE <sub>IFD</sub>	$\Delta$ PE	new_ IFD Score _1	new_ IFD Score _5	new_ IFD Score _10	new_ IFD Score _20	new_ IFD Score _30	new_ IFD Score _40	new_ IFD Score _50	new_ IFD Score _60	new_ IFD Score _70	new_ IFD Score _80	new_ IFD Score _90	new_ IFD Score _100
1	0.8	0.9	-576	-13.0	-11297	-62.8	-13.7	-16.2	-19.3	-25.6	-31.9	-38.2	-44.4	-50.7	-57.0	-63.3	-69.6	-75.8
2	1.8	0.8	-575	-12.8	-11297	-62.2	-13.5	-16.0	-19.1	-25.3	-31.5	-37.7	-43.9	-50.1	-56.4	-62.6	-68.8	-75.0
3	0.8	0.8	-575	-12.9	-11262	-28.1	-13.1	-14.3	-15.7	-18.5	-21.3	-24.1	-26.9	-29.7	-32.5	-35.3	-38.1	-41.0
4	1.5	0.9	-574	-12.1	-11289	-55.0	-12.7	-14.9	-17.6	-23.1	-28.6	-34.1	-39.6	-45.1	-50.6	-56.1	-61.6	-67.1

Table S7: 12 in 1DM2, Experiment 7

Entry	ligand RMSD	BS RMSD	old_IFD Score	Glide Score	PE <sub>IFD</sub>	ΔPE	new_IFD Score_1	new_IFD Score_5	new_IFD Score_10	new_IFD Score_20	new_IFD Score_30	new_IFD Score_40	new_IFD Score_50	new_IFD Score_60	new_IFD Score_70	new_IFD Score_80	new_IFD Score_90	new_IFD Score_100
1	1.8	0.8	-578	-12.9	-11335	-110.7	-14.0	-18.4	-24.0	-35.0	-46.1	-57.2	-68.2	-79.3	-90.4	-101.4	-112.5	-123.6
2	1.9	0.7	-578	-13.2	-11324	-99.3	-14.1	-18.1	-23.1	-33.0	-42.9	-52.9	-62.8	-72.7	-82.6	-92.6	-102.5	-112.4
3	4.0	0.8	-577	-11.8	-11324	-99.2	-12.7	-16.7	-21.7	-31.6	-41.5	-51.4	-61.4	-71.3	-81.2	-91.1	-101.1	-111.0
4	4.2	0.9	-576	-10.9	-11324	-99.2	-11.9	-15.8	-20.8	-30.7	-40.6	-50.5	-60.5	-70.4	-80.3	-90.2	-100.1	-110.0
5	4.6	0.7	-576	-11.0	-11322	-97.4	-11.9	-15.8	-20.7	-30.4	-40.2	-49.9	-59.7	-69.4	-79.1	-88.9	-98.6	-108.3
6	4.7	0.9	-576	-10.7	-11317	-92.3	-11.6	-15.3	-19.9	-29.2	-38.4	-47.6	-56.9	-66.1	-75.3	-84.6	-93.8	-103.0
7	2.3	1.0	-575	-9.9	-11342	-117.3	-11.1	-15.8	-21.7	-33.4	-45.1	-56.9	-68.6	-80.3	-92.0	-103.8	-115.5	-127.2
8	5.6	1.0	-575	-10.1	-11330	-104.9	-11.2	-15.4	-20.6	-31.1	-41.6	-52.1	-62.6	-73.1	-83.5	-94.0	-104.5	-115.0
9	2.6	1.2	-574	-9.3	-11339	-114.2	-10.5	-15.0	-20.7	-32.2	-43.6	-55.0	-66.4	-77.8	-89.3	-100.7	-112.1	-123.5
10	5.9	0.9	-573	-8.2	-11337	-112.3	-9.4	-13.9	-19.5	-30.7	-41.9	-53.2	-64.4	-75.6	-86.9	-98.1	-109.3	-120.6
11	3.2	1.1	-572	-8.4	-11337	-112.2	-9.5	-14.0	-19.6	-30.8	-42.0	-53.2	-64.5	-75.7	-86.9	-98.1	-109.4	-120.6
12	6.5	1.0	-570	-6.5	-11334	-109.6	-7.5	-11.9	-17.4	-28.4	-39.3	-50.3	-61.3	-72.2	-83.2	-94.2	-105.1	-116.1
13	6.9	0.9	-569	-4.5	-11323	-97.9	-5.5	-9.4	-14.3	-24.1	-33.9	-43.7	-53.5	-63.2	-73.0	-82.8	-92.6	-102.4

Table S8: 12 in 1DM2, Experiment 8

## Ligand 11 in 4EK3

Entry	ligand RMSD	BS RMSD	old_IFD Score	Glide Score	PE <sub>IFD</sub>	ΔPE	new_IFD Score_1	new_IFD Score_5	new_IFD Score_10	new_IFD Score_20	new_IFD Score_30	new_IFD Score_40	new_IFD Score_50	new_IFD Score_60	new_IFD Score_70	new_IFD Score_80	new_IFD Score_90	new_IFD Score_100
1	5.6	1.5	-621	-7.9	-12119	-37.8	-8.3	-9.8	-11.7	-15.5	-19.3	-23.1	-26.8	-30.6	-34.4	-38.2	-42.0	-45.8
2	4.2	1.4	-620	-7.7	-12112	-30.7	-8.0	-9.2	-10.8	-13.8	-16.9	-20.0	-23.1	-26.1	-29.2	-32.3	-35.3	-38.4
3	3.3	1.4	-620	-7.8	-12120	-38.5	-8.2	-9.7	-11.7	-15.5	-19.3	-23.2	-27.0	-30.9	-34.7	-38.6	-42.4	-46.3
4	7.9	1.6	-620	-6.9	-12125	-43.6	-7.4	-9.1	-11.3	-15.6	-20.0	-24.4	-28.7	-33.1	-37.4	-41.8	-46.1	-50.5
5	7.8	1.6	-620	-6.5	-12121	-39.8	-6.9	-8.5	-10.5	-14.5	-18.5	-22.5	-26.4	-30.4	-34.4	-38.4	-42.4	-46.4
6	8.5	1.5	-619	-6.3	-12125	-43.0	-6.7	-8.4	-10.6	-14.9	-19.2	-23.5	-27.8	-32.1	-36.4	-40.7	-45.0	-49.3
7	8.1	1.5	-619	-6.1	-12114	-32.5	-6.5	-7.8	-9.4	-12.7	-15.9	-19.2	-22.4	-25.7	-28.9	-32.2	-35.4	-38.7
8	8.7	1.6	-619	-6.7	-12123	-41.6	-7.1	-8.7	-10.8	-15.0	-19.2	-23.3	-27.5	-31.7	-35.8	-40.0	-44.1	-48.3
9	7.8	1.6	-619	-6.1	-12119	-37.7	-6.4	-8.0	-9.8	-13.6	-17.4	-21.1	-24.9	-28.7	-32.4	-36.2	-40.0	-43.7
10	8.8	1.6	-619	-6.3	-12114	-33.0	-6.7	-8.0	-9.6	-12.9	-16.2	-19.5	-22.8	-26.1	-29.4	-32.7	-36.0	-39.3
11	5.9	1.7	-618	-6.0	-12114	-32.5	-6.3	-7.6	-9.2	-12.5	-15.7	-19.0	-22.2	-25.4	-28.7	-31.9	-35.2	-38.4
12	7.4	1.6	-618	-5.6	-12120	-38.7	-6.0	-7.5	-9.4	-13.3	-17.2	-21.0	-24.9	-28.8	-32.7	-36.5	-40.4	-44.3
13	7.2	1.6	-618	-5.3	-12120	-38.9	-5.7	-7.2	-9.2	-13.1	-17.0	-20.9	-24.8	-28.6	-32.5	-36.4	-40.3	-44.2
14	8.5	1.5	-618	-5.2	-12111	-29.5	-5.5	-6.6	-8.1	-11.1	-14.0	-17.0	-19.9	-22.9	-25.8	-28.8	-31.7	-34.7

Table S9: 11 in 4EK3, Experiment 1

Entry	ligand RMSD	BS RMSD	old_IFD Score	Glide Score	PE <sub>IFD</sub>	ΔPE	new_IFD Score _1	new_IFD Score _5	new_IFD Score _10	new_IFD Score _20	new_IFD Score _30	new_IFD Score _40	new_IFD Score _50	new_IFD Score _60	new_IFD Score _70	new_IFD Score _80	new_IFD Score _90	new_IFD Score _100
1	4.4	1.1	-621	-9.2	-12100	-15.4	-9.4	-10.0	-10.7	-12.3	-13.8	-15.4	-16.9	-18.4	-20.0	-21.5	-23.1	-24.6
2	4.0	1.1	-621	-8.8	-12104	-19.1	-9.0	-9.8	-10.7	-12.6	-14.5	-16.4	-18.3	-20.2	-22.2	-24.1	-26.0	-27.9
3	5.0	0.9	-621	-8.6	-12107	-21.9	-8.8	-9.7	-10.8	-13.0	-15.2	-17.4	-19.6	-21.8	-24.0	-26.2	-28.4	-30.6
4	5.1	0.9	-621	-9.0	-12107	-22.1	-9.2	-10.1	-11.2	-13.4	-15.6	-17.8	-20.0	-22.2	-24.4	-26.6	-28.8	-31.1
5	4.5	1.2	-621	-8.8	-12103	-18.2	-8.9	-9.7	-10.6	-12.4	-14.2	-16.0	-17.9	-19.7	-21.5	-23.3	-25.2	-27.0
6	5.9	1.2	-621	-8.2	-12109	-24.4	-8.5	-9.4	-10.7	-13.1	-15.5	-18.0	-20.4	-22.8	-25.3	-27.7	-30.2	-32.6
7	5.7	0.9	-621	-8.6	-12107	-22.3	-8.8	-9.7	-10.8	-13.0	-15.3	-17.5	-19.7	-22.0	-24.2	-26.4	-28.7	-30.9
8	4.4	1.3	-620	-8.4	-12094	-8.9	-8.5	-8.8	-9.3	-10.2	-11.0	-11.9	-12.8	-13.7	-14.6	-15.5	-16.4	-17.3
9	4.1	1.2	-620	-8.4	-12102	-17.2	-8.6	-9.3	-10.1	-11.9	-13.6	-15.3	-17.0	-18.8	-20.5	-22.2	-23.9	-25.7
10	4.5	1.2	-620	-7.6	-12101	-15.9	-7.8	-8.4	-9.2	-10.8	-12.4	-14.0	-15.6	-17.2	-18.8	-20.3	-21.9	-23.5
11	5.9	1.2	-620	-7.7	-12102	-17.0	-7.8	-8.5	-9.4	-11.1	-12.8	-14.5	-16.2	-17.9	-19.6	-21.3	-23.0	-24.7
12	4.5	1.1	-619	-7.3	-12102	-16.6	-7.5	-8.1	-8.9	-10.6	-12.3	-13.9	-15.6	-17.3	-18.9	-20.6	-22.3	-23.9
13	5.1	1.1	-619	-7.5	-12113	-27.9	-7.8	-8.9	-10.3	-13.1	-15.9	-18.7	-21.5	-24.3	-27.0	-29.8	-32.6	-35.4
14	7.1	1.4	-619	-7.9	-12095	-10.1	-8.0	-8.4	-8.9	-9.9	-10.9	-11.9	-12.9	-13.9	-14.9	-15.9	-16.9	-18.0
15	5.6	1.2	-618	-6.3	-12116	-31.4	-6.6	-7.9	-9.5	-12.6	-15.8	-18.9	-22.0	-25.2	-28.3	-31.5	-34.6	-37.8
16	5.4	1.0	-618	-6.7	-12105	-19.7	-6.9	-7.7	-8.7	-10.7	-12.7	-14.6	-16.6	-18.6	-20.5	-22.5	-24.5	-26.4
17	7.5	1.1	-618	-7.0	-12099	-13.6	-7.1	-7.7	-8.3	-9.7	-11.0	-12.4	-13.8	-15.1	-16.5	-17.8	-19.2	-20.5

Table S10: 11 in 4EK3, Experiment 2

Entry	ligand RMSD	BS RMSD	old_IFD Score	Glide Score	PE <sub>IFD</sub>	ΔPE	new_IFD Score <sub>_1</sub>	new_IFD Score <sub>_5</sub>	new_IFD Score <sub>_10</sub>	new_IFD Score <sub>_20</sub>	new_IFD Score <sub>_30</sub>	new_IFD Score <sub>_40</sub>	new_IFD Score <sub>_50</sub>	new_IFD Score <sub>_60</sub>	new_IFD Score <sub>_70</sub>	new_IFD Score <sub>_80</sub>	new_IFD Score <sub>_90</sub>	new_IFD Score <sub>_100</sub>
1	4.7	1.2	-621	-8.4	-12118	-36.5	-8.7	-10.2	-12.0	-15.7	-19.3	-23.0	-26.6	-30.3	-33.9	-37.6	-41.2	-44.9
2	5.2	1.3	-621	-8.4	-12122	-40.8	-8.9	-10.5	-12.5	-16.6	-20.7	-24.8	-28.9	-33.0	-37.0	-41.1	-45.2	-49.3
3	3.7	1.4	-620	-7.6	-12119	-37.9	-7.9	-9.5	-11.4	-15.1	-18.9	-22.7	-26.5	-30.3	-34.1	-37.9	-41.7	-45.5
4	4.0	1.2	-620	-7.8	-12121	-39.5	-8.2	-9.8	-11.8	-15.7	-19.7	-23.6	-27.5	-31.5	-35.4	-39.4	-43.3	-47.3
5	3.3	1.4	-620	-7.4	-12117	-35.3	-7.7	-9.2	-10.9	-14.4	-18.0	-21.5	-25.0	-28.6	-32.1	-35.6	-39.1	-42.7
6	4.1	1.1	-619	-7.8	-12120	-38.0	-8.2	-9.7	-11.6	-15.4	-19.2	-23.0	-26.8	-30.6	-34.4	-38.2	-42.0	-45.8
7	3.5	1.2	-619	-7.8	-12118	-36.5	-8.2	-9.7	-11.5	-15.1	-18.8	-22.4	-26.1	-29.7	-33.4	-37.0	-40.7	-44.3
8	5.1	1.2	-619	-7.6	-12115	-33.6	-7.9	-9.3	-11.0	-14.3	-17.7	-21.0	-24.4	-27.7	-31.1	-34.5	-37.8	-41.2
9	5.5	1.4	-619	-7.3	-12117	-35.1	-7.7	-9.1	-10.8	-14.3	-17.9	-21.4	-24.9	-28.4	-31.9	-35.4	-38.9	-42.4
10	5.5	1.3	-619	-7.6	-12116	-34.6	-8.0	-9.4	-11.1	-14.6	-18.0	-21.5	-25.0	-28.4	-31.9	-35.4	-38.8	-42.3
11	3.9	1.4	-619	-7.7	-12119	-37.2	-8.0	-9.5	-11.4	-15.1	-18.8	-22.5	-26.3	-30.0	-33.7	-37.4	-41.1	-44.8
12	5.3	1.2	-619	-7.6	-12114	-32.6	-7.9	-9.2	-10.8	-14.1	-17.3	-20.6	-23.9	-27.1	-30.4	-33.6	-36.9	-40.1
13	5.1	1.2	-619	-7.7	-12116	-34.4	-8.1	-9.4	-11.1	-14.6	-18.0	-21.5	-24.9	-28.3	-31.8	-35.2	-38.7	-42.1
14	4.7	1.4	-619	-7.4	-12112	-30.1	-7.7	-8.9	-10.4	-13.4	-16.4	-19.4	-22.4	-25.4	-28.4	-31.5	-34.5	-37.5
15	5.4	1.4	-619	-7.4	-12121	-39.5	-7.8	-9.3	-11.3	-15.3	-19.2	-23.2	-27.1	-31.1	-35.0	-39.0	-42.9	-46.9
16	4.6	1.4	-618	-7.3	-12118	-36.6	-7.7	-9.1	-10.9	-14.6	-18.3	-21.9	-25.6	-29.2	-32.9	-36.6	-40.2	-43.9
17	5.4	1.3	-618	-7.3	-12122	-40.4	-7.7	-9.3	-11.3	-15.3	-19.4	-23.4	-27.5	-31.5	-35.6	-39.6	-43.6	-47.7
18	4.6	1.4	-618	-6.6	-12115	-34.0	-6.9	-8.3	-10.0	-13.4	-16.7	-20.1	-23.5	-26.9	-30.3	-33.7	-37.1	-40.5
19	7.5	1.5	-617	-5.3	-12118	-36.5	-5.7	-7.1	-8.9	-12.6	-16.2	-19.9	-23.5	-27.2	-30.9	-34.5	-38.2	-41.8

Table S11: 11 in 4EK3, Experiment 3



Entry	ligand RMSD	BS RMSD	old_IFD Score	Glide Score	PE <sub>IFD</sub>	ΔPE	new_IFD Score <sub>_1</sub>	new_IFD Score <sub>_5</sub>	new_IFD Score <sub>_10</sub>	new_IFD Score <sub>_20</sub>	new_IFD Score <sub>_30</sub>	new_IFD Score <sub>_40</sub>	new_IFD Score <sub>_50</sub>	new_IFD Score <sub>_60</sub>	new_IFD Score <sub>_70</sub>	new_IFD Score <sub>_80</sub>	new_IFD Score <sub>_90</sub>	new_IFD Score <sub>_100</sub>
1	1.4	1.1	-622	-9.5	-12131	-49.5	-10.0	-12.0	-14.5	-19.4	-24.3	-29.3	-34.2	-39.2	-44.1	-49.1	-54.0	-59.0
2	5.4	1.3	-622	-8.9	-12126	-44.3	-9.4	-11.1	-13.3	-17.8	-22.2	-26.6	-31.1	-35.5	-39.9	-44.4	-48.8	-53.2
3	2.9	1.2	-621	-8.7	-12123	-41.0	-9.1	-10.7	-12.8	-16.9	-21.0	-25.1	-29.2	-33.3	-37.4	-41.5	-45.6	-49.7
4	4.0	1.5	-621	-8.1	-12129	-47.4	-8.6	-10.5	-12.8	-17.6	-22.3	-27.1	-31.8	-36.6	-41.3	-46.0	-50.8	-55.5
5	5.6	1.4	-621	-7.8	-12131	-49.0	-8.2	-10.2	-12.7	-17.6	-22.5	-27.4	-32.3	-37.2	-42.1	-47.0	-51.9	-56.8
6	4.3	1.4	-621	-7.7	-12133	-51.2	-8.2	-10.3	-12.8	-18.0	-23.1	-28.2	-33.3	-38.4	-43.5	-48.7	-53.8	-58.9
7	5.5	1.4	-621	-7.7	-12128	-46.0	-8.2	-10.0	-12.3	-16.9	-21.5	-26.1	-30.7	-35.3	-39.9	-44.5	-49.1	-53.7
8	4.0	1.4	-621	-7.5	-12127	-45.7	-8.0	-9.8	-12.1	-16.7	-21.2	-25.8	-30.4	-34.9	-39.5	-44.1	-48.6	-53.2
9	4.6	1.2	-621	-8.2	-12127	-45.7	-8.6	-10.4	-12.7	-17.3	-21.9	-26.4	-31.0	-35.6	-40.1	-44.7	-49.2	-53.8
10	3.5	1.2	-621	-7.7	-12125	-43.1	-8.1	-9.9	-12.0	-16.3	-20.7	-25.0	-29.3	-33.6	-37.9	-42.2	-46.5	-50.8
11	3.9	1.3	-620	-7.6	-12124	-42.6	-8.0	-9.7	-11.8	-16.1	-20.3	-24.6	-28.8	-33.1	-37.3	-41.6	-45.9	-50.1
12	5.4	1.5	-620	-7.7	-12122	-40.6	-8.1	-9.7	-11.8	-15.8	-19.9	-23.9	-28.0	-32.1	-36.1	-40.2	-44.2	-48.3
13	4.5	1.8	-620	-7.6	-12130	-49.0	-8.1	-10.1	-12.5	-17.4	-22.3	-27.2	-32.1	-37.0	-41.9	-46.8	-51.7	-56.6
14	5.5	1.1	-620	-6.7	-12131	-49.3	-7.2	-9.2	-11.7	-16.6	-21.5	-26.5	-31.4	-36.3	-41.2	-46.2	-51.1	-56.0
15	4.4	1.3	-619	-7.3	-12124	-42.8	-7.7	-9.4	-11.6	-15.9	-20.1	-24.4	-28.7	-33.0	-37.3	-41.6	-45.8	-50.1
16	5.5	1.4	-619	-6.1	-12124	-42.0	-6.5	-8.2	-10.3	-14.5	-18.7	-22.9	-27.1	-31.3	-35.5	-39.7	-43.9	-48.1
17	3.9	1.3	-619	-6.3	-12127	-45.8	-6.7	-8.5	-10.8	-15.4	-20.0	-24.6	-29.1	-33.7	-38.3	-42.9	-47.5	-52.0
18	6.0	1.7	-618	-5.8	-12124	-42.3	-6.2	-7.9	-10.1	-14.3	-18.5	-22.8	-27.0	-31.2	-35.5	-39.7	-43.9	-48.2
19	8.9	1.4	-618	-5.4	-12127	-45.7	-5.8	-7.7	-10.0	-14.5	-19.1	-23.7	-28.2	-32.8	-37.4	-41.9	-46.5	-51.1

Table S12: 11 in 4EK3, Experiment 4

Entry	ligand RMSD	BS RMSD	old_IFD Score	Glide Score	PE <sub>IFD</sub>	ΔPE	new_IFD Score _1	new_IFD Score _5	new_IFD Score _10	new_IFD Score _20	new_IFD Score _30	new_IFD Score _40	new_IFD Score _50	new_IFD Score _60	new_IFD Score _70	new_IFD Score _80	new_IFD Score _90	new_IFD Score _100
1	2.5	0.9	-623	-9.8	-12131	-45.7	-10.2	-12.0	-14.3	-18.9	-23.5	-28.0	-32.6	-37.2	-41.8	-46.3	-50.9	-55.5
2	4.3	1.1	-622	-8.9	-12132	-47.3	-9.3	-11.2	-13.6	-18.3	-23.0	-27.8	-32.5	-37.2	-42.0	-46.7	-51.4	-56.1
3	5.1	0.9	-621	-8.2	-12135	-50.2	-8.7	-10.7	-13.2	-18.3	-23.3	-28.3	-33.3	-38.4	-43.4	-48.4	-53.4	-58.4
4	4.3	0.9	-621	-8.6	-12117	-31.8	-8.9	-10.2	-11.8	-14.9	-18.1	-21.3	-24.5	-27.7	-30.9	-34.0	-37.2	-40.4
5	5.0	0.9	-621	-8.4	-12120	-34.8	-8.7	-10.1	-11.9	-15.3	-18.8	-22.3	-25.8	-29.3	-32.8	-36.3	-39.7	-43.2
6	4.5	1.1	-621	-7.9	-12129	-44.0	-8.3	-10.1	-12.3	-16.7	-21.1	-25.5	-29.9	-34.3	-38.7	-43.1	-47.5	-51.9
7	5.0	0.9	-621	-7.9	-12127	-42.4	-8.3	-10.0	-12.1	-16.4	-20.6	-24.9	-29.1	-33.4	-37.6	-41.8	-46.1	-50.3
8	5.7	1.2	-621	-7.7	-12130	-44.8	-8.1	-9.9	-12.2	-16.7	-21.1	-25.6	-30.1	-34.6	-39.1	-43.5	-48.0	-52.5
9	5.6	1.1	-621	-7.8	-12128	-43.0	-8.3	-10.0	-12.1	-16.4	-20.7	-25.0	-29.3	-33.6	-37.9	-42.2	-46.5	-50.8
10	3.1	0.9	-621	-8.0	-12127	-41.9	-8.5	-10.1	-12.2	-16.4	-20.6	-24.8	-29.0	-33.2	-37.4	-41.5	-45.7	-49.9
11	5.0	0.9	-621	-7.9	-12130	-45.5	-8.3	-10.2	-12.4	-17.0	-21.5	-26.1	-30.6	-35.2	-39.7	-44.3	-48.8	-53.4
12	5.2	1.1	-620	-7.9	-12139	-53.9	-8.5	-10.6	-13.3	-18.7	-24.1	-29.5	-34.9	-40.3	-45.6	-51.0	-56.4	-61.8
13	5.1	1.7	-620	-7.6	-12129	-44.2	-8.0	-9.8	-12.0	-16.4	-20.9	-25.3	-29.7	-34.1	-38.6	-43.0	-47.4	-51.8
14	4.7	1.1	-620	-7.4	-12128	-43.2	-7.8	-9.5	-11.7	-16.0	-20.3	-24.7	-29.0	-33.3	-37.6	-42.0	-46.3	-50.6
15	4.9	1.1	-619	-7.5	-12132	-47.0	-7.9	-9.8	-12.2	-16.9	-21.6	-26.3	-31.0	-35.6	-40.3	-45.0	-49.7	-54.4
16	4.4	1.3	-619	-6.8	-12129	-43.9	-7.2	-9.0	-11.1	-15.5	-19.9	-24.3	-28.7	-33.1	-37.5	-41.8	-46.2	-50.6
17	4.8	1.1	-619	-6.4	-12145	-60.5	-7.0	-9.4	-12.4	-18.5	-24.5	-30.6	-36.6	-42.7	-48.8	-54.8	-60.9	-66.9
18	7.5	1.3	-619	-6.6	-12133	-47.9	-7.1	-9.0	-11.4	-16.2	-21.0	-25.8	-30.6	-35.4	-40.2	-45.0	-49.8	-54.6
19	5.0	1.9	-618	-6.1	-12125	-40.0	-6.5	-8.1	-10.1	-14.1	-18.1	-22.1	-26.1	-30.1	-34.1	-38.1	-42.1	-46.1
20	8.6	1.3	-618	-5.9	-12130	-45.5	-6.4	-8.2	-10.5	-15.0	-19.6	-24.1	-28.7	-33.2	-37.8	-42.3	-46.8	-51.4

Table S13: 11 in 4EK3, Experiment 5

Entry	ligand RMSD	BS RMSD	old_IFD Score	Glide Score	PE <sub>IFD</sub>	ΔPE	new_IFD Score _1	new_IFD Score _5	new_IFD Score _10	new_IFD Score _20	new_IFD Score _30	new_IFD Score _40	new_IFD Score _50	new_IFD Score _60	new_IFD Score _70	new_IFD Score _80	new_IFD Score _90	new_IFD Score _100
1	4.4	0.9	-622	-9.1	-12127	-42.1	-9.5	-11.2	-13.3	-17.5	-21.7	-25.9	-30.1	-34.3	-38.5	-42.7	-46.9	-51.1
2	3.4	0.9	-622	-8.6	-12132	-46.6	-9.1	-11.0	-13.3	-17.9	-22.6	-27.3	-31.9	-36.6	-41.3	-45.9	-50.6	-55.3
3	6.0	1.2	-621	-7.8	-12139	-54.2	-8.3	-10.5	-13.2	-18.6	-24.0	-29.4	-34.8	-40.3	-45.7	-51.1	-56.5	-61.9
4	5.8	0.9	-621	-8.3	-12129	-44.0	-8.7	-10.5	-12.7	-17.1	-21.5	-25.9	-30.3	-34.7	-39.1	-43.5	-47.9	-52.3
5	4.6	1.1	-621	-8.3	-12126	-41.2	-8.8	-10.4	-12.5	-16.6	-20.7	-24.8	-29.0	-33.1	-37.2	-41.3	-45.5	-49.6
6	3.5	1.3	-621	-8.1	-12130	-45.1	-8.5	-10.3	-12.6	-17.1	-21.6	-26.1	-30.6	-35.1	-39.7	-44.2	-48.7	-53.2
7	6.0	1.2	-620	-7.3	-12134	-49.1	-7.8	-9.8	-12.2	-17.1	-22.0	-26.9	-31.9	-36.8	-41.7	-46.6	-51.5	-56.4
8	4.7	1.2	-620	-7.4	-12133	-47.7	-7.9	-9.8	-12.2	-17.0	-21.7	-26.5	-31.3	-36.0	-40.8	-45.6	-50.3	-55.1
9	3.7	1.3	-620	-7.6	-12128	-43.5	-8.1	-9.8	-12.0	-16.3	-20.7	-25.0	-29.4	-33.8	-38.1	-42.5	-46.8	-51.2
10	5.1	1.1	-620	-7.2	-12139	-54.2	-7.8	-10.0	-12.7	-18.1	-23.5	-28.9	-34.3	-39.7	-45.2	-50.6	-56.0	-61.4
11	5.7	0.9	-620	-6.7	-12137	-51.8	-7.3	-9.3	-11.9	-17.1	-22.3	-27.5	-32.7	-37.8	-43.0	-48.2	-53.4	-58.6
12	5.8	0.9	-620	-6.8	-12136	-50.6	-7.3	-9.4	-11.9	-16.9	-22.0	-27.1	-32.1	-37.2	-42.2	-47.3	-52.3	-57.4
13	5.9	0.9	-620	-6.7	-12134	-49.5	-7.2	-9.2	-11.6	-16.6	-21.5	-26.5	-31.4	-36.4	-41.3	-46.3	-51.2	-56.2
14	7.7	1.3	-619	-6.4	-12133	-47.8	-6.8	-8.7	-11.1	-15.9	-20.7	-25.5	-30.2	-35.0	-39.8	-44.6	-49.3	-54.1
15	7.0	0.9	-618	-5.9	-12129	-44.4	-6.4	-8.1	-10.4	-14.8	-19.2	-23.7	-28.1	-32.6	-37.0	-41.4	-45.9	-50.3
16	6.4	1.3	-618	-5.4	-12127	-42.4	-5.8	-7.5	-9.6	-13.8	-18.1	-22.3	-26.6	-30.8	-35.1	-39.3	-43.5	-47.8

Table S14: 11 in 4EK3, Experiment 6

Entry	ligand RMSD	BS RMSD	old_IFD Score	Glide Score	PE <sub>IFD</sub>	ΔPE	new_IFD Score <sub>_1</sub>	new_IFD Score <sub>_5</sub>	new_IFD Score <sub>_10</sub>	new_IFD Score <sub>_20</sub>	new_IFD Score <sub>_30</sub>	new_IFD Score <sub>_40</sub>	new_IFD Score <sub>_50</sub>	new_IFD Score <sub>_60</sub>	new_IFD Score <sub>_70</sub>	new_IFD Score <sub>_80</sub>	new_IFD Score <sub>_90</sub>	new_IFD Score <sub>_100</sub>
1	3.2	1.3	-621	-8.0	-12130	-48.5	-8.5	-10.4	-12.9	-17.7	-22.6	-27.4	-32.3	-37.1	-42.0	-46.8	-51.7	-56.5
2	5.6	1.5	-621	-8.0	-12125	-43.3	-8.4	-10.2	-12.3	-16.7	-21.0	-25.3	-29.6	-34.0	-38.3	-42.6	-46.9	-51.3
3	5.2	1.3	-620	-7.3	-12127	-45.3	-7.8	-9.6	-11.8	-16.4	-20.9	-25.4	-30.0	-34.5	-39.0	-43.6	-48.1	-52.6
4	5.4	1.2	-619	-6.4	-12129	-47.9	-6.9	-8.8	-11.2	-16.0	-20.8	-25.6	-30.4	-35.2	-40.0	-44.8	-49.6	-54.3
5	7.8	1.6	-619	-7.2	-12105	-23.7	-7.4	-8.4	-9.5	-11.9	-14.3	-16.7	-19.0	-21.4	-23.8	-26.1	-28.5	-30.9
6	6.4	1.1	-619	-6.9	-12127	-45.8	-7.3	-9.2	-11.5	-16.0	-20.6	-25.2	-29.8	-34.3	-38.9	-43.5	-48.1	-52.7
7	8.9	1.5	-619	-6.5	-12124	-42.1	-6.9	-8.6	-10.7	-14.9	-19.1	-23.4	-27.6	-31.8	-36.0	-40.2	-44.4	-48.6
8	8.8	1.5	-619	-6.9	-12124	-42.5	-7.3	-9.0	-11.1	-15.4	-19.6	-23.9	-28.1	-32.4	-36.6	-40.9	-45.1	-49.4
9	7.3	1.6	-619	-6.5	-12124	-42.1	-6.9	-8.6	-10.7	-14.9	-19.1	-23.3	-27.5	-31.7	-35.9	-40.1	-44.3	-48.5
10	7.6	1.6	-619	-6.3	-12122	-40.4	-6.7	-8.3	-10.3	-14.3	-18.4	-22.4	-26.4	-30.5	-34.5	-38.6	-42.6	-46.6
11	7.9	1.5	-619	-6.0	-12127	-45.2	-6.5	-8.3	-10.5	-15.0	-19.6	-24.1	-28.6	-33.1	-37.6	-42.2	-46.7	-51.2
12	8.8	1.5	-619	-6.4	-12120	-38.8	-6.8	-8.3	-10.3	-14.1	-18.0	-21.9	-25.8	-29.6	-33.5	-37.4	-41.3	-45.2
13	5.6	1.6	-618	-6.7	-12121	-39.5	-7.1	-8.7	-10.6	-14.6	-18.5	-22.5	-26.4	-30.4	-34.4	-38.3	-42.3	-46.2
14	8.8	1.6	-618	-6.0	-12117	-35.7	-6.4	-7.8	-9.6	-13.2	-16.7	-20.3	-23.9	-27.4	-31.0	-34.6	-38.1	-41.7
15	8.4	1.8	-618	-6.1	-12128	-46.0	-6.6	-8.4	-10.7	-15.3	-19.9	-24.5	-29.1	-33.7	-38.3	-42.9	-47.5	-52.1
16	8.5	1.5	-618	-5.6	-12118	-36.6	-5.9	-7.4	-9.2	-12.9	-16.6	-20.2	-23.9	-27.6	-31.2	-34.9	-38.5	-42.2
17	8.9	1.5	-618	-6.1	-12114	-32.3	-6.5	-7.8	-9.4	-12.6	-15.8	-19.1	-22.3	-25.5	-28.7	-32.0	-35.2	-38.4
18	7.2	1.5	-617	-5.4	-12103	-21.5	-5.6	-6.5	-7.6	-9.7	-11.9	-14.0	-16.2	-18.3	-20.5	-22.6	-24.8	-26.9

Table S15: 11 in 4EK3, Experiment 7

Entry	ligand RMSD	BS RMSD	old_IFD Score	Glide Score	PE <sub>IFD</sub>	ΔPE	new_IFD Score _1	new_IFD Score _5	new_IFD Score _10	new_IFD Score _20	new_IFD Score _30	new_IFD Score _40	new_IFD Score _50	new_IFD Score _60	new_IFD Score _70	new_IFD Score _80	new_IFD Score _90	new_IFD Score _100
1	4.2	1.1	-623	-9.3	-12132	-46.9	-9.8	-11.7	-14.0	-18.7	-23.4	-28.1	-32.8	-37.5	-42.2	-46.9	-51.6	-56.3
2	3.2	0.9	-622	-9.1	-12134	-49.4	-9.6	-11.6	-14.1	-19.0	-23.9	-28.9	-33.8	-38.8	-43.7	-48.6	-53.6	-58.5
3	2.5	0.9	-622	-9.5	-12130	-45.4	-10.0	-11.8	-14.0	-18.6	-23.1	-27.6	-32.2	-36.7	-41.3	-45.8	-50.3	-54.9
4	4.9	0.9	-622	-8.6	-12132	-46.8	-9.0	-10.9	-13.3	-17.9	-22.6	-27.3	-32.0	-36.6	-41.3	-46.0	-50.7	-55.3
5	4.4	0.8	-622	-8.7	-12123	-37.8	-9.0	-10.6	-12.4	-16.2	-20.0	-23.8	-27.6	-31.4	-35.1	-38.9	-42.7	-46.5
6	5.3	0.9	-621	-8.3	-12126	-41.3	-8.7	-10.3	-12.4	-16.5	-20.6	-24.8	-28.9	-33.0	-37.2	-41.3	-45.4	-49.5
7	5.8	1.2	-621	-8.1	-12124	-38.6	-8.5	-10.0	-12.0	-15.8	-19.7	-23.6	-27.4	-31.3	-35.1	-39.0	-42.9	-46.7
8	4.4	1.1	-621	-8.3	-12121	-36.3	-8.6	-10.1	-11.9	-15.5	-19.2	-22.8	-26.4	-30.1	-33.7	-37.3	-41.0	-44.6
9	4.5	1.2	-621	-7.8	-12125	-39.7	-8.2	-9.8	-11.8	-15.8	-19.7	-23.7	-27.7	-31.7	-35.6	-39.6	-43.6	-47.6
10	5.8	1.2	-621	-7.7	-12124	-39.3	-8.1	-9.7	-11.6	-15.6	-19.5	-23.4	-27.4	-31.3	-35.2	-39.2	-43.1	-47.0
11	5.0	0.9	-620	-7.5	-12130	-44.8	-8.0	-9.8	-12.0	-16.5	-20.9	-25.4	-29.9	-34.4	-38.8	-43.3	-47.8	-52.3
12	4.6	1.1	-620	-7.2	-12123	-37.9	-7.5	-9.1	-10.9	-14.7	-18.5	-22.3	-26.1	-29.9	-33.7	-37.5	-41.3	-45.1
13	5.0	1.7	-620	-7.4	-12130	-45.1	-7.8	-9.6	-11.9	-16.4	-20.9	-25.4	-29.9	-34.4	-38.9	-43.5	-48.0	-52.5
14	5.2	1.1	-620	-7.8	-12131	-45.9	-8.2	-10.0	-12.3	-16.9	-21.5	-26.1	-30.7	-35.3	-39.9	-44.5	-49.1	-53.7
15	5.0	1.1	-619	-7.4	-12126	-41.4	-7.8	-9.4	-11.5	-15.6	-19.8	-23.9	-28.1	-32.2	-36.4	-40.5	-44.6	-48.8
16	4.3	1.3	-619	-6.4	-12131	-45.7	-6.9	-8.7	-11.0	-15.6	-20.1	-24.7	-29.3	-33.9	-38.4	-43.0	-47.6	-52.1
17	4.8	1.1	-619	-6.4	-12132	-46.9	-6.9	-8.8	-11.1	-15.8	-20.5	-25.2	-29.9	-34.6	-39.2	-43.9	-48.6	-53.3
18	8.1	1.8	-618	-6.0	-12123	-37.7	-6.4	-7.9	-9.8	-13.5	-17.3	-21.1	-24.9	-28.6	-32.4	-36.2	-40.0	-43.7
19	8.8	1.3	-618	-5.8	-12130	-45.1	-6.3	-8.1	-10.4	-14.9	-19.4	-23.9	-28.4	-32.9	-37.4	-42.0	-46.5	-51.0

Table S16: 11 in 4EK3, Experiment 8

## Ligand 12 in 4EK3

Entry	ligand RMSD	BS RMSD	old_IFD Score	Glide Score	PE <sub>IFD</sub>	ΔPE	new_IFD Score _1	new_IFD Score _5	new_IFD Score _10	new_IFD Score _20	new_IFD Score _30	new_IFD Score _40	new_IFD Score _50	new_IFD Score _60	new_IFD Score _70	new_IFD Score _80	new_IFD Score _90	new_IFD Score _100
1	2.1	1.2	-617	-10.0	-12099	-17.8	-10.2	-10.9	-11.8	-13.6	-15.4	-17.2	-18.9	-20.7	-22.5	-24.3	-26.0	-27.8
2	2.0	1.6	-616	-9.0	-12109	-27.2	-9.3	-10.4	-11.8	-14.5	-17.2	-19.9	-22.6	-25.3	-28.1	-30.8	-33.5	-36.2
3	5.6	1.4	-616	-8.8	-12125	-43.2	-9.2	-11.0	-13.1	-17.4	-21.8	-26.1	-30.4	-34.7	-39.0	-43.4	-47.7	-52.0
4	6.3	1.7	-616	-8.5	-12129	-47.9	-9.0	-10.9	-13.3	-18.1	-22.9	-27.7	-32.4	-37.2	-42.0	-46.8	-51.6	-56.4
5	6.4	1.7	-616	-8.4	-12132	-50.2	-8.9	-10.9	-13.4	-18.4	-23.5	-28.5	-33.5	-38.5	-43.5	-48.6	-53.6	-58.6
6	6.3	1.7	-616	-7.8	-12129	-47.7	-8.3	-10.2	-12.6	-17.4	-22.1	-26.9	-31.7	-36.4	-41.2	-46.0	-50.7	-55.5
7	2.1	1.6	-616	-8.1	-12125	-43.4	-8.5	-10.3	-12.4	-16.8	-21.1	-25.5	-29.8	-34.1	-38.5	-42.8	-47.2	-51.5
8	5.7	1.7	-616	-8.6	-12111	-29.7	-8.9	-10.1	-11.6	-14.5	-17.5	-20.5	-23.5	-26.4	-29.4	-32.4	-35.3	-38.3
9	5.8	1.6	-615	-8.0	-12102	-20.1	-8.2	-9.1	-10.1	-12.1	-14.1	-16.1	-18.1	-20.1	-22.1	-24.1	-26.1	-28.1
10	1.9	1.3	-615	-7.9	-12125	-43.2	-8.4	-10.1	-12.3	-16.6	-20.9	-25.2	-29.6	-33.9	-38.2	-42.5	-46.8	-51.2
11	6.3	1.7	-615	-7.8	-12120	-38.7	-8.2	-9.7	-11.7	-15.5	-19.4	-23.3	-27.1	-31.0	-34.9	-38.7	-42.6	-46.5
12	5.6	1.6	-615	-7.2	-12128	-46.8	-7.7	-9.6	-11.9	-16.6	-21.3	-25.9	-30.6	-35.3	-40.0	-44.6	-49.3	-54.0
13	9.4	1.6	-614	-7.4	-12110	-28.1	-7.7	-8.8	-10.2	-13.0	-15.8	-18.6	-21.5	-24.3	-27.1	-29.9	-32.7	-35.5
14	5.5	1.9	-614	-6.8	-12114	-32.5	-7.2	-8.5	-10.1	-13.3	-16.6	-19.9	-23.1	-26.4	-29.6	-32.9	-36.1	-39.4
15	6.7	1.6	-613	-6.2	-12117	-35.6	-6.5	-8.0	-9.8	-13.3	-16.9	-20.4	-24.0	-27.6	-31.1	-34.7	-38.2	-41.8

Table S17: 12 in 4EK3, Experiment 1

Entry	ligand RMSD	BS RMSD	old_IFD Score	Glide Score	PE <sub>IFD</sub>	ΔPE	new_IFD Score _1	new_IFD Score _5	new_IFD Score _10	new_IFD Score _20	new_IFD Score _30	new_IFD Score _40	new_IFD Score _50	new_IFD Score _60	new_IFD Score _70	new_IFD Score _80	new_IFD Score _90	new_IFD Score _100
1	4.8	1.0	-619	-10.7	-12115	-30.0	-11.0	-12.2	-13.7	-16.7	-19.7	-22.7	-25.7	-28.7	-31.7	-34.7	-37.7	-40.7
2	2.2	1.1	-619	-10.0	-12132	-46.6	-10.4	-12.3	-14.6	-19.3	-24.0	-28.6	-33.3	-37.9	-42.6	-47.3	-51.9	-56.6
3	5.9	1.1	-617	-8.9	-12120	-34.8	-9.3	-10.7	-12.4	-15.9	-19.4	-22.8	-26.3	-29.8	-33.3	-36.8	-40.3	-43.7
4	5.5	1.4	-616	-8.7	-12127	-41.9	-9.1	-10.7	-12.8	-17.0	-21.2	-25.4	-29.6	-33.8	-38.0	-42.2	-46.4	-50.6
5	2.2	1.4	-616	-8.1	-12133	-48.3	-8.6	-10.5	-12.9	-17.8	-22.6	-27.4	-32.3	-37.1	-41.9	-46.8	-51.6	-56.4
6	4.8	1.3	-615	-7.9	-12122	-37.5	-8.3	-9.8	-11.6	-15.4	-19.1	-22.9	-26.6	-30.4	-34.1	-37.9	-41.6	-45.4
7	8.8	1.3	-612	-4.2	-12127	-41.7	-4.6	-6.3	-8.4	-12.5	-16.7	-20.9	-25.1	-29.2	-33.4	-37.6	-41.8	-45.9

Table S18: 12 in 4EK3, Experiment 2

Entry	ligand RMSD	BS RMSD	old_IFD Score	Glide Score	PE <sub>IFD</sub>	$\Delta$ PE	new_IFD Score <sub>_1</sub>	new_IFD Score <sub>_5</sub>	new_IFD Score <sub>_10</sub>	new_IFD Score <sub>_20</sub>	new_IFD Score <sub>_30</sub>	new_IFD Score <sub>_40</sub>	new_IFD Score <sub>_50</sub>	new_IFD Score <sub>_60</sub>	new_IFD Score <sub>_70</sub>	new_IFD Score <sub>_80</sub>	new_IFD Score <sub>_90</sub>	new_IFD Score <sub>_100</sub>
1	2.1	1.4	-617	-9.0	-12132	-50.2	-9.5	-11.5	-14.0	-19.0	-24.0	-29.1	-34.1	-39.1	-44.1	-49.2	-54.2	-59.2
2	5.7	1.6	-617	-8.9	-12132	-50.4	-9.4	-11.5	-14.0	-19.0	-24.1	-29.1	-34.1	-39.2	-44.2	-49.3	-54.3	-59.3
3	5.7	1.4	-616	-8.7	-12125	-43.8	-9.2	-10.9	-13.1	-17.5	-21.9	-26.2	-30.6	-35.0	-39.4	-43.7	-48.1	-52.5
4	5.8	1.6	-616	-8.1	-12134	-52.7	-8.6	-10.7	-13.3	-18.6	-23.9	-29.2	-34.4	-39.7	-45.0	-50.2	-55.5	-60.8
5	5.7	1.6	-616	-8.1	-12134	-52.5	-8.6	-10.7	-13.3	-18.6	-23.8	-29.1	-34.3	-39.6	-44.8	-50.1	-55.3	-60.6
6	6.3	1.7	-615	-8.1	-12121	-39.6	-8.5	-10.1	-12.1	-16.1	-20.0	-24.0	-28.0	-31.9	-35.9	-39.8	-43.8	-47.8
7	4.7	1.8	-615	-7.8	-12129	-47.3	-8.3	-10.2	-12.5	-17.3	-22.0	-26.7	-31.5	-36.2	-40.9	-45.6	-50.4	-55.1
8	5.8	1.8	-615	-6.9	-12132	-50.4	-7.4	-9.4	-12.0	-17.0	-22.0	-27.1	-32.1	-37.2	-42.2	-47.2	-52.3	-57.3
9	6.4	1.8	-614	-6.7	-12121	-39.7	-7.1	-8.7	-10.7	-14.7	-18.7	-22.6	-26.6	-30.6	-34.6	-38.5	-42.5	-46.5
10	5.7	1.6	-614	-6.7	-12130	-48.5	-7.2	-9.2	-11.6	-16.4	-21.3	-26.1	-31.0	-35.9	-40.7	-45.6	-50.4	-55.3
11	5.6	1.8	-614	-6.7	-12114	-32.4	-7.0	-8.3	-9.9	-13.2	-16.4	-19.6	-22.9	-26.1	-29.4	-32.6	-35.9	-39.1
12	5.8	1.8	-613	-5.9	-12128	-46.6	-6.3	-8.2	-10.5	-15.2	-19.9	-24.5	-29.2	-33.8	-38.5	-43.2	-47.8	-52.5
13	6.7	1.6	-613	-5.9	-12131	-49.4	-6.4	-8.4	-10.8	-15.8	-20.7	-25.7	-30.6	-35.5	-40.5	-45.4	-50.4	-55.3

Table S19: 12 in 4EK3, Experiment 3



Entry	ligand RMSD	BS RMSD	old_IFD Score	Glide Score	PE <sub>IFD</sub>	ΔPE	new_IFD Score <sub>_1</sub>	new_IFD Score <sub>_5</sub>	new_IFD Score <sub>_10</sub>	new_IFD Score <sub>_20</sub>	new_IFD Score <sub>_30</sub>	new_IFD Score <sub>_40</sub>	new_IFD Score <sub>_50</sub>	new_IFD Score <sub>_60</sub>	new_IFD Score <sub>_70</sub>	new_IFD Score <sub>_80</sub>	new_IFD Score <sub>_90</sub>	new_IFD Score <sub>_100</sub>
1	5.7	1.6	-617	-9.0	-12125	-44.0	-9.4	-11.2	-13.4	-17.8	-22.2	-26.6	-31.0	-35.4	-39.8	-44.2	-48.6	-53.0
2	5.8	1.4	-617	-8.9	-12123	-41.7	-9.3	-11.0	-13.1	-17.3	-21.4	-25.6	-29.8	-34.0	-38.1	-42.3	-46.5	-50.7
3	2.3	1.4	-617	-8.3	-12133	-51.1	-8.9	-10.9	-13.5	-18.6	-23.7	-28.8	-33.9	-39.0	-44.1	-49.2	-54.3	-59.4
4	6.3	1.7	-616	-7.7	-12141	-59.2	-8.3	-10.7	-13.6	-19.5	-25.5	-31.4	-37.3	-43.2	-49.1	-55.1	-61.0	-66.9
5	5.7	1.3	-615	-8.4	-12114	-32.6	-8.7	-10.0	-11.6	-14.9	-18.2	-21.4	-24.7	-27.9	-31.2	-34.4	-37.7	-41.0
6	5.7	1.6	-615	-8.3	-12115	-33.7	-8.6	-9.9	-11.6	-15.0	-18.4	-21.7	-25.1	-28.5	-31.8	-35.2	-38.6	-41.9
7	6.5	1.7	-615	-7.1	-12133	-51.9	-7.6	-9.7	-12.3	-17.5	-22.7	-27.9	-33.1	-38.2	-43.4	-48.6	-53.8	-59.0
8	5.3	2.0	-615	-7.8	-12127	-45.3	-8.2	-10.0	-12.3	-16.8	-21.4	-25.9	-30.4	-34.9	-39.5	-44.0	-48.5	-53.0
9	4.8	1.5	-615	-6.3	-12133	-51.9	-6.8	-8.9	-11.5	-16.7	-21.9	-27.1	-32.3	-37.5	-42.7	-47.9	-53.1	-58.3
10	5.8	1.8	-615	-7.3	-12125	-43.2	-7.7	-9.4	-11.6	-15.9	-20.2	-24.6	-28.9	-33.2	-37.5	-41.8	-46.2	-50.5
11	5.7	1.6	-615	-7.4	-12124	-42.1	-7.8	-9.5	-11.6	-15.8	-20.0	-24.2	-28.5	-32.7	-36.9	-41.1	-45.3	-49.5
12	4.5	1.3	-614	-6.9	-12116	-34.9	-7.2	-8.6	-10.4	-13.8	-17.3	-20.8	-24.3	-27.8	-31.3	-34.8	-38.2	-41.7
13	5.8	1.8	-613	-6.4	-12128	-46.7	-6.8	-8.7	-11.0	-15.7	-20.4	-25.0	-29.7	-34.4	-39.0	-43.7	-48.4	-53.0

Table S20: 12 in 4EK3, Experiment 4

Entry	ligand RMSD	BS RMSD	old_IFD Score	Glide Score	PE <sub>IFD</sub>	ΔPE	new_IFD Score _1	new_IFD Score _5	new_IFD Score _10	new_IFD Score _20	new_IFD Score _30	new_IFD Score _40	new_IFD Score _50	new_IFD Score _60	new_IFD Score _70	new_IFD Score _80	new_IFD Score _90	new_IFD Score _100
1	2.1	1.1	-618	-9.8	-12132	-46.6	-10.3	-12.1	-14.5	-19.1	-23.8	-28.4	-33.1	-37.8	-42.4	-47.1	-51.7	-56.4
2	2.4	1.1	-617	-9.5	-12118	-32.9	-9.8	-11.1	-12.7	-16.0	-19.3	-22.6	-25.9	-29.2	-32.5	-35.8	-39.0	-42.3
3	2.3	1.5	-617	-8.8	-12120	-35.0	-9.2	-10.6	-12.3	-15.8	-19.3	-22.8	-26.3	-29.8	-33.3	-36.8	-40.3	-43.8
4	5.5	1.5	-617	-8.7	-12130	-45.3	-9.2	-11.0	-13.3	-17.8	-22.3	-26.8	-31.4	-35.9	-40.4	-44.9	-49.5	-54.0
5	5.5	1.5	-616	-8.6	-12129	-44.2	-9.0	-10.8	-13.0	-17.4	-21.8	-26.2	-30.7	-35.1	-39.5	-43.9	-48.3	-52.8
6	6.6	1.4	-616	-7.8	-12143	-58.0	-8.4	-10.7	-13.6	-19.4	-25.2	-31.0	-36.8	-42.6	-48.4	-54.2	-60.0	-65.8
7	5.5	1.9	-615	-8.0	-12126	-41.2	-8.4	-10.1	-12.1	-16.3	-20.4	-24.5	-28.6	-32.8	-36.9	-41.0	-45.1	-49.3
8	5.9	1.2	-615	-7.6	-12127	-41.6	-8.0	-9.7	-11.8	-15.9	-20.1	-24.2	-28.4	-32.5	-36.7	-40.9	-45.0	-49.2
9	6.5	1.4	-614	-7.5	-12108	-22.9	-7.7	-8.6	-9.8	-12.1	-14.4	-16.7	-19.0	-21.2	-23.5	-25.8	-28.1	-30.4
10	2.8	1.3	-614	-6.6	-12131	-45.7	-7.1	-8.9	-11.2	-15.8	-20.4	-24.9	-29.5	-34.1	-38.6	-43.2	-47.8	-52.4
11	6.0	1.4	-613	-5.2	-12128	-43.2	-5.6	-7.3	-9.5	-13.8	-18.2	-22.5	-26.8	-31.1	-35.4	-39.8	-44.1	-48.4

Table S21: 12 in 4EK3, Experiment 5

Entry	ligand RMSD	BS RMSD	old_IFD Score	Glide Score	PE <sub>IFD</sub>	ΔPE	new_IFD Score _1	new_IFD Score _5	new_IFD Score _10	new_IFD Score _20	new_IFD Score _30	new_IFD Score _40	new_IFD Score _50	new_IFD Score _60	new_IFD Score _70	new_IFD Score _80	new_IFD Score _90	new_IFD Score _100
1	1.6	1.1	-618	-10.7	-12120	-35.2	-11.1	-12.5	-14.2	-17.7	-21.3	-24.8	-28.3	-31.8	-35.3	-38.8	-42.4	-45.9
2	2.0	1.1	-618	-10.1	-12119	-33.7	-10.4	-11.8	-13.5	-16.8	-20.2	-23.6	-26.9	-30.3	-33.7	-37.1	-40.4	-43.8
3	5.5	1.5	-616	-8.9	-12125	-40.1	-9.3	-10.9	-12.9	-16.9	-20.9	-24.9	-28.9	-33.0	-37.0	-41.0	-45.0	-49.0
4	2.4	1.2	-616	-9.2	-12116	-31.2	-9.5	-10.7	-12.3	-15.4	-18.5	-21.6	-24.8	-27.9	-31.0	-34.1	-37.2	-40.3
5	5.5	1.3	-616	-8.8	-12132	-46.8	-9.3	-11.2	-13.5	-18.2	-22.9	-27.5	-32.2	-36.9	-41.6	-46.3	-50.9	-55.6
6	6.0	1.2	-615	-8.4	-12115	-30.4	-8.7	-9.9	-11.4	-14.5	-17.5	-20.5	-23.6	-26.6	-29.7	-32.7	-35.8	-38.8
7	3.3	1.2	-615	-8.4	-12124	-39.0	-8.8	-10.3	-12.3	-16.2	-20.1	-24.0	-27.9	-31.8	-35.7	-39.6	-43.5	-47.4
8	5.7	1.2	-614	-7.6	-12115	-29.9	-7.9	-9.1	-10.6	-13.6	-16.6	-19.6	-22.6	-25.6	-28.6	-31.6	-34.6	-37.6
9	5.8	1.2	-614	-6.9	-12117	-32.4	-7.2	-8.5	-10.1	-13.4	-16.6	-19.9	-23.1	-26.3	-29.6	-32.8	-36.1	-39.3
10	5.8	1.5	-613	-6.7	-12116	-31.4	-7.0	-8.2	-9.8	-13.0	-16.1	-19.2	-22.4	-25.5	-28.7	-31.8	-34.9	-38.1
11	7.0	1.1	-612	-5.5	-12118	-33.4	-5.8	-7.2	-8.8	-12.2	-15.5	-18.9	-22.2	-25.5	-28.9	-32.2	-35.6	-38.9

Table S22: 12 in 4EK3, Experiment 6

Entry	ligand RMSD	BS RMSD	old_IFD Score	Glide Score	PE <sub>IFD</sub>	ΔPE	new_IFD Score <sub>_1</sub>	new_IFD Score <sub>_5</sub>	new_IFD Score <sub>_10</sub>	new_IFD Score <sub>_20</sub>	new_IFD Score <sub>_30</sub>	new_IFD Score <sub>_40</sub>	new_IFD Score <sub>_50</sub>	new_IFD Score <sub>_60</sub>	new_IFD Score <sub>_70</sub>	new_IFD Score <sub>_80</sub>	new_IFD Score <sub>_90</sub>	new_IFD Score <sub>_100</sub>
1	2.1	1.4	-618	-9.5	-12133	-51.3	-10.1	-12.1	-14.7	-19.8	-24.9	-30.1	-35.2	-40.3	-45.4	-50.6	-55.7	-60.8
2	1.9	1.2	-618	-10.1	-12114	-32.5	-10.4	-11.7	-13.3	-16.6	-19.8	-23.1	-26.3	-29.6	-32.9	-36.1	-39.4	-42.6
3	2.1	1.3	-617	-9.5	-12112	-30.5	-9.8	-11.0	-12.5	-15.6	-18.6	-21.7	-24.7	-27.8	-30.8	-33.9	-36.9	-40.0
4	2.1	1.3	-617	-9.4	-12114	-32.5	-9.7	-11.0	-12.7	-15.9	-19.2	-22.4	-25.7	-28.9	-32.2	-35.4	-38.7	-41.9
5	6.4	1.6	-615	-7.5	-12121	-39.2	-7.9	-9.5	-11.4	-15.4	-19.3	-23.2	-27.1	-31.0	-34.9	-38.9	-42.8	-46.7
6	5.7	1.9	-614	-7.0	-12126	-44.2	-7.4	-9.2	-11.4	-15.8	-20.3	-24.7	-29.1	-33.5	-37.9	-42.3	-46.8	-51.2
7	8.1	1.7	-611	-3.5	-12133	-51.1	-4.0	-6.0	-8.6	-13.7	-18.8	-23.9	-29.0	-34.1	-39.2	-44.3	-49.4	-54.5

Table S23: 12 in 4EK3, Experiment 7

Entry	ligand RMSD	BS RMSD	old_IFD Score	Glide Score	PE <sub>IFD</sub>	$\Delta$ PE	new_IFD Score _1	new_IFD Score _5	new_IFD Score _10	new_IFD Score _20	new_IFD Score _30	new_IFD Score _40	new_IFD Score _50	new_IFD Score _60	new_IFD Score _70	new_IFD Score _80	new_IFD Score _90	new_IFD Score _100
1	2.2	1.1	-617	-9.9	-12115	-29.6	-10.2	-11.4	-12.8	-15.8	-18.8	-21.7	-24.7	-27.7	-30.6	-33.6	-36.6	-39.5
2	2.5	1.1	-617	-8.8	-12131	-45.6	-9.2	-11.0	-13.3	-17.9	-22.4	-27.0	-31.6	-36.1	-40.7	-45.2	-49.8	-54.4
3	5.6	1.5	-616	-8.5	-12134	-49.3	-9.0	-11.0	-13.4	-18.4	-23.3	-28.2	-33.1	-38.1	-43.0	-47.9	-52.8	-57.8
4	4.0	1.1	-616	-8.0	-12129	-43.7	-8.5	-10.2	-12.4	-16.8	-21.1	-25.5	-29.9	-34.3	-38.6	-43.0	-47.4	-51.8
5	5.9	1.1	-616	-8.6	-12121	-35.9	-8.9	-10.4	-12.2	-15.7	-19.3	-22.9	-26.5	-30.1	-33.7	-37.3	-40.9	-44.5
6	6.6	1.4	-616	-7.8	-12142	-56.8	-8.3	-10.6	-13.4	-19.1	-24.8	-30.5	-36.2	-41.8	-47.5	-53.2	-58.9	-64.6
7	5.8	1.1	-616	-8.4	-12121	-36.0	-8.8	-10.2	-12.0	-15.6	-19.2	-22.8	-26.4	-30.0	-33.6	-37.2	-40.8	-44.4
8	2.4	1.1	-615	-7.9	-12130	-44.6	-8.4	-10.2	-12.4	-16.8	-21.3	-25.8	-30.2	-34.7	-39.1	-43.6	-48.0	-52.5
9	6.6	1.5	-614	-7.4	-12115	-30.2	-7.7	-8.9	-10.4	-13.4	-16.4	-19.4	-22.4	-25.5	-28.5	-31.5	-34.5	-37.5
10	6.1	1.3	-614	-6.9	-12122	-36.6	-7.2	-8.7	-10.5	-14.2	-17.8	-21.5	-25.2	-28.8	-32.5	-36.1	-39.8	-43.4
11	5.8	1.5	-614	-6.8	-12128	-43.1	-7.2	-9.0	-11.1	-15.4	-19.7	-24.0	-28.4	-32.7	-37.0	-41.3	-45.6	-49.9
12	5.8	1.5	-613	-6.3	-12129	-43.8	-6.8	-8.5	-10.7	-15.1	-19.5	-23.9	-28.2	-32.6	-37.0	-41.4	-45.8	-50.1

Table S24: 12 in 4EK3, Experiment 8

Ligand **14** in 4NCKH

Entry	ligand RMSD	BS RMSD	old_IFD Score	Glide Score	PE <sub>IFD</sub>	ΔPE	new_IFD Score _1	new_IFD Score _5	new_IFD Score _10	new_IFD Score _20	new_IFD Score _30	new_IFD Score _40	new_IFD Score _50	new_IFD Score _60	new_IFD Score _70	new_IFD Score _80	new_IFD Score _90	new_IFD Score _100
1	9.0	2.3	-983	-9.9	-19206	26.3	-9.7	-8.6	-7.3	-4.7	-2.0	0.6	3.2	5.8	8.5	11.1	13.7	16.3
2	9.7	2.8	-983	-9.2	-19216	16.0	-9.0	-8.4	-7.6	-6.0	-4.4	-2.8	-1.2	0.4	2.0	3.6	5.2	6.8
3	9.7	2.0	-983	-9.0	-19227	5.7	-8.9	-8.7	-8.4	-7.8	-7.2	-6.7	-6.1	-5.5	-4.9	-4.4	-3.8	-3.2
4	9.3	2.1	-983	-9.4	-19224	8.6	-9.3	-9.0	-8.5	-7.7	-6.8	-6.0	-5.1	-4.2	-3.4	-2.5	-1.7	-0.8
5	8.8	2.4	-983	-9.7	-19203	29.4	-9.4	-8.2	-6.7	-3.8	-0.8	2.1	5.1	8.0	10.9	13.9	16.8	19.8
6	8.6	2.3	-982	-9.2	-19210	22.7	-8.9	-8.0	-6.9	-4.6	-2.4	-0.1	2.2	4.5	6.7	9.0	11.3	13.5
7	10.0	2.6	-982	-8.3	-19224	8.4	-8.2	-7.8	-7.4	-6.6	-5.7	-4.9	-4.0	-3.2	-2.4	-1.5	-0.7	0.2
8	8.9	2.3	-982	-8.9	-19212	20.8	-8.7	-7.9	-6.8	-4.7	-2.6	-0.6	1.5	3.6	5.7	7.8	9.9	11.9
9	9.2	2.4	-982	-9.3	-19198	34.5	-9.0	-7.6	-5.9	-2.4	1.0	4.5	7.9	11.4	14.8	18.3	21.7	25.2
10	9.0	2.5	-982	-9.3	-19200	32.4	-9.0	-7.7	-6.1	-2.9	0.4	3.6	6.9	10.1	13.4	16.6	19.9	23.1
11	8.9	2.2	-982	-8.6	-19214	18.4	-8.4	-7.7	-6.8	-4.9	-3.1	-1.3	0.6	2.4	4.2	6.1	7.9	9.7
12	8.9	2.4	-981	-8.8	-19201	31.0	-8.5	-7.3	-5.7	-2.6	0.5	3.6	6.7	9.8	12.9	16.0	19.1	22.1
13	8.9	2.4	-981	-8.1	-19222	10.3	-8.0	-7.5	-7.0	-6.0	-5.0	-3.9	-2.9	-1.9	-0.8	0.2	1.2	2.3
14	10.9	2.1	-981	-8.3	-19206	26.3	-8.0	-7.0	-5.7	-3.0	-0.4	2.2	4.9	7.5	10.1	12.8	15.4	18.0

Table S25: **14** in 4NCKH, Experiment 1

Entry	ligand RMSD	BS RMSD	old_IFD Score	Glide Score	PE <sub>IFD</sub>	ΔPE	new_IFD Score _1	new_IFD Score _5	new_IFD Score _10	new_IFD Score _20	new_IFD Score _30	new_IFD Score _40	new_IFD Score _50	new_IFD Score _60	new_IFD Score _70	new_IFD Score _80	new_IFD Score _90	new_IFD Score _100
1	2.4	1.0	-985	-8.7	-19282	-50.0	-9.2	-11.2	-13.7	-18.7	-23.7	-28.7	-33.7	-38.7	-43.7	-48.7	-53.7	-58.7
2	2.7	0.9	-985	-8.8	-19283	-50.4	-9.3	-11.3	-13.8	-18.9	-23.9	-29.0	-34.0	-39.0	-44.1	-49.1	-54.1	-59.2
3	6.7	0.9	-984	-7.4	-19262	-29.2	-7.7	-8.9	-10.3	-13.2	-16.2	-19.1	-22.0	-24.9	-27.8	-30.7	-33.7	-36.6
4	6.9	0.9	-984	-7.1	-19265	-33.0	-7.5	-8.8	-10.4	-13.7	-17.0	-20.3	-23.6	-26.9	-30.2	-33.5	-36.8	-40.1
5	9.6	0.8	-984	-7.4	-19268	-35.3	-7.8	-9.2	-10.9	-14.5	-18.0	-21.5	-25.1	-28.6	-32.1	-35.7	-39.2	-42.7
6	2.7	0.8	-984	-8.1	-19270	-37.6	-8.5	-10.0	-11.9	-15.7	-19.4	-23.2	-26.9	-30.7	-34.5	-38.2	-42.0	-45.8
7	11.7	1.0	-983	-7.1	-19269	-36.4	-7.5	-8.9	-10.7	-14.4	-18.0	-21.7	-25.3	-28.9	-32.6	-36.2	-39.9	-43.5
8	2.4	0.7	-983	-7.1	-19258	-25.4	-7.3	-8.3	-9.6	-12.1	-14.7	-17.2	-19.8	-22.3	-24.9	-27.4	-29.9	-32.5
9	6.5	1.0	-983	-7.1	-19254	-22.0	-7.3	-8.2	-9.3	-11.5	-13.7	-15.9	-18.1	-20.3	-22.5	-24.7	-26.9	-29.1
10	10.0	0.9	-983	-7.6	-19250	-17.2	-7.8	-8.5	-9.3	-11.1	-12.8	-14.5	-16.2	-17.9	-19.6	-21.4	-23.1	-24.8
11	2.4	0.9	-983	-6.8	-19258	-25.6	-7.1	-8.1	-9.4	-11.9	-14.5	-17.1	-19.6	-22.2	-24.8	-27.3	-29.9	-32.4
12	2.5	0.8	-983	-6.6	-19274	-41.2	-7.0	-8.7	-10.7	-14.8	-19.0	-23.1	-27.2	-31.3	-35.4	-39.6	-43.7	-47.8
13	2.2	0.8	-983	-7.0	-19274	-41.3	-7.4	-9.1	-11.1	-15.3	-19.4	-23.5	-27.6	-31.8	-35.9	-40.0	-44.2	-48.3
14	11.8	1.0	-982	-6.9	-19261	-28.7	-7.2	-8.4	-9.8	-12.7	-15.5	-18.4	-21.3	-24.1	-27.0	-29.9	-32.8	-35.6
15	2.9	0.8	-982	-6.4	-19262	-29.6	-6.7	-7.9	-9.3	-12.3	-15.3	-18.2	-21.2	-24.1	-27.1	-30.0	-33.0	-36.0
16	1.9	0.8	-982	-5.9	-19275	-42.4	-6.3	-8.0	-10.1	-14.3	-18.6	-22.8	-27.1	-31.3	-35.5	-39.8	-44.0	-48.3
17	10.2	0.8	-981	-5.4	-19253	-20.7	-5.6	-6.4	-7.4	-9.5	-11.6	-13.6	-15.7	-17.8	-19.9	-21.9	-24.0	-26.1

Table S26: 14 in 4NCKH, Experiment 2

Entry	ligand RMSD	BS RMSD	old_IFD Score	Glide Score	PE <sub>IFD</sub>	ΔPE	new_IFD Score _1	new_IFD Score _5	new_IFD Score _10	new_IFD Score _20	new_IFD Score _30	new_IFD Score _40	new_IFD Score _50	new_IFD Score _60	new_IFD Score _70	new_IFD Score _80	new_IFD Score _90	new_IFD Score _100
1	9.1	2.3	-985	-9.9	-19224	8.9	-9.8	-9.4	-9.0	-8.1	-7.2	-6.3	-5.4	-4.5	-3.7	-2.8	-1.9	-1.0
2	9.4	1.9	-985	-9.6	-19231	1.6	-9.6	-9.6	-9.5	-9.3	-9.2	-9.0	-8.8	-8.7	-8.5	-8.3	-8.2	-8.0
3	8.7	2.3	-984	-9.1	-19246	-13.5	-9.3	-9.8	-10.5	-11.9	-13.2	-14.6	-15.9	-17.3	-18.6	-20.0	-21.3	-22.7
4	8.8	2.4	-984	-9.1	-19227	4.9	-9.1	-8.9	-8.6	-8.2	-7.7	-7.2	-6.7	-6.2	-5.7	-5.2	-4.7	-4.2
5	8.8	2.3	-984	-9.0	-19226	6.6	-9.0	-8.7	-8.4	-7.7	-7.0	-6.4	-5.7	-5.1	-4.4	-3.7	-3.1	-2.4
6	10.4	2.0	-984	-9.1	-19230	2.1	-9.1	-9.0	-8.9	-8.7	-8.5	-8.3	-8.1	-7.9	-7.7	-7.4	-7.2	-7.0
7	8.9	2.3	-984	-9.1	-19221	11.3	-8.9	-8.5	-7.9	-6.8	-5.7	-4.5	-3.4	-2.3	-1.2	0.0	1.1	2.2
8	8.7	2.4	-984	-9.2	-19220	12.0	-9.1	-8.6	-8.0	-6.8	-5.6	-4.4	-3.2	-2.0	-0.8	0.4	1.6	2.8
9	9.1	2.1	-984	-9.8	-19215	16.9	-9.6	-8.9	-8.1	-6.4	-4.7	-3.0	-1.3	0.4	2.1	3.8	5.5	7.1
10	9.1	2.2	-984	-8.8	-19228	4.4	-8.8	-8.6	-8.4	-7.9	-7.5	-7.1	-6.6	-6.2	-5.7	-5.3	-4.9	-4.4
11	8.8	2.2	-984	-9.4	-19222	9.9	-9.3	-8.9	-8.4	-7.4	-6.4	-5.4	-4.4	-3.5	-2.5	-1.5	-0.5	0.5
12	8.9	2.2	-983	-8.9	-19219	13.1	-8.7	-8.2	-7.6	-6.3	-4.9	-3.6	-2.3	-1.0	0.3	1.6	2.9	4.2
13	7.7	2.2	-983	-8.7	-19223	9.3	-8.6	-8.3	-7.8	-6.9	-6.0	-5.0	-4.1	-3.2	-2.2	-1.3	-0.4	0.5
14	10.9	2.2	-983	-8.9	-19222	10.5	-8.8	-8.4	-7.8	-6.8	-5.7	-4.7	-3.6	-2.6	-1.5	-0.5	0.6	1.6
15	10.2	2.0	-983	-8.8	-19230	2.4	-8.8	-8.7	-8.6	-8.3	-8.1	-7.8	-7.6	-7.4	-7.1	-6.9	-6.6	-6.4
16	9.3	1.9	-982	-8.8	-19235	-2.2	-8.8	-8.9	-9.0	-9.3	-9.5	-9.7	-9.9	-10.2	-10.4	-10.6	-10.8	-11.1

Table S27: 14 in 4NCKH, Experiment 3



Entry	ligand RMSD	BS RMSD	old_IFD Score	Glide Score	PE <sub>IFD</sub>	ΔPE	new_IFD Score _1	new_IFD Score _5	new_IFD Score _10	new_IFD Score _20	new_IFD Score _30	new_IFD Score _40	new_IFD Score _50	new_IFD Score _60	new_IFD Score _70	new_IFD Score _80	new_IFD Score _90	new_IFD Score _100
1	10.2	1.3	-985	-8.9	-19246	-13.8	-9.0	-9.6	-10.3	-11.7	-13.0	-14.4	-15.8	-17.2	-18.6	-19.9	-21.3	-22.7
2	9.2	1.3	-985	-8.1	-19259	-26.8	-8.4	-9.4	-10.8	-13.4	-16.1	-18.8	-21.5	-24.2	-26.8	-29.5	-32.2	-34.9
3	9.8	1.3	-985	-8.1	-19257	-24.8	-8.3	-9.3	-10.5	-13.0	-15.5	-18.0	-20.5	-22.9	-25.4	-27.9	-30.4	-32.9
4	9.8	1.3	-985	-8.0	-19252	-20.0	-8.2	-9.0	-10.0	-12.0	-14.0	-16.0	-18.0	-20.0	-22.0	-24.0	-26.0	-28.0
5	9.3	1.3	-984	-7.7	-19257	-24.9	-8.0	-9.0	-10.2	-12.7	-15.2	-17.7	-20.2	-22.7	-25.1	-27.6	-30.1	-32.6
6	9.5	1.3	-984	-7.6	-19258	-26.0	-7.8	-8.9	-10.2	-12.8	-15.4	-18.0	-20.6	-23.2	-25.8	-28.4	-31.0	-33.6
7	10.1	1.3	-984	-8.4	-19225	7.5	-8.4	-8.0	-7.7	-6.9	-6.2	-5.4	-4.7	-3.9	-3.2	-2.4	-1.6	-0.9
8	7.9	1.5	-984	-7.4	-19259	-26.8	-7.7	-8.8	-10.1	-12.8	-15.4	-18.1	-20.8	-23.5	-26.1	-28.8	-31.5	-34.2
9	11.7	1.3	-983	-7.1	-19255	-23.1	-7.3	-8.3	-9.4	-11.7	-14.0	-16.3	-18.6	-20.9	-23.2	-25.6	-27.9	-30.2
10	6.6	1.3	-982	-6.1	-19253	-21.1	-6.3	-7.2	-8.2	-10.3	-12.5	-14.6	-16.7	-18.8	-20.9	-23.0	-25.1	-27.2
11	8.7	1.4	-982	-6.5	-19248	-15.6	-6.6	-7.3	-8.0	-9.6	-11.2	-12.7	-14.3	-15.9	-17.4	-19.0	-20.5	-22.1
12	6.0	1.5	-982	-6.7	-19254	-21.6	-7.0	-7.8	-8.9	-11.1	-13.2	-15.4	-17.5	-19.7	-21.8	-24.0	-26.2	-28.3
13	5.0	1.5	-981	-5.9	-19252	-19.4	-6.1	-6.8	-7.8	-9.8	-11.7	-13.6	-15.6	-17.5	-19.5	-21.4	-23.3	-25.3

Table S28: 14 in 4NCKH, Experiment 4

Entry	ligand RMSD	BS RMSD	old_IFD Score	Glide Score	PE <sub>IFD</sub>	ΔPE	new_IFD Score _1	new_IFD Score _5	new_IFD Score _10	new_IFD Score _20	new_IFD Score _30	new_IFD Score _40	new_IFD Score _50	new_IFD Score _60	new_IFD Score _70	new_IFD Score _80	new_IFD Score _90	new_IFD Score _100
1	10.1	0.8	-986	-8.8	-19263	-30.2	-9.1	-10.3	-11.8	-14.8	-17.8	-20.9	-23.9	-26.9	-29.9	-33.0	-36.0	-39.0
2	9.7	0.7	-985	-8.6	-19264	-31.9	-8.9	-10.2	-11.8	-15.0	-18.1	-21.3	-24.5	-27.7	-30.9	-34.1	-37.3	-40.5
3	9.9	0.8	-985	-8.3	-19252	-19.8	-8.5	-9.3	-10.3	-12.3	-14.3	-16.2	-18.2	-20.2	-22.2	-24.2	-26.1	-28.1
4	9.7	1.2	-985	-8.0	-19257	-24.9	-8.3	-9.3	-10.5	-13.0	-15.5	-18.0	-20.5	-23.0	-25.5	-28.0	-30.5	-32.9
5	9.6	1.3	-984	-7.4	-19277	-44.4	-7.8	-9.6	-11.8	-16.2	-20.7	-25.1	-29.6	-34.0	-38.4	-42.9	-47.3	-51.8
6	6.7	0.8	-984	-7.1	-19262	-29.9	-7.4	-8.6	-10.1	-13.1	-16.0	-19.0	-22.0	-25.0	-28.0	-31.0	-34.0	-37.0
7	7.7	0.9	-984	-7.3	-19255	-22.8	-7.5	-8.4	-9.6	-11.8	-14.1	-16.4	-18.7	-21.0	-23.3	-25.5	-27.8	-30.1
8	11.1	0.9	-984	-7.2	-19260	-27.2	-7.5	-8.6	-10.0	-12.7	-15.4	-18.1	-20.9	-23.6	-26.3	-29.0	-31.7	-34.5
9	7.8	1.5	-983	-7.2	-19255	-22.5	-7.4	-8.3	-9.5	-11.7	-14.0	-16.2	-18.5	-20.7	-23.0	-25.2	-27.4	-29.7
10	9.4	1.0	-983	-6.9	-19268	-35.4	-7.3	-8.7	-10.5	-14.0	-17.5	-21.1	-24.6	-28.1	-31.7	-35.2	-38.8	-42.3
11	9.4	1.3	-983	-5.8	-19279	-46.8	-6.3	-8.2	-10.5	-15.2	-19.9	-24.5	-29.2	-33.9	-38.6	-43.2	-47.9	-52.6
12	2.6	0.9	-983	-6.8	-19256	-23.2	-7.0	-7.9	-9.1	-11.4	-13.7	-16.0	-18.4	-20.7	-23.0	-25.3	-27.6	-29.9

Table S29: 14 in 4NCKH, Experiment 5

Entry	ligand RMSD	BS RMSD	old_IFD Score	Glide Score	PE <sub>IFD</sub>	ΔPE	new_IFD Score _1	new_IFD Score _5	new_IFD Score _10	new_IFD Score _20	new_IFD Score _30	new_IFD Score _40	new_IFD Score _50	new_IFD Score _60	new_IFD Score _70	new_IFD Score _80	new_IFD Score _90	new_IFD Score _100
1	9.6	1.9	-986	-9.8	-19233	-0.5	-9.8	-9.8	-9.8	-9.9	-10.0	-10.0	-10.1	-10.1	-10.2	-10.2	-10.3	-10.3
2	9.1	2.0	-985	-9.8	-19227	4.9	-9.8	-9.6	-9.3	-8.8	-8.3	-7.9	-7.4	-6.9	-6.4	-5.9	-5.4	-4.9
3	9.2	2.2	-985	-9.7	-19217	15.0	-9.6	-9.0	-8.2	-6.7	-5.3	-3.8	-2.3	-0.8	0.7	2.2	3.7	5.2
4	9.3	2.0	-985	-9.4	-19241	-8.6	-9.5	-9.9	-10.3	-11.1	-12.0	-12.9	-13.7	-14.6	-15.4	-16.3	-17.2	-18.0
5	9.3	1.9	-985	-9.1	-19230	2.4	-9.1	-9.0	-8.9	-8.6	-8.4	-8.2	-7.9	-7.7	-7.5	-7.2	-7.0	-6.8
6	10.1	1.9	-985	-9.0	-19239	-6.3	-9.0	-9.3	-9.6	-10.2	-10.8	-11.5	-12.1	-12.7	-13.4	-14.0	-14.6	-15.2
7	10.3	2.1	-985	-8.7	-19231	1.1	-8.7	-8.6	-8.5	-8.4	-8.3	-8.2	-8.1	-8.0	-7.9	-7.7	-7.6	-7.5
8	9.0	2.1	-985	-9.4	-19231	1.1	-9.4	-9.3	-9.2	-9.1	-9.0	-8.9	-8.8	-8.7	-8.6	-8.5	-8.3	-8.2
9	10.3	2.2	-985	-9.0	-19232	0.0	-9.0	-9.0	-9.0	-9.0	-9.0	-9.0	-9.0	-9.0	-9.0	-9.0	-9.0	-9.0
10	9.2	2.0	-985	-8.9	-19235	-2.6	-9.0	-9.1	-9.2	-9.5	-9.7	-10.0	-10.2	-10.5	-10.7	-11.0	-11.3	-11.5
11	9.3	1.9	-985	-9.3	-19233	-0.2	-9.3	-9.3	-9.3	-9.3	-9.3	-9.3	-9.3	-9.4	-9.4	-9.4	-9.4	-9.4
12	9.6	1.7	-985	-8.4	-19233	-0.7	-8.5	-8.5	-8.5	-8.6	-8.7	-8.7	-8.8	-8.9	-9.0	-9.0	-9.1	-9.2
13	10.3	2.2	-985	-8.5	-19237	-4.2	-8.5	-8.7	-8.9	-9.3	-9.8	-10.2	-10.6	-11.0	-11.4	-11.8	-12.2	-12.7
14	9.6	2.0	-984	-8.6	-19230	2.7	-8.6	-8.5	-8.3	-8.1	-7.8	-7.5	-7.3	-7.0	-6.7	-6.4	-6.2	-5.9
15	8.7	2.2	-984	-8.9	-19231	1.2	-8.9	-8.8	-8.8	-8.6	-8.5	-8.4	-8.3	-8.2	-8.1	-7.9	-7.8	-7.7
16	9.1	1.9	-983	-8.4	-19244	-11.3	-8.5	-8.9	-9.5	-10.6	-11.8	-12.9	-14.0	-15.1	-16.3	-17.4	-18.5	-19.6
17	9.0	2.1	-983	-7.7	-19226	6.4	-7.7	-7.4	-7.1	-6.4	-5.8	-5.2	-4.5	-3.9	-3.2	-2.6	-2.0	-1.3
18	10.2	1.8	-983	-7.9	-19225	7.5	-7.9	-7.6	-7.2	-6.4	-5.7	-4.9	-4.2	-3.4	-2.7	-1.9	-1.2	-0.4

Table S30: 14 in 4NCKH, Experiment 6

Entry	ligand RMSD	BS RMSD	old_IFD Score	Glide Score	PE <sub>IFD</sub>	ΔPE	new_IFD Score _1	new_IFD Score _5	new_IFD Score _10	new_IFD Score _20	new_IFD Score _30	new_IFD Score _40	new_IFD Score _50	new_IFD Score _60	new_IFD Score _70	new_IFD Score _80	new_IFD Score _90	new_IFD Score _100
1	9.7	1.2	-985	-8.4	-19253	-20.6	-8.6	-9.4	-10.5	-12.5	-14.6	-16.6	-18.7	-20.7	-22.8	-24.9	-26.9	-29.0
2	3.0	0.8	-985	-9.0	-19253	-20.8	-9.2	-10.0	-11.1	-13.2	-15.2	-17.3	-19.4	-21.5	-23.6	-25.6	-27.7	-29.8
3	9.2	1.0	-985	-8.1	-19255	-23.1	-8.3	-9.2	-10.4	-12.7	-15.0	-17.3	-19.6	-21.9	-24.2	-26.5	-28.9	-31.2
4	9.1	1.1	-984	-7.9	-19254	-21.4	-8.1	-9.0	-10.1	-12.2	-14.4	-16.5	-18.6	-20.8	-22.9	-25.1	-27.2	-29.3
5	9.7	1.0	-984	-8.1	-19271	-38.1	-8.4	-10.0	-11.9	-15.7	-19.5	-23.3	-27.1	-30.9	-34.8	-38.6	-42.4	-46.2
6	9.8	1.0	-984	-8.0	-19263	-30.1	-8.3	-9.5	-11.0	-14.0	-17.0	-20.0	-23.1	-26.1	-29.1	-32.1	-35.1	-38.1
7	7.2	0.9	-984	-8.1	-19244	-11.3	-8.2	-8.7	-9.2	-10.4	-11.5	-12.6	-13.7	-14.9	-16.0	-17.1	-18.2	-19.4
8	7.4	0.8	-983	-7.3	-19247	-14.4	-7.5	-8.0	-8.8	-10.2	-11.6	-13.1	-14.5	-16.0	-17.4	-18.8	-20.3	-21.7
9	10.1	0.9	-983	-8.0	-19242	-10.0	-8.1	-8.5	-9.0	-10.0	-11.0	-12.0	-13.0	-14.0	-15.0	-16.0	-17.0	-18.0
10	11.8	1.1	-983	-7.1	-19266	-34.0	-7.5	-8.8	-10.5	-13.9	-17.3	-20.7	-24.1	-27.5	-30.9	-34.3	-37.7	-41.1
11	6.4	0.9	-983	-6.3	-19258	-25.2	-6.5	-7.5	-8.8	-11.3	-13.8	-16.4	-18.9	-21.4	-23.9	-26.5	-29.0	-31.5
12	2.4	0.9	-982	-6.5	-19247	-14.8	-6.7	-7.3	-8.0	-9.5	-11.0	-12.4	-13.9	-15.4	-16.9	-18.4	-19.9	-21.3
13	10.3	0.9	-982	-6.7	-19250	-17.8	-6.9	-7.6	-8.5	-10.3	-12.0	-13.8	-15.6	-17.4	-19.1	-20.9	-22.7	-24.5
14	7.9	1.0	-982	-6.1	-19247	-14.4	-6.2	-6.8	-7.5	-9.0	-10.4	-11.9	-13.3	-14.7	-16.2	-17.6	-19.1	-20.5

Table S31: 14 in 4NCKH, Experiment 7

Entry	ligand RMSD	BS RMSD	old_IFD Score	Glide Score	PE <sub>IFD</sub>	ΔPE	new_IFD Score _1	new_IFD Score _5	new_IFD Score _10	new_IFD Score _20	new_IFD Score _30	new_IFD Score _40	new_IFD Score _50	new_IFD Score _60	new_IFD Score _70	new_IFD Score _80	new_IFD Score _90	new_IFD Score _100
1	8.7	1.9	-986	-9.7	-19242	-10.1	-9.8	-10.2	-10.7	-11.7	-12.7	-13.7	-14.7	-15.7	-16.7	-17.7	-18.7	-19.7
2	9.5	2.1	-986	-10.1	-19218	14.6	-10.0	-9.4	-8.7	-7.2	-5.7	-4.3	-2.8	-1.4	0.1	1.5	3.0	4.5
3	10.0	2.1	-986	-9.5	-19230	2.7	-9.5	-9.4	-9.2	-9.0	-8.7	-8.4	-8.2	-7.9	-7.6	-7.4	-7.1	-6.8
4	9.0	2.2	-986	-9.7	-19229	3.5	-9.7	-9.5	-9.3	-9.0	-8.6	-8.3	-8.0	-7.6	-7.3	-6.9	-6.6	-6.2
5	9.8	1.9	-986	-8.8	-19252	-19.1	-9.0	-9.8	-10.8	-12.7	-14.6	-16.5	-18.4	-20.3	-22.2	-24.2	-26.1	-28.0
6	9.3	2.1	-986	-8.9	-19242	-9.5	-9.0	-9.4	-9.9	-10.8	-11.8	-12.7	-13.7	-14.6	-15.6	-16.5	-17.5	-18.4
7	10.2	2.1	-985	-8.3	-19263	-30.2	-8.6	-9.8	-11.3	-14.4	-17.4	-20.4	-23.4	-26.4	-29.4	-32.5	-35.5	-38.5
8	8.9	2.2	-985	-9.5	-19228	4.3	-9.4	-9.3	-9.1	-8.6	-8.2	-7.8	-7.4	-6.9	-6.5	-6.1	-5.6	-5.2
9	8.9	2.2	-985	-8.9	-19250	-17.9	-9.1	-9.8	-10.7	-12.5	-14.3	-16.1	-17.8	-19.6	-21.4	-23.2	-25.0	-26.8
10	9.1	2.1	-985	-9.0	-19241	-8.7	-9.1	-9.4	-9.9	-10.7	-11.6	-12.5	-13.4	-14.2	-15.1	-16.0	-16.8	-17.7
11	9.3	1.9	-985	-8.8	-19240	-7.4	-8.9	-9.2	-9.5	-10.3	-11.0	-11.8	-12.5	-13.2	-14.0	-14.7	-15.5	-16.2
12	9.4	2.1	-985	-9.2	-19224	8.4	-9.2	-8.8	-8.4	-7.6	-6.7	-5.9	-5.0	-4.2	-3.4	-2.5	-1.7	-0.8
13	9.4	2.0	-985	-8.5	-19247	-14.7	-8.6	-9.2	-9.9	-11.4	-12.9	-14.4	-15.8	-17.3	-18.8	-20.2	-21.7	-23.2
14	8.9	2.3	-984	-8.1	-19243	-10.6	-8.2	-8.6	-9.1	-10.2	-11.3	-12.3	-13.4	-14.5	-15.5	-16.6	-17.6	-18.7
15	4.3	1.5	-983	-7.3	-19250	-17.3	-7.4	-8.1	-9.0	-10.7	-12.5	-14.2	-15.9	-17.7	-19.4	-21.1	-22.8	-24.6
16	5.0	1.7	-983	-6.6	-19258	-25.9	-6.8	-7.8	-9.1	-11.7	-14.3	-16.9	-19.5	-22.1	-24.7	-27.2	-29.8	-32.4

Table S32: 14 in 4NCKH, Experiment 8

Ligand **15** in 4NCKH

Entry	ligand RMSD	BS RMSD	old_IFD Score	Glide Score	PE <sub>IFD</sub>	$\Delta$ PE	new_IFD Score_1	new_IFD Score_5	new_IFD Score_10	new_IFD Score_20	new_IFD Score_30	new_IFD Score_40	new_IFD Score_50	new_IFD Score_60	new_IFD Score_70	new_IFD Score_80	new_IFD Score_90	new_IFD Score_100
1	10.6	1.2	-992	-11.3	-19239	-6.5	-11.4	-11.6	-11.9	-12.6	-13.2	-13.9	-14.5	-15.2	-15.8	-16.5	-17.1	-17.8
2	6.3	1.9	-991	-11.3	-19239	-6.5	-11.3	-11.6	-11.9	-12.6	-13.2	-13.9	-14.5	-15.2	-15.8	-16.5	-17.1	-17.8
3	5.5	2.4	-991	-10.6	-19246	-14.0	-10.7	-11.3	-12.0	-13.4	-14.8	-16.2	-17.6	-19.0	-20.4	-21.8	-23.2	-24.6
4	10.6	1.2	-991	-9.7	-19253	-21.1	-9.9	-10.7	-11.8	-13.9	-16.0	-18.1	-20.2	-22.3	-24.4	-26.5	-28.6	-30.7
5	10.7	2.1	-989	-9.6	-19247	-14.3	-9.7	-10.3	-11.0	-12.4	-13.9	-15.3	-16.7	-18.1	-19.6	-21.0	-22.4	-23.8
6	7.0	1.3	-988	-8.2	-19245	-12.2	-8.4	-8.8	-9.5	-10.7	-11.9	-13.1	-14.3	-15.6	-16.8	-18.0	-19.2	-20.5
7	8.8	1.3	-986	-6.4	-19242	-10.0	-6.5	-6.9	-7.4	-8.4	-9.4	-10.4	-11.4	-12.4	-13.4	-14.4	-15.4	-16.4

Table S33: **15** in 4NCKH, Experiment 1

Entry	ligand RMSD	BS RMSD	old_IFD Score	Glide Score	PE <sub>IFD</sub>	ΔPE	new_IFD Score <sub>_1</sub>	new_IFD Score <sub>_5</sub>	new_IFD Score <sub>_10</sub>	new_IFD Score <sub>_20</sub>	new_IFD Score <sub>_30</sub>	new_IFD Score <sub>_40</sub>	new_IFD Score <sub>_50</sub>	new_IFD Score <sub>_60</sub>	new_IFD Score <sub>_70</sub>	new_IFD Score <sub>_80</sub>	new_IFD Score <sub>_90</sub>	new_IFD Score <sub>_100</sub>
1	6.2	1.2	-991	-9.4	-19263	-30.2	-9.7	-10.9	-12.5	-15.5	-18.5	-21.5	-24.6	-27.6	-30.6	-33.6	-36.6	-39.7
2	11.0	1.2	-990	-9.6	-19262	-29.5	-9.9	-11.1	-12.6	-15.5	-18.5	-21.4	-24.4	-27.3	-30.3	-33.2	-36.1	-39.1
3	8.7	1.2	-990	-9.7	-19253	-20.2	-9.9	-10.7	-11.7	-13.7	-15.7	-17.8	-19.8	-21.8	-23.8	-25.8	-27.8	-29.9
4	6.7	1.0	-989	-8.9	-19257	-24.6	-9.1	-10.1	-11.4	-13.8	-16.3	-18.7	-21.2	-23.6	-26.1	-28.6	-31.0	-33.5
5	9.2	1.2	-988	-7.9	-19255	-22.7	-8.1	-9.0	-10.1	-12.4	-14.7	-16.9	-19.2	-21.5	-23.8	-26.0	-28.3	-30.6
6	6.1	1.3	-988	-7.6	-19267	-34.9	-8.0	-9.4	-11.1	-14.6	-18.1	-21.6	-25.1	-28.6	-32.1	-35.6	-39.1	-42.6
7	8.0	1.2	-988	-7.7	-19265	-32.7	-8.0	-9.3	-10.9	-14.2	-17.5	-20.7	-24.0	-27.3	-30.5	-33.8	-37.1	-40.3
8	6.1	1.1	-987	-7.2	-19276	-43.9	-7.6	-9.3	-11.5	-15.9	-20.3	-24.7	-29.1	-33.5	-37.9	-42.3	-46.6	-51.0
9	5.8	1.1	-986	-6.8	-19270	-37.5	-7.1	-8.6	-10.5	-14.2	-18.0	-21.7	-25.5	-29.2	-33.0	-36.7	-40.5	-44.2
10	11.4	1.2	-986	-5.9	-19271	-39.1	-6.3	-7.9	-9.8	-13.8	-17.7	-21.6	-25.5	-29.4	-33.3	-37.2	-41.1	-45.0

Table S34: 15 in 4NCKH, Experiment 2

Entry	ligand RMSD	BS RMSD	old_IFD Score	Glide Score	PE <sub>IFD</sub>	ΔPE	new_IFD Score <sub>_1</sub>	new_IFD Score <sub>_5</sub>	new_IFD Score <sub>_10</sub>	new_IFD Score <sub>_20</sub>	new_IFD Score <sub>_30</sub>	new_IFD Score <sub>_40</sub>	new_IFD Score <sub>_50</sub>	new_IFD Score <sub>_60</sub>	new_IFD Score <sub>_70</sub>	new_IFD Score <sub>_80</sub>	new_IFD Score <sub>_90</sub>	new_IFD Score <sub>_100</sub>
1	10.7	1.2	-992	-10.8	-19247	-14.5	-11.0	-11.6	-12.3	-13.7	-15.2	-16.6	-18.1	-19.5	-21.0	-22.4	-23.9	-25.3
2	6.6	1.1	-991	-10.1	-19250	-17.7	-10.2	-10.9	-11.8	-13.6	-15.4	-17.1	-18.9	-20.7	-22.5	-24.2	-26.0	-27.8
3	10.7	1.1	-990	-9.4	-19258	-25.8	-9.6	-10.7	-11.9	-14.5	-17.1	-19.7	-22.2	-24.8	-27.4	-30.0	-32.6	-35.1
4	3.0	1.1	-990	-9.6	-19275	-42.2	-10.1	-11.8	-13.9	-18.1	-22.3	-26.5	-30.8	-35.0	-39.2	-43.4	-47.7	-51.9
5	5.7	1.9	-989	-9.5	-19248	-16.1	-9.7	-10.3	-11.1	-12.7	-14.3	-15.9	-17.6	-19.2	-20.8	-22.4	-24.0	-25.6
6	5.9	1.1	-988	-7.9	-19282	-49.9	-8.4	-10.4	-12.9	-17.9	-22.9	-27.9	-32.9	-37.9	-42.8	-47.8	-52.8	-57.8
7	9.5	1.3	-987	-7.4	-19255	-22.5	-7.6	-8.5	-9.6	-11.9	-14.1	-16.4	-18.6	-20.9	-23.1	-25.4	-27.6	-29.9

Table S35: 15 in 4NCKH, Experiment 3

Entry	ligand RMSD	BS RMSD	old_IFD Score	Glide Score	PE <sub>IFD</sub>	ΔPE	new_IFD Score_1	new_IFD Score_5	new_IFD Score_10	new_IFD Score_20	new_IFD Score_30	new_IFD Score_40	new_IFD Score_50	new_IFD Score_60	new_IFD Score_70	new_IFD Score_80	new_IFD Score_90	new_IFD Score_100
1	6.5	1.2	-991	-10.5	-19253	-20.4	-10.7	-11.5	-12.6	-14.6	-16.6	-18.7	-20.7	-22.8	-24.8	-26.9	-28.9	-30.9
2	6.4	1.2	-991	-10.0	-19252	-20.0	-10.2	-11.0	-12.0	-14.0	-16.0	-18.0	-20.0	-22.0	-24.0	-26.0	-28.0	-30.0
3	6.5	1.3	-990	-9.7	-19251	-18.2	-9.8	-10.6	-11.5	-13.3	-15.1	-17.0	-18.8	-20.6	-22.4	-24.2	-26.1	-27.9
4	6.6	1.2	-990	-9.3	-19252	-19.5	-9.5	-10.2	-11.2	-13.2	-15.1	-17.1	-19.0	-21.0	-22.9	-24.9	-26.8	-28.8
5	10.7	1.0	-989	-9.1	-19242	-9.5	-9.2	-9.5	-10.0	-11.0	-11.9	-12.9	-13.8	-14.8	-15.8	-16.7	-17.7	-18.6
6	7.1	1.3	-989	-8.8	-19252	-19.9	-9.0	-9.8	-10.8	-12.7	-14.7	-16.7	-18.7	-20.7	-22.7	-24.7	-26.6	-28.6
7	6.8	1.3	-987	-6.9	-19259	-26.7	-7.2	-8.2	-9.6	-12.2	-14.9	-17.6	-20.2	-22.9	-25.6	-28.2	-30.9	-33.6
8	8.6	1.4	-987	-7.3	-19255	-22.8	-7.6	-8.5	-9.6	-11.9	-14.2	-16.5	-18.7	-21.0	-23.3	-25.6	-27.9	-30.1
9	8.5	1.4	-987	-7.0	-19258	-25.2	-7.2	-8.2	-9.5	-12.0	-14.5	-17.0	-19.6	-22.1	-24.6	-27.1	-29.6	-32.2
10	8.4	1.4	-987	-7.2	-19257	-24.3	-7.4	-8.4	-9.6	-12.0	-14.5	-16.9	-19.3	-21.8	-24.2	-26.6	-29.1	-31.5
11	5.8	1.2	-986	-6.8	-19268	-35.9	-7.2	-8.6	-10.4	-14.0	-17.6	-21.2	-24.8	-28.3	-31.9	-35.5	-39.1	-42.7

Table S36: 15 in 4NCKH, Experiment 4



Entry	ligand RMSD	BS RMSD	old_IFD Score	Glide Score	PE <sub>IFD</sub>	ΔPE	new_IFD Score _1	new_IFD Score _5	new_IFD Score _10	new_IFD Score _20	new_IFD Score _30	new_IFD Score _40	new_IFD Score _50	new_IFD Score _60	new_IFD Score _70	new_IFD Score _80	new_IFD Score _90	new_IFD Score _100
1	6.7	1.2	-990	-9.3	-19261	-28.9	-9.6	-10.7	-12.2	-15.1	-17.9	-20.8	-23.7	-26.6	-29.5	-32.4	-35.3	-38.2
2	9.4	1.0	-990	-8.9	-19280	-47.7	-9.3	-11.2	-13.6	-18.4	-23.2	-27.9	-32.7	-37.5	-42.3	-47.0	-51.8	-56.6
3	8.8	1.1	-988	-8.3	-19266	-34.1	-8.6	-10.0	-11.7	-15.1	-18.5	-21.9	-25.3	-28.7	-32.1	-35.6	-39.0	-42.4
4	7.4	1.2	-988	-7.9	-19254	-21.9	-8.1	-9.0	-10.1	-12.3	-14.4	-16.6	-18.8	-21.0	-23.2	-25.4	-27.5	-29.7
5	5.8	1.2	-987	-7.9	-19257	-24.3	-8.1	-9.1	-10.3	-12.7	-15.2	-17.6	-20.0	-22.4	-24.9	-27.3	-29.7	-32.2
6	8.9	1.2	-987	-7.4	-19243	-10.5	-7.5	-7.9	-8.4	-9.5	-10.5	-11.6	-12.7	-13.7	-14.8	-15.8	-16.9	-17.9
7	9.0	1.1	-987	-7.7	-19256	-23.4	-8.0	-8.9	-10.1	-12.4	-14.7	-17.1	-19.4	-21.8	-24.1	-26.5	-28.8	-31.2
8	9.0	1.1	-987	-7.5	-19256	-23.2	-7.8	-8.7	-9.8	-12.2	-14.5	-16.8	-19.1	-21.4	-23.7	-26.1	-28.4	-30.7
9	9.0	1.1	-987	-7.5	-19256	-23.2	-7.7	-8.7	-9.8	-12.1	-14.5	-16.8	-19.1	-21.4	-23.8	-26.1	-28.4	-30.7
10	5.9	1.2	-987	-7.3	-19258	-25.1	-7.5	-8.5	-9.8	-12.3	-14.8	-17.3	-19.8	-22.4	-24.9	-27.4	-29.9	-32.4
11	6.3	1.0	-987	-7.1	-19251	-19.0	-7.3	-8.0	-9.0	-10.9	-12.8	-14.7	-16.6	-18.5	-20.4	-22.3	-24.2	-26.1
12	5.9	1.1	-986	-6.7	-19260	-27.5	-7.0	-8.1	-9.5	-12.2	-15.0	-17.7	-20.5	-23.2	-26.0	-28.7	-31.5	-34.2
13	5.8	1.1	-986	-6.6	-19257	-24.3	-6.8	-7.8	-9.0	-11.4	-13.9	-16.3	-18.7	-21.2	-23.6	-26.0	-28.5	-30.9
14	6.9	1.0	-986	-6.0	-19256	-23.9	-6.2	-7.2	-8.4	-10.7	-13.1	-15.5	-17.9	-20.3	-22.7	-25.1	-27.4	-29.8
15	5.8	1.1	-985	-5.7	-19258	-25.9	-6.0	-7.0	-8.3	-10.9	-13.5	-16.1	-18.6	-21.2	-23.8	-26.4	-29.0	-31.6

Table S37: 15 in 4NCKH, Experiment 5

Entry	ligand RMSD	BS RMSD	old_IFD Score	Glide Score	PE <sub>IFD</sub>	ΔPE	new_IFD Score _1	new_IFD Score _5	new_IFD Score _10	new_IFD Score _20	new_IFD Score _30	new_IFD Score _40	new_IFD Score _50	new_IFD Score _60	new_IFD Score _70	new_IFD Score _80	new_IFD Score _90	new_IFD Score _100
1	10.5	1.2	-990	-10.6	-19224	8.2	-10.5	-10.2	-9.8	-9.0	-8.2	-7.3	-6.5	-5.7	-4.9	-4.1	-3.2	-2.4
2	6.0	2.2	-990	-10.6	-19235	-3.0	-10.7	-10.8	-10.9	-11.2	-11.5	-11.8	-12.1	-12.4	-12.7	-13.0	-13.3	-13.6
3	8.8	1.3	-990	-10.0	-19232	-0.1	-10.0	-10.0	-10.0	-10.0	-10.0	-10.0	-10.0	-10.0	-10.0	-10.0	-10.0	-10.0
4	2.9	1.2	-988	-7.9	-19255	-22.6	-8.1	-9.0	-10.1	-12.4	-14.6	-16.9	-19.1	-21.4	-23.7	-25.9	-28.2	-30.4
5	3.4	0.9	-988	-8.3	-19244	-11.7	-8.5	-8.9	-9.5	-10.7	-11.8	-13.0	-14.2	-15.3	-16.5	-17.7	-18.8	-20.0
6	8.3	1.1	-987	-7.2	-19259	-26.1	-7.5	-8.5	-9.8	-12.4	-15.1	-17.7	-20.3	-22.9	-25.5	-28.1	-30.7	-33.4
7	9.4	1.1	-987	-7.9	-19231	1.1	-7.9	-7.8	-7.8	-7.7	-7.6	-7.5	-7.4	-7.3	-7.1	-7.0	-6.9	-6.8
8	10.7	1.1	-987	-7.6	-19242	-10.0	-7.7	-8.1	-8.6	-9.6	-10.6	-11.6	-12.6	-13.6	-14.6	-15.6	-16.6	-17.6

Table S38: 15 in 4NCKH, Experiment 6

Entry	ligand RMSD	BS RMSD	old_IFD Score	Glide Score	PE <sub>IFD</sub>	ΔPE	new_IFD Score _1	new_IFD Score _5	new_IFD Score _10	new_IFD Score _20	new_IFD Score _30	new_IFD Score _40	new_IFD Score _50	new_IFD Score _60	new_IFD Score _70	new_IFD Score _80	new_IFD Score _90	new_IFD Score _100
1	6.6	1.3	-991	-10.1	-19250	-18.0	-10.3	-11.0	-11.9	-13.7	-15.5	-17.3	-19.1	-20.9	-22.7	-24.5	-26.3	-28.2
2	7.2	1.5	-990	-8.7	-19255	-22.6	-8.9	-9.8	-11.0	-13.2	-15.5	-17.7	-20.0	-22.2	-24.5	-26.8	-29.0	-31.3
3	10.6	1.2	-989	-9.0	-19247	-14.9	-9.1	-9.7	-10.5	-12.0	-13.4	-14.9	-16.4	-17.9	-19.4	-20.9	-22.4	-23.8
4	7.2	1.4	-989	-9.1	-19253	-20.6	-9.3	-10.1	-11.1	-13.2	-15.2	-17.3	-19.4	-21.4	-23.5	-25.6	-27.6	-29.7
5	4.7	1.4	-988	-8.0	-19254	-22.1	-8.2	-9.1	-10.2	-12.4	-14.6	-16.8	-19.0	-21.2	-23.4	-25.7	-27.9	-30.1
6	10.6	1.2	-988	-7.4	-19257	-24.6	-7.6	-8.6	-9.8	-12.3	-14.8	-17.2	-19.7	-22.2	-24.6	-27.1	-29.6	-32.0
7	12.9	1.2	-988	-8.0	-19248	-15.4	-8.1	-8.7	-9.5	-11.0	-12.6	-14.1	-15.7	-17.2	-18.7	-20.3	-21.8	-23.3
8	11.5	1.2	-988	-7.5	-19251	-18.3	-7.7	-8.4	-9.3	-11.1	-13.0	-14.8	-16.6	-18.5	-20.3	-22.1	-24.0	-25.8
9	11.6	1.1	-987	-7.5	-19260	-27.9	-7.8	-8.9	-10.3	-13.1	-15.9	-18.7	-21.5	-24.2	-27.0	-29.8	-32.6	-35.4
10	8.5	1.3	-987	-7.1	-19261	-28.7	-7.4	-8.5	-10.0	-12.8	-15.7	-18.6	-21.4	-24.3	-27.2	-30.0	-32.9	-35.8
11	9.3	1.1	-987	-7.0	-19259	-26.3	-7.3	-8.3	-9.6	-12.3	-14.9	-17.5	-20.2	-22.8	-25.4	-28.0	-30.7	-33.3
12	8.5	1.4	-986	-6.7	-19253	-21.1	-6.9	-7.7	-8.8	-10.9	-13.0	-15.1	-17.2	-19.3	-21.4	-23.6	-25.7	-27.8
13	11.5	1.2	-986	-6.4	-19262	-30.0	-6.7	-7.9	-9.4	-12.4	-15.4	-18.4	-21.4	-24.4	-27.4	-30.4	-33.4	-36.4

Table S39: 15 in 4NCKH, Experiment 7

Entry	ligand RMSD	BS RMSD	old_IFD Score	Glide Score	PE <sub>IFD</sub>	ΔPE	new_IFD Score _1	new_IFD Score _5	new_IFD Score _10	new_IFD Score _20	new_IFD Score _30	new_IFD Score _40	new_IFD Score _50	new_IFD Score _60	new_IFD Score _70	new_IFD Score _80	new_IFD Score _90	new_IFD Score _100
1	10.7	1.1	-992	-10.4	-19263	-30.4	-10.7	-12.0	-13.5	-16.5	-19.6	-22.6	-25.6	-28.7	-31.7	-34.7	-37.8	-40.8
2	<b>6.0</b>	2.0	-992	-11.3	-19234	-1.4	<b>-11.3</b>	-11.4	-11.5	-11.6	-11.7	-11.9	-12.0	-12.2	-12.3	-12.4	-12.6	-12.7
3	10.9	1.0	-992	-10.1	-19261	-28.8	-10.4	<b>-11.5</b>	<b>-13.0</b>	<b>-15.8</b>	-18.7	-21.6	-24.5	-27.4	-30.2	-33.1	-36.0	-38.9
4	<b>6.0</b>	2.2	-991	-10.8	-19233	-0.3	-10.8	-10.8	-10.8	-10.8	-10.9	-10.9	-10.9	-11.0	-11.0	-11.0	-11.1	-11.1
5	10.4	2.8	-989	-9.1	-19238	-6.1	-9.1	-9.4	-9.7	-10.3	-10.9	-11.5	-12.1	-12.7	-13.3	-14.0	-14.6	-15.2
6	10.8	1.2	-989	-8.4	-19254	-21.7	-8.7	-9.5	-10.6	-12.8	-14.9	-17.1	-19.3	-21.4	-23.6	-25.8	-27.9	-30.1
7	9.6	1.2	-988	-8.1	-19270	-37.8	-8.5	-10.0	-11.9	-15.7	<b>-19.4</b>	<b>-23.2</b>	<b>-27.0</b>	<b>-30.8</b>	<b>-34.6</b>	<b>-38.4</b>	<b>-42.2</b>	<b>-45.9</b>
8	10.4	1.2	-986	-5.4	-19268	-36.1	-5.7	-7.2	-9.0	-12.6	-16.2	-19.8	-23.4	-27.0	-30.6	-34.2	-37.8	-41.4

Table S40: 15 in 4NCKH, Experiment 8

Ligand **13** in 1ZHUB

Entry	ligand RMSD	BS RMSD	old_IFD Score	Glide Score	PE <sub>IFD</sub>	$\Delta$ PE	new_IFD Score _1	new_IFD Score _5	new_IFD Score _10	new_IFD Score _20	new_IFD Score _30	new_IFD Score _40	new_IFD Score _50	new_IFD Score _60	new_IFD Score _70	new_IFD Score _80	new_IFD Score _90	new_IFD Score _100
1	<b>2.0</b>	0.7	-1001	-10.7	-19562	-19.5	<b>-10.8</b>	-11.6	-12.6	-14.6	-16.5	-18.5	-20.4	-22.4	-24.3	-26.3	-28.2	-30.2
2	2.1	0.8	-1001	-10.4	-19569	-27.0	-10.7	-11.7	-13.1	-15.8	-18.5	-21.2	-23.9	-26.6	-29.3	-32.0	-34.7	-37.4
3	2.2	0.6	-1001	-10.4	-19574	-32.4	-10.7	<b>-12.0</b>	<b>-13.6</b>	<b>-16.9</b>	<b>-20.1</b>	<b>-23.4</b>	<b>-26.6</b>	<b>-29.8</b>	-33.1	-36.3	-39.6	-42.8
4	3.2	0.7	-999	-9.3	-19565	-23.1	-9.6	-10.5	-11.6	-14.0	-16.3	-18.6	-20.9	-23.2	-25.5	-27.8	-30.1	-32.4
5	2.4	0.9	-998	-8.5	-19577	-35.4	-8.9	-10.3	-12.1	-15.6	-19.1	-22.7	-26.2	-29.7	<b>-33.3</b>	<b>-36.8</b>	<b>-40.4</b>	<b>-43.9</b>
6	2.9	0.8	-998	-9.4	-19561	-19.3	-9.6	-10.3	-11.3	-13.2	-15.2	-17.1	-19.0	-20.9	-22.9	-24.8	-26.7	-28.6
7	6.0	0.8	-998	-8.7	-19572	-29.5	-8.9	-10.1	-11.6	-14.6	-17.5	-20.5	-23.4	-26.4	-29.3	-32.3	-35.2	-38.2
8	2.9	0.8	-998	-8.5	-19572	-29.8	-8.8	-10.0	-11.5	-14.5	-17.5	-20.5	-23.4	-26.4	-29.4	-32.4	-35.4	-38.4
9	3.3	0.8	-998	-8.9	-19574	-32.5	-9.2	-10.5	-12.1	-15.4	-18.6	-21.9	-25.1	-28.4	-31.6	-34.9	-38.1	-41.4
10	5.8	0.9	-997	-8.1	-19577	-34.6	-8.5	-9.9	-11.6	-15.1	-18.5	-22.0	-25.4	-28.9	-32.3	-35.8	-39.3	-42.7
11	5.8	0.9	-997	-7.7	-19570	-27.8	-7.9	-9.0	-10.4	-13.2	-16.0	-18.8	-21.5	-24.3	-27.1	-29.9	-32.7	-35.4

Table S41: **13** in 1ZHUB, Experiment 1

Entry	ligand RMSD	BS RMSD	old_IFD Score	Glide Score	PE <sub>IFD</sub>	ΔPE	new_IFD Score _1	new_IFD Score _5	new_IFD Score _10	new_IFD Score _20	new_IFD Score _30	new_IFD Score _40	new_IFD Score _50	new_IFD Score _60	new_IFD Score _70	new_IFD Score _80	new_IFD Score _90	new_IFD Score _100
1	2.2	0.7	-998	-10.1	-19551	-8.1	-10.1	-10.5	-10.9	-11.7	-12.5	-13.3	-14.1	-14.9	-15.7	-16.6	-17.4	-18.2
2	2.1	0.7	-998	-9.4	-19563	-19.6	-9.6	-10.4	-11.3	-13.3	-15.3	-17.2	-19.2	-21.2	-23.1	-25.1	-27.1	-29.0
3	2.2	0.7	-998	-10.1	-19556	-13.6	-10.2	-10.8	-11.4	-12.8	-14.1	-15.5	-16.9	-18.2	-19.6	-20.9	-22.3	-23.6
4	2.2	0.7	-998	-9.6	-19551	-8.0	-9.7	-10.1	-10.5	-11.3	-12.1	-12.9	-13.7	-14.5	-15.3	-16.1	-16.9	-17.7
5	2.0	0.8	-997	-8.7	-19557	-14.0	-8.9	-9.4	-10.1	-11.5	-12.9	-14.3	-15.7	-17.2	-18.6	-20.0	-21.4	-22.8
6	2.1	0.8	-997	-8.1	-19570	-26.8	-8.4	-9.5	-10.8	-13.5	-16.2	-18.8	-21.5	-24.2	-26.9	-29.5	-32.2	-34.9
7	2.3	0.8	-997	-8.8	-19561	-18.4	-9.0	-9.7	-10.6	-12.4	-14.3	-16.1	-18.0	-19.8	-21.6	-23.5	-25.3	-27.2
8	3.1	0.7	-997	-9.0	-19554	-11.2	-9.1	-9.5	-10.1	-11.2	-12.3	-13.4	-14.6	-15.7	-16.8	-17.9	-19.0	-20.1
9	3.2	0.7	-997	-8.8	-19555	-12.0	-8.9	-9.4	-10.0	-11.2	-12.4	-13.6	-14.8	-16.0	-17.2	-18.4	-19.6	-20.8
10	2.0	0.8	-997	-8.5	-19563	-20.2	-8.7	-9.5	-10.6	-12.6	-14.6	-16.6	-18.6	-20.6	-22.7	-24.7	-26.7	-28.7
11	2.1	0.8	-997	-8.3	-19544	-1.5	-8.3	-8.4	-8.4	-8.6	-8.7	-8.9	-9.0	-9.2	-9.3	-9.5	-9.6	-9.8
12	2.3	0.9	-996	-8.1	-19534	9.2	-8.0	-7.6	-7.1	-6.2	-5.3	-4.4	-3.4	-2.5	-1.6	-0.7	0.3	1.2
13	2.9	0.9	-995	-7.7	-19556	-12.7	-7.8	-8.3	-9.0	-10.2	-11.5	-12.8	-14.1	-15.3	-16.6	-17.9	-19.1	-20.4

Table S42: 13 in 1ZHUB, Experiment 2

Entry	ligand RMSD	BS RMSD	old_IFD Score	Glide Score	PE <sub>IFD</sub>	ΔPE	new_IFD Score _1	new_IFD Score _5	new_IFD Score _10	new_IFD Score _20	new_IFD Score _30	new_IFD Score _40	new_IFD Score _50	new_IFD Score _60	new_IFD Score _70	new_IFD Score _80	new_IFD Score _90	new_IFD Score _100
1	2.3	0.8	-1001	-10.6	-19577	-33.7	-11.0	-12.3	-14.0	-17.4	-20.8	-24.1	-27.5	-30.9	-34.3	-37.6	-41.0	-44.4
2	2.2	0.8	-1001	-10.0	-19592	-48.9	-10.5	-12.4	-14.9	-19.8	-24.7	-29.6	-34.5	-39.4	-44.3	-49.1	-54.0	-58.9
3	2.0	0.7	-1000	-9.7	-19591	-47.8	-10.2	-12.1	-14.5	-19.3	-24.0	-28.8	-33.6	-38.4	-43.2	-47.9	-52.7	-57.5
4	2.1	0.9	-1000	-9.2	-19594	-51.2	-9.7	-11.7	-14.3	-19.4	-24.5	-29.6	-34.8	-39.9	-45.0	-50.1	-55.2	-60.3
5	2.0	0.7	-1000	-9.2	-19601	-58.4	-9.8	-12.1	-15.1	-20.9	-26.7	-32.6	-38.4	-44.3	-50.1	-55.9	-61.8	-67.6
6	3.3	0.9	-1000	-9.1	-19569	-26.4	-9.4	-10.5	-11.8	-14.4	-17.0	-19.7	-22.3	-25.0	-27.6	-30.2	-32.9	-35.5
7	3.2	0.8	-999	-8.5	-19597	-53.7	-9.0	-11.2	-13.9	-19.2	-24.6	-30.0	-35.3	-40.7	-46.1	-51.4	-56.8	-62.2
8	6.6	0.8	-998	-7.2	-19593	-50.2	-7.7	-9.7	-12.2	-17.2	-22.2	-27.3	-32.3	-37.3	-42.3	-47.3	-52.3	-57.4
9	7.4	0.9	-997	-7.4	-19592	-48.7	-7.9	-9.8	-12.3	-17.1	-22.0	-26.9	-31.7	-36.6	-41.5	-46.3	-51.2	-56.1

Table S43: **13** in 1ZHUB, Experiment 3

Entry	ligand RMSD	BS RMSD	old_IFD Score	Glide Score	PE <sub>IFD</sub>	ΔPE	new_IFD Score _1	new_IFD Score _5	new_IFD Score _10	new_IFD Score _20	new_IFD Score _30	new_IFD Score _40	new_IFD Score _50	new_IFD Score _60	new_IFD Score _70	new_IFD Score _80	new_IFD Score _90	new_IFD Score _100
1	2.0	0.7	-999	-10.2	-19562	-19.1	-10.4	-11.1	-12.1	-14.0	-15.9	-17.8	-19.8	-21.7	-23.6	-25.5	-27.4	-29.3
2	2.0	0.8	-998	-9.8	-19538	5.4	-9.8	-9.6	-9.3	-8.8	-8.2	-7.7	-7.2	-6.6	-6.1	-5.6	-5.0	-4.5
3	2.4	0.8	-998	-9.5	-19559	-15.6	-9.6	-10.2	-11.0	-12.6	-14.1	-15.7	-17.3	-18.8	-20.4	-22.0	-23.5	-25.1
4	2.4	1.0	-998	-9.8	-19533	9.6	-9.7	-9.3	-8.9	-7.9	-6.9	-6.0	-5.0	-4.1	-3.1	-2.1	-1.2	-0.2
5	6.0	0.8	-997	-8.7	-19560	-17.1	-8.9	-9.6	-10.5	-12.2	-13.9	-15.6	-17.3	-19.0	-20.7	-22.4	-24.1	-25.9
6	3.2	0.8	-997	-9.1	-19550	-7.0	-9.2	-9.5	-9.8	-10.5	-11.2	-11.9	-12.7	-13.4	-14.1	-14.8	-15.5	-16.2
7	6.4	0.9	-997	-9.2	-19573	-29.8	-9.5	-10.6	-12.1	-15.1	-18.1	-21.1	-24.0	-27.0	-30.0	-33.0	-36.0	-38.9
8	6.1	0.9	-997	-8.8	-19560	-17.2	-8.9	-9.6	-10.5	-12.2	-13.9	-15.6	-17.4	-19.1	-20.8	-22.5	-24.2	-26.0
9	6.4	0.9	-997	-8.8	-19573	-30.1	-9.1	-10.3	-11.8	-14.8	-17.8	-20.8	-23.8	-26.9	-29.9	-32.9	-35.9	-38.9
10	5.7	0.9	-997	-8.4	-19557	-14.1	-8.6	-9.1	-9.8	-11.2	-12.6	-14.0	-15.5	-16.9	-18.3	-19.7	-21.1	-22.5
11	5.6	0.9	-996	-8.1	-19569	-25.8	-8.3	-9.3	-10.6	-13.2	-15.8	-18.4	-20.9	-23.5	-26.1	-28.7	-31.2	-33.8
12	5.6	0.8	-996	-7.9	-19556	-13.1	-8.0	-8.6	-9.2	-10.5	-11.9	-13.2	-14.5	-15.8	-17.1	-18.4	-19.7	-21.0

Table S44: **13** in 1ZHUB, Experiment 4



Entry	ligand RMSD	BS RMSD	old_IFD Score	Glide Score	PE <sub>IFD</sub>	ΔPE	new_IFD Score_1	new_IFD Score_5	new_IFD Score_10	new_IFD Score_20	new_IFD Score_30	new_IFD Score_40	new_IFD Score_50	new_IFD Score_60	new_IFD Score_70	new_IFD Score_80	new_IFD Score_90	new_IFD Score_100
1	2.9	0.8	-998	-9.2	-19558	-15.3	-9.4	-10.0	-10.8	-12.3	-13.8	-15.4	-16.9	-18.4	-20.0	-21.5	-23.0	-24.6
2	2.1	0.8	-998	-9.3	-19558	-14.8	-9.4	-10.0	-10.8	-12.2	-13.7	-15.2	-16.7	-18.1	-19.6	-21.1	-22.6	-24.1
3	2.0	0.8	-998	-9.2	-19552	-9.5	-9.3	-9.7	-10.2	-11.1	-12.1	-13.0	-14.0	-14.9	-15.9	-16.8	-17.8	-18.7
4	6.0	0.9	-998	-9.4	-19564	-21.3	-9.6	-10.4	-11.5	-13.6	-15.8	-17.9	-20.0	-22.1	-24.3	-26.4	-28.5	-30.7
5	3.1	0.8	-998	-8.6	-19561	-18.5	-8.8	-9.6	-10.5	-12.3	-14.2	-16.0	-17.9	-19.7	-21.6	-23.4	-25.3	-27.1
6	1.9	0.7	-998	-8.7	-19558	-14.9	-8.9	-9.5	-10.2	-11.7	-13.2	-14.7	-16.2	-17.7	-19.2	-20.7	-22.1	-23.6
7	2.8	0.8	-997	-9.4	-19547	-4.3	-9.4	-9.6	-9.8	-10.3	-10.7	-11.1	-11.5	-12.0	-12.4	-12.8	-13.3	-13.7
8	2.2	0.9	-997	-8.6	-19551	-8.5	-8.7	-9.1	-9.5	-10.3	-11.2	-12.0	-12.9	-13.7	-14.6	-15.4	-16.2	-17.1
9	2.2	0.8	-997	-8.7	-19551	-7.6	-8.8	-9.1	-9.5	-10.2	-11.0	-11.7	-12.5	-13.3	-14.0	-14.8	-15.6	-16.3
10	3.2	0.7	-997	-8.3	-19561	-17.9	-8.5	-9.2	-10.1	-11.9	-13.7	-15.5	-17.2	-19.0	-20.8	-22.6	-24.4	-26.2
11	6.0	0.9	-997	-8.3	-19560	-16.8	-8.4	-9.1	-9.9	-11.6	-13.3	-15.0	-16.7	-18.3	-20.0	-21.7	-23.4	-25.0
12	5.7	0.8	-996	-8.0	-19565	-21.9	-8.3	-9.1	-10.2	-12.4	-14.6	-16.8	-19.0	-21.2	-23.3	-25.5	-27.7	-29.9
13	6.7	0.9	-996	-7.9	-19564	-21.2	-8.2	-9.0	-10.1	-12.2	-14.3	-16.4	-18.5	-20.7	-22.8	-24.9	-27.0	-29.1
14	2.0	0.7	-996	-7.6	-19563	-20.5	-7.8	-8.6	-9.7	-11.7	-13.8	-15.8	-17.9	-19.9	-21.9	-24.0	-26.0	-28.1
15	3.1	0.8	-996	-8.0	-19550	-7.2	-8.1	-8.4	-8.8	-9.5	-10.2	-10.9	-11.6	-12.4	-13.1	-13.8	-14.5	-15.3
16	6.8	1.0	-996	-7.7	-19567	-24.2	-7.9	-8.9	-10.1	-12.5	-14.9	-17.4	-19.8	-22.2	-24.6	-27.0	-29.5	-31.9
17	5.8	0.8	-995	-7.8	-19553	-10.2	-7.9	-8.3	-8.9	-9.9	-10.9	-11.9	-12.9	-14.0	-15.0	-16.0	-17.0	-18.0

Table S45: 13 in 1ZHUB, Experiment 5

Entry	ligand RMSD	BS RMSD	old_IFD Score	Glide Score	PE <sub>IFD</sub>	ΔPE	new_IFD Score _1	new_IFD Score _5	new_IFD Score _10	new_IFD Score _20	new_IFD Score _30	new_IFD Score _40	new_IFD Score _50	new_IFD Score _60	new_IFD Score _70	new_IFD Score _80	new_IFD Score _90	new_IFD Score _100
1	2.0	0.7	-1000	-10.1	-19562	-19.3	-10.3	-11.0	-12.0	-13.9	-15.9	-17.8	-19.7	-21.6	-23.6	-25.5	-27.4	-29.4
2	2.0	0.8	-999	-9.6	-19584	-40.6	-10.0	-11.6	-13.6	-17.7	-21.8	-25.8	-29.9	-34.0	-38.0	-42.1	-46.1	-50.2
3	2.2	0.9	-999	-8.9	-19586	-43.4	-9.3	-11.0	-13.2	-17.5	-21.9	-26.2	-30.6	-34.9	-39.2	-43.6	-47.9	-52.2
4	3.0	0.9	-999	-9.2	-19574	-31.1	-9.5	-10.7	-12.3	-15.4	-18.5	-21.6	-24.7	-27.8	-31.0	-34.1	-37.2	-40.3
5	3.0	0.8	-998	-8.8	-19586	-43.5	-9.2	-11.0	-13.1	-17.5	-21.8	-26.2	-30.5	-34.9	-39.2	-43.6	-47.9	-52.3
6	3.1	0.8	-998	-8.3	-19586	-43.5	-8.8	-10.5	-12.7	-17.0	-21.4	-25.7	-30.1	-34.4	-38.8	-43.1	-47.5	-51.8
7	2.2	0.8	-998	-8.3	-19578	-35.4	-8.7	-10.1	-11.9	-15.4	-19.0	-22.5	-26.0	-29.6	-33.1	-36.7	-40.2	-43.8
8	3.2	0.7	-998	-8.2	-19576	-33.5	-8.6	-9.9	-11.6	-14.9	-18.3	-21.7	-25.0	-28.4	-31.7	-35.1	-38.4	-41.8
9	2.6	0.8	-998	-8.8	-19578	-35.0	-9.1	-10.5	-12.3	-15.7	-19.2	-22.7	-26.2	-29.7	-33.2	-36.7	-40.2	-43.7
10	2.3	0.9	-998	-8.8	-19567	-24.3	-9.1	-10.1	-11.3	-13.7	-16.1	-18.6	-21.0	-23.4	-25.9	-28.3	-30.7	-33.2
11	2.1	0.8	-998	-8.3	-19577	-34.2	-8.6	-10.0	-11.7	-15.1	-18.6	-22.0	-25.4	-28.8	-32.3	-35.7	-39.1	-42.5
12	3.2	0.8	-997	-8.4	-19569	-25.7	-8.7	-9.7	-11.0	-13.5	-16.1	-18.7	-21.2	-23.8	-26.4	-28.9	-31.5	-34.1
13	3.2	0.8	-997	-8.4	-19568	-25.5	-8.7	-9.7	-11.0	-13.5	-16.1	-18.6	-21.2	-23.7	-26.3	-28.8	-31.4	-33.9
14	2.1	0.8	-997	-8.1	-19556	-13.2	-8.2	-8.8	-9.4	-10.7	-12.1	-13.4	-14.7	-16.0	-17.3	-18.7	-20.0	-21.3

Table S46: **13** in 1ZHUB, Experiment 6

Entry	ligand RMSD	BS RMSD	old_IFD Score	Glidecore	PE <sub>IFD</sub>	ΔPE	new_IFD Score _1	new_IFD Score _5	new_IFD Score _10	new_IFD Score _20	new_IFD Score _30	new_IFD Score _40	new_IFD Score _50	new_IFD Score _60	new_IFD Score _70	new_IFD Score _80	new_IFD Score _90	new_IFD Score _100
1	2.2	0.8	-999	-9.6	-19561	-18.6	-9.7	-10.5	-11.4	-13.3	-15.1	-17.0	-18.8	-20.7	-22.6	-24.4	-26.3	-28.1
2	2.2	0.7	-998	-10.1	-19549	-5.8	-10.1	-10.4	-10.7	-11.2	-11.8	-12.4	-13.0	-13.6	-14.1	-14.7	-15.3	-15.9
3	2.0	0.8	-998	-10.1	-19538	5.3	-10.1	-9.9	-9.6	-9.1	-8.5	-8.0	-7.5	-6.9	-6.4	-5.9	-5.3	-4.8
4	2.1	0.7	-998	-9.4	-19558	-15.4	-9.5	-10.1	-10.9	-12.4	-14.0	-15.5	-17.0	-18.6	-20.1	-21.7	-23.2	-24.7
5	2.0	0.7	-998	-9.1	-19564	-21.0	-9.3	-10.1	-11.2	-13.3	-15.4	-17.4	-19.5	-21.6	-23.7	-25.8	-27.9	-30.0
6	2.0	0.7	-998	-9.9	-19554	-10.8	-10.0	-10.4	-10.9	-12.0	-13.1	-14.2	-15.3	-16.3	-17.4	-18.5	-19.6	-20.7
7	2.1	0.8	-998	-9.6	-19547	-4.0	-9.7	-9.8	-10.0	-10.4	-10.8	-11.2	-11.6	-12.0	-12.4	-12.8	-13.2	-13.6
8	3.2	0.9	-997	-8.8	-19557	-13.9	-9.0	-9.5	-10.2	-11.6	-13.0	-14.4	-15.8	-17.2	-18.5	-19.9	-21.3	-22.7
9	2.1	0.8	-997	-8.9	-19552	-9.4	-9.0	-9.4	-9.8	-10.8	-11.7	-12.7	-13.6	-14.6	-15.5	-16.5	-17.4	-18.3
10	3.2	0.8	-997	-9.0	-19549	-6.5	-9.1	-9.3	-9.7	-10.3	-11.0	-11.6	-12.2	-12.9	-13.5	-14.2	-14.8	-15.5
11	2.0	0.8	-997	-8.8	-19547	-3.7	-8.8	-9.0	-9.2	-9.5	-9.9	-10.3	-10.7	-11.0	-11.4	-11.8	-12.1	-12.5
12	3.4	0.8	-997	-8.5	-19560	-16.7	-8.7	-9.3	-10.2	-11.8	-13.5	-15.2	-16.8	-18.5	-20.2	-21.8	-23.5	-25.2
13	2.1	0.8	-997	-8.9	-19534	9.1	-8.8	-8.4	-8.0	-7.1	-6.2	-5.3	-4.4	-3.4	-2.5	-1.6	-0.7	0.2
14	2.2	0.8	-996	-8.2	-19560	-17.0	-8.4	-9.1	-9.9	-11.6	-13.3	-15.0	-16.7	-18.4	-20.1	-21.8	-23.5	-25.3
15	8.8	0.8	-995	-6.7	-19565	-22.5	-6.9	-7.8	-9.0	-11.2	-13.5	-15.7	-18.0	-20.2	-22.5	-24.7	-27.0	-29.2

Table S47: 13 in 1ZHUB, Experiment 7

Entry	ligand RMSD	BS RMSD	old_IFD Score	Glide Score	PE <sub>IFD</sub>	ΔPE	new_IFD Score _1	new_IFD Score _5	new_IFD Score _10	new_IFD Score _20	new_IFD Score _30	new_IFD Score _40	new_IFD Score _50	new_IFD Score _60	new_IFD Score _70	new_IFD Score _80	new_IFD Score _90	new_IFD Score _100
1	2.0	0.7	-1002	-10.3	-19597	-53.6	-10.9	-13.0	-15.7	-21.1	-26.4	-31.8	-37.1	-42.5	-47.9	-53.2	-58.6	-64.0
2	2.1	0.7	-1000	-10.5	-19570	-27.0	-10.8	-11.9	-13.2	-15.9	-18.6	-21.3	-24.0	-26.7	-29.4	-32.1	-34.8	-37.5
3	2.5	0.9	-1000	-9.6	-19581	-37.9	-10.0	-11.5	-13.4	-17.2	-21.0	-24.8	-28.6	-32.4	-36.2	-39.9	-43.7	-47.5
4	2.4	0.9	-1000	-9.6	-19590	-46.8	-10.0	-11.9	-14.2	-18.9	-23.6	-28.3	-33.0	-37.6	-42.3	-47.0	-51.7	-56.4
5	2.0	0.8	-1000	-9.9	-19577	-34.6	-10.2	-11.6	-13.3	-16.8	-20.2	-23.7	-27.1	-30.6	-34.1	-37.5	-41.0	-44.4
6	3.1	0.8	-1000	-9.5	-19588	-45.2	-9.9	-11.7	-14.0	-18.5	-23.0	-27.6	-32.1	-36.6	-41.1	-45.7	-50.2	-54.7
7	1.9	0.7	-1000	-9.5	-19579	-36.0	-9.8	-11.3	-13.1	-16.7	-20.3	-23.9	-27.5	-31.1	-34.7	-38.3	-41.9	-45.5
8	2.1	0.8	-999	-9.0	-19574	-31.4	-9.3	-10.5	-12.1	-15.2	-18.4	-21.5	-24.7	-27.8	-30.9	-34.1	-37.2	-40.3
9	9.4	0.9	-998	-7.7	-19581	-38.3	-8.1	-9.6	-11.5	-15.4	-19.2	-23.0	-26.9	-30.7	-34.5	-38.4	-42.2	-46.0
10	6.7	0.9	-997	-7.5	-19597	-53.7	-8.0	-10.1	-12.8	-18.2	-23.6	-28.9	-34.3	-39.7	-45.0	-50.4	-55.8	-61.1

Table S48: **13** in 1ZHUB, Experiment 8

Ligand **15** in 1ZHUB

Entry	ligand RMSD	BS RMSD	old_IFD Score	Glide Score	PE <sub>IFD</sub>	$\Delta$ PE	new_IFD Score_1	new_IFD Score_5	new_IFD Score_10	new_IFD Score_20	new_IFD Score_30	new_IFD Score_40	new_IFD Score_50	new_IFD Score_60	new_IFD Score_70	new_IFD Score_80	new_IFD Score_90	new_IFD Score_100
1	<b>8.9</b>	1.5	-1002.8	-10.5	-19577	-33.6	<b>-10.9</b>	<b>-12.2</b>	-13.9	-17.3	-20.6	-24.0	-27.3	-30.7	-34.0	-37.4	-40.8	-44.1
2	9.0	1.2	-1002.3	-9.2	-19595	-51.8	-9.7	-11.8	-14.3	-19.5	-24.7	-29.9	-35.1	-40.3	-45.4	-50.6	-55.8	-61.0
3	9.2	1.1	-1002.1	-8.8	-19591	-48.1	-9.3	-11.2	-13.6	-18.4	-23.2	-28.1	-32.9	-37.7	-42.5	-47.3	-52.1	-56.9
4	9.1	0.9	-1001.9	-9.1	-19581	-38.2	-9.4	-11.0	-12.9	-16.7	-20.5	-24.3	-28.2	-32.0	-35.8	-39.6	-43.5	-47.3
5	9.4	1.0	-1001.9	-8.5	-19597	-53.7	-9.1	-11.2	-13.9	-19.3	-24.6	-30.0	-35.4	-40.7	-46.1	-51.5	-56.9	-62.2
6	9.5	1.2	-1001.9	-8.8	-19598	-54.7	-9.4	-11.6	-14.3	-19.8	-25.2	-30.7	-36.2	-41.6	-47.1	-52.6	-58.1	-63.5
7	<b>8.9</b>	1.0	-1001.8	-8.9	-19602	-59.3	-9.5	-11.8	<b>-14.8</b>	<b>-20.7</b>	<b>-26.6</b>	<b>-32.6</b>	<b>-38.5</b>	<b>-44.4</b>	<b>-50.3</b>	<b>-56.3</b>	<b>-62.2</b>	<b>-68.1</b>
8	9.3	0.9	-1001.8	-8.9	-19586	-42.8	-9.3	-11.0	-13.1	-17.4	-21.7	-26.0	-30.3	-34.6	-38.8	-43.1	-47.4	-51.7
9	9.0	1.0	-1000.2	-7.9	-19583	-39.9	-8.3	-9.9	-11.8	-15.8	-19.8	-23.8	-27.8	-31.8	-35.8	-39.7	-43.7	-47.7
10	9.0	1.1	-1000.1	-7.9	-19587	-43.9	-8.4	-10.1	-12.3	-16.7	-21.1	-25.5	-29.9	-34.3	-38.7	-43.1	-47.5	-51.9

Table S49: **15** in 1ZHUB, Experiment 1

Entry	ligand RMSD	BS RMSD	old_IFD Score	Glide Score	PE <sub>IFD</sub>	ΔPE	new_IFD Score _1	new_IFD Score _5	new_IFD Score _10	new_IFD Score _20	new_IFD Score _30	new_IFD Score _40	new_IFD Score _50	new_IFD Score _60	new_IFD Score _70	new_IFD Score _80	new_IFD Score _90	new_IFD Score _100
1	9.0	1.1	-1004	-9.6	-19588	-45.5	-10.1	-11.9	-14.1	-18.7	-23.2	-27.8	-32.3	-36.9	-41.4	-46.0	-50.5	-55.1
2	9.1	1.1	-1003	-9.2	-19592	-48.8	-9.7	-11.7	-14.1	-19.0	-23.9	-28.7	-33.6	-38.5	-43.4	-48.2	-53.1	-58.0
3	9.5	1.1	-1003	-9.6	-19598	-54.9	-10.2	-12.4	-15.1	-20.6	-26.1	-31.6	-37.1	-42.6	-48.1	-53.5	-59.0	-64.5
4	9.1	1.1	-1003	-9.7	-19585	-42.2	-10.1	-11.8	-13.9	-18.2	-22.4	-26.6	-30.8	-35.0	-39.3	-43.5	-47.7	-51.9
5	8.7	1.2	-1003	-9.7	-19581	-38.5	-10.1	-11.6	-13.5	-17.4	-21.2	-25.1	-28.9	-32.8	-36.7	-40.5	-44.4	-48.2
6	8.9	1.2	-1003	-8.2	-19604	-61.3	-8.9	-11.3	-14.4	-20.5	-26.6	-32.8	-38.9	-45.1	-51.2	-57.3	-63.5	-69.6
7	9.0	1.0	-1003	-8.9	-19585	-42.6	-9.3	-11.0	-13.2	-17.4	-21.7	-25.9	-30.2	-34.4	-38.7	-42.9	-47.2	-51.5
8	9.1	1.1	-1002	-8.5	-19586	-43.2	-8.9	-10.6	-12.8	-17.1	-21.4	-25.8	-30.1	-34.4	-38.7	-43.0	-47.3	-51.7
9	8.7	1.2	-1002	-9.2	-19587	-44.6	-9.7	-11.5	-13.7	-18.1	-22.6	-27.1	-31.5	-36.0	-40.4	-44.9	-49.4	-53.8
10	8.7	1.1	-1002	-8.8	-19589	-45.9	-9.3	-11.1	-13.4	-18.0	-22.6	-27.2	-31.8	-36.4	-41.0	-45.6	-50.2	-54.8
11	8.8	1.2	-1002	-9.0	-19587	-44.0	-9.4	-11.2	-13.4	-17.8	-22.2	-26.6	-31.0	-35.4	-39.8	-44.2	-48.6	-53.0
12	9.5	1.1	-1002	-8.8	-19593	-50.2	-9.3	-11.3	-13.8	-18.8	-23.9	-28.9	-33.9	-38.9	-44.0	-49.0	-54.0	-59.0
13	9.1	1.1	-1002	-8.6	-19581	-37.9	-9.0	-10.5	-12.4	-16.2	-20.0	-23.7	-27.5	-31.3	-35.1	-38.9	-42.7	-46.5
14	8.7	1.1	-1002	-8.6	-19581	-37.6	-9.0	-10.5	-12.3	-16.1	-19.9	-23.6	-27.4	-31.2	-34.9	-38.7	-42.5	-46.2
15	9.9	1.1	-1001	-7.6	-19591	-47.9	-8.1	-10.0	-12.4	-17.2	-22.0	-26.8	-31.6	-36.4	-41.1	-45.9	-50.7	-55.5
16	9.4	1.1	-1001	-7.5	-19590	-47.6	-8.0	-9.9	-12.3	-17.1	-21.8	-26.6	-31.3	-36.1	-40.8	-45.6	-50.4	-55.1
17	7.6	1.0	-1001	-7.3	-19588	-44.9	-7.7	-9.5	-11.8	-16.3	-20.7	-25.2	-29.7	-34.2	-38.7	-43.2	-47.7	-52.2

Table S50: 15 in 1ZHUB, Experiment 2

Entry	ligand RMSD	BS RMSD	old_IFD Score	Glide Score	PE <sub>IFD</sub>	ΔPE	new_IFD Score _1	new_IFD Score _5	new_IFD Score _10	new_IFD Score _20	new_IFD Score _30	new_IFD Score _40	new_IFD Score _50	new_IFD Score _60	new_IFD Score _70	new_IFD Score _80	new_IFD Score _90	new_IFD Score _100
1	9.1	1.0	-1002	-9.0	-19574	-31.4	-9.3	-10.6	-12.2	-15.3	-18.4	-21.6	-24.7	-27.8	-31.0	-34.1	-37.3	-40.4
2	8.9	1.0	-1001	-8.7	-19564	-21.3	-8.9	-9.8	-10.8	-13.0	-15.1	-17.2	-19.4	-21.5	-23.6	-25.8	-27.9	-30.0
3	9.2	1.0	-1001	-8.2	-19584	-40.8	-8.7	-10.3	-12.3	-16.4	-20.5	-24.6	-28.7	-32.7	-36.8	-40.9	-45.0	-49.1
4	9.4	1.0	-1001	-8.4	-19573	-29.9	-8.7	-9.9	-11.4	-14.4	-17.4	-20.3	-23.3	-26.3	-29.3	-32.3	-35.3	-38.3
5	9.2	1.0	-1001	-8.7	-19572	-29.1	-9.0	-10.1	-11.6	-14.5	-17.4	-20.3	-23.2	-26.2	-29.1	-32.0	-34.9	-37.8
6	9.2	1.1	-1001	-8.9	-19563	-20.2	-9.1	-9.9	-11.0	-13.0	-15.0	-17.0	-19.0	-21.1	-23.1	-25.1	-27.1	-29.2
7	9.4	0.9	-999	-7.2	-19583	-39.7	-7.6	-9.2	-11.2	-15.2	-19.1	-23.1	-27.1	-31.0	-35.0	-39.0	-42.9	-46.9
8	9.4	1.0	-999	-7.5	-19572	-29.5	-7.8	-8.9	-10.4	-13.4	-16.3	-19.3	-22.2	-25.2	-28.1	-31.0	-34.0	-36.9
9	9.1	1.0	-999	-7.5	-19583	-39.7	-7.9	-9.5	-11.5	-15.5	-19.4	-23.4	-27.4	-31.3	-35.3	-39.3	-43.2	-47.2

Table S51: **15** in 1ZHUB, Experiment 3

Entry	ligand RMSD	BS RMSD	old_IFD Score	Glide Score	PE <sub>IFD</sub>	ΔPE	new_IFD Score <sub>_1</sub>	new_IFD Score <sub>_5</sub>	new_IFD Score <sub>_10</sub>	new_IFD Score <sub>_20</sub>	new_IFD Score <sub>_30</sub>	new_IFD Score <sub>_40</sub>	new_IFD Score <sub>_50</sub>	new_IFD Score <sub>_60</sub>	new_IFD Score <sub>_70</sub>	new_IFD Score <sub>_80</sub>	new_IFD Score <sub>_90</sub>	new_IFD Score <sub>_100</sub>
1	8.9	1.1	-1002	-9.0	-19575	-32.6	-9.4	-10.7	-12.3	-15.5	-18.8	-22.1	-25.3	-28.6	-31.8	-35.1	-38.4	-41.6
2	9.0	1.1	-1001	-9.0	-19560	-17.1	-9.2	-9.9	-10.7	-12.4	-14.2	-15.9	-17.6	-19.3	-21.0	-22.7	-24.4	-26.2
3	8.8	1.0	-1001	-9.2	-19563	-19.9	-9.4	-10.2	-11.2	-13.2	-15.1	-17.1	-19.1	-21.1	-23.1	-25.1	-27.1	-29.1
4	9.0	1.0	-1001	-9.1	-19560	-17.6	-9.3	-10.0	-10.8	-12.6	-14.4	-16.1	-17.9	-19.6	-21.4	-23.1	-24.9	-26.7
5	9.2	1.0	-1001	-8.8	-19565	-22.1	-9.1	-9.9	-11.1	-13.3	-15.5	-17.7	-19.9	-22.1	-24.3	-26.5	-28.7	-31.0
6	9.0	1.0	-1001	-8.7	-19567	-23.8	-9.0	-9.9	-11.1	-13.5	-15.8	-18.2	-20.6	-23.0	-25.3	-27.7	-30.1	-32.5
7	9.2	1.1	-1001	-8.7	-19577	-34.2	-9.1	-10.4	-12.2	-15.6	-19.0	-22.4	-25.9	-29.3	-32.7	-36.1	-39.6	-43.0
8	9.3	1.0	-1001	-8.7	-19575	-31.8	-9.0	-10.2	-11.8	-15.0	-18.2	-21.4	-24.5	-27.7	-30.9	-34.1	-37.2	-40.4
9	8.9	1.0	-1001	-8.5	-19570	-26.7	-8.7	-9.8	-11.2	-13.8	-16.5	-19.2	-21.8	-24.5	-27.2	-29.8	-32.5	-35.2
10	9.4	1.2	-1001	-8.3	-19560	-17.2	-8.5	-9.2	-10.0	-11.8	-13.5	-15.2	-16.9	-18.6	-20.3	-22.1	-23.8	-25.5
11	9.1	1.0	-1001	-8.3	-19569	-26.3	-8.6	-9.6	-11.0	-13.6	-16.2	-18.8	-21.5	-24.1	-26.7	-29.4	-32.0	-34.6
12	9.3	1.0	-1001	-8.5	-19573	-30.2	-8.8	-10.0	-11.5	-14.5	-17.6	-20.6	-23.6	-26.6	-29.6	-32.7	-35.7	-38.7
13	9.2	1.0	-1000	-8.2	-19572	-28.6	-8.4	-9.6	-11.0	-13.9	-16.8	-19.6	-22.5	-25.3	-28.2	-31.1	-33.9	-36.8
14	9.4	1.1	-1000	-7.7	-19585	-42.0	-8.1	-9.8	-11.9	-16.1	-20.3	-24.5	-28.7	-32.9	-37.1	-41.3	-45.5	-49.8
15	9.2	1.1	-1000	-8.0	-19575	-31.7	-8.3	-9.6	-11.2	-14.4	-17.5	-20.7	-23.9	-27.1	-30.2	-33.4	-36.6	-39.7
16	9.2	1.1	-1000	-8.1	-19570	-26.9	-8.4	-9.4	-10.8	-13.5	-16.2	-18.8	-21.5	-24.2	-26.9	-29.6	-32.3	-35.0
17	9.1	1.1	-1000	-7.7	-19581	-38.1	-8.1	-9.6	-11.5	-15.3	-19.1	-23.0	-26.8	-30.6	-34.4	-38.2	-42.0	-45.8
18	9.1	1.1	-1000	-7.6	-19576	-32.7	-7.9	-9.2	-10.9	-14.1	-17.4	-20.7	-23.9	-27.2	-30.5	-33.7	-37.0	-40.3
19	9.8	1.0	-999	-6.8	-19582	-39.1	-7.2	-8.8	-10.7	-14.7	-18.6	-22.5	-26.4	-30.3	-34.2	-38.1	-42.0	-46.0
20	10.2	1.1	-998	-6.9	-19575	-32.4	-7.2	-8.5	-10.1	-13.4	-16.6	-19.8	-23.1	-26.3	-29.6	-32.8	-36.1	-39.3

Table S52: 15 in 1ZHUB, Experiment 4



Entry	ligand RMSD	BS RMSD	old_IFD Score	Glide Score	PE <sub>IFD</sub>	ΔPE	new_IFD Score _1	new_IFD Score _5	new_IFD Score _10	new_IFD Score _20	new_IFD Score _30	new_IFD Score _40	new_IFD Score _50	new_IFD Score _60	new_IFD Score _70	new_IFD Score _80	new_IFD Score _90	new_IFD Score _100
1	9.5	1.1	-1003	-10.2	-19583	-39.8	-10.6	-12.2	-14.1	-18.1	-22.1	-26.1	-30.1	-34.0	-38.0	-42.0	-46.0	-49.9
2	9.2	1.0	-1002	-8.8	-19584	-40.7	-9.2	-10.8	-12.8	-16.9	-21.0	-25.0	-29.1	-33.1	-37.2	-41.3	-45.3	-49.4
3	8.9	1.0	-1002	-10.0	-19587	-44.2	-10.4	-12.2	-14.4	-18.8	-23.2	-27.7	-32.1	-36.5	-40.9	-45.3	-49.7	-54.2
4	9.4	1.0	-1002	-9.2	-19586	-43.0	-9.7	-11.4	-13.5	-17.8	-22.1	-26.4	-30.7	-35.0	-39.3	-43.7	-48.0	-52.3
5	9.5	1.0	-1002	-9.1	-19589	-45.8	-9.6	-11.4	-13.7	-18.3	-22.9	-27.5	-32.0	-36.6	-41.2	-45.8	-50.4	-54.9
6	9.1	1.0	-1002	-9.1	-19576	-32.9	-9.4	-10.7	-12.4	-15.7	-19.0	-22.3	-25.5	-28.8	-32.1	-35.4	-38.7	-42.0
7	9.2	1.0	-1002	-8.8	-19576	-33.3	-9.1	-10.5	-12.1	-15.5	-18.8	-22.1	-25.4	-28.8	-32.1	-35.4	-38.7	-42.1
8	8.7	1.1	-1002	-8.9	-19578	-34.9	-9.3	-10.7	-12.4	-15.9	-19.4	-22.9	-26.4	-29.9	-33.4	-36.9	-40.4	-43.9
9	9.1	1.0	-1002	-9.0	-19562	-19.5	-9.2	-10.0	-10.9	-12.9	-14.8	-16.8	-18.7	-20.7	-22.6	-24.6	-26.5	-28.5
10	9.4	1.0	-1002	-8.9	-19584	-41.5	-9.3	-11.0	-13.0	-17.2	-21.3	-25.5	-29.6	-33.8	-37.9	-42.1	-46.2	-50.3
11	8.7	1.1	-1001	-8.3	-19575	-31.9	-8.6	-9.9	-11.5	-14.7	-17.9	-21.1	-24.3	-27.4	-30.6	-33.8	-37.0	-40.2
12	9.4	1.0	-1001	-7.9	-19592	-49.4	-8.4	-10.4	-12.8	-17.8	-22.7	-27.7	-32.6	-37.5	-42.5	-47.4	-52.3	-57.3
13	9.0	1.2	-1001	-8.3	-19574	-30.7	-8.6	-9.8	-11.4	-14.4	-17.5	-20.6	-23.6	-26.7	-29.8	-32.8	-35.9	-39.0
14	9.3	1.1	-1000	-7.4	-19591	-48.5	-7.9	-9.9	-12.3	-17.1	-22.0	-26.8	-31.7	-36.5	-41.4	-46.2	-51.1	-55.9
15	7.8	1.0	-1000	-7.8	-19581	-38.6	-8.2	-9.7	-11.6	-15.5	-19.4	-23.2	-27.1	-30.9	-34.8	-38.7	-42.5	-46.4
16	9.5	1.1	-999	-7.3	-19581	-37.7	-7.7	-9.2	-11.1	-14.9	-18.7	-22.4	-26.2	-30.0	-33.7	-37.5	-41.3	-45.0

Table S53: 15 in 1ZHUB, Experiment 5

Entry	ligand RMSD	BS RMSD	old_IFD Score	Glide Score	PE <sub>IFD</sub>	ΔPE	new_IFD Score _1	new_IFD Score _5	new_IFD Score _10	new_IFD Score _20	new_IFD Score _30	new_IFD Score _40	new_IFD Score _50	new_IFD Score _60	new_IFD Score _70	new_IFD Score _80	new_IFD Score _90	new_IFD Score _100
1	9.3	1.0	-1004	-9.6	-19587	-44.2	-10.1	-11.9	-14.1	-18.5	-22.9	-27.3	-31.7	-36.1	-40.6	-45.0	-49.4	-53.8
2	9.8	1.1	-1003	-9.1	-19587	-44.0	-9.5	-11.3	-13.5	-17.9	-22.3	-26.7	-31.1	-35.5	-39.9	-44.3	-48.7	-53.1
3	9.2	1.0	-1003	-8.6	-19590	-46.8	-9.1	-11.0	-13.3	-18.0	-22.7	-27.4	-32.0	-36.7	-41.4	-46.1	-50.8	-55.5
4	9.4	1.1	-1003	-9.2	-19588	-45.4	-9.7	-11.5	-13.8	-18.3	-22.8	-27.4	-31.9	-36.4	-41.0	-45.5	-50.1	-54.6
5	8.2	1.2	-1003	-9.4	-19583	-40.1	-9.8	-11.4	-13.4	-17.4	-21.4	-25.4	-29.4	-33.4	-37.4	-41.4	-45.5	-49.5
6	8.4	1.1	-1003	-9.3	-19587	-44.2	-9.7	-11.5	-13.7	-18.1	-22.6	-27.0	-31.4	-35.8	-40.2	-44.6	-49.1	-53.5
7	9.2	1.1	-1003	-8.4	-19593	-50.6	-9.0	-11.0	-13.5	-18.6	-23.6	-28.7	-33.7	-38.8	-43.8	-48.9	-54.0	-59.0
8	7.0	1.1	-1002	-8.6	-19577	-34.4	-9.0	-10.4	-12.1	-15.5	-19.0	-22.4	-25.9	-29.3	-32.7	-36.2	-39.6	-43.1
9	9.3	1.1	-1002	-8.4	-19592	-49.3	-8.9	-10.8	-13.3	-18.2	-23.2	-28.1	-33.0	-38.0	-42.9	-47.8	-52.8	-57.7
10	9.5	1.1	-1002	-8.4	-19593	-50.4	-9.0	-11.0	-13.5	-18.5	-23.6	-28.6	-33.6	-38.7	-43.7	-48.7	-53.8	-58.8
11	8.8	1.0	-1002	-8.6	-19584	-41.3	-9.0	-10.7	-12.7	-16.9	-21.0	-25.1	-29.3	-33.4	-37.5	-41.7	-45.8	-49.9
12	9.0	1.2	-1002	-8.5	-19589	-46.4	-9.0	-10.9	-13.2	-17.8	-22.5	-27.1	-31.7	-36.4	-41.0	-45.7	-50.3	-54.9
13	9.6	1.1	-1001	-7.8	-19589	-46.2	-8.3	-10.1	-12.5	-17.1	-21.7	-26.3	-30.9	-35.6	-40.2	-44.8	-49.4	-54.0
14	9.3	1.1	-1000	-6.9	-19594	-51.3	-7.4	-9.4	-12.0	-17.1	-22.3	-27.4	-32.5	-37.7	-42.8	-47.9	-53.1	-58.2

Table S54: 15 in 1ZHUB, Experiment 6

Entry	ligand RMSD	BS RMSD	old_IFD Score	Glide Score	PE <sub>IFD</sub>	ΔPE	new_IFD Score _1	new_IFD Score _5	new_IFD Score _10	new_IFD Score _20	new_IFD Score _30	new_IFD Score _40	new_IFD Score _50	new_IFD Score _60	new_IFD Score _70	new_IFD Score _80	new_IFD Score _90	new_IFD Score _100
1	9.1	1.1	-1002	-9.1	-19586	-42.7	-9.5	-11.2	-13.4	-17.6	-21.9	-26.2	-30.5	-34.7	-39.0	-43.3	-47.5	-51.8
2	9.1	1.0	-1002	-9.1	-19572	-29.4	-9.4	-10.6	-12.0	-15.0	-17.9	-20.8	-23.8	-26.7	-29.6	-32.6	-35.5	-38.4
3	9.3	1.0	-1001	-9.3	-19575	-32.3	-9.6	-10.9	-12.5	-15.7	-19.0	-22.2	-25.4	-28.7	-31.9	-35.1	-38.4	-41.6
4	9.1	1.1	-1001	-9.1	-19570	-27.5	-9.4	-10.5	-11.9	-14.6	-17.4	-20.1	-22.9	-25.6	-28.3	-31.1	-33.8	-36.6
5	9.1	1.1	-1001	-9.3	-19578	-34.6	-9.7	-11.0	-12.8	-16.2	-19.7	-23.2	-26.6	-30.1	-33.5	-37.0	-40.5	-43.9
6	9.0	1.0	-1001	-9.3	-19564	-20.8	-9.5	-10.3	-11.4	-13.4	-15.5	-17.6	-19.7	-21.8	-23.9	-25.9	-28.0	-30.1
7	9.1	1.0	-1001	-8.8	-19574	-31.1	-9.1	-10.3	-11.9	-15.0	-18.1	-21.2	-24.3	-27.4	-30.5	-33.7	-36.8	-39.9
8	9.1	1.0	-1001	-8.5	-19576	-33.2	-8.8	-10.1	-11.8	-15.1	-18.4	-21.7	-25.1	-28.4	-31.7	-35.0	-38.4	-41.7
9	8.9	1.0	-1001	-8.9	-19566	-23.2	-9.2	-10.1	-11.3	-13.6	-15.9	-18.2	-20.5	-22.9	-25.2	-27.5	-29.8	-32.1
10	9.4	1.0	-1001	-8.4	-19575	-31.8	-8.7	-10.0	-11.6	-14.8	-17.9	-21.1	-24.3	-27.5	-30.6	-33.8	-37.0	-40.2
11	9.1	1.0	-1001	-8.5	-19577	-34.4	-8.8	-10.2	-11.9	-15.4	-18.8	-22.2	-25.7	-29.1	-32.6	-36.0	-39.5	-42.9
12	9.0	1.0	-1000	-8.3	-19571	-27.7	-8.5	-9.6	-11.0	-13.8	-16.6	-19.3	-22.1	-24.9	-27.7	-30.4	-33.2	-36.0
13	9.0	1.0	-1000	-8.6	-19561	-18.2	-8.7	-9.5	-10.4	-12.2	-14.0	-15.8	-17.6	-19.4	-21.3	-23.1	-24.9	-26.7
14	9.2	1.0	-1000	-8.3	-19567	-23.6	-8.5	-9.4	-10.6	-13.0	-15.3	-17.7	-20.0	-22.4	-24.8	-27.1	-29.5	-31.8
15	9.3	1.0	-1000	-8.5	-19577	-34.1	-8.8	-10.2	-11.9	-15.3	-18.7	-22.1	-25.5	-28.9	-32.4	-35.8	-39.2	-42.6
16	9.1	1.0	-999	-7.7	-19573	-30.3	-8.0	-9.3	-10.8	-13.8	-16.8	-19.9	-22.9	-25.9	-29.0	-32.0	-35.0	-38.1
17	9.3	1.0	-999	-8.0	-19559	-16.1	-8.1	-8.8	-9.6	-11.2	-12.8	-14.4	-16.0	-17.6	-19.2	-20.8	-22.4	-24.0

Table S55: 15 in 1ZHUB, Experiment 7

Entry	ligand RMSD	BS RMSD	old_IFD Score	Glide Score	PE <sub>IFD</sub>	ΔPE	new_IFD Score _1	new_IFD Score _5	new_IFD Score _10	new_IFD Score _20	new_IFD Score _30	new_IFD Score _40	new_IFD Score _50	new_IFD Score _60	new_IFD Score _70	new_IFD Score _80	new_IFD Score _90	new_IFD Score _100
1	9.3	1.1	-1004	-10.4	-19581	-38.2	-10.8	-12.3	-14.2	-18.0	-21.8	-25.6	-29.5	-33.3	-37.1	-40.9	-44.7	-48.6
2	9.3	1.1	-1004	-10.6	-19585	-41.9	-11.0	-12.7	-14.8	-19.0	-23.2	-27.4	-31.6	-35.8	-40.0	-44.2	-48.4	-52.6
3	9.0	1.0	-1004	-9.4	-19585	-41.7	-9.8	-11.5	-13.6	-17.7	-21.9	-26.1	-30.2	-34.4	-38.6	-42.8	-46.9	-51.1
4	9.4	1.1	-1004	-10.0	-19581	-37.7	-10.4	-11.9	-13.8	-17.6	-21.3	-25.1	-28.9	-32.6	-36.4	-40.2	-44.0	-47.7
5	9.3	1.1	-1003	-10.1	-19568	-24.9	-10.4	-11.4	-12.6	-15.1	-17.6	-20.1	-22.6	-25.1	-27.6	-30.0	-32.5	-35.0
6	9.6	1.1	-1003	-9.3	-19588	-45.2	-9.8	-11.6	-13.8	-18.4	-22.9	-27.4	-31.9	-36.4	-41.0	-45.5	-50.0	-54.5
7	9.0	1.1	-1002	-9.1	-19574	-30.8	-9.4	-10.6	-12.2	-15.2	-18.3	-21.4	-24.5	-27.5	-30.6	-33.7	-36.8	-39.9
8	8.8	1.2	-1002	-8.9	-19591	-48.2	-9.4	-11.3	-13.7	-18.5	-23.3	-28.2	-33.0	-37.8	-42.6	-47.5	-52.3	-57.1
9	9.3	1.1	-1002	-8.7	-19583	-39.8	-9.1	-10.7	-12.7	-16.7	-20.6	-24.6	-28.6	-32.6	-36.5	-40.5	-44.5	-48.5
10	9.3	1.2	-1002	-8.1	-19593	-50.1	-8.6	-10.6	-13.1	-18.1	-23.1	-28.1	-33.1	-38.2	-43.2	-48.2	-53.2	-58.2
11	9.5	1.0	-1001	-7.5	-19602	-58.9	-8.1	-10.5	-13.4	-19.3	-25.2	-31.1	-37.0	-42.8	-48.7	-54.6	-60.5	-66.4
12	9.3	1.0	-1001	-7.2	-19586	-42.8	-7.7	-9.4	-11.5	-15.8	-20.1	-24.4	-28.6	-32.9	-37.2	-41.5	-45.7	-50.0
13	9.6	1.1	-1001	-7.5	-19589	-46.5	-7.9	-9.8	-12.1	-16.8	-21.4	-26.1	-30.7	-35.4	-40.0	-44.7	-49.3	-54.0

Table S56: 15 in 1ZHUB, Experiment 8

Ligand **13** in 7WZYC

Entry	ligand RMSD	BS RMSD	old_IFD Score	Glide Score	PE <sub>IFD</sub>	$\Delta$ PE	new_IFD Score _1	new_IFD Score _5	new_IFD Score _10	new_IFD Score _20	new_IFD Score _30	new_IFD Score _40	new_IFD Score _50	new_IFD Score _60	new_IFD Score _70	new_IFD Score _80	new_IFD Score _90	new_IFD Score _100
1	1.6	1.1	-2142	-9.2	-41919	-84.6	-10.0	-13.4	-17.6	-26.1	-34.5	-43.0	-51.4	-59.9	-68.4	-76.8	-85.3	-93.7
2	1.8	1.1	-2142	-9.9	-41797	37.5	-9.6	-8.1	-6.2	-2.4	1.3	5.1	8.8	12.6	16.3	20.1	23.8	27.6
3	1.5	1.1	-2142	-10.0	-41860	-25.8	-10.2	-11.3	-12.6	-15.1	-17.7	-20.3	-22.9	-25.4	-28.0	-30.6	-33.2	-35.8
4	2.4	1.1	-2141	-9.9	-41848	-13.3	-10.0	-10.6	-11.2	-12.6	-13.9	-15.2	-16.6	-17.9	-19.2	-20.6	-21.9	-23.2
5	2.3	1.1	-2141	-9.1	-41862	-28.0	-9.4	-10.5	-11.9	-14.7	-17.5	-20.3	-23.1	-25.9	-28.7	-31.5	-34.3	-37.1
6	2.6	1.1	-2141	-9.1	-41862	-27.8	-9.4	-10.5	-11.9	-14.7	-17.4	-20.2	-23.0	-25.8	-28.5	-31.3	-34.1	-36.9
7	2.1	1.1	-2141	-9.4	-41855	-20.7	-9.6	-10.4	-11.4	-13.5	-15.6	-17.6	-19.7	-21.8	-23.9	-25.9	-28.0	-30.1
8	2.3	1.1	-2141	-9.4	-41803	30.8	-9.1	-7.8	-6.3	-3.2	-0.1	3.0	6.1	9.1	12.2	15.3	18.4	21.5
9	2.2	1.1	-2141	-8.8	-41903	-69.2	-9.5	-12.2	-15.7	-22.6	-29.5	-36.5	-43.4	-50.3	-57.2	-64.1	-71.1	-78.0

Table S57: **13** in 7WZYC, Experiment 1

Entry	ligand RMSD	BS RMSD	old_IFD Score	Glide Score	PE <sub>IFD</sub>	ΔPE	new_IFD Score <sub>_1</sub>	new_IFD Score <sub>_5</sub>	new_IFD Score <sub>_10</sub>	new_IFD Score <sub>_20</sub>	new_IFD Score <sub>_30</sub>	new_IFD Score <sub>_40</sub>	new_IFD Score <sub>_50</sub>	new_IFD Score <sub>_60</sub>	new_IFD Score <sub>_70</sub>	new_IFD Score <sub>_80</sub>	new_IFD Score <sub>_90</sub>	new_IFD Score <sub>_100</sub>
1	2.3	1.2	-2140	-9.0	-41849	-14.9	-9.1	-9.7	-10.5	-12.0	-13.5	-15.0	-16.5	-18.0	-19.5	-21.0	-22.5	-23.9
2	3.3	1.4	-2140	-10.1	-41773	61.1	-9.5	-7.0	-4.0	2.1	8.2	14.4	20.5	26.6	32.7	38.8	44.9	51.0
3	3.1	1.4	-2140	-10.2	-41889	-54.9	-10.7	-12.9	-15.7	-21.2	-26.6	-32.1	-37.6	-43.1	-48.6	-54.1	-59.6	-65.1
4	2.2	1.4	-2140	-9.1	-41781	53.7	-8.5	-6.4	-3.7	1.7	7.0	12.4	17.8	23.2	28.5	33.9	39.3	44.6
5	2.2	1.3	-2140	-9.3	-41836	-1.7	-9.3	-9.4	-9.4	-9.6	-9.8	-9.9	-10.1	-10.3	-10.4	-10.6	-10.8	-10.9
6	4.4	1.0	-2139	-8.8	-41870	-35.4	-9.2	-10.6	-12.4	-15.9	-19.5	-23.0	-26.5	-30.1	-33.6	-37.2	-40.7	-44.2
7	1.9	1.4	-2139	-9.5	-41855	-21.2	-9.7	-10.5	-11.6	-13.7	-15.8	-18.0	-20.1	-22.2	-24.3	-26.4	-28.6	-30.7

Table S58: 13 in 7WZYC, Experiment 2

Entry	ligand RMSD	BS RMSD	old_IFD Score	Glide Score	PE <sub>IFD</sub>	ΔPE	new_IFD Score _1	new_IFD Score _5	new_IFD Score _10	new_IFD Score _20	new_IFD Score _30	new_IFD Score _40	new_IFD Score _50	new_IFD Score _60	new_IFD Score _70	new_IFD Score _80	new_IFD Score _90	new_IFD Score _100
1	2.3	1.2	-2143	-10.9	-41911	-76.5	-11.6	-14.7	-18.5	-26.2	-33.8	-41.5	-49.1	-56.8	-64.4	-72.0	-79.7	-87.3
2	2.0	1.0	-2142	-9.5	-41903	-68.3	-10.2	-12.9	-16.3	-23.1	-30.0	-36.8	-43.6	-50.5	-57.3	-64.1	-71.0	-77.8
3	2.6	1.2	-2142	-10.1	-41856	-21.6	-10.3	-11.2	-12.2	-14.4	-16.6	-18.7	-20.9	-23.0	-25.2	-27.3	-29.5	-31.7
4	5.0	1.3	-2141	-10.3	-41902	-67.6	-11.0	-13.7	-17.1	-23.8	-30.6	-37.4	-44.1	-50.9	-57.7	-64.4	-71.2	-78.0
5	2.0	1.1	-2141	-9.7	-41897	-62.7	-10.4	-12.9	-16.0	-22.3	-28.6	-34.8	-41.1	-47.4	-53.6	-59.9	-66.2	-72.5
6	2.2	1.1	-2141	-8.7	-41870	-36.0	-9.1	-10.5	-12.3	-15.9	-19.5	-23.1	-26.7	-30.3	-33.9	-37.5	-41.1	-44.7
7	3.0	1.0	-2141	-9.0	-41800	33.8	-8.7	-7.3	-5.6	-2.3	1.1	4.5	7.9	11.2	14.6	18.0	21.4	24.8
8	3.0	1.3	-2141	-9.5	-41850	-15.6	-9.7	-10.3	-11.1	-12.6	-14.2	-15.8	-17.3	-18.9	-20.4	-22.0	-23.6	-25.1
9	3.3	1.0	-2141	-8.8	-41865	-30.7	-9.1	-10.3	-11.8	-14.9	-18.0	-21.1	-24.1	-27.2	-30.3	-33.4	-36.4	-39.5
10	3.0	1.2	-2141	-9.3	-41856	-21.9	-9.5	-10.4	-11.5	-13.7	-15.9	-18.0	-20.2	-22.4	-24.6	-26.8	-29.0	-31.2
11	2.4	1.1	-2141	-9.4	-41898	-63.5	-10.0	-12.6	-15.8	-22.1	-28.5	-34.8	-41.2	-47.5	-53.9	-60.2	-66.6	-72.9
12	9.2	1.0	-2140	-8.6	-41868	-33.4	-9.0	-10.3	-12.0	-15.3	-18.7	-22.0	-25.3	-28.7	-32.0	-35.3	-38.7	-42.0

Table S59: **13** in 7WZYC, Experiment 3

Entry	ligand RMSD	BS RMSD	old_IFD Score	Glide Score	PE <sub>IFD</sub>	ΔPE	new_IFD Score _1	new_IFD Score _5	new_IFD Score _10	new_IFD Score _20	new_IFD Score _30	new_IFD Score _40	new_IFD Score _50	new_IFD Score _60	new_IFD Score _70	new_IFD Score _80	new_IFD Score _90	new_IFD Score _100
1	2.8	1.1	-2141	-10.4	-41871	-37.3	-10.7	-12.2	-14.1	-17.8	-21.5	-25.3	-29.0	-32.7	-36.4	-40.2	-43.9	-47.6
2	3.0	1.0	-2140	-9.8	-41889	-55.0	-10.4	-12.6	-15.3	-20.8	-26.3	-31.8	-37.3	-42.8	-48.3	-53.8	-59.3	-64.8
3	3.0	1.1	-2140	-9.4	-41888	-53.5	-10.0	-12.1	-14.8	-20.1	-25.5	-30.8	-36.2	-41.5	-46.8	-52.2	-57.5	-62.9
4	2.4	1.2	-2140	-9.0	-41891	-57.1	-9.6	-11.9	-14.7	-20.4	-26.1	-31.8	-37.6	-43.3	-49.0	-54.7	-60.4	-66.1
5	9.1	1.4	-2140	-9.3	-41911	-76.4	-10.0	-13.1	-16.9	-24.5	-32.2	-39.8	-47.5	-55.1	-62.7	-70.4	-78.0	-85.7
6	5.4	1.2	-2139	-9.2	-41871	-36.6	-9.6	-11.1	-12.9	-16.6	-20.2	-23.9	-27.5	-31.2	-34.8	-38.5	-42.1	-45.8
7	4.2	1.5	-2139	-9.4	-41892	-57.6	-9.9	-12.2	-15.1	-20.9	-26.6	-32.4	-38.2	-43.9	-49.7	-55.5	-61.2	-67.0
8	2.1	1.0	-2139	-9.1	-41793	41.2	-8.7	-7.0	-5.0	-0.8	3.3	7.4	11.5	15.6	19.7	23.9	28.0	32.1
9	8.9	1.6	-2139	-9.5	-41882	-47.4	-10.0	-11.9	-14.3	-19.0	-23.8	-28.5	-33.2	-38.0	-42.7	-47.5	-52.2	-56.9
10	2.4	1.0	-2139	-9.1	-41870	-35.8	-9.5	-10.9	-12.7	-16.3	-19.9	-23.4	-27.0	-30.6	-34.2	-37.7	-41.3	-44.9
11	9.3	1.5	-2138	-8.7	-41835	-0.9	-8.7	-8.7	-8.8	-8.9	-9.0	-9.0	-9.1	-9.2	-9.3	-9.4	-9.5	-9.5
12	9.2	1.3	-2138	-8.0	-41901	-66.9	-8.7	-11.3	-14.7	-21.4	-28.1	-34.8	-41.4	-48.1	-54.8	-61.5	-68.2	-74.9
13	8.7	1.6	-2138	-9.0	-41885	-50.3	-9.5	-11.5	-14.0	-19.1	-24.1	-29.1	-34.2	-39.2	-44.2	-49.3	-54.3	-59.3
14	3.1	1.4	-2138	-8.0	-41888	-53.7	-8.6	-10.7	-13.4	-18.8	-24.1	-29.5	-34.9	-40.2	-45.6	-51.0	-56.3	-61.7
15	8.7	1.4	-2138	-8.2	-41903	-68.8	-8.9	-11.7	-15.1	-22.0	-28.9	-35.8	-42.7	-49.5	-56.4	-63.3	-70.2	-77.1
16	9.1	1.7	-2137	-7.3	-41854	-19.3	-7.5	-8.3	-9.2	-11.2	-13.1	-15.0	-17.0	-18.9	-20.8	-22.8	-24.7	-26.6

Table S60: 13 in 7WZYC, Experiment 4



Entry	ligand RMSD	BS RMSD	old_IFD Score	Glide Score	PE <sub>IFD</sub>	ΔPE	new_IFD Score _1	new_IFD Score _5	new_IFD Score _10	new_IFD Score _20	new_IFD Score _30	new_IFD Score _40	new_IFD Score _50	new_IFD Score _60	new_IFD Score _70	new_IFD Score _80	new_IFD Score _90	new_IFD Score _100
1	2.2	1.3	-2141	-8.9	-41812	22.0	-8.7	-7.8	-6.7	-4.5	-2.3	-0.1	2.1	4.3	6.5	8.7	10.9	13.1
2	7.0	1.5	-2141	-8.6	-41872	-37.4	-9.0	-10.5	-12.3	-16.1	-19.8	-23.6	-27.3	-31.0	-34.8	-38.5	-42.3	-46.0
3	2.3	1.3	-2141	-9.1	-41887	-53.0	-9.6	-11.7	-14.4	-19.7	-25.0	-30.3	-35.6	-40.9	-46.2	-51.5	-56.8	-62.1
4	3.0	1.3	-2141	-9.5	-41860	-25.8	-9.7	-10.8	-12.1	-14.6	-17.2	-19.8	-22.4	-24.9	-27.5	-30.1	-32.7	-35.2
5	2.4	1.0	-2141	-9.3	-41863	-28.7	-9.6	-10.8	-12.2	-15.1	-18.0	-20.8	-23.7	-26.6	-29.4	-32.3	-35.2	-38.0
6	2.9	1.2	-2141	-8.6	-41872	-37.8	-9.0	-10.5	-12.4	-16.2	-19.9	-23.7	-27.5	-31.3	-35.0	-38.8	-42.6	-46.4
7	2.7	1.2	-2141	-9.5	-41786	48.4	-9.0	-7.1	-4.7	0.2	5.0	9.8	14.7	19.5	24.3	29.2	34.0	38.9
8	3.1	1.0	-2141	-8.9	-41914	-79.6	-9.7	-12.8	-16.8	-24.8	-32.7	-40.7	-48.7	-56.6	-64.6	-72.5	-80.5	-88.4

Table S61: 13 in 7WZYC, Experiment 5

Entry	ligand RMSD	BS RMSD	old_IFD Score	Glide Score	PE <sub>IFD</sub>	ΔPE	new_IFD Score _1	new_IFD Score _5	new_IFD Score _10	new_IFD Score _20	new_IFD Score _30	new_IFD Score _40	new_IFD Score _50	new_IFD Score _60	new_IFD Score _70	new_IFD Score _80	new_IFD Score _90	new_IFD Score _100
1	2.3	1.2	-2142	-10.8	-41906	-71.6	-11.6	-14.4	-18.0	-25.2	-32.3	-39.5	-46.7	-53.8	-61.0	-68.2	-75.3	-82.5
2	2.9	1.1	-2142	-10.1	-41803	30.7	-9.8	-8.5	-7.0	-3.9	-0.9	2.2	5.3	8.4	11.4	14.5	17.6	20.7
3	2.3	1.3	-2141	-10.6	-41881	-47.2	-11.0	-12.9	-15.3	-20.0	-24.7	-29.5	-34.2	-38.9	-43.6	-48.3	-53.1	-57.8
4	2.6	1.2	-2141	-10.3	-41888	-53.7	-10.8	-12.9	-15.6	-21.0	-26.4	-31.7	-37.1	-42.5	-47.8	-53.2	-58.6	-64.0
5	2.9	1.1	-2141	-9.6	-41917	-82.9	-10.4	-13.7	-17.8	-26.1	-34.4	-42.7	-51.0	-59.3	-67.6	-75.9	-84.2	-92.5
6	4.6	1.1	-2141	-9.3	-41900	-65.6	-10.0	-12.6	-15.9	-22.4	-29.0	-35.5	-42.1	-48.7	-55.2	-61.8	-68.3	-74.9
7	2.9	1.2	-2140	-9.3	-41859	-24.6	-9.6	-10.6	-11.8	-14.3	-16.7	-19.2	-21.6	-24.1	-26.5	-29.0	-31.4	-33.9
8	3.0	1.2	-2140	-9.7	-41842	-7.7	-9.7	-10.1	-10.4	-11.2	-12.0	-12.7	-13.5	-14.3	-15.0	-15.8	-16.6	-17.3
9	2.2	1.4	-2140	-9.6	-41840	-5.6	-9.7	-9.9	-10.2	-10.7	-11.3	-11.9	-12.4	-13.0	-13.5	-14.1	-14.6	-15.2
10	3.3	1.1	-2140	-9.4	-41893	-59.2	-10.0	-12.4	-15.4	-21.3	-27.2	-33.1	-39.0	-44.9	-50.9	-56.8	-62.7	-68.6
11	3.3	1.0	-2140	-8.7	-41874	-40.2	-9.1	-10.7	-12.7	-16.8	-20.8	-24.8	-28.8	-32.8	-36.9	-40.9	-44.9	-48.9
12	7.8	1.1	-2139	-8.2	-41866	-31.6	-8.5	-9.8	-11.4	-14.5	-17.7	-20.9	-24.0	-27.2	-30.3	-33.5	-36.7	-39.8
13	6.4	1.1	-2139	-8.0	-41792	42.5	-7.5	-5.8	-3.7	0.5	4.8	9.0	13.3	17.5	21.8	26.0	30.3	34.5
14	6.9	1.2	-2139	-8.1	-41913	-79.2	-8.9	-12.0	-16.0	-23.9	-31.8	-39.8	-47.7	-55.6	-63.5	-71.4	-79.3	-87.3

Table S62: **13** in 7WZYC, Experiment 6

Entry	ligand RMSD	BS RMSD	old_IFD Score	Glide Score	PE <sub>IFD</sub>	ΔPE	new_IFD Score_1	new_IFD Score_5	new_IFD Score_10	new_IFD Score_20	new_IFD Score_30	new_IFD Score_40	new_IFD Score_50	new_IFD Score_60	new_IFD Score_70	new_IFD Score_80	new_IFD Score_90	new_IFD Score_100
1	2.4	1.0	-2143	-10.0	-41927	-92.8	-10.9	-14.6	-19.3	-28.5	-37.8	-47.1	-56.4	-65.7	-75.0	-84.2	-93.5	-102.8
2	3.2	1.1	-2142	-9.2	-41885	-50.6	-9.7	-11.7	-14.2	-19.3	-24.3	-29.4	-34.5	-39.5	-44.6	-49.7	-54.7	-59.8
3	3.2	1.0	-2142	-9.6	-41871	-36.9	-10.0	-11.4	-13.3	-17.0	-20.7	-24.4	-28.1	-31.7	-35.4	-39.1	-42.8	-46.5
4	2.9	1.1	-2142	-9.6	-41869	-35.0	-9.9	-11.3	-13.1	-16.6	-20.1	-23.6	-27.1	-30.6	-34.1	-37.6	-41.1	-44.6
5	2.9	0.9	-2142	-9.4	-41809	25.4	-9.2	-8.2	-6.9	-4.4	-1.8	0.7	3.3	5.8	8.4	10.9	13.5	16.0
6	2.9	1.2	-2142	-9.4	-41816	18.6	-9.2	-8.5	-7.5	-5.7	-3.8	-2.0	-0.1	1.8	3.6	5.5	7.4	9.2
7	2.2	1.0	-2142	-9.0	-41868	-33.7	-9.3	-10.6	-12.3	-15.7	-19.1	-22.5	-25.8	-29.2	-32.6	-36.0	-39.3	-42.7
8	3.1	1.1	-2141	-9.6	-41801	32.9	-9.3	-8.0	-6.3	-3.1	0.2	3.5	6.8	10.1	13.4	16.7	20.0	23.2
9	2.5	1.2	-2141	-8.8	-41801	33.6	-8.5	-7.1	-5.4	-2.1	1.3	4.6	8.0	11.4	14.7	18.1	21.4	24.8

Table S63: **13** in 7WZYC, Experiment 7

Entry	ligand RMSD	BS RMSD	old_IFD Score	Glide Score	PE <sub>IFD</sub>	ΔPE	new_IFD Score_1	new_IFD Score_5	new_IFD Score_10	new_IFD Score_20	new_IFD Score_30	new_IFD Score_40	new_IFD Score_50	new_IFD Score_60	new_IFD Score_70	new_IFD Score_80	new_IFD Score_90	new_IFD Score_100
1	2.1	1.2	-2142	-10.4	-41891	-57.1	-11.0	-13.3	-16.1	-21.9	-27.6	-33.3	-39.0	-44.7	-50.4	-56.1	-61.8	-67.5
2	2.0	1.0	-2141	-9.6	-41909	-75.3	-10.4	-13.4	-17.2	-24.7	-32.2	-39.8	-47.3	-54.8	-62.3	-69.9	-77.4	-84.9
3	3.0	1.1	-2141	-9.8	-41850	-16.2	-10.0	-10.6	-11.4	-13.0	-14.7	-16.3	-17.9	-19.5	-21.2	-22.8	-24.4	-26.0
4	3.1	1.2	-2141	-9.2	-41855	-20.4	-9.4	-10.2	-11.2	-13.2	-15.3	-17.3	-19.4	-21.4	-23.4	-25.5	-27.5	-29.5
5	2.2	1.3	-2141	-10.3	-41888	-54.1	-10.8	-13.0	-15.7	-21.1	-26.5	-31.9	-37.4	-42.8	-48.2	-53.6	-59.0	-64.4
6	3.0	1.2	-2140	-8.4	-41904	-69.8	-9.1	-11.9	-15.4	-22.4	-29.4	-36.4	-43.3	-50.3	-57.3	-64.3	-71.3	-78.3
7	2.2	1.0	-2139	-8.8	-41797	36.9	-8.4	-7.0	-5.1	-1.4	2.3	6.0	9.6	13.3	17.0	20.7	24.4	28.1
8	4.5	1.1	-2139	-7.7	-41892	-57.6	-8.3	-10.6	-13.5	-19.2	-25.0	-30.8	-36.5	-42.3	-48.1	-53.8	-59.6	-65.4

Table S64: **13** in 7WZYC, Experiment 8

Ligand **14** in 7WZYC

Entry	ligand RMSD	BS RMSD	old_IFD Score	Glide Score	PE <sub>IFD</sub>	ΔPE	new_IFD Score <sub>_1</sub>	new_IFD Score <sub>_5</sub>	new_IFD Score <sub>_10</sub>	new_IFD Score <sub>_20</sub>	new_IFD Score <sub>_30</sub>	new_IFD Score <sub>_40</sub>	new_IFD Score <sub>_50</sub>	new_IFD Score <sub>_60</sub>	new_IFD Score <sub>_70</sub>	new_IFD Score <sub>_80</sub>	new_IFD Score <sub>_90</sub>	new_IFD Score <sub>_100</sub>
1	1.9	0.8	-2141	-9.3	-41906	-72.2	-10.1	-13.0	-16.6	-23.8	-31.0	-38.2	-45.5	-52.7	-59.9	-67.1	-74.3	-81.6
2	1.8	0.8	-2141	-10.4	-41873	-39.3	-10.8	-12.3	-14.3	-18.2	-22.2	-26.1	-30.0	-33.9	-37.9	-41.8	-45.7	-49.6
3	2.9	0.8	-2141	-9.6	-41813	21.6	-9.3	-8.5	-7.4	-5.2	-3.1	-0.9	1.3	3.4	5.6	7.7	9.9	12.1
4	3.0	0.8	-2141	-9.4	-41873	-38.8	-9.8	-11.3	-13.3	-17.1	-21.0	-24.9	-28.8	-32.7	-36.6	-40.4	-44.3	-48.2
5	1.8	0.8	-2140	-8.8	-41912	-77.3	-9.6	-12.7	-16.6	-24.3	-32.0	-39.8	-47.5	-55.2	-63.0	-70.7	-78.4	-86.2
6	2.2	0.8	-2140	-8.8	-41806	28.6	-8.6	-7.4	-6.0	-3.1	-0.3	2.6	5.4	8.3	11.2	14.0	16.9	19.7
7	2.0	1.0	-2140	-9.2	-41792	42.1	-8.8	-7.1	-5.0	-0.8	3.5	7.7	11.9	16.1	20.3	24.5	28.7	33.0
8	2.6	0.8	-2140	-9.0	-41799	35.4	-8.6	-7.2	-5.4	-1.9	1.7	5.2	8.7	12.3	15.8	19.4	22.9	26.5
9	1.7	0.8	-2139	-8.8	-41798	36.6	-8.5	-7.0	-5.2	-1.5	2.2	5.8	9.5	13.2	16.8	20.5	24.2	27.8
10	5.1	0.8	-2139	-8.5	-41866	-32.2	-8.8	-10.1	-11.7	-14.9	-18.2	-21.4	-24.6	-27.8	-31.0	-34.2	-37.5	-40.7
11	3.6	1.2	-2139	-8.8	-41859	-24.5	-9.1	-10.0	-11.3	-13.7	-16.2	-18.6	-21.0	-23.5	-25.9	-28.4	-30.8	-33.3
12	2.5	0.8	-2139	-8.1	-41810	24.5	-7.9	-6.9	-5.7	-3.2	-0.8	1.7	4.1	6.6	9.0	11.5	13.9	16.4
13	2.7	0.8	-2138	-8.0	-41800	34.4	-7.7	-6.3	-4.6	-1.2	2.3	5.7	9.2	12.6	16.0	19.5	22.9	26.4

Table S65: **14** in 7WZYC, Experiment 1

Entry	ligand RMSD	BS RMSD	old_IFD Score	Glide Score	PE <sub>IFD</sub>	ΔPE	new_IFD Score <sub>_1</sub>	new_IFD Score <sub>_5</sub>	new_IFD Score <sub>_10</sub>	new_IFD Score <sub>_20</sub>	new_IFD Score <sub>_30</sub>	new_IFD Score <sub>_40</sub>	new_IFD Score <sub>_50</sub>	new_IFD Score <sub>_60</sub>	new_IFD Score <sub>_70</sub>	new_IFD Score <sub>_80</sub>	new_IFD Score <sub>_90</sub>	new_IFD Score <sub>_100</sub>
1	4.7	0.9	-2140	-9.1	-41857	-23.0	-9.3	-10.2	-11.4	-13.7	-16.0	-18.3	-20.6	-22.9	-25.2	-27.5	-29.8	-32.1
2	2.4	0.9	-2140	-9.2	-41801	33.7	-8.9	-7.5	-5.9	-2.5	0.9	4.3	7.6	11.0	14.4	17.7	21.1	24.5
3	2.6	0.8	-2140	-9.1	-41796	37.9	-8.8	-7.3	-5.4	-1.6	2.2	6.0	9.8	13.6	17.4	21.2	25.0	28.8
4	3.1	0.8	-2140	-8.7	-41909	-74.4	-9.4	-12.4	-16.1	-23.6	-31.0	-38.5	-45.9	-53.3	-60.8	-68.2	-75.7	-83.1
5	2.4	0.8	-2140	-8.9	-41797	37.2	-8.5	-7.1	-5.2	-1.5	2.2	6.0	9.7	13.4	17.1	20.8	24.6	28.3
6	3.1	0.8	-2139	-9.4	-41781	53.2	-8.8	-6.7	-4.1	1.3	6.6	11.9	17.2	22.5	27.9	33.2	38.5	43.8
7	3.0	0.8	-2139	-8.8	-41901	-66.4	-9.5	-12.1	-15.4	-22.1	-28.7	-35.4	-42.0	-48.7	-55.3	-62.0	-68.6	-75.2
8	3.0	0.8	-2139	-8.9	-41867	-32.9	-9.2	-10.6	-12.2	-15.5	-18.8	-22.1	-25.4	-28.6	-31.9	-35.2	-38.5	-41.8
9	4.6	0.8	-2139	-8.9	-41777	56.8	-8.3	-6.1	-3.2	2.5	8.2	13.8	19.5	25.2	30.9	36.6	42.3	47.9
10	2.4	0.8	-2139	-8.5	-41791	43.4	-8.0	-6.3	-4.1	0.2	4.5	8.9	13.2	17.6	21.9	26.2	30.6	34.9
11	3.1	0.9	-2139	-8.8	-41777	57.6	-8.2	-5.9	-3.0	2.8	8.5	14.3	20.0	25.8	31.5	37.3	43.0	48.8
12	3.3	1.0	-2138	-7.7	-41788	46.6	-7.3	-5.4	-3.1	1.6	6.2	10.9	15.6	20.2	24.9	29.5	34.2	38.8

Table S66: 14 in 7WZYC, Experiment 2

Entry	ligand RMSD	BS RMSD	old_IFD Score	Glide Score	PE <sub>IFD</sub>	ΔPE	new_IFD Score _1	new_IFD Score _5	new_IFD Score _10	new_IFD Score _20	new_IFD Score _30	new_IFD Score _40	new_IFD Score _50	new_IFD Score _60	new_IFD Score _70	new_IFD Score _80	new_IFD Score _90	new_IFD Score _100
1	2.2	0.7	-2139	-9.2	-41789	44.9	-8.7	-7.0	-4.7	-0.2	4.3	8.8	13.2	17.7	22.2	26.7	31.2	35.7
2	3.1	0.9	-2139	-9.3	-41850	-16.2	-9.5	-10.1	-10.9	-12.5	-14.2	-15.8	-17.4	-19.0	-20.6	-22.2	-23.8	-25.5
3	2.2	0.7	-2139	-9.0	-41777	57.6	-8.4	-6.1	-3.2	2.5	8.3	14.0	19.8	25.5	31.3	37.1	42.8	48.6
4	4.7	0.9	-2139	-8.8	-41897	-62.5	-9.4	-11.9	-15.0	-21.3	-27.5	-33.8	-40.0	-46.3	-52.5	-58.8	-65.0	-71.3
5	2.4	0.8	-2139	-8.7	-41853	-19.2	-8.8	-9.6	-10.6	-12.5	-14.4	-16.3	-18.3	-20.2	-22.1	-24.0	-26.0	-27.9
6	2.7	0.8	-2139	-9.1	-41906	-71.7	-9.8	-12.7	-16.3	-23.5	-30.6	-37.8	-45.0	-52.1	-59.3	-66.5	-73.6	-80.8
7	4.9	0.8	-2139	-8.5	-41848	-13.6	-8.6	-9.1	-9.8	-11.2	-12.5	-13.9	-15.2	-16.6	-18.0	-19.3	-20.7	-22.0
8	2.5	0.9	-2138	-8.6	-41902	-68.3	-9.3	-12.0	-15.4	-22.2	-29.1	-35.9	-42.7	-49.5	-56.4	-63.2	-70.0	-76.9
9	2.5	0.8	-2138	-8.3	-41897	-63.1	-8.9	-11.4	-14.6	-20.9	-27.2	-33.5	-39.8	-46.1	-52.4	-58.8	-65.1	-71.4
10	2.5	0.8	-2138	-8.2	-41789	45.1	-7.8	-6.0	-3.7	0.8	5.3	9.8	14.3	18.8	23.3	27.8	32.3	36.9
11	2.1	0.8	-2138	-8.2	-41790	43.8	-7.7	-6.0	-3.8	0.6	5.0	9.3	13.7	18.1	22.5	26.9	31.2	35.6
12	2.5	0.9	-2138	-8.5	-41785	49.3	-8.0	-6.0	-3.5	1.4	6.4	11.3	16.2	21.2	26.1	31.0	36.0	40.9

Table S67: 14 in 7WZYC, Experiment 3

Entry	ligand RMSD	BS RMSD	old_IFD Score	Glide Score	PE <sub>IFD</sub>	ΔPE	new_IFD Score _1	new_IFD Score _5	new_IFD Score _10	new_IFD Score _20	new_IFD Score _30	new_IFD Score _40	new_IFD Score _50	new_IFD Score _60	new_IFD Score _70	new_IFD Score _80	new_IFD Score _90	new_IFD Score _100
1	4.8	0.9	-2140	-9.0	-41843	-9.1	-9.1	-9.4	-9.9	-10.8	-11.7	-12.6	-13.5	-14.4	-15.3	-16.2	-17.1	-18.0
2	2.8	0.7	-2140	-9.1	-41862	-28.3	-9.4	-10.5	-12.0	-14.8	-17.6	-20.4	-23.3	-26.1	-28.9	-31.8	-34.6	-37.4
3	5.2	0.9	-2139	-8.8	-41908	-74.1	-9.5	-12.5	-16.2	-23.6	-31.0	-38.4	-45.8	-53.2	-60.6	-68.0	-75.4	-82.8
4	5.3	0.9	-2139	-8.8	-41905	-70.3	-9.5	-12.3	-15.8	-22.8	-29.9	-36.9	-43.9	-51.0	-58.0	-65.0	-72.1	-79.1
5	2.4	0.8	-2139	-8.6	-41892	-58.2	-9.1	-11.5	-14.4	-20.2	-26.0	-31.8	-37.7	-43.5	-49.3	-55.1	-60.9	-66.7
6	2.3	0.8	-2139	-8.8	-41899	-65.2	-9.5	-12.1	-15.3	-21.8	-28.4	-34.9	-41.4	-47.9	-54.4	-60.9	-67.4	-74.0
7	2.9	0.8	-2139	-9.0	-41797	37.7	-8.6	-7.1	-5.2	-1.5	2.3	6.1	9.8	13.6	17.4	21.1	24.9	28.7
8	1.9	0.8	-2139	-8.2	-41802	32.6	-7.9	-6.6	-5.0	-1.7	1.5	4.8	8.0	11.3	14.6	17.8	21.1	24.3
9	7.7	0.8	-2139	-8.5	-41891	-56.7	-9.1	-11.4	-14.2	-19.9	-25.5	-31.2	-36.9	-42.5	-48.2	-53.9	-59.5	-65.2
10	2.7	1.0	-2138	-8.7	-41884	-50.1	-9.2	-11.2	-13.7	-18.7	-23.7	-28.7	-33.7	-38.7	-43.7	-48.7	-53.7	-58.7
11	2.1	0.9	-2138	-8.2	-41859	-24.7	-8.4	-9.4	-10.6	-13.1	-15.6	-18.1	-20.5	-23.0	-25.5	-27.9	-30.4	-32.9
12	7.5	0.9	-2138	-8.0	-41891	-57.0	-8.6	-10.9	-13.7	-19.4	-25.1	-30.8	-36.5	-42.2	-47.9	-53.6	-59.3	-65.0
13	3.1	1.0	-2138	-7.6	-41785	48.8	-7.1	-5.2	-2.7	2.1	7.0	11.9	16.8	21.6	26.5	31.4	36.3	41.1
14	7.8	0.9	-2137	-7.7	-41843	-9.2	-7.8	-8.2	-8.6	-9.6	-10.5	-11.4	-12.3	-13.2	-14.2	-15.1	-16.0	-16.9

Table S68: **14** in 7WZYC, Experiment 4

Entry	ligand RMSD	BS RMSD	old_IFD Score	Glide Score	PE <sub>IFD</sub>	ΔPE	new_IFD Score _1	new_IFD Score _5	new_IFD Score _10	new_IFD Score _20	new_IFD Score _30	new_IFD Score _40	new_IFD Score _50	new_IFD Score _60	new_IFD Score _70	new_IFD Score _80	new_IFD Score _90	new_IFD Score _100
1	2.7	0.7	-2141	-9.7	-41860	-25.5	-9.9	-10.9	-12.2	-14.8	-17.3	-19.9	-22.4	-25.0	-27.5	-30.1	-32.6	-35.2
2	2.8	1.0	-2141	-9.5	-41866	-31.9	-9.8	-11.1	-12.7	-15.9	-19.1	-22.3	-25.5	-28.7	-31.8	-35.0	-38.2	-41.4
3	4.7	0.9	-2140	-9.5	-41896	-62.0	-10.1	-12.6	-15.7	-21.9	-28.1	-34.3	-40.5	-46.7	-52.9	-59.1	-65.3	-71.5
4	4.7	0.9	-2140	-9.2	-41788	45.7	-8.7	-6.9	-4.6	0.0	4.5	9.1	13.7	18.3	22.8	27.4	32.0	36.6
5	2.4	0.8	-2140	-8.9	-41906	-71.5	-9.6	-12.5	-16.1	-23.2	-30.4	-37.5	-44.6	-51.8	-58.9	-66.1	-73.2	-80.4
6	7.7	0.8	-2140	-8.8	-41915	-80.7	-9.6	-12.9	-16.9	-25.0	-33.0	-41.1	-49.2	-57.2	-65.3	-73.4	-81.4	-89.5
7	2.2	0.8	-2140	-8.9	-41861	-27.2	-9.1	-10.2	-11.6	-14.3	-17.0	-19.7	-22.5	-25.2	-27.9	-30.6	-33.3	-36.1
8	7.7	0.8	-2140	-8.8	-41903	-68.5	-9.5	-12.3	-15.7	-22.5	-29.4	-36.2	-43.1	-49.9	-56.8	-63.7	-70.5	-77.4
9	2.3	0.8	-2139	-8.6	-41900	-66.1	-9.3	-11.9	-15.3	-21.9	-28.5	-35.1	-41.7	-48.3	-54.9	-61.6	-68.2	-74.8
10	7.7	1.3	-2139	-9.2	-41833	1.1	-9.2	-9.1	-9.1	-8.9	-8.8	-8.7	-8.6	-8.5	-8.4	-8.3	-8.2	-8.0

Table S69: 14 in 7WZYC, Experiment 5



Entry	ligand RMSD	BS RMSD	old_IFD Score	Glide Score	PE <sub>IFD</sub>	ΔPE	new_IFD Score _1	new_IFD Score _5	new_IFD Score _10	new_IFD Score _20	new_IFD Score _30	new_IFD Score _40	new_IFD Score _50	new_IFD Score _60	new_IFD Score _70	new_IFD Score _80	new_IFD Score _90	new_IFD Score _100
1	4.8	0.8	-2141	-9.8	-41795	39.1	-9.4	-7.8	-5.9	-2.0	1.9	5.8	9.8	13.7	17.6	21.5	25.4	29.3
2	2.6	0.8	-2140	-9.4	-41798	36.0	-9.0	-7.6	-5.8	-2.2	1.4	5.0	8.6	12.2	15.8	19.4	23.0	26.6
3	4.7	0.9	-2140	-9.4	-41897	-62.4	-10.0	-12.5	-15.6	-21.8	-28.1	-34.3	-40.5	-46.8	-53.0	-59.2	-65.5	-71.7
4	2.5	1.0	-2140	-9.7	-41792	42.7	-9.3	-7.6	-5.4	-1.2	3.1	7.4	11.7	15.9	20.2	24.5	28.7	33.0
5	5.5	0.9	-2140	-9.4	-41898	-63.6	-10.0	-12.6	-15.8	-22.1	-28.5	-34.8	-41.2	-47.5	-53.9	-60.3	-66.6	-73.0
6	2.4	0.8	-2140	-9.3	-41799	35.6	-9.0	-7.5	-5.8	-2.2	1.4	4.9	8.5	12.1	15.6	19.2	22.7	26.3
7	3.0	0.9	-2140	-9.4	-41794	40.2	-9.0	-7.4	-5.4	-1.3	2.7	6.7	10.7	14.7	18.7	22.8	26.8	30.8
8	3.3	0.8	-2139	-8.8	-41857	-22.9	-9.0	-9.9	-11.1	-13.4	-15.7	-17.9	-20.2	-22.5	-24.8	-27.1	-29.4	-31.7
9	3.3	0.9	-2139	-8.8	-41793	40.8	-8.4	-6.7	-4.7	-0.6	3.5	7.5	11.6	15.7	19.8	23.9	28.0	32.0
10	2.8	0.7	-2139	-8.9	-41892	-58.1	-9.5	-11.8	-14.7	-20.5	-26.3	-32.1	-38.0	-43.8	-49.6	-55.4	-61.2	-67.0
11	3.0	0.9	-2139	-8.5	-41801	32.8	-8.1	-6.8	-5.2	-1.9	1.4	4.7	8.0	11.2	14.5	17.8	21.1	24.4
12	4.4	0.9	-2139	-7.9	-41860	-25.9	-8.2	-9.2	-10.5	-13.1	-15.7	-18.3	-20.9	-23.5	-26.1	-28.6	-31.2	-33.8
13	2.7	0.9	-2139	-8.0	-41799	34.9	-7.6	-6.2	-4.5	-1.0	2.5	6.0	9.5	13.0	16.4	19.9	23.4	26.9

Table S70: 14 in 7WZYC, Experiment 6

Entry	ligandR MSD	BS RMSD	old_IFD Score	Glide Score	PE <sub>IFD</sub>	ΔPE	new_IFD Score _1	new_IFD Score _5	new_IFD Score _10	new_IFD Score _20	new_IFD Score _30	new_IFD Score _40	new_IFD Score _50	new_IFD Score _60	new_IFD Score _70	new_IFD Score _80	new_IFD Score _90	new_IFD Score _100
1	2.3	0.7	-2141	-9.6	-41860	-25.9	-9.9	-10.9	-12.2	-14.8	-17.4	-20.0	-22.6	-25.2	-27.8	-30.4	-33.0	-35.6
2	4.7	0.9	-2141	-9.7	-41895	-61.1	-10.3	-12.7	-15.8	-21.9	-28.0	-34.1	-40.2	-46.3	-52.4	-58.5	-64.6	-70.7
3	2.4	0.8	-2140	-9.0	-41807	27.3	-8.7	-7.6	-6.2	-3.5	-0.8	2.0	4.7	7.4	10.1	12.9	15.6	18.3
4	2.2	0.8	-2140	-9.1	-41798	35.9	-8.7	-7.3	-5.5	-1.9	1.7	5.3	8.9	12.4	16.0	19.6	23.2	26.8
5	2.8	0.8	-2140	-8.8	-41804	30.7	-8.5	-7.3	-5.8	-2.7	0.4	3.4	6.5	9.6	12.6	15.7	18.8	21.8
6	3.2	0.8	-2140	-8.8	-41915	-81.1	-9.6	-12.8	-16.9	-25.0	-33.1	-41.2	-49.3	-57.4	-65.5	-73.7	-81.8	-89.9
7	2.2	0.8	-2140	-8.8	-41799	35.7	-8.5	-7.0	-5.2	-1.7	1.9	5.4	9.0	12.6	16.1	19.7	23.3	26.8
8	2.9	0.8	-2139	-8.9	-41864	-30.2	-9.2	-10.4	-11.9	-14.9	-17.9	-21.0	-24.0	-27.0	-30.0	-33.1	-36.1	-39.1
9	2.3	0.7	-2139	-9.0	-41793	40.7	-8.6	-6.9	-4.9	-0.8	3.3	7.3	11.4	15.5	19.6	23.6	27.7	31.8
10	1.8	0.8	-2139	-8.8	-41794	40.4	-8.4	-6.8	-4.8	-0.8	3.3	7.3	11.4	15.4	19.4	23.5	27.5	31.5
11	2.3	0.9	-2138	-8.1	-41782	52.1	-7.6	-5.5	-2.9	2.3	7.5	12.7	18.0	23.2	28.4	33.6	38.8	44.0

Table S71: 14 in 7WZYC, Experiment 7

Entry	ligand RMSD	BS RMSD	old_IFD Score	Glide Score	PE <sub>IFD</sub>	ΔPE	new_IFD Score _1	new_IFD Score _5	new_IFD Score _10	new_IFD Score _20	new_IFD Score _30	new_IFD Score _40	new_IFD Score _50	new_IFD Score _60	new_IFD Score _70	new_IFD Score _80	new_IFD Score _90	new_IFD Score _100
1	2.9	0.8	-2140	-8.9	-41856	-22.3	-9.1	-10.0	-11.1	-13.3	-15.6	-17.8	-20.0	-22.3	-24.5	-26.7	-28.9	-31.2
2	3.1	0.8	-2140	-9.3	-41790	44.0	-8.8	-7.1	-4.9	-0.5	3.9	8.3	12.7	17.1	21.5	25.9	30.3	34.7
3	4.9	1.2	-2139	-8.6	-41887	-52.7	-9.2	-11.3	-13.9	-19.2	-24.4	-29.7	-35.0	-40.3	-45.5	-50.8	-56.1	-61.3
4	3.3	0.8	-2138	-8.6	-41897	-63.1	-9.2	-11.7	-14.9	-21.2	-27.5	-33.8	-40.1	-46.4	-52.8	-59.1	-65.4	-71.7

Table S72: 14 in 7WZYC, Experiment 8

